INFORMATION TO USERS

This manuscript has been reproduced from the microfilm master. UMI films the text directly from the original or copy submitted. Thus, some thesis and dissertation copies are in typewriter face, while others may be from any type of computer printer.

The quality of this reproduction is dependent upon the quality of the copy submitted. Broken or indistinct print, colored or poor quality illustrations and photographs, print bleedthrough, substandard margins, and improper alignment can adversely affect reproduction.

In the unlikely event that the author did not send UMI a complete manuscript and there are missing pages, these will be noted. Also, if unauthorized copyright material had to be removed, a note will indicate the deletion.

Oversize materials (e.g., maps, drawings, charts) are reproduced by sectioning the original, beginning at the upper left-hand corner and continuing from left to right in equal sections with small overlaps. Each original is also photographed in one exposure and is included in reduced form at the back of the book.

Photographs included in the original manuscript have been reproduced xerographically in this copy. Higher quality 6" x 9" black and white photographic prints are available for any photographs or illustrations appearing in this copy for an additional charge. Contact UMI directly to order.

UMI®

NOTE TO USERS

This reproduction is the best copy available

UMI

University of Alberta

Molecular Order, Miscibility, and Rheology of Molten Polyethylenes

by

Ibnelwaleed Ali Hussein ©

A thesis submitted to the Faculty of Graduate Studies and Research in partial fulfillment of the requirements for the degree of **Doctor of Philosophy**

in

Chemical Engineering

Department of Chemical and Materials Engineering

Edmonton, Alberta

Spring 1999

0-612-39542-1

Canada

University of Alberta

Library Release Form

Name of Author: Ibnelwaleed Ali Hussein
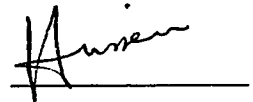
Title of Thesis: Molecular Order, Miscibility, and Rheology of Molten Polyethylenes

Degree: Doctor of Philosophy

Year this Degree Granted: 1999

Permission is hereby granted to the University of Alberta Library to reproduce single copies of this thesis and to lend or sell such copies for private, scholarly, or scientific research purposes only.

The author reserves all other publication and other rights in association with the copyright in the thesis, and except as hereinbefore provided, neither the thesis nor any substantial portion thereof may be printed or otherwise reproduced in any material form whatever without the author's prior written permission.

401 Michener Park
Edmonton, Alberta
Canada T6H 4M5

Date Submitted to the Faculty of Graduate Studies and Research

April 14, 99

University of Alberta

Faculty of Graduate Studies and Research

The undersigned certify that they have read, and recommended to the Faculty of Graduate studies and Research for acceptance, a thesis entitled **Molecular Order, Miscibility, and Rheology of Molten Polyethylenes** submitted by **Ibnelwaleed A. Hussein** in partial fulfillment of the requirements for the degree of Doctor of Philosophy in Chemical Engineering.

Professor Michael C. Williams
(Thesis Supervisor)

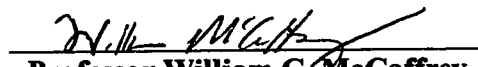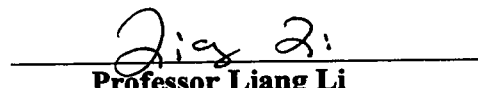Professor Sieghard E. Wanke
(Chair)

Professor Morton M. Denn
(External Examiner)

Professor Reg L. Eadie
(Member of Supervisory Committee)

Professor William C. McCaffrey
(Member of Supervisory Committee)

Professor Liang Li
(Member)

April 12, 99

ABSTRACT

New evidence of high-temperature transitions and molecular order in molten polyethylenes is presented, and its influence on the miscibility of polyethylenes is discussed. Thermal and rheological techniques were used to investigate commercial HDPE, LDPE and Ziegler-Natta and Metallocene LLDPEs. Adequate amounts of extra antioxidants were added to the polyethylenes during melt conditioning, following a separate investigation. Polystyrene was utilized to demonstrate the typical behavior of isotropic polymer melts. Temperature sweeps during torque measurements in a melt blender, and when using a rheometer and DSC, showed thermal transitions at about 208°C and 227°C. Torque in the blender over the temperature range 208°-227°C showed a flat profile or an increase in torque near 227°C, unique behavior associated with thermotropic liquid crystal polymers (LCP). Additional support for the liquid-state order that agree with theoretical predictions for a LCP is found. These include indications of an approach to a sign change in the first normal stress difference, $N_1(\dot{\gamma})$, at low values of the steady shear rate, $\dot{\gamma}$, and a kink in the non-Newtonian viscosity $\eta(\dot{\gamma})$. A rheological investigation found no evidence of the attainment of the isotropic state at high temperature and suggested the persistence of order above these transitions. However, highly branched metallocene LLDPE (~40 CH_3/1000 C) did not show transitions or any evidence of molecular order. It is suggested that polyethylenes possess different molecular conformation in the melt state ranging from the chain-folded HDPE to the amorphous highly-branched LLDPE. It is this molecular order and mismatch of the molecular conformations of different polyethylene structures that provide an explanation

for the immiscibility of polyethylenes, as revealed by the dependence of their rheological properties on blend composition. The influence of molecular weight, comonomer type, and mixing temperature on the miscibility of LLDPE and LDPE is discussed. Partial miscibility is observed in blends mixed at a temperature below 208°C, whereas blends mixed above that temperature were almost immiscible. Increasing the branch length of the LLDPE from butene to octene increased miscibility slightly. Literature reporting polyethylene melt behavior is critically reviewed over the last four decades and found to contain many anomalies of molecular order and structural transformations. The scientific community and the polyethylene processing industry need to investigate the implications of these findings.

Acknowledgements

Table of Contents

List of Tables

List of Figures

Nomenclature

a_0, a_1, a_2, a_3	constants (equations 6.1 and 6.6)
A	constant in the Arrhenius viscosity-temperature relationship
E	flow activation energy
g	gram
G'	storage (elastic) modulus
G''	loss modulus
G_m	modulus for the matrix (equation 6.6)
h	gap spacing between parallel plates
H_0	null hypothesis
L	lamellae thickness (equation 5.4)
m_1, m_2	fitting parameters in Carreau Model (equation 6.4) related to the powerlaw exponent by equation 6.5
M_n, M_w, M_z	molecular weights
n	powerlaw exponent
n_1, n_2	sample sizes
N_1	first normal stress difference
N_2	second normal stress difference
Q	volumetric flow rate
r	radius
R	gas constant
S_D	standard deviation
S_1, S_2	individual sample variances

S_p	common variance defined by equation 5.6
t_o	random variable of the t distribution defined by equation 5.5
T	temperature
T_m	melting temperature
T_{mix}	melt conditioning temperature in the blender
T_{test}	test temperature in the RMS
X_c	percentage crystallinity
y_1, y_2	sample means (equation 5.5)
γ	strain
γ^o	strain amplitude in dynamic shear ($\gamma = \gamma^o \sin \omega t$)
$\dot{\gamma}$	strain rate; steady shear rate
$\dot{\gamma}_R$	steady shear rate at the rim
δ	phase angle (tan $\delta = G''/G'$)
Δ	difference
η	non-Newtonian viscosity
η^*	complex viscosity ($= \eta' - i\,\eta''$)
η'	dynamic viscosity
η''	elastic component of the complex viscosity
η_o	zero shear viscosity
θ	mean relaxation time (equation 6.4)
λ	viscosity ratio ($= \lambda_2/\lambda_1$)
λ_1	matrix viscosity (equation 6.8)
λ_2	droplet viscosities (equation 6.8)

μ Newtonian viscosity

μ_1, μ_2 population means

ρ density

σ_y yield stress

τ stress

ϕ volume fraction

ω frequency in dynamic shear

I. Introduction

Today there are hundreds of homopolymers commercially available. Usually one type of polymer does not possess all the physical and/or mechanical properties desired in a finished product. So it is natural to try to blend two or more polymers to meet the requirements. This, besides other factors, generated the current interest, both academic and industrial, in the performance and processing and properties of polymer blends. Most commonly, a mixture of two or more polymers composed of chemically different monomers forms two or more distinct phases in the molten state. This gives rise to an emulsion-like dispersion in which one component, the discrete phase, is suspended in the other component, which forms the continuous phase (Han, 1981).

Intramolecular phase separation, of the sort exhibited by block copolymers with immiscible (incompatible) blocks was proposed for polyolefin copolymers by Wardhaugh and Williams (1995). They estimated the solubility parameter, δ, for linear and branched blocks within polyolefins, using the group contribution method, and one can infer that the same technique can be used for calculating δ for independent chain molecules as well as for blocks of those compositions. Their work on many specific branch structures in polyolefin molecules, predicted sufficient thermodynamic immiscibility between linear polyethylene (LPE) and a variety of unlike nonlinear structures containing CH_2 groups in linear and branched arrays to induce phase separation at the molecular level (microphase separation). A lot of unpublished experimental work of Williams' group on the rheology of polyethylene blends showed the presence of macroscopic phase separation in the melt, which opposes the conventional view that

polyethylene of all sorts (all composed primarily of $-CH_2-$ groups) should be completely miscible.

The experimental work published by Hill's group in UK (Barham et al., 1993, Hill et al., 1991, 1993, Hill and Barham, 1992 & 1993, Thomas et al., 1993) suggested that 'liquid-liquid' phase separation could occur in blends of linear and branched polyethylene (LPE, BPE) blends prepared at temperatures lower than 220°C, over certain wide ranges of fractional compositions.

The observed phase separation in the blends of molten polyethylenes, and other anomalous behavior reported in the literature, raised some new questions about the 'pure' polymers. In this research we carried out an investigation of 'pure' polymers, taking a major change in the direction of the current research in polyethylenes and their blends. The investigation was directed toward possible ordered microstructures in the melt being the reason behind the phase separation. This is expected to give new insight and help explain the observed nonuniformities in melt blends.

The suspicion of structure in the melt was triggered by the sudden ease of flow of LPE (also known as high-density polyethylene, HDPE) when heated past 210°C on a flame in a test tube. This observation was unusual since HDPE possesses solid-state crystals that have a melting range of 135°-140°C, and it is usually understood that when the temperature exceeds the solid-state crystalline melting range (characterized by T_m ≈137°C), then by definition HDPE is a melt and is usually thought to be amorphous, with molecules in the classical random coil form (Flory, 1953). Despite its molecular simplicity, HDPE in the solid crystalline state exhibits numerous thermal transitions at temperatures below T_m, such as α, β, γ, γ' transitions (Popli et al., 1984).

In this study linear and branched polyethylenes from different producers were investigated using three different rheological instruments which included a Rheometrics Mechanical Spectrometer 800 (RMS), a Haake Rheocord 90, and a Kayeness 7053 Melt Indexer. We primarily used the RMS rotational rheometer to obtain viscometric steady and dynamic shear data at different temperatures and to study the viscosity-temperature behavior of 'pure' polyethylenes and their blends. The Rheocord 90 blender was used to investigate the torque-temperature dependence for pure HDPE, linear low-density polyethylene (LLDPE), and low-density polyethylene (LDPE) in addition to similar data in blend studies. The Melt Indexer was used somewhat as a capillary rheometer, where melt flow rate was measured at constant load (pressure) and different wall temperatures.

Thermal analysis was carried out in a Differential Scanning Calorimeter (DSC, TA 2200) to search for possible evidence of high temperature transitions in the melts of 'pure' polethylenes. Further support from density measurements was obtained in a densitometer. Polyethylene characterization such as temperature rising elution fractionation (TREF) and Gel Permeation Chromatography (GPC) were provided by the Lynch/Wanke group and the rest of the analysis (NMR, FTIR ..., etc.) was carried out at Nova Chemicals Ltd. Laboratories in Calgary.

All of the above-mentioned rheological and thermal analysis tools were used to characterize 'pure' polyethylenes of different average molecular weights and different molecular structures (branching). The miscibility/immiscibility of different LLDPEs (different comonomer type) with LDPE was studied. Rheological and thermal evidence of high-temperature phase transitions in Ziegler-Natta (Z-N) HDPE, Z-N LLDPE, and LDPE (produced by a high-pressure free radical process) was discovered, strongly

resembling similar data reported for liquid crystal polymers, as will be discussed along with literature reports on the anomalous behavior of polyethylenes which support our research findings. The influences of melt order and high-temperature phase transitions on the miscibility and/or immiscibility of blends of polyethylenes were investigated and parameters which could affect the miscibility of branched polyethylenes, were identified.

II. Anomalous Behavior: A Review of Literature

It is conventionally believed that when the temperature of a semicrystalline polymer, like polyethylene, exceeds T_m then it is sufficient to model the melt as being isotropic, amorphous, and unstructured at rest, with molecular orientation arising only due to a flow field. A major exception is the liquid-crystal polymer (LCP) whose molecules normally contain rigid structural units, and whose melts contain regions of strong local order and can experience phase transitions at high temperatures.

The "conventional belief" was questioned in the light of my experimental observations, motivating a search of the literature for possible anomalous behavior (rheological and other) of molten polyethylene. To my surprise, it was found that the last four decades of polyethylene literature were full of anomalies that support my experimental observations and, together, present a coherent picture of a LCP-like, if not strictly LCP, behavior. In this chapter, some of these anomalies will be reported and introduce LCPs and their rheology to the reader.

A. Anomalies in Molten Polyethylenes

Despite the frequent success of the general concept of disorder in polymer melts, it can now be challenged by data that have emerged in recent years about polyethylene (PE), the most common of all polymers and normally regarded as having the simplest and most flexible molecular structure (polymethylene chains, $-CH_2-$). In this laboratory, Muhammed (1995) observed evidence of a yield stress in melts of high-density polyethylene (HDPE), persisting to over 240°C (whereas $T_m \cong 137°C$). This seems consistent with NMR studies of Charlesby and co-workers. Kamel and Charlesby (1981)

investigated the temperature range 140°-204°C for HDPE using NMR spin-spin relaxations (T_2). Earlier reports of the Charlesby group (Folland and Charlesby, 1978) found that T_2 values for molten PE of low M_W ($M_W = 7,000$-$8,000$) follow a single exponential decay similar to the behavior found in normal liquid n-alkanes (C_{15} - C_{40}) with long T_2 values (in the hundreds of msec). At the other extreme, they found that molten ultra-high-molecular-weight polyethylene (UHMWPE) with M_W of 2-8×10^6, has a relatively short T_2 decay patterns (0.5 - 1.5 msec) which was best expressed as the sum of two exponentials. Kamel and Charlesby (1981) results on HDPE ($M_W = 2 \times 10^5$) identified three regions (or phases) of the melt. The three phases of the melt were identified as: (a) the "ordered", not so far observed in other polymers; (b) the "mobile entangled network", as observed generally in amorphous polymers that are either crosslinked or at high enough M_W to be entangled ; and (c) the "amorphous" phase, found also in other polymer melts, which arises from molecules which are essentially free, i.e. too short to form part of the entangled network.

NMR studies of Bremner and Rudin (1992) showed a substantial amount of ordered phase exists in high and low density polyethylene melts (HDPE, M_W=112,000, $M_n = 18,000$, $T_m = 130^\circ$C; LDPE, $M_W = 84,600$, $M_n = 18,600$, $T_m = 113.6^\circ$C) even after equilibrium for long times at 150°C. Bremner and Rudin (1992) compared the DSC and NMR measurements and showed that the actual volume fraction of the "ordered" phase seems to be dependent on the particular polymer (HDPE or LDPE) and previous thermal history.

Aharoni and co-workers (1979) using TEM found that the radius of gyration for Br-tagged molecules UHMWPE (M_V =2.8×10^6) remains essentially the same in the melt

and in the crystallized bulk. The X-ray diffraction patterns and percent crystallinity of the Br-tagged and the untagged blanks of UHMWPE were about the same. This would not be possible if molecules in the melt had a Gausian spatial distribution as historically believed for the "amorphous" melt state.

Petermann and Gleiter (1973) studied the molecular structure of molten polyethylene films (thickness ~20 nm) by TEM and electron diffraction. The films (M_w = 5300, 10K, 90K, 800K) were prepared using different supporting liquids of different molecular structure, and at different cooling rates. Under all conditions the solidified film was a single crystal with a thickness of ~ 20 nm independent of the cooling rate, the supporting liquid, and the molecular weight. The electron diffraction pattern of a melt heated to 190°C, showed five concentric rings. The molten film was assumed to consist of folded molecules the axes of which are normal to the plane of the film; similar to that of the crystalline state (Keller, 1957). Due to the liquid crystal-like structure of the melt, the size of the single crystals should be practically independent of cooling rate as was observed. Furthermore, the diffuse rings correspond to interatomic distances different from that of bonded carbon atoms in solid-state polyethylene (0.152 nm). Hence, the observed ring pattern cannot be explained by assuming a random coil conformation of the molecules in the molten film, while a chain folded model can easily explain these observations. Moreover, the shortest interchain distance for the molten film, was estimated from the packing density of the molecules in a single crystal and the observed thermal expansion during melting as 4.65 $\overset{o}{A}$, in agreement with the interchain distance calculated from the first diffuse ring. No change in the molecular structure was noticed when the film was annealed at 200°C for several hours. The annealing experiment

indicated a relation between the stability of the structure (equilibrium or metastable) and the molecular weight. The annealing temperature was close to a recently discovered melt-transition temperature, 208°C (Hussein and Williams, 1998a); and, hence, the stability of the structure reported by Petermann and Gleiter (M_w=5-800K) could suggest a molecular weight dependency of transition temperature as proposed for low M_w liquid crystals by Keller et al. (1990).

Kruger and co-workers (1979, 1980) determined the shift in sound frequencies in acoustic tests of low- molecular weight LPE (M_w=6,600, M_w/M_n=2). They observed a bend in the sound frequency-temperature curve at ca. 230°C interpreted as a transition from locally nematic structure to isotropic melt. Balta'-Calleja et al. (1976), who measured the diamagnetic susceptibility, χ_M, reported the existence of a mesophase with a smectic-like order in melt-crystallized and solution-crystallized monodisperse n-paraffins (C_{12}-C_{44}) above T_m. Their findings regarding stability of the mesophase are in line with the scheme proposed for liquid crystals by Keller and Ungar (1991).

Phuong-Nguyen and Delmas (1992a) used a sensitive and stable scanning microcalorimeter (room temp. to 200°C) at low heating/cooling rates (0.5 K/h) to detect the presence of an unmelted crystal in molten UHMWPE (Mw =$0.9*10^6$) at T>T_m. Furthermore, the constrained melting/crystallization was studied in the range 110°-210°C under a variety of thermal treatments and showed the persistence of "partial melting" above T_m. In an effort to explain the "partial melting" (or liquid crystal) behavior, they tentatively suggested that tight knots between crystals in the liquid state may be responsible for their observations. Phuong-Nguyen and Delmas (1992a) used the same technique to study medium MWPE (10^4 - 10^5). They observed the same "partial melting"

and explained it as due to strain developed in the unmelted crystals through the tie molecules. They ruled out the same explanation for the constrained crystals of UHMWPE where more strain and network structures are expected because of the high M_w (10^6-10^7). Birefringence (ability to rotate the plane of polarized light, a characteristic of order) was observed at high temperature in the PE melt by Gopalan and Mandelkern (Phuong-Nguyen and Delmas, 1992a). They separately dissolved and annealed at 190°C fractions of HDPE (M_w = 10^4-10^5) and UHMWPE in Decalin (0.2% v) for a week. The most striking result of the DSC work of Phuong-Nguyen and Delmas (1992b) was that during the dissolution, total randomization had not taken place in the cooling (198°-108°C) of the high temperature exotherms of these samples. This showed that some kind of order was preferred by polyethylene molecules even in a solution.

Wunder and Merajver (1986) observed optical anisotropy (birefringence) for UHMWPE in the temperature interval 135°-208°C using the Raman spectrum. Their Raman spectra indicated a two-phase system of ordered and disordered regions for T< 208°C, with the ordered regions becoming progressively more disordered with increasing temperature above 208°C. Zachariades and Logan (1983), using a Zeiss Photomicroscope III equipped with a Mettler FP6 hot stage for the range 25°-300°C, observed birefringence in UHMWPE below 220°C. Furthermore, they observed the persistence of melt anisotropy in unperturbed samples above 220°C. The simultaneous change in the melt anisotropy of UHMWPE, detected by the Photomicroscope at 220°C, appears to be similar to that encountered in the polymorphic modification of the smectic S_E liquid-crystalline phase to S_B phase observed on heating paraffins (D. Coates and G.W. Gray, 1976).

Earlier, Rabesiaka and Kovacs (1961) concluded from their isothermal crystallization measurement (at ~170°C) in a dilatometer that HDPE melt ($M_W \sim 10^5$) was not in a true thermodynamic equilibrium at 170°C and, furthermore, that the melt structure was dependent on the molding and mechanical history of the pre-melt solid polymer. The thermal analysis work on linear HDPE ($M_W=2.5\times10^5$) is consistent with this idea, and identifies thermo-mechanical history effects similar to those observed in low-M_W liquid crystals.

Recently published work of the Williams group (Ghosh et al., 1996) on Melt Index-M_w relation for HDPEs implied $\eta_0 \propto M_w^n$ with n=5.4, which is far from the n=3.3-3.4 value reported for isotropic polymer melts and close to values (3.5< n <5) obtained by Heberer et al. (1994) for thermotropic liquid crystal polymers. Dealy and Wissbrun (1990, p. 174) reported that the Cox-Merz rule $\{\,|\eta^*(\omega)| \approx \eta(\gamma)$, where η^* is the complex viscosity and η is the steady shear viscosity$\}$, which applies for amorphous polymer melts and solutions, does not apply for polyethylenes and rigid molecules.

Waddon and Keller (1990, 1992) and Keller et al. (1990, 1991) observed, when increasing melt temperature during the extrusion of HDPE ($M_W = 4\times10^5$) at constant flow rate ("throughput") through a cylindrical capillary, the existence of a narrow temperature window (150°-152°C) with low flow resistance, interpreted as due to transition from an ordered (hexagonal) phase (T<150°) to an isotropic phase (T>152°C). In a later publication, Kolnaar and Keller (1995) investigated this temperature window further, and concluded that the rheological singularity at 150°C originated within the straight section of the capillary in contrast to their previously held view (Kolnaar and Keller, 1994) that the elongational flow at the capillary entrance was responsible for the effect.

Furthermore, they suggested that this phase transition was initiated by simple shear flow-induced chain extension at the wall (this could explain "slip" and sharkskin phenomenon), and they suggested a formation of a transient, hexagonal, 'mobile' crystal phase. In a later publication (Kolnaar and Keller, 1997) they mentioned that such a singularity cannot arise from the constitutive properties of the melt alone along lines of traditional rheology (e.g., normal $\eta(T)$ variation) and a sharp change with temperature suggests a thermodynamic origin and specifically a phase change and associated structure formation. This was supported by the fact that for a short chain branched PE (LLDPE), where all melting and crystallization effects are shifted to lower temperatures compared to the unbranched linear material, the window temperature is also lower, specifically T_{min} (corresponds to P_{min} in the extrusion window) is 146°C. They concluded from their most recent experiments that the location of such distortions in flow must lie within the entry orifice violating their original interpretations. As regards the nature of the phase transition they concluded that it was not of the flow induced crystallization type since that would be expected to hinder the flow and not promote it as observed. While, so it seems, they have found the answer to the central question of the nature and the origin of the 'window' effect; their work generated some unexpected new questions. They found that η (measured in capillary rheometer) is proportional to $M^{4.0}$ giving n (powerlaw exponent) larger than the empirically well established relation: $\eta_0 \propto M^{3.4}$. Their results on the molecular weight dependency of viscosity are along the lines of the previous work of the Williams group (Ghosh et al., 1996) which produced a power n of 5.4 in a slit die Melt Indexer. The difference between the numerical values of the power n, could be attributed to the geometrical differences of the dies used in the two independent studies and the

consequent influence on the orientation of the melt . Kolnaar and Keller (1997) results were obtained in an "orifice" die, which will give rise to more orientation in the melt, and hence lower viscosities, a known feature of liquid crystal polymers.

Ungar had earlier (1986) shown from high-pressure static studies that the PE mesophase ("hexagonal" or "rotator") is stable at pressures $\geq$ 3 k bar with a triple point of 215°C. In Chapter 4, rheological and thermal evidence of a thermal transition in the range 208°-210°C obtained at atmospheric pressure (1 bar) will be shown.

The existence of structural phase transitions in molten PE might be expected for a polymer with three reported transitions in the solid state. Popli et al. (1984) reported the α transition in the range (30 to 120°C); the β transition (-30 to 10°C); and the γ transition (-150°C to -120°C) that originate within the crystal structure and this might be relevant to liquids too.

Linster and Meissner (1986) measured the elongational viscosity, η_e, of different HDPEs (M_w=150-263x10^3, 2-8 branchs/1000 C) at constant elongational strain rate, $\dot{\varepsilon}$, and found that there was more strain hardening at 170°C than at 150°C. This observation contradicts the possible hypothesis that crystallization is induced by the extension of a molten polymeric material that is semicrystalline in the solid state. The strain hardening parameter, defined as $\partial \log \eta_e / \partial \log \varepsilon$, at 170°C was 1.8-2.6 times higher than at 150°C. This could be another manifestation of the Kolnaar and Keller 150°C transition discussed earlier.

Kavassalis and Sundararajan (1993) performed molecular dynamics (MD) simulations of LPE chains (1000 CH$_2$ units) and reported that the occurrence of a few

gauche states promotes long range attractive interactions between segments and causes the chain to fold into lamellae, via a global collapse mechanism. The predominance of trans conformation even at a high temperature (600 K) is indicative of sustained local order in the polyethylene melt. In another MD study Choi et al. (1995) observed the immiscibility of linear polyethylene and polypropylene at temperatures well above the crystal melting points of the homopolymers. Furthermore, they observed that the degree of order in the collapsed state increased with melt annealing time.

Hill's group (Barham et al., 1993, Hill et al., 1991, 1993, Hill and Barham, 1992 & 1993, Thomas et al., 1993) experimental work with PE blends indicated that the melt for 20% LPE (M_W=98,000, M_n=28,200) and 80% LLDPE (M_W = 208,100, M_n = 25,300 with long branch content 10/1000 C, and short branch content 16/1000 C backbone atoms) is a single phase at 220°C and is biphasic at 170°C. They concluded that there is a liquid-liquid phase boundary of the UCT type between 170 and 220°C. Transmission electron microscopy (TEM) was carried out after lightly crosslinking thin films of the polymer in the melt by irradiation. Using the hot stage TEM technique they were able to determine the mix and/or demix boundary to within ± 5°C. Their TEM results showed that phase separation occurred in blends of LLDPE and LPE with composition <50% LPE (Hill and Barham, 1995), while blends of LPE fractions of differing M_w showed absence of liquid-liquid phase separation (LLPS). Hill et al. (1997) reported that the branch content is the most important factor influencing the extent of LLPS; and the phase behavior is rather insensitive to the M_w of the linear component.

Hill et al. (1991) performed rheological measurements (RMS 800) of tan δ (= G''/G') for blends of LLDPE ($T_m \cong 112$°C) and LPE ($T_m \cong 140$°C). At 215°C, tan δ was

observed to vary continuously (with positive deviation from linear additivity rule, see Figure 8) with blend composition suggesting that the melt was homogeneously mixed at all compositions. However, at 140°C a different picture had emerged. For blend compositions of 100-50% LPE much the same variation in tan δ as the higher temperature was observed; while for compositions of 40% to 0% LPE a much lower value of tan δ which was fairly insensitive to composition was detected. They suggested that the melts of composition <40% LPE were biphasic, and that the LLDPE formed the continuous phase. In their rheological measurements, they encountered a significant complication not shown in their presented figures. The observed complication was particularly pronounced in the pure linear polymer. In this case a continuous decrease in tan δ (T) was observed as melt temperatures were increased above 200°C. This decrease was not repeatable and was accompanied by a decrease in viscosity suggesting thermal or oxidative degradation of polymer. However, the branched polymer did not behave the same way. They explained this in terms of suggested differences in the amount and/or effectiveness of stabilizers in the polymers. Their observation could be looked at as a variation of dynamic properties with time (thixotropy) similar to that observed by Done and Baird (1987) in their G' measurements for liquid crystal polymers.

Micic et al. (1996) measured the melt strength (related to η_e) for blends of LLDPE/LDPE at 190°C and 220°C. Blends at 220°C showed a melt strength-composition curve which followed the linear additivity rule (suggesting miscibility) while those at 190°C resulted in melt strength higher than that of either of the pure polymers (suggesting immiscibility). The positive deviation from the linear additivity rule was observed in the

more elastic LDPE-rich blends. Their finding was similar to Hill's group earlier observations.

Minkova and Mihailov (1987) reported what they called "flow temperature" for UHMWPE at 215°C measured by a polarized light microscope. They recognized the network structure in fibers and as-received polymer. They explained reflections observed in the melt as due to strain on crystals and tie molecules resulting from polymerization, the same way Kresteva et al. (1985) explained similar findings. Their thermal analysis of a 50/50(w) blend of UHMWPE and normal MWPE showed one melting peak for blends mixed at 220°C or above (up to 280°C), suggesting miscibility, while two peaks (suggesting immiscibility) and melt segregation were obtained for blends mixed at 190°C.

The above literature survey indicates the existence of partial molecular and microstructural order in molten PEs, mainly the UHMWPEs (unbranched structure), which suggests the study of the possibility of melt order and high-temperature phase transitions in commercial PEs. This was the focus of the first part of this study, as will be reported in Chapter 4.

B. Liquid Crystal Polymers (LCPs)

1. General

Materials that exhibit partially ordered fluid phases, are intermediate between the three-dimensionally ordered crystalline state and the disordered or isotropic fluid states are called liquid crystals (sometimes named mesomorphic phases). Some call it the fourth state of matter (Franklin, 1979). Phases with positional and/or orientational long-range order in one or two dimensions are termed mesophases. Because of the molecular order,

liquid crystalline phases are anisotropic, i.e. their properties are a function of direction. Liquid crystals in solution are called lyotropic and those in the melt are termed thermotropic. Within the molecule, there is usually a rigid unit responsible for the liquid crystalline behavior. This unit is referred to as the mesogen. Side-chain LCPs (prepared by attaching a mesogen hanged to a flexible polymer backbone) have generated interest for such applications as nonlinear optics, filters and optical storage devices (Ober and Weiss, 1989). LCs are further classified into nematic, cholesteric, chiral and the smectics, according to the type of 3D order they possess in the liquid state (Franklin, 1979; Wunderlich and Grebowicz, 1984).

All current commercial and nearly commercial thermotropic LCPs show nematic, one-dimensional order, which results from the semirigid, essentially linear architecture of the molecules. They can form aggregates, known as domains, in the nematic melt state with a characteristic interdomain spacing detectable by X-ray diffraction measurements. In general, the "clearing" temperature or disordering point (nematic/isotropic transition) is well above the solid/nematic liquid phase transition, which is commonly referred to as the melting point although, strictly speaking, the clearing point is the true melting point (the nematic structures "melt"). The nematic-isotropic transition is often in a temperature range at which the polymer thermally decomposes.

Because the melt viscosity increases by a factor of two to ten (McChesney, 1988) when the polymer passes from the nematic to isotropic state, processing becomes extremely difficult as melt temperatures exceed the clearing point. One other important point is that the true melting (LC→isotropic) transition is accompanied by a very low enthalpy change, so there is little crystallization on cooling compared to conventional

melting (Wunderlich, 1997; McChensy, 1988). This allows a fast molding cycle and low mold shrinkage but makes detection of liquid state transitions by thermal analysis rather difficult (McChesney, 1988).

The anisotropy is responsible for many of the characteristic properties of liquid crystals such as birefringence and NMR line splitting. The order in LCs is represented conceptually by a "director", a vector whose direction is aligned with the molecular or domain or microstructural preferred average direction. Brownian motion fluctuations of the director and of the molecules with respect to the director give rise to intense light scattering, which accounts for the turbidity of liquid crystals as reported by Wissbrun (1981) in his review paper on LCPs.

The LCP-like order in molten PEs may explain the phase separation in the blends of linear and branched PEs reported by Hill's group and observed in much of the unpublished work of the Williams group. Furthermore, phase separation can also be explained for LCPs on the basis of a distribution of molar masses. This distribution will lead to a range of clearing temperatures for a given polydisperse polymer. Experiments which have elegantly demonstrated this point were made using LCPs in which the isotropic and mesomorphic melts were allowed to separate due to difference in phase density (D'Allest et al., 1988). Upon analysis, the nematic component was shown to be of a higher M_W than the isotropic phase. Theoretical and experimental work of Stupp (1988) has also demonstrated that biphasic systems can arise from chemical heterogeneity (tacticity) in nominally 'pure' nematic polymers. Stupp (1989), using optical microscopy, showed for random copolyesters of LCP type that such chemical heterogeneity causes

broadened nematic/ isotropic biphase transition and leads with increasing temperature to the separation of the nematic phase into "ordered" and "amorphous" biphases.

Rheological testing is frequently used to study order in the melt and there is a good literature on the rheology of LCPs, especially lyotropic LCP. It must be kept in mind that preparation of samples, beginning with the synthesis of the chemical architecture, and including the mechanical and thermal history just prior to testing, is an integral part of the measurement procedure (Wissbrun, 1980). More work is still needed to generalize the current findings on certain families of LCPs like polyesters and polyethers.

2. Rheology of LCPs

The rheology of liquid crystalline polymers (LCPs) is characterized by a number of phenomena that are unusual for typical amorphous polymer melts and solutions: extreme shear-thinning viscosity behavior, normal forces that can change sign with change of $\dot{\gamma}$ are often negative at low shear rates, and low extrudate swell (Dealy and Wissbrun, 1990). Even negative extrudate swell (i.e., shrinkage to a diameter less than that of the capillary) was observed by Wissbrun (1994).

Lyotropic systems received most of the early attention, and here it was first reported (Kiss and Porter, 1978, 1980) that the normal stress function $N_1(\dot{\gamma})$ measured in a cone-and-plate geometry as a function of steady shear rate $\dot{\gamma}$ was observed to change sign as $\dot{\gamma}$ passed a specific value. Other researchers (Moldenaers and Mewis, 1986a) later obtained similar results. The short-term stress transients of the LCP can also appear peculiar. This was well exemplified by another lyotropic polymer system (Moldenaers

and Mewis, 1986b, 1987), with the start-up transient viscosity $\eta^+(t)$ exhibiting a sequence of sharp maxima unlike the more gradual single stress overshoot phenomenon of most viscoelastic polymer solutions.

Rheological theory has not been entirely successful in predicting and interpreting the behavior cited above for lyotropic systems. Non-dilute solutions are not well characterized by rheological molecular models of any kind. The dilute-solution molecular theories can be formulated for polymers of any degree of rigidity but seem incapable by definition of establishing local order. Despite this handicap, some of the lyotropic LCP transient behavior was described quite well by an approximate representation of the dilute-solution internal viscosity (IV) model (Manke and Williams, 1989), in the limit of high values of the IV ratio ϕ/f. Here, ϕ is the IV parameter for the chain and f is the bead/solvent friction coefficient that contains solvent viscosity η_s. In this high-ϕ limit, predictions for the intrinsic property $[\eta^+(t)]$ gave precisely the correct response (Manke and Williams, 1989, their Figure 6) to agree with the LCP transient data (Moldenaers and Mewis, 1986b, 1987). While $N_1^+(t)$ was not predicted to change sign, $N_2^+(t)$ exhibited a positive maximum and slowly drifted into negative values before eventually going to zero at the steady state. This transient sign change in $N_2^+(t)$ predicted by a model based on the random-coil Gaussian chain, was duplicated by dilute-suspension rigid-rod dumbbell theory (Strand et al., 1987), which could be regarded as a closer model for the rigid molecules found in most LCP systems. The absence of changes of sign in $N_1^+(t)$ predictions could be attributed to the lack of long-range order in all dilute-solution models. In any event, no data on either N_2 or N_1 are available in truly dilute LCP

solutions, and N_2 has apparently never been reported for concentrated lyotropic systems either.

For the melt state, of far greater interest for polymer processing purposes (Baird et al., 1985) researchers have thus far produced no correspondingly peculiar thermotropic LCP normal stress behavior. There has been no observation of a sign change in $N_1(\dot{\gamma})$. Indeed, conducting such rheometry with LCP melts has proved to be more than challenging. The ordering produced in such flows can be virtually macroscopic and calls into question some of the basic tenets of conventional simple-shear rheometry. Moreover, some of these melts are not chemically stable under common test conditions. For example, it seems likely that a polyester LCP could hydrolyze in situ if contacting even moderate levels of ambient humidity. It is not clear whether these experimental difficulties, collectively, could be responsible for the absence of data indicating, for example, a sign change in $N_1(\dot{\gamma})$. However, start-up transients in LCP melts have shown peculiarities similar to those of lyotropic systems, in that a double-overshoot in $\eta^+(t)$ and $N_1^+(t)$ has been reported (Baird et al., 1985).

However, theoretical progress has been made recently, and various rheological anomalies in LCP liquid systems have been predicted that parallel the behavior of lyotropic LCP fluids. It appears likely that these theories should apply also to the LCP melt state. Of particular note is the work of Marrucci and Maffettone (1989, 1990, 1991), used to characterize normal and shear stress for rodlike polymers assembled in a nematic phase to establish a polydomain structure. In their model, $N_1(\dot{\gamma})$ is predicted to change sign twice as $\dot{\gamma}$ increases and $\eta(\dot{\gamma})$ is predicted to have a "kink" in the $\dot{\gamma}$-range just above the first sign change in N_1 (see Figure 1 of Marrucci and Maffettone, 1990 or

Figure 4.5a in Chapter 4 of this thesis). The viscosity kink has been found in lyotropic LCP systems (Kiss and Porter, 1978, 1980; Moldenaers and Mewis, 1986b, 1987), but this and the N_1 sign change have not yet been observed in bulk LCP melts. The theory predicts no yield stress, but a Newtonian viscosity plateau at low $\dot{\gamma}$ that develops into shear-thinning behavior at a $\dot{\gamma}$ corresponding to the low-$\dot{\gamma}$ maximum in $N_1(\dot{\gamma})$. Similar predictions have also been made lately by Larson (1990) with a comparable but more refined theory.

A good literature review on LCP rheology is given by Wissbrun (1981). His review points out that LCPs can possess very long stress relaxation times, perhaps 100 times longer than those of isotropic materials. Furthermore, Wissbrun (1980) observed, upon start-up of steady shear at very low $\dot{\gamma}$, a sharp maximum in the transient shear stress. Normally, with isotropic melts, a mild maximum is sometimes observed but only at very high $\dot{\gamma}$ such that the product of shear rate and relaxation time is in the order of unity. He further observed occasionally a form of thixotropy (increase of viscoelastic properties with time) in dynamic testing which was also observed later by Done and Baird (1987) in the G' measurements of LCPs. Hill and Barham (1993) reported similar behavior in tan δ for LPE. Baird et al. (1985) reported stress relaxation of thermotropic liquid crystalline copolyesters which was considerably faster than would be expected for a flexible polymer.

Heberer et al. (1994) observed that $\eta(T)$ increased with T (unlike most liquid behavior) for thermotropic polyethers, with the isotropic viscosity (at high T) being about an order of magnitude higher than the liquid crystalline (lower T) viscosity. They

observed that the variations in viscosity due to temperature changes affected the viscosity of the isotropic phase more than the LC phase. Han and Rey (1995) presented a comprehensive nonlinear numerical analysis of the temperature dependent nematorheological shear behavior of rod-like liquid crystals. The computed steady state viscosity of 8CBP (4-n-octyl-4'-cyanobiphenyl), a thermotropic liquid crystal, was found to increase sharply with temperature across the transition temperature for aligning to non-aligning transition. Wissbrun and Griffin (1982), reported increase of viscosity with temperature for thermotropic LC polyesters and referred to other reports about the same observation. Kiss (1986) made similar reports for thermotropic LCPs.

Double stress overshoot peaks upon the inception of shear were observed by Wissbrun (1980) and by Baird et al. (1985). The experimental work of Viola and Baird (1986) showed the transient flow behavior of polymers is sensitive to changes in structure during flow. Therefore, stress growth and stress relaxation experiments may provide an insight into the differences between isotropic and LCPs and the changes in structure which may take place in LCPs during deformation. Apart from the above mentioned behavior, however, the steady shear behavior of LCPs seems to resemble closely that of isotropic flexible chain systems (Wissbrun, 1981).

The foregoing rheological properties, generated as a result of the existence of order in the melt, provide distinct processing advantages over isotropic melts. For example, processing in the liquid crystalline state, even at low shear rate, can result in high molecular alignment and consequently high modulus and mechanical anisotropy in the solid. Moreover, the LCP has low η because of shear thinning, so smaller pressures and forces are needed to sustain a flow. These properties are thought to originate from the

alignment of liquid-crystalline domains that can be sheared easily in the aligned direction.

The explanations of the rheological behavior of liquid crystals have concentrated predominantly on the effect of shear on the domain texture of the liquid crystal. A rheo-optical study of Onogi and Asada (1980) led them to propose a mechanism to account for the anomalous viscosity of LCPs. A log-log plot of the viscosity, η, versus the shear rate, $\dot{\gamma}$, shows three distinct regions (Figure 2.1). Region I encompasses low shear rates, where the material is shear thinning and flow occurs by the relative motion of the separated liquid crystal domains without a collective orientation of the all the directors. Flow properties in this region are strongly affected by the texture or bulk structure of liquid crystals and vary greatly with the preparation procedure and history of the sample. Marrucci and Greco (1992) reported theoretical support for the observed behavior of LCP at low shear. In region II the viscosity is nearly constant and the increased shear rate breaks down some of the domains whose molecules then act as a solvent for the remaining domains. Lastly, in region III, the material is again shear thinning and the texture becomes a continuous but diluted monodomain structure defined by molecular orientation in the shear direction. Onogi and Asada (1980) used a polarized photomicrograph of solid-state HDPE film for comparison with polarized photomicrographs of a LCP (see Figure 4 of the same reference) and they mentioned that "polydomain texture of the liquid crystal resembles the superstructure of polyethylene, a typical semicrystalline polymer".

**Fig 2.1 The shear rate dependence of apparent viscosity
for liquid crystal polymers.**
Redrawn from Onogi and Asada (1980)
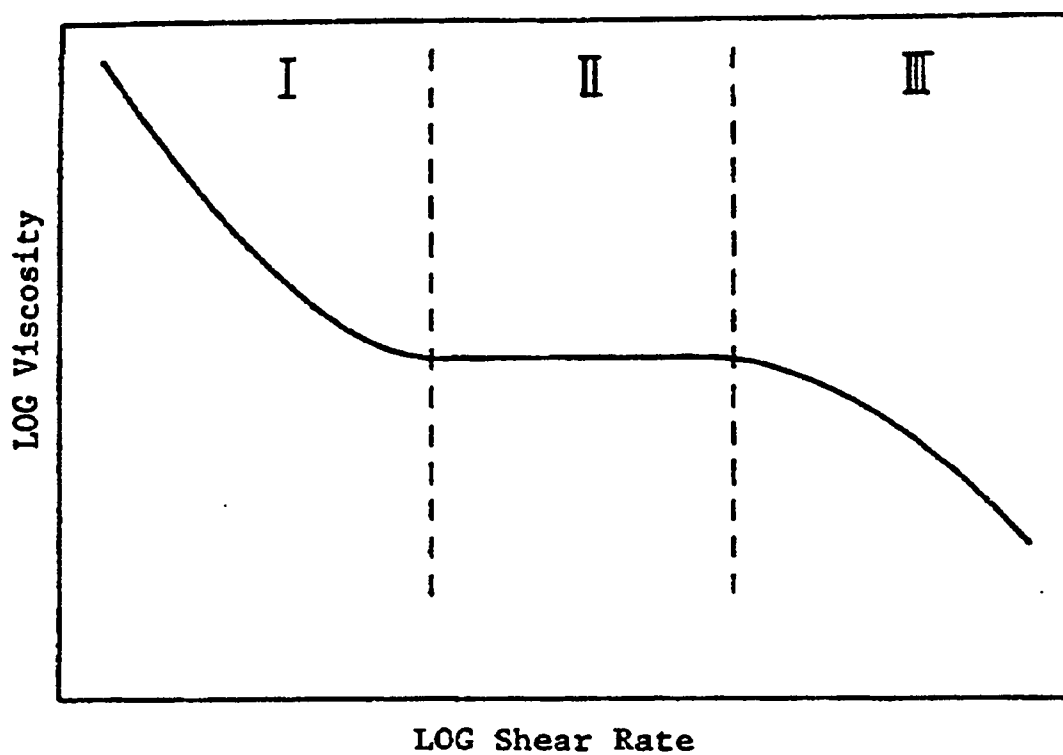
In the present work, a different experimental approach was taken in seeking these predicted LCP melt phenomena. Polyethylene melts, particularly those of HDPE, were reason possess sufficient molecular order to be likely candidates for exhibiting thermotropic LCP-type rheology. Moreover, HDPE is not affected by ambient humidity and is chemically inert at the primary temperature of testing used here (190°C); thermal degradation occurs only above 345°C (Zachariades and Logan, 1983) and oxidative degradation is prevented by a blanket of nitrogen gas and the presence of antioxidants in the melt.

This initial part of the Ph.D. project is primarily a rheological investigation for the question of melt order in polyethylene, to be supplemented by thermal analysis and other experiments. In this work I will present new rheological evidence of a liquid crystalline behavior in polyethylene melts such as high-temperature phase transitions in the processing range observed for the first time, negative normal force, overshoot in stress growth upon start-up, and stress relaxation. The interdependence of the phase behavior, viscosity, temperature and shear rate are also presented. Further support will be presented from thermal analysis (DSC), melt index measurements, and evidence from mixing melts of unlike kinds of PE. Most of the data, however, were obtained with the simplest molecular PE structure, the linear molecules of HDPE and later extended to investigate melt order in branched polyethylenes and its influence on the miscibility of LLDPEs in LDPE. Most of the data presented on HDPE were obtained on the pure, unblended polymers. Samples of linear HDPE from seven different producers were used in this study in addition to different branched polyethylenes from Nova Chemicals. For comparison, a commercial sample of atactic polystyrene from Dow Canada was tested in

an identical fashion; it, too, contained anti-oxidant. This polymer was selected as a reference because it has no solid-state crystals and is known to be an amorphous melt in the temperature range explored in this research.

III. Experimental

A. Materials

General-purpose commodity grade HDPE samples prepared by Ziegler-Natta (Z-N) catalysis were obtained from seven different resin producers. All were then characterized independently as to solid-state density (a measure of fractional crystallinity), molecular weight distribution by gel permeation chromatography, GPC, melt index (inversely proportional to viscosity), and temperature-rising elution fractionation, TREF, (to confirm that samples were free of branched components). Sample densities at 25°C were similar (0.951 – 0.964 g/cm^3), well within the HDPE range. Most of the samples had density values of 0.960 g/cm^3 or more at room temperature, corresponding to the accepted HDPE category, indicating they should not have side branches (Bourgeois and Blackett, 1988), which reduce crystallinty and hence density; this was consistent with the TREF results. The molecular weight distributions were obtained from GPC measurements in chlorobenzene at 140°C and interpreted with calibrations utilizing near-monodisperse HDPE standards. Molecular weights obtained in this way for LDPE and LLDPE can be only approximate. These services were provided by staff of the research group of Professors Wanke and Lynch. Other features varied significantly: the weight-average molecular weight M_w from 36,000 to 137,000 (far below UHMWPE levels), the breadth of molecular weight distribution (characterized by polydispersity, M_w/M_n) from 3.3 to 5.9, and melt index (M.I., ASTM D-1238) from 0.65 to 50 g/10 min (190°C). These characterization data (M_n, M_w, M_z, and polydispersity, M_w/M_n) are shown in Table 3.1. Also shown is the melt index information provided by

the producers (which was closely replicated by our own measurements, as described in

Chapter IV).

Table 3.1: Characterization of linear HDPEs from different producers

Resin Producer and our lab code	Density g/cm^3	M_n	M_w	M_w/M_n	M_z	M.I.*
Union Carbide(UC)	0.961	13,340	78,292	5.87	224,055	0.8
Solvay	0.960	16,970	79,689	4.70	264,826	0.7
Quantum	0.960	17,347	85,149	4.93	269,093	0.7
Phillips	0.964	16,545	78,031	4.73	260,835	0.65
Exxon 6750	0.951	10,823	35,946	3.32	79,871	50
Exxon 6705	0.953	13,376	46,891	3.51	109,818	20
Paxon	0.960	17,449	82,960	4.76	274,329	0.7
Nova S221	0.957	28,000	137,000	4.89	758,000	1.0
Nova S215	0.960	19,400	251,500	12.96	1,375,000	0

* Melt Index, a measure of $1/\eta$.

All samples contained normal antioxidant additives (AO) for protection from oxidative degradation at typical processing temperatures, the regime intended for study. Additional antioxidants (Irganox B225, 50/50 blend of Irganox 1010 and Irgafos 168) were mixed with commercial resins to avoid degradation during the mixing process or the testing in the RMS. This avoidance of oxidation was confirmed by carrying out a high-pressure liquid chromatography (HPLC) analysis for the residual AO, which showed the presence of enough active AO at the end of the mixing experiment to demonstrate it had not been "used up" (by oxidation) to leave the resin unprotected. Results will be discussed in Chapter V. Further support for the HPLC results was obtained from

rheological testing in the RMS. Results obtained for linear and branched polyethylenes, with additional AO, will be discussed later.

Other important additives are the polymer processing aids (ppa) or lubricants, which form a large group of chemicals used to improve the processing of plastics. They may be characterized as either internal or external (Radian Corporation, 1987). Both may be blended with the resin preceding processing; however, their function vary. Internal lubricants reduce shear stress between individual resin molecules, whereas external lubricants reduce this stress on a macroscopic level (e.g., between resin particles and or polymer-metal surfaces). External lubricants have a lower compatibility with the polymer than do internal lubricants. There is overlap between these two roles and many lubricants serve both functions. Polyethylene waxes (ultra-low-molecular-weight polyethylene, M_w=500 to 10,000) are usually used as ppa for polyethylenes (Lindner, 1996; Radian Corporation, 1987).

The melt order in branched polyethylenes was investigated using samples obtained from Nova Chemicals and Exxon. LLDPE samples of different comonomer type (butene, hexene, octene) and molecular weights were used in this study. All LLDPEs polyethylenes were Z-N commercial resins (mainly from Nova Chemicals), except one metallocene sample (Exxon 4033). Sample densities at 25°C were similar (0.918 – 0.924 g/cm^3) for the Z-N resins while that of the metallocene sample was lower (0.88 g/cm^3); a direct consequence of the high branch content and possibly the uniform branch distribution. The molecular weight characterization data varied significantly: the weight-average molecular weight M_w from 50,836 to 120,000, the polydispersity from 3.2-6.5

for Z-N resins and 2.14 for the metallocene sample. These characterization data (M_n, M_w, M_z, M_w/M_n) are shown in Table 3.2 for branched polyethylenes.

Table 3.2: Molecular weight characterization of branched polyethylenes

Sample #	Density	Polymer Type	M_n	M_w	M_w/M_n	M_z
S229	0.918	LLDPE(butene)	29,503	105,313	3.57	268,153
S237	0.918	LLDPE(hexene)	34,000	110,000	3.2	298,000
S226	0.920	LLDPE(octene)	17,000	106,000	6.2	343,000
S225	0.919	LLDPE(butene)	25,000	120,000	4.8	N/A
S227	0.924	LLDPE(butene)	14,708	50,836	3.46	114,884
S236	0.920	LDPE	27,000	119,000	4.4	N/A
S231	0.918	LDPE	13,377	71,797	5.37	182,785
S216	0.919	LDPE	15,458	99,464	6.45	281,431
Exxon 4033	0.880	LLDPE (butene) Metallocene	51,859	110,086	2.14	170,686
Dow	N/A	LLDPE	N/A	N/A	N/A	N/A
Dow-123 C	0.923	LDPE	17,849	95,114	5.33	268,095

The melt index (M.I.) varied from 0.75 to 20 g/10 min (190°C) while the corresponding melt flow ratios (MFR, ratio of MI at two different standard loads) were $\geq$ 26. The branch content for the Z-N LLDPEs (obtained from NMR-FTIR analysis) was similar (14.7-22.1 CH_3/1000 C) while that for the metallocene is somewhat higher (36.2 CH_3/1000 C). These additional characterization data (M.I., MFR, and branch content) are shown in Table 3.3.

For comparison, a commercial sample of atactic polystyrene (PS, Dow Styron 666D resin, $M_w \cong 200K$, $\rho = 1.04$ g/cm^3) was tested in an identical fashion; it, too, contained antioxidant. This polymer was selected as a reference because PS has no solid-state crystals and is also known to be an amorphous melt in the temperature range explored in this research.

Table 3.3: Additional characterization data of branched polyethylenes

Sample #	Polymer Type	CH$_3$/1000 C	M$_w$	MI	MFR
S229	LLDPE(butene)	22.1	105,313	1.0	26
S237	LLDPE(hexene)	17.2	110,000	1.0	27
S226	LLDPE(octene)	14.7	106,000	1.0	30
S225	LLDPE(butene)	16.1	120,000	0.75	32
S227	LLDPE(butene)	20.7	50,836	20	N/A
S216	LDPE	*	99,464	0.75	>30
S231	LDPE	**	71,797	7.0	v. high
S236	LDPE	N/A	119,000	0.31	N/A
Exxon 4033	Butene Metallocene	36.2	110,086	0.8	N/A
Dow-123 C	LDPE	N/A	95,114	0.28	N/A
Dow	LLDPE	N/A	N/A	N/A	N/A

*1(Me), 6(Et), 1(Pr), 8(Bu), 3(Pe), 3(He+)
**1(Me), 7(Et), 1(Pr), 8(Bu), 2(Pe), 4(He+)

B. Rheological Measurements

Observation by the Williams group of 'pure' HDPEs and their corresponding blends has accumulated a large body of evidence that HDPEs might be 'structured' in the melt i.e. HDPEs could be special forms of LCPs. A simple test-tube experiment, which supports this contention, was carried out. Pellets of HDPE were placed in a test tube and heated over a flame with continuous shaking. The test tube was moved away from the flame and placed in an inclined position to see if the HDPE sample would flow under gravity. A thermocouple was dipped in the melt for the measurement of its temperature. The experiment was repeated and an increase in ease of flow was observed around 210°C. This observation, together with the literature reports mentioned earlier, inspired more testing on polyethylene melts.

Rheological measurements were performed using three different types of equipment: the Rheometrics Mechanical Spectrometer 800 (RMS), where different dynamic and steady shear viscometric tests were carried out; Haake Rheocord 90 mixer used for the measurement of torque and melt temperature in a ramp heating or at constant wall temperature; and Kayeness 7053 melt indexer for the measurement of M.I. according to ASTM D-1238 (2.16 Kg) in the temperature range 190-230°C, from the ASTM conventional value (190°C) to values in excess of those used often in processing (~ 220°C).

1. Measurements in the RMS

The RMS is equipped with a 2000g.cm / 2000 g rated capacity torque and normal force transducer of the force rebalance type. The RMS was employed for steady-shear and dynamic (small strain oscillatory) tests. The oven attachment allowed isothermal or

programmed temperature measurements over a wide range of temperatures, encompassing the higher temperatures characteristic of melt processing operations. Samples were sheared with two platen geometries, a cone-and-plate (CP) set and a parallel-plate (PP) set; and all platen diameters were 25 mm. The cone angle was 0.1 radian with a 53 μm truncated "apex". A gap spacing of 1.5 mm was used for the testing in parallel plates. The independently measured gap correction of 3 μm/°C was used in temperature sweep tests to account for the thermal expansion or contraction of the test fixtures. The rheometer was serviced regularly, twice a year, by Rheometrics and was calibrated according to the standard procedures just prior to the measurements.

An independent study on the effect of polymer processing aid at a concentration of 0.1%, showed no effect of the ppa on the rheology (results are discussed in Chapter V). We also repeated experiments under the same conditions but different PP gap spacings (1-2 mm) and results showed no gap dependence indicating the absence of slip. Rheological measurements carried out using air heating were found to be different from those obtained in a nitrogen atmosphere. Hence, all measurements were conducted using nitrogen, obtained from a nitrogen cylinder, as the heating medium to alleviate the suspected oxidative sample degradation.

In all cases, the polyethylene samples were given a controlled thermo/mechanical history (molding) before introduction into the RMS for shear testing. Circular disc samples were prepared by compression molding in a Carver press (mold: 15 cm × 15 cm ×2 mm, 9 holes for discs 25 mm dia each), preheated to 170°C, by placing 1.1-1.2 g of pellets in the hole. A preheat time of 5 minutes was allowed to ensure complete melting, while slowly lowering the upper press surface to the touching position. Load on the

sample was increased to 3 metric tons for 5 minutes, followed by another 5 minutes at 7 metric tons and then water cooling for 10 minutes to room temperature. The molding operation produced air-free flat discs (25 mm diameter, 2mm thick) for insertion between the RMS platens. Mylar sheets were used to secure a "clean" release of disks from the mold. No attempt was done to study the influence of molding conditions [T, or P (t)] since Rabesiaka and Kovacs (1961) concluded that the melt structure of HDPE (Mw ~ 10^5) melt was dependent on the molding and mechanical history of the pre-melt solid polymer (see Chapter II).

The disk was inserted between the RMS platens that had been pre-heated in mounted position within the RMS oven, to achieve the intended working temperature as measured with a thermocouple embedded in the lower platen and contacting the melt during the testing procedure. With the sample in position, the oven closed and the polymer heated for 3 minutes, the upper platen force transducer assembly was then lowered to the proper working position. For both platen configurations, the vertical force to accomplish this had to be carefully monitored to avoid overstressing the transducer, and the procedure was terminated when the PP were separated by 1.5 mm or the cone flattened tip position separated from the opposing platen by 53 μm. Because of considerable resistance by the HDPE melt, which has a rubbery and not free-flowing consistency even at high temperatures, the platen-positioning step for the CP geometry was time consuming; qualitatively, the melt resisted deformation and flow as might be expected from a yield-stress fluid. Melt extruded beyond the platen rim by this procedure was removed by a razor blade. With the system at operating temperature and the nitrogen blanket in place, a holding period of 2 minutes was allowed for thermal equilibrium

before beginning measurements. Temperature variations, during tests performed at nominally constant temperature, were $<1°C$ from the set temperature.

The RMS force rebalance transducer is capable of measuring simultaneously both torque and normal force. With CP platens, if expected hydrodynamics prevail (e.g., no secondary flows and no slip at platen surfaces), shear rate $\dot{\gamma}$ is uniform and one obtains two rheological properties, the viscosity $\eta(\dot{\gamma})$ and the first normal stress function $N_1(\dot{\gamma})$ where $\dot{\gamma}=\Omega R/\psi$ (with Ω the steady angular platen speed, R the platen radius, and ψ the cone angle, Bird et al., 1988; Walters 1975). With the PP, the non-uniform $\dot{\gamma}(r)$ creates well-known complications (Bird et al., 1988; Walters 1975) that will not be discussed here; instead, we follow the conventional practice of characterizing the flow by the "Newtonian equivalent" value of shear rate at the platen rim, $\dot{\gamma}_R=\Omega R/h$ (with h the inter-platen spacing) and report the corresponding $\eta(\dot{\gamma}_R)$ and normal stress function (N_1-N_2) as functions of $\dot{\gamma}_R$.

Different dynamic and steady rheological tests were used in this study. The temperature sweep tests, which approximate a slow linear ramp of T(t), were performed to study the temperature dependence of the melt viscosity. The tests were carried out at small torsional strain and frequency with T increased at small increments $(10°C/step)$. Time sweep tests assessed rheological properties over a long period of time at constant temperature, strain and frequency, and were carried out to study the thermal stability of the melts. Steady shear rate experiments were carried out mainly for the observation of viscosity, stress and normal force (NF) behavior when $\dot{\gamma}$ was varied. In these steady-$\dot{\gamma}$ tests, the transient build-up of stresses to their steady-state values could also be tracked.

In another test mode ("transient") the transient stages of stress development could be measured even more accurately.

When dynamic (oscillatory) testing was the objective, a shear strain amplitude (γ^o) of 10% or less was used, after a strain sweep showed that this γ^o was sufficiently small to produce sinusoidal torque responses and dynamic properties independent of γ^o (i.e., linear properties were obtained). The angular frequency (ω) was usually extended to 10^2 rad/s. A delay time of 3 seconds (time between the moment the motor starts deforming the sample and the beginning of the test measurement) was used before measurement for the frequency sweep experiments. Some experiments were then carried out in a descending-ω order (from 10^2 -10^{-2} rad/s) to examine whether molecular degradation had occurred during the increasing-ω sequence. Excellent reproducibility always prevailed.

Small strain dynamic testing was used to study the temperature effects. Molded discs of different polyethylenes from different producers were used to measure the temperature dependence of melt viscosity. Polystyrene (PS) from Dow-Canada was used for comparison as an example of a typical amorphous polymer. Strain sweep tests were performed at a frequency of 0.1 and 1 rad/s for polyethylenes and 1.0 rad/s for PS and a strain in the linear range of viscosity-strain log-log curve was selected (10% or less for polyethylenes and 15% for PS). Temperature sweep tests were carried out in the range 260 - 160°C with all samples being heated to 260°C and then cooled to 160°C in steps of $\Delta T = 10^o$ with a thermal soak time of one minute at each step. All resins were loaded in the RMS as discs prepared either from the as-received resins or from samples of the air-cooled "torqued" resins. The "torqued" resins were as-received samples that had a torque

experience in the Rheocord 90 melt blender. The term "torqued" was used instead of "sheared" since the flow field in the blender is a combination of shear as well as elongational flows. (Later, the blending of different polyethylenes, followed the same procedure, so those materials were also "torqued").

Steady-shear testing was always conducted with a fresh sample. Tests began at the lowest shear rate ($\dot{\gamma}$) and continued up to the hydrodynamic stability limit, when secondary flow caused radial ejection of the sample. Steady-shear measurements were made with unidirectional platen rotation. The normal practice of taking a stress value for clockwise (CW) platen rotation followed immediately by one taken for counterclockwise (CCW) rotation, and then reporting an average of the two, was abandoned when early tests showed that

(i) Stress transients upon start-up from rest, and after changing shear direction, were usually too long to make the dual-run procedure practical, and

(ii) The flow reversal caused anomalous transients that made the averaging process meaningless. Such behavior has apparently not been reported for HDPE heretofore.

Separate runs with fresh samples sheared in CW and CCW directions showed that there was no geometrical bias of the sort associated with platen misalignment, and independent calibrations confirmed this. However, even with unidirectional shear, the steady-stress state could not be achieved quickly with polyethylene melts at any temperature.

It was found by experience that these transients passed within about 5 minutes in most cases, so the RMS was programmed to perform a $\dot{\gamma}$-sweep in the following fashion:

Begin at the lowest $\dot{\gamma}$ and wait for 5 minutes, then collect torque and normal stress data for 30 s and average it (to be reported as the steady state result), then step to the next $\dot{\gamma}$ and repeat the procedure at intervals that were selected by the operator to achieve an equal number of data points per decade of $\dot{\gamma}$.

2. *Torque measurements in the Rheocord 90 Mixer*

Because liquid-state mechanical properties of the polymer should be especially sensitive to morphological changes, rheological testing was desired. However, the determination of specific rheological properties was not the objective; rather, a rheological signal of thermal transitions was intended. It was therefore decided to use a melt-blending device (Haake Rheocord 90) and follow the torque as a function of melt temperature under standard testing conditions. The Haake Rheocord 90 is a computer-controlled torque rheometer, which can also be operated as an extruder or a mixer. In this research, only the mixer was used.

In this mixer, torque is generated by the resistance of the fluid in a heated mixing bowl to the rotation of two offset blades moving at constant angular speed. The flow field is complex, producing many shearing and extensional elements of the deformation rate tensor, and the torque is therefore a complex function of all elements of the stress tensor. However, any thermal transitions in the melt must have impact simultaneously on all rheological properties that contribute to the measured torque. Because this blender has very effective thermal mixing, near-isothermal conditions prevail throughout the polymer. Electrical heaters are embedded in heavy steel walls surrounding the bowl and controlled by computer to achieve a programmed rate of temperature change. Melt

temperature, monitored by computer, is sensed by a thermocouple at the bowl bottom, contacting the melt directly.

The standard test procedure was to establish in the blender a starting condition at 160°C with a rotor speed of 50 rev/min, load the bowl with ~ 50-52 g of solid pellets (depending on $\rho_{25°c}$), initiate a nitrogen flow through a plunger supported upon the pellets, to purge oxygen from the bowl, and then to compress the melting mass with a weight on the plunger. Torque stabilized in two minutes, but this 160°C condition at 50 rpm was held for three minutes to break up any persistent residues of the melted solid crystals and assist their diffusion into a homogeneous state. Thereafter, heating was increased to achieve a linear ramp in the wall temperature from 160° to 260°C at a rate of 5°C/min, while rotor speed continued at 50 rpm. Torque and melt temperature were sampled every six seconds, during the holding period and thereafter, producing more than 200 points for each torque curve.

To study the influence of operating conditions on the obtained results the rotor speed was varied from 20-100 rpm, and the heating rate from 2-5°C/min. The effect of nitrogen atmosphere was also studied.

The mixer was then used in a more classical fashion for blending different polymers at constant temperature and rpm for a fixed time. A separate study (will be discussed later) was conducted to select optimum blending conditions. The standard conditions were chosen as: 190° or 220°C, 50 rpm and 10 minutes.

3. Melt Index Measurements in a Melt Indexer

Kayeness 7053 melt indexer was used for the measurement of M.I. according to ASTM D-1238 (2.16 kg) in the temperature range 190-230°C, from the ASTM conventional value (190°C) to values in excess of those used often in processing (~ 220°C).

C. Thermal Analysis

Samples of 5-10 mg were sliced from the as-received pellets then compressed into aluminum sample pans for testing in a TA Instruments DSC 2910 equipped with a Thermal Analyst 2200, and a nitrogen gas flow established from a liquid nitrogen vessel; this further protected the samples from oxidation as well as assisted in temperature regulation. Various T-scan rates were used, in the range of 1-20°C/min, for both heating and subsequent cooling parts of the heat/cool cycle for each sample. Only low heating and cooling rates (1°-3°C) were capable of revealing the high temperature transitions of polyethylenes. Each sample was tested in two heating and cooling cycles from 30° - 280°C, carried out under nitrogen in nonhermetic pans with a one-minute isothermal program at 30°C and 280°C.

D. Density Measurements

The density-temperature behavior of polymers in the solid and liquid states is very important for polymer processing as well as reflecting a variety of thermodynamic transitions. The first method to determine the density-temperature behavior of polymers was developed by Zoller et al. (1976). Their apparatus could measure pressure-volume-temperature relationship of polymers up to 350°C and 2200 kg/cm^2, but the design was complicated and required high precision calibration. A simple apparatus for measuring

the density of solid and liquid polymers as function of temperature (25-250°C) was constructed in our laboratory (Muhammed, 1995). The measurement was based on the specific gravity method defined by ASTM D 792 (Shah, 1984, p. 239), which simply uses Archimedes law.

The set-up was composed of an electronic balance (Ohaus; TS120); a temperature controlled oil bath (Haake F3) mounted on a jack and a copper wire, from which a sample was hung and its weight measured in air (W_a) and oil (W_L). W_L was determined at different temperatures. From values of W_L and W_a the density of the immersed sample (ρ_s) or oil (ρ_L) was computed according to:

$$\rho_s = \frac{\rho_L}{\left(1-\frac{W_L}{W_a}\right)}$$

A high temperature oil (Fisher bath oil) was initially the heated immersion fluid. Stainless steel standard weights were used for calibration of the oil. Polymer samples were press-molded plaques, 1-2 g weight and 1-2 mm thick.

This method is capable of reproducing the density of silicone oil (Dow Corning 710 fluid) as well as its thermal expansion coefficient. Density measurements were able to detect several transition temperatures in linear and branched commercial polyethylenes (HDPE, LLDPE, LDPE) with T_m (melting point) being of primary interest (Muhammad et al., 1997). Good detailed agreement between the melting transition results of the densitometer and the DSC was observed. Furthermore, the simple densitometer revealed the subtle polyethylene α-transition (Popli et al., 1984) in the range of 40°-70°C, which was again supported by the sophisticated DSC. The set-up and the established procedure

were also used to detect structures in molten HDPE at high temperature (200°-250°C), using silicone oil. The silicone oil is the Dow Corning 710 fluid (phenylmethyl polysiloxane) that is serviceable from −18°C to 260°C. It shows very low volatility even at elevated temperatures, and is highly resistant to oxidation and gumming.

In this research, a different experimental approach was taken in seeking possible LCP melt phenomena, in that acknowledged LCPs were not used. We reason that polyethylene melts, particularly those of HDPE, possess sufficient molecular order to be likely candidates for exhibiting thermotropic LCP-type rheology. Moreover, polyethylene is not affected by ambient humidity (as many LCP polyesters, etc. are) and is chemically inert at the primary temperature of testing used here (160°-260°C); thermal degradation occurs only above 345°C (Zachariades and Logan, 1983) and oxidative degradation in the RMS, the DSC, and the Mixer was prevented by a blanket of nitrogen gas and the presence of antioxidants at high levels in the polymers.

IV. Results: Melt Order in 'Pure' Polyethylenes

'Pure' polyethylenes studied in this research, are commercial resins of linear high-density, linear low-density, and nonlinear low-density polyethylenes that contain antioxidants, polymer processing aid, and possibly other additives (UV and heat stabilizers, antistatic agents, ..etc.). The possibility that 'pure' polyethylene resins are likely ordered in the liquid state is investigated and experimental results that support liquid-state order in linear and branched Z-N polyethylenes are discussed below. The new support for liquid-state order in 'pure' polyethylenes was obtained from the measurements of different rheological and thermal properties carried out in different rheological and thermal analysis devices. Temperature sweep measurements in the RMS, Rheocord 90, Melt Indexer, DSC, and the Densitometer, showed evidence of high-temperature transitions in polyethylene. Furthermore, the RMS was extensively used to study the steady and dynamic shear properties of linear high-density polyethylene melts, which produced unique low-shear rheological behavior in agreement with the experimental and theoretical predictions of liquid crystal polymers.

Experimental results on different polyethylenes, from different producers (Chapter III), were obtained in three different rheological instruments: the RMS, the Rheocord 90 Mixer, and the Melt Indexer. Further support was provided by thermal analysis carried out in the DSC and the Densitometer.

A. *Dynamic and Steady shear testing in the RMS*

The RMS was used to collect rheological data in two different modes of operation: the dynamic and the steady shear. Different tests were conducted in the

dynamic mode: temperature sweeps (T-sweep) at constant frequency, ω and strain amplitude, γ^o, ω-sweeps at constant T and γ^o, and time sweeps at constant T, ω, and γ^o. The T-sweep data were used to explore the high-temperature liquid-state transitions by tracking the viscosity-temperature relationship, and the ω-sweep tests were employed for comparison with steady shear results, while the time sweeps were utilized in steady-state oscillatory shear for studying the thermal stability of the polyethylene resins. On the other hand, the steady mode was used to obtain steady shear non-Newtonian viscosity and normal stress (N_1 or N_1-N_2), as well as transient normal force (NF) and stress growth-and-relaxation data after abrupt change of $\dot{\gamma}$ (e.g., from the rest condition $\dot{\gamma}=0$ to some selected steady $\dot{\gamma}>0$, or from $\dot{\gamma}$ to $\dot{\gamma}=0$).

1. Viscosity-Temperature Relationship

(i) *General*

The temperature dependence of the viscosity of amorphous polymer melts, at temperatures far enough above the glass transition ($T>T_g+100$), follows a simple Arrhenius-type relationship: $\eta = A\,e^{E/RT}$ where, E is the activation energy for viscous flow, R is the gas constant, and A is a constant. This expression was first formulated for low-M_w liquids by Andrade (1930). Eyring and co-workers (1940, 1941) interpreted this equation with the aid of their hole theory of liquids. This approximate theory illustrated the mechanisms involved and did permit rough estimation of viscosity-temperature relation from other physical properties. According to the hole theory, a liquid contains unoccupied sites or holes, which move at random throughout the liquid as they are filled and created again by molecules jumping from one site to another. Each jump is made by overcoming an energy barrier of height E. This energy of activation was (for low M_w

liquids) experimentally found to be related to the energy of vaporization of the liquid, E_{vap}, ($E=1/4\ E_{vap}$) since the removal of a molecule from the environment of its neighbors forms part of both processes.

In polymers, however, E (M_w) levels at quite low M_w at a value that at higher M_w is independent of M_w (Kauzmann and Eyring, 1940). This means that in long chains (like linear polyethylene) the unit of flow is considerably smaller than the complete molecule. Kauzmann and Eyring suggested that viscous flow in polymers takes place by successive jumps of segments ($M_{seg}<<M_w$) until the whole chain has shifted. The work required to form a hole for the unit of flow is thus less than the ¼ E_{vap} that would be necessary if the unit consisted of the whole molecule. It is evident that with increasing number of carbon atoms the flow unit becomes a decreasing proportion of the whole chain and in very long chains LPE (or n-alkanes) the unit attains an average length that is approximately constant and contains 20-25 carbon atoms. The activation energy of flow for such a unit, estimated from values of ¼ E_{vap} (from alkane evaporation), is 6 to 7 kcal (25-29 kJ/mol), in excellent agreement with the viscometrically measured activation energies for HDPE that were reported to be in the range 5.5-7.5 kcal/mol (Bersted, 1985; Mark et al., 1986).

When log η is plotted against 1/T over wide ranges of temperature ($T>T_g+100$), even for liquids of low M_w, the apparent value of E decreases as T increases (Krevelen, 1972). This phenomenon may be explained by the fact that viscosity is sensitive to the extra free volume created by thermal expansion. This was suggested by Batschinski in 1913.

If the Eyring hole theory is to be extended to LCPs that undergo thermal transitions, another important factor that influences viscosity (besides the availability of

unoccupied sites or holes) should be considered. That is the mobility of the unit of flow or chain segment, which will be different below and above a thermal transition. Past their thermal transitions, LCPs lose part (or all) of their molecular order; and gain more chain flexibility. The volume occupied by the molecules above the transition would then be larger than that below the transition; and, hence, less holes or accessible free volume will be available for the segmental jumps. Therefore, the energy barrier, E, will increase leading to higher viscosities above the transition point. This might explain the observed and predicted increase in viscosity of LCPs above their transition temperatures (Heberer et al., 1994; Han and Rey, 1995); and the ease of the processing in the liquid crystalline state (McChesney, 1988).

For a Newtonian material, viscosity is independent of shear stress, τ, or shear rate, $\dot{\gamma}$, and is a constant at any one temperature at a fixed pressure. However, for a non-Newtonian material, viscosity at fixed temperature is dependent on shear stress or shear rate and, thus, the Andrade equation would be: $\eta(\tau$ or $\dot{\gamma})=A\ e^{\ E/RT}$. Hence, either A, or E, or both must be considered as functions of τ or $\dot{\gamma}$. In order to make quantitative evaluation of the variation of viscosity with temperature; it is therefore necessary to deal with variations under some kind of fixed conditions of shear stress or shear rate. The variations are expressed as apparent flow activation energy, E_τ or $E_{\dot{\gamma}}$ given by $R[\delta\ln \eta/\delta(1/T)]_\tau$ or $R[\delta\ln \eta/\delta(1/T)]\dot{\gamma}$ (Bestul and Belcher, 1953) with $E_\tau \cong E_{\dot{\gamma}} \cong E$ at low shear rate (i.e., in the Newtonian limit).

The relation between E_τ and $E_{\dot{\gamma}}$ was mathematically derived as $E_\tau/E_{\dot{\gamma}}=1-\dot{\gamma}\times (\delta\eta/\delta\tau)_T$; and $(\delta\eta/\delta\tau)_T$ is either negative or zero in shear flows (Sabia, 1964). Bestul and

Belcher collected quantitative experimental data on several different systems of linear amorphous polymers, both solvent-free and in solution (not including polyethylene). Their results indicated that the variation of viscosity with temperature at fixed shear stress is independent of shear stress. However, the variation at fixed shear rate is always less than that at very low shear stress, and decreases with increasing shear rate. Bestul and Belcher results on different polymer solutions and melts showed that E_τ and $E_{\dot\gamma}$ were independent of τ and $\dot\gamma$ respectively.

The flow behavior of molten polyethylene resins (mainly LDPE) was studied with rotational viscometers and piston- or gas-driven capillary rheometers. Results obtained from different types of instruments were often in disagreement (Schott and Kaghan, 1961). Furthermore, different anomalies were reported on the viscosity-temperature relationship for LDPE and widely attributed to long-chain branching (Porter and Johnson, 1966). Mendelson (1965a) studied the viscosity-temperature behavior of LDPE (M_w=730-1580K) and observed that the apparent viscosities at constant shear stress may be adequately fitted to an Arrhenius equation (using E_τ) over the $180°$ temperature range covered ($120°$-$300°$C, 6 data points). However, such an equation does not adequately represent the constant shear rate data over this temperature range. An observed break in $\eta_{\dot\gamma}$ (1/T) data (Mendelson, 1965a), hints to a possibility of a thermal transition in the temperature range $200°$-$250°$C, where no experimental data were taken. Mendelson observed a decrease in E_τ with increasing τ. On the other hand, Philippoff and Gaskins (1956) reported (LDPE; 3-5 data points; only one above $210°$C) an increase in E_τ from 12.8 to 19 kcal/mol following an increase in τ from zero to 10^5 Pa.

Meissner (1963) reported a relatively slow decrease in E_τ with increasing τ disagreeing with previous reports. His experimental results (125°-240°C; 4 data points) fitted Arrhenius behavior with E_τ and $E_{\dot\gamma}$ independent of τ and $\dot\gamma$ respectively. Porter and Johnson (1960) observed an increase in activation energy of LDPEs with increasing M_w. Dexter (1954) results on LDPE show that E_τ is independent of τ. Reduced curves (η_a/η_0 vs $\dot\gamma \lambda_1$, where λ_1 is the longest relaxation time) obtained for the branched and linear polyethylenes encountered wide scatter of the data (Mendelson et al., 1970), and time-temperature shifting of LDPE data yielded only an approximate superposition (Dealy and Wissbrun, 1990, p. 92). Mendelson (1965b) reported that the plot of log $a_T(T)$ vs. $1/T$ (120°-300°C; 6 data points) for LDPE was linear and followed Arrhenius behavior in contrast to the results of Horio et al. who reported a linear behavior of log $a_T(T)$ vs. T (140°-200°C). Sabia (1964) studied a series of HDPEs and found that the non-Newtonian $\eta(T)$ measured at constant shear rate (150°-220°C) appeared to follow Arrhenius behavior.

In general, E_τ and $E_{\dot\gamma}$ were used only as a convenient and readily compared means of expressing the variations of $\eta(T)$, and their use is not necessarily meant to imply that in non-Newtonian flow they hold the full significance attached to activation energies in Newtonian flow.

In most, if not all, of the above-cited literature few data points were taken, at intervals too spread out to define any thermal transition. The fact that linear polyethylene has the smallest activation energy ever described for a molten polymer (Philippoff and Gaskins, 1956), makes detecting these transitions even harder. Therefore, a close look at the viscosity-temperature relation, especially in the high temperature range, is needed to

clarify the above-cited anomalous behavior; and more data are required to clearly define any thermal transition. The relation $\eta(\dot{\gamma})=A(\dot{\gamma}) \ e^{E(\dot{\gamma})/RT}$ or $\eta(\tau)=A(\tau) \ e^{E(\tau)/RT}$ should apply to the temperature range above the melting point regardless of the flow regime. The RMS 800 can provide full control of the oscillatory shear rate rather than the shear stress, and hence, constant shear rate operation was selected. At constant shear rate, $\eta_{\dot{\gamma}} = A_{\dot{\gamma}} \ e^{E_{\dot{\gamma}}/RT}$; and in the absence of any thermal transitions, a plot of $\ln \eta_{\gamma}$ vs. $1/T$ should yield a straight line with a slope of $E\dot{\gamma}/R$. Small-strain T-sweeps were used to measure the complex viscosity, η^*, (at constant ω and γ^o) of different linear and branched polyethylenes. Results will be discussed below.

(ii) Linear High-Density Polyethylenes

Small-strain T-sweep tests of $\eta^*(\omega;T)$ were carried out on different Z-N linear HDPEs from different resin producers (see Table 3.1). Quantum high-density polyethylene (Q-HDPE) was chosen, as an example for linear polyethylenes, to study the effect of different parameters (to be discussed later) on the viscosity-temperature behavior. All T-sweep tests were preceded by γ^o-sweep testing at constant ω and T, to select γ^o in the linear viscoelastic range of the polymer of interest. The range covered by the temperature sweeps was 160°-260^oC at a step size of $\Delta T=10^o$ and a thermal soak time of 1 minute. Hence, strain sweep data were obtained (at constant ω) at 160^oC and 260^oC. The Q-HDPE as-received resin was highly stabilized by adding 3000 ppm of AO (in addition to the amounts already present in the commercial resin) and mixing at 180^oC for 10 min. Results for Q-HDPE, obtained at 160^oC, are shown in Figure 4.1. Data on similar measurements taken at 260^oC are given in the Appendix (Figure A.1). The viscous (η')

Figure 4.1 Strain sweep test for Q-HDPE at 160°C
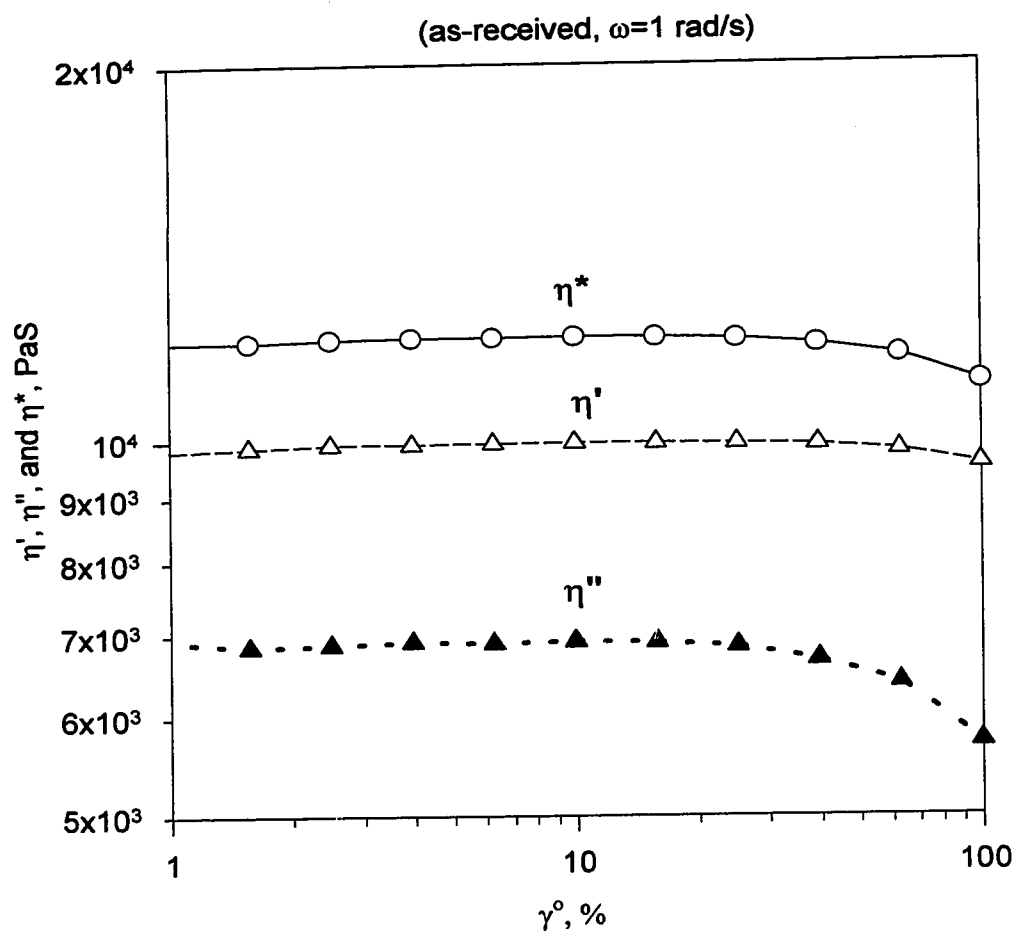
and elastic (η'') properties were both linear for γ° up to 30%. A value of γ°= 10% was normally selected for all linear-HDPEs studied in this research; and later used in temperature, frequency, and time sweep tests. The same test was repeated for Dow polystyrene (PS) at 160° and 260°C, and a strain of 15% (at ω= 1 rad/s) was picked. The independently measured PP gap correction of 3 $\mu m/^{\circ}C$ was used in all T-sweep tests to correct for thermal expansion or contraction.

The complex viscosity, η^*, was measured for HDPEs and PS (used as reference for typical amorphous behavior) at different temperatures in the range 260°-160°C. Arrhenius plots (Figure 4.2a) of log η^* vs. 1/T are characteristic of the melt state(s) with a slope of $E_{\dot{\gamma}}/2.303R$, where $E_{\dot{\gamma}}$ is the apparent activation energy for viscous flow. $E_{\dot{\gamma}}$ obtained at low frequencies could be compared to reported values of the activation energy for viscous flow. However, when measured at high frequencies (i.e. in the non-Newtonian flow regime), $E_{\dot{\gamma}}$ could only be used as a convenient and sensitive measure of expressing the variations of $\eta(T)$. Hence, for the purpose of this study $E_{\dot{\gamma}}$ (now and hereafter referred to by E) will be adopted to test the viscosity-temperature relation for Arrhenius behavior. The presence of a liquid-state transition temperature, i.e. evidence of liquid crystal behavior, is implied by obtaining data that can be well fitted by two straight lines above and below the melt transition temperature.

Independent T-sweep testing, at constant ω and γ°, was carried out for the Q-HDPE and PS. Arrhenius plots of $\eta^*(1/T)$ for Q-HDPE (obtained at ω=0.1 rad/s) and PS are shown in Figure 4.2a. As expected for amorphous melts, the PS (dotted line) showed linear behavior over the whole range (r^2 = 0.999) with calculated activation energy of

Figure 4.2a Arrhenius plot of $\eta^*(1/T)$ for Q-HDPE[+] and PS

(+with 3000 ppm A/O mixed for 10 min. at 180°C, 50 rpm)
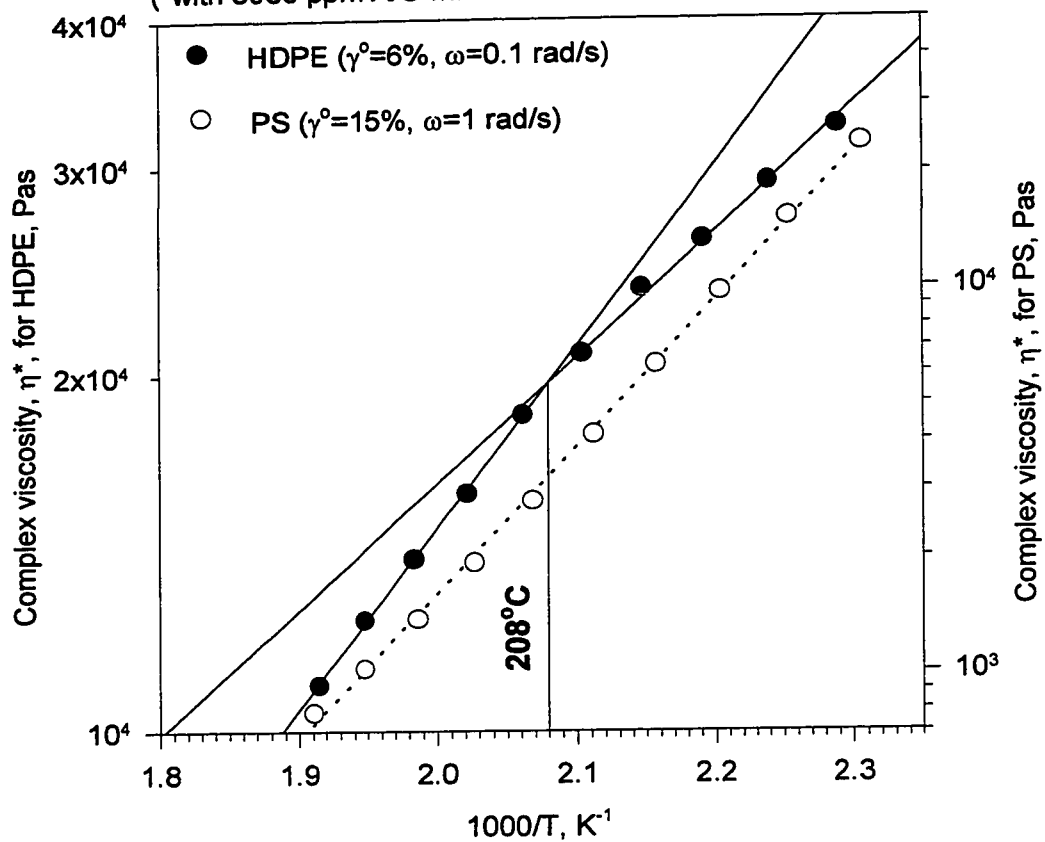
17.4 kcal/mol (72.8 kJ/mol) in excellent uniformity with previous literature reports (Krevelen, 1976, p. 345; Philippoff and Gaskins, 1956). On the other hand, the Q-HDPE showed an obvious break in the curve near T=208°C (1000/T=2.08K^{-1}). The plot shows linear behavior above and below the break (transition point). Activation energies below, E_B, (160°< T < 208°C) and above, E_A, (208°< T < 260°C) were calculated from the linear regression fitting of the data. The activation energies were found to be E_A= 7.0 kcal/mol (r^2=0.997) and E_B= 4.7 kcal/mol (r^2=0.999). Fitting the whole collection of data above and below the transition by a straight line (as would happen for widely scattered data) resulted in an activation energy of 5.8 kcal/mol (r^2=0.990) in excellent agreement with earlier-cited theoretical predictions and experimental observations that reported E to be in the range 5.5-7.5 kcal/mol (Kauzmann and Eyring, 1940; Bersted, 1985; Mark et al., 1986). The transition temperature, T_1, was obtained as the intersection of the two straight lines representing the behavior below and above the phase transition.

The previous testing on the highly stabilized Q-HDPE was repeated at a higher frequency (ω= 1 rad/s). Results are shown in Figure 4.2b with PS shown as dotted line. The curve showed a break at the same transition temperature (208°C) with E_A=5.7 kcal/mol (r^2=0.999) and E_B= 4.1 kcal/mol (r^2=0.995). Both E_A and E_B were lower than those obtained at ω=0.1 rad/s, in agreement with theoretical predictions (Bestul and Belcher, 1953; Sabia, 1964) and previous experimental observations on different polyethylenes (Philippoff and Gaskins, 1956; Schott and Kaghan, 1961; Meissner, 1963; Sabia, 1964; Mendelson, 1965a; Porter and Johnson, 1966).

Surprisingly, the energy barrier above the 208°C transition is always higher than that below (E_A=1.5 E_B). This observation cannot be explained by either Eyring's hole

Figure 4.2b Arrhenius plot of η*(1/T) for Q-HDPE with A/O⁺
(ω=1 rad/s, T= 260°-160°C, thermal soak=1 min.)
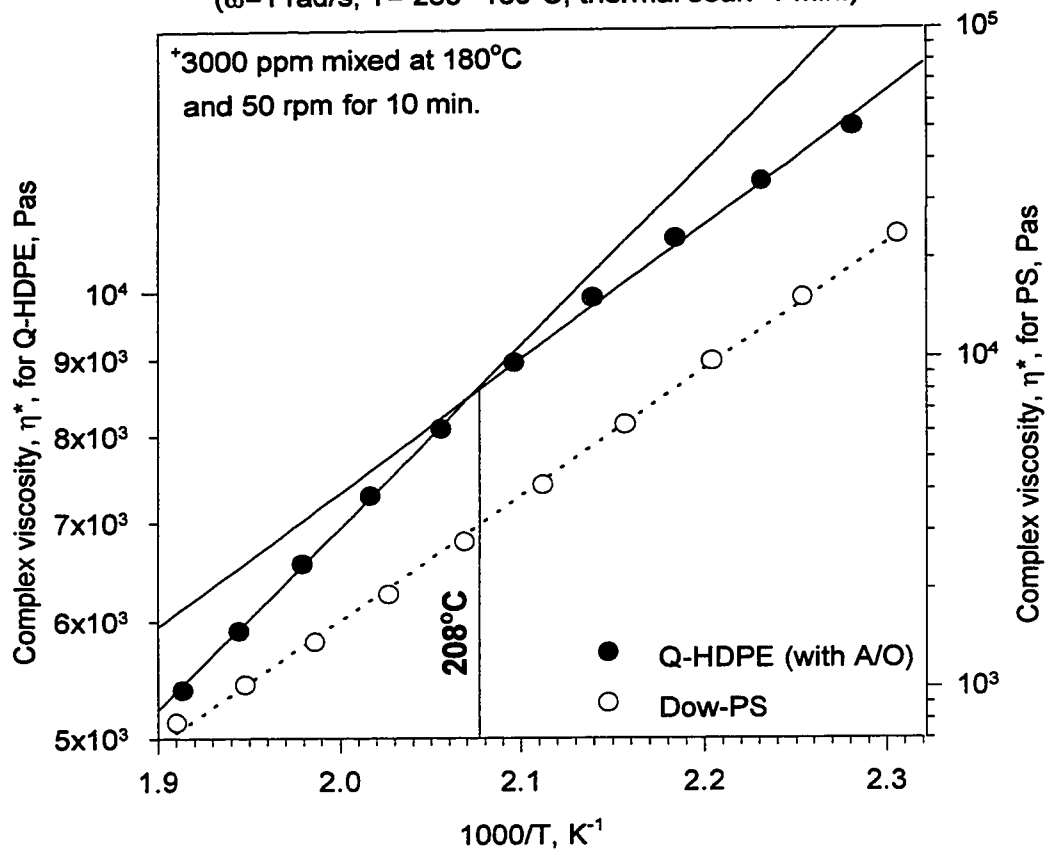
theory or by Batschinski's free volume approach, since the activation energy is predicted to be constant or decrease at high temperatures. The two theories would explain the increase in activation energy as either an increase in the number of occupied sites or a decrease in the accessible free volume, which could be a direct result of the molecular freedom (partial or total) gained by the ordered melt past the transition temperature. Moreover, this observation is in agreement with the theoretical predictions and the experimental observations for LCPs discussed earlier.

Furthermore, as-received commercial resins of Q-HDPE were tested (ω=1 rad/s) for comparison with the highly stabilized torqued samples. Data obtained for the as-received sample, along with previous data collected for the highly AO-stabilized resin (at the same frequency), are shown in Figure 4.2c. The η*(1/T) plot for the as-received resins produced the same results as the highly stabilized torqued samples. Thus, the commercial resin was already stable and there is no need for additional AO. Furthermore, the results suggest there are no shear history effects on the T_1 thermal transition. Thus, the observed transition is neither a result of oxidative degradation, nor a product of the thermal and/or mechanical histories in the blender, but rather a pure molecular state phenomenon. Therefore, samples prepared from the as-received commercial resins were used in testing other commercial HDPEs. Nova S221 (HDPE) was tested in the as-received form at ω=1 rad/s; and results are shown in Figure 4.3a. Again, the 208°C transition was observed and the activation energies were found to be E_A=5.5 kcal/mol (r^2=0.9997) and E_B=4.2 kcal/mol (r^2=0.9977).

Results for other linear HDPEs from Paxon, Solvay, and Union Carbide (UC), (obtained separately for each resin) are shown in Figure 4.3b. All the Arrhenius plots

Figure 4.2c η^*(T) for Q-HDPE with[+] and w/o A/O

(γ°= 6%, ω=1 rad/s, T= 260°-160°C, thermal soak=1 min.)

[+]3000 ppm mixed at 180°C and 50 rpm for 10 min.

- ● with extra AO
- ○ w/o extra AO
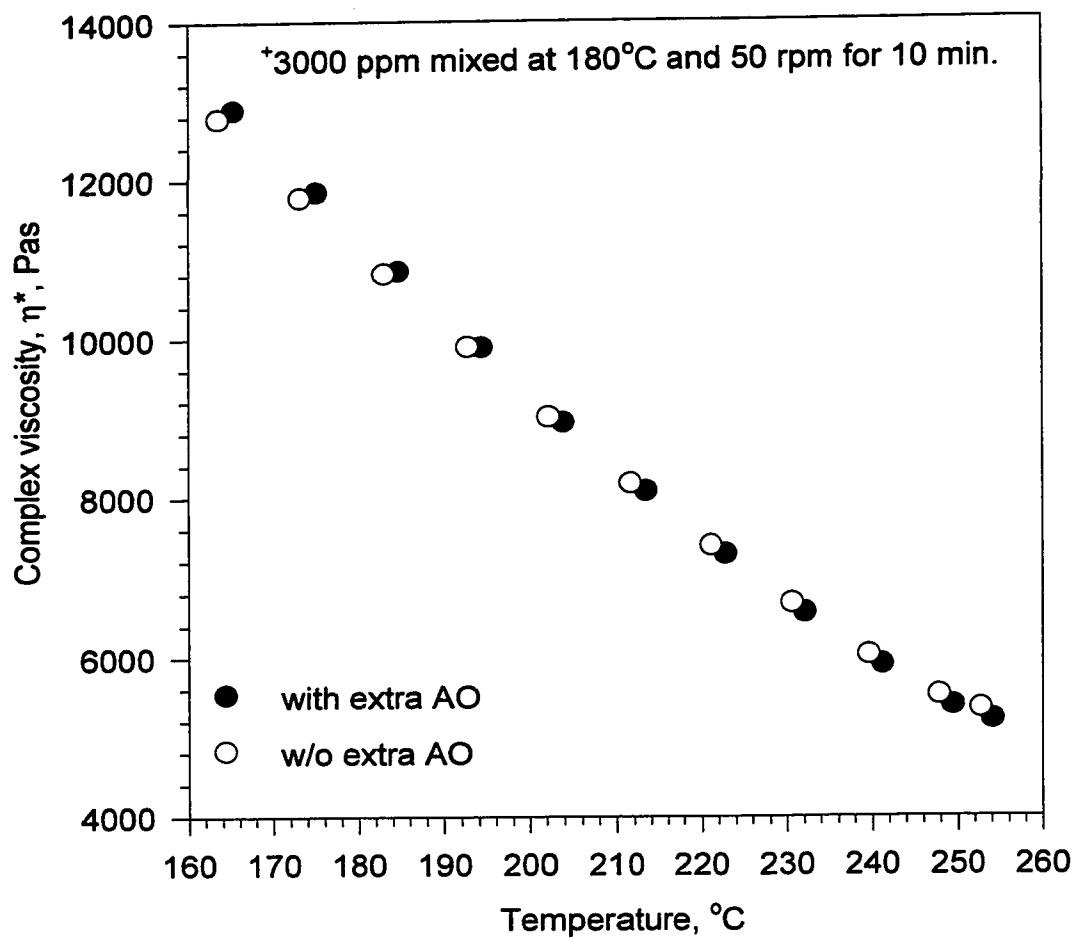
Figure 4.3a Arrhenius plot of $\eta^*(1/T)$ for Nova S221(HDPE)

(as-received, γ°=10%, ω=1 rad/s, 260°-160°C)
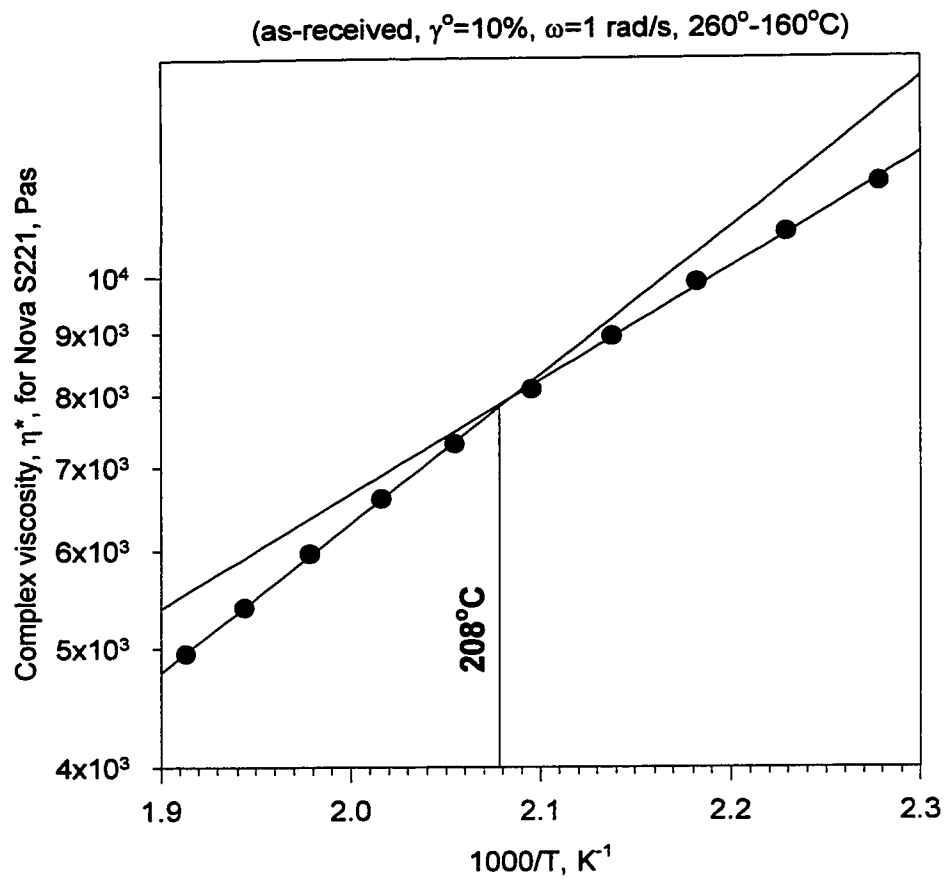
Figure 4.3b η*(T) for different HDPEs and PS
(temperature sweeps from 260° to 160°C, ω=0.1 rad/s)
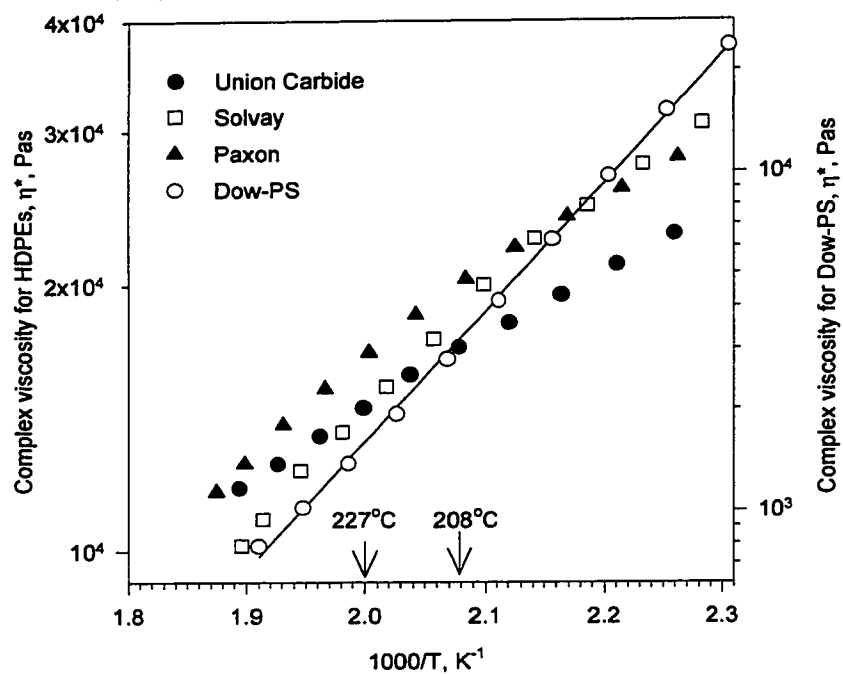
produced a break near 208°C, accompanied by a linear behavior above and below the T_1 transition. Data on PS are shown in Figure 4.3b as a solid-line. Activation energies, E_A and E_B, for different HDPEs are given in Table 4.1.

Activation energy E_B, corresponding to the temperature range 160°-208°C, ranged from 3.3-4.9 kcal/mol. On the other hand, E_A, corresponding to the temperature range 208°-260°C, ranged from 4.1–7.0 kcal/mol. E_A was greater than E_B for all samples, with E_A/E_B ranging from 1.2 to 1.6. This suggests that the T_1 transition signals a <u>change</u> in order leading to more interactions, and, hence, higher activation energies.

Table 4.1: Activation energies for HDPEs (T-sweeps in the RMS @ 0.1 rad/s)

Resin Producer	E_B (kcal/mol)	r_b^2	E_A (kcal/mol)	r_a^2	E_A/E_B
Paxon	3.486	0.9989	5.430	0.9975	1.558
Quantum	4.667	0.9966	7.011	0.9992	1.50
Solvay	4.850	0.9907	6.729	0.9951	1.387
UC	3.280	0.9997	4.057	0.9995	1.237
Nova S221*	4.201	0.9977	5.494	0.9997	1.308

*Measured at 1 rad/s.

As discussed earlier, the temperature sweep testing of torqued and as-received samples of Q-HDPE produced almost identical results suggesting the absence of 'shear' (mechanical) history effects on the reported thermal transitions and order in the liquid state. It remains to investigate the effect of thermal history (or annealing) on the order and the transitions.

A small-γ° temperature-sweep test for $\eta^*(T)$ was carried out for Q-HDPE at $\omega=1$ rad/s. The test started by heating from 160° to 260°C, followed by cooling from 260° to 160°C, and finally ended by another heating to 260°C. Complex viscosities, $\eta^*(1/T)$, are given in Figure 4.3c. Viscosities obtained in the first heating were always lower than the corresponding values during later heating and cooling. The results for the as-received and highly stabilized samples were almost identical. Therefore, the possibility of oxidative degradation as the reason for this observation is remote. Thermal cycling (annealing) had the general effect of continuing to increase viscosity as the highly stabilized material was 'conditioned' by each half cycle. An increase, of about 16%, in the viscosity at low temperature was observed when the sample was heated from 160° to 260°C and then cooled back to 160°C.

The effect of thermal history on thermotropic LCPs was investigated by Wissbrun et al. (1987) and Done and Baird (1987). Wissbrun et al. (1987) carefully studied (using rheology and DSC) the thermal history effects on as-received resins and extrudates of LCPs. They attributed the increase in viscosity to changes in the molecular order rather than changes in the molecular weight (degradation). It is believed that "annealing" increases the liquid crystalline order of the polymer. This explanation is further supported by the molecular dynamics studies of PE (Choi et al., 1995) where an increase in the degree of order of PE with annealing time was observed.

Activation energies, E_A and E_B, calculated from the Arrhenius plots of $\eta^*(1/T)$ (Figure 4.3c) are given in Table 4.2. In the second heating, the activation energies and, hence, the resistance to flow, were higher than the corresponding values of the first heating. These observations support the previous explanations of Wissbrun et al. (1987).

Figure 4.3c Arrhenius plot of $\eta^*(1/T)$ for Q-HDPE[+]

(T=160°-260°-160°-260°C, $\gamma°$=10%, ω=1 rad/s)

[+]3000 ppm of A/O mixed for 10 min at 180°C and 50 rpm

○ 1st heating (160°-260°C)
● 1st cooling (260°-160°C)
△ 2nd heating (160°-260°C)
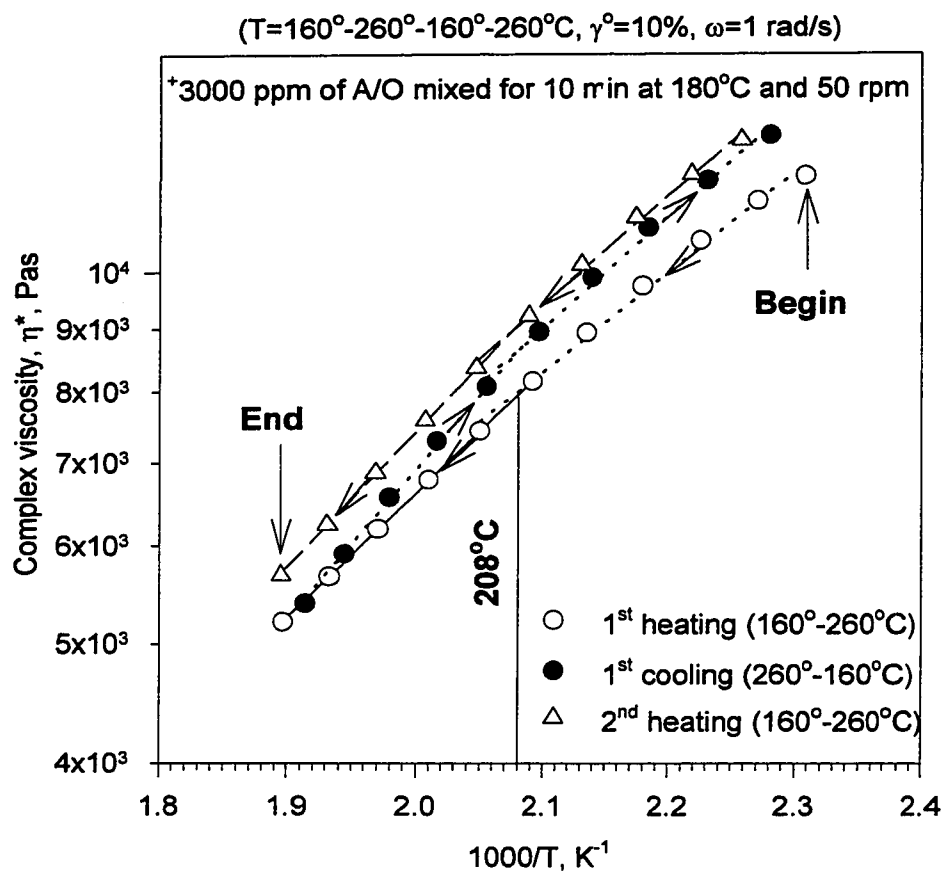
Table 4.2: Activation energies for Q-HDPE (T-sweeps in the RMS @ 1.0 rad/s)

Thermal history	E_B (kcal/mol)	r_b^2	E_A (kcal/mol)	r_a^2	E_A/E_B
1st heating	3.680	0.9938	4.581	0.9999	1.245
1st cooling	4.110	0.9947	5.529	0.9985	1.345
2nd heating	3.988	0.9956	4.994	0.9997	1.252

(iii) Branched Polyethylenes

Polyethylenes with short (LLDPEs) and long (LDPE) chain branching were studied for possible order in the liquid state. All LLDPE polyethylenes used were Z-N products of Nova (identified with Sample #), except one metallocene resin from Exxon. The characterization data for these resins were given in Tables 3.1 and 3.2. The Z-N LLDPEs, were of different comonomer type, namely butene, hexene, and octene. Their branch contents were of the same order of magnitude (14.7-22.1 branches/1000 C). Small-strain temperature sweep testing was conducted at constant frequency ($\omega=1$ rad/s) and strain-amplitude ($\gamma^o=10\%$) in the range 160°-260°C, similar to that carried out for HDPEs. All resins were highly stabilized by adding extra AO and mixing at 190°C and 50 rpm for 10 minutes (1000 ppm for the Z-N resins and 6000 ppm for the metallocene resin).

Results obtained for S229 (butene) by heating from 160°C to 260°C, are shown in Figure 4.4a as a plot of η^* vs. 1/T. Again, collected data didn't fit a single straight line, but rather two lines above and below 204°C. Furthermore, the temperature sweep test was carried out by heating from 160°C to 260°C and then cooling back to 160°C. This kind of full-cycle temperature sweep testing was usually performed to check for reproducibility

Figure 4.4a Arrhenius plot of η*(1/T) for S229 (butene)⁺

(160°-260°C, ω=1 rad/s, γ°=10%, 22.1 branches/1000 C)

⁺with additional 1000 ppm of A/O
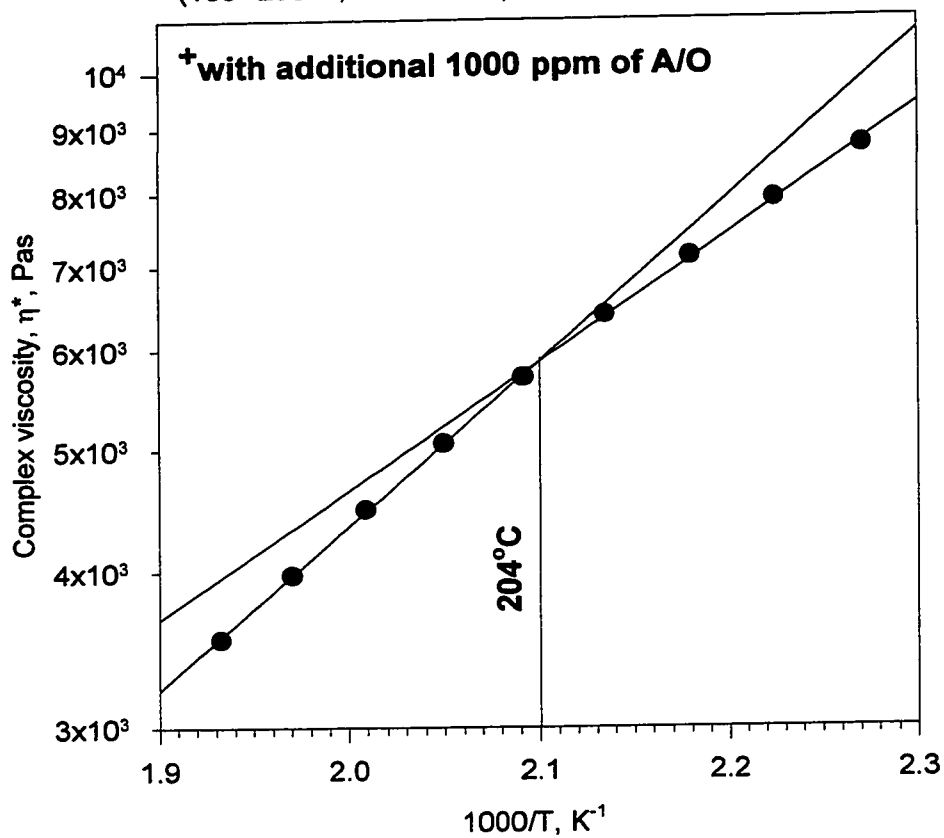
of data and possible degradation. Typical results, given for S229, showed the excellent agreement between data obtained in heating and that collected in cooling (see Appendix, Figure A.2). Other LLDPEs (S237, hexene; S226, octene) were tested in the same fashion and under the same experimental conditions. Results for S237 and S226 showed behavior similar to, S229 with transition temperatures at 203°C and 201°C respectively (Appendix A, Figures A.3 and A.4).

Another branched polyethylene with short and long chain branching (S216, LDPE) was studied. The resin was a product of a free radical polymerization process. The data obtained in the temperature sweep test are shown in Figure 4.4b as Arrhenius plot of $\eta^*(1/T)$. Results on the LDPE showed a behavior similar to that observed for the LLDPEs with a transition at 206°C (similar to HDPEs $T_1 \cong 208°C$, too). Activation energies above and below the transition, in addition to the transition temperatures for the different Z-N branched polyethylenes are given in Table 4.3.

The above results on branched polyethylenes indicate that the order in the liquid state is not limited to linear polyethylenes, but rather is very likely a characteristic of the methylene ($-CH_2-$) unit present in the different polyethylenes covered by this study. Moreover, the branching resulted in the lowering of the liquid-state transition temperature T_1 (melting point of liquid crystals) by 2° to 7°C, with the high end (204°C) associated with the shortest-branched LLDPEs. The results given in Table 4.3 show a decrease (to 201°C) in the transition temperature with the increase in branch length. The short chain branching and its length influenced the liquid-state transition temperature in a way similar to their observed influence (Wunderlich, 1980; Mathot et al., 1998) on the solid-state transition temperature (T_m).

Figure 4.4b Arrhenius plot of $\eta^*(1/T)$ for S216 (LDPE)$^+$

(160°-260°C, ω=1rad/s, γ°=10%, thermal soak=1min.)

$^+$**with additional 1000 ppm of AO**
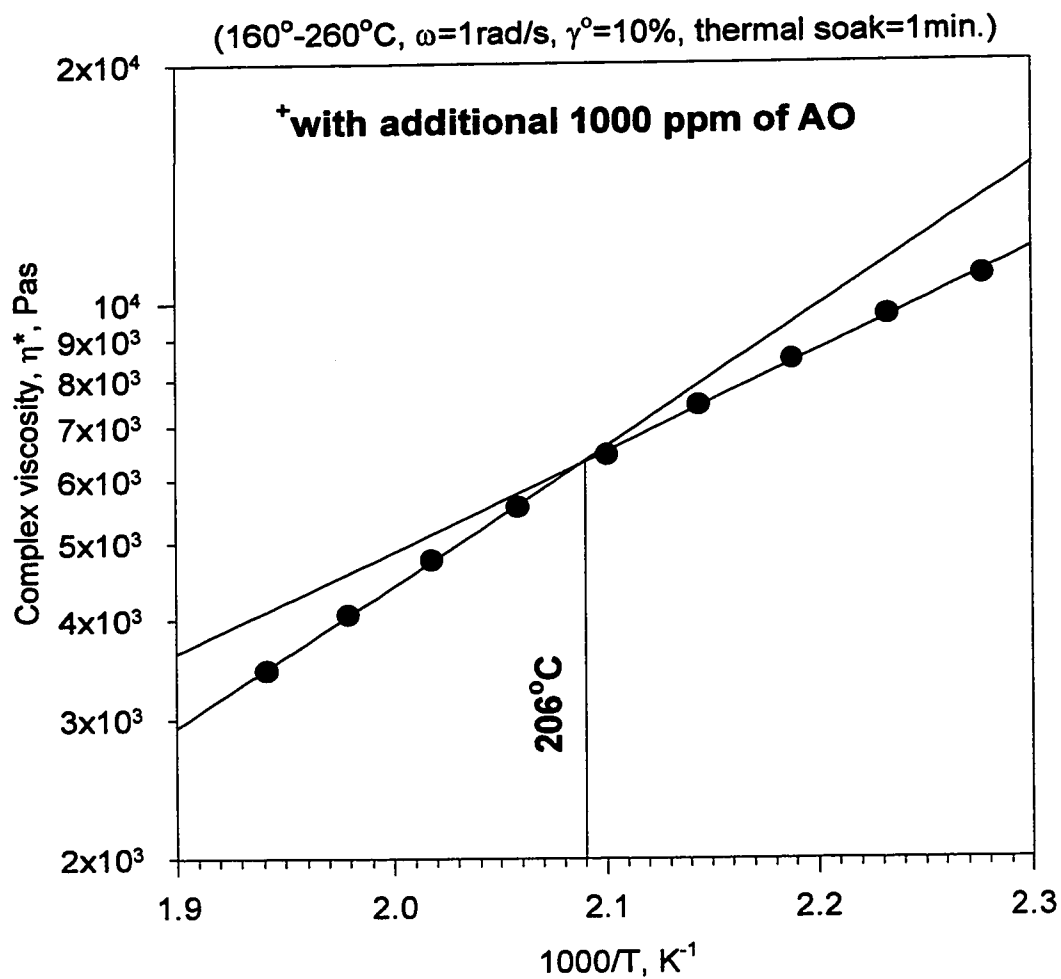
Table 4.3: Activation energies for Nova Branched Polyethylenes measured at 1 rad/s

Resin	E_B (kcal/mol)	r_b^2	E_A (kcal/mol)	r_a^2	E_A/E_B	T_1, °C
S229 (butene)	4.679	0.9981	5.990	0.9996	1.28	204
S237 (hexene)	4.710	0.9943	6.137	0.9999	1.30	203
S226 (octene)	4.657	0.9952	5.955	0.9998	1.28	201
S216 (LDPE)	5.794	0.9992	8.054	0.9979	1.33	206
Q-HDPE*	4.110	0.9947	5.529	0.9985	1.345	208°C

*For comparison with the different branched samples

However, the activation energies of the three LLDPEs (given in Table 4.3) show weak or no dependency on branch length. Figure 4.4c shows a correlation of E_A, E_B, and T_1 to the branch length reported here as the number of carbon atoms in the branch. The abscissa numbers 2, 4, and 6 stand for Butene, Hexene, and Octene LLDPEs respectively, with 0 representing the linear Q-HDPE. The branch densities ($CH_3/1000$ C) of the LLDPE are given in parenthesis.

Furthermore, the temperature sweep testing was extended to a highly branched metallocene resin that contained 36.2 branches/1000C. The test was carried out under the same conditions of constant γ^0 and ω, and in the same temperature range. The results obtained showed a very interesting behavior, totally different from the previous observations [see Figure 4.4d for a plot of $\eta^*(1/T)$]. No evidence of a liquid-state transition in the temperature range 160°-260°C was detected. This time, the data fitted a single straight line (r^2=0.999). The heating and cooling cycles reproduced the same results (Appendix, Figure A.5). This interesting observation could be related to the influence of both the high branch content and the uniform branch distribution on the

Figure 4.4c Effect of branching on E_A, E_B, and T_1

Figure 4.4c Effect of branching on E_A, E_B, and T_1
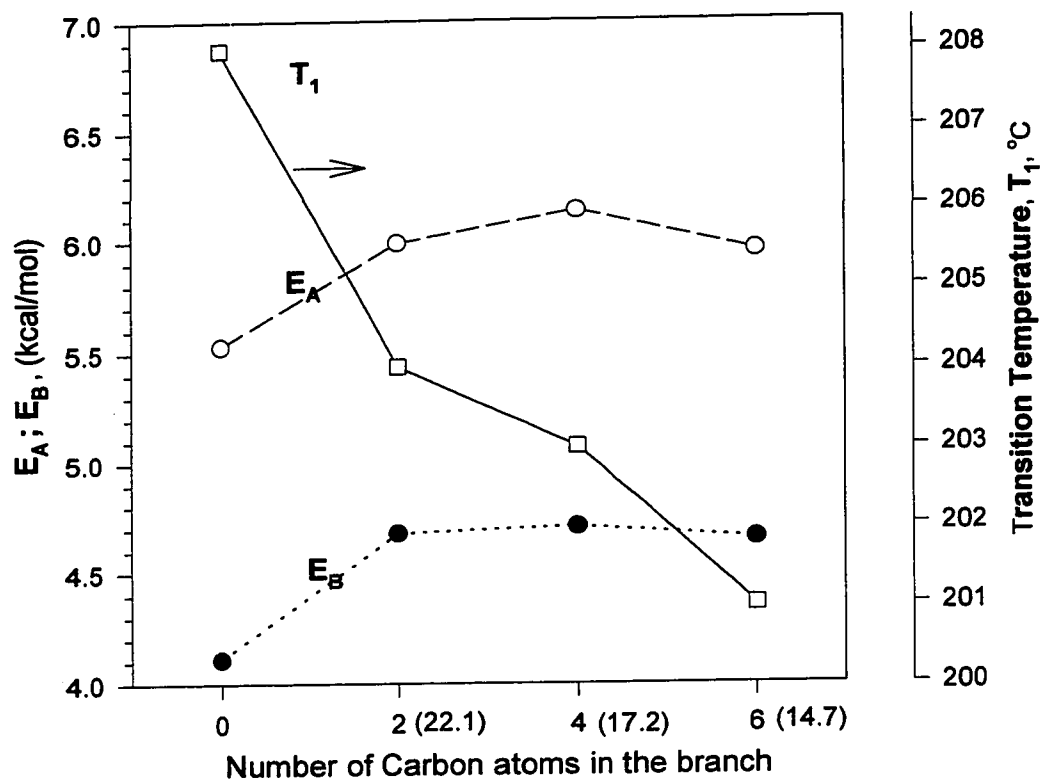
Figure 4.4d Arrhenius plot of η*(1/T) for Exxon 4033 (Met.)[+]

$(\gamma^\circ=10\%, \omega=1\text{rad/s}, \text{Butene}, 36.2 \text{ Branches/1000})$

[+]with additional 6000 ppm of AO

(E=6.791 kcal/mol, r^2=0.9985)
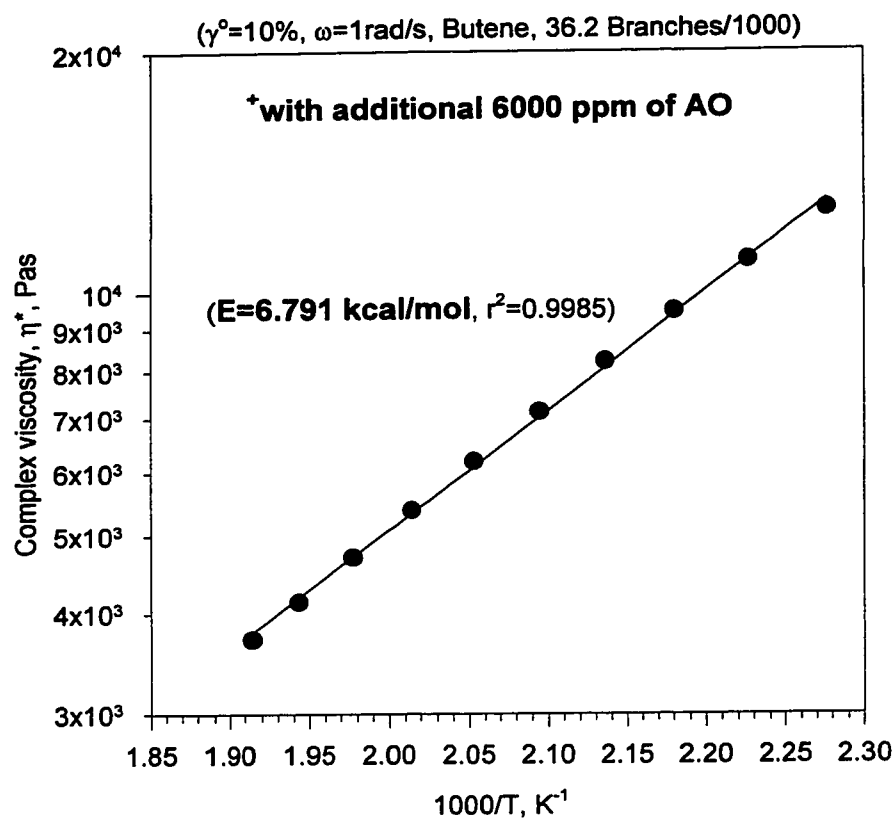
molecular order in the liquid state. The influence of the short-chain branching (content and length) on the liquid and solid-state chain folding was found to be similar. This might be the reason behind the disappearance of thermal transitions (and hence molecular order) for the high-branch content resin, where branching is expected to reduce molecular order (chain folding). The branching produced effect is similar.

In summary, all linear and branched Z-N polyethylenes studied in this research, showed a high-temperature transition in the range 200° to 208°C with $E_A > E_B$, indicating liquid state molecular order. The introduction of branching on the linear polyethylene chain depressed the liquid-crystal melting temperature (transition temperature), and eventually led to no detectable transitions and possible amorphous melt in highly branched chains as observed for the metallocene resin. The depression of the liquid-crystal melting point T_l as a result of branching (content, length) is in agreement with predictions of classical thermodynamics for depression of T_m; more work is needed to define this relation properly.

2. Stress Transients and Steady Shear behavior

(i) Steady (constant-γ) Shear flow

The primary focus here is on steady state shear flow behavior, so the dynamic results will be mentioned later only for specific comparison purposes and the transients will be reported separately in the following section. Steady shear measurements were carried out on HDPEs from different resin producers. Again Q-HDPE was selected for in-depth study and tested following the earlier described procedure. Each data point on the steady shear curve was recorded by the RMS following a 5-minute time-before-measurement (tbm) and a 30 seconds measurement-time (mt). The resulting anomalous

behavior in steady shear viscosity and normal force will later be compared to the theoretical predictions of Marrucci and Maffettone (1990) shown in Figure 4.5a.

Figure 4.5b displays results for Q-HDPE at 190°C, obtained with parallel plates. The anomalous drop in N_1-N_2, with a minimum at about $\dot{\gamma}_R$=0.05 s^{-1}, is interpreted here as the same phenomenon as predicted in Figure 4.5a near a dimensionless shear rate G=1.2, namely the trend of N_1 changing sign. A plot resembling Figure 4.5b was presented earlier for a lyotropic LCP system (Moldenaers and Mewis, 1986a; Huang et al., 1999). Further support for this LCP-type interpretation is the obvious kink in $\eta(\dot{\gamma})$ at $\dot{\gamma}_R$=0.8 s^{-1}, which strongly resembles the kink in Figure 4.5a near G=2. The fact that the normal stress function does not actually change sign in Figure 4.5b could be attributed to the contribution of N_2, which is normally expected to have a sign opposite to N_1; thus, as N_1 approaches zero at the $\dot{\gamma}_R$ of its sign change, the non-zero values of N_2 would begin to dominate the function N_1-N_2 and the sign change of N_1 would not be measurable. Of course, the logarithmic stress scale cannot show negative values, but a plunge of the data towards zero would take the values below the RMS sensitivity in the region $0.04<\dot{\gamma}<0.05$ s^{-1} anyway. In this steady-shear mode of operation, no negative normal stresses could be detected in this $\dot{\gamma}$-regime.

There are several resemblances between Figures 4.5a and 4.5b, in addition to the viscosity kink and descent of N from both directions toward an apparent sign change. One such similarity is the fact that the low-$\dot{\gamma}_R$ maximum in normal stress in Figure 4.5b occurs at a value of $\dot{\gamma}_R$ close to that at which $\eta(\dot{\gamma}_R)$ departs from its Newtonian plateau, just as shown in Figure 4.5a for $N_{max}(G)$ relative to $\eta(G)$. Another is the quantitative similarity of the spacings along the shear rate axis between the two branches of the

Figure 4.5a Steady state shear viscosity and normal stress difference vs. shear rate.
Redrawn from Marrucci and Maffetone (1990).
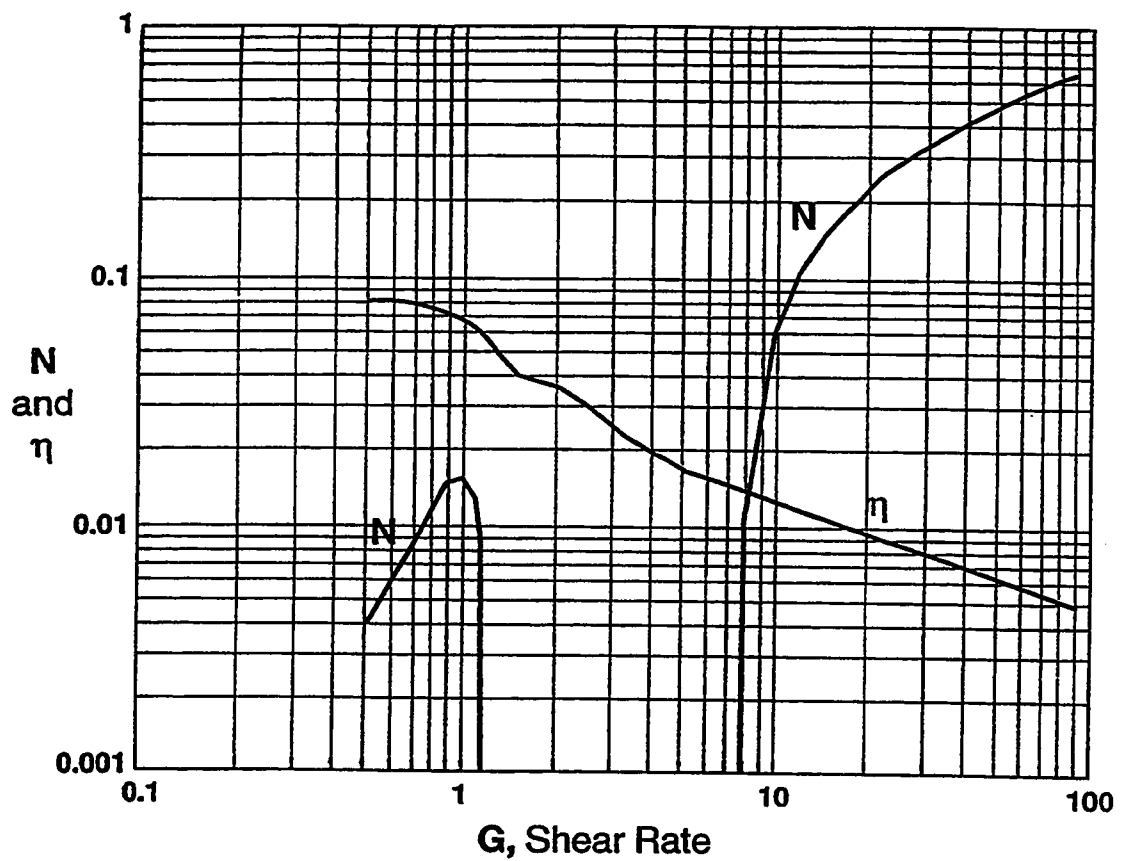
Figure 4.5b Steady shear viscosity and Normal stress for Q-HDPE

(PP, T=190°C, tbm=5 min., mt= 30 sec)
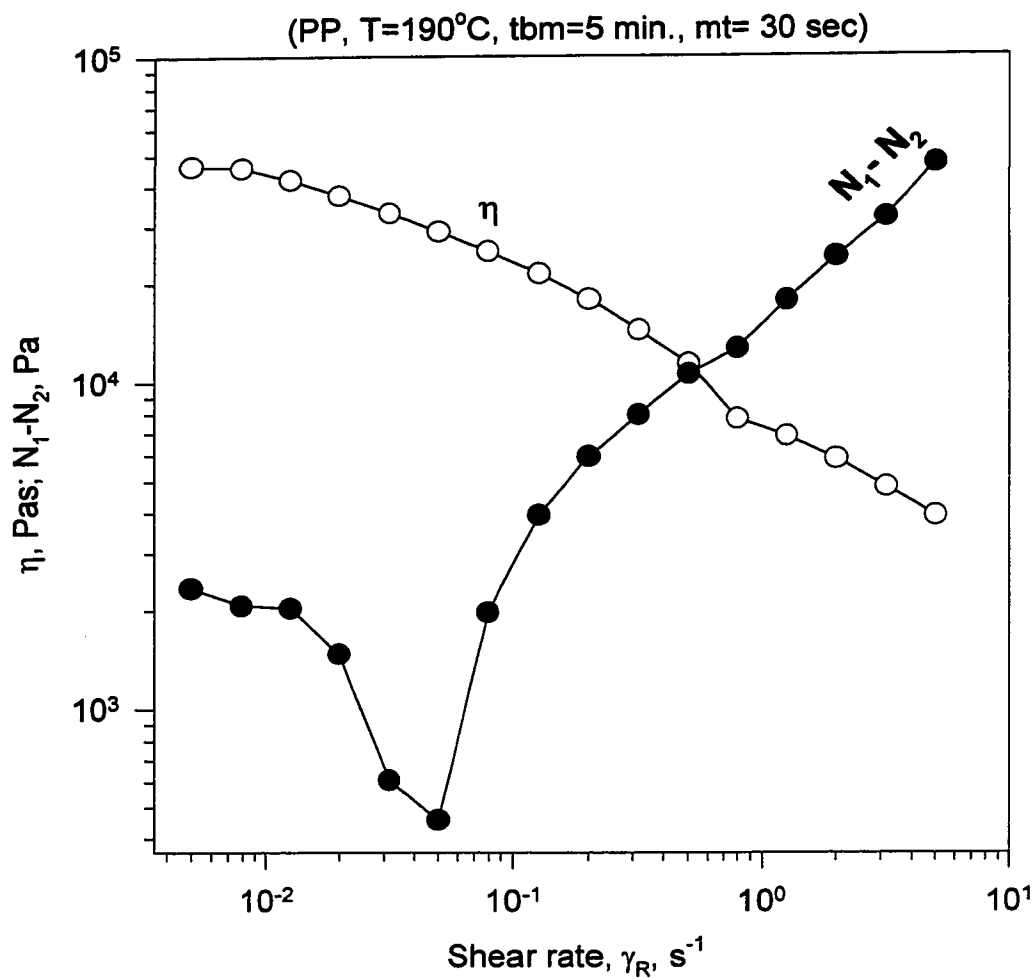
normal stress functions descending toward the sign change (i.e.,toward zero). In Figure 4.5b the peak at low $\dot\gamma_R$ has a shoulder at $\dot\gamma_R = 0.013$ s^{-1}. Moving across to higher $\dot\gamma_R$, one encounters the high-$\dot\gamma_R$ normal stress branch at $\dot\gamma_R = 0.08$ to 0.09 s^{-1}, a factor of 7 further along the $\dot\gamma_R$ axis. Similarly, in Figure 4.5a the low-G peak has a right-hand "corner" at about G=1.2, and a line extended horizontally to the right from that point intersects the descending right-hand N branch at about G=8.4, also higher by a factor of 7.

The question about the role of N_2 in parallel-plate (PP) testing has no counterpart in cone-and-plate (CP) testing, where N_2 is not involved in the interpretation of the vertical thrust. Thus, most of the subsequent tests employed the CP platens.

The nature of the unexpected minimum in N_1-N_2 discovered in the PP tests required more complete definition, so the following CP test was designed to utilize more data points per decade of $\dot\gamma$ (increasing from 5 points/decade in Figure 4.5b to 10 points /decade). Results, for the same HDPE (Q-HDPE), are given in Figure 4.5c. Again the normal stress minimum is seen, even more dramatically than in Figure 4.5b, at the same value of shear rate (i.e., 0.05 s^{-1}) despite the different meanings of $\dot\gamma$ and $\dot\gamma_R$ in the two geometries. The maximum in N_1 at low $\dot\gamma$ in Figure 4.5c was better resolved than the one in Figure 4.5b, showing a sharp right-hand corner/shoulder that clearly resembles a similar feature in Figure 4.5a. As measured from this corner, the $N_1(\dot\gamma)$ branch descending toward zero from the right was located at a $\dot\gamma$-value higher by a factor of 7, just as in Figure 4.5b. Values of the normal stress maxima in Figures 4.5b and 4.5c agree, at about 2000 Pa. Collectively, these extensive similarities between the PP and CP tests reinforce the reliability of the basic rheological observations. However, the $\eta(\dot\gamma)$ kink in Figure 4.5c has a somewhat different character than in Figure 4.5b, possibly because the

Figure 4.5c Steady shear properties of Q-HDPE

(C&P, T=190°C, tbm=5 min, mt=30sec)
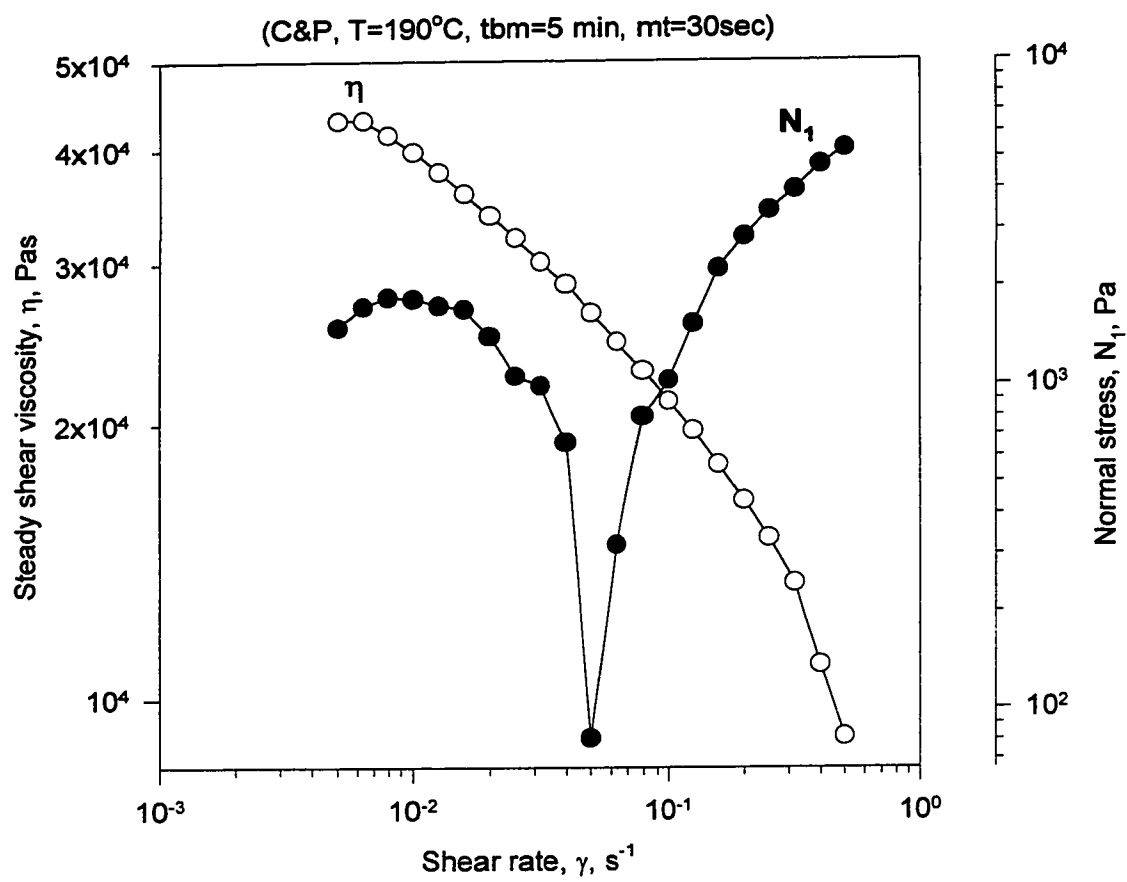
range of shear rate is less and therefore the nature of $\eta(\dot{\gamma})$ is less easy to determine. To investigate the source of this difference, we repeated the CP testing but returned to the use of only 5 data points per decade of $\dot{\gamma}$. The result, in Figure 4.5d, demonstrates both that the sign change (descent of N_1 toward zero) has almost been lost, along with the low-$\dot{\gamma}$ maximum which has now only a few points to define it. Because the data in Figure 4.5d extend to higher $\dot{\gamma}$ than in Figure 4.5c, it is possible to see that the viscosity kink is still present in the CP data, looking much as it did with PP testing.

The earlier work (Hussein and Williams, 1998a) with HDPE phase transitions at high temperatures (208°, 227°C) also showed that the rheological behavior at even higher temperatures was anomalous, suggesting that microstructural order of some sort could still be present. This work will be discussed in detail later.

Based on the supposition that HDPE could still be in a LCP molecular conformation at those high temperatures, we used the RMS to test sample UC-HDPE at 230°C. Results, given in Figure 4.6, showed both the viscosity kink and a clearly defined normal stress anomaly. This result led to testing well above the T_1 transition. Q-HDPE was tested at 240°C, with steady-shear PP data displayed in Figure 4.7. Once more, the viscosity kink and the normal stress anomaly appeared which encouraged testing at still higher temperatures. Paxon-HDPE was therefore examined in the CP at 250°C (Figure 4.8). Here, $N_1(\dot{\gamma})$ was measured, and the anomaly is just as well defined as for N_1-N_2 with Q-HDPE in Figure 4.7. A similar test at 250°C was performed on a Solvay-HDPE sample, and results (see Appendix, Figure A.6) were similar to those displayed here in Figures 4.5b to 4.8. It seems clear that LCP order prevails for a wide range of

Figure 4.5d Steady shear measurements for Q-HDPE

(C&P, T=190°C, tbm=5 min, mt=30 sec)
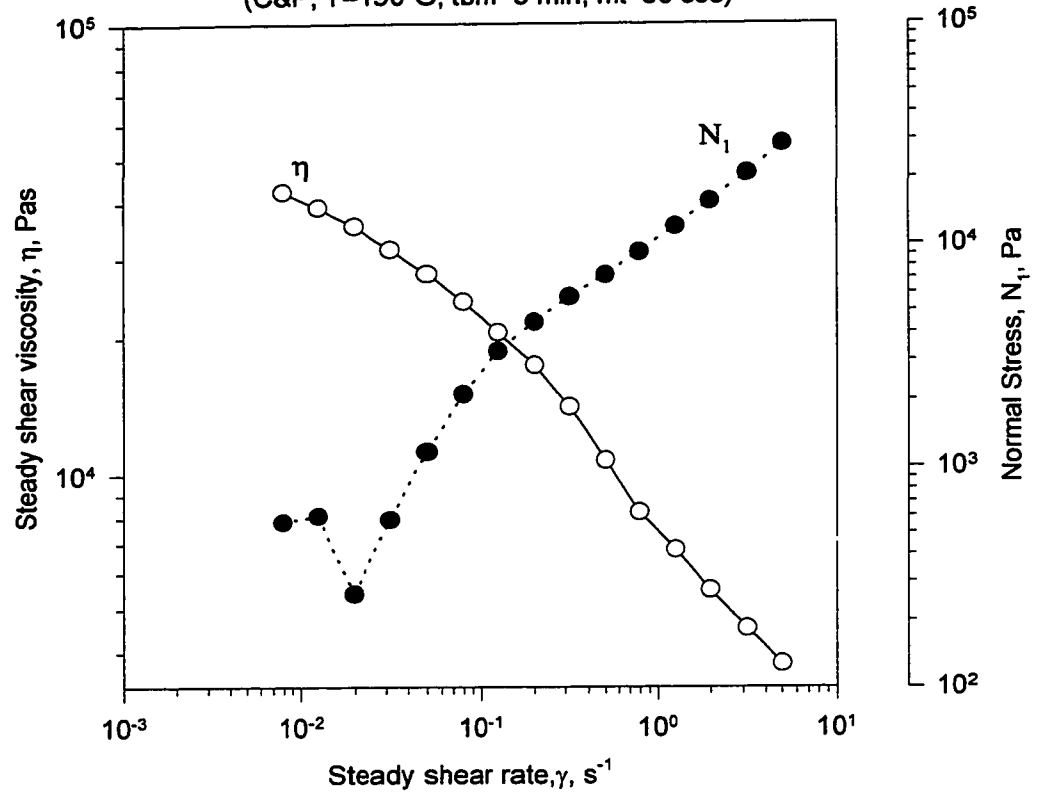
Figure 4.6 Normal stress and viscosity functions for UC-HDPE
(PP, T=230°C, tbm=5min., mt=30 s)
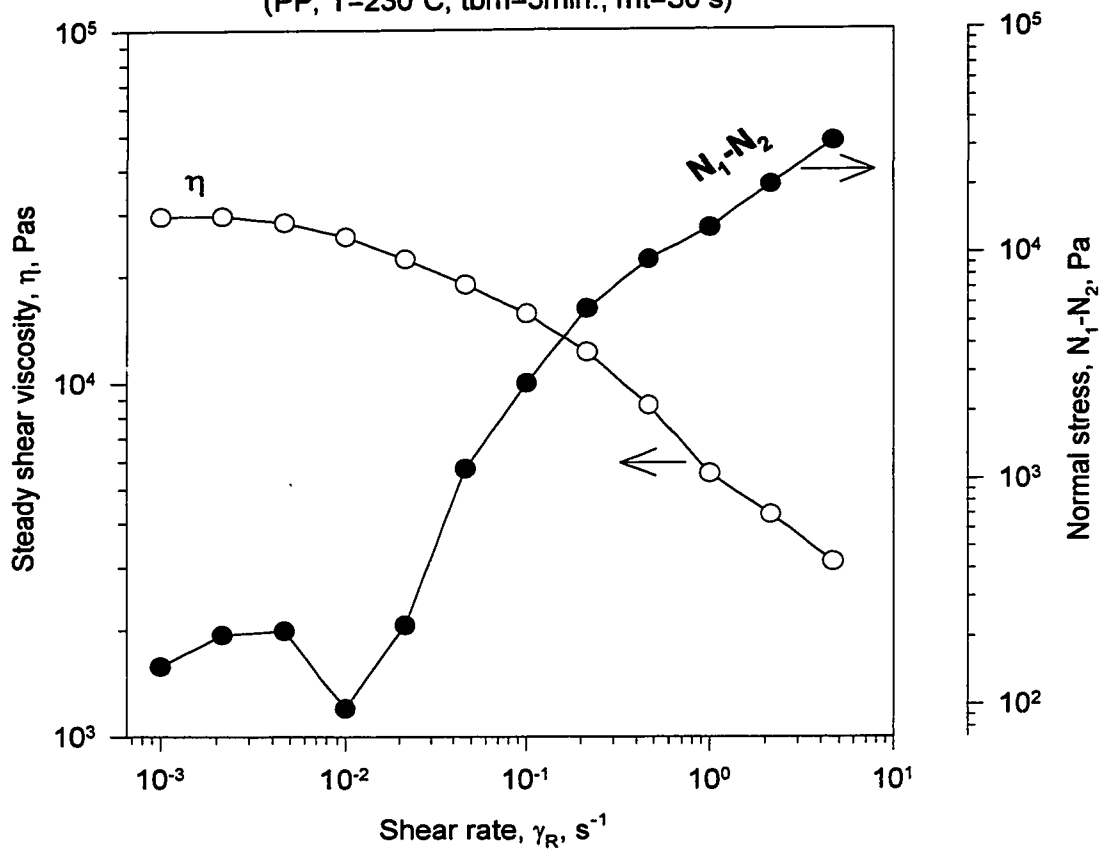
Figure 4.7 Steady shear properties for Q-HDPE

(PP, T=240°C, tbm=5 min, mt=30 sec)
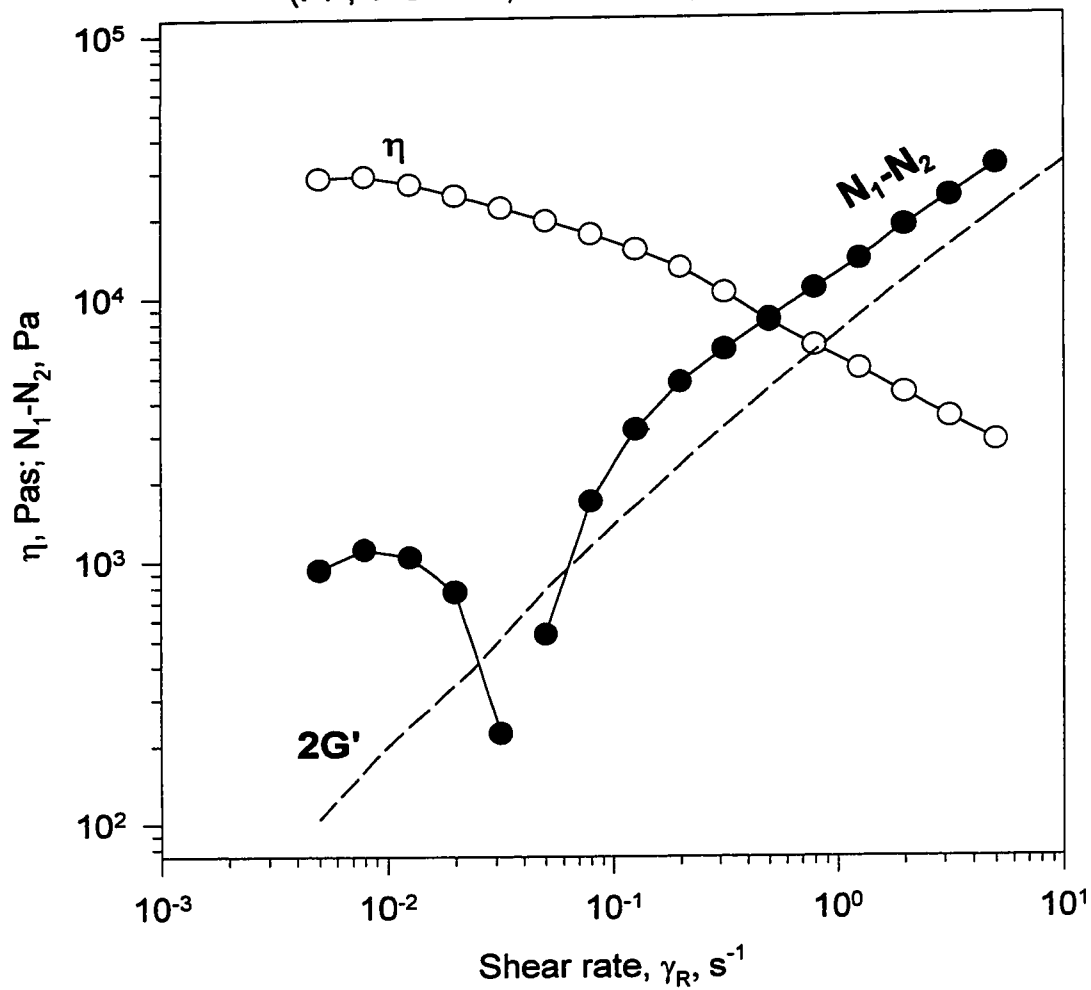
Figure 4.8 Steady shear properties for Paxon-HDPE

(C&P, T=250°C, tbm=2min, mt=30 sec)

Steady shear rate, γ, s^{-1}
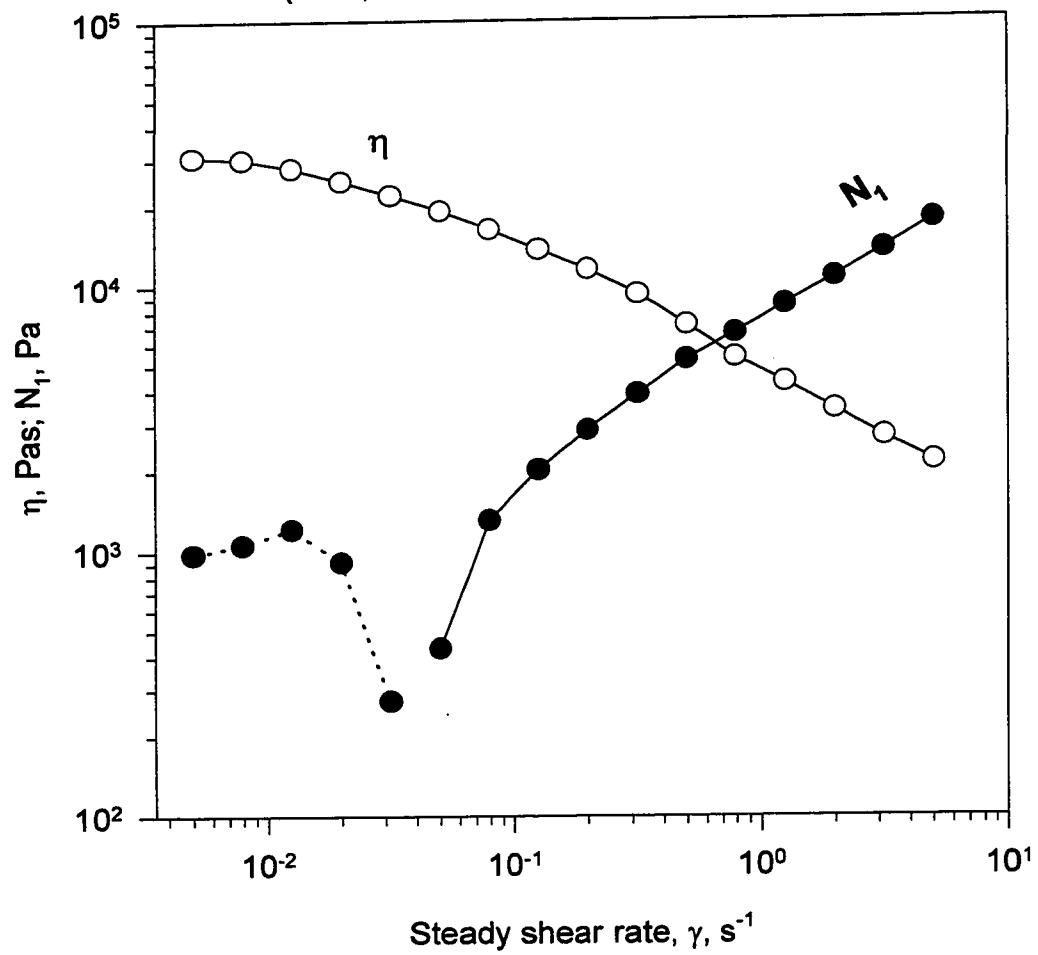
temperatures above the 208°C transition, implying that the latter is not a transition to the isotropic state. It is important to recognize that the normal stress minima displayed in all these figures are well defined and reproducible. The minimum points correspond to transducer force values well above the noise level; transducer sensitivity is about 2 g weight, whereas all the normal stress minima were represented by points in the range 2-20 g weight.

These observations were also not a consequence of wall slip, which sometimes accompanies the shear flow of PE melts. Slip is reported to begin at a wall shear stress of about 0.1-0.3 MPa (Dealy and Wissbrun, 1990; Wang and Drda, 1997), for HDPE melts far above the maximum stresses achieved here (on the order of 0.02 MPa) and enormously beyond the stress minima and viscosity kink anomalies. Furthermore, the results being observed here are not changed by variation of the parallel-plate spacing (h); h-dependence is often taken as evidence of slip (Macosko, 1994). Additionally, the fact that CP and PP results are virtually identical (see Appendix, Figure A.7) is strong support for the contention that the results are true rheological phenomena and not dominated by secondary flows and other hydrodynamic stability problems that tend to be specific for one kind of platen geometry.

There is also ample evidence that the RMS was performing well. In addition to frequent calibration by a Rheometrics service engineer, the instrument detected no anomalies when used to test familiar amorphous melts; this is demonstrated in Figure 4.9 for polystyrene at 190°C, using parallel plates. No spurious indication of a normal stress minimum (or approach to zero) is observed in the $\dot{\gamma}_R$-range (10^{-2} to 10^{-1} s^{-1}) wherein such an indication appeared with HDPE, or at any other $\dot{\gamma}_R$, and the RMS is clearly shown to

Figure 4.9 Comparison of steady and dynamic shear properties of polystyrene

(PP, T=190°C, $\gamma°$=10%, tbm=2 min, mt=30 sec)

- ○ η (steady shear)
- □ η' (dynamic)
- ● η* (dynamic)
- △ N_1-N_2 (steady shear)
- ▲ 2G' (dynamic)

y-axis: η, η*, Pas; G'; N_1-N_2, Pa

x-axis: Shear rate, γ_R; frequency, ω, s^{-1}
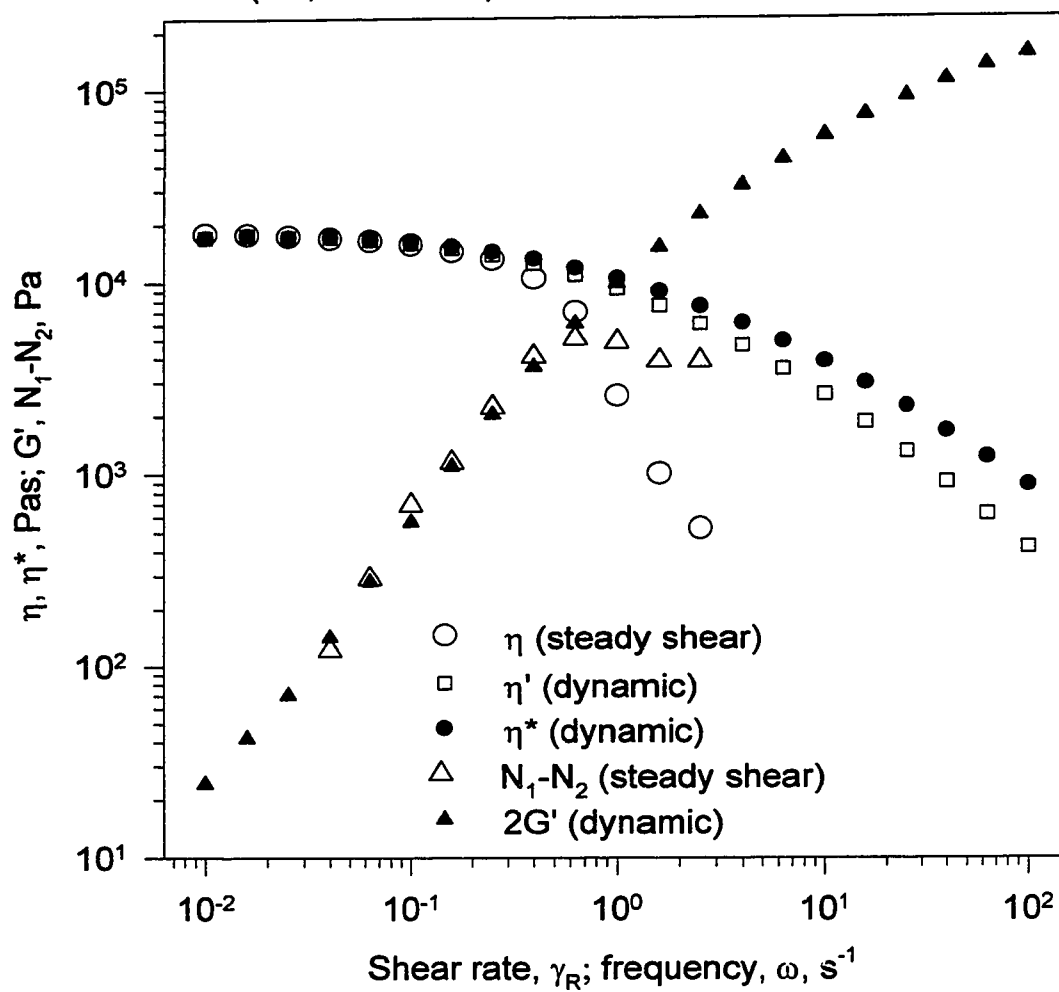
be capable of responding accurately to fluid normal stress down to about $N_1-N_2=130$ Pa (and the HDPE minima are defined by collections of data points well above this). Furthermore, the polystyrene dynamic properties in Figure 4.9 confirm that the low-$\dot{\gamma}_R$ nonlinear properties are being sensed properly: Values of $\eta(\dot{\gamma}_R)$ and $\eta^*(\omega)$ superimpose well (conforming to the Cox-Merz relation) until strong non-Newtonian behavior begins, and – more importantly here – the normal stress function is well matched by $2G'(\omega)$ up to the same $\dot{\gamma}_R$. Equally important is the fact that $2G'(\omega)$ matches $N(\dot{\gamma}_R)$ (Wissbrun et al., 1987) down to the lowest ω and $\dot{\gamma}_R$ at which the two can be measured. Such results verify both that the polystyrene melt was behaving as a classical unstructured viscoelastic fluid, rheologically simple, and also that the RMS was functioning properly. (The transition in normal stress, with a maximum at about $\dot{\gamma}_R = 0.8$ s^{-1}, corresponded to the hydrodynamic stability limit, observed visually, and means that both η and N_1-N_2 plotted for higher $\dot{\gamma}_R$ are artifactual.)

(ii) *Stress Transients in Steady Shear*

It remains to be demonstrated that the sequence of data acquisition used here produced steady-state stress information. First, we address the low-$\dot{\gamma}$ range, which was most relevant to the major goals of this work. My general observation was that when $\dot{\gamma}<0.1$ s^{-1} the normal stress transient $N(t)$ was a well behaved function of time, either monotonically increasing or demonstrating a gradual overshoot, and achieved its steady state within 5 minutes. Examples are given in Figure 4.10a, for Q-HDPE at 190°C. When $\dot{\gamma}\geq1$ s^{-1}, there was generally a sharp initial overshoot with a non-smooth decay to steady state. Examples of shear stress and normal stress starting from rest to $\dot{\gamma}=1$ s^{-1} are given in

Figure 4.10a Transient normal force
for Q-HDPE

(PP, gap=1.5 mm, T=190°C)

γ_R=0.1 s^{-1}

γ_R=0.05 s^{-1}

N$^+$(t), Pa

Time, s
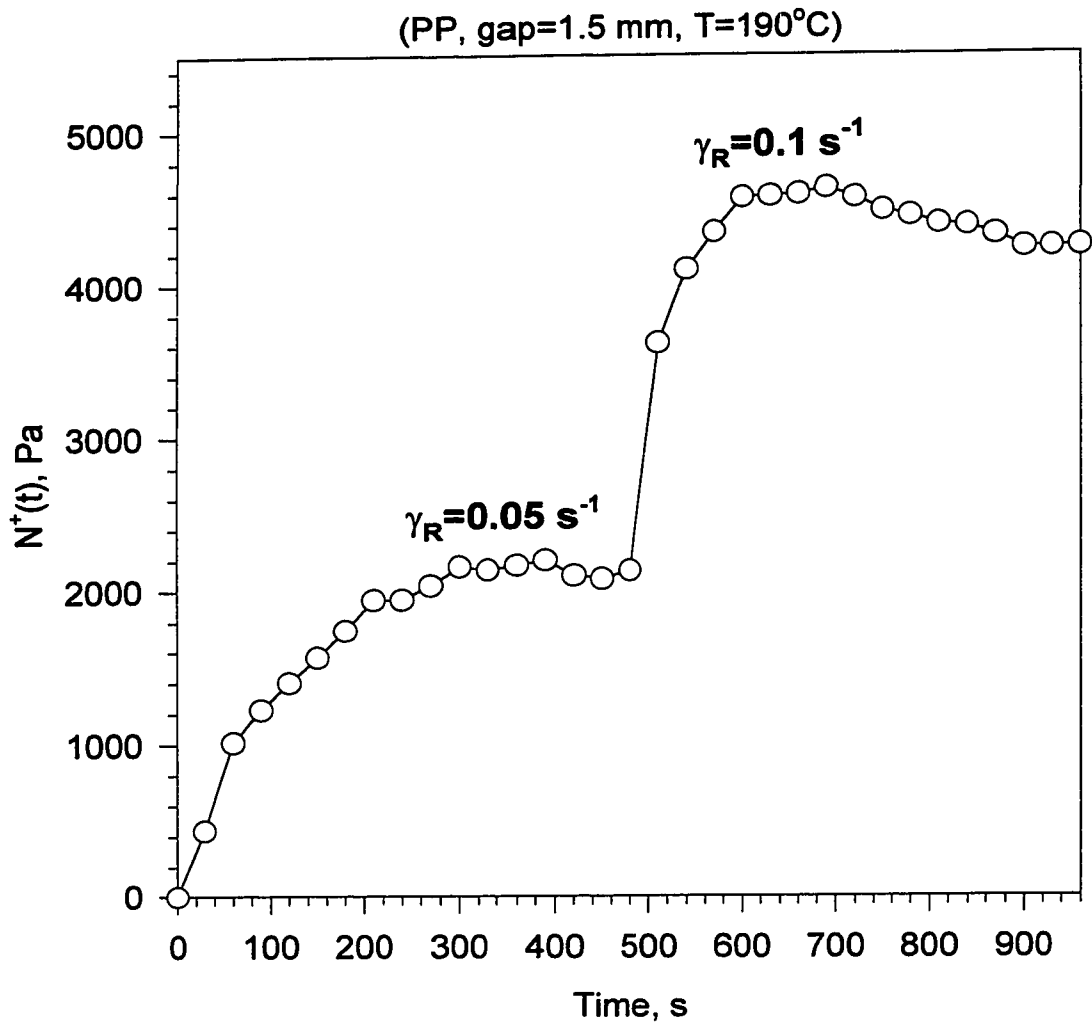
Figures 4.10b and 4.10c. The shear stress reached its plateau value after 5 min. (although long-term oscillations were seen), but the normal stress required 20-25 min. and the 5-minute point was essentially a stress decay half-life. Recording the normal stress at 5 min. would essentially over-represent its steady state magnitude by 25%. Errors of this sort are diminished when the higher $\dot{\gamma}$ are achieved by the sequential-step sweep program, which is illustrated in Figure 4.10d for the normal stress. Here, $\dot{\gamma}$ begins from rest with a step into the low-$\dot{\gamma}$ regime ($\dot{\gamma}=0.1$ s^{-1}) which leads monotonically to its steady state after 5 minutes. Then, when $\dot{\gamma}$ is stepped up into the high-$\dot{\gamma}$ regime ($\dot{\gamma}=1$ s^{-1}), a sharp peak results but it is less high than it would be if starting from rest with a jump to $\dot{\gamma}=1$ s^{-1}. The result is that steady state is achieved in less than 5 min. longer. This type of behavior justifies the method used here to achieve steady-state data over the whole range of $\dot{\gamma}$. (The reason that the two normal stress steady states at $\dot{\gamma}=1$ s^{-1}, in Figures 4.10c and 4.10d do not seem to agree is that they represent PP and CP normal stress functions, respectively). Stress transients of this character have been reported for LCP melts (Wissbrun and Griffin, 1982; Viola and Baird, 1986, Cogswell and Wissbrun, 1996).

One of the rheological phenomena displayed by LCPs is that the normal stress function (N_1) changes sign at low shear rates in steady or transient testing. In addition, stress and NF overshoot at start-up associated with the orientation of the domains, and short stress relaxation times (upon cessation of shear) were reported for LCPs (Baird, 1985; Viola and Baird, 1986; Baird et al. 1985; Wissbrun, 1980). In Figure 4.10e shear stress growth and relaxation, experiments on Q-HDPE are displayed for different temperatures below and above the transition (208°C). These showed similar sharp overshoot at start-up and similar rapid relaxations upon cessation of shear. The

Figure 4.10b Transient viscosity for Q-HDPE

(PP, gap=1.5 mm, T=190°C)

γ_R=1 s^{-1}
T=190°C
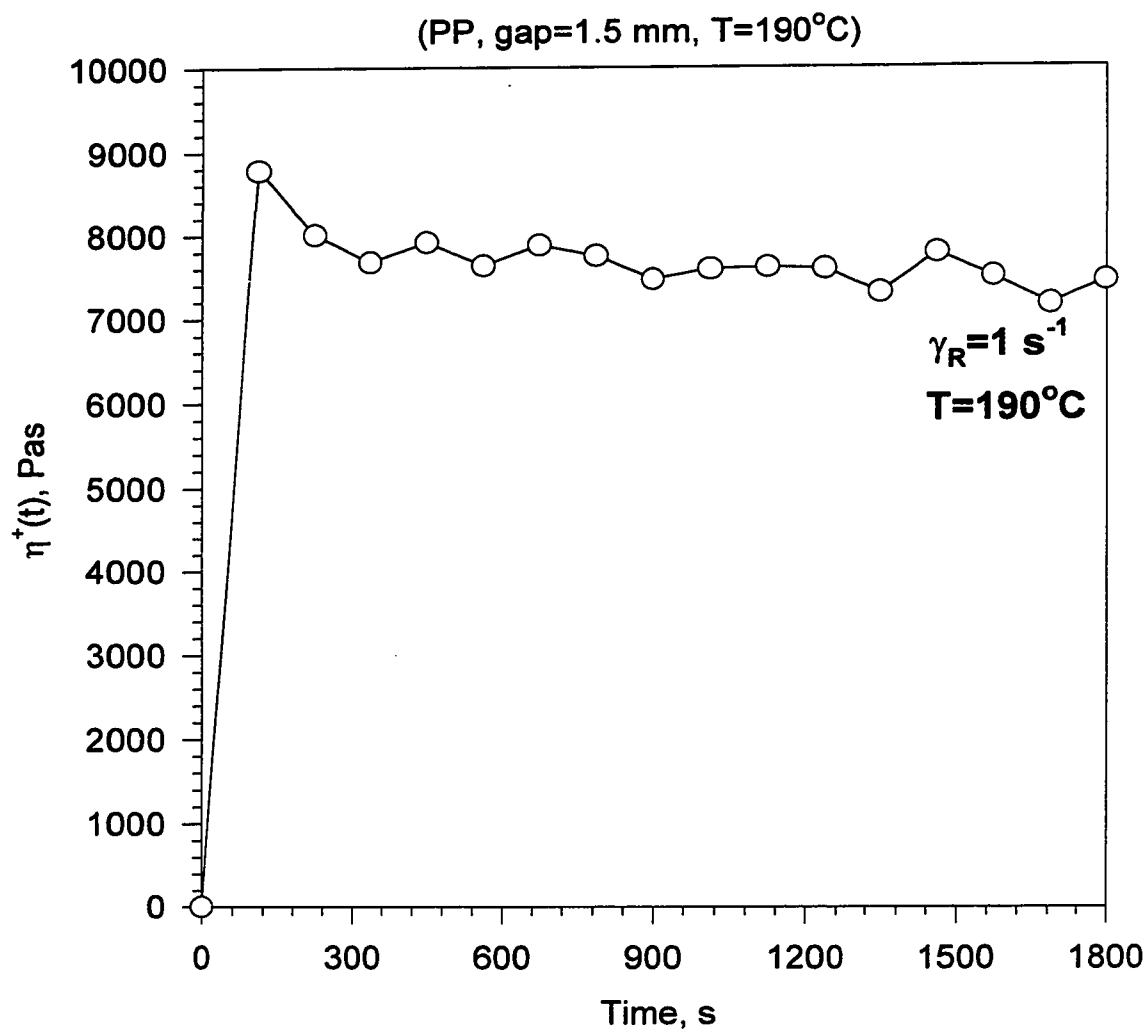
Figure 4.10c Transient normal stress for Q-HDPE

(PP, gap=1.5 mm, T=190°C)

γ_R=1 s^{-1}
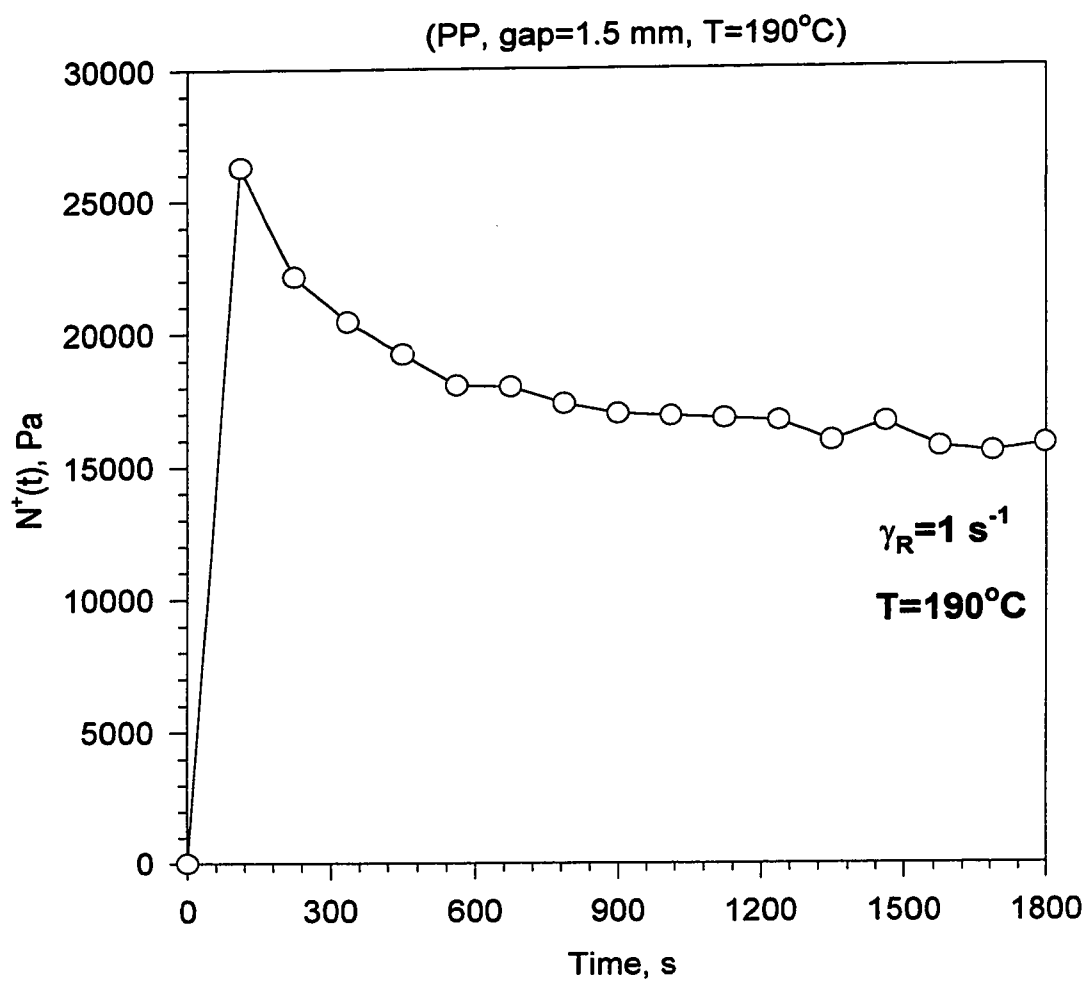
T=190°C

Figure 4.10d Transient normal stress for Q-HDPE

(C&P, cone angle=0.1 rad, T=190°C)
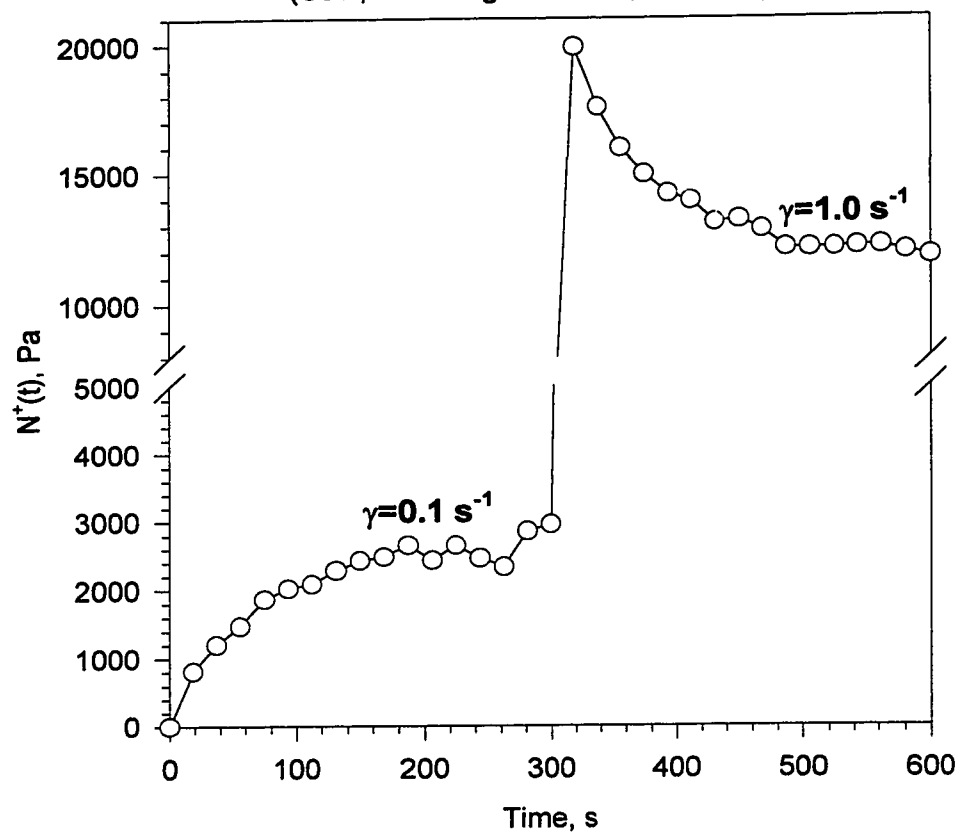
Figure 4.10e Shear stress growth and relaxation for Q-HDPE at different temperatures
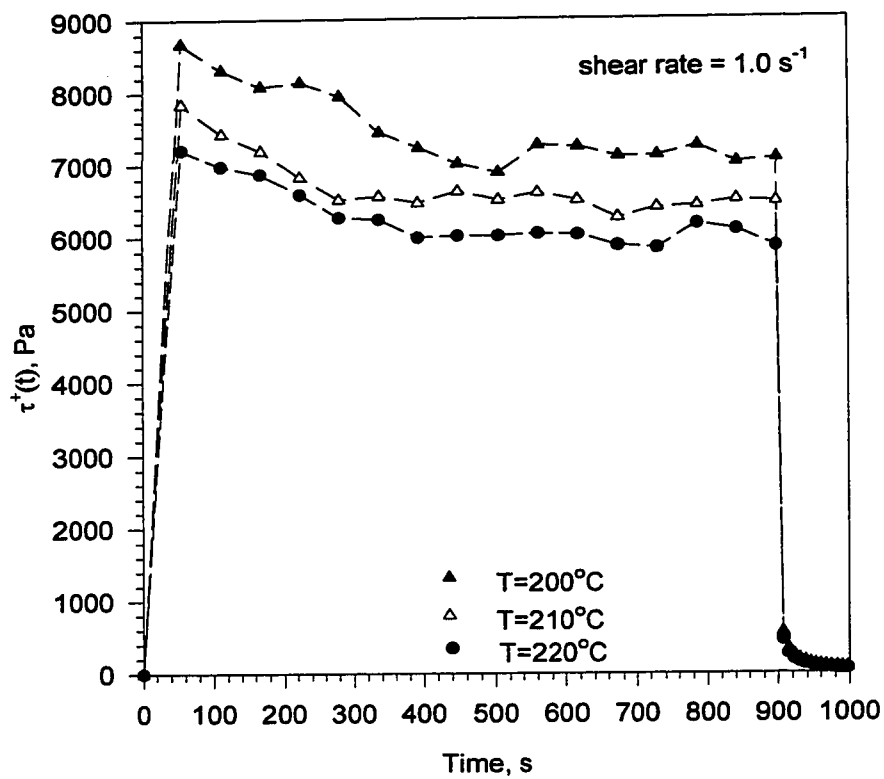
simultaneous normal stress transients were given in Figure 4.10f. Values of normal stress overshoots were about twice the steady state value as represented by the levels achieved at t = 900 s, when shear stopped.

For liquid crystallites formed by flexible chains, the stress overshoot phenomenon occurs at values of $\dot{\gamma}$ comparable to the reciprocal of the longest relaxation time (λ_1). The value of λ_1 is usually obtained from the corresponding $\dot{\gamma}_1$ that marks the onset of shear thinning in the steady-shear non-Newtonian viscosity curve $(\lambda_1=1/\dot{\gamma}_1)$. The steady-shear results at 190°C, shown in Figure 4.5b, suggest that the onset of shear thinning occurs at shear rates lower than 0.01 s^{-1}, which implies an overshoot time of more than 100 seconds. The observed shear stress and NF relaxation occurs in a shorter time, but not instantaneous. According to Viola and Baird (1986), this form of relaxation suggests a yield stress behavior.

Steady shear viscosity and NF measured at 190°C (Figures 4.5b & 4.5c) showed shear thinning even at low shear rates (0.01-0.1 s^{-1}). The strange drop in the NF in the $\dot{\gamma}$ range 0.01-0.05 s^{-1} led to further investigation of the transient behavior in this range. The results of transient NFs at four different shear rates in the range of 0.005-0.1 s^{-1} are shown in Figure 4.10g. Surprisingly, negative NFs as large as 800 Pa (~10 g), well above the sensitivity limit of the RMS (2 g), were measured for Q-HDPE at low shear rates (0.005 & 0.01s^{-1}). Negative NF was observed in another experiment with shear rates covering three decades of $\dot{\gamma}_R$, as shown in Figure 4.10h. The low-shear-rate data were observed to be more sensitive to large step sizes in shear and produced more fluctuations, unlike data collected at small step sizes where shorter step changes (i.e. more data points) led to shorter transients. At shear rates higher than 0.1 s^{-1} no fluctuations were observed

Figure 4.10f Transient normal stress for Q-HDPE
at different temperatures
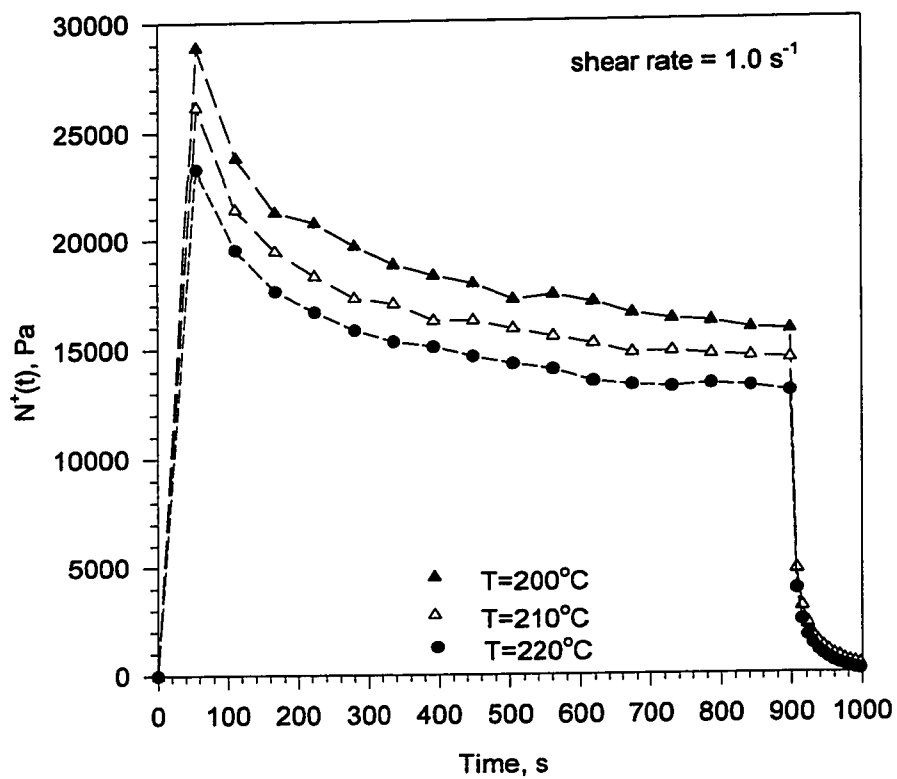
Figure 4.10g Transient normal stress for Q-HDPE at 190°C
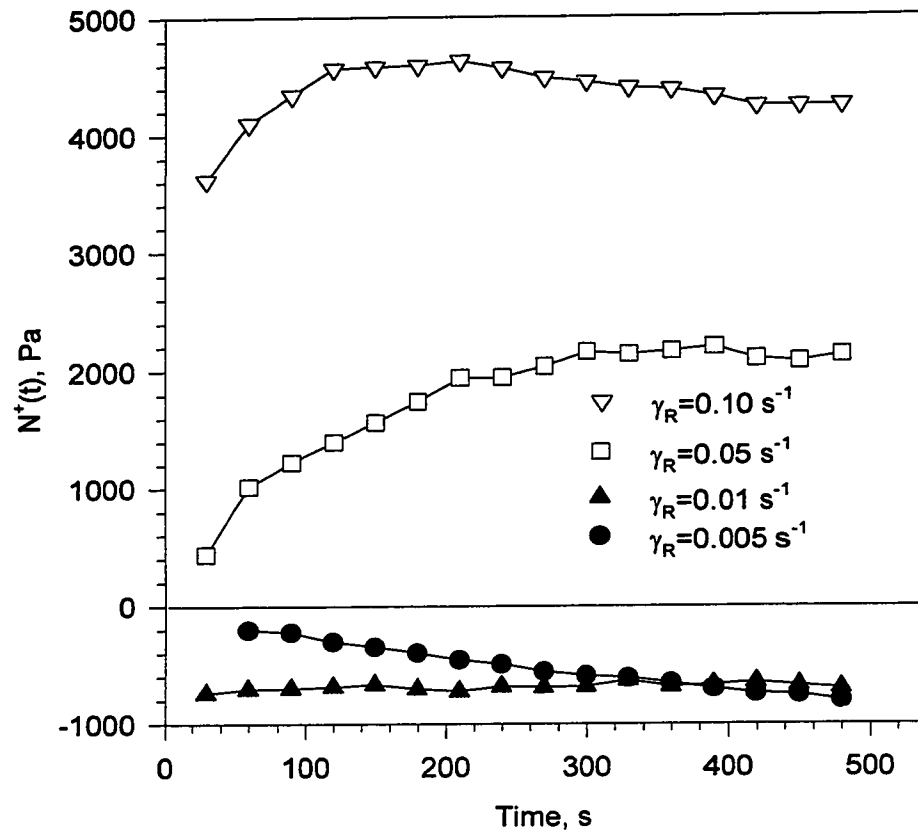
Figure 4.10h Transient PP normal stress for Q-HDPE at 190°C
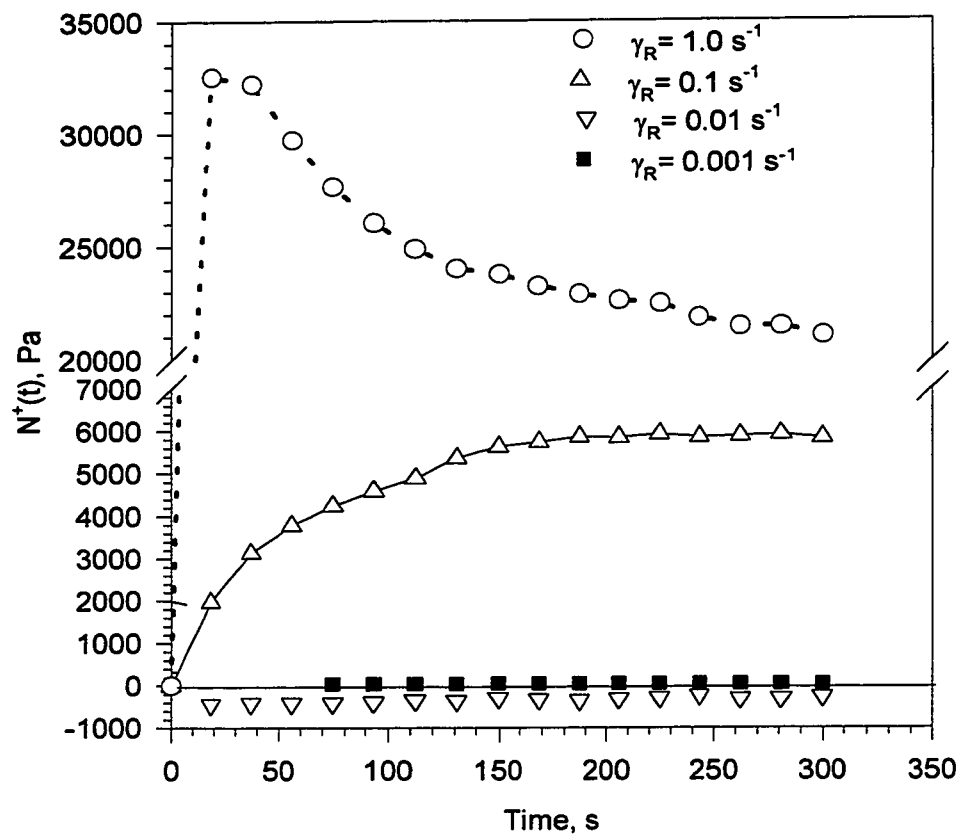
regardless of the step size. This suggests that past the low-shear regime, a stable orientation of the director in the direction of flow has been achieved.

Negative NF is usually observed in LCPs at low shear rates (0.01-0.05 s^{-1}) where piled and dispersed-polydomains prevail (Onogi and Asada, 1980). At high shear, the polydomains are reduced to a monodomain continuous phase, and the behavior of LCPs is similar to isotropic polymers, where orientation in the direction of the flow takes place. Figures 4.10g & 4.10h showed that for $\dot{\gamma} \leq 0.1$ s^{-1} the normal stress transient was a well-behaved function monotonically increasing with time, while $\dot{\gamma}=1$ s^{-1} demonstrated a sudden but smooth overshoot. Furthermore, the 5 minutes "tbm" was found sufficient for the normal force to achieve steady state in the range of shear studied.

The negative normal stress observed in the transient PP measurements of Q-HDPE motivated testing of other HDPEs. This time we used Solvay-HDPE in a different flow field, the cone-and-plate. Four levels of shear rates representing the four decades of shear covered in this study, were selected. The test proceeded from low to high shear rates to explore the polydomain morphology before its destruction at high shear rates. The transient results (given in Figure 4.10i) showed that the normal stress was negative at low $\dot{\gamma}$ (0.001 and 0.01 s^{-1}), and positive at high $\dot{\gamma}$ (0.1 and 1.0 s^{-1}). The CP data at $\dot{\gamma}=0.001$ s^{-1} showed a sharp positive overshoot (~600Pa) before dropping to negative values (~ -1000 Pa). The normal stress continued to be negative at $\dot{\gamma}=0.01$ s^{-1} and reached steady values (~ −2000 Pa). It worth noting that the negative normal stress is usually observed at shear rates that fall below the normal stress anomaly (observed in steady shear measurements), while positive normal stress correspond to the range above it.

Figure 4.10i Transient normal stress for Solvay-HDPE

(CP, T=190°C)

$\gamma=1.0$ s^{-1}

$\gamma=0.1$ s^{-1}

$\gamma=0.01$ s^{-1}

$\gamma=0.001$ s^{-1}

N$^+$(t), Pa

Time, s
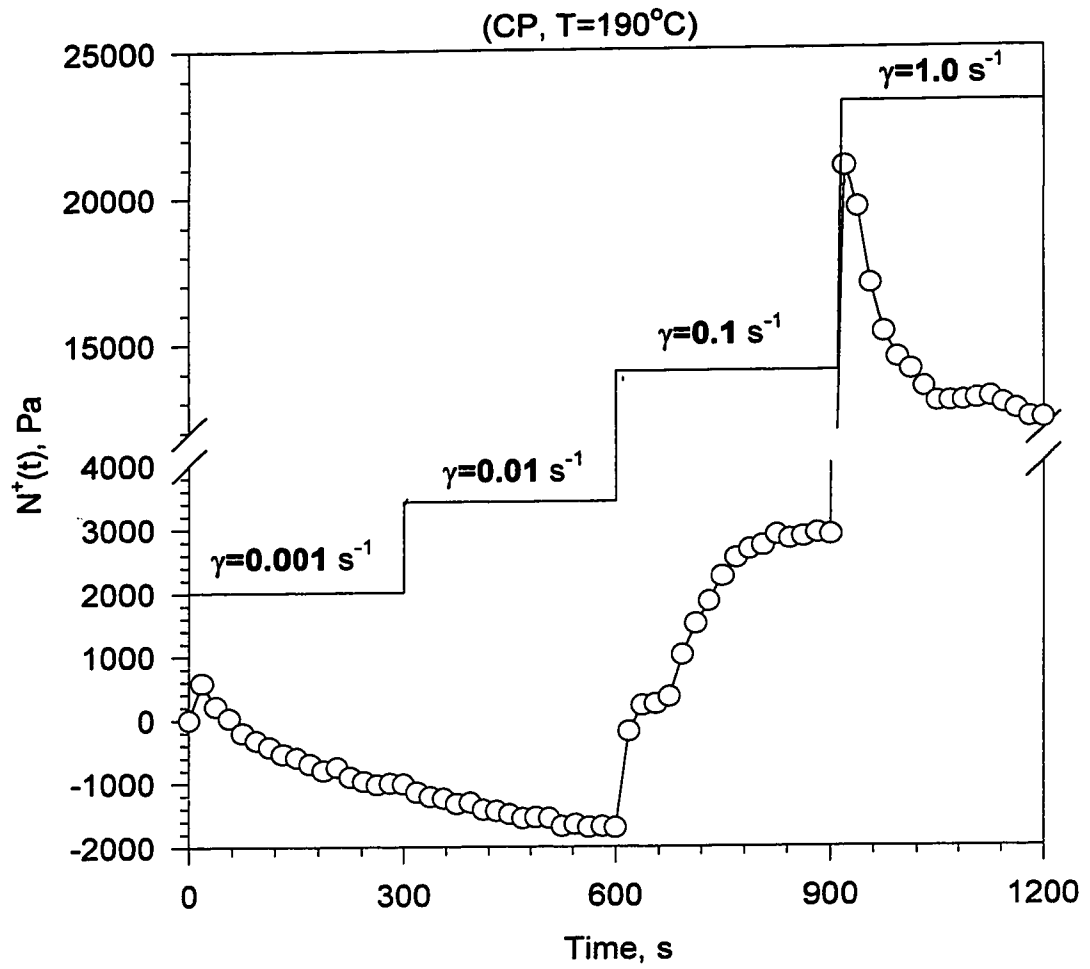
Similar behavior was detected in CP geometry for Paxon-HDPE (see Appendix, Figure A.8). The same test was then repeated under the same conditions for Dow-PS. The transient normal stress was found positive in the whole shear range (low or high) indicating typical amorphous behavior (see Appendix, Figure A.9) and confirming the confidence in the RMS operation.

We don't have a definite answer why negative NFs were observed in the steady-$\dot{\gamma}$ transient stress testing (Figures 4.10g, h, i and A.8) while the steady auto sweep test (Figures 4.5b & 4.5c) used for steady-$\dot{\gamma}$ steady stress tests showed a drop in the NF in the same range but still remained positive. (Marrucci and Maffettone (1990) had theoretically predicted totally unrealistic transient response at low $\dot{\gamma}$ when they extended the simplifying assumption of negligible interdomain interactions to the transient calculations).

(iii) What is the possibility of alternative explanations?

In seeking alternative explanations for the rheological anomalies presented here, one is drawn to the possibility that fluid mechanical instabilities and secondary flows of well-known kinds or inertia may be responsible for either the normal stress or viscosity-kink anomaly, or both. We believe this is not the case.

Part of my belief is because these results reflect so closely the acknowledged behavior of LCP fluids, both data and theory. Moreover, these HDPE results are totally unlike the behavior of other melts (e.g., polystyrene) and solutions tested in Williams' laboratories over a 30-year period of rheological investigation.

In the cone-and-plate, inertia forces tend to pull the plates together rather than push them apart. This "negative" normal force can be expressed in terms of stress distribution (Walters, 1975) as: $(\tau_{\theta\theta})_{inert} = 0.15 \, \rho \, \Omega^2 \, (r^2\text{-}R^2)$ or $N_1 = 2 \, F_Z/\pi R^2 - 0.15 \, \rho \, \Omega^2 \, R^2$. Several studies indicated that this correction is valid for Newtonian and non-Newtonian fluids (Macosco, 1994). The drop in the normal force was observed around a shear rate of $0.05 \, s^{-1}$. The calculation of the correction for N_1 for HDPE at 190°C gives:

$$(N_1)_{correc} = 0.15 \, \rho_{190} \, \Omega^2 \, R^2 = 0.15 \, (760 \, kg/m^3) \, (0.05 \, S^{-1})^2 \, (0.0125 \, m)^2 = +4.45 \times 10^{-5} \, Pa$$

which is insignificant in comparison with the N_1 values reported here. Furthermore, inertia effects were automatically subtracted by RMS software from NF measurements. Inertia also generates secondary flows in the rθ plane. Secondary flow will increase the torque from M_o to M where: $M/M_o = 1 + 6.1 \times 10^{-4} \, Re^2$, $Re = \rho \, \Omega \beta^2 \, R^2/\eta_o$ (Macosko, 1994). The calculation of Re number gives:

$$Re = \rho \, \Omega \beta^2 \, R^2/\eta_o = (760 \, kg/m^3) \, (0.05 \, S^{-1}) \, (0.1)^2 \, (0.0125 \, m)^2/ \, (4 \times 10^4 \, PaS) = 1.48 \times 10^{-9}$$

indicating that the possibility of altered torque due to secondary flows because of inertia is quite remote. We have also examined the literature on flow instabilities in these shearing geometries (Macosko, 1994; Macosko and Morse, 1976) and found no evidence for instabilities that could give the results reported here. Furthermore, flow instability in simple shear at low Re number has never been established (Denn, 1987). We recognize that secondary flows can exist with viscoelastic liquids at shear rates well below that at which sample ejection occurs. One such instability, for example, is known as an "edge effect" and manifested externally at the platen rim by the fluid appearing to cut in at the mid-plane and flow out along each of the platen surfaces (Macosko, 1994; Macosko and Morse, 1976). When it occurs, this phenomenon can be seen visually within 15 seconds

after shearing is initiated (when $\dot{\gamma}$ is in the range 5-10 s^{-1}). The consequences on measured torque and normal thrust are the onset of a slow drift downward, so that the transient appears not to be approaching a steady-state limit. Furthermore, Shipman et al. (1991) reported that rheological measurements (torque and normal force) in torsional PP rheometry were insensitive to free-surface distortions of polymer melts. In my tests, however, none of these indicators (drift, etc.) appeared. Moreover, the $\dot{\gamma}$-range in which the normal stress anomaly occurred (around 0.05 s^{-1}) is two orders of magnitude lower than that at which the edge effect is commonly reported (Macosko, 1994).

We have also explored the possibility of thermal heating (electrical sources vs thermal sources) of the force rebalance transducer and consequent expansion of the system (Niemiec et al., 1996). A weight of 20 g was hung on the upper platen and the steady shear and transient NF measurements were repeated under the same testing conditions. Neither the steady-shear anomalous NF behavior, nor the negative transient NF was detected, but rather stable measurements.

Another intriguing question about these anomalies is why have they not been reported before? One might expect that such a common polymer, as HDPE would have received abundant rheological attention over the years. Indeed, the literature contains many examples (Mendelson, 1965; Mendelson et al., 1970) of such work, including superposition of $\eta(\dot{\gamma})$ data from many instruments to cover wide range of $\dot{\gamma}$. We suspect that the viscosity kink may have been overlooked because it is a rather subtle effect, and because the procedures we followed (similar to those of LCP investigators) have not been common. For example, in rotational viscometry, it has been standard procedure to average consecutive CW and CCW torque measurements. However, for a structured fluid

like HDPE melts, this sequence of shearing alters the structure in a major way (perhaps destroying it), as my early tests showed. The stress transients are surprisingly long, so most workers would not let either a CW or subsequent CCW test run long enough to achieve steady state. In this case, unidirectional shearing for at least 5 minutes for each sample was used. We cannot project how the kink phenomenon would affect measurements in capillary viscometry, but possibly structural damage near the wall would obscure the effect, and residence times within the capillary might not be long enough to achieve steady state.

We note that the more dramatic anomaly is in the normal stress, at very low $\dot{\gamma}$, but most HDPE melt work in the past has not included N_1 measurements, being focussed instead on $\eta(\dot{\gamma})$. There has also been little incentive to examine the very low-$\dot{\gamma}$ regime. Moreover, the academic community has preferred to bypass polyethylene for studies of fundamental fluid rheology; the favorite materials were solutions and melts of polymers that had molecular weight distributions which could be easily measured and were, ideally, monodisperse. Neither of these attributes describes HDPE. Thus, academic laboratories have used HDPE (and other polyethylenes) primarily for melt processing studies, and their industrial counterparts had relatively little interest in N_1 (or in very low $\dot{\gamma}$). (However, the negative N_1 could account for "anomalous" data or extrudate swelling that have recently been reported on LCPs. The swelling is normally explained as a positive N_1 effect, the reported (Wissbrun, 1994) extrudate contraction is either a surface tension effect [not seen with other polymers] or due to negative N_1). If the latter is true, then extrusion processing in PE may have to be re-evaluated.

In Williams' laboratory, abundant evidence of many types supports the LCP nature of HDPE. For example, the RMS temperature sweeps discussed earlier and the blender torque curves, melt index, and DSC evidences to be discussed later.

3. Comparison of steady and dynamic shear results

Steady-shear tests of the HDPE melts were normally accompanied by oscillatory-shear dynamic tests (on fresh samples) as well, analogous to that shown for polystyrene in Figure 4.9. The Q-HDPE was selected for this study. The first test carried out in this comparison is to see if there is any dependency on the direction (ascending or descending) or duration during dynamic measurement. The complex viscosity, η^*, and elastic modulus, G', were obtained at $190°$ and $240°C$. The measurements carried out in an ascending order of ω (0.01 to 100 rad/s) were compared to those taken in descending order (100-0.01 rad/s). Perfect match between the measurement in both directions for both temperatures was observed (see Appendix, Figure A.10). Furthermore, a time sweep test was performed at $190°C$. The low strain (6%) and frequency (0.1 rad/s) were used. The elastic modulus (G') and tan δ were measured over a period of 30 minutes (Appendix, Figure A.11). The variations are within 5-6% and hence we conclude that there is no direction or time dependency for the dynamic testing.

Moreover, the observation that LCP order prevails for a wide range of temperatures above the $230°C$ transition, motivated a study of the dynamic and steady shear rheology above and below the reported transitions (Hussein and Williams, 1998a). In particular, $\eta(\dot{\gamma})$ and $\eta^*(\omega)$ were compared and normal stress and $2G'$ were compared at two temperatures, one below the transition ($190°C$) and one above the transition

(240°C). In addition, normal stress, and $2G'$ obtained at the same temperature were compared with predictions based on the viscoelastic theory of isotropic melts.

A representative set of such data obtained in the parallel-plate geometry is given in Figure 4.11a, for Q-HDPE at 240°C. Measurements performed at 190°C are given in Figure 4.11b for the same resin. Here, η and $\eta^* = [(\eta')^2 + (\eta'')^2]^{1/2}$ are displayed together; $2G'(\omega)$ rather than $\eta''(\omega)$ is given to facilitate comparison with the $\dot{\gamma}$-dependent function N_1-N_2 in Figures 4.11a & b. These dynamic data for Q-HDPE are just as unexceptional as those for polystyrene, in Figure 4.9. The function $\eta^*(\omega)$ has no kink at any ω, and at low ω it appears to superimpose with $\eta(\dot{\gamma})$ at low $\dot{\gamma}$ (Figures 4.11a &b). The function N_1-N_2, however, does not come close to superposition with $2G'(\omega)$, as it does for PS in Figure 4.9. This is emphasized in Figures 4.11a & b by the dotted line showing N_1-N_2. Only at high $\dot{\gamma}$ (high ω) is their behavior similar, with the two functions running parallel with N_1-N_2 higher than $2G'$ for both temperatures. For low ω, $2G'(\omega)$ fails totally to mimic the normal stress function, so should never be used as a means of predicting the latter. Similar results have emerged from a previous study of other LCP melts (Wissbrun and Griffin, 1982).

The absence of a kink in the dynamic viscosity functions and the absence of a sharp minimum in $G'(\omega)$ are reasonable and expected. In steady shear, those phenomena arise because at that $\dot{\gamma}$, the liquid-crystal domains change their motion from tumbling to one of steady oriented flow, according to the theoretical models (Marrucci and Maffettone, 1989, 1990 & 1991; Larson, 1990), and there is no mechanism in small-amplitude strain for such a transition to occur.

Figure 4.11a Dynamic and steady shear properties for Q-HDPE

(PP, gap=1.5 mm, T=240°C, $\gamma°$=10%)

η (steady shear viscosity)

η^* (complex viscosity)

2G' (2 x elastic modulus)
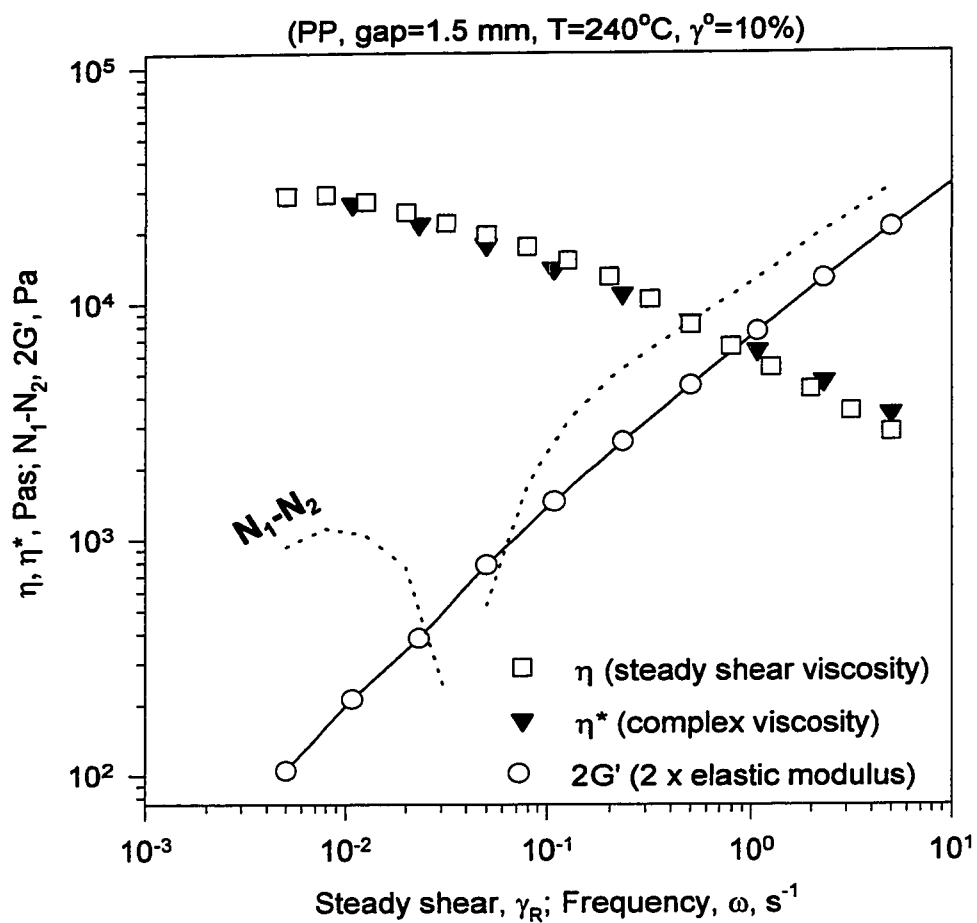
Figure 4.11b Dynamic and steady shear properties for Q-HDPE

(PP, gap=1.5 mm, T=190°C, γ°=10%)

N_1-N_2

□ η (steady shear viscosity)

▼ η* (complex viscosity)

○ 2G' (2 x elastic modulus)

η, η*, Pas; N_1-N_2, 2G', Pa

Shear rate,γ_R; Frequency,ω, s^{-1}
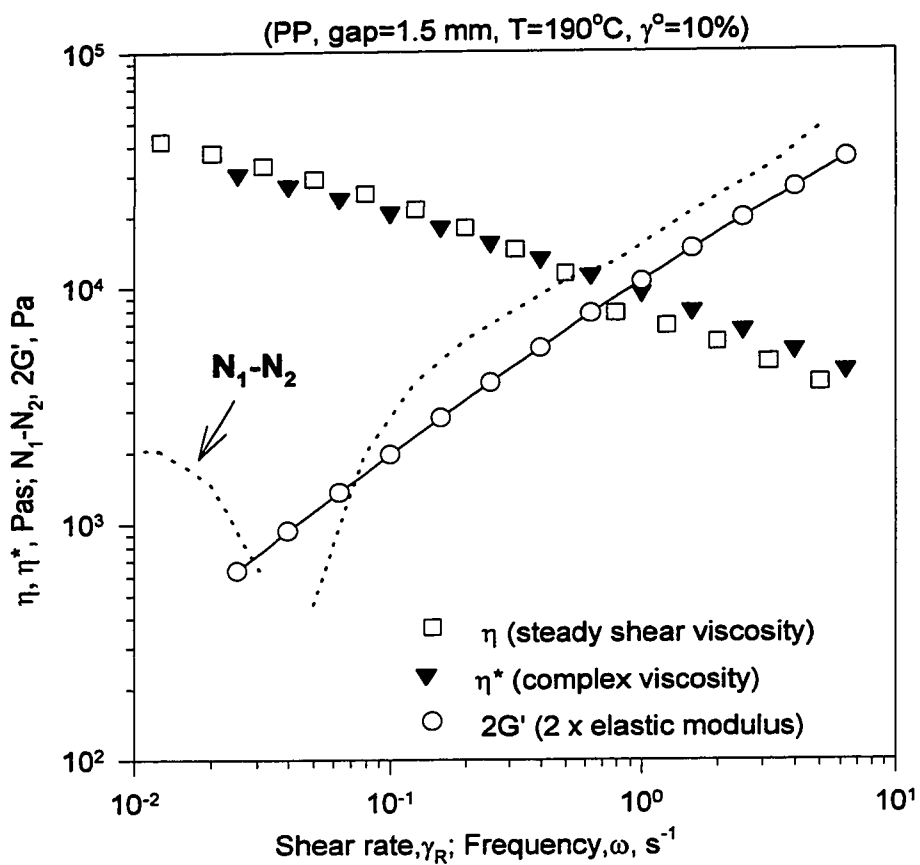
Comparison of the slopes of the curves below and above the transition was carried out similar to the work of Wissbrun and Griffin on LCPs (1982). Results are shown in Table 4.4.

Table 4.4: Comparison of the slopes of Figures 4.11a & b for Q-HDPE and Figure 4.9 for PS

	190°C	$\dot{\gamma}$ or ω, s⁻¹	r²	240°C	$\dot{\gamma}$ or ω, s⁻¹	r²
δ [log(N_1-N_2)]/δ [log $\dot{\gamma}$], Q-HDPE	0.695	0.5 - 5	0.9974	0.455	0.1 - 3	0.9974
δ (log G')/ δ (log ω) , Q-HDPE	0.828	0.01-0.1	0.9995	0.903	0.01 - 0.1	0.9954
δ (log G')/ δ (log ω), Q-HDPE	0.668	0.5 - 5	0.9997	0.659	0.1 - 100	0.9978
δ [log (N_1-N_2)]/ δ [log $\dot{\gamma}$], PS	1.499	0.04-0.6	0.9910			
δ (log G')/ δ (log ω), PS	1.389	0.01-1	0.9983			
δ (log G')/ δ (log ω), PS	0.427	10-100	0.9918			

The steady and dynamic shear properties of polystyrene (a typical amorphous polymer) at 190°C, were shown earlier in Figure 4.9. The slopes of the N_1-N_2 and 2G' curves are given in Table 4.4. For PS, the slope, δ (log G')/δ (log ω), at low ω is more than three times that at high shear; and at low $\dot{\gamma}$ (or ω) δ [log (N_1-N_2)]/ δ [log $\dot{\gamma}$]≅δ (log G')/δ (log ω). For Q-HDPE, the behavior at 190°C and 240°C is almost similar. The slope, δ (log G')/δ (log ω)≅0.7-0.9 for both temperatures regardless of the level of ω. At 190°C, the slope δ [log (N_1-N_2)]/ δ [log $\dot{\gamma}$]=δ (log G')/δ (log ω)=0.7 at high shear rates

$[\dot{\gamma}$(or ω)=0.5 to 5 s^{-1}], while at 240°C the slope is ~0.5-0.7. From the above analysis, it is clear that:

a) for PS, the slope δ (log G')/δ (log ω) showed a strong dependency on the level of ω, while for HDPE the slope was almost independent of ω.

b) for HDPE, the slopes δ [log (N$_1$-N$_2$)]/ δ [log $\dot{\gamma}$] and δ (log G')/δ (log ω), obtained below and above the transitions, didn't show any significant differences.

The results in (a) & (b) show <u>differences</u> relative to PS, which <u>is</u> amorphous. These findings suggest the following: first, HDPE melts are not amorphous like those of PS; and second, the melt order persists (although weakened) at temperatures above the transitions.

Furthermore, a similar analysis was carried out in the cone-and-plate geometry for Paxon-HDPE at 170° and 250°C. Results are shown in Figures 4.11c & d. For both temperatures, the "kink" in the steady shear viscosity was displayed and the match between η and η^* at low $\dot{\gamma}$ was observed. The behavior of the normal force (N$_1$) and 2G' at 170°C, for low and high $\dot{\gamma}$ or ω, was similar to that of Q-HDPE (i.e., mismatched) regardless of the testing geometry (CP as well as PP). Results obtained at 250°C emphasized my previous observations (the NF anomaly and the "kink" in viscosity) at low shear; but produced a remarkable agreement between N$_1$ and 2G' over a wide range of $\dot{\gamma}$ (or ω) past the normal force anomaly. This latter match at 250°C could be a direct influence of the high temperature and/or shear on the order in the liquid-state. Results obtained at 250°C for Solvay-HDPE (see Appendix, Figure A.12) showed the NF

Figure 4.11c Dynamic and steady shear properties for Paxon-HDPE

(C&P, T=170°C, tbm=2min, mt=30 sec)
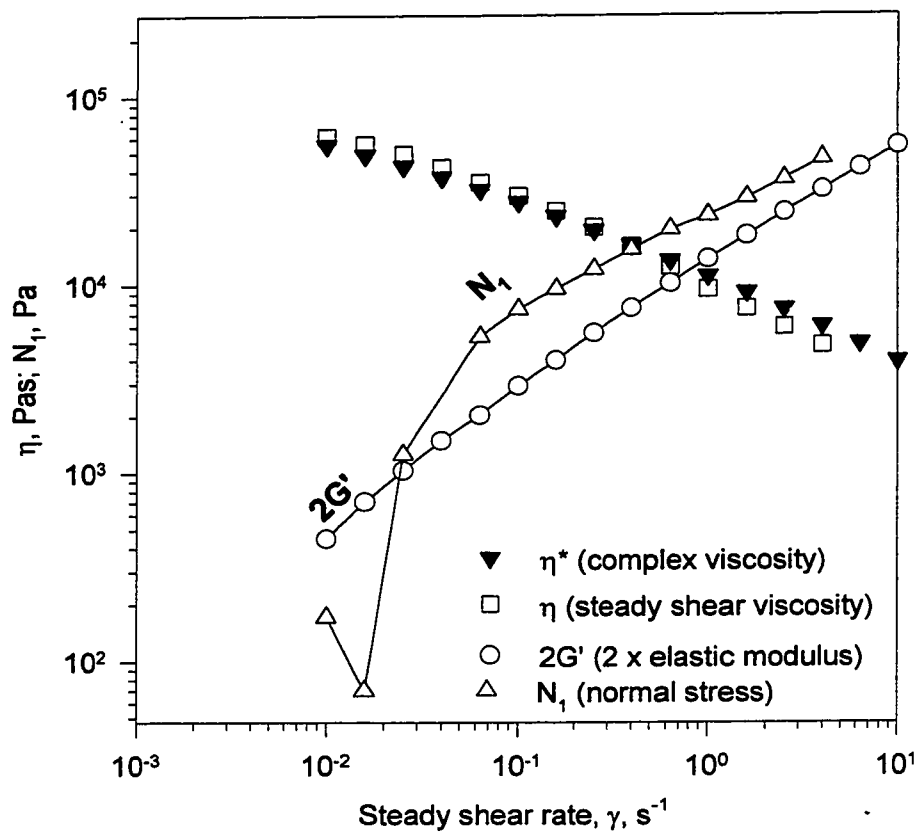
Figure 4.11d Dynamic and steady shear properties for Paxon-HDPE

(C&P, T=250°C, tbm=2min, mt=30 sec)

- ▼ η^* (complex viscosity)
- ☐ η (steady shear viscosity)
- ○ $2G'$ (2 x elastic modulus)

N_1

$2G'$

η, Pas; N_1, Pa

Steady shear rate, γ, s^{-1}
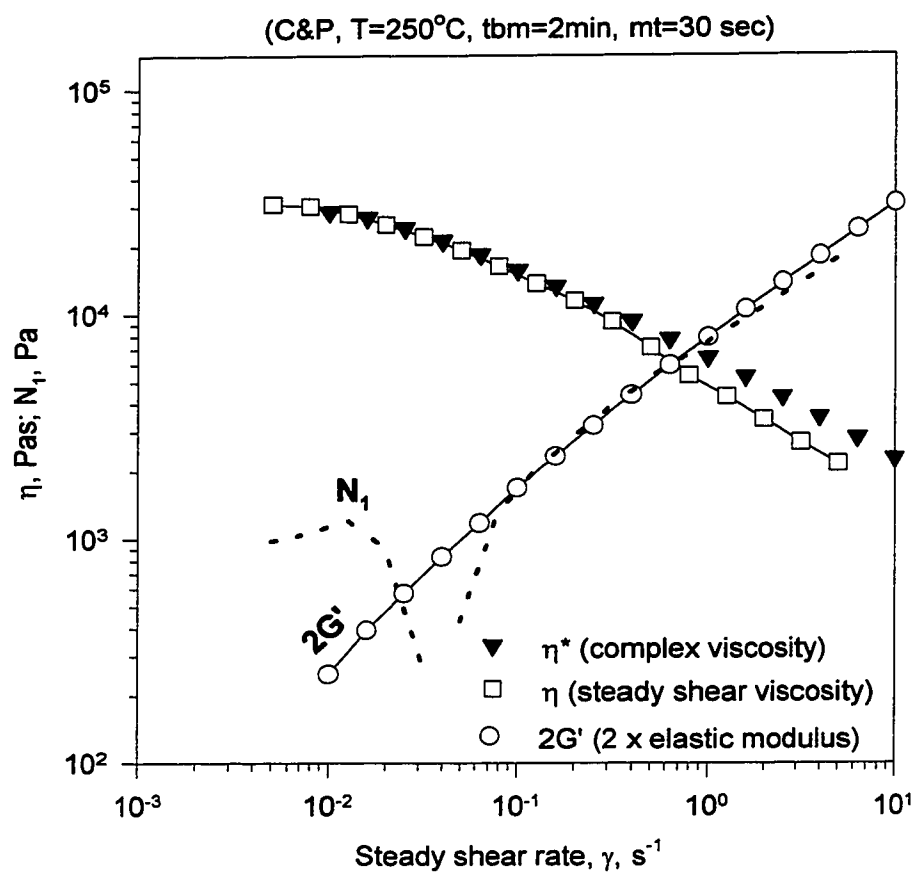
anomaly, but not the match of N_1–N_2 and $2G'$ (may be because the PP function N_1–N_2 ≠ N_1 from CP, and also $\dot{\gamma}_R$ ≠ $\dot{\gamma}$. Thus, Figure A.12 <u>may not</u> be in disagreement with Q-HDPE).

The similarity of the rheology below and above the transition coupled with its significant difference from that of polystyrene suggests that order in the HDPE melt persists even above the transition.

B. *Torque - Melt Temperature Behavior in Mixing*

Torque and melt temperature of six linear HD and five-branched PE resins were measured separately in a Haake Rheocord 90 mixer. The melt temperature was measured by a thermocouple positioned in direct contact with the melt in the middle of the mixing chamber between the rotating blades, but not exactly, where the torque is measured. This leads to a melt temperature measurement a few degrees lower than the actual temperature at the blades except at low heating rates where a uniform temperature distribution is expected as will be shown later. The standard conditions used here were: 3 minutes hold-up time at initial temperature; 50 rpm rotor speed; 5°C/min. heating rate. Visual observations (videotaping of the mixing operation) showed that 3 minutes was long enough for complete melting. The effect of varying these parameters was studied and will be reported later. Polystyrene was used for comparison purposes, and "torqued" under the same conditions. The initial temperature in most of these experiments was 160°C, about 20°C above the normal melting point of HDPE, and heating continued to about 260°C. The torque-melt temperature behavior of linear and branched polyethylenes will be discussed separately.

1. Torque-melt temperature relation for linear polyethylenes

The torque-melt temperature responses showed some minor differences among the six HDPE samples, though similar reproducible behavior was displayed by all. The two responses that differed the most widely were shown in Figures 4.12a for Phillips-HDPE and 4.12b for Solvay-HDPE. For ease of comparison, the PS melt behavior was superimposed on both figures. Clearly, the HDPE melts exhibit a complex series of transitions that occur at temperatures far beyond the disappearance of the solid-state crystals at about 140°C. The PS behaves as expected, with the torque declining regularly with temperature in a fashion akin to the viscosity of most liquids. The PS behavior serves not only to highlight the anomalous HDPE performance, but also to demonstrate that the latter is not an artifact of the equipment or its operation or of oxidation.

The main distinguishing features of the HDPE behavior appear for all six samples (without any dependence on M_w) in the temperature range of roughly 208° to 225°C; however, other anomalies can be seen too. The torque for HDPE in the Haake Rheocord 90 melt blender did not decay with temperature as $\exp(E/RT)$. The Arrhenius form is seen with typical amorphous polymers (e.g., PS) and small-molecule liquids where viscosity behaves this way at temperatures far above T_g. For example, for T>225°C, the torque decrease is distinctly non-Arrhenius, being almost linear as far as 260°C. This suggests that the polymer chains remain ordered in some fashion and do not "melt" into the amorphous random coil conformation until T>260°C, if at all. For 208° >T>160°C the torque also descends in non-Arrhenius fashion (again, more linear), as is more evident for Phillips-HDPE in Figure 4.12a than for Solvay-HDPE in Figure 4.12b. However, the most dramatic features are the midrange ones. The initial torque decreases in Figure

Figure 4.12a Torque-melt temperature curve for Phillips-HDPE

(hold at 160°C for 3 min, 50 rpm, 5°C/min, with N_2)
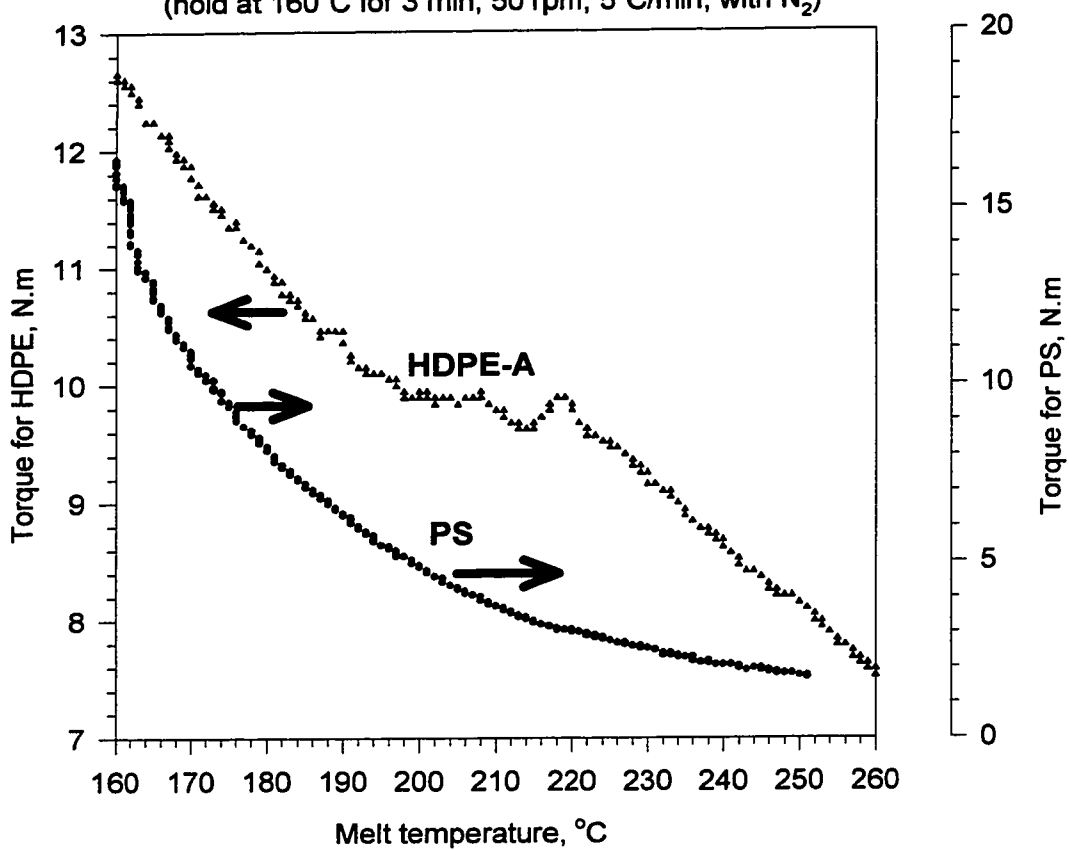
Figure 4.12b Torque-melt temperature curve for Solvay-HDPE

(hold at 160°C for 3 min, 50 rpm, 5°C/min., with N_2)
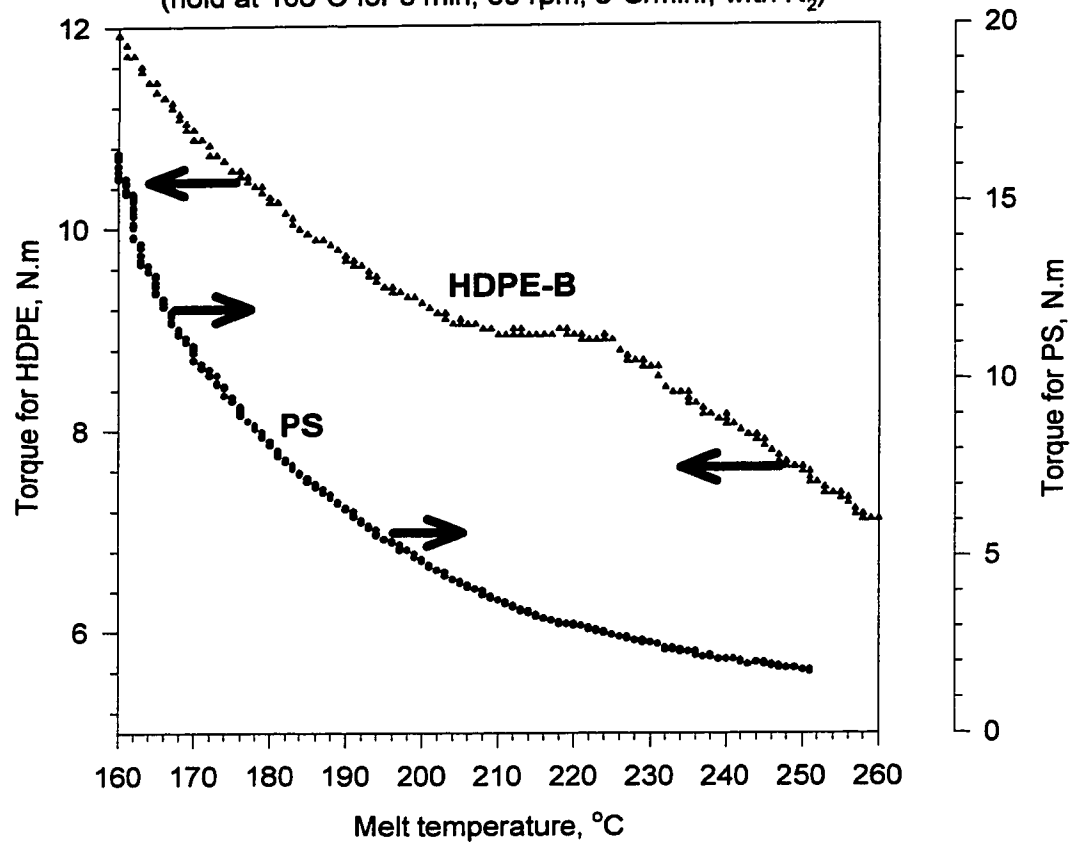
4.12b ends at about 208°C, moving into a plateau and a subsequent transition at 227° where the plateau ends. In Figure 4.12a, the initial decrease merges with a short plateau that terminates at 208°C, followed by a sharp minimum at 215° and a major peak that subsides before the final decrease commences at about 227°C. In Figure 4.12a, there is also considerable irregularity in the decline over 188°-208°C.

To demonstrate that these phenomena do not represent chemical changes due to oxidation, we display in Figure 4.12c the same behavior, with a large excess of antioxidant (6000 ppm) added to Nova S221 (HDPE). By the end of this experiment samples were collected and analyzed for residual AO using high-pressure liquid chromatography. The samples contained more than 93% of active AO available for guarding the HDPE from oxidation. This further supports the LCP interpretations for this phenomenon. (The double peak is probably due to molecular structure features of this sample, which had a small degree of branching not shared by other samples.)

Furthermore, the torque measurements were extended to Solvay-HDPE (in the presence of AO), Quantum, Paxon, and Union Carbide-HDPEs. Results are shown in the Appendix (Figures A.13 to A.16). All HDPEs showed the same distinct regions of torque-melt temperature behavior: (a) T<208°C, (b) 208<T<225°C, and (c) T>225°C. (Figure A.15 for Paxon-HDPE almost loses the two transitions, and is also the only case that shows a match between N_1 and $2G'$ at high shear rates (see Figure 4.11d) suggesting the weakness of the melt order.

The torque experiments reinforced the temperature sweep results by showing the 208°C-transition; displayed the 227°C-transition; and showed the persistence of order above these transitions, in direct agreement with the previous analysis of the rheology

Figure 4.12c Torque-melt temperature curve for Nova S221*

(50 rpm, T_{hold}=160°C, ramp to 260°C at 5°C/min)

*with additional 6000 ppm of antioxidant
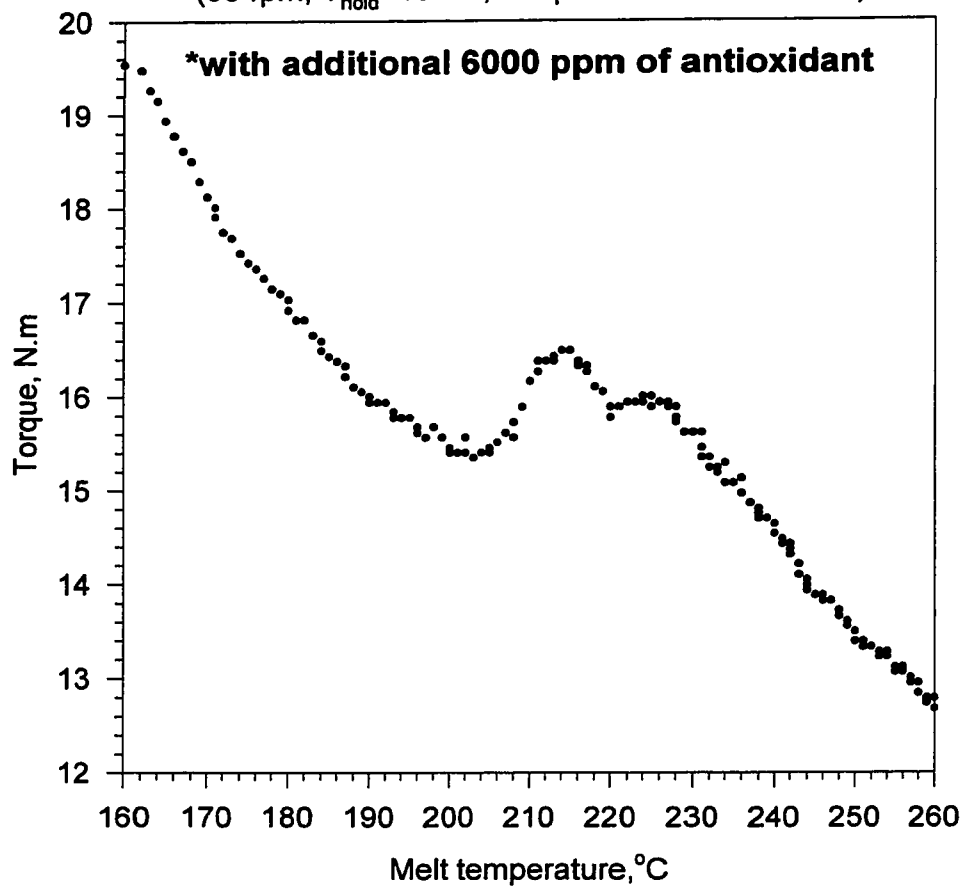
below and above the transitions. The 3-regime temperature behavior is not observed for amorphous polymers and the increase of viscosity at any temperature is rarely seen for any liquids, being unique to thermotropic LCPs (Heberer et al., 1994; Han and Rey, 1995).

However, HDPE melts have previously been associated with other fluid mechanical anomalies, such as slip at solid boundaries (Dealy and Wissbrun, 1990) - e.g., in pressure-driven capillary die extrusion. This prompts one to question whether the behavior displayed in Figures 4.12a, b and c (and Appendix A.13 to A.16) could be attributed to some kind of slip or slip/stick flow. This possibility must be rejected, however, since slip is known to correlate with the magnitude of the wall shear stress. A given shear stress is achieved for polymers of different M_w and viscosities at different temperatures, unlike the case here where the same transitions at 208° and 227°C were displayed by samples whose viscosities varied by a factor of approximately 100 in this temperature range.

My contention is that the 208° and 227° transitions found in the torque data are rheological manifestations of liquid-crystal transitions that are characteristic of the methylene chain structure and not necessarily related to other exaggerated behavior displayed by UHMWPE that is usually interpreted as due to long relaxation times (Wunder and Merajvar, 1983). The transitions are thus independent of M_w and the number of entanglements per chain.

The study of UHMWPE by Raman spectroscopy (Wunder and Merajvar, 1983) demonstrated strong tendencies toward all-trans chain order in melts, consistent with liquid-crystal structures, and that study terminated at 208°C (identical to the lower-T

transition found here) without comment by the authors. At the higher-temperature end, acoustic measurements (Kruger et al., 1980) have detected a change in sound velocity in LPE (M_w=6600) melts at about 230°C, again in agreement with the data but without molecular interpretation.

Rheological support for the fundamental LCP interpretation of HDPE melts below 208°C was recently presented by Williams' laboratory (Ghosh et al., 1996) using these same six samples at 190°C, with the finding that the M_w-dependence of melt index implied that viscosity varied as M_w $^{5.5}$ (as opposed to M_w $^{3.4}$ for entangled amorphous melts such as PS), a result previously associated only with the LCP (Heberer et al., 1994).

Additional rheological support for the LCP interpretation of HDPE melts below 208° was found in the work of Kolnaar and Keller (1994, 1995, 1996, and 1997) that reported a transition in the interval 148°-152°C (observed in the extrusion of HDPE, M_w=2.8×10^5). Moreover, the torque measurement technique was capable of reproducing the 150°C-transition. Three HDPEs (Nova S221, Phillips, and Solvay) were selected for this study.

The HDPEs were heated from 135° to 260°C with a hold for 3 minutes at 135°C for complete melting followed by heating at 5°C/min. All samples reproduced the 3-regime distinct behavior, but here the attention was focused on the range 130°-190°C. The three resins (M_w~80 to 140×10^3) displayed a low-T maximum in the torque-T curves (usually associated with crystal melting) at 138°C (see Figure 4.13). For Nova-HDPE (M_w=1.4×10^5) the torque showed a significant drop (from 36 to 20 N.m) in the temperature window 148°-152°C. Phillips and Solvay-HDPE (M_w~80×10^3) showed

Figure 4.13 Comparison of torque-melt temperature behavior for HDPEs

(50 rpm, hold at 135°C for 3 min, 5°C/min.)
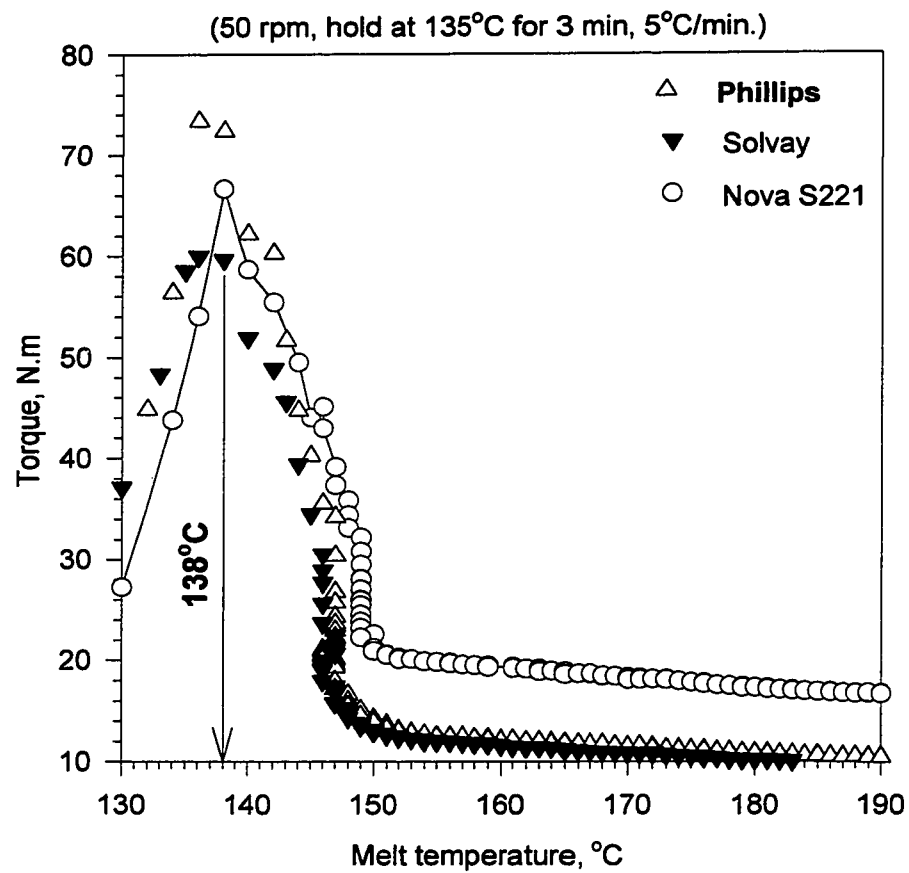
similar behavior in the interval 146°-150°C. The observed drop in the torque (in a blender) reinforces Kolnaar and Keller findings on pressure drop (in extrusion) in the same temperature window. Furthermore, these observations suggest a weak dependency of the 150°C-transition on M_w.

The observed torque-T behavior in HDPEs suggests at least two and perhaps three distinct microstructural forms over the range measured (160°-260°C). Arrhenius plots (see Appendix, A.17 to A.20) were generated from torque-T data to calculate the activation energy for these distinct phases. These positive variations are interpreted as structural transformations leading to more freedom and thus interaction of the polymer molecules and, hence, an increase in viscosity (Heberer et al., 1994; Han and Rey, 1995).

Activation energies calculated from Arrhenius plots are shown in Table 4.5. The obtained values are of the same order of magnitude as those obtained from the temperature sweep tests to get $\eta^*(T)$ using RMS (Table 4.1). Activation energies above the transition, E_A, were found higher than those below it, E_B, as in $\eta^*(T)$ temperature sweep tests, with E_A/E_B in about the same range.

The torque measurements were obtained from a complicated flow pattern with more disentangling effects (high rpm is equivalent to high $\dot{\gamma}$) that resulted in lowering the activation energy. The activation energy for PS was calculated as 11 kcal/mol (r^2= 0.9963); less than that obtained in $\eta^*(T)$ temperature sweep tests by a factor of 1.6. The same observation applies for HDPEs (see Tables 4.1 and 4.5). These results are supported by theoretical predictions (Bestul and Belcher, 1953; Sabia, 1964) and experimental observations on polyethylene (Philippoff and Gaskins, 1956; Schott and Kaghan, 1961; Meissner, 1963; Sabia, 1964; Mendelson, 1965a; Porter and Johnson, 1966).

Variation of the parameters selected for the standard test (blade rotational speed, holding time at 160°C, T-ramp speed, etc.) had only minor influences on the behavior seen in Figures 4.12 (a to c), without altering the major features cited above. Results will be discussed below.

Table 4.5: Activation energy for HDPEs (in the Rheocord 90 blender)

Resin Producer	E_B (kcal/mol)	r_b^2	E_A (kcal/mol)	r_a^2	E_A/E_B
Nova S221	2.166	0.9898	3.605	0.9920	1.669
Paxon	2.293	0.9949	3.184	0.9818	1.389
Quantum	2.167	0.9951	3.808	0.9962	1.757
Solvay	2.533	0.9939	3.392	0.9925	1.339
UC	1.927	0.9935	3.530	0.9926	1.832

2. Influence of mixing Conditions

The effect of the mixing conditions: temperature and heating-rate; rotor speed and use of a nitrogen gas purge; were studied using Solvay-HDPE. Low heating rates of 2°C/min were used with other parameters kept at the standard values mentioned earlier. Results are shown in Figure 4.14 and compared to the results at 5°C/min. The flat region (208°-225°C) found when using 5°C/min was converted (using 2°C/min) into a shallow minimum with a flat bottom, followed by an increase in torque (viscosity) with increasing temperature in the range 210 - 230°C as seen with other manufacturers' samples. The range shows a positive shift of 5°C in the start-up of the flat plateau. As was pointed out earlier, lower heating rates reduce the temperature differences between the rotating blades and the melt, the latter temperature measured by a thermocouple positioned close to the

Figure 4.14 Torque - melt temperature curve for
Solvay-HDPE at different heating rates

(hold at 160°C for 3 min, 50 rpm, with N_2)
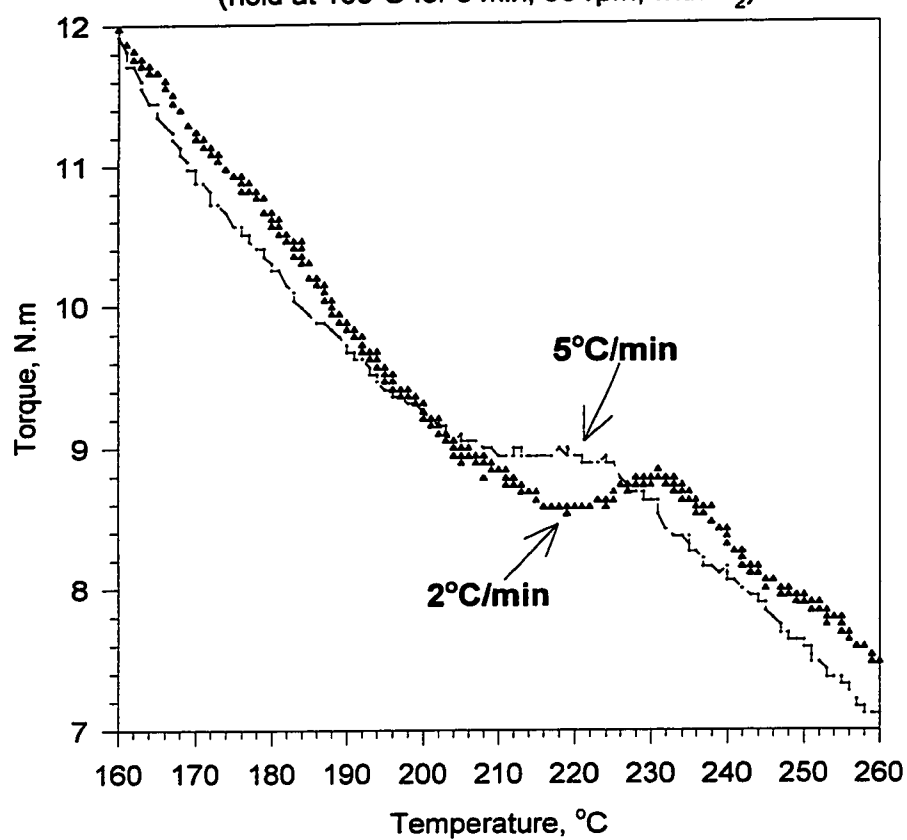
wall. Lower heating rates gave more time for the heat generated due to viscous heating to distribute in the melt, and hence reduce the differences between the actual and measured temperatures. This explains the positive shift (on melt temperature scale) in the onset of the transition range at lower heating rates. Furthermore, these results indicate that oxidation is not the reason for the observed phenomenon, since longer times of exposure (at low heating rates), should have resulted in oxidation taking place at lower temperatures (i.e. negative shift of the transition range). In general, both torque and $\eta^*(T)$ measurements in the RMS show the 208°C transition.

The effect of the rotor speed is shown in Appendix (Figure A.21). All three curves show T_2, but T_1 is not easy to see. T_2 is $\cong 220°C$ for $\Omega=20$ and 50 rpm, but at 200°C at $\Omega=100$ rpm. The Ω-dependence of transition temperature shows a decrease in T_2 with the increase in Ω suggesting altering of the melt order.

The effect of nitrogen atmosphere was also studied by repeating the same experiments under the same conditions but without nitrogen. Phillips-HDPE was used for this study. Exact or excellent agreement (see Appendix, Figure A.22) between the two experiments was found all over the entire temperature range except in the flat (or peak) region. The exact agreement of the torque-temperature curves at high temperatures (up to 260°C) for both cases verified that oxidative degradation was not a problem, even without N_2, and for most purposes the expensive and tedious use of N_2 could be discontinued since all commercial samples are well protected with anti-oxidant. The increase in torque with temperature observed in the transition range ($\sim 200°$-$220°C$) in the experiment with nitrogen may be a result of limited oxidation due to trapped oxygen. This is further supported by the fact that the pressure inside the mixer is higher than the atmospheric (a 5

kg weight and stopper were used to keep the mixing chamber closed) giving no chance for air to get in and cause oxidation.

3. Torque-melt temperature relation for branched polyethylenes

The torque-melt temperature behavior of branched polyethylenes was studied in the Haake Rheocord 90 melt blender at different rotor speeds and heating rates. The branched PEs investigated by this technique included three Butene LLDPE samples [Exxon metallocene (36.2 CH_3/1000 C), and two Z-N Nova polymers S225 (16.1 CH_3/1000 C), and S229 (22.1 CH_3/1000 C)] and Nova S216 LDPE. All commercial resins were highly stabilized by adding 6000 ppm of AO.

The metallocene resin was torqued at 30 rpm and heated from 160° to 260°C beginning with a hold for 3 minutes at 160°C followed by heating at 3°C/min. Results are given in Figure 4.15. The displayed data show no sign of transitions in the temperature range 160°-260°C and fit Arrhenius behavior (see Appendix, Figure A.23). The test was repeated at 20 rpm and similar results (Appendix, Figures A.24 and A.25) were obtained. This suggests amorphous behavior of the highly branched polymer when $T > T_m$. These results reinforce the previous observations in the temperature sweep testing in the RMS (i.e., η^* showed no T_1 transition).

Torque measurements for the LDPE were carried out at 20 rpm and 2°C/min. in the presence of 6000 ppm of additional AO. The test failed to show any distinct behavior (neither T_1 nor T_2) in the temperature range covered by this study (see Appendix, Figures A.26 and A.27 for LDPE). Similar results (Appendix, Figures A.28 to A.31) were obtained for the LLDPEs (S225 and S229).

Figure 4.15 Torque-T behavior of Exxon LLDPE metallocene*

(hold at 160°C for 3 min., 30 rpm, 3°C/min)

*with additional 6000 ppm of A/O
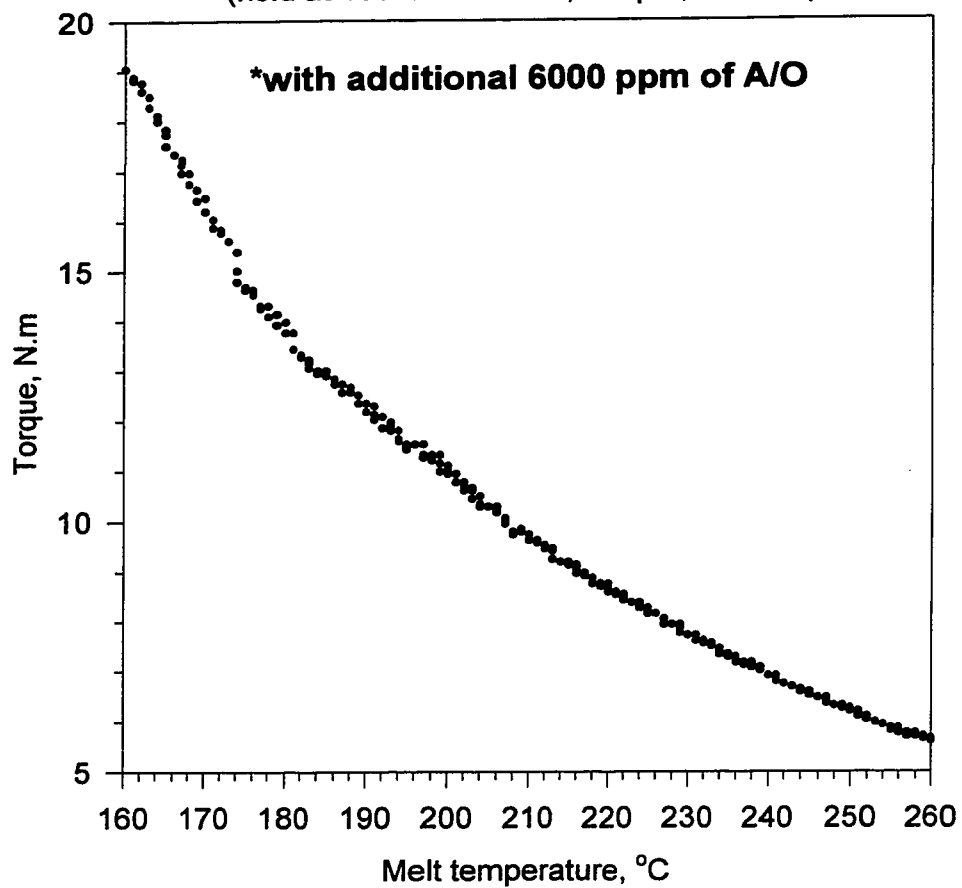
The small-strain RMS measurements of $\eta^*(T)$ showed the existence of high temperature transition in Z-N LLDPEs and LDPE (see Table 4.3) that were later supported by DSC (to be shown below). On the other hand, the high shear (high rpm) torque measurements in the blender did not reveal these transitions. This suggests that the melt order that did exist at low $\dot\gamma$ in the RMS was either destroyed or weakened by the high shear, and hence not picked up by the blender.

The activation energies for all LLDPEs and LDPEs were calculated from the Arrhenius plots of torque-T curves and are given in Table 4.6. In general, the E values calculated from torque measurements data are lower than both E_A and E_B obtained from the RMS measurements. For S229 (LLDPE) E was 6 and 36% lower than E_A and E_B respectively, while for S216 (LDPE) E was 14 and 59% lower. For the metallocene

Table 4.6: Activation energies for BPEs (in the Rheocord 90 blender)

Resin	Branch density	M_w	E (kcal/mol)	r^2	Conditions
Exxon Met.(butene)	36.2	110,086	5.386	0.9969	30 rpm, 3°C/min
Exxon Met.(butene)	36.2	110,086	5.778	0.9977	20 rpm, 3°C/min
Nova S229 (butene)	22.1	105,313	4.411	0.9987	30 rpm, 3°C/min
Nova S225 (butene)	16.1	120,000	4.219	0.9986	30 rpm, 3°C/min
Nova S216 (LDPE)	*	99,464	5.074	0.9990	20 rpm, 3°C/min

*see Table 3.3

resin, the effect of high rotor speed (30 vs. 20 rpm) on activation energy is similar to that of high shear in well-defined flow fields. Exxon metallocene and Z-N Nova S229 that were both butene LLDPEs and have almost the same M_w, showed different activation energies when tested under the same experimental conditions (30 rpm, 3°C/min). Vega et

al. (1996) reported higher activation energies for metallocene-catalyzed HDPE (7-9 kcal/mol) over that of Z-N HDPE (6-7 kcal/mol) of the same M_w.

The activation energy of the Exxon metallocene resin is 22% higher than that of the Nova Z-N resin, which could be explained by the significant differences in the molecular conformations resulting from the different branch contents (the metallocene is 63% higher). Furthermore, the high shear blender produced similar E values for Z-N butene LLDPEs and LDPE. Similar results where obtained for butene LLDPEs and LDPEs by Sabia (1964) in a capillary rheometer. The similarity of activation energies of Z-N LLDPE and LDPE suggests that at high Ω (or $\dot{\gamma}$) the melt molecular conformations were influenced by the high shear rather than short or long branching. Alternatively, the similarity could be due to the fact that both LDPE and LLDPE contain many short branches. [S216 (LDPE) has the same total number of short branches as S229 (LLDPE), see Table 3.3].

C. Melt Flow-Temperature relation in a Melt Indexer

The investigation of the effect of temperature on the flow properties of HDPEs in the range 210°-230°C took a further step in another rheological equipment, the Melt Indexer, which is totally different from the controlled shear fields of the RMS and the complicated flow field of the blender. The Melt Indexer is a simple device, which resembles the capillary viscometer. This device is widely used in industry for molecular weight characterization. Although it is a simple instrument, little has been published about the fluid mechanics of the melt going through the device, except for the work of the Williams group (Ghosh et al., 1996).

Although the melt index (MI) is usually defined at a temperature of 190°C, the melt flow can also be measured in the temperature range of 190°-230°C. Testing at higher temperatures was not considered to avoid degradation since the melt indexer doesn't have an arrangement for nitrogen atmosphere. The oxidation temperature obtained in air for PE with "normal" AO using a DSC is 235°C (will be discussed in Chapter V). The MI(T) behavior of Q-HDPE, UC-HDPE, and Dow-LDPE are shown in Figure 4.16. The reported MI is an average of three samples taken 3 minutes apart during a single piston descent. The weight of the three samples was approximately the same suggesting the steadiness of the flow during this period of measurement, as reported by Gosh et al. (1996). Measurements were taken at a temperature interval of 5°C for Q-HDPE and 10°C for UC-HDPE and Dow-LDPE. Fresh loadings were used for each T.

To estimate the activation energy from the melt flow data we assumed the applicability of Hagen-Poiseuille law for flow in circular tubes, where the volumetric flow rate (Q), the pressure drop (ΔP), the tube radius (R) and length (L) are related by $Q = \pi R^4 \Delta P / 8 \eta_0 L$. Since (melt flow)$/\rho = Q \propto 1/\eta_0 \propto e^{-E/RT}$, neglecting the small T-dependence of $\rho(T)$, then an Arrhenius plot of (melt flow/ρ) vs. $1/T(K)$ would give the activation energy (E). Activation energies calculated from the melt flow data (Figure A.32) in the range of 190°-210°C (E_B) are 5.9, 7.4, and 11.4 kcal/mol for Q-HDPE, UC-HDPE, and Dow-LDPE respectively. These values are in excellent, if not exact, agreement with theoretical predictions and experimental observations discussed earlier, indicating the reliability of the MI measurements. Furthermore, the results suggest that the shear at the wall of the melt indexer is low enough such that Newtonian flow prevailed and therefore $\eta = \eta_0$ and hence $E_{\dot{\gamma}} \cong E_\tau \cong E$.

Results for Q-HDPE (dotted line) revealed a distinctive MI-T behavior in the range 210°C≤T≤230°C. The MI-T curve displayed a flat upper plateau followed by a drop (increase of viscosity) with a minimum of MI at about 225°C and then an increase in MI, resembling the torque-T curve in the blender. A similar performance is demonstrated by UC-HDPE. The drop in the MI and the increase in the blender torque (see Figure A.16), were caused by the increase in viscosity. The results obtained in the two different rheological devices (with totally different flow fields) were mirror images, and presented the 'distinctive' behavior at the same temperatures. Furthermore, the same behavior was duplicated by UC-HDPE. It is interesting to note that the drop in MI was proportional to the increase in torque exhibited by both resins. A comparison of the torque-T curves shown in Appendix (Figures A.14 and A.16) to the MI data in Figure 4.16 reveals this interesting observation.

For the LDPE, both the MI (Figure 4.16) and the torque measurements (see Appendix, Figures A.33 and A.34) implied ease of flow above 210°C. The LDPE showed a decrease in the torque [see Appendix, Figure A.34], and an increase in the MI (Figure 4.16) at T>210°C; however, the responses were not as strong as that of HDPEs which is not a surprise for a branched polyethylene.

D. *Density measurements*

The apparatus used for measuring the densities of solid and liquid polymers as functions of temperature (25°-250°C) was constructed in Williams' laboratory (Muhammed, 1995). The measurement is based on Archimedes law; and the density of the polymer sample was computed according to the previously mentioned equation (see Chapter 3). Stainless steel standard weights were used for the calibration of the

Figure 4.16 Polyethylene melt flow in a melt indexer

Figure 4.16 Polyethylene melt flow in a melt indexer
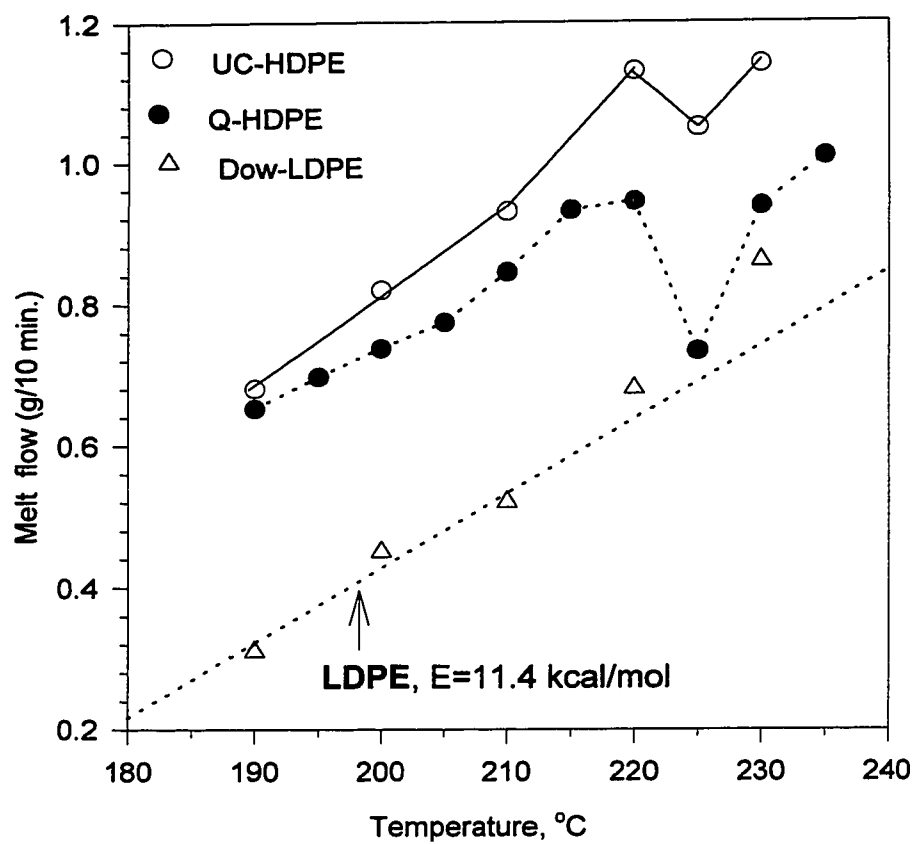
immersion fluid density. Initially, the heated immersion fluid was a high-temperature mineral oil, but later replaced by a silicone oil, which is more stable at high temperatures.

Density calibrations of the two oils are shown in Appendix (Figures A.35 and A.36). Figure A.35 shows the reproducibility of the data regardless of who performs the measurements. Furthermore, the density and the thermal expansion coefficient of the silicone oil reported by the suppliers were reproduced by the densitometer (difference is <0.1%).

The possibility of anomalous swelling of the polymer sample by the oil was also investigated. A sample of Q-HDPE was soaked in the silicone oil at 220°C for ~3 min. and then left to cool in air. The weight of the sample, measured to the fourth decimal, before and after heating in the oil was the same. The sample was then scanned by SEM for Si inside the sample and the result was negative.

Moreover, the density of a polymer sample (Q-HDPE) was measured using different oil baths. The agreement of the results (Appendix, Figure A.37) provided more confidence in the technique and the procedure. Density measurements were able to detect several transition temperatures in linear and branched commercial polyethylenes (Muhammad et al., 1997). In addition, the densitometer revealed the subtle (see Appendix, Figure A.38) polyethylene α-transition (Popli et al., 1984; Boyd, 1985; Ashcraft and Boyd, 1976) in the range of 40°-70°C, which was again supported by the DSC.

It is now clear that the simple densitometer is reliable and sensitive enough to detect solid-state transitions. For that reason, we are encouraged to extend the technique to measure the density of HDPE above its melting point, hoping to find thermal evidence

for the LCP behavior of polyethylenes already observed in different rheological devices. One of the interesting findings in the density measurements is the observation that the HDPE melt can support a weight (0.1-0.2 g) at temperatures as high as 250°C, which could be a result of buoyancy forces ($\rho_{HDPE} < \rho_{oil}$) or another anecdotal manifestation of melt order.

Density measurements were carried out for Q-HDPE in the range 135°-250°C. Results for Q-HDPE are displayed in Figure 4.17 as $\rho^{-1}(T)$. The curve shows a break in the specific volume at 208°C with linear behavior above and below the transition. More data were taken above 190°C to clearly define the 208°C-transition. No attempt was made to take more measurements around 150°C or 230°C to define these transitions. The break at 208°C is comparable to that of the α-transition (see Figure A.38), hence, it should not be confused with simple data scatter. Besides, the specific volume thermal expansion coefficient of Q-HDPE has increased from 1.003×10^{-3} to 1.254×10^{-3} cm^3/g/°C above the transition. The 25% increase in thermal expansion coefficient suggests a difference in the molecular ordering below and above the transition. Finally, the density measurement technique provided additional support for the previous rheological interpretations of the LCP-like behavior of polyethylene.

E. Thermal Analysis

The possibility that the previous rheological anomalies represented LCP-like microstructural or molecular phase transitions suggested that, if so, thermal evidence of such transitions might be observed by differential scanning calorimetry (DSC). We report here that such thermal evidence has been found, apparently for the first time.

Figure 4.17 ρ^{-1} (T) for Q-HDPE measured in a densitometer
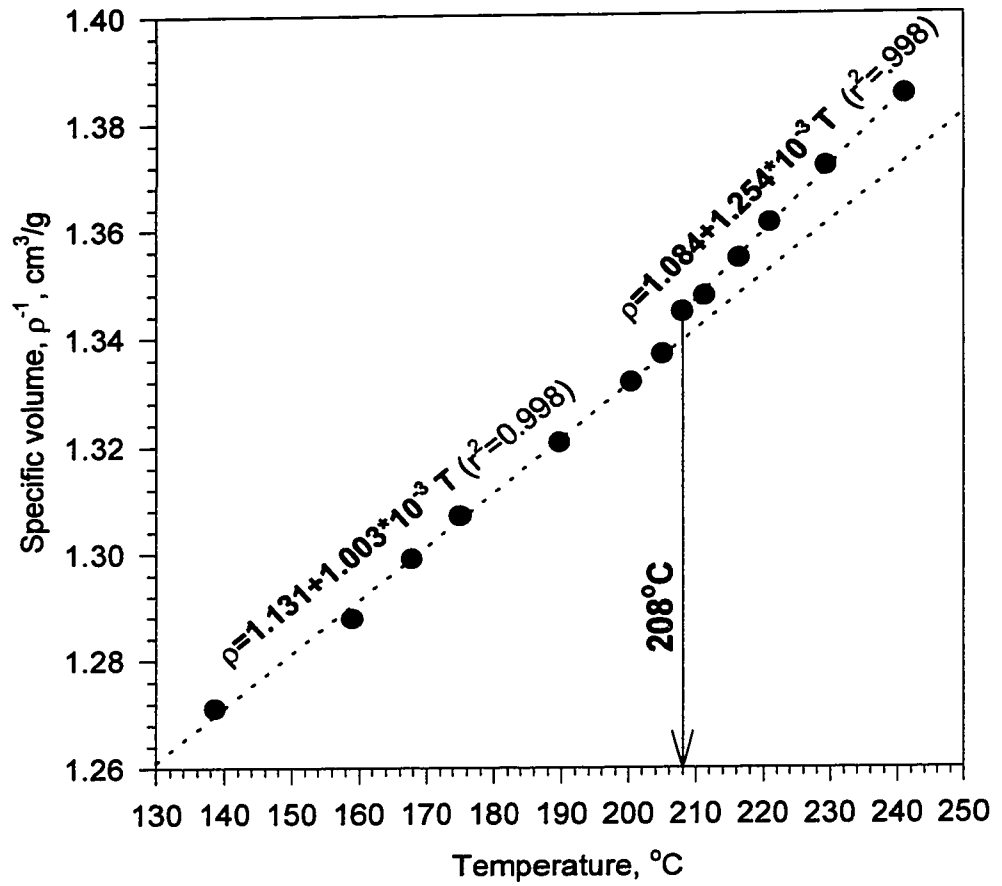
The reason that DSC evidence of these two transitions has not been previously reported is probably related to the fact that the DSC signals are small. Contributing factors could be that a systematic search has not been motivated by any industrial need, together with the fact that the molecular structure of PE is so simple that transitions would not be expected. Moreover, we found that high scan rates (e.g., 10°C/min) were not effective in revealing the transitions in either heating or cooling scans, and the high scan rates are generally favored by most DSC operators. Finally, the heating scan (which usually receives most of the attention) is less effective in detecting the LCP-like order "melting" phenomenon than is the cooling scan in detecting the "freezing" phenomenon (the terminology here is borrowed from ordinary crystalline phase-change behavior, though LCP order-change is believed to be occurring), and thus the more useful half of the DSC cycle (cooling) has often not been explored.

Wunderlich and Grebowicz (1984) and Wunderlich (1997) found that, for LCPs the enthalpy (and hence entropy) of the second-order transitions is rather small and much more reversible than the normal melting transition. In addition, on cooling of LCPs partial crystallization to small crystals is common (i.e., LCs are observed in cooling only). Furthermore, Keller and Ungar (1991) proposed a scheme for phase stability in LCPs that illustrated the possibility of having the LCP mesophases appear on one half of the heating/cooling cycle (i.e. monotropic behavior) depending on the kinetics of crystallization. Here, we report the thermal evidence for high-T transitions in linear and branched Z-N polyethylenes, demonstrating behavior similar to that cited above for LCPs.

1. Linear HDPEs

Results for Z-N Exxon-HDPE are displayed in Figures 4.18 a&b. Two full cycles of heat/cool scans were employed, all at rates of 1.5°C/min. Figure 4.18a expands the T_2 ("freezing") region, while Figure 4.18b stretches the temperature scale to incorporate the conventional melting peak (T_m) for comparison. Both heating scans (Figure 4.18a) failed to show a high-T melting peak, and they reproduced each other very well, diverging only slightly at about 218°C. The two cooling scans in Figure 4.18 a and b both exhibit freezing peaks in the range 227°-230°C and are only slightly displaced vertically from each other. The reproducibility (reversibility) of the T_2 transition in the second cool after a complete cycle of cooling and heating is quite remarkable and indicates the validity and reliability of these observations. Figure 4.18b shows the relative sizes of the "conventional" melting peak, T_m, and the peak at the T_2 transition temperature. At T_2, the net heat evolved (ΔH_2) in the first cooling was 0.0855 J/g (Appendix, Figure A.39) while that evolved in the second cooling (Figure A.40) was 0.0938 J/g. For T_m, the heat of fusion was 146 J/g and 163 J/g in the first and second heating respectively. Hence, the heat evolved at T_2 (ΔH_2) was rather small when compared to that of conventional melting. The small ΔH_2 also means that the corresponding entropy $\Delta S_2 = \Delta H_2/T_2$ is small, too; akin to entropy changes in previous reports on LCPs (Wunderlich and Grebowicz, 1984; Wunderlich, 1997).

In Figure 4.19a, the two cooling scans for a specimen of Nova S215 are shown, here at a scan rate of 3°C/min. The peaks in the two curves show greater complexity than in Figure 4.18 and are more displaced in T from each other than in Figure 4.18. However,
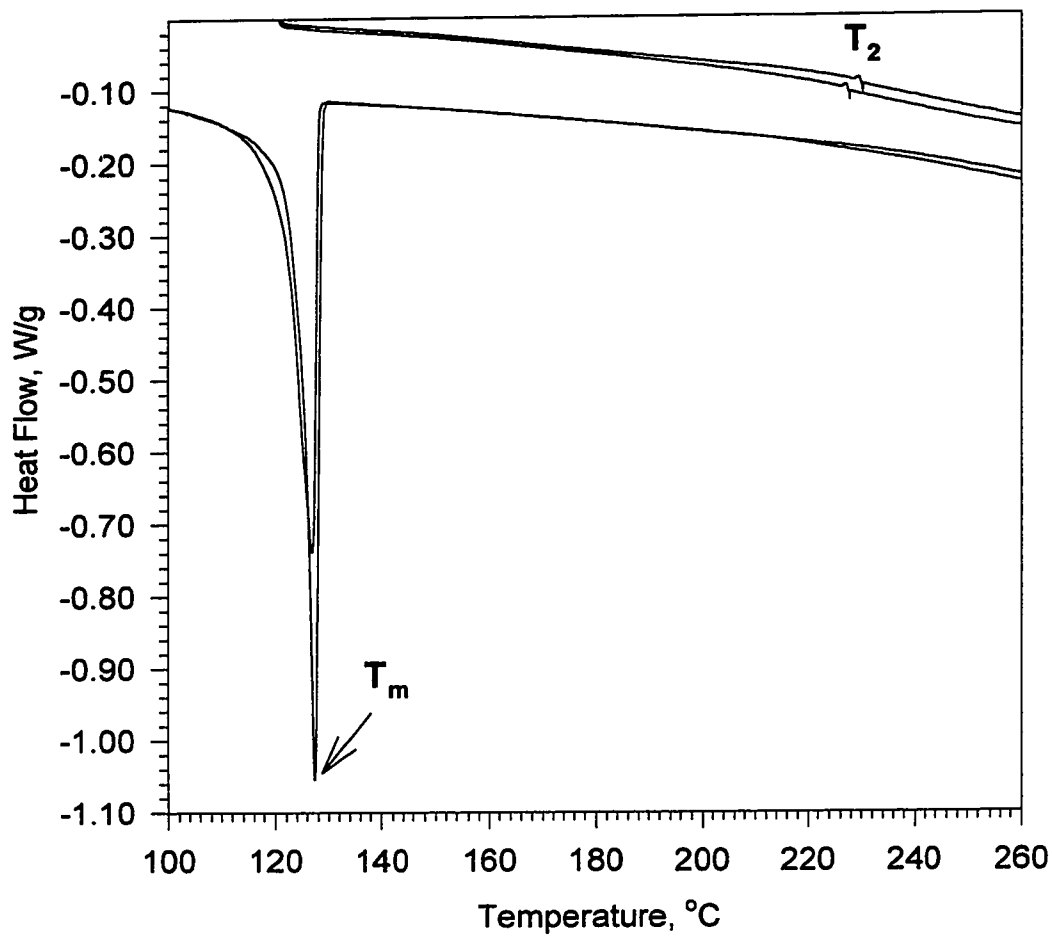
Figure 4.18a DSC plot for as-received Exxon-HDPE (6750)
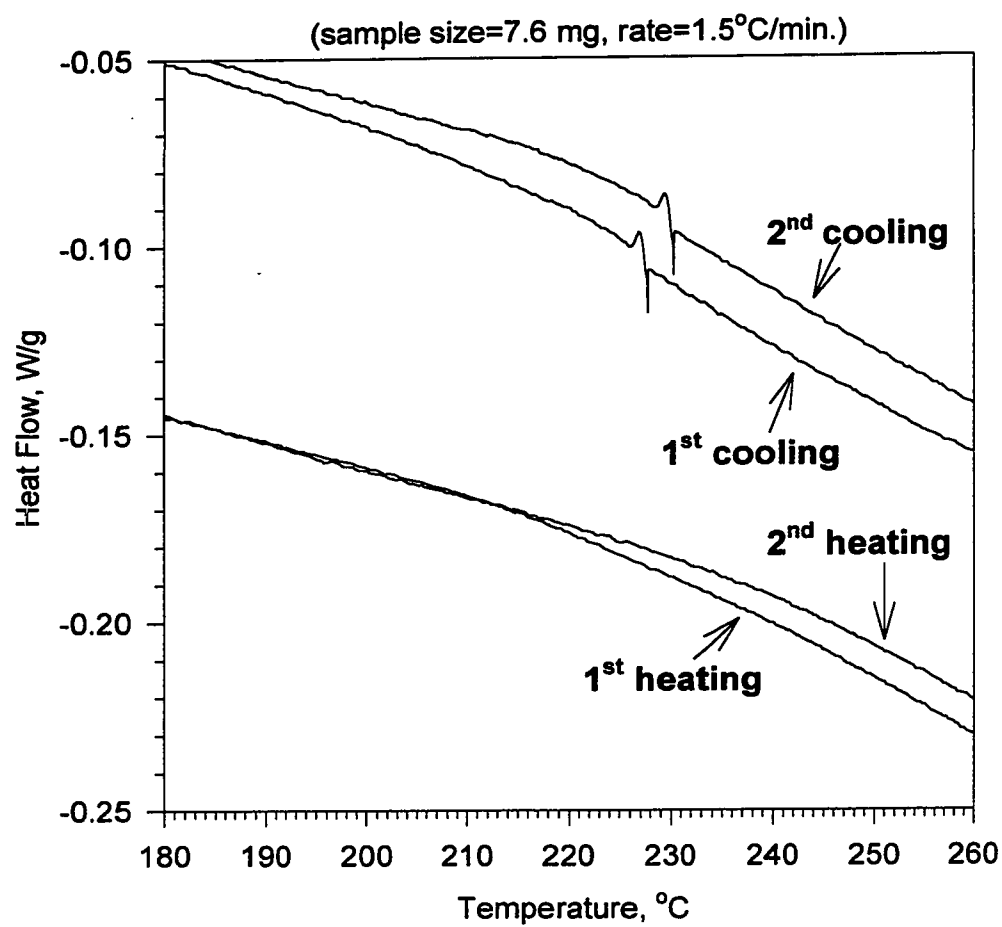
Figure 4.18b DSC plot for as-received Exxon-HDPE (6750)

(sample size=7.6 mg, rate=1.5°C/min.)

Figure 4.19a DSC plot for S215 (HMWHDPE)

(sample size=9.1 mg, rate=3°C/min.)
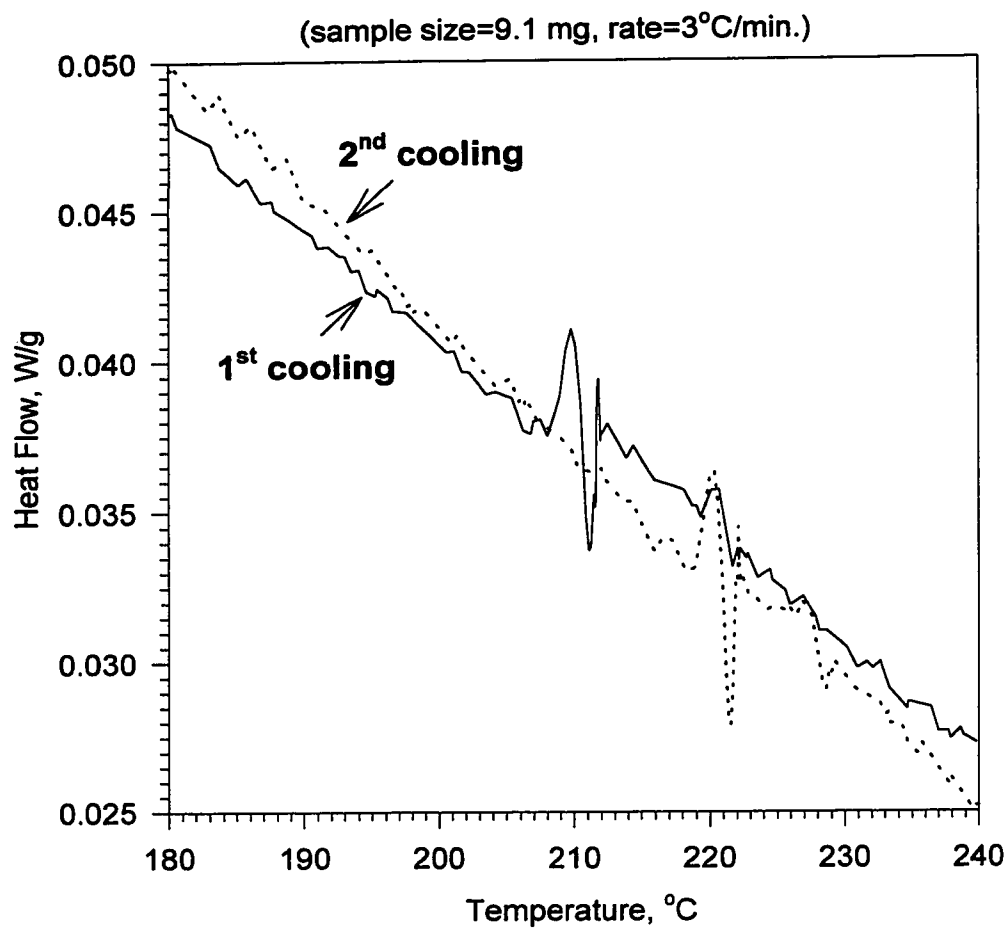
the Figure 4.19a curves display evidence of a lower-T peak at 210°C (T₁) and a higher-T peak (T₂) at 227°C, which matches well the mechanical evidence of torque-T from the blender, MI, and temperature sweeps in the RMS. A second specimen of Nova S215, tested at a scan rate of 1°C/min. gives equivalent results in the single cooling curve shown in Figure 4.19b, though both transitions are shifted slightly to lower T. The shift of the transition at lower cooling rates (1.5°C/min in Figure 4.18 vs. 3°C/min in Figure 4.19a) is another manifestation that these observations are real responses to a physical phenomenon.

It is important to note that the T_2 transition shown above for HDPE is not a consequence of oxidation or other degradation reactions; HDPE is extremely stable under these DSC testing conditions (Hawkins 1984; Chartoff, 1997).

The minor differences in results for the above resins, for cooling from their melts at 280°C ($\cong T_m + 140$°C), are not understood, but may be related to the considerable differences in the molecular weight, thus viscosity and diffusion time scale (which could affect the formation of order in the melt). There is also no certainty that their microstructures were exactly the same when the cooling scans began at 280°. High temperature transitions in DSC tests were also displayed by Q-HDPE (Appendix, Figures A.41 to A.43).

2. Branched PEs

The short-branched resin (Dow-LLDPE, Figure 4.20), and the chaotically-branched (Dow-LDPE), with both long and short branches (Figure 4.21a), made with high-pressure free radical techniques, were both tested at cooling rates of 2°C/min. For both specimens, a first and second scan are shown, displaying good reproducibility, and

Figure 4.19b DSC plot for S215 (HMWHDPE)

(sample size=7.7 mg, rate=1°C/min.)
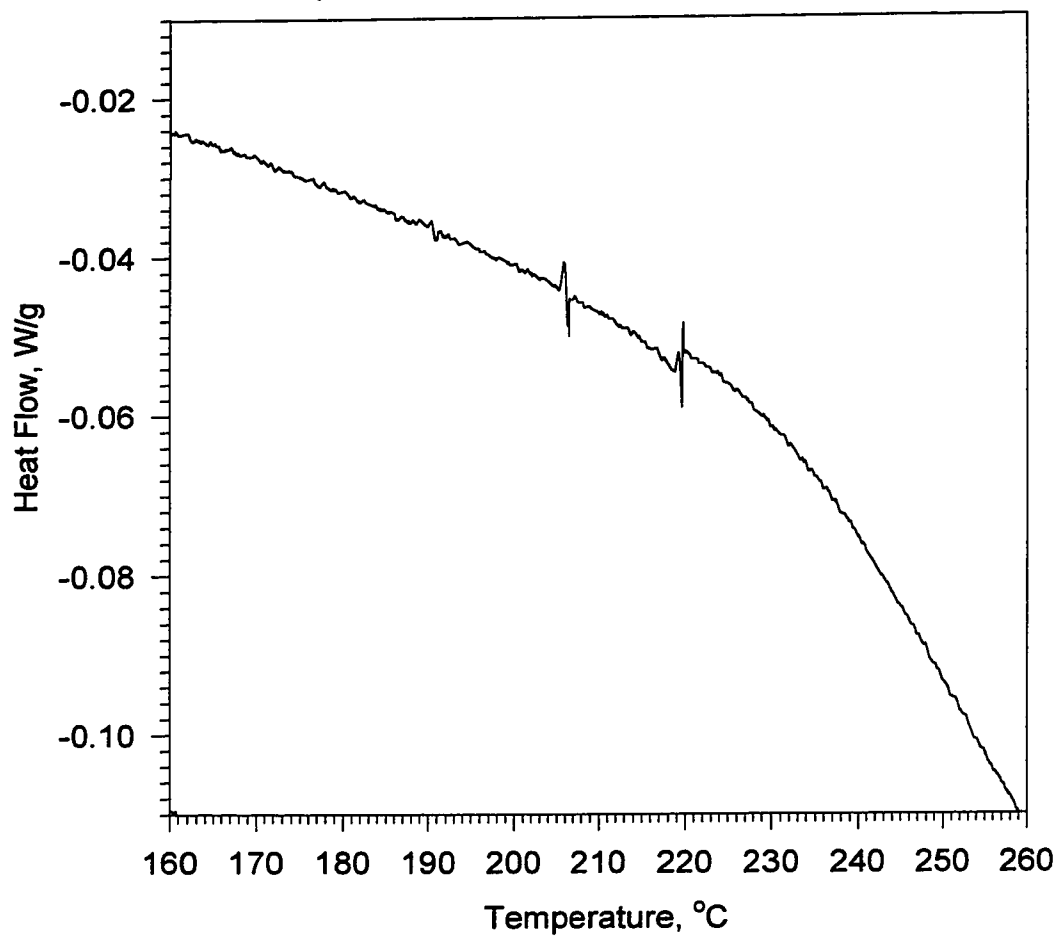
Figure 4.20 DSC plot for Dow (LLDPE-A)

(sample size 9.6 mg, rate=2°C/min)
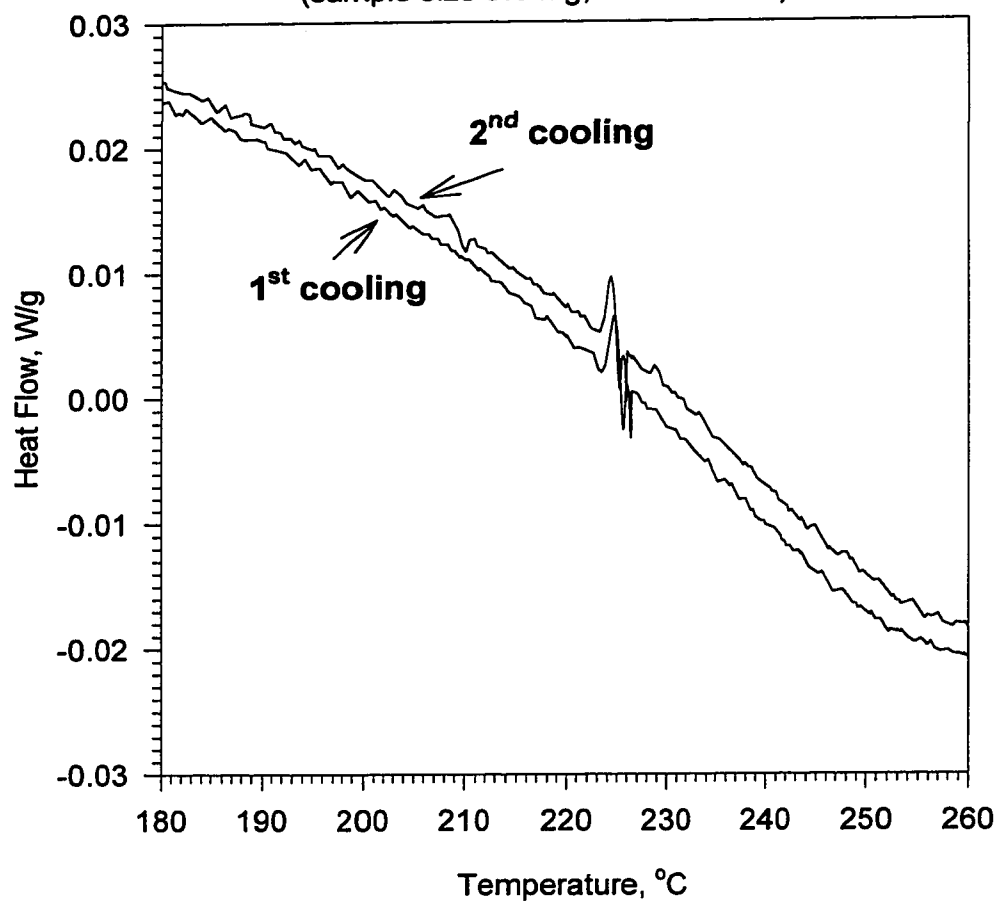
Figure 4.21a DSC plot for Dow (LDPE)

(sample size 8.7 mg, rate=2°C/min)
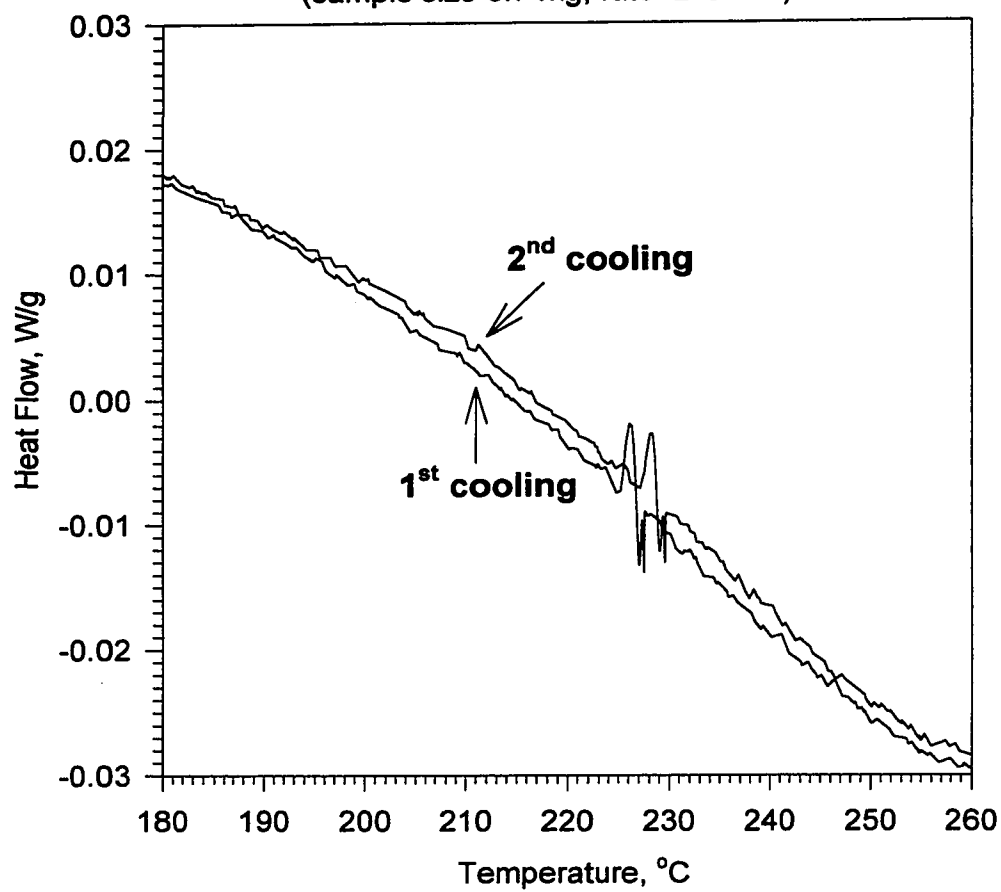
the data for the two resin types resemble each other closely, with a major peak near 227-230°C (T_2). Heat released during these transitions are given in Appendix (Figures A.44 to A.47). One difference between the Dow LLDPE and the LDPE is that the former displays a small but clear peak near 208°-210°C (T_1), resembling in this detail the behavior of the unbranched linear chains of Exxon and Nova HDPEs. On the other hand, the Dow LDPE does not show evidence of T_1. The 208°-210°C transition was detected in another LDPE (Nova S216) with different molecular weight characteristics. Results are displayed in Figures 4.21b and Appendix (Figures A.48 and A.49). Thus, we might infer that the absence or presence of the 208°C peak could be due to differences in the structural and molecular weight characteristics of linear and branched polyethylenes.

The DSC software was utilized to integrate the peaks and calculate the net heat released during the transitions. The percentage of liquid state crystallinity (LC-type) was calculated for all polyethylenes with reference to solid state crystallinity, for which a value of ΔH=290 J/g (Wunderlich, 1997) was used. Results are shown in Table 4.7.

Table 4.7: Entropy change for linear and branched PEs (the T_2-transition in the DSC)

Resin	MI (g/10 min.)	M_n	ΔH_2 (J/g) 1st, 2nd cooling	ΔS_2 (J/g K)×10^4 1st, 2nd cooling
Exxon 6750 (HDPE)	40.2	10,823	0.0855, 0.0938	1.7, 1.9
Nova S215 (HDPE)	0	19,400	0.0385, 0.0280	0.8, 0.6
Dow-LLDPE	N/A	N/A	0.0799, 0.1032	1.6, 2.1
Dow-LDPE	0.21	17,849	0.0570, 0.1097	1.1, 2.2
Nova S216 (LDPE)	0.75	15,458	0.0090, 1.201	0.2, 24.0

Figure 4.21b DSC plot for S216 (LDPE)

(sample size 7.0 mg, rate=1.5°C/min)
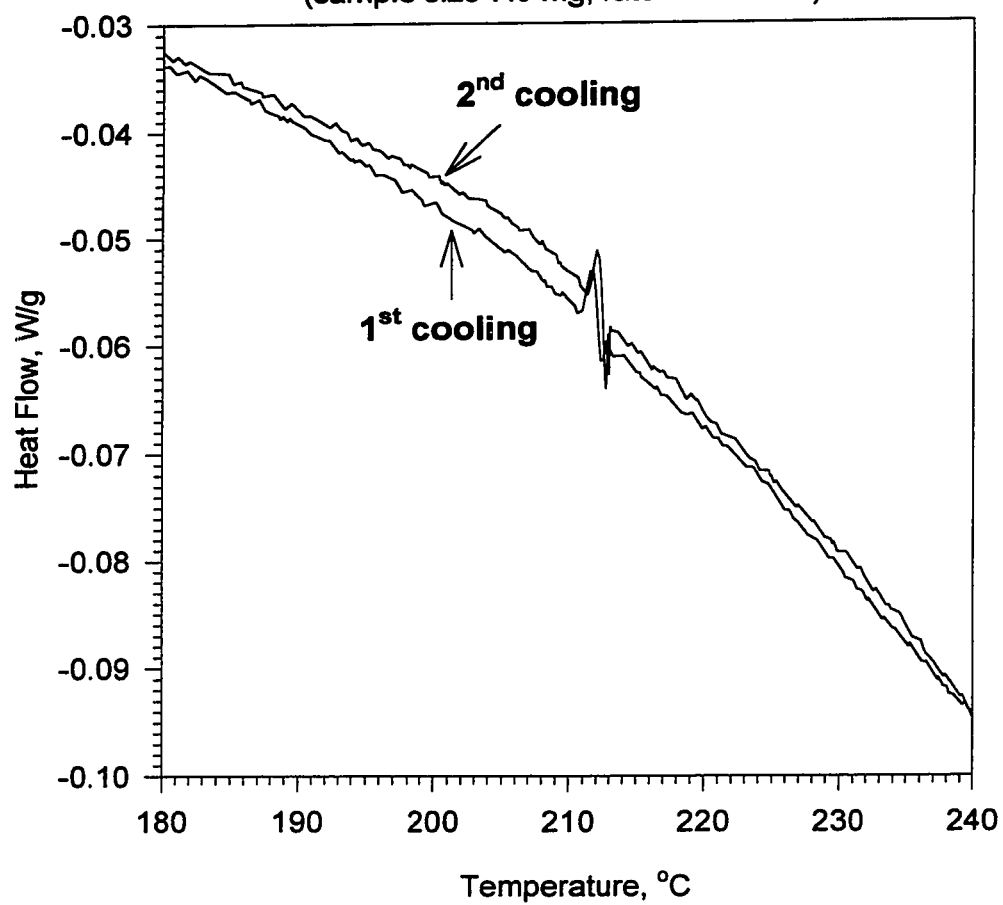
The entropy change associated with the 227°C-transition was calculated as $\Delta S_2 = \Delta H_2/T_2$ ($\Delta G_2 \cong 0$ at the transition). The entropy changes are quite small and for most PEs the second cooling cycle produced higher values of ΔH and ΔS. This could be a consequence of "annealing" which was reported for LCPs (Wissbrun et al., 1987; Done and Baird, 1987) to promote order in the liquid-state as discussed earlier in section 4-A-1-ii.

3. Interpretation of transitions

The 227°C transition was seen in most PE resins, regardless of supplier (i.e., regardless of various proprietary additives and their concentrations) and regardless of whether branching was present in the molecules. This might suggest an origin in polymethylene chemical reaction, but thermal decomposition under N_2 can be dismissed (it occurs at 345°C) and oxidative degradation seems unlikely because of the repeatability with different suppliers, amounts and types of antioxidants, differing lengths of time spent by each specimen in the DSC sample pan (due to different scan rates, and second-scan results that replicated first-scan results. Instead, we believe the collective evidence supports the view that the 227°C transition represents a LCP-like transition of some sort, meaning that ordinary polymethylene sequences (independent of length and unimpeded by occasional branches) are capable of either localized chain order or collective assembly behavior that provides other forms of ordering. Somewhat similar concepts have appeared before, though never based on DSC evidence. For example, Balta-Calleja et al. analyzed data on diamagnetic susceptibility of low-M_w paraffin melts and proposed that they possessed order akin to that of smectic liquid crystals. Kruger et al. used acoustic measurements with low-M_w PE over 130°-390°C to identify a transition in the range

220°-230°C, which they attributed to a transformation from an ordered phase (not characterized in molecular terms) to an isotropic phase.

However, we doubt that the 227°C transition represents conversion to isotropy, since the earlier rheology studies above and below the transitions showed the persistence of order above 227°C and apparently continuing to 250°C. However, transition from one type of order to some other type is common for liquid crystals.

The 208°C transition always presented a smaller DSC peak than at 227°C, which is consistent with the torque-T evidence that much sharper rheological transitions occurred at 220-230°C than at 208°C. Indeed, the latter transition was not at all abrupt in the torque-T curve, but seemed to signal the nearly smooth merger of regimes above and below 208°C. This could indicate that polymethylene chains possess substantial sequential order from solid-crystal melting point T_m (i.e., in the highly regular planar zigzag crystalline form with dominant trans bond sequences) but lose it progressively as T increases towards 208°C, the latter being a point where some "equilibrium" is established between trans and gauche isomeric states along the chain. This picture is consistent with Raman spectroscopic studies that detected strong trans-trans bond sequencing in HDPE melts at lower temperatures; the data were reported only up to 208°C, which is unlikely to be merely coincidence but remained without commentary by the authors (Wunder and Merajver, 1986). This gradual-transition molecular explanation, however, is not easy to reconcile with the appearance of 208°C peaks in DSC cooling curves (Figures 4.19, 4.21b, and A.41), though it seems consistent with the absence of 208°C peaks in DSC heating curves. The weakening of evidence for the 208°C transition in DSC cooling curves with the presence of branching to interrupt the polymethylene

sequences is compatible with increased difficulty (geometric or energetic) in achieving sequential isomeric order along the molecular backbone or any long polymethylene chain within the molecule.

The experimental investigation of order in "pure" polyethylenes, carried out in different rheological and thermal analysis devices, showed clear evidences of LCP-like behavior for linear and branched Z-N polyethylenes. The results of this investigation could be summarized as:

(a) The rheology of HDPE proves to be more complex than previously believed, especially at low shear rates where the first normal stress function appears capable of changing sign twice as γ increases, and the viscosity function exhibits a kink.

(b) Inasmuch as these rheological features had been predicted (and, in some cases, found) only for liquid-crystal polymers, we conclude that HDPE should be considered to be a special kind of LCP from a rheological and melt processing viewpoint. This may ultimately explain some of the HDPE special properties, such as unusual orientability in the melt and consequent high melt strength and subsequent superior properties in the solid state.

(c) HDPE appears to fulfill the predictions of LCP rheological theories as well as or better than polymers of acknowledged LCP molecular structure. Since those theories had received little experimental support from other sources, they must now be regarded as validated for the first time.

(d) The rheological and thermal investigations presented new evidence that confirms the existence of molecular and microstructural transitions near 208°C and 227°C in Z-N HDPE and LLDPE, and also in high-pressure LDPE. The evidence

strongly implies that PE melts are structured liquids and mimic in many ways the characteristics of LCPs.

(e) These transitions are independent of molecular weight and nearly independent of details of molecular structure (e.g., branching). This behavior is not explicitly related to various anomalies reported for UHMWPE many of which can be traced to extremely high melt viscosity, relaxation times, and segmental diffusion times, none of which prevail in the ordinary PE samples tested here.

(f) Recognition of the LCP nature of PE melts, and especially the 208°C and 227°C transition, should induce the melt processing industry to re-examine the conditions (e.g., the temperatures) at which their processes operate, in view of the potential to make those processes more effective and to optimize product quality.

Some of the work discussed in this Chapter has already been published or accepted in refereed Journals (Hussein and Williams, 1998 a & b) as well as presented (Hussein and Williams, 1998 c &d) or will be presented (Hussein and Williams, 1999) in international conferences.

V. Results: Melt Blender and Degradation of Polyethylenes

Polyethylenes are usually processed above their melting point. The potential for saving energy and increasing output because of the reduction in the melt viscosity is an incentive for processing at higher temperatures. The conditions for processing polymers, namely high temperature, the presence of oxygen, and substantial shear stresses, can cause chemical reactions to occur. Even a small extent of reaction has an enormous effect on the physical properties of the polymer (Moss and Zweifel, 1989). The buildup or breakdown of polymer chains can considerably influence the liquid and solid-state properties of the polymer.

Hence, in all studies that involve melt "conditioning" (either in an extruder or in a melt blender) care should be given to prevent degradation of polymers during the "conditioning" process. Here, a Rheocord 90 melt blender was used to prepare samples to study the miscibility of HDPE, different LLDPEs and LDPE as well as to condition the pure components. Consequently, the question of stability of all polyethylenes in the melt blender has to be answered before we proceed with the miscibility study.

The objective of this study was to make sure that the degradation of polyethylenes was prevented during the "conditioning" process. In this investigation, different techniques were employed to examine the stability of polyethylenes in the Rheocord 90 melt blender. Batch blenders (e.g., Brabenders, Rheocord 90) are widely used in polymer research laboratories, yet little consideration (in the public literature) has been given to study of the mechano-thermal degradation of polymers in these devices. On the other hand, a lot of research has focused on degradation during melt processing in extruders (as

will be discussed below). Furthermore, most of these latter degradation studies were carried out by introducing a <u>foreign</u> material (mostly peroxide initiators). Thus, the present study of the possible mechano-thermally-induced degradation in the Rheocord 90 batch melt blender has another significant advantage.

Small-strain dynamic oscillatory measurements of viscoelastic properties in the RMS as well as average molecular weight and MWD from GPC analysis were used to assess the stability of S229 (LLDPE) and S216 (LDPE) in the melt blender. The rheological and GPC analyses were supported by NMR, and DSC testing. The study covered torqued resins with and without additional antioxidants; results were compared to the properties of as-received polymers.

In this Chapter, we will introduce the degradation of polymers in general and polyethylenes in particular, followed by discussion of the results of the present degradation study. The different techniques integrate to explain: the modifications that can occur due to melt blending of polyethylenes; relation to the polymer chemistry; and the possible means for detection and prevention of degradation.

A. *Degradation of Polymers: General*

Polymers vary widely in their ability to withstand deterioration when exposed to a "degradation" environment. These differences in stability are due primarily to chemical structure, but also may be caused by impurities or residual monomers. Polymeric degradation can be caused by both reactive chemicals such as oxygen or water and by various sources of energy such as heat, UV radiation, or mechanical stress. It is well known that heat accelerates the degradation of polymers in the presence and absence of chemical reactants.

Thermal degradation of thermoplastics occurs by three primary mechanisms: random scission, depolymerization (or "unzipping"), and degradation involving thermally labile defects or "weak links". However, degradation is often a complex process involving combinations of these mechanisms. Other mechanisms are also encountered, including intramolecular cyclizations and eliminations, side group scission, intermolecular cross-linking, and radical chain transfer reactions (Chartoff, 1997).

The most common types of degradation occur through chemical reactions at the molecular level. Degradation resulting from various reactions with oxygen (especially at high temperatures) is the most important mechanism that influences the liquid and solid-state properties of the polymer. Even during processing in enclosed equipment, sufficient oxygen is still present for oxidation reactions to take place. Degradation by heat alone (thermal degradation or thermolysis) is important, however, since in a restricted-oxygen atmosphere these reactions may take place simultaneously with thermal oxidation. By definition, thermolysis of a polymer is thermal degradation in the complete absence of any external reactant (Hawkins, 1984). As energy is absorbed and distributed through the molecules, a point is reached at which the energy concentrated at one bond in the molecule exceeds its dissociation energy. Thermal degradation, however, usually results from the combined effects of thermolysis and thermal oxidation.

Most processing equipment restricts access of oxygen to the molten polymer and thermolysis may be the predominating degradation reaction during processing. However, the contribution of thermal oxidation cannot be ignored. Polymers pyrolyze by one of three general mechanisms or by combinations of two or more of these mechanisms. Random scission, which is the predominant reaction in polyolefins, occurs through

scission of carbon-carbon bonds along the backbone chain. As the term implies, scission is a random event, and polymer molecules are first broken into large macroradicals (Hawkins, 1984). There is a rapid decrease in average molecular weight (especially in M_w and M_z) and almost no monomer is formed in the early stages.

The chemical structure of hydrocarbon polymers plays an important role in autoxidation (low-temperature oxidation). This is evident in differences observed in the rates of oxidation of linear polyethylene, branched polyethylene, and polypropylene. The susceptibility to oxidation increases with the increase in the number of branch points. At those points where branching occurs in the backbone chain, hydrogen is attached to a tertiary carbon atom. The bond between carbon and the hydrogen at these branch points has a lower dissociation energy than that between hydrogen and carbons in the methylene groups along the unbranched sections of the chain. These weak hydrogens are likely points for initiation of autoxidation and consequently LLDPE is more susceptible to oxidation than linear PE (see Figure 108 of Chartoff, 1997). The extent to which hydrogen at branch sites in LDPE promotes oxidation, however, decreases at higher temperatures (Hawkins, 1984). Under these conditions, oxidation proceeds too rapidly for selective hydrogen attack to take place. These differences in resistance to autoxidation are reflected in the amounts of stabilizers required to provide protection to these polymers. In general, LDPE needs less than LLDPE under the same conditions (as we have found; to be reported in section C).

As would be expected, the rate of oxidation increases with temperature, and excessive oxidation is quite likely to occur under processing conditions - unless the polymer has been adequately stabilized. Antioxidants are but one type of stabilizer, used

primarily to inhibit thermal oxidation. Other types of stabilizers have been developed to protect polymers against photooxidation and ozone-induced degradation. The chain reaction responsible for autoxidation is initiated by free radicals, and hence reactions that deactivate or reduce the reactivity of initiating radicals will contribute to stability. Scavenging or trapping of radicals responsible for degradation is one obvious approach. Hydroperoxides are assumed to be the primary source of radicals which initiate oxidation in polymers, but various additives including stabilizers may be involved in the initiation step.

The chemical and physical properties of most commercial plastics can be improved, in some instances dramatically, by blending one or more additives into a polymer. Successful selection of an additive system for a polymer can markedly increase the resin's chances of meeting its intended design lifetime. The choice of a particular additive or additives for a resin formulation is based on knowledge of a polymer's inherent weakness and the conditions under which it will be processed and used. The concentration of additives in a polymer depends on its intended function. For instance, to inhibit thermal oxidation in polyolefins, as little as 0.05%w of an antioxidant additive may be needed (Bair, 1997).

Antioxidants for polymers are generally categorized by their mode of action during degradation. *Primary antioxidants* act through chain transfer and chain termination by trapping or deactivating radicals after they are formed. *Secondary antioxidants* prevent the formation of free radicals through nonradical decomposition of peroxides and hydroperoxides. In general, primary antioxidants can be used alone more or less successfully, whereas secondary antioxidants are used to enhance the performance

of the primary antioxidant and are hence rarely employed alone. For the best stabilization, combinations of primary and secondary antioxidants are often used. If their combined effect exceeds the sum of the effects of the individual components, the behavior is referred to as synergistic.

B. *Degradation and Stabilization of Polyethylenes: A review of literature*

Although polyethylene is a comparatively stable polymer, it is susceptible to oxidation during processing, storage, and use. The degradation of a polyolefin involves the breaking of primary chemical bonds. The mechanisms of polyethylene oxidation have been reviewed and described as free radical chain reactions (Pospíšil and Klemchuk, 1990; Pospíšil and Nešpůrek, 1995). Free radicals ($R^{\bullet}$) are formed and combine with oxygen to create peroxy radicals:

$$R^{\bullet} + O_2 \rightarrow ROO^{\bullet}. \tag{5.1}$$

These radicals can remove a hydrogen atom from another portion of the polymer to form hydroperoxide and a polymer free radical:

$$ROO^{\bullet} + RH \rightarrow ROOH + R^{\bullet}. \tag{5.2}$$

Hence, a repetitive cyclic chain reaction results with the addition of oxygen to the newly formed free radical. The hydroperoxides that have been generated along the polyethylene's backbone are unstable and decompose to form free radicals that initiate more chain reactions. Control of the peroxy-radicals and the hydroperoxide groups is the key to successful stabilization of polymers. Metal salts have been shown to cause a catastrophic acceleration of polyethylene degradation with the formation of ketonic products similar to that observed in simple hydrocarbons (Kamiya and Niki, 1978).

The oxidative degradation of polyethylene can be delayed by adding small amounts of labile-hydrogen donors such as hindered phenols or secondary aromatic amines. Hindered phenols are the most widely used primary antioxidants. They function in a sacrificial role as peroxy radical traps and are used to impart both processing and long-term stability. Hindered phenols (AH) donate an $H^\bullet$ radical to deactivate peroxy-free radicals,

$$ROO^\bullet + AH \rightarrow ROOH + A^\bullet \qquad (5.3)$$

thereby breaking the propagation step of the oxidative reaction. Ideally, the antioxidant radical ($A^\bullet$) is stable and does not react with the polymer to initiate new radicals. However, it can react with one additional polymer peroxy-radical (see Figure 14.1 of Drake, 1996a).

Sterically hindered phenols are commercially the most important class of primary antioxidants. In this study Irganox 1010 {Phenol B, tetrakis[methylene 3-(3′,5′–di-t-butylphenol) propionate]methane, M_w=1178} was used as the primary antioxidant and the phosphorous-containing compound Irgafos 168 {P-1, tris[2,4-di-t-butylphenol] phosphite, M_w=646} as the secondary antioxidant. Synergism occurs when phosphites are added to sterically hindered phenols for the melt stabilization of polyolefins. Normally, 0.1% (1000 ppm) or less of primary and secondary antioxidants are used for polyolefins (Bair, 1997).

The proper selection of the stabilizer formulation depends not only on preventing degradation during processing, but also on the final application. With recent emphasis on recycling, the stabilizer formulation must not only provide optimum service-life for the original article, but should be available for subsequent recycling applications (Drake,

1996b). The optimal composition of the stabilizer formulation depends most critically on the temperature selected for melt processing (Malik et al., 1995; Bharel et al. 1992).

The molecular weight (M_w) of most commercial thermoplastics falls between 2×10^4 and 5×10^5; however, in this range T_g and T_m are relatively insensitive to moderate changes in M_w resulting from oxidative degradation (Bair, 1997). Hence, transition measurements of partially oxidized polyolefins by DSC would not be expected to show any significant shifts in T_g or T_m. Similarly, tensile strength only shows a weak response to changes in M_w. However, tensile elongation, impact strength, and melt viscosity measurements are sensitive to degradative M_w changes.

Konar and Ghosh (1988) studied the oxidation of LDPE in the presence of permanganate using FTIR. They reported that the extents of oxidation of LDPE, as well as the nature of the oxidative degradation products vary with catalyst cation. Konar et al. (1988) observed small differences in melting peak temperature and in percentage crystallinity of LDPE and degraded LDPE. They concluded that permanganate-oxidized LDPEs do not undergo a random scission type of degradation when heated in the temperature range from ambient to 450°C. Instead, both chain cleavage and molecular enlargement reactions occur.

Ghosh et al. (1997) investigated the effect of dicumyl peroxide (DCP) action on polymer structure, melt rheology and relaxation behavior in reactive melt processing of LDPE in a Brabender (170°C, 50 rpm, 25 min). They observed enhancement of the melt viscosity (pseudoplastic flow behavior) as a result of mild cross-linking in LDPE due to peroxide action. The melts of LDPE and modified LDPE (oxidized) both showed pseudoplastic flow behavior (Ghosh et al. 1997; Ghosh and Dev, 1998). However, before

the strongly shear-thinning behavior commenced with increasing shear, the moderately low-shear viscosity was greater in the presence of the higher dose of DCP (greater by 50% to > 400%). This larger magnitude of $\eta(\dot{\gamma})$ was observed to be less pronounced at higher rates of shear, where the two $\eta(\dot{\gamma})$ curves were almost coinciding. This could indicate that the oxidation produced large aggregates of PE molecules (leading to enhanced viscosity at low shear). Such gel-like aggregates might disassemble and be separated into their component molecules at high ω, however, making the gelled systems and non-gelled systems to have very similar $\eta(\dot{\gamma})$ in the high-ω regime. However, no firm evidence of other sorts is available to support this speculation.

Similarly, Hinsken et al. (1991) examined the thermo-oxidative and thermo-mechanical stability of HDPE (Cr-catalyst technology) using multiple extrusions. They used GPC, MI, and FTIR to investigate the degradation process. Depending on the type of polymer and even the catalyst used to produce it, HDPE may undergo many radical reactions; chain scission and chain branching leading to cross-linking are generally favored. Moreover, heterogeneity of oxidation was observed in photo-oxidized γ-irradiated LLDPE films, which may result from, for example, limited oxygen diffusion or non-uniform initiation (Lacoste, 1995). Furthermore, the oxidation of HDPE and LDPE melts was studied by Egorenkov et al. (1975) who found that the oxidation rate depends on the nature of the metal (and metal-containing compounds) with which they had been in contact. The metals used in their study were classified as high-activity (Cu, Pb, Ag, Zn) and low-activity metals (Al, Au).

There are certain difficulties in studying the kinetics of degradation during polymer processing. This is due to the short period during which the polymer is in the

extruder and the non-uniform distribution of temperature and the mechanical stress on the polymer melt which are major sources of initiation of chemical reaction. El'darov et al. (1986) studied the kinetics changes during the extrusion of polyethylene by measuring the MI and M_w. They observed that in the presence of the stabilizer Ionol, the M_w decreases at a constant rate, while in the absence of the stabilizer the M_w of linear PE either increases or decreases depending on the oxygen content of the processing environment. Oxygen performs a double function: it increases the rate of radical initiation due to hydroperoxide decomposition and affects the competition between M_w degradation and cross-linking in the secondary reactions of the radicals. They attributed the slow increase in M_w, observed in extrusion experiments carried out under nitrogen, to secondary reactions of free radicals formed only as a result of mechano-chemical initiation.

The results for different studies of polymer reactive extrusion may appear to conflict if the effects due to different flow geometry are not taken into account. In a single-screw extruder the extent of reaction increases with increasing screw rotation rates while in a counter-rotating twin-screw extruder, the extent of reaction does not vary monotonically with screw rotation rates (Polance and Jayaraman, 1995). Polance and Jayaraman studied the reactive extrusion of LLDPE and LDPE in a co-rotating twin-screw extruder. They reported that LLDPE is significantly more reactive than the LDPE. They attributed this observation to the high concentration of tertiary carbons in LLDPE. Their shear viscosity measurements showed an order of magnitude increase at low shear rates but much less at higher rates. [i.e., η_0 is more sensitive to M_w and MWD than is the shear-thinning $\eta(\dot{\gamma})$].

Bremner and Rudin (1990) investigated the modification of HDPE by reaction with various levels of the free radical initiator DCP. The peroxide action was found to broaden the MWD, especially towards the higher molecular weight end (strongly affecting M_w and M_z). The low molecular weight end of the MWD, which affects mainly M_n, remained virtually unchanged at all temperatures (180°-200°C). An increase in the M_w and M_z with increasing temperature was observed in the range 180°-200°C suggesting an intermolecular coupling. At higher temperatures (225°-250°C), M_w and M_z decreased with increasing temperature. The long chain branching and crystallinity of HDPE oxidized at 180°C were observed to drop continuously with increasing concentrations of peroxide.

The rheological data of Wasserman and Foster (1996) indicated an increase in viscosity magnitude of unstabilized LLDPE base resin. Flow activation energy increased dramatically with the degree of processing. Similar trends were apparent in the extensional viscosity, as well as other simple flow parameters. The increase in the level of branching in the polymer system was reflected in an increase in the breadth of the relaxation time distribution.

Moss and Zweifel (1989) studied the thermo-oxidative degradation of HDPE using multiple extrusions. Unstabilized Phillips HDPE (Cr-catalyst) showed a tendency towards cross-linking whereas unstabilized Ziegler-type HDPE (Ti-catalyst) favored chain scission. The MWD and polydispersity of the polymers changed during processing. Vinyl group ($CH_2=CH-$) reactions were found primarily responsible for the increase in molecular weight as suggested by the FTIR measurements.

However, before I proceed with the investigation of degradation in the batch melt blender, I would like to show that our results were not influenced by the presence of other additives in the polymer (like the polymer processing aid).

The effect of the polymer processing aid (ppa) on rheological properties was investigated. Two hexene LLDPEs (ρ=0.918; MI=1) with (S213) and without (S214) ppa (FX 9613, 1000 ppm) were used as model PEs. The two polymers were "conditioned" by torquing for 12 minutes at 180°C and 50 rpm. Dynamic oscillatory and steady shear testing was carried out at 190°C and 230°C using PP geometry. Excellent match of dynamic (η'; η'') as well as steady shear (η; N_1-N_2) measurements was obtained for S213 (with ppa) and S214 (w/o ppa). The excellent reproducibility of data (obtained on a fresh sample of the same resin) suggested no influence of ppa on rheological measurements. Results are given in Appendix B (Figures B.1 to B.8). [In Figure B.5 the normal force data collected at $\dot{\gamma} \leq 0.06$ s^{-1} were below the nominal sensitivity limit of the transducer (most of the data were equivalent to $\approx$ 1 g while the sensitivity limit is 2 g). However, the excellent reproducibility of the data suggests validity of anomalous normal stress behavior of LLDPE (akin to that of HDPEs). The ppa obviously was not responsible. Likewise, the normal force data in Figure B.8 for $\dot{\gamma}$ <0.2 were under 2 g, but the same anomalous trends noted earlier appear here too, and there is no significant difference between the ppa case and no ppa case. The N_1-N_2 maximum at $\dot{\gamma}$=2 s^{-1} is due to hydrodynamic instabilities at "high" $\dot{\gamma}$ (observed visually), as we saw earlier with PS. Note; $\eta(\dot{\gamma})$ also is taking a "nosedive" in the $\dot{\gamma}$-regime. It is still not a ppa effect].

The above rheological measurements were supported by DSC analysis carried out on specimens prepared from "conditioned" samples of the two polymers (with and w/o

ppa). Two heating/ cooling cycles were employed at 5°C/min. The DSC results (see Appendix B, Figures B.9 to B. 12) indicated agreement of melting and crystallization peaks as well as crystallinity (calculated from the second melting) for S213 (with ppa) and S214 (w/o ppa). Hence, it was concluded that under the above-mentioned conditions the ppa has <u>no</u> influence on rheological and thermal properties.

In another DSC study, the effect of AO was examined by using Dowlex 2045 (LLDPE) as model PEs. Stabilized (Dowlex 2045AC) and unstabilized (Dowlex 2045) resins were heated in air at a rate of 10°C/min. The melting peak (T_m), onset of oxidation (T_{oo}) and oxidation peak (T_{op}) temperatures as well as the crystallinity of the two polymers are displayed on Figures B.13 and B.14. The T_{oo} and the T_{op} for the stabilized polymer were increased by 14°C over that of the unstabilized resin (with little influence on crystallinity) <u>without</u> affecting the melting peak.

The influence of the blender "conditioning" process on the possible degradation of polyethylene was studied using model polymers. Q-HDPE was used as an example for linear polyethylenes. S229 (LLDPE) and S216 (LDPE) were chosen for a thorough investigation taking into consideration their higher susceptibility to degradation (Chartoff, 1997; Hawkins, 1984). The objective was to prevent structural modifications (chain buildup or breakdown) that could influence the pair miscibility (Chapter VI) interpretations.

Most of the commercial HDPEs studied in this research either were used in the as-received form or shown to be stable (as discussed in the previous Chapter). Hence, the study of their degradation was limited to rheological characterization. Temperature sweep (160°-260°C) testing on Q-HDPE in the RMS showed (see Figure B.15) the agreement of

η*(T) measurements for as-received and torqued resin (with and w/o AO). Hence, it was considered that melt "conditioning" in the blender imparts no structural modifications on commercial HDPEs. This further confirms the known stability of the linear PE (Chartoff, 1997; Hawkins, 1984). The results for LLDPE and LDPE will be discussed below.

Furthermore, to check for the reproducibility of the HDPE torque data (discussed in Chapter IV) in the presence of additional 1000 ppm AO, the following experiment was performed. Nova S221 (HDPE) was torqued for 23 minutes at 50 rpm with the temperature ramped from 160°C to 260°C. Samples from three different batches were analyzed by HPLC for residual AO at the end of the torquing experiment. Results (see Table 5.1) showed the presence of 93% active AO demonstrating that the AO had not been "used up" (by oxidation), which would have left the resin unprotected. Although this experiment has helped testing the reproducibility of torque data (as discussed earlier), its other important significance is to indicate that the AO is essentially not used regardless of the high T (average T=210°C) and residence time (23 minutes). This analysis suggests the stability of HDPEs during melt "conditioning" particularly when performed at lower temperatures and for shorter times (i.e., the standard blending conditions of 190°C and 10 minutes in our case).

Table 5.1: HPLC analysis for residual AO in Nova S221 (HDPE) after torquing for 23 minutes with T=160°-260°C

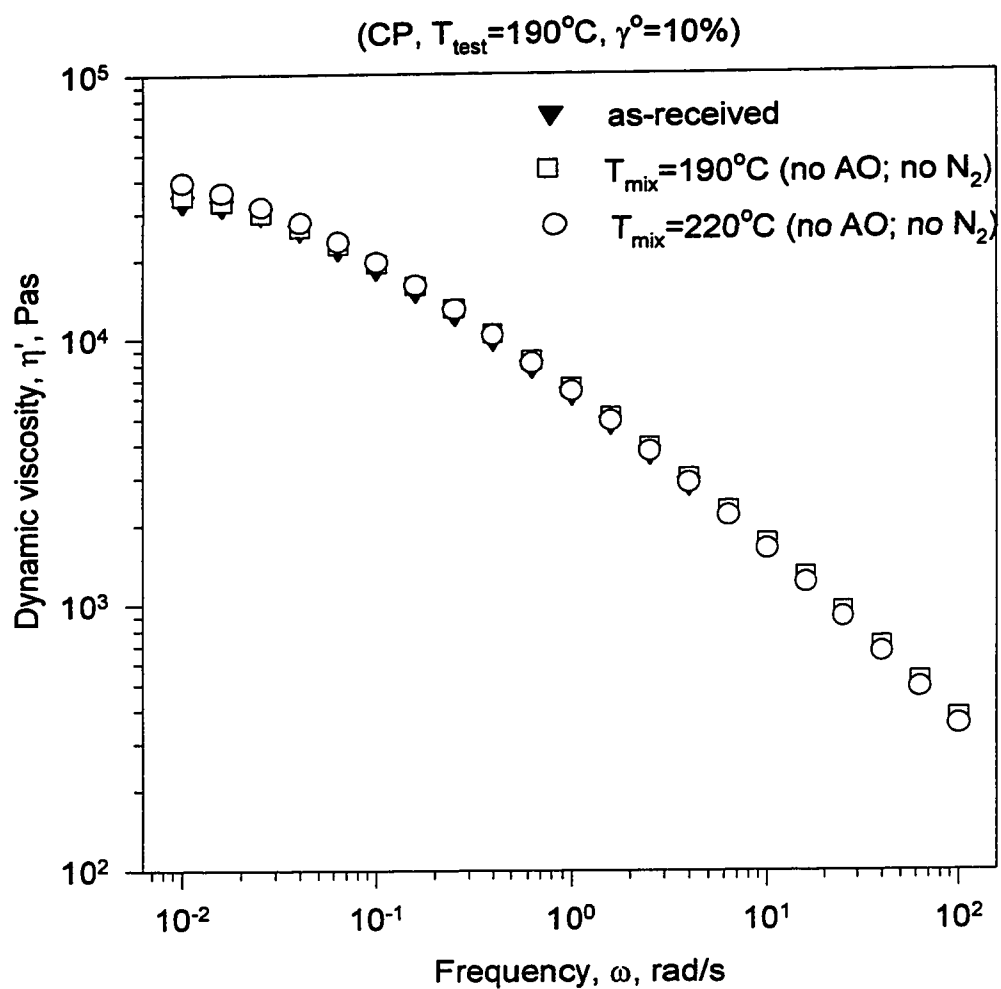| Batch #	Active Primary AO (ppm)	Active Secondary AO (ppm)	Degraded Secondary AO (ppm)	Total active AO ×100% (Total active+Degraded) AO
1	2408	2412	356	93.1
2	2485	2474	345	93.5
3	2508	2525	347	93.6

The resins used in this study were torqued in the Rheocord 90 melt blender at 50 rpm for 10 minutes. The influence of the blender mixing temperature (T_{mix}) on the degradation was investigated at 190°C and 220°C. The effect of antioxidant (AO) on degradation was examined by mixing the polymer(s) with and without (w/o) the AO. The "conditioned" samples were then air-cooled and characterized by different techniques. The as-received resins were used in this study as <u>control</u> samples.

Different techniques were used to study the possible degradation of S229 (LLDPE) and S216 (LDPE). Melt rheology was utilized to investigate viscoelastic properties before and after mixing with and without additional antioxidants. Further support was obtained from ^{13}C-NMR where the influence of mixing conditions on branch density of LLDPE was examined. Furthermore, DSC was employed in seeking differences between additionally stabilized and commercial resins. The results of all of these measurements will be discussed in the above-mentioned order.

C. Rheological Measurements

The RMS was used to examine the degradation of LLDPE and LDPE that might have occurred in the melt blender. Small-strain frequency (ω) sweep testing (0.01-100 rad/s) was employed to avoid any modifications that could result from the large strains inherent in steady shear. All tests were carried out using the cone-and-plate (CP) test geometry and strain amplitude (γ^{o}) of 10% was selected following γ^{o}-sweep test. Most of the tests were performed at 190°C. The two polymers examined were S229 (LLDPE) and S216 (LDPE).

Figure 5.1 displays the ω-sweep test results for S216 (LDPE) torqued at 190° and 220°C without AO. Only at very low ω is there a tendency for the case of T_{mix}=220°C to
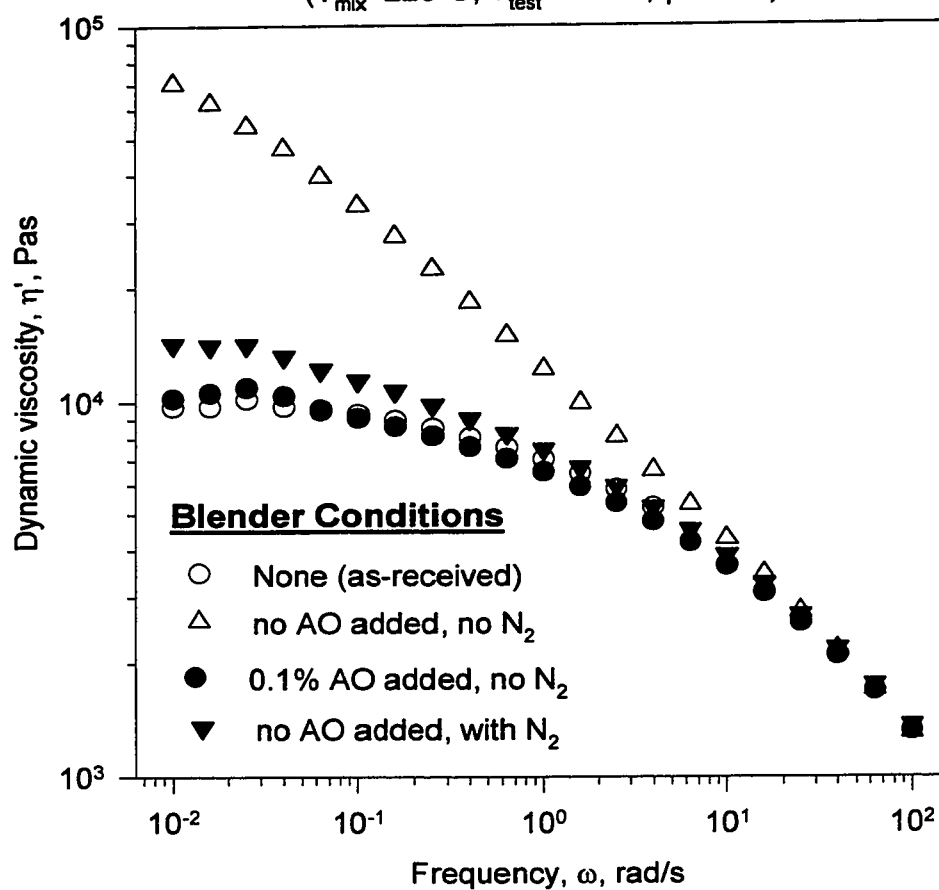
Figure 5.1 Effect of T_{mix} on η' for S216 (LDPE)

(CP, T_{test}=190°C, $\gamma°$=10%)

Legend:
- ▼ as-received
- □ T_{mix}=190°C (no AO; no N_2)
- ○ T_{mix}=220°C (no AO; no N_2)

X-axis: Frequency, ω, rad/s

Y-axis: Dynamic viscosity, η', Pas

show $\eta'(\omega)$ exceeding slightly the case of $T_{mix}=190^{\circ}C$. Results for the as-received resin are shown as well. The dynamic viscosity measurements, $\eta'(\omega)$, showed excellent agreement between results obtained at 190° or $220^{\circ}C$ and that of the as-received resin, suggesting no influence of the "conditioning" process on the LDPE. These results suggest that LDPE (made by high-pressure free radical polymerization) was very stable and did not undergo degradation despite the fact that it contained no AO. To check the reproducibility of the data, the ω-sweep test was repeated on a sample prepared in Calgary by Dr. Kam Ho of Nova Chemicals. Excellent agreement, if not exact results, was obtained (see Appendix, Figure B.16).

The rheological characterization of S229 (LLDPE) was examined after torquing under different blender conditions. The blender conditions included the use of added AO (1000 ppm) in the absence of N_2 as well as under a N_2 blanket without adding extra AO (indicated in the following Figures as "no AO"). Results for S229 mixed at $220^{\circ}C$ in the presence of extra AO and under N_2 blanket are displayed in Figure 5.2a as $\eta'(\omega)$. The $\eta'(\omega)$ curve for the "control" sample showed a Newtonian behavior at low ω with $\eta_0\sim10^4$ Pas. Measurements obtained for the resin torqued in the absence of both extra AO and N_2 blanket (the norm in melt blending) showed enhancement of viscosity at low ω by up to a factor of 7 over the range $\omega=0.01$ to ~10 rad/s without showing a Newtonian limit at low ω. For high ω (10 to 100 rad/s), the curve matched that of the as-received resin. On the other hand, measurements obtained for S229 torqued under N_2 blanket in the absence of added AO showed less enhancement in viscosity ($\eta_0\sim1.4*10^4$ Pas) but did not eliminate degradation. Results obtained in the presence of AO without using N_2 agreed with the as-received measurements over the whole ω-range. The effect of T_{mix} was examined by

Figure 5.2a Effect of blender conditions on η' for S229 (LLDPE)

$(T_{mix}=220°C, T_{test}=190°C, \gamma°=10\%)$

Blender Conditions

○ None (as-received)

△ no AO added, no N_2

● 0.1% AO added, no N_2

▼ no AO added, with N_2

comparing $\eta'(\omega)$ for S229 torqued, in the absence of both AO and N_2, at 190°C and 220°C. Results that show the effect of T_{mix} as well as reproducibility of data are given in the Appendix (Figure B.17).

An attempt was made to resolve the effects of heat and torque on the oxidative degradation of S229 (LLDPE). The as-received polymer was placed in a preheated oven for 10 minutes at 220°C (same time and T as the melt blender). Rheological characterization of the "statically" heated samples showed (Figure 5.2b) essentially the same $\eta'(\omega)$ and $G'(\omega)$ as the as-received resin. This result suggests the significance of the combined effect of stress and heat in the melt blender on the degradation process.

The adequacy of the amount of the AO was checked by mixing S229 with an extra 2000 ppm of AO at 190° and 220°C. $\eta'(\omega)$ curves for different levels of AO and different mixing temperatures are shown in Figure 5.3. The $\eta'(\omega)$ curve obtained for samples mixed with 1000 ppm of AO showed a close match of the as-received data. Data obtained for the 2000-ppm case (at low ω) were lower than those of the as-received sample, which could be a direct result of the low M_w of the AO. This shows that 1000 ppm of AO was adequate to prevent polymer degradation.

The above observations of degradation in S229 (butene) motivated the investigation of another LLDPE. This time S237 (hexene) was used. Results on $\eta'(\omega)$ for S237 samples mixed with and w/o AO at different temperatures are given in Figure 5.4a. A behavior similar to that of S229 was obtained. Again, $\eta'(\omega)$ for the resin with 1000 ppm additional AO matched that of the as-received sample. The torquing at 190° and 220°C in the absence of extra AO resulted in enhancement of viscosity at low ω, and the higher the temperature the higher the increase in $\eta'(\omega)$. The validity of some of the

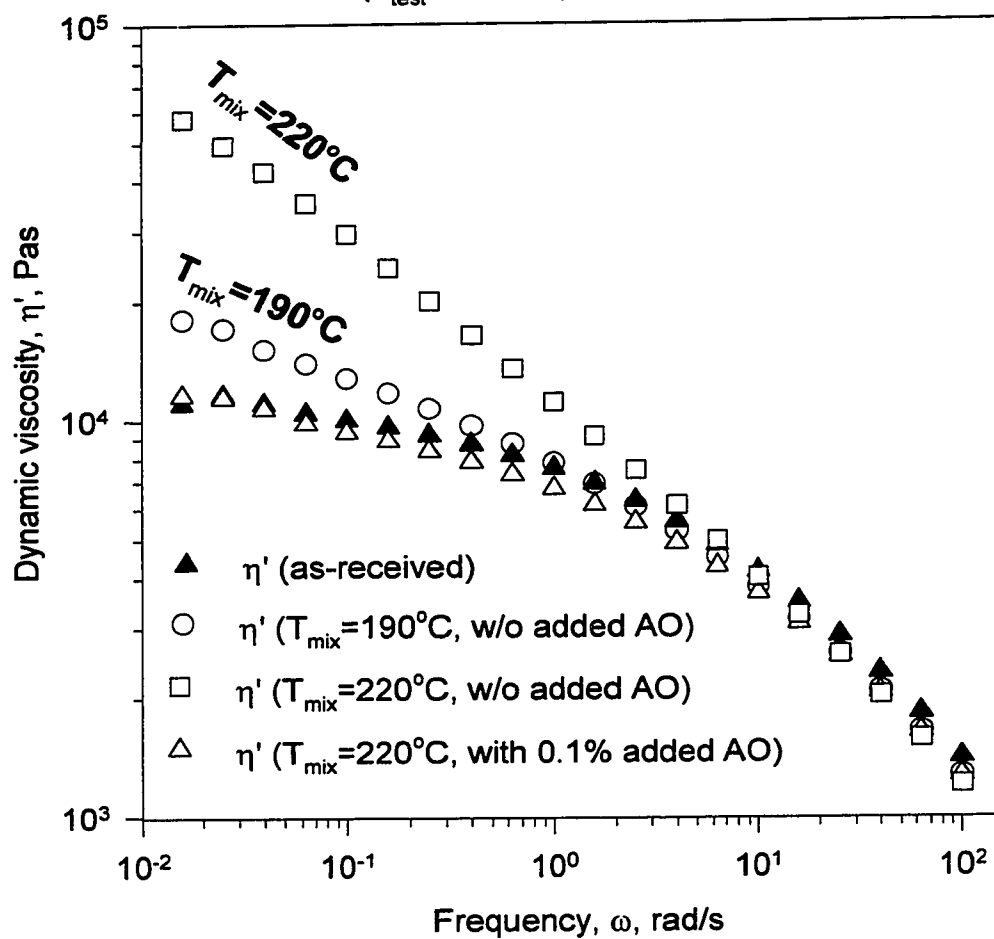Figure 5.2b $\eta'(\omega)$ and $G'(\omega)$ for as-received and statically heated S229 (LLDPE)
(CP, T_{test}=190°C, $\gamma°$=10%)
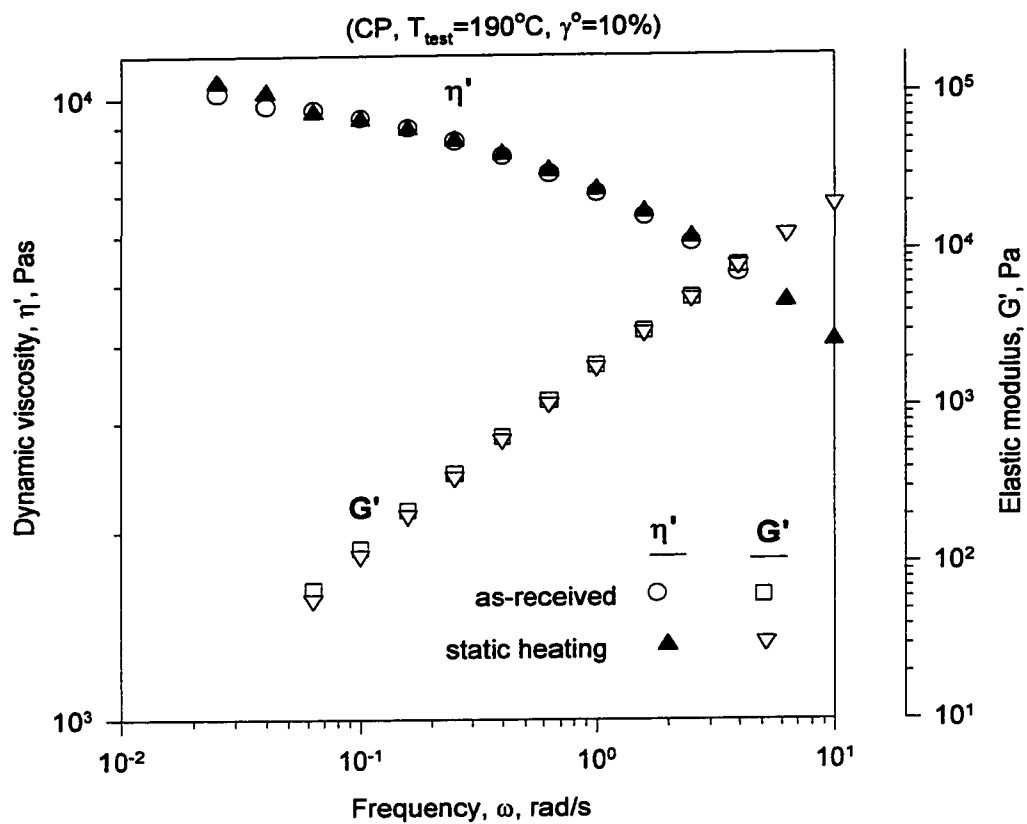
Figure 5.3 Effect of AO level on η' for S229
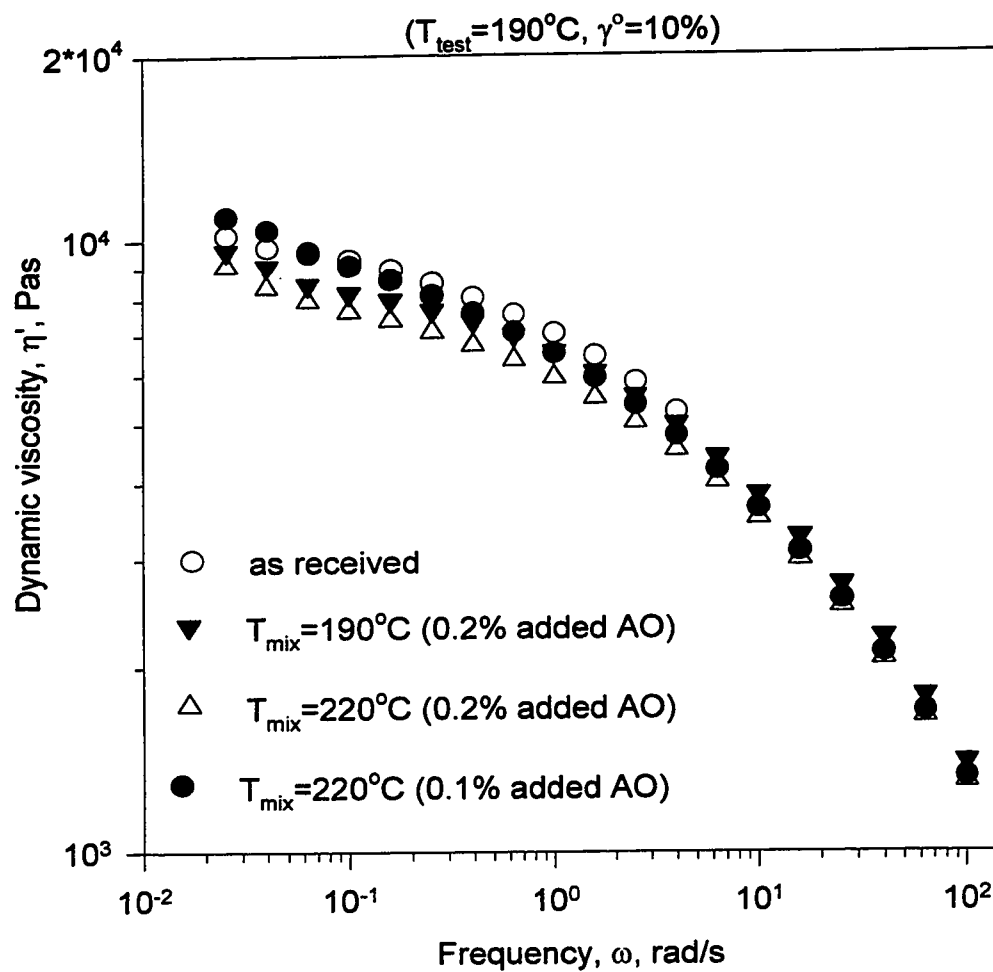
Figure 5.4a Effect of AO and T_{mix} on η'
for S237 (LLDPE)

$(T_{test}=190°C, \gamma°=10\%, C\&P)$

$T_{mix}=220°C$

$T_{mix}=190°C$

- ▲ η' (as-received)
- ○ η' ($T_{mix}=190°C$, w/o added AO)
- □ η' ($T_{mix}=220°C$, w/o added AO)
- △ η' ($T_{mix}=220°C$, with 0.1% added AO)

Dynamic viscosity, η', Pas

Frequency, ω, rad/s

presented data was checked by running a steady shear test on as-received samples of S237. Results that show the excellent match of $\eta(\dot{\gamma})$ and $\eta'(\omega)$ [Cox-Merz rule] for as-received resin at low $\dot{\gamma}$ (or ω) are given in the Appendix (Figure B.18).

The enhancement of the viscosity of S237 (hexene) at 190°C relative to the as-received resin was less than that of S229 (butene), at the same temperature, by a factor of ~5/2. If the two polymers were prepared under similar conditions and had the same original dose of extra AO, then these differences could be related to post reactor processing or possible differences in susceptibility to oxidation with different branch types. Nevertheless, for both LLDPEs 1000 ppm of extra AO had to be added to prevent degradation.

The rheological investigation of degradation in LLDPEs was then extended to the Exxon metallocene. Results of $\eta'(\omega)$ are shown in Figure 5.4b for the metallocene resin obtained after torquing the polymer at 190°C without extra AO and at 220°C in the presence of 1000 ppm of extra AO. The measurements indicated a significant enhancement in the low-ω viscosity over that of the as-received polymer, with less difference in the high-ω regime. The low-ω viscosity of the metallocene resin (torqued at 190°C without extra AO) has increased by a factor of ~15, while that obtained for the Z-N LLDPE (S229) (at the same conditions) increased by a factor of ~ 5 (Figures 5.2a and B.17) by comparison to the as-received resins. Furthermore, the addition of 1000 ppm of AO to the metallocene polymer did not prevent degradation as it did with the Z-N resins (S229 and S237). Possible explanations for the substantial enhancement of the low-ω viscosity are:

Figure 5.4b Effect of blender conditions on η' for Exxon (LLDPE) metallocene resin

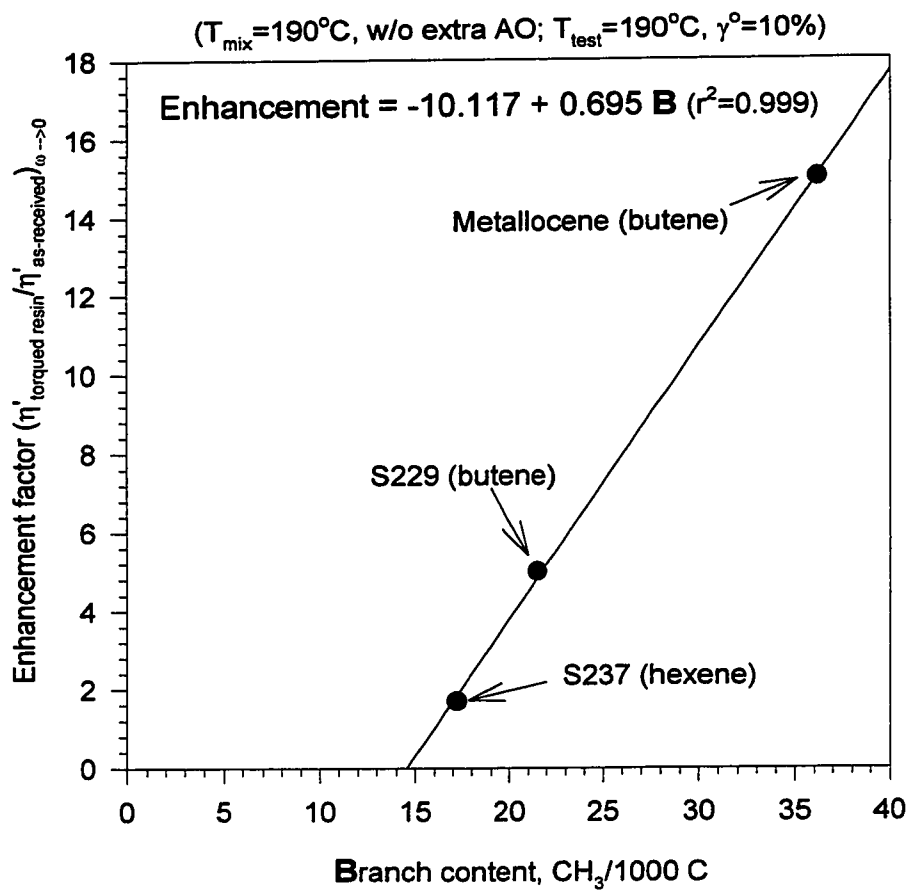$(T_{test}=190°C, \gamma°=10\%, \omega=0.01\text{-}100\ rad/s)$
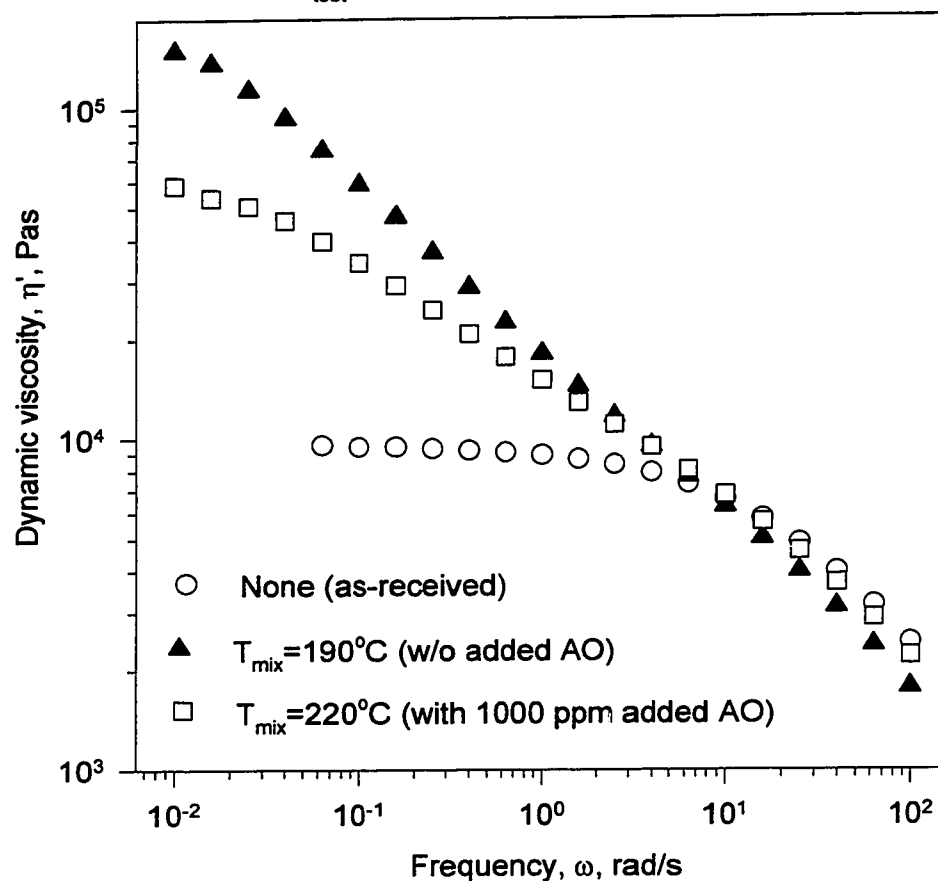
1. The high branch content of the metallocene resin (36.2) compared to Z-N S237 (17.2) and S229 (21.5) is indicated in Figure 5.4c [Enhancement factor = $(\eta'_{torqued\ resin}/\eta'_{as-received})_{\omega\to 0}$]. Previous reports (Chartoff, 1997; Hawkins, 1984) suggested the increase in susceptibility of LLDPEs to degradation with increased branching.

2. The different metal residues in Z-N and metallocene resins could result in different influences on the degree of degradation.

It is clear that torquing under standard conditions (i.e. no additional AO and no N_2) can lead to a substantial increase in viscosity at low ω as shown for LLDPEs, both alone and during blending with LDPE. Low-ω data were usually used to assess the miscibility of polymer blends. Therefore, the "conditioning" process that took place by torquing in the melt blender can strongly influence the interpretations of blend miscibility data if adequate amount of extra AO is not added.

The enhancement of viscosity at low shear was observed when LLDPEs (S229 and S237 and metallocene resins) were torqued without adding extra AO. It was also observed that the enhancement was less at high frequencies. Similar observations were reported for LLDPE and LDPE and their blends (Abraham et al., 1998; Ghosh et al., 1997) where degradation was induced by reactive processing (adding peroxides) and cross-linking was assumed to take place. Hinsken et al. (1991) suggested that the increase in MI (because of multiple extrusions) of HDPE (Cr-catalyst) might be caused by chain branching and cross-linking. Their interpretations were supported by GPC and FTIR analysis. In general, the enhancement of viscosity or the decrease in MI were caused by cross-linking (Ghosh et al., 1997; Hinsken et al., 1991; Moss and Zweifel, 1989; Polance

Figure 5.4c Enhancement of low-ω viscosity for Z-N and metallocene LLDPEs

(T_{mix}=190°C, w/o extra AO; T_{test}=190°C, γ°=10%)

Enhancement = -10.117 + 0.695 B (r^2=0.999)

Metallocene (butene)

S229 (butene)

S237 (hexene)

Branch content, CH_3/1000 C

and Jayaraman, 1995). Moss and Zweifel (1989) indicated that a few cross-links could lead to gelation, which can considerably influence the properties of the polymer.

In the current study, no foreign material was added and the mixing device was different than in the previous studies, however, similar behavior was obtained. The enhancement of viscosity at low shear rate could result from:

1. Cross-linking (chain buildup) which would lead to increase in branching or molecular weight, and hence an increase in viscosity. However, this kind of "permanent" chemical reaction cannot explain why $\eta'(\omega)$ for cross-linked molecules match that of as-received resin. OR

2. Gel-like aggregates of PE molecules produced by oxidation (pre-cross-linked structure) that disassemble at high ω making the gelled systems have $\eta'(\omega)$ very similar to that of the as-received polymer.

The above rheological characterization revealed the structural modifications that can occur in LLDPEs due to the conditioning in the melt blender. It was also observed that the higher the temperature the higher the increase in the low-shear viscosity signaling the influence of chemical reactions. In addition, rheology has shown that the addition of 1000 ppm of AO prevented the degradation from taking place.

In section D, NMR and DSC results will be shown that reproduce the same trends predicted by the rheological characterization. The reasons behind the low-shear enhancement of viscosity will be discussed in light of the NMR and GPC analysis (sections D and E). In section F we will try to address the question of what could happen if the usual practice of not adding antioxidants was followed.

D. *NMR and DSC Analysis*

1. NMR Results

The NMR analysis for S229 (LLDPE) was carried out by Nova Chemicals in Calgary. The as-received resin was torqued in the melt blender under different temperatures (190° and 220°C) with and without AO. Five such "conditioned" samples were analyzed for branch content and compared to as-received resin. The six NMR spectra are shown in the Appendix (Figures B.19 to B.24). The branch content for the six samples is given in Table 5.2 below.

Table 5.2: NMR Characterization of S229 (LLDPE)

Blender Conditions	Branch Content (CH$_3$/ 1000 C)	Spectrum
none (as-received)	21.5	Figure B.19
torqued at 190°C with added 1000 ppm of added AO	21.9	Figure B.20
torqued at 190°C w/o added AO	17.8	Figure B.21
torqued at 220°C w/o added AO	16.6	Figure B.22
torqued at 220°C with 2000 ppm of added AO	19.9	Figure B.23
torqued at 220°C with 1000 ppm of added AO	18.8	Figure B.24

Table 5.2 shows no difference in branch content between the as-received resin (21.5) and that mixed at 190°C in the presence of extra 1000 ppm of AO (21.9), indicating no modifications in the structure of the LLDPE. On the other hand, samples mixed at the same temperature (190°C) but without additional AO, suffered a loss of branches (branch content 17.8). The loss of branches at 220°C without extra AO was higher (content 16.6) than that at 190°C, suggesting the sensitivity to temperature of the

reactions that lead to the loss of branches. The effect of mixing temperature and added AO on NMR data followed the same previous trend of the rheological characterization. First, in both cases the degradation (loss of branches) at 190°C was prevented by adding 1000 ppm of AO. Second, the low-ω viscosities as well as the loss of branches increased with increasing mixing temperature.

Samples mixed at 220°C in the presence of 1000 and 2000 ppm of AO showed less loss of branches (content 18.8 and 19.9, respectively) than that mixed w/o additional AO (content 16.6). Higher amounts of AO resulted in lesser loss of branches and hence a better protection against degradation. However, the addition of 2000 ppm of AO did not eliminate the loss of branches at 220°C. A possible explanation for this observation is the partial loss of the low M_w AO by volatilization (Bair, 1997; Drake, 1996).

Under these mixing conditions stress, residual Z-N metals in the polymer, and heat act to initiate (in the absence of AO) free radicals that attack the H-C bond on the tertiary carbon atoms in Z-N LLDPE and possibly form ethylene through intramolecular or intermolecular hydrogen transfer reactions (Nyden et al., 1992). The NMR analysis has also shown that the frequency of long chain branches in all samples after torquing was < 1 branch/1000 C, indicating little or no cross-linking on the side groups. Hence, NMR analysis shows little or no support for growth of long-chain branching during torquing. Therefore, the NMR and the high-ω rheology data could be a result of a development of degradation products into a pre-cross-linked structure, or a formation of gel-like systems due to light cross-linking.

The stability of LDPE under similar conditions can be explained by the absence of Z-N metals, since Z-N catalysis is not used in polymerization. However, this opens the

possibility that LDPE might degrade in those blends wherein it is mixed with LLDPE components containing Z-N metals.

2. DSC Results

The DSC analysis was carried out after torquing samples of S229 (190°C) and S216 (220°C), with and w/o added AO. In both cases, results were compared to that of the as-received resin. All samples were heated in the DSC under N_2 from 30° to 160°C at a scan rate of 10°C/min. DSC data were analyzed for possible differences in the melting peak (T_m) and the weight fraction crystallinity (X_c). Results for as-received S229 (LLDPE) and S216 (LDPE) are displayed in the Appendix (Figures B.25 and B.26). DSC curves for S216 torqued with and w/o added AO are shown in the Figures B.27 and B.28 respectively. A comparison of S229 (LLDPE) torqued with and w/o additional AO is given in Figure 5.5.

The summary of T_m and X_c for both polymers is given in Table 5.2. It is important to note that our previous oxidation experiments on Dowlex 2045 (LLDPE) stabilized and unstabilized resin indicated (Figures B.13 and B.14) that added AO had some influence on X_c but not T_m.

Table 5.3 suggests no change in the melting peak of S216 due to torquing with or w/o added AO and the values of T_m were very close to that of the as-received resin ($\Delta \leq 0.5^\circ$C). This result indicates the stability of the LDPE and supports the previous rheology data. Similar behavior was obtained in comparison of the T_m between the as-received LLDPE and that torqued with additional AO ($\Delta = 0.2^\circ$C).

On the other hand, the melting peak of LLDPE torqued w/o additional AO showed an increase of T_m (to 124.1°C). Similar increases in T_m were reported by Konar et

Figure 5.5 DSC melting curve for S229 (LLDPE) with and w/o added AO

(T_{mix}=190°C; sample size=5.6 mg, heating rate=10°C/min)
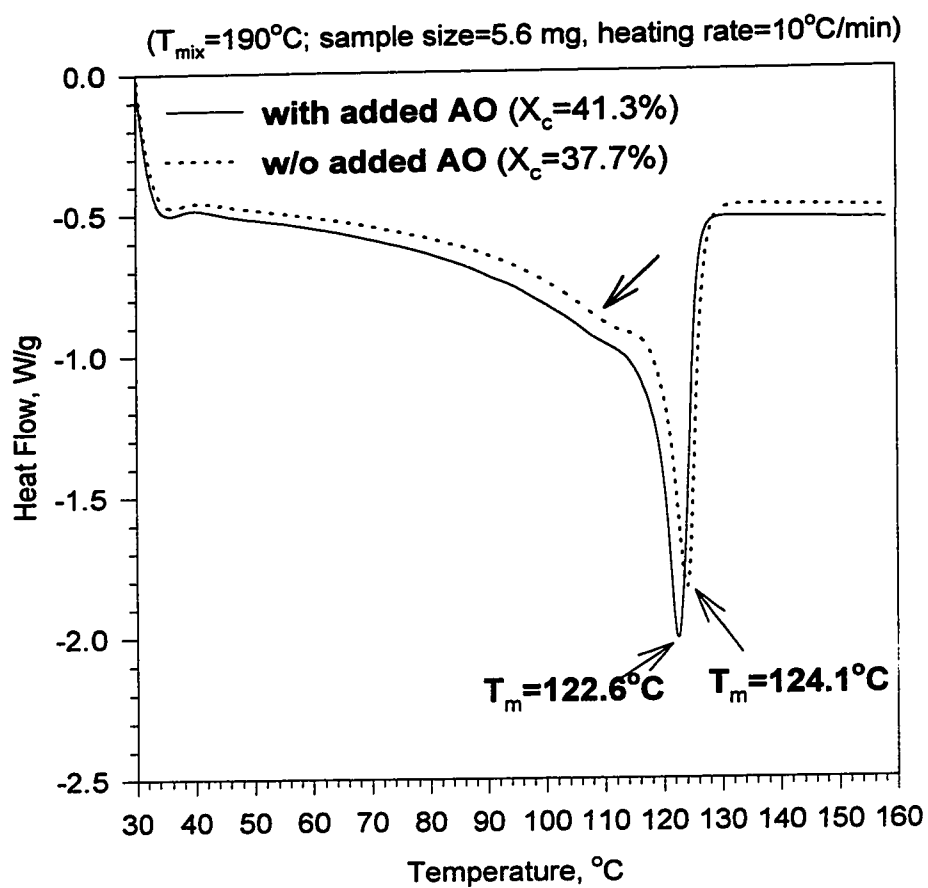
al. (1988) for chemically degraded LDPE. The increase in T_m of degraded LLDPE could be explained by the possible increase in the lamellae thickness, L, (as shown in equation 5.4) that results from the loss of the branches (NMR data) or the formation of gel-like systems that melt at high temperatures. The loss of branches leads to more linearity in the molecule and hence increased T_m and X_c (Chartoff, 1977). An empirical fit to $T_m(L)$ data has been given by Wunderlich (1997, Figure 59):

$$T_m(K) = 414.2 \left[1 - 0.627/L \text{ (nm)} \right] \tag{5.4}$$

Table 5.3: DSC Characterization of S216 (LDPE) and S229 (LLDPE)

Blender Conditions	T_m, °C	X_c, %	DSC curve
S216: none (as-received)	110.1	41.0	Figure B.26
S216: with 1000 ppm of added AO	109.6	40.0	Figure B.27
S216: w/o added AO	109.7	38.0	Figure B.28
S229: none (as-received)	122.8	39.7	Figure B.25
S229: with 1000 ppm of added AO	122.6	41.3	Figure 5.5
S229: w/o added AO	124.1	37.7	Figure 5.5

In general, the DSC results on T_m support the previous rheology and NMR data with regard to the stability of the LDPE and the degradation of the LLDPE when torqued in the absence of additional AO. Again, the degradation of LLDPE was prevented by the addition of 1000 ppm of AO as shown by the rheology, NMR and DSC data.

The changes in crystallinity (Table 5.3) could be due to the influence of the AO (as discussed earlier) or the long- chain branching. The percent crystallinity is anticipated

to _increase_ in branched polymers if the branches are getting longer (Konar et al., 1988; see Figure 60 of Chartoff, 1997). However, in our case X_c was observed to _decrease_ and a "shoulder" in the DSC curve was more visible (see Figure 5.5) in S229 torqued w/o additional AO. The arise of the shoulder indicates the presence of a different molecular structure such as gel-like aggregates. This observation could be used to support the NMR data that suggested little or no long-chain branching in torqued LLDPEs.

The above mentioned techniques show excellent agreement in showing the following:

a. the S216 (LDPE) torqued at 190°C and 220°C was stable and did not undergo any detectable degradation.

b. the degradation in Z-N LLDPE (torqued at 50 rpm for 10 min.) could be prevented by adding 1000 ppm of AO. No attempt was done to see if lesser amounts would be sufficient.

Additional results were obtained from the different measurements that could be summarized as follows:

a. Rheology: the match of the high-ω data for degraded and as-received resins.

b. NMR: long-chain branches were <1 branch/1000C.

c. DSC: the decrease of X_c and the increase of T_m in degraded LLDPE.

These observations integrate to support a degradation model involving the formation of gel-like aggregates of LLDPE molecules that could be produced by oxidation or light cross-linking (Hinsken, 1991) rather than the creation of long-chain branching as observed in chemically induced degradation.

E. GPC Characterization

The GPC characterization was performed on S229 (LLDPE) and S216 (LDPE) after torquing at 190°C and 220°C without additional antioxidants. The 'pure' polymers were characterized, too, and used as control samples for comparison purposes. If degradation is to take place, then M_w will increase (chain buildup) or decrease (chain breakdown) and the polydispersity (PD) will be broadened (Hinsken et al., 1991; Moss and Zweifel, 1989). Four measurements were carried out for each of the six samples. Results are shown in Table 5.4. The M_w and PD of the four different measurements were averaged and the standard deviation (S_D), given in parenthesis, was calculated for each case.

Statistical decision theory was used to test the significance of the differences in M_w and PD (reported in Table 5.4) between the torqued and as-received resins. Here, we will compare M_w and PD of torqued (at 190° or 220°C) resin to that of the as-received. The null hypothesis H_0: $\mu_1 = \mu_2$ (where μ can be either M_w or PD from the two different populations that are compared) is that the two means (M_w or PD) are equal and the samples (represented by the two sets of four data points) were withdrawn from the same population. A 95% confidence level was chosen and the t-test was performed. Even for small sample size, the t-test is usually relatively accurate (Perry and Green, 1997).

For 95% confidence level, if the value of t_0 (defined by equation 5.5, following) is *less than or equal to* 2.447 then the null hypothesis is true and the differences are not significant. Otherwise, the hypothesis is rejected and one concludes that the samples represent two different populations. The values of t_0 calculated for the torqued polymers in comparison with as-received resins are reported in Table 5.4. Values that are *less than*

or equal to 2.447 are shown in boldface representing the cases where the null hypothesis is true.

$$t_o = \frac{y_1 - y_2}{S_p\sqrt{\dfrac{1}{n_1} + \dfrac{1}{n_2}}} \qquad (5.5)$$

where y_1 and y_2 are the sample means, n_1 and n_2 are the sample sizes (here $n_1=n_2=4$), S_p^2 is an estimate of the common variance computed from:

$$S_p^2 = \frac{(n_1 - 1)S_1^2 + (n_2 - 1)S_2^2}{n_1 + n_2 - 2} \qquad (5.6)$$

and S_1^2 and S_2^2 are the two individual sample variances.

Table 5.4: GPC Characterization of S216 (LDPE) and S229 (LLDPE)

Blender Conditions	M_w (S_D)	t_o	PD (S)	t_o
S229: none	105,313 (*1285*)	–	3.57 (*0.07*)	–
S229: T$_{torque}$= 190°C	95,794 (*1750*)	8.770	3.32 (*0.10*)	4.096
S229: T$_{torque}$ = 220°C	93,530 (*2163*)	9.367	3.39 (*0.22*)	4.097
S216: none	99,464 (*902*)	–	6.45 (*0.36*)	–
S216: T$_{torque}$ = 190°C	100,255 (*1818*)	**0.78**	5.98 (*0.14*)	**2.434**
S216: T$_{torque}$ = 220°C	108,934 (*1696*)	9.86	6.48 (*0.56*)	**0.090**

The results show that M_w and PD for S216 (LDPE) torqued at 190°C are (with 95% confidence) the same as those of the as-received resin. For S216 torqued at 220°C, the analysis of PD suggests no significant difference between torqued and as-received resins, while that of M_w predicts an increase in M_w. This rather misleading latter finding

is not a surprise for GPC analysis (Hinsken et al., 1991). Furthermore, the PD is more reliable than M_w measurement (Wanke, 1999). The predicted increase in M_w is not substantiated by the low-ω viscosity measurements shown in Figure 5.1 and hence rejected on physical grounds. Therefore, it was concluded that S216 (LDPE) did not undergo any detectable degradation, as predicted by the previous rheological and DSC characterization.

However, all the results displayed in Table 5.4 for S229 (LLDPE) suggest that the torquing at 190°C and 220°C produced significant differences between the torqued and as-received resins leading to a decrease in M_w. This observation supports the previous rheology, NMR and DSC characterization. The decrease in M_w could be directly related to the loss of branching in torqued LLDPE.

Figure 5.6 relates M_w and branching of S229 for different blender conditions. A linear relation was obtained between M_w and branch content. The loss of branches contributes to the decrease in M_w but cannot explain the observed large decrease in M_w. Hence, another mechanism that leads to a decrease in M_w such as the filtering of high-M gel molecules in the GPC filter is possible. The effectiveness of the filter with known pore size may help to identify the size of gel particles.

In summary, the rheology, NMR, DSC and GPC analysis has shown that S229 (LLDPE) did undergo degradation as a result of torque and heat in the melt blender. The degradation in LLDPE was prevented by adding 1000 ppm of AO. However, S216 (LDPE) that does not contain any AO is very stable. The different techniques suggest that the enhancement of the low-ω $\eta'(\omega)$ is caused by the formation of gel-like aggregates.

Figure 5.6 Effect of blender conditions on M_w and branch content for S229 (LLDPE)

$M_w = 52665 + 2444\,B\ (r^2=0.997)$
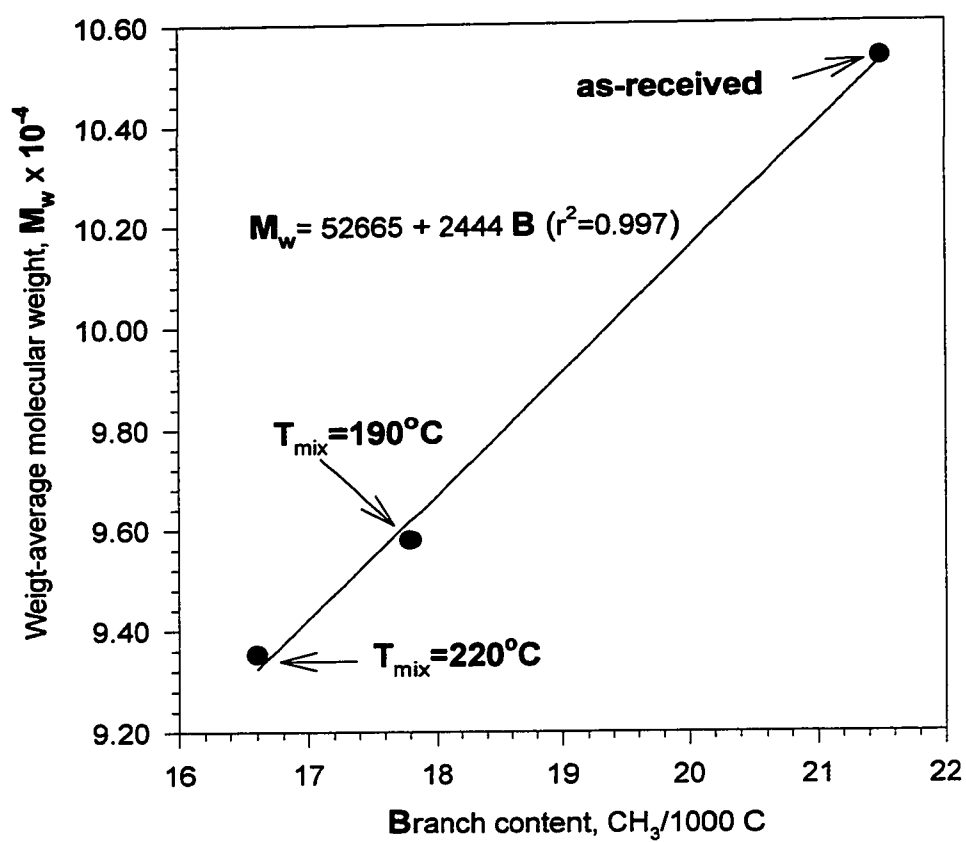
F. *What could happen in the absence of additional AO?*

To answer this question the normal practice of preparing melt blends was followed and hence no extra antioxidants were added. Blends of S229 (LLDPE) and S216 (LDPE) as well as the 'pure' resins were torqued in the melt blender at 220°C and 50 rpm for 10 minutes. The LLDPE concentration in the blend was 10, 30, 50, 70, 80 and 90% by weight. Dynamic oscillatory ω-sweep testing on blends and 'pure' resins was carried out in the RMS at 190°C and 240°C and $\gamma^o=10\%$.

As noted earlier, the high-pressure LDPE (S216) did <u>not</u> contain any AO; however, the polymer was very stable and tests on samples prepared from different batches showed excellent reproducibility ("batch reproducibility"; see Figure B.16). The reproducibility of the $\eta'(\omega)$ data for LLDPE (S229) samples prepared from the same batch was excellent, too (see Figure B.17). On the other hand, the batch reproducibility of $\eta'(\omega)$ for LLDPE was poor (see Figure B.29). To check the batch reproducibility of $\eta'(\omega)$ for blends of S229 and S216, a blend of 80% S229 was studied. Samples from three batches prepared under the same blender conditions were used. One of the batches was prepared by Dr. Kam Ho of Nova Chemicals in Calgary. The rheological characterization of the 80% LLDPE blend produced significant differences among the three batches in the low-ω viscosity. Results given in Figure 5.7 show values of η' that are different by a factor of up to ~3. It is clear that the batch reproducibility of the degraded samples is very poor, and hence this test could be used as a quick check for degradation. Furthermore, the poor batch reproducibility could be the reason behind the observed peculiar behavior of $\eta'(\phi)$ curves that will be discussed below.

Figure 5.7 Comparison of η' for 80% S229 from three different batches

$(T_{mix}=220°C, T_{test}=190°C, \gamma°=10\%, w/o \text{ added AO})$
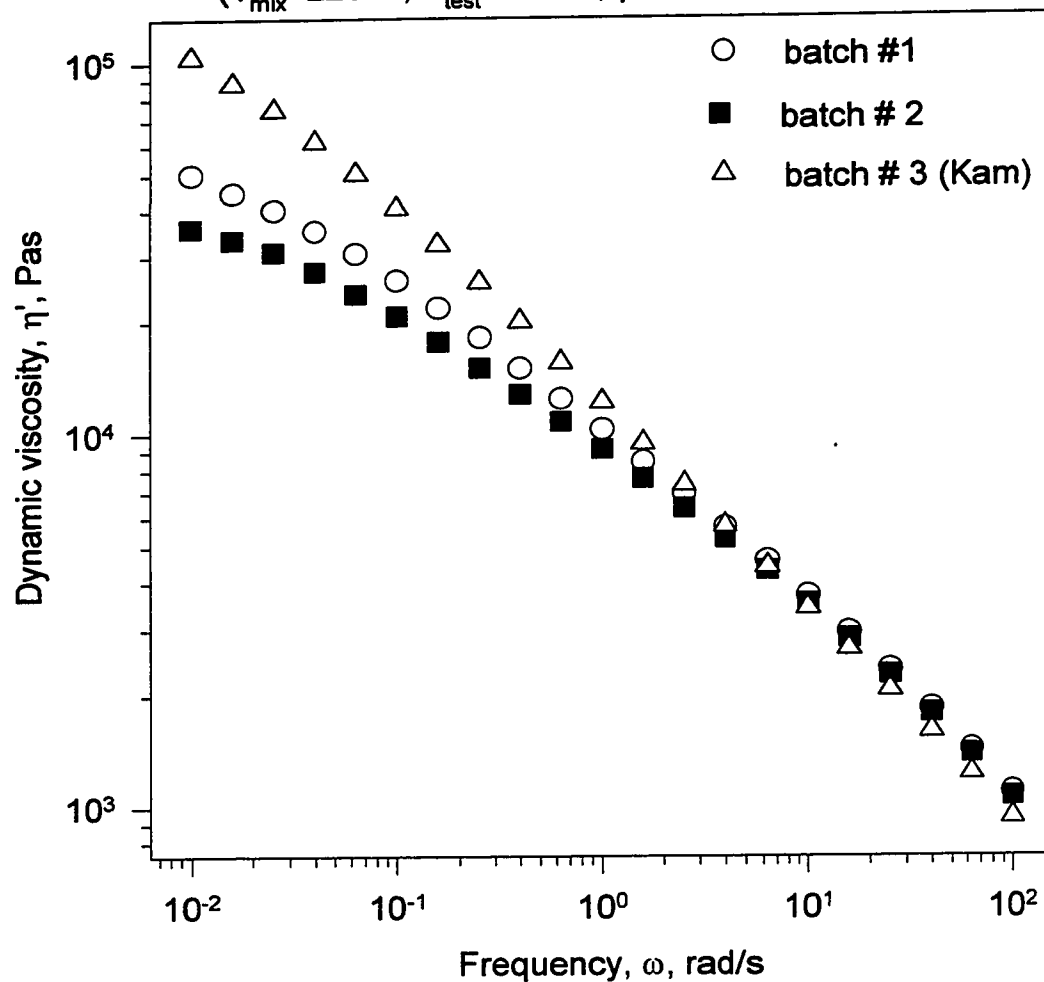
The ω-sweep data obtained for the blends of different compositions of S229 (LLDPE) and S216 (LDPE) as well as the 'pure' resins were analyzed and plots of $\eta'(\phi)$ and $G'(\phi)$ at constant ω are given in Figure 5.8 and the Appendix (Figures B.30 and B.31). Figure 5.8 displays $\eta'(\phi)$ data for $\omega=0.1$ rad/s obtained at $190^{\circ}C$. The solid straight line that connects points for the 'pure' resins represents the expected behavior of the blend if a linear additivity rule were followed (which would suggest miscibility across the entire ϕ-range). The linear additivity rule was approximately followed for $\phi\leq50\%$ LLDPE, while negative deviation behavior (NDB) was observed for $50<\phi<100\%$ LLDPE. The NDB and the minimum in $\eta(\phi)$ and $N_1(\phi)$ curves were previously reported for HDPE-PS blends which are known to be immiscible (Van Oene, 1978).

The NDB was explained by interlayer slip (Utracki, 1989a) or through a free volume approach (Lipatov et al., 1981; Shumski et al., 1979). However, the data displayed in Figure 5.8 could be simply explained by looking into the influence of degradation on the batch reproducibility of these results. The values of η' for the 80% LLDPE obtained at $\omega=0.1$ rad/s from the second and third batch data given in Figure 5.7 were superimposed on Figure 5.8. While η' for batch # 2 supports that of batch # 1 and shows NDB, the batch # 3 value was far above the linear additivity line, suggesting a positive deviation behavior (PDB). Moreover, all data on the curve would look like showing a PDB if AO was added to the 'pure' LLDPE. NDB was also observed in $\eta'(\phi)$ and $G'(\phi)$ curves for the same blend at $\omega=1$ rad/s (Figure B.30).

Previous reports that examined HDPE/LDPE melt blends (Manero et al., 1987) observed increase in the viscosity of pure components due to shear i.e., they observed what is known in the literature as "shear modification". These modifications had

Figure 5.8 $\eta'(\phi)$ for blends of LLDPE and LDPE

(T_{mix}=220°C, T_{test}=190°C, $\gamma°$=10%, ω=0.1 rad/s, w/o added AO)
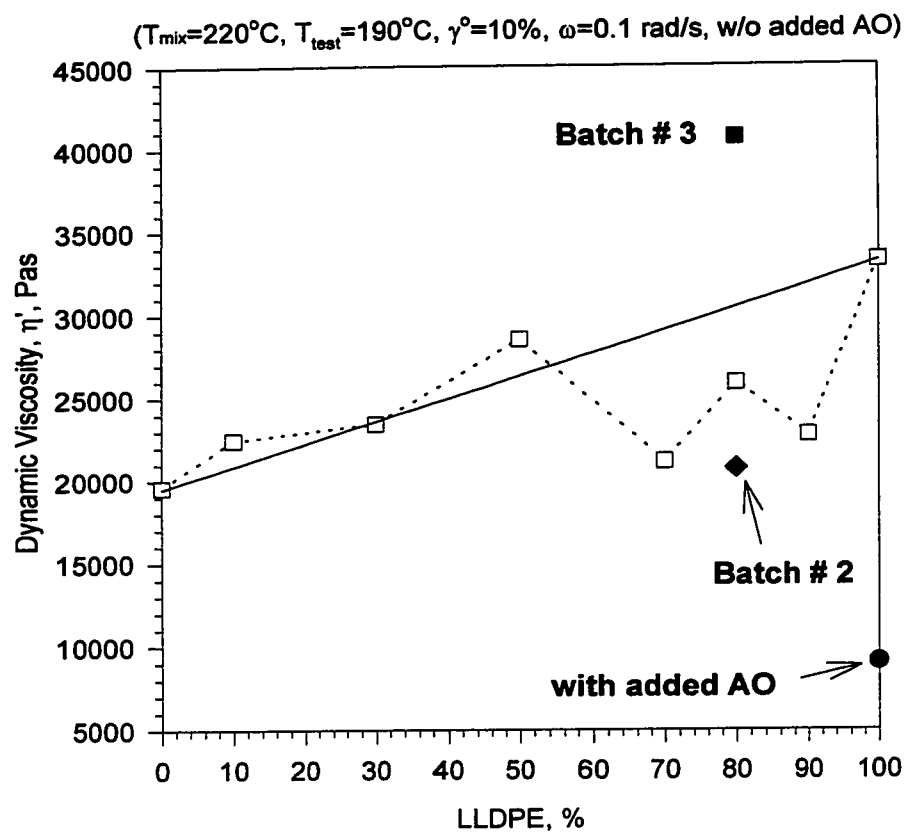
significantly influenced the interpretations of the blend viscosity and resulted in NDB when the torqued pure components were taken as reference. The shear modifications were explained in terms of intermolecular interactions induced through the extra entanglements generated by the shearing forces (Rudin, 1970; Heitmiller et al., 1964). It is valid to question whether the observed modifications were due to extra entanglements or simply a result of degradation that could have been prevented by adding extra AO, taking into consideration the long torquing time (20 minutes in the Manero et al. study).

The influence of the test temperature on the NDB was checked by repeating the previous testing at 240°C. The same overall behavior (including the NDB) was reproduced at 240°C (Figure B.31).

The above analysis clearly shows very important observations that strongly influence the interpretation of the miscibility data. These observations could be summarized as follows:

a. poor "batch reproducibility" is a possible reason for the peculiar NDB in blends of LLDPE and LDPE.

b. lack of 'batch reproducibility' could be a sign of degradation in one (or more) of the blend components. The test might be introduced as a routine check for degradation.

c. the test temperature has no influence on the general shape of the $\eta'(\phi)$ curve.

d. it is difficult to conclude anything about the miscibility of a blend if one (or more) of the components is undergoing degradation since the reproducibility of the data is very poor.

e. It is important to check the influences of melt conditioning or sample preparation steps on the 'pure' polymers before proceeding with melt blending.

Some of the work discussed in this Chapter has already been presented in national and international conferences (Hussein et al., 1997; Hussein and Williams, 1997).

VI. Results: Rheology and Miscibility of LLDPE and LDPE Blends

In this Chapter, the rheology of LLDPE and LDPE blends was studied. The aim of this investigation was to examine the effect of M_w, MWD, and molecular architecture (branch type, content) on the miscibility of LLDPE blends in the 'liquid' state. In this thesis, only the effect of M_w and branch type will be discussed. Two pairs of LLDPE and LDPE were selected to study the effect of M_w. S229 (LLDPE) and S216 (LDPE) was the high-M_w pair; and S237 (LLDPE) and S231 (LDPE) was chosen as the low-M_w pair. The effect of the branch type was investigated by testing blends of S226 (octene LLDPE) and S216 and comparing results to those of S229 (butene LLDPE) and S216. The influence of the torquing temperature (T_{mix}) was examined by preparing blends of the high-M_w pair at 190°C and 220°C. The low-M_w pair was mixed at 190°C and the polymers were quite runny, hence, no results are given to compare the influence of T_{mix}. The characterization of the above-mention resins is given in Chapter III.

The torquing of the 'pure' polymers and their blends was carried out in the Haake Rheocord 90 blender at 50 rpm and for 10 minutes in the presence of 1000 ppm of additional antioxidant (AO) except for the low-M_w pair where no AO was added. The previous degradation study (discussed in Chapter V) showed that this level of AO is adequate to prevent degradation of the Z-N LLDPEs. The LDPE (S216) was found to be very stable at 190° and 220°C. The melt blending in the Rheocord 90 was followed by specimen preparation in the Carver press and then dynamic oscillatory testing in the RMS (as explained earlier in Chapter III). The small strain dynamic shear testing was chosen to avoid possible morphological changes as might result from the high-strain steady

shearing. Frequency and temperature sweeps were carried out in the linear viscoelastic range of γ^o for S229 (butene) and S226 (octene) blends with S216 (LDPE) as well as the 'pure' polymers.

The uniform shear cone-and-plate (CP) and the nonuniform shear parallel plates (PP) geometries were used for the ω- and T-sweeps respectively. Strain amplitude in the linear viscoelastic range was achieved with a value of $\gamma^o=10\%$, used in the ω- and T-sweep testing. The ω-sweep testing was performed at 190°C over the range $\omega=10^{-2}-10^{2}$ rad/s except for the low-M_w pair which was tested at 140°C; and the T-sweep measurements were carried out over the range 160°-260°C.

In the following, a brief review of the literature on the rheology and miscibility of polymer blends in general and polyethylenes in particular is discussed in section A. Furthermore, section A will elucidate the relation between the rheology and the morphology of multi-phase systems. Rheological measurements (ω-sweeps) for the high- and low-M_w pairs involving butene-based LLDPE; as well as the octene-based LLDPE and LDPE pair are discussed in sections B and C respectively. Results for the T-sweep measurements are given in section D.

A. *Rheology and miscibility of polymer blends:* A brief review of Literature

The relation between equilibrium thermodynamic functions, ΔH_m or ΔG_m as measured by inverse gas chromatography and the shear viscosity η (determined in capillary viscometer) were studied by Lipatov et al. (1982 a & b). Their results show a definite correlation between the viscosity-concentration relationship and the thermodynamic state of a system in the melt at a given temperature. A positive deviation of the blend viscosity from additivity is taken to indicate immiscibility of the components

(Lipatov et al. 1982b). They confirm that this phenomenon is common for both the mixtures of different polymers and those of different M_w for the same molecular structure.

There is an extensive literature on polymer blends, including the blend rheology that has been reviewed by a number of authors. Most reviews have concentrated on two-phase systems (Han, 1976 and 1981; Utracki, 1987 and 1989a). The rheology of various kinds of polyolefin blends was surveyed by Plochocki (1978) and that of polyethylenes in particular was reviewed by Utracki (1989b). For polyethylenes, with the same molecular unit (methylene, $-CH_2-$) in each blend component, the simple study of the phase morphology of the melt tends to be unhelpful (due to similarity of the molecular structure), and in general, individual methods (methods that study blend components individually) are inconclusive (Groves et al., 1996).

In the flow of polymer blends, three types of behavior can be identified when a rheological function (e.g., η_0, η', G') is plotted vs. composition (ϕ). The blend can exhibit deviations that are positive (PDB), negative (NDB) or both: positive and negative (PNDB) from the linear-additivity or log-additivity rules ($\eta=\Sigma\phi_i\ \eta_i$; $\log\ \eta=\Sigma\phi_i\ \log\ \eta_i$). In miscibile systems, the non-additive blend rheology is a reflection of thermodynamics, in particular, the specific interactions and free volume variation with ϕ. If two polymers show a partial miscibility, then they are miscible in a certain range of ϕ but immiscible in another. In immiscible systems, the rheological functions depend on the form and concentration of the dispersed phase, the interfacial interactions (including surface tension), and relative rheological properties of the two polymers (Utracki and Schlund, 1987).

It is estimated that 60 to 70% of LLDPE enters the market as blends (Utracki, 1989a), primarily with other member of the polyolefin family, e.g. LDPE or polypropylene (PP). The blending may be mechanical using two commercial products or in a reactor, merging two streams of LLDPE in solution/suspension process using multi-site catalyst or changing the feed stock during the fluidized bed polymerization. The PE/PP systems are known to be immiscible (Utracki, 1989b; Dumoulin et al., 1991, Fujiyama and Kawasaki, 1991 a & b; Choi et al., 1995), while those of PE/PE show a quite diverse behavior as discussed below.

The new catalysts (metallocenes) produce random copolymers as opposed to the older kinetically controlled ones that tend to have higher degrees of short chain branching in the lower M_w components (Freed and Dudowicz, 1996).

The compositional asymmetry is present in polyolefin blends even if the two components have equivalent overall molecular volumes. Adding a small amount of a highly branched component to a lightly branched melt is more likely to cause liquid-liquid phase separation than the addition of a small amount of a lightly branched component to a highly branched melt. The *conformational* and *architectural* "mismatch" between components of polyolefin blends are important factors that influence the miscibility of polyolefin (Frerickson and Liu, 1995).

Dobrescu (1980) studied HDPE/LDPE blends of different M_w of the components using a capillary rheometer. In most cases the $\eta(\phi)$ plot showed PDB from the log-additivity rule, and the stronger the mismatch between the 'pure' polymers viscosities the larger was the PDB. Garcia-Rejon and Alvarez (1987) reported the incompatibility (immiscibility) of HDPE/LDPE blends, too. They observed that low concentrations of

HDPE (10%) had increased the LDPE G' by 50% (strong PDB). However, Curto et al. (1983) indicated good superposition of reduced $\eta(\dot{\gamma})$ capillary flow data for a series of HDPE/LDPE blends at T=160° to 200°C, interpreted as support for likely miscibility or stable morphology. In general, HDPE/LDPE blends are immiscible, but with stable morphology they may generate a time-temperature master curve (Utracki, 1989a).

Blends of HDPE/HDPE and LDPE/LDPE (different M_w fractions) were reported to be miscibile (Munoz-Escalona, 1997; Utracki 1989 a & b, Hill and Barham, 1995) and the viscosity vs. composition followed the log-additivity rule. However, due to the diversity of composition, molecular structure, M_w and MWD the LLDPE/LLDPE blends may or may not be miscible (Utracki 1989a). A pair of high-M_w LLDPE (butene, Ti catalyst) and LLDPE (hexene, Vanadium catalyst) were found to be immiscible (Utracki, 1989a) with $\eta'(\phi)$ following a third order polynomial and showing positive-negative deviation behavior (PNDB).

However, a very similar blend (LLDPE/LLDPE) containing polymers of high-M_w was miscible (Utracki and Schlund, 1987). On the other hand, a blend of LLDPE (high-M_w)/LDPE (low-M_w) was found to be immiscible (Utracki and Schlund, 1987) and another blend of LLDPE (high-M_w)/LDPE (high-M_w) was partially miscible (Datta and Birley 1983; Utracki, 1989b). Hence, blends of LLDPE with other LLDPE or LDPE may show a widely diverse behavior, dependent on small changes in molecular structure caused by e.g., different catalyst, polymerization method or composition (Utracki, 1989b). The equations for homologous and miscible blends due to Tsenoglou (1987, 1988, 1991) did not provide a precise prediction of the rheology of a series of linear with

short-branched polyethylene blends unless the molecular weights and rheology are of a similar magnitude (Groves et al., 1996).

Wardhaugh and Williams (1995) have suggested that there may be blockiness in branching, which may lead to phase separation in LLDPEs. Phase separation was also detected in melts of several LLDPEs (Hill and Puig, 1997). If LLDPEs can undergo phase separation in the melt, it would not be surprising if blends of LLDPEs with other polyethylenes did so, too.

In Chapter IV, rheological data presented for highly branched LLDPE (Exxon metallocene resin) suggested that the melt was amorphous (random coil conformation), while that for other Z-N LLDPEs (less branched) showed molecular order (assumed to be chain-folded conformation). This difference in the molecular conformation in the melt-state might be the reason for the miscibility or immiscibility of blends of LLDPE/LLDPE or LLDPE/LDPE systems. Furthermore, the same argument could be extended to explain the reported (Hill and Puig, 1997) liquid-liquid phase separation in 'pure' LLDPEs that are known for their intra- and intermolecular heterogeneity (Usami et al., 1986). In 'pure' Z-N LLDPEs, the presence of highly branched low M_w molecules and highly linear high M_w chains could result in different molecular conformations in the melt that induce liquid-liquid phase separation.

Lee et al. (1997) studied the effect of branch distribution on the miscibility of LLDPE/HDPE blends. Z-N LLDPE (butene) and a metallocene-catalyzed LLDPE (butene) of about the same M_w and branch content were blended with HDPE. The branch distribution was assumed to be uniform in the metallocene and heterogeneous in the Z-N resin. It was observed that Z-N LLDPE were miscible with HDPE over a wider range of

composition in comparison to the metallocene-catalyzed LLDPE. Their results suggest that chain structure in terms of distribution of branches determines the miscibility behavior of the blend. However, their observation is not conclusive since the two LLDPEs possessed different MWDs (PD=3.9 for Z-N and 2.4 for the metallocene-catalyzed LLDPEs).

The rheology of 'pure' LLDPEs of different comonomer types was studied by Kalyon et al. (1988). They concluded that increasing comonomer length (from butene to octene) in LLDPEs appears to generate higher normal stress (N_1) in shear and extensional flows, but the differences are not as pronounced as those found between LLDPE and LDPE.

For immiscible blend systems, the state of dispersion and specifically the shape of the dispersed phase (i.e. droplets) greatly influence the rheological responses of immiscible polymer blends. Both the theoretical and experimental studies indicated that the highest degree of dispersion can be obtained by blending two liquids with similar viscosities at the same stress level as that expected during mixing: η_2/η_1=0.3 to 1.0 where subscript 1 indicates the matrix and 2 indicates the dispersed polymer (Utracki, 1987, 1989 a&b).

For a polymer with narrow MWD, in the terminal (low-ω) region of the plot of the storage and loss moduli (G' and G'') versus the frequency of oscillation ω, yields G' α ω^2 and G'' α ω (Ferry, 1980). This behavior is temperature independent and is referred to as the "homogeneous phase rheological behavior". In the terminal region $\omega\lambda_t<1$, where λ_t is the terminal relaxation time, and viscous behavior dominates over elastic behavior. A blend of two monodisperse homopolymers (linear PEs: Hill et al., 1991; Barham et al.,

1993; hydrogenated and deuterated polybutadiene: Nesarikar, 1995 a&b) showed the homogeneous-phase rheological behavior (miscibility) in its homogeneous melt state, and deviation from this was seen in the phase-separated melts (Hill et al., 1991; Barham et al., 1993; Ajji and Choplin, 1991; Han and Kim, 1993; Nesarikar, 1995 a&b). Departure from miscibility can be brought about by varying the weight fraction of the blend, and it was due to the change in the melt morphology when the melt phase separates. For the phase-separated melt in the terminal region, the slope of log G'-log ω is less than one (Ferry, 1980).

In the above information, it is assumed that during phase separation the equilibrium properties are not affected by the dynamic shearing of the blend. As illustrated by Chuang and Han (1994) rheological behavior of immiscible blends is strongly affected by the type of applied shear (whether it is oscillatory or steady shear). While shear-induced mixing is observed in some steady shear experiments (Larson, 1992; Minale et al., 1997), no such effects are reported for small amplitude dynamic shear (Utracki, 1988; Chuang and Han, 1994).

As a basic rule, phase separation causes G' and G'' to increase, due to the presence of droplets of dispersed phase. The increase is a result of "emulsion morphology" present in phase separated systems. The emulsion morphology gives rise to a non-zero storage modulus (G') even in a mixture of two Newtonian liquids (which, by themselves have $G'=0$). That is, their emulsion exhibits elastic behavior in addition to the viscous nature (Taylor, 1932; Oldroyd, 1953).

Earlier hydrodynamic calculations (Taylor, 1932; Frölich and Sack, 1946) for such systems were for dilute emulsions, and an extension to concentrated emulsions

(blend viscosity expression contains a ϕ^2 term) was given by Choi and Schowalter (1975). They derived expressions for G' and G'' for an emulsion of two Newtonian liquids, which can also be applied to a phase separated polymeric system in the Newtonian regime (Scholz et al., 1989; Gramespacher and Meissner, 1992), where the G' had increased due to the presence of droplets. The storage modulus $G'(\omega)$ obtained at low-ω was found to be higher than those of the components in the case of immiscible blends of PP/HDPE (Fujiyama and Kawasaki, 1991b); PS/Poly(Methyl Methacrylate) (PMMA) (Graebling et al., 1993; Gramespacher and Meissner, 1992; Chuang and Han, 1984); PP/Polyamide 6, PA6, (Scholz et al., 1989). This principle was applied to differentiate between miscible and phase-separated polymeric blends. Similar to the concentrated-emulsion model, Ajji and Choplin (1991) found the effects of phase separation on G' to be more pronounced than on G''.

Earlier work of Williams' group (Martinez and Williams, 1980) showed similar increase in $\eta'(\phi)$ and $\eta(\dot{\gamma})$ for HDPE/PMMA system. Their rheological measurements were supported by SEM micrographs. The low-shear data showed excellent agreement with the predictions of the dilute emulsion model (Taylor, 1932; Oldroyd, 1953). Karbashewski et al. (1993) observed that the addition of HDPE to LLDPE, of the same M_w or lower, resulted in an increase in extrudate swell and a "decrease in processability" both in terms of viscosity and melt elasticity. Their observations could easily be explained in view of phase separation in the liquid state.

Recently, stress relaxation measurements were used as a microstructural probe for immiscible blends (Vinckier et al., 1997). On the other hand, the time-temperature superposition is non- rigorous for immiscible blends (Han and Kim, 1993) since plots of

G' vs. G" were independent of temperature for both miscible and immiscible blends (Chuang and Han, 1984). Furthermore, and as pointed out earlier, immiscible polyethylenes (HDPE/LDPE) with stable morphology can generate a time-temperature master curve (Utracki, 1989a).

An alternative approach to the time-temperature superposition was suggested by Chuang and Han (1984) to assess the miscibility of polymer blends. It made use of a modified Cole-Cole plot (log G' vs. log G"). They measured the steady and oscillatory-shear flow properties of compatible (miscible) and incompatible (immiscible) polymer blend systems as functions of composition and temperature, using a CP rheometer. Their study was supported by photomicrographs for the immiscible blend. The miscible blend system investigated by Chuang and Han (1984) was a blend of two LDPE (with different M_w) and the immiscible blend studied was a blend of PMMA and Poly(vinylidene fluoride) (PVDF). It was found that:

a. Plots of log G' vs. log G" for the miscible blends of LDPE become independent of blend composition and the type of shear flow. Similar results were reported (Muñoz-Escalona et al., 1997) for blends of metallocene-catalyzed HDPE of different molecular weights (M_w=14K and 238K)

b. Plots of log G' vs. log G" for the PMMA/PVDF blends become dependent upon blend composition and the type of shear flow.

Consider a spherical droplet suspended in a continuous medium, which is subjected to either a steady-shear flow or an oscillatory-shear flow. Under the steady-shear flow, the droplet is deformed in the direction of the shear plane, and the greater the shear rate the longer the droplet will be stretched. On the other hand, under the oscillatory

shear flow, the shape of the droplet will also oscillate, corresponding to the frequency of the oscillation imposed on the fluid. When the viscosity of the dispersed phase is very large compared to the viscosity of the matrix phase, the oscillatory motion of the cone (or plate) of the rheometer may little affect the shape of the droplet; but when the viscosity of the dispersed phase is very small compared to that of the matrix phase, the shape of the droplet will oscillate greatly.

Therefore, the similarity of dynamic and shear properties e.g., between η and η', and between N_1 and G' must <u>not</u> be expected for inmmiscible blends (Utracki and Schlund, 1987; Chuang and Han, 1984). However, while the lack of superposition of dynamic and steady shear viscosities indicates immiscibility, its absence cannot be taken as a proof of the reverse (Utracki and Schlund, 1987). It should also be mentioned that the shape of the droplets in a two-phase blend in a *uniform* flow field might be different from that in a *nonuniform* flow field. Hence, there is no presumable reason for expecting that the rheological data obtained with a capillary viscometer should agree with that measured with the CP rheometer. However, the use of capillary viscometer should not be overlooked since it is more likely to represent the behavior of the material under true processing conditions such as extrusion (Utracki et al., 1986).

The rheological consequences of blending short-branched (LLDPEs) and long-branched polymers (LDPEs) have received far less attention than have linear/linear or linear/branched blends (Groves et al., 1996). A closer examination of this case will be very important in shedding light on the molecular mechanisms, which control the miscibility of polymer blends.

The aim of this study is to investigate the miscibility of polyethylene blends that combine the advantageous mechanical properties of the LLDPE with the ease of processing of LDPE. Since these properties are not necessarily additive but depend on the complex balance between thermodynamic miscibility and blending and cooling kinetics, it has been attempted to find a correlation between the miscibility of the blends and the rheological properties of the 'pure' polymers and their blends.

B. ω-sweep Measurements for Blends of the Low- and high-M_w pairs

The premolded specimens were tested in the RMS under nitrogen. The low- and high-M_w pairs were tested at $140°$ and $190°C$ respectively. The cone-and-plate with 25-mm diameter and a cone angle of 0.1 rad was used. A strain amplitude, $\gamma°$, of 10% was selected following a $\gamma°$-sweep to ascertain that subsequent ω-sweeps were done within the linear viscoelastic range as discussed earlier in Chapters IV and V. The stability of the blends was established from G' measurements at different temperatures (Appendix C, Figure C.1) and repeat measurements as shown for 10% and 90% S229 blends with S216 (Appendix C, Figures C.2 and C.3 respectively).

1. Blends of the Low-M_w Pair

The dynamic flow measurements were obtained at $140°C$ for S227 and S231 (see Tables 3.2 and 3.3 for characterization data) and their blends. Lower T_{test} was selected for use of these low-viscosity components to assure that the torque signal was above the sensitivity level of the RMS. The blends were mainly characterized by the following rheological functions: dynamic viscosity, η', storage, G', and loss, G'' moduli as functions of composition, ϕ, and frequency, ω. The viscous component of the ω-sweep measurements is shown in Figure 6.1 as $\eta'(\omega)$ for 5 blends of the low-M_w pair in addition

Figure 6.1 $\eta'(\omega)$ for blends of S227 (LLDPE) and S231 (LDPE)

$(T_{mix}=190°C; T_{test}=140°C, \gamma°=10\%, \omega=1\text{-}100 \text{ rad/s})$

Dynamic viscosity, η', Pas

10^3

10^2

- ○ 0% (S231)
- ■ 10%
- △ 30%
- ▼ 50%
- ▽ 70%
- □ 90%
- ● 100% S227

10^0 10^1 10^2
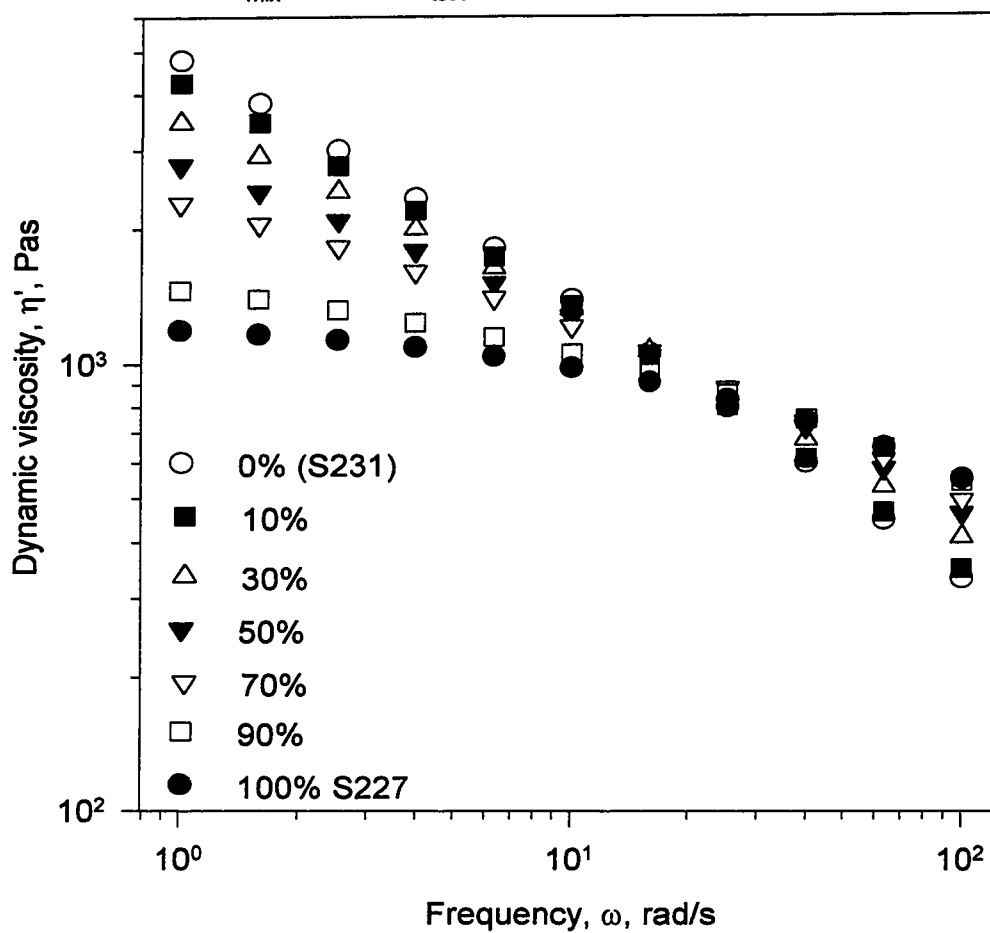
Frequency, ω, rad/s

to the two 'pure' resins. Results were obtained in the frequency range $\omega=1-100$ rad/s. In Figure 6.2 the same data are given as η' vs. stress, τ, calculated as $\tau = \eta^* \times \omega$ as employed by Wissbrun and Griffin, (1982), [the expression $\tau = \eta^* \times (\gamma^\circ\omega)$ could also be used]. Figures 6.1 and 6.2 show the similarity of $\eta'(\omega)$ and $\eta'(\tau)$.

The composition dependence of the rheological properties was obtained by plotting the property vs. ϕ data measured at constant ω (or τ). For example, the ϕ-dependence of η' for the low-M_w pair at $\omega=1$ rad/s was picked from data displayed in Figure 6.2 and is shown in Figure 6.3. The $\eta'(\phi)$ data (obtained at low ω) followed the linear additivity rule (indicated by a solid straight line) suggesting the miscibility of the low-M_w pair. Results obtained at high ω ($\omega=100$ rad/s) show similar behavior (see Appendix, Figure C.4).

Another way of presenting the dynamic shear data is the Cole-Cole plot that was reviewed by Nakajima and Harrell (1987), and widely used in the polymer blends literature (Dumoulin et al., 1991; Graebling et al., 1993; Scholz et al., 1989; Han and Kim, 1993; Fairley and Prud'homme, 1989; Nesarikar, 1995; Fujiyama and Kawasaki, 1991; Chuang and Han, 1984). The Cole-Cole plot is a linear plot of η' vs. η'' or G' vs. G'' that corresponds to the linear additivity rule of property-composition curve. On the other hand, the modified Cole-Cole (mCC) is a log-log plot similar to the log-additivity rule. The log-log plot of G' vs. G'' was reported (Chuang and Han, 1984; Muñoz-Escalona et al., 1997) to be independent of composition for miscible blends generating a master curve. The lack of superposition suggests immiscibility of blends (Chuang and Han, 1984).

Figure 6.2 $\eta'(\tau)$ curve for blends of S227 (LLDPE) and S231 (LDPE)

$(T_{mix}=190°C; T_{test}=140°C, \gamma°=10\%, \omega=1\text{-}100 \text{ rad/s})$

Dynamic viscosity, η', Pas

○ 0%
■ 10%
△ 30%
▼ 50%
▽ 70%
□ 90%
● 100% S227

Stress $(\tau = \eta^* \times \omega)$, Pa
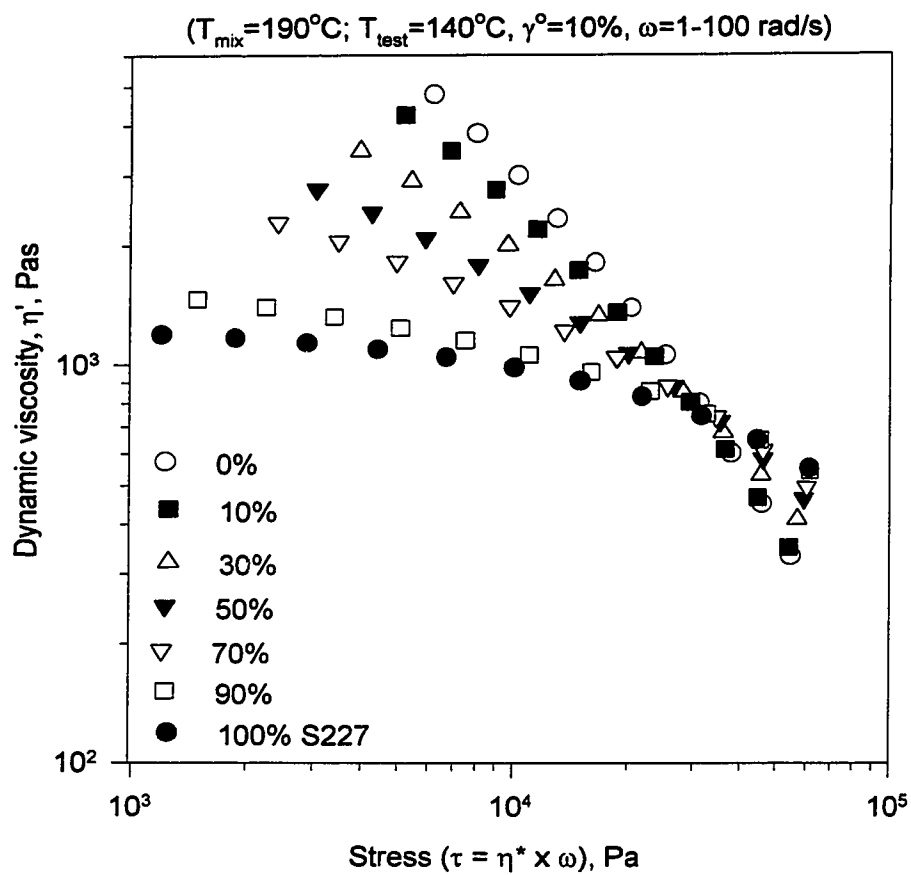
Figure 6.3 $\eta'(\phi)$ for blends of S227 (LLDPE) and S231 (LDPE)

$(T_{mix}=190^{\circ}C; T_{test}=140^{\circ}C, \gamma^{\circ}=10\%, \omega=1.0 \text{ rad/s})$
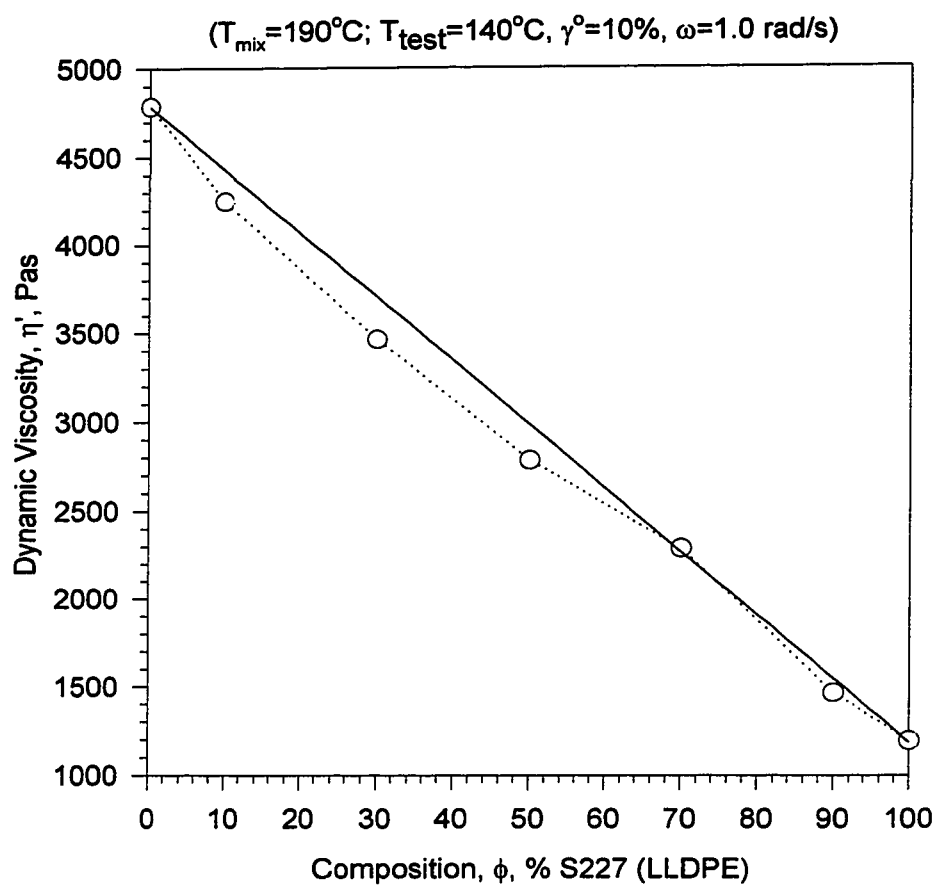
Here, the mCC plot was used to predict the liquid-state miscibility of the low-M_w pair. The G' vs. G'' data for the low-M_w pair are given in Figure 6.4a. The log G' vs. log G'' data were linear and lines for different compositions are distinctly separated and almost parallel. The data in Figure 6.4a were next used to construct a master curve by a procedure analogous to time-temperature superposition. The line representing each value of blend concentration, ϕ, was vertically shifted downward and superimposed on the S227 (LLDPE) line. Results are given in Figure 6.4b and the shift factor, $a_\phi(\phi)$, is shown in Appendix C (Figure C.5). The mCC plot showed a good degree of superposition, but not excellent, (see the solid line in Figure 6.4b). Such superposition is comparable to that of the $\eta'(\phi)$ data shown in Figure 6.3 above. The $a_\phi(\phi)$ plot was linear. These results suggest that the low-M_w pair is <u>almost</u> miscible. Therefore, the dynamic shear measurements attest to the nature of miscibility of the low-M_w pair over almost the whole composition range regardless of the method of presenting the data ($T_{test}=140^\circ C$). The experimental measurements for the low-M_w pair were obtained by Dr. Phillip Choi[*].

2. Blends of the high-M$_w$ Pair

Blends of S229 (LLDPE) and S216 (LDPE), as well as the 'pure' polymers, were torqued at 190° and $220^\circ C$ in the presence of extra 1000 ppm of AO. The adequate amount of the AO was added following a degradation study that was discussed earlier in Chapter V. The dynamic flow properties on premolded specimens were obtained at $190^\circ C$ ($\gamma^\circ=10\%$; $\omega=0.01$-100 rad/s) using the CP geometry.

The dynamic shear measurements obtained for the set of the high-M_w pair that was torqued at $190^\circ C$ were picked for detailed analysis. The analysis was aimed at

---

[*] Former PDF in Williams' group and currently an Assistant Professor of Chemical Engineering at U of A.

Figure 6.4a G' vs. G" for blends of S231 (LDPE) and S227 (LLDPE)

$(T_{mix}=190°C; T_{test}=140°C, \gamma°=10\%, \omega=1\text{-}100\%)$
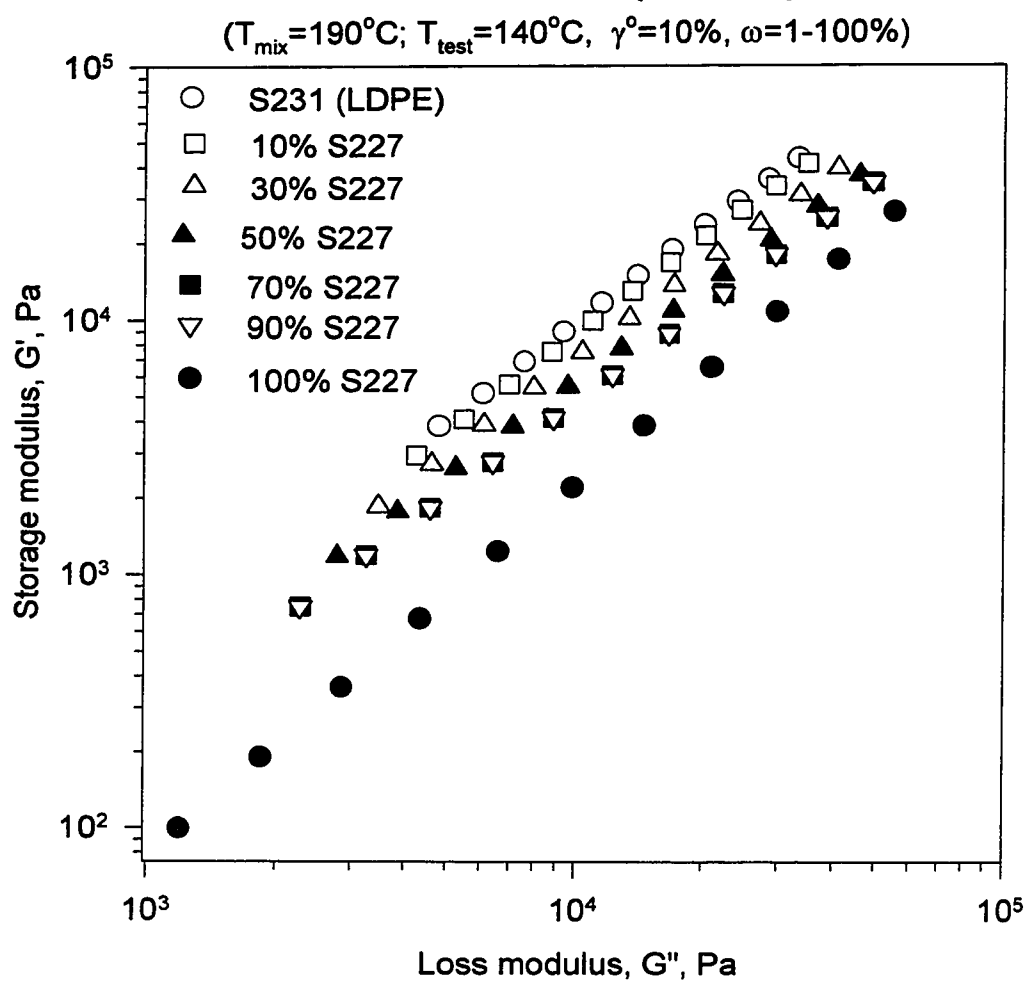
Figure 6.4b Superposition of G' vs. G"
for blends of S231 and S227

$(T_{mix}=190^\circ C; T_{test}=140^\circ C, \gamma^\circ=10\%, \omega=1\text{-}100\%)$
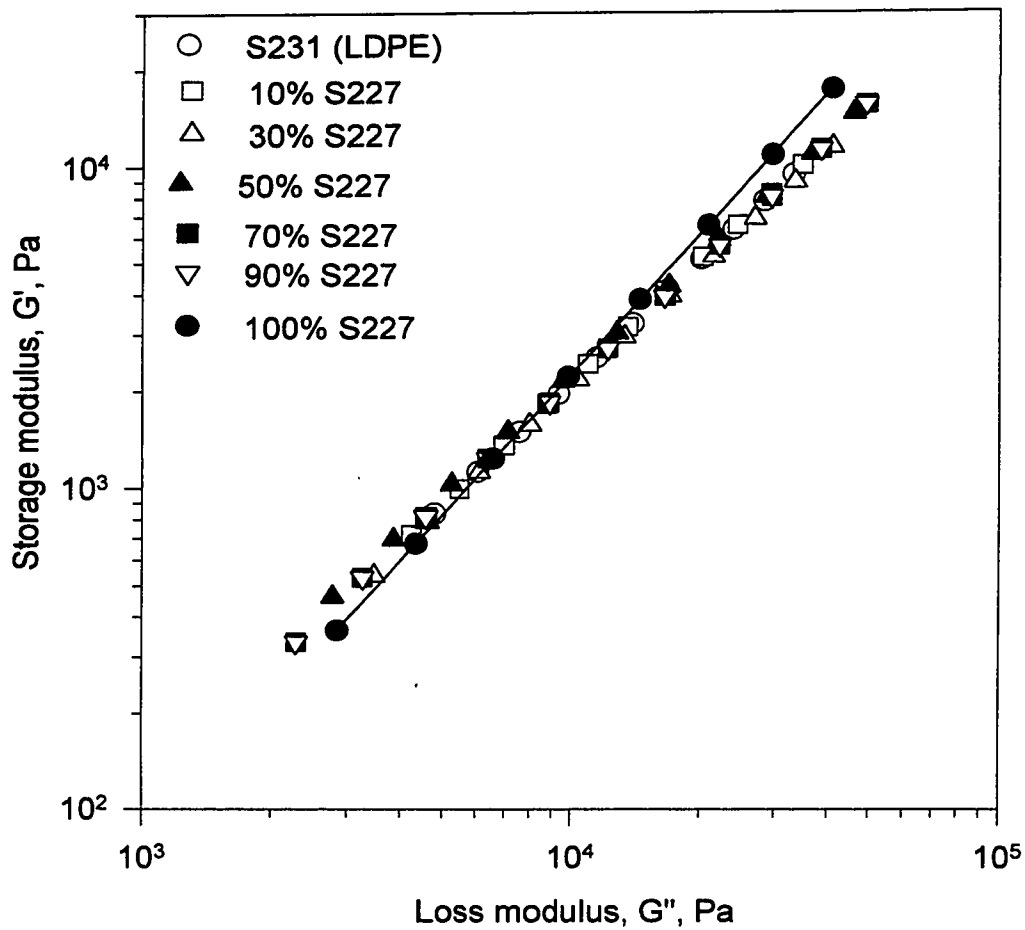
presenting the rheological data in different formats to facilitate the assessment of the miscibility, and possibly help scrutinize the different methods. The dynamic shear data were examined as:

a. $\eta'(\omega)$ and $\eta'(\tau)$ for all compositions ($\tau = \eta^* \times \omega$).

b. $\eta'(\phi)|_{\omega=const}$ obtained directly from the ω-sweep measurements (widely used in the literature).

c. $\eta'(\phi)|_{\tau=const}$ obtained through curve fitting of $\eta'(\tau)$ data (suggested by Van Oene, 1978 since the boundary conditions at the fluid-fluid interfaces require the continuity of the shear stress). The ϕ-dependence evaluated at constant τ is larger than that evaluated at constant ω $\{(\partial\eta'/\partial\phi)_\tau = (\partial\eta'/\partial\phi)_\omega [1-\omega(\partial\eta'/\partial\tau)_\phi]\}$ since $(\partial\eta'/\partial\tau)_\phi$ is negative.

d. Comparison of $\eta'(\omega)$ and steady shear viscosity, $\eta(\dot{\gamma})$. Lack of superposition of $\eta'(\omega)$ and $\eta(\dot{\gamma})$ indicates immiscibility (Utracki and Schlund, 1987).

e. log G' vs. log G'' or mCC plots. Lack of superposition (ϕ-dependency) of reduced plots was observed for immiscible blends (as discussed earlier).

f. $\eta_0(\phi)$ extracted from fitting the $\eta'(\omega)$ data to a rheological model.

In Figure 6.5, plots of $\eta'(\omega)$ are given for blends and 'pure' components of the high-M_w pair. The addition of up to 30% of S229 (lower η_0) to S216 (higher η_0) did <u>not</u> result in a drop of η_0 to values below that of S216, but rather led to blend η_0 values higher than that of the higher-η_0 component. This phenomenon was also observed at higher ω, (where $\eta'<\eta_0$); indeed, throughout the intermediate ω-range ($0.1<\omega<2$ rad/s). In the absence of specific interactions (like polar or hydrogen bonding), the increase of

Figure 6.5 $\eta'(\omega)$ for blends* of S229 (LLDPE) and S216 (LDPE)

$(T_{mix}=190°C,\ 50\ rpm\ for\ 10\ min.;\ T_{test}=190°C,\ \gamma°=10\%,\ C\&P)$

**with additional 1000 ppm of A/O*

high-M_w pair

- ● S216 (LDPE)
- ○ 10% S229
- △ 30% S229
- ▽ 50% S229
- ▲ 70% S229
- □ 90% S229
- ○ S229 (LLDPE)

Dynamic viscosity, η', Pas

Frequency, ω, rad/s
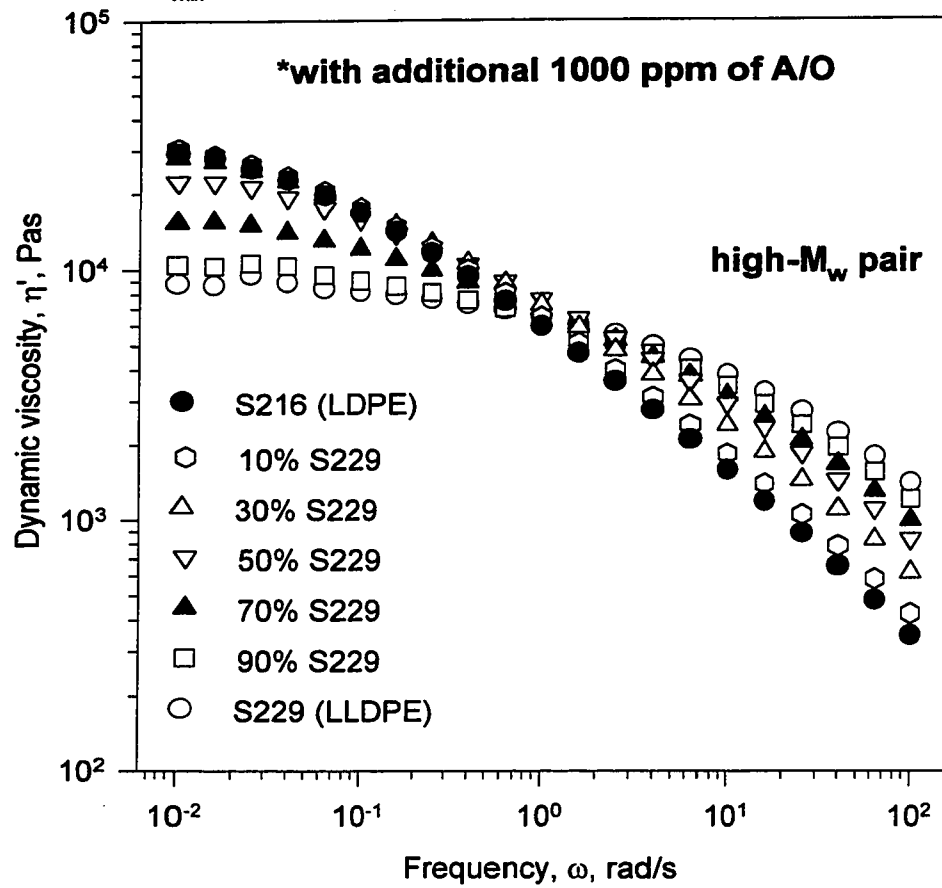
viscosity of a polymer blend beyond the viscosity of its 'pure' components is not consistent with any of the mixing rules (like linear- or log-additivity rules). On the other hand, two-phase models (like emulsion models) can easily explain our observations.

At low ω, $\eta'(\omega)$ for the 10 and 30% S229 (LLDPE) blends are almost the same as that of S216 (LDPE), i.e. the addition of the less viscous polymer to the more viscous polymer did not result in a blend of a lower viscosity. Again, this observation is difficult (if not impossible) to explain with the above-mentioned mixing rules. At high ω ($\omega>10$ rad/s), the blend viscosities were bounded by those of the 'pure' polymers and the increase/decrease in viscosity followed the increase of one component or the other. This behavior might suggest the miscibility of the blend at high shear rate (typical for polymer processing). At high ω ($\omega>10$ rad/s), Schloz et al. (1989) reported that the values of the dynamic moduli for the immiscible blend of PP/PA6 were intermediate between those of PA6 and PP. Therefore, the high ω data should <u>not</u> be used for the interpretation of the miscibility of a blend. This 'apparent' miscibility of the melt will likely be lost as soon as it gets a chance to relax, restoring immiscibility in the melt and possibly leading to phase separation locked into the solid state.

The ϕ-dependence of the previous $\eta'(\omega)$ data are presented in Figures 6.6 a, b and c as linear plots of $\eta'(\phi)_{\omega=const}$ for $\omega=0.04$, 0.1, and 10 rad/s respectively. Semi-log plots of $\eta'(\phi)_{\omega=const}$ are given in the Appendix (Figures C.6 to C.9). The low ω data ($\omega=0.04$; 0.1 rad/s) showed a strong PDB from linear-additivity (Figures 6.6 a, b) and log-additivity (Figures C.6 and C.7) rules in the LDPE-rich blends and around $\phi=50\%$ with the blend viscosity exceeding (in some cases) the viscosity of the more viscous component. The $\eta'(\phi)$ for LLDPE-rich blends tended to follow the linear-additivity rule.

Figure 6.6a $\eta'(\phi)$ for blends* of S229 (LLDPE) and S216 (LDPE)

(T_{mix}=190°C, 50 rpm, 10 min.; T_{test}=190°C, $\gamma°$=10%, ω=0.04 rad/s)

*with additional 1000 ppm of A/O

high-M_w pair

Dynamic viscosity, η', Pas

S229 (LLDPE), ϕ, %

Figure 6.6b η'(φ) for blends* of S229 (LLDPE) and S216 (LDPE)

$(T_{mix}=190°C, 50\ rpm, 10\ min.; T_{test}=190°C, \gamma=10\%, \omega=0.1\ rad/s)$

high-M_w pair

*with additional 1000 ppm of A/O
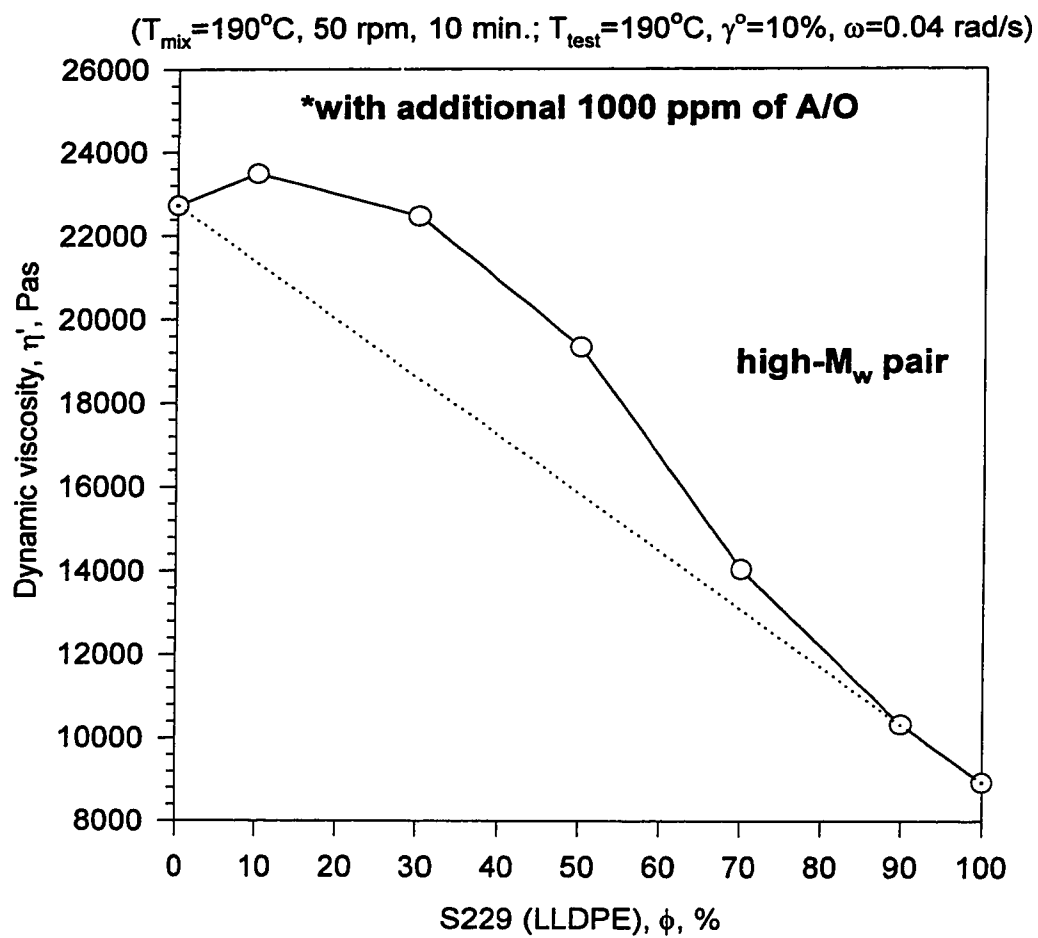
S229 (LLDPE), φ, %
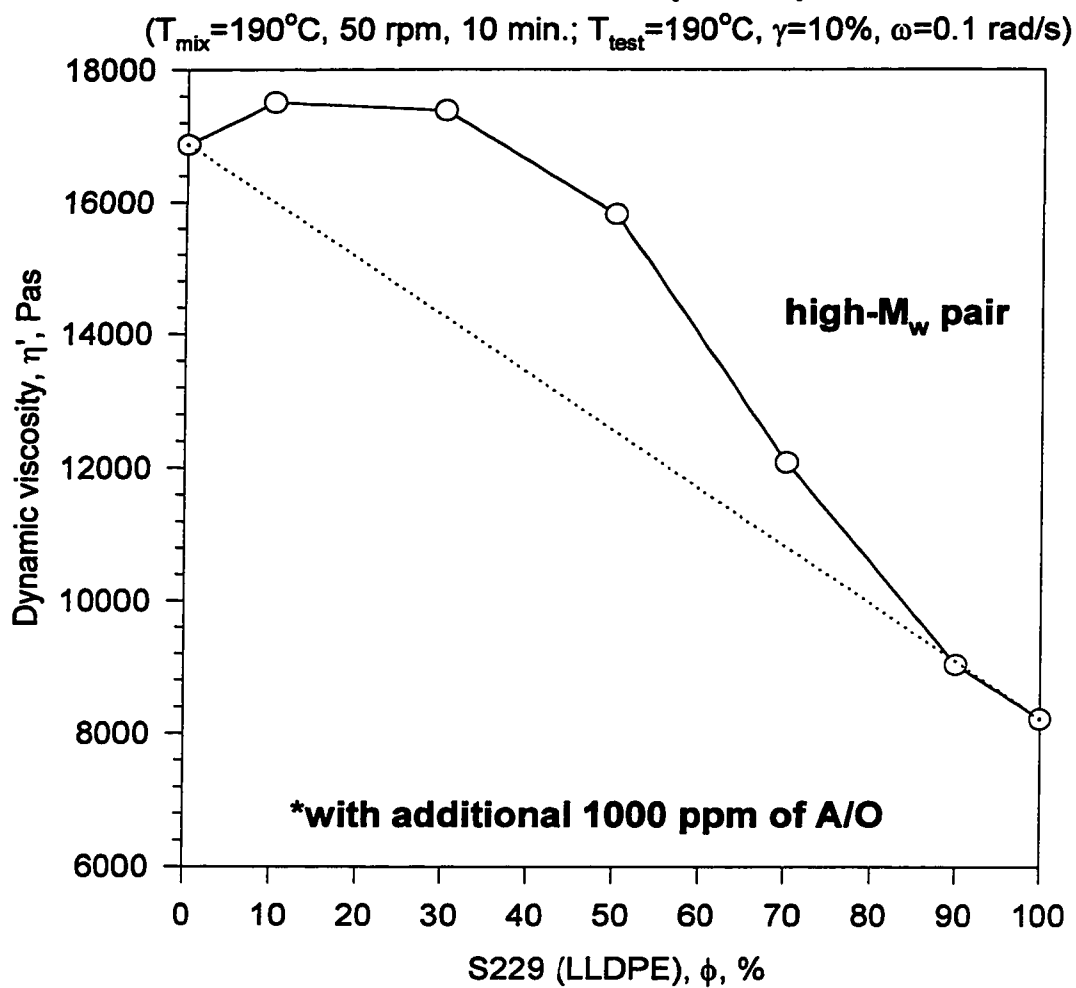
However, the semi-log plots of $\eta'(\phi)_{\omega=const}$ (used to check the applicability of the log-additivity rule) were generally showing much stronger PDB compared to the linear additivity rule. Furthermore, 'apparent' miscibility was observed (Figures 6.6c and C.8; C.9) at high ω ($\omega=10$, 100 rad/s).

The previous set of $\eta'(\omega)$ data, given in Figure 6.5, are displayed in Figure 6.7 as $\eta'(\tau)$, where τ was calculated as: $\tau = \eta^* \times \omega$. The log-log plots of $\eta'(\tau)$ were fitted by the following 3rd order polynomial:

$$\log \eta' = a_o + a_1 x + a_2 x^2 + a_3 x^3, \; x = \log \tau \qquad (6.1)$$

The parameters a_o to a_3 as well as the regression coefficients are given in Table 6.1.

Table 6.1: Results of the regression analysis for Equation 6.1

Composition	a_o	a_1	a_2	a_3	r^2
S216 (LDPE)	4.4544	-0.1898	0.2107	-0.0531	1.0000
10% S229	4.4117	-0.0521	0.1363	-0.0414	0.9999
30% S229	4.5457	-0.1088	0.1059	-0.0309	0.9998
50% S229	4.5570	-0.1976	0.1129	-0.0268	0.9995
70% S229	5.4051	-1.0729	0.3432	-0.0438	0.9994
90% S229	5.9850	-1.7472	0.5292	-0.0577	0.9994
100% S229 (LLDPE)	6.0709	-1.9104	0.5793	-0.0611	0.9996

The continuous lines in Figure 6.7 represent the curve fit of the data using equation 6.1. The plots of $\eta'(\tau)$ followed the same previous trend of $\eta'(\omega)$, but, here, the curves are distinctly separated from each other. This observation supports the suggestion of Van Oene (1978) that:

Figure 6.6c $\eta'(\phi)$ **for blends* of S229 (LLDPE) and S216 (LDPE)**

(T_{mix}=190°C, 50 rpm, 10 min.; T_{test}=190°C, $\gamma°$=10%, ω=10 rad/s)

*with additional 1000 ppm of A/O

high-M_w pair
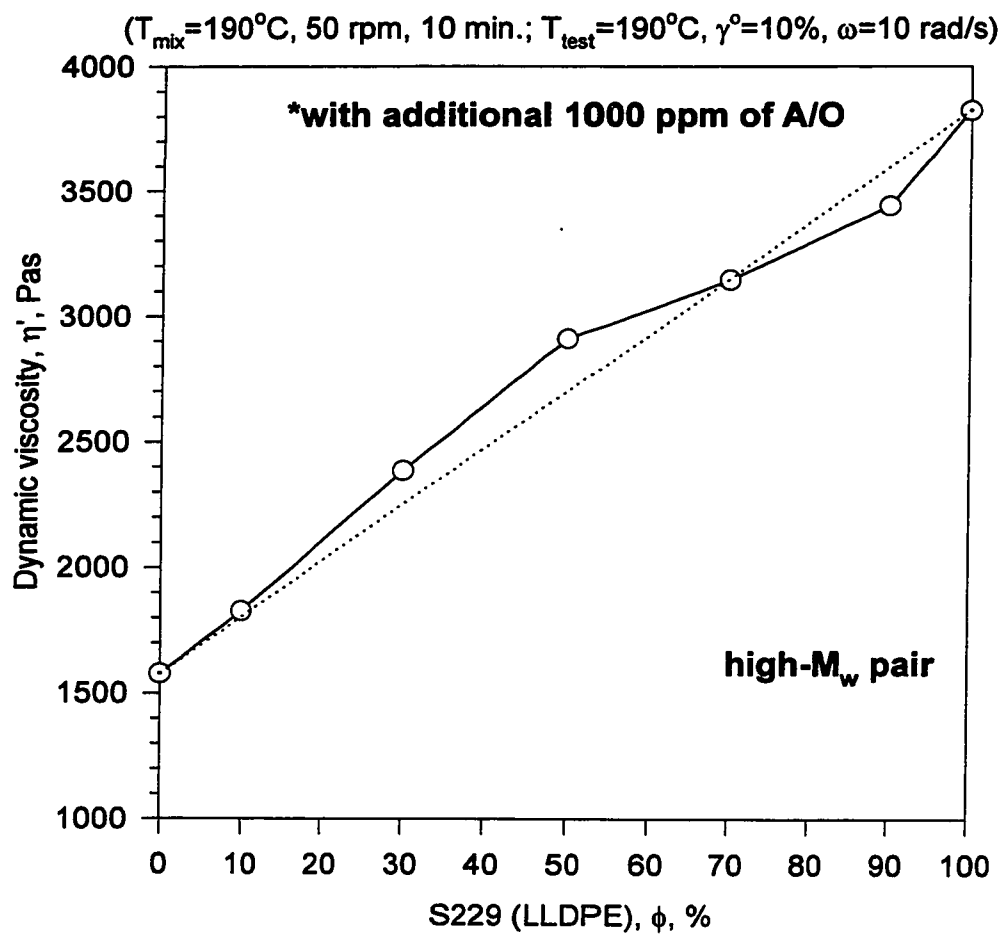
Figure 6.7 $\eta'(\tau)$ for blends* of S216 (LDPE) and S229 (LLDPE)

$(T_{mix}=190^{\circ}C; T_{test}=190^{\circ}C, \gamma=10\%, \omega=0.01\text{-}100 \text{ rad/s})$

*with additional 1000 ppm of A/O

high-M_w pair

○ S216 (LDPE)
▲ 10% S229
▽ 30%S229
▼ 50% S229
△ 70% S229
□ 90% S229
● S229 (LLDPE)

Dynamic viscosity, η', Pas

Stress,τ, ($\eta^* \times \omega$), Pa
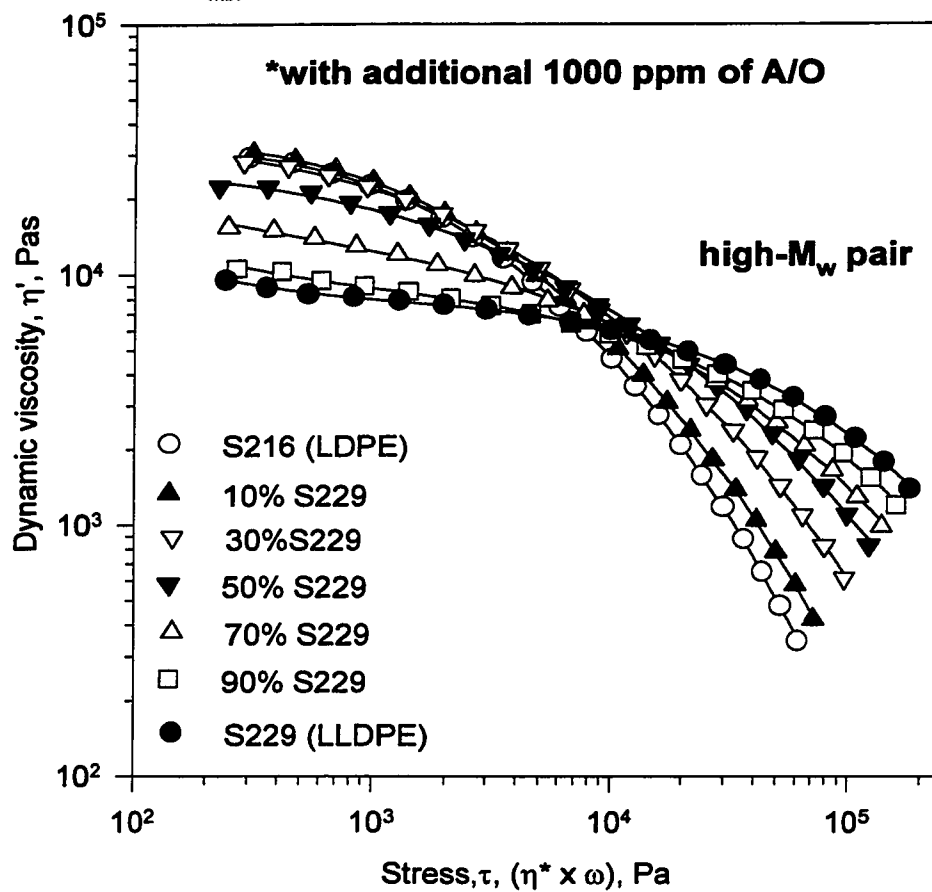
$$(\partial\eta'/\partial\phi)_\tau > (\partial\eta'/\partial\phi)_\omega, \quad \text{for } (\partial\eta'/\partial\tau)_\phi < 0 \tag{6.2}$$

Again, the LDPE-rich and the 50/50 % blends are showing viscosities that are either equal or higher than that of LDPE (the more viscous component) in the range $\tau=2\times10^2$-10^4 Pa.

Equation 6.1 was used to calculate $\eta'(\phi)_\tau$ for $\tau=300$ and 1000 Pa. The $\eta'(\phi)_{\tau=300}$ (Figure 6.8) represents the low stress range which provides the most information about the morphology of the blend. However, the other set of data for $\eta'(\phi)_{\tau=1000}$ (Figure C.10) was used to demonstrate the effect of high τ (or high ω) on the miscibility of the blend. Results for $\eta'(\phi)_\tau$ (Figures 6.8 and C.10) were similar to the previous plots of $\eta'(\phi)_\omega$ (Figures 6.6 a &b) suggesting the immiscibility of the high-M_w pair in the 50/50 composition range as well as the LDPE-rich ($\phi<0.5$) blends. On the other hand, the LLDPE-rich ($\phi>0.5$) blends are likely to be miscible.

The different methods of presenting the dynamic shear data, discussed so far, suggested that the LDPE-rich blends are likely immiscible; and the LLDPE-rich blends are likely miscible. Hence, in a blend of S229 (LLDPE) and S216 (LDPE) a 10% S229 blend is likely to be immiscible while that of 90% S229 is likely miscible. To investigate further the miscibility at the two ends of the composition spectrum, steady shear measurements were performed. As suggested by Utracki and Schlund (1987),

$$\eta'(\omega) \cong \eta(\dot\gamma) \quad \text{for } \omega = \dot\gamma \tag{6.3}$$

and lack of superposition of $\eta'(\omega)$ and $\eta(\dot\gamma)$ is taken as an indication of immiscibility. The steady shear measurements were obtained in the CP geometry in the range $\dot\gamma = 0.01$-1.0 s^{-1}; 3 minutes of steady shearing were allowed as time before measurement (tbm) followed by 30 seconds measurement time (mt).

Figure 6.8 η'(φ) for blends* of S229 and S216 for τ=300 Pa

$(T_{mix}=190°C; T_{test}=190°C, \gamma°=10\%, \omega=0.01\text{-}100 \text{ rad/s})$

*with additional 1000 ppm of AO

high-M_w pair

S229 (LLDPE), φ, %

Dynamic viscosity, η', Pas
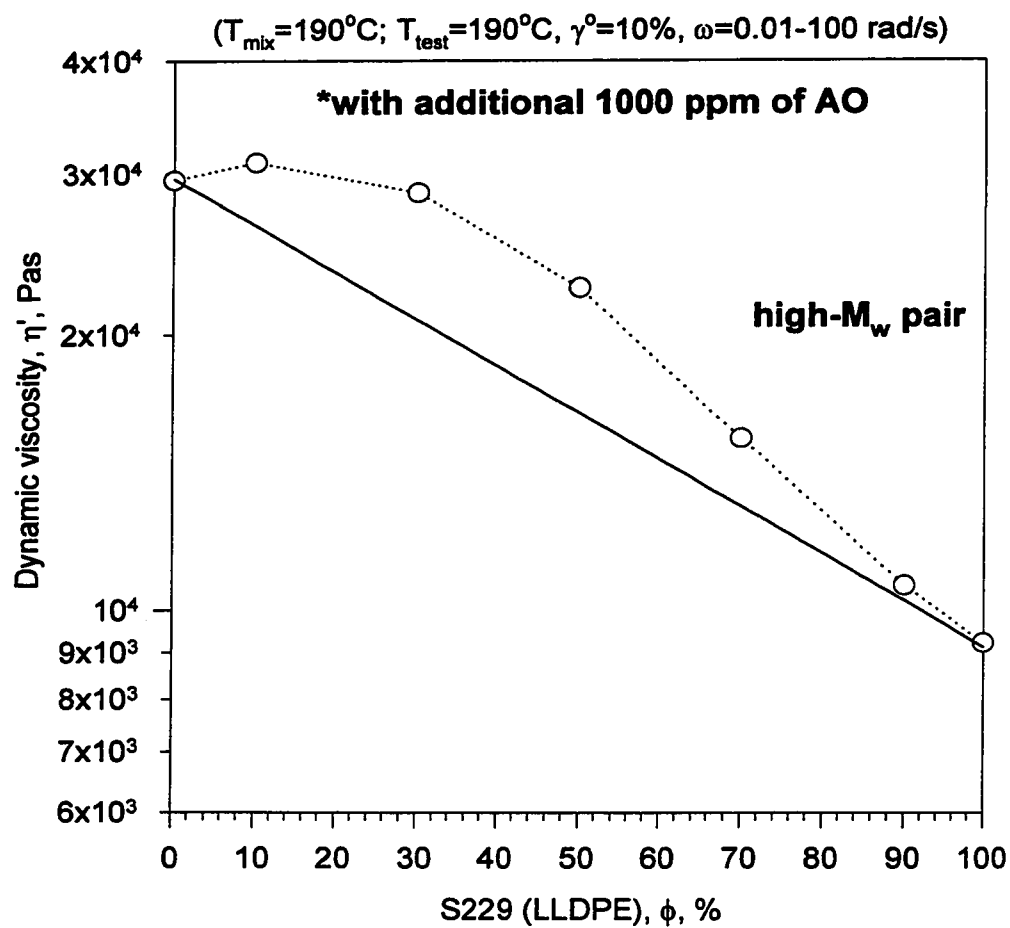
The steady and dynamic shear measurements for the 10% and 90% S229 blend are displayed in Figures 6.9 [as $\eta'(\omega)$ and $\eta(\dot{\gamma})$] and C.11 [as $\eta'(\tau)$ and $\eta(\tau)$]. The 90% blend (LLDPE-rich blend, suggested to be miscible) showed a very good degree of superposition of $\eta'(\omega)$ and $\eta(\dot{\gamma})$ over the whole range of shear confirming the previous interpretations. On the other side, the steady and dynamic shear results for the 10% S229 (LDPE-rich blend, suggested to be immiscible) lacked superposition over the same shear range. Similar observations can be made about $\eta'(\tau)$ and $\eta(\tau)$ data given in Appendix (Figure C.11). This comparison of steady and dynamic shear viscosities on selected compositions that represent the LLDPE-rich and LDPE-rich blends reinforce the findings of the previous methods of data treatment.

In the following paragraphs, other methods of data treatment will be discussed. It is useful to characterize the material behavior with quantifiable parameters, such as $\eta'(\phi)$ at constant ω or τ. The zero-shear viscosity, $\eta_0(\phi)$, is another important parameter. However, for high M_w high-PD materials it is often difficult to observe a Newtonian plateau. This was the case for several samples of the high-M_w pair (see Figures 6.5 and 6.7). In these cases, it is appropriate to use rheological models that can be extrapolated to obtain η_0.

Utracki (1987) proposed a simple generalization of the Carreau 'Model A' relation between viscosity and rate of deformation in steady shear (Carreau, 1972). Utracki and coworkers (Utracki and Schlund, 1987, Utracki, 1989 a& b, Dumoulin et al., 1991) used the following generalization of the $\eta(\dot{\gamma})$ model to describe their $\eta'(\omega)$ data:

$$\eta' = \frac{\eta_o}{\left[1 + (\omega\theta)^{m_1}\right]^{m_2}} \tag{6.4}$$

Figure 6.9 Comparison of $\eta(\gamma)$ and $\eta'(\omega)$ for blends of S229 and S216

$(\gamma^0=10\%, \omega=0.01\text{-}100$ rad/s; tbm=3 min., mt=30 s, $\gamma=0.01\text{-}1$ s$^{-1})$
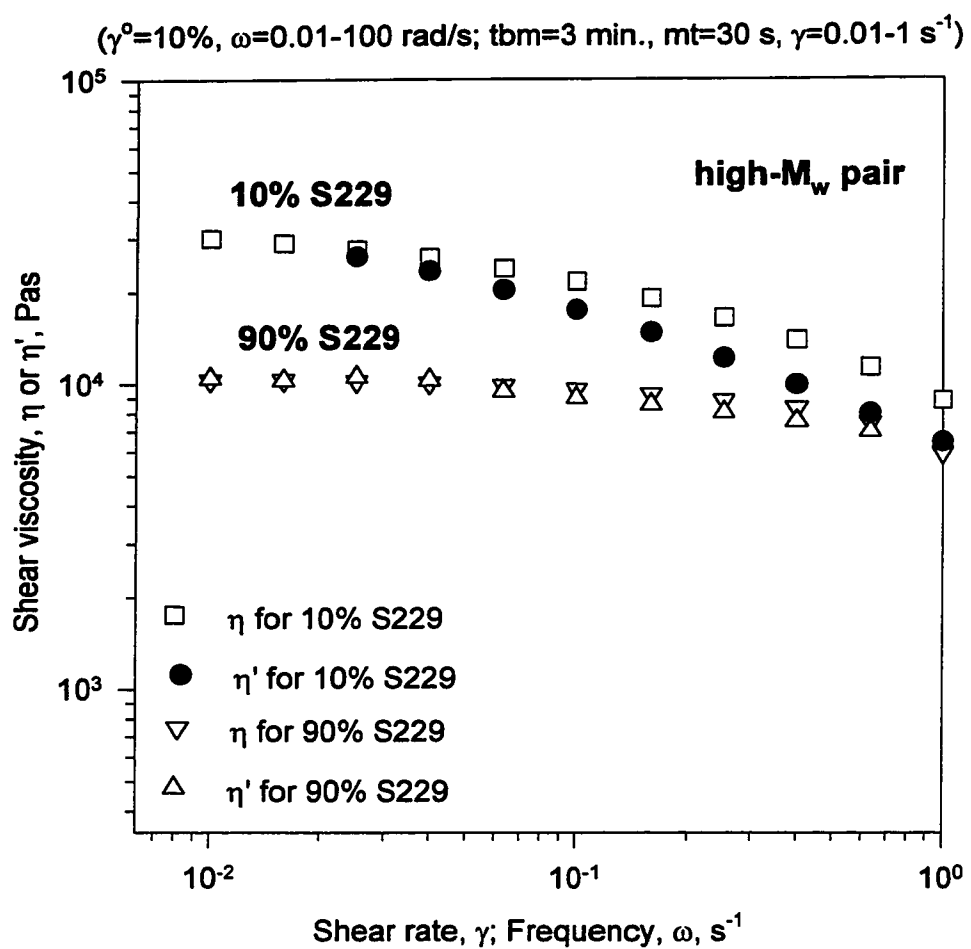
where η_0 is one of the adjustable parameters, the other three being: θ, the mean relaxation time and the two exponents, m_1 and m_2. It can be seen that for large dimensionless frequencies ($\omega\theta \gg 1$), a 'power law', $\eta' = \left(\dfrac{\eta_o}{\theta^{m_1 m_2}}\right) \omega^{-m_1 m_2}$ is recovered. In the context of a traditional powerlaw model, $\tau \propto \omega^n$ so $\eta' = \tau/\omega \propto \omega^{n-1}$. This gives the power law exponent:

$$n = 1 - m_1 m_2 \qquad (6.5)$$

Since $0 \leq n \leq 1$, the values of the product $m_1 m_2$ should also be within these limits. A value outside this range indicates either an experimental error in the data or error in the curve fitting procedure or significant changes in the melt structure (Dumoulin et al., 1991).

The SigmaPlot nonlinear curve fitter was used to fit equation (6.4). It works by modifying the parameters (coefficients) of an equation, and finds the parameters that give the 'best fit' of the data. The $\eta'(\omega)$ data were fitted to equation 6.4 after subtracting the apparent yield stress (will be discussed later). The parameters obtained from the regressions as well as the power law exponent calculated from equation (6.5) are listed in Table 6.2.

The computed $\eta_0(\phi)$, $n(\phi)$, and $\theta(\phi)$ are plotted in Figures 6.10 a & b and C.12 respectively. Typical examples of the curve fitted data are shown in Figures 6.11 and C.13. The shape of the curve of $\eta_0(\phi)$ displayed in Figure 6.10a is similar to those of $\eta'(\phi)_\omega$ given in Figures 6.6a & b ($\omega = 0.04$; 0.1 rad/s respectively) and $\eta'(\phi)_\tau$ shown in Figures 6.8 and C.10 (τ=300; 1000 Pa respectively). The computed $\eta_0(\phi)$ values reinforce the previous observations of the dynamic and steady shear measurement. Blend

Figure 6.10a $\eta_o(\phi)$ for blends of S229 (LLDPE) and S216 (LDPE)

$(T_{mix}=190°C; T_{test}=190°C, \gamma°=10\%)$

Figure 6.10b n(ϕ) for blends of S229 (LLDPE) and S216 (LDPE)

(T_{mix}=190°C; T_{test}=190oC, $\gamma°$=10%, ω=0.01-100 rad/s)
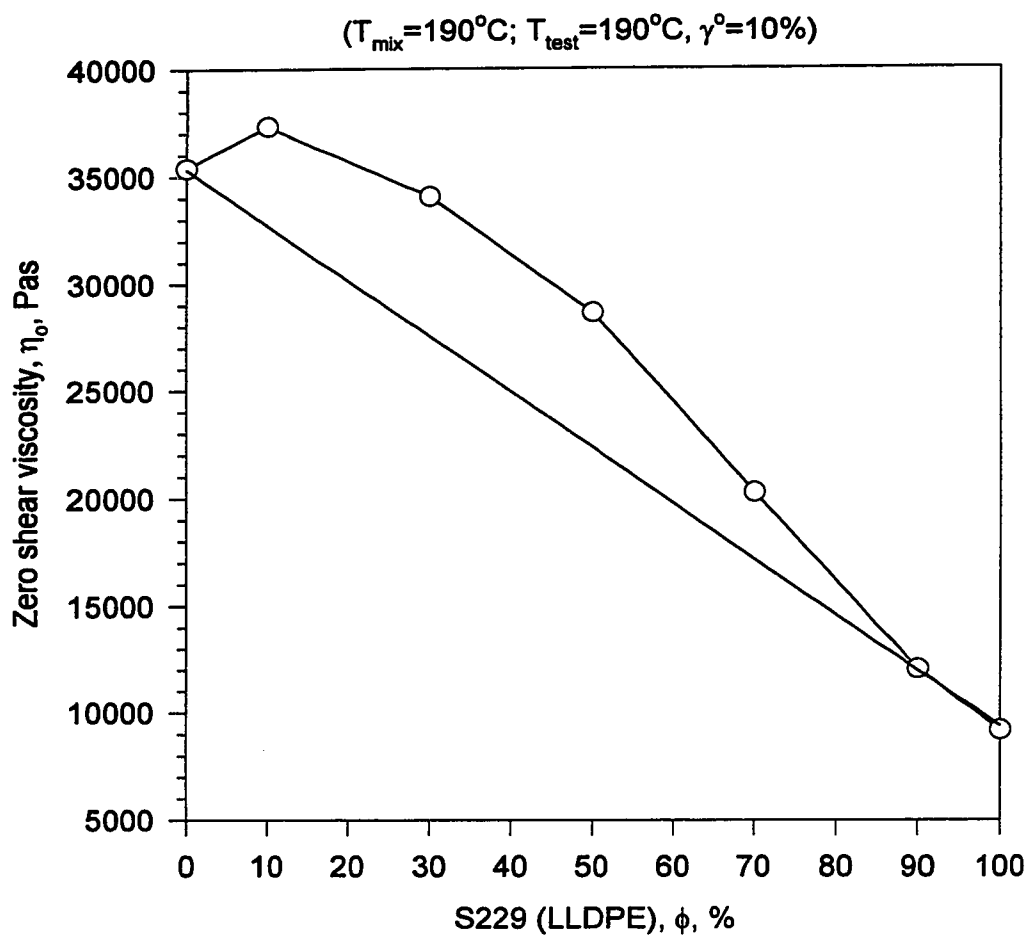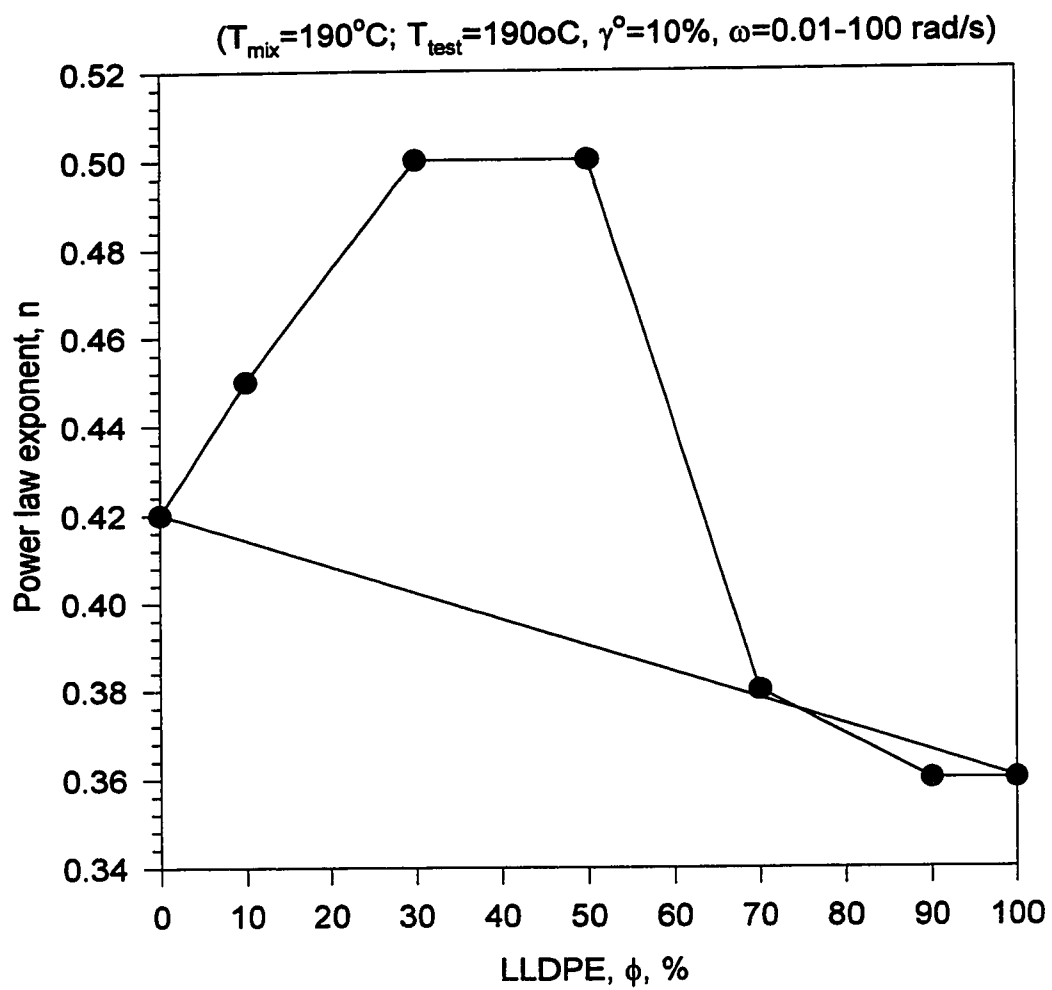
Figure 6.11 $\eta'(\omega)$ for 90% S229 (LLDPE)

$(T_{mix}=190°C; T_{test}=190°C, \gamma°=10\%)$

Experimental data

Curve fit (Table 6.2 parameters used with Carreau Model)
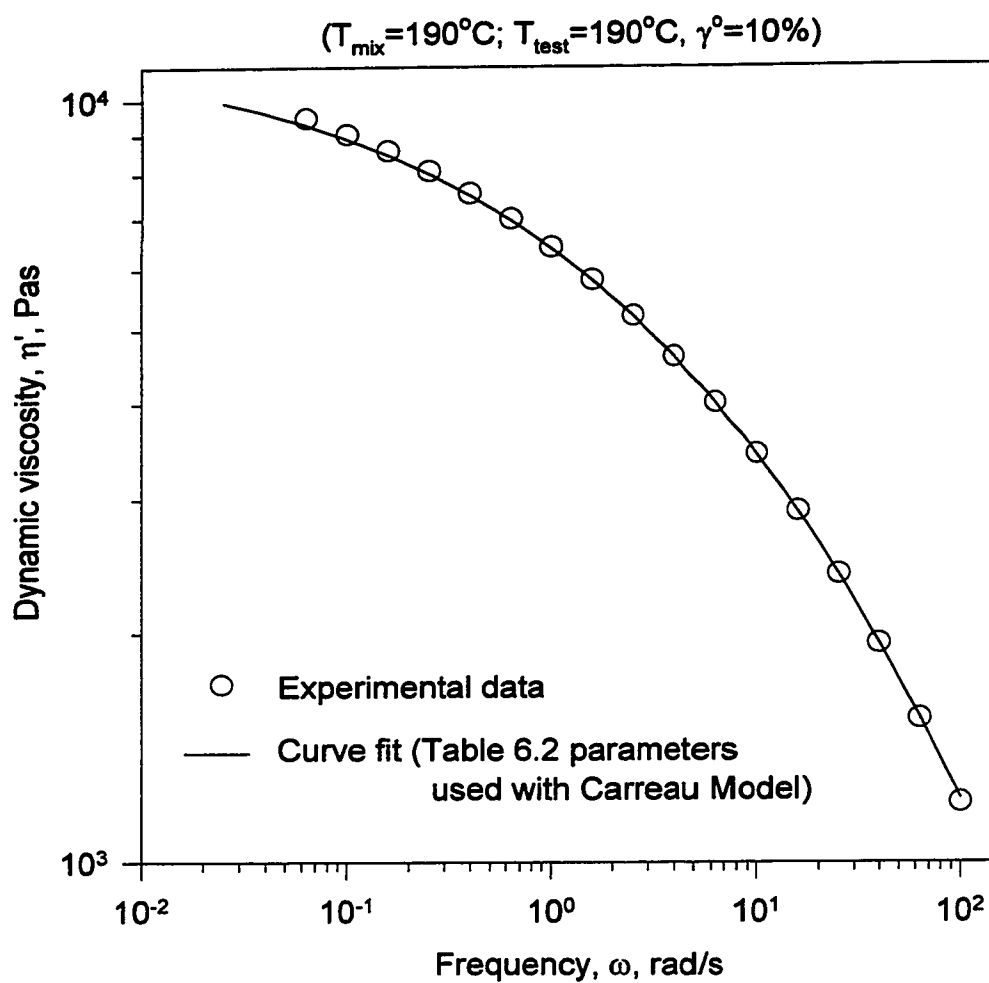
viscosities higher than any of the 'pure' polymers are obtained, and the immiscibility of the LDPE-rich range is suggested by the strong PDB.

Table 6.2: Blends of S229 and S216: Parameters for Equation 6.4 (T_{mix}=190°C)

Composition	η_o (Pas)	θ (s)	m_1	m_2	n
S216 (LDPE)	35390	19.6	0.78	0.74	0.42
10% S229	37340	21.3	0.75	0.74	0.45
30% S229	34060	20.1	0.73	0.68	0.50
50% S229	31610	9.8	0.50	1.0	0.50
70% S229	20270	0.7	0.37	1.68	0.38
90% S229	12040	0.16	0.40	1.61	0.36
100% S229 (LLDPE)	9188	0.13	0.53	1.2	0.36

The mean relaxation time, θ, closely followed the log-additivity rule (see Figure C.12) in the LLDPE-rich range ($\phi \geq 70\%$). However, the 50/50 and the LDPE-rich blends showed a strong PDB. The θ values were high and insensitive to changes in composition in the range $\phi \geq 30\%$ LDPE suggesting the presence of a multiphase system (Scholz et al., 1989; Graebling et al., 1993).

The power law exponent, n, was found to be 0.4<n<0.5, i.e., within the acceptable limit. In this analysis, the power law exponent as function of composition, $n(\phi)$, has emerged as a sensitive and a strong measure of miscibility. It shows a very strong PDB (see Figure 6.10b) in the likely immiscible range of LDPE-rich blends; and followed a linear-additivity behavior in the likely miscible LLDPE-rich blends.

In fitting $\eta'(\omega)$ data to equation (6.4) the apparent yield stress, σ_y, was subtracted from the rheological measurements. The objective of this exercise is to correct the original stress data (σ' and σ'') leading to the calculated $\eta'(\omega)$ [or $\eta''(\omega)$] properties for apparent yield stress (σ_y' or σ_y''), that is usually associated with a structured material or a three-dimensional network (Dumoulin et al., 1991). In the following, the details of the procedure will be discussed.

The numerical values of σ_y' σ_y'' were evaluated by using a modified Casson equation (Utracki and Schlund, 1987; Utracki, 1989 a & b; Dumoulin et al., 1991) as follows:

$$(G')^{1/2} = (\sigma_y')^{1/2} + a_o(G'_m)^{1/2} \tag{6.6a}$$

$$(G'')^{1/2} = (\sigma_y'')^{1/2} + a_o(G''_m)^{1/2} \tag{6.6b}$$

where G', G'' are respectively the storage and loss moduli for the blend, and G'_m G''_m are respectively the storage and loss moduli for the matrix. From dynamic test data, a yield stress, σ_y', corresponding to the storage component, G', and σ_y'' for the loss component were computed. Following the modified Casson equation approach, σ_y' was obtained by plotting $\sqrt{G'(\omega)}$ for each blend vs. $\sqrt{G'_m(\omega)}$ of the corresponding matrix (at the same ω) and then extrapolated to $G'_m=0$ (as suggested by equation 6.6a), with the intercept being $\sqrt{\sigma_y'}$. A similar procedure with the loss moduli yielded σ_y''. The values of σ_y' and σ_y'' as well as the material taken as the matrix are shown for the high-M_w pair, mixed at 190°C, in Appendix D (Table D.1).

This Casson approach is illustrated in Figures 6.12 and C.14 for the 90% S229 (LLDPE). The LLDPE was taken as the matrix for the (immiscible) blend. An alternative

Figure 6.12 Calculation of $\sigma_y{}''$ for 90% S229 (LLDPE)

$(T_{mix}=190°C; T_{test}=190°C, \gamma°=10\%)$
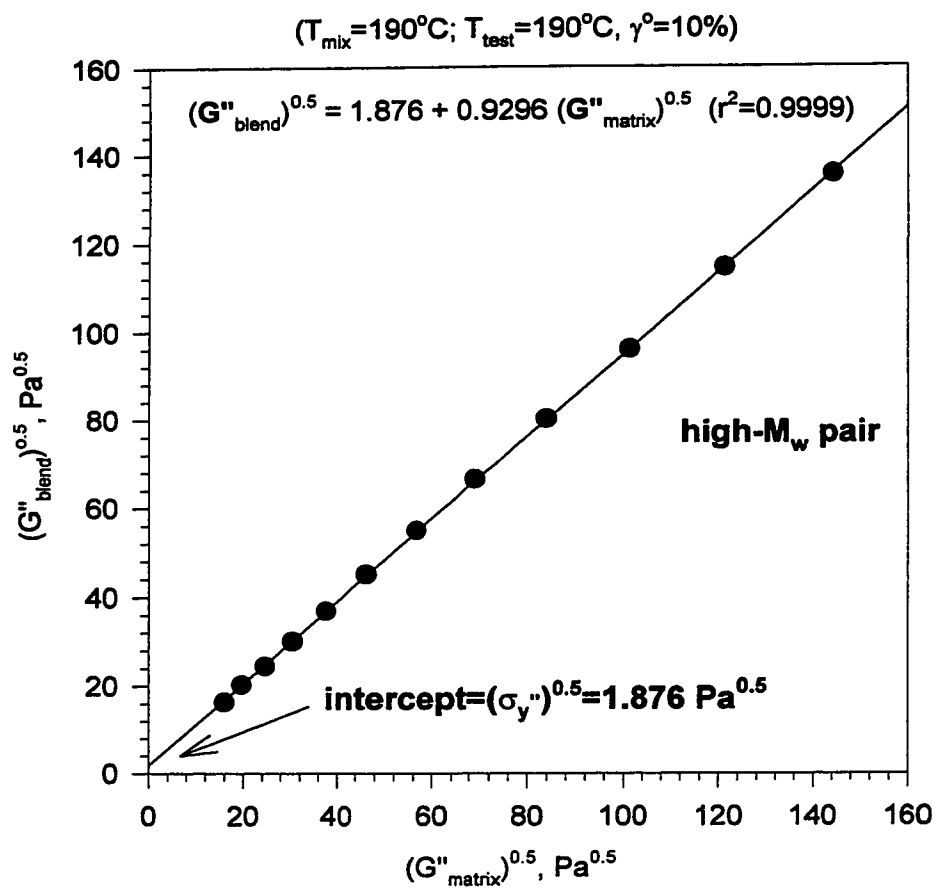
approach to finding σ_y' and σ_y'' is discussed in Appendix D. It extracts σ_y' and σ_y'' for each blend from the corresponding $G''(\omega)$ and $G'(\omega)$ data from a single dynamic measurement. Results are same as those of the modified Casson equation.

It is clear that the values of σ_y' and σ_y'' are small. Nevertheless, the values of σ_y'' were subtracted from the corresponding $G''(\omega)$ and then the corrected $\eta'(\omega)$ was obtained as: $\eta'(\omega)=G''(\omega)/\omega$. The $\eta'(\omega)$ data used in fitting equation (6.4) were corrected in this fashion. Similarly, it is possible to calculate other rheological functions that are free from the yield stress phenomenon.

The analysis above has centered on the viscous component of the melt dynamic response $[\eta'(\omega)]$. Here, the focus will next be turned to the behavior of the elastic component for different compositions, such as $G'(\omega)$ and $G'(\phi)_{\omega=const}$. Plots of $G'(\omega)$ are given in Figure 6.13 for blends of S229 and S216 mixed at 190°C. The overall behavior is similar to that of $\eta'(\omega)$ shown earlier in Figure 6.5. At low ω, the $G'(\omega)$ plots are separated from each other with G' showing composition independency for the LDPE-rich blends. This observation is manifested in the linear plots of $G'(\phi)_\omega$ displayed in Figures 6.14 a, b & c and C.15 (ω=0.04 to 100 rad/s). The semi-log plots of $G'(\phi)_\omega$ given in Appendix (Figures C.16 to C.19) show the same behavior with much stronger PDB in the low ω range (sensitive to morphology). The LDPE-rich blends are suggested to be immiscible while the LLDPE-rich blends are miscible. At high ω (Figure 6.14c), 'apparent' miscibility is indicated.

At this stage, we would like to give a tentative explanation for the high η' (and G'') at low ω of the LDPE-rich blends. The likelihood of these blends being two-phase

Figure 6.13 G'(ω) for blends* of S229 (LLDPE) and S216 (LDPE)
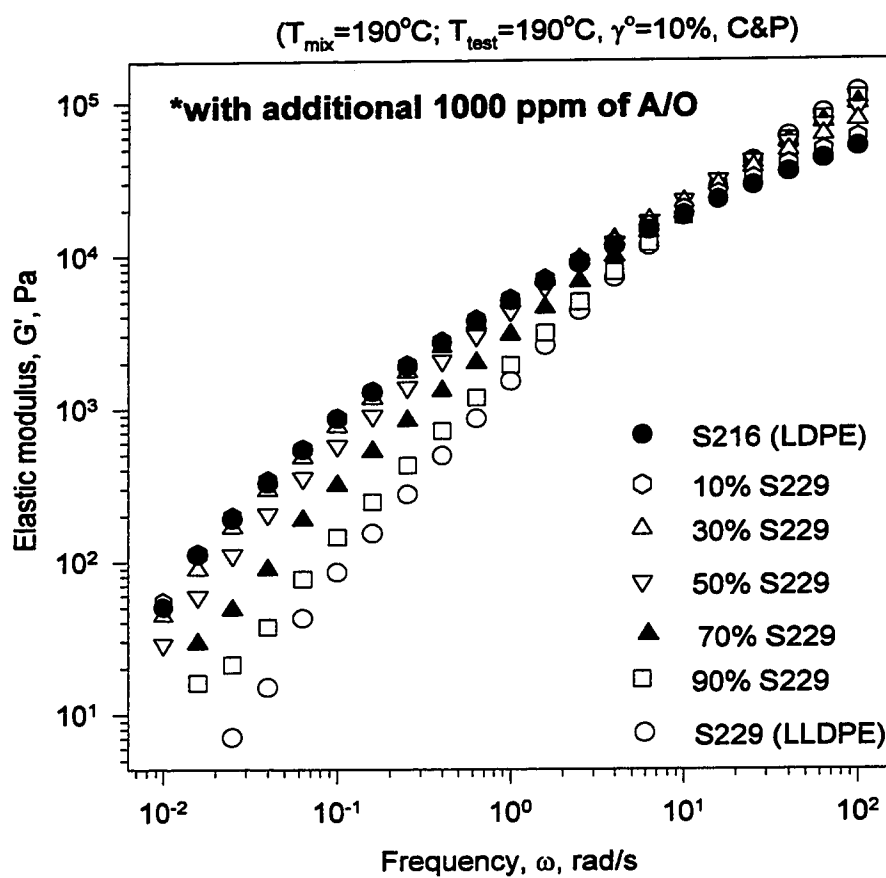
$(T_{mix}=190°C; T_{test}=190°C, \gamma°=10\%, C\&P)$

*with additional 1000 ppm of A/O

- ● S216 (LDPE)
- ○ 10% S229
- △ 30% S229
- ▽ 50% S229
- ▲ 70% S229
- □ 90% S229
- ○ S229 (LLDPE)

Elastic modulus, G', Pa

Frequency, ω, rad/s

Figure 6.14a G'(φ) for blends* of S229 (LLDPE) and S216 (LDPE)

(T_{mix}=190°C, 50 rpm, 10 min.; T_{test}=190°C, γ=10%, ω=0.04 rad/s)

*with additional 1000 ppm of A/O

Figure 6.14b G'(φ) for blends* of S229 (LLDPE) and S216 (LDPE)

(T$_{mix}$=190°C; T$_{test}$=190°C, γ°=10%, ω=0.1 rad/s)

Figure 6.14c G'(φ) for blends* of S229 (LLDPE) and S216 (LDPE)

(T_{mix}=190°C; T_{test}=190°C, γ°=10%, ω=100 rad/s)

*with additional 1000 ppm of A/O
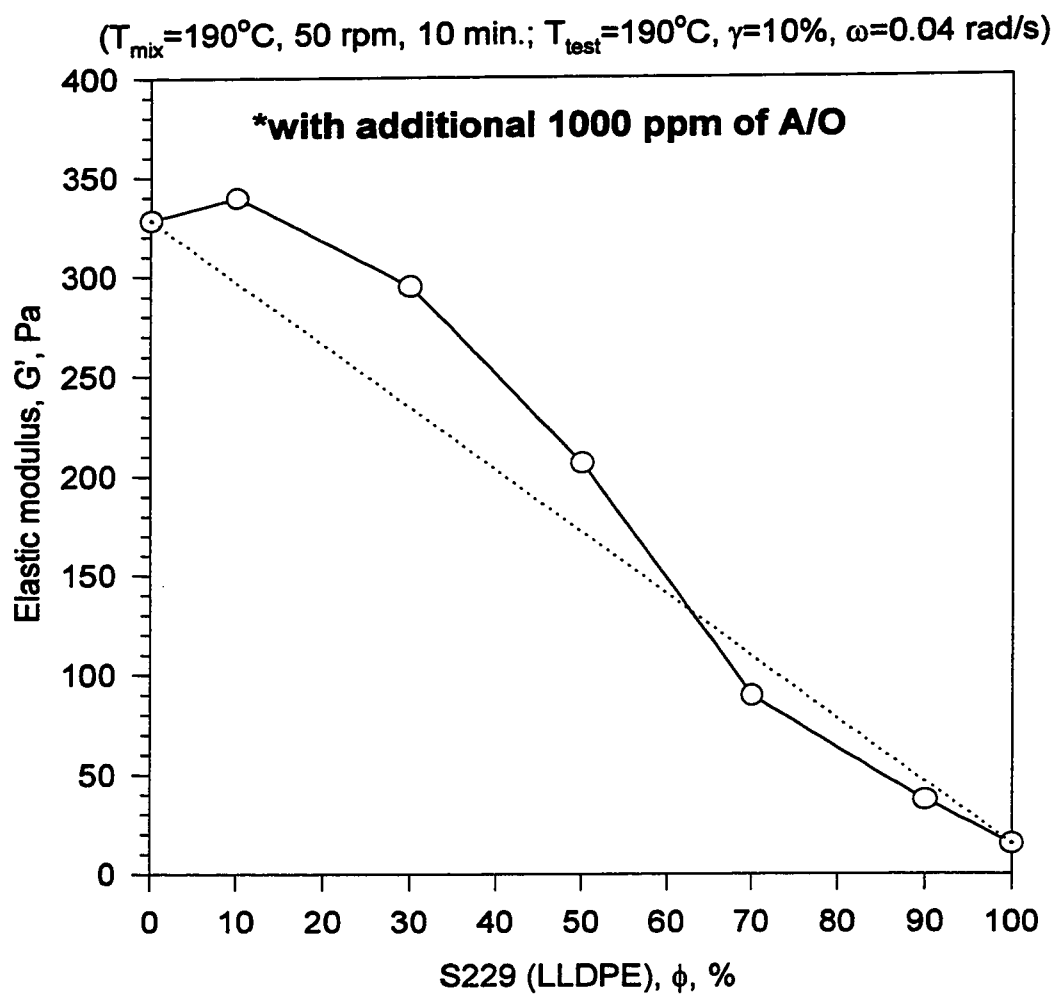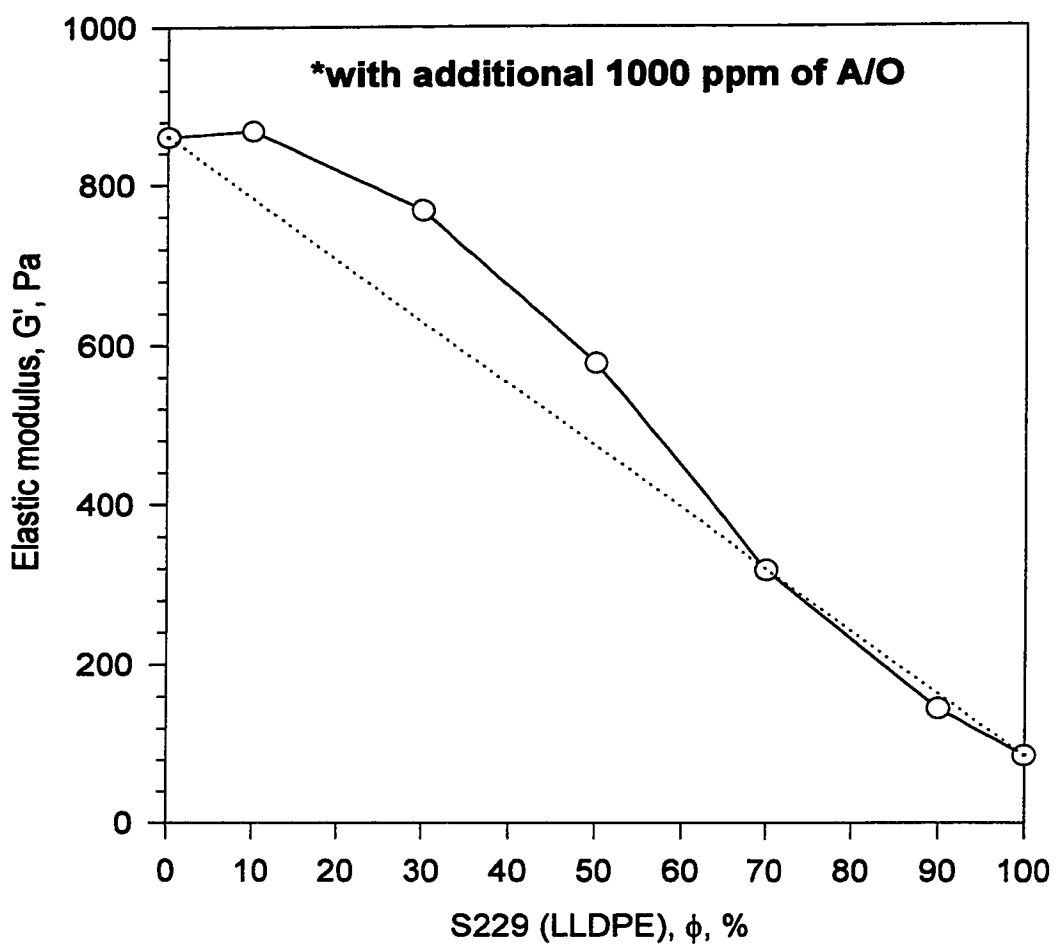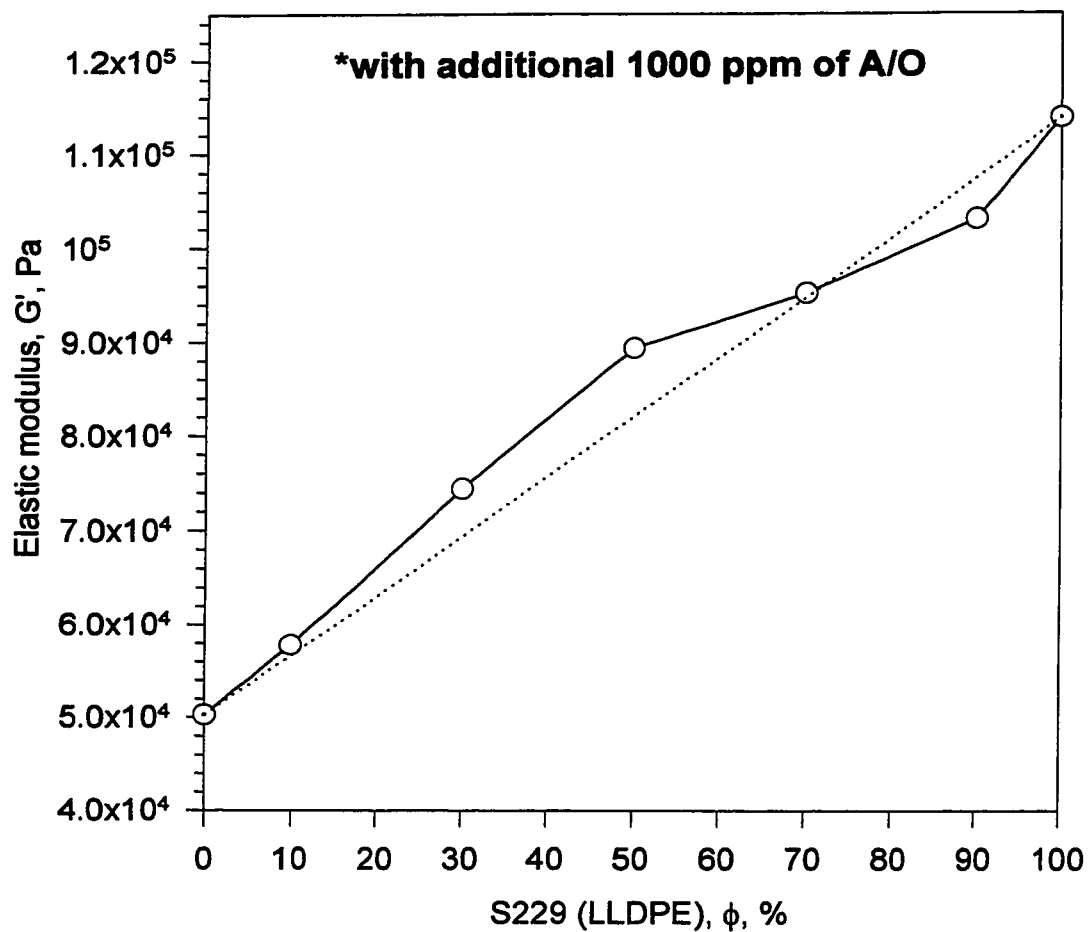
systems (already supported by various arguments above), will be analyzed in terms of rheological models of dilute emulsions developed for noninteracting, spherical monodisperse droplets of Newtonian liquids. The two liquids are assumed to be incompressible, and totally immiscible. The dilute emulsion models were previously used to explain the two-phase behavior of other polymeric blend systems (Martinez and Williams, 1980; Scholz et al., 1989; and Graebling et al. 1993). It is well founded to consider this simplified situation only in the near-Newtonian limit (at $\omega<0.2$ rad/s) where dynamic viscosities of both phases are almost independent of ω (Scholz et al., 1989), and where elasticity can be neglected ($G'<<G''$).

For small-γ° dynamic shear experiments, Scholz et al. (1989) showed that the expressions of the loss modulus of the emulsion reduce to:

$$\frac{G''(\omega)}{\omega} = \eta'(\omega) = \eta_1\left[1+\left(\frac{1+2.5\lambda}{1+\lambda}\right)\phi\right]$$ (6.7)

$$\lambda = \frac{\eta_2}{\eta_1}$$ (6.8)

where: η_1 and η_2 are respectively the matrix and droplet viscosities, and ϕ is the volume fraction. The viscosity of the 10% S229 blend ($\phi=0.1$) was estimated using equation (6.7). The emulsion viscosity of the 10% blend was calculated using $\eta'_{\omega=0.1}$, $\eta'_{\omega=0.04}$, and η_0. Results are given in Table 6.3. The viscosities η_1 and η_2 for $\omega=0$ are the zero-shear viscosities, η_0, calculated by equation (6.4).

As shown in Table 6.3, the emulsion model gives good prediction of the blend viscosity especially at low ω. Further, this simple model predicts and explains the

increase in the viscosity of LDPE due to the addition of 10% LLDPE. The above calculations could be repeated to explain the PDB observed for LDPE-rich blends.

Table 6.3: Viscosities for the 10% S229 Blend (T_{mix}=190°C)

ω rad/s	Matrix	η_1' Pas	η_2' Pas	η_{theor}' Pas	η_{exp}' Pas	$\Delta\eta' / \eta_{theor}'$ (%)
0	LDPE	35,390	9,188	40,020	37,340	6.7
0.04	LDPE	22,730	8,925	25,964	23,490	9.5
0.1	LDPE	16,870	8,213	19,386	17,510	9.7

Further, the mCC plot was used to evaluate the miscibility of the high-M_w pair. The G' vs. G'' data for the high-M_w pair are given in Figure 6.15a. The log G' vs. log G'' data for the LDPE-rich blends were overlapping at low ω (low G' and G''). The data in Figure 6.15a were then shifted to construct a master curve (Figure 6.15b) by superposition, similar to that explained in Figure 6.4b. The shift factor, $a_*(\phi)$, is shown in Appendix (Figure C.20). The mCC plot showed a very good degree of superposition in the high ω range (high G' and G''). In the low ω range, which is significant for miscibility interpretations, the superposition was poor, suggesting immiscibility. Such superposition is comparable to that of the $\eta'(\phi)$ and $G'(\phi)$ data discussed earlier. Unlike the low-M_w pair, the $a_*(\phi)$ plot for the high-M_w pair was <u>not</u> linear.

In summary, several data-treatment approaches were used. First, plots of $\eta'(\omega)$, $\eta'(\phi)|_{\omega=const}$, $\eta'(\tau)$, $G'(\omega)$, $G'(\phi)|_{\omega=const}$ were shown to be beneficial; making it possible to identify the miscible and phase-separated regions in the high-M_w blends. Second, the comparison of $\eta'(\omega)$ and $\eta(\dot{\gamma})$ was found to be an important indicator of miscibility.

Figure 6.15a G' vs. G" for blends of S216 (LDPE) and S229 (LLDPE)

$(T_{mix}=190°C, \gamma°=10\%, \omega=0.01\text{-}100\%)$
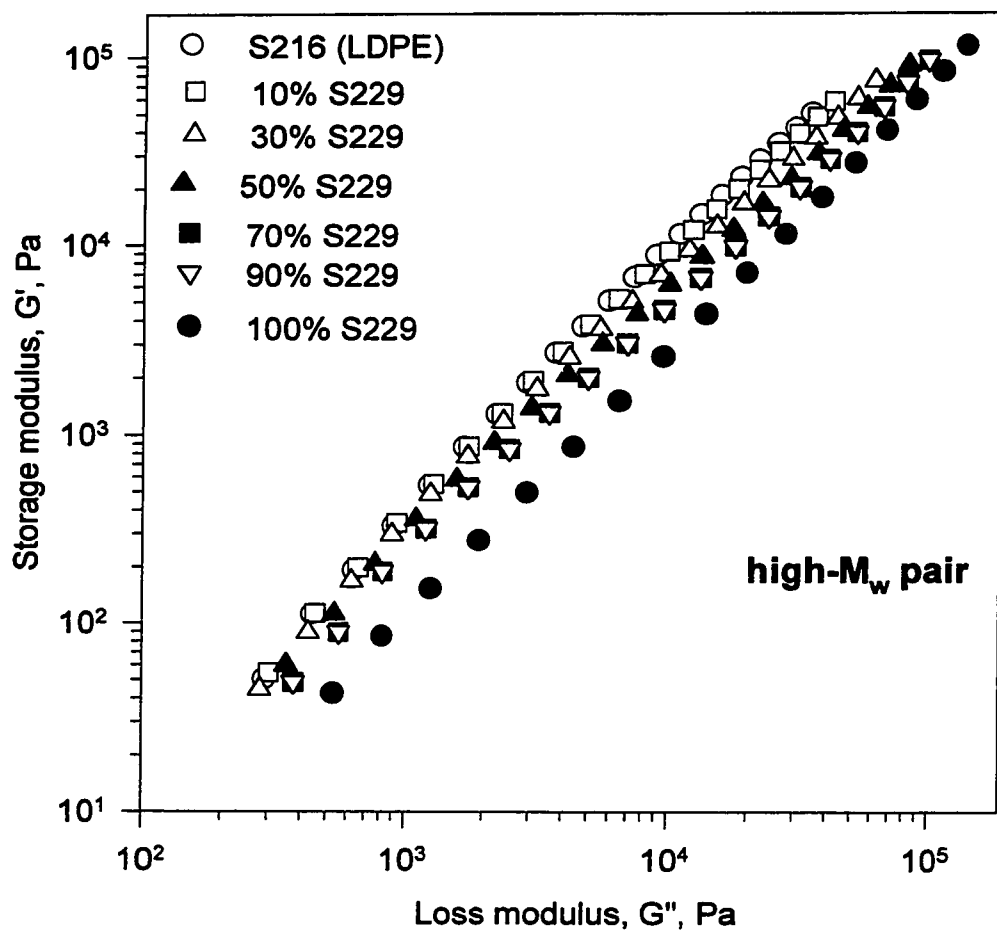
Figure 6.15b G' vs. G" for blends of S216 (LDPE) and S229 (LLDPE)

$(T_{mix}=190°C; T_{test}=190°C, \gamma°=10\%, \omega=0.01\text{-}100\%)$
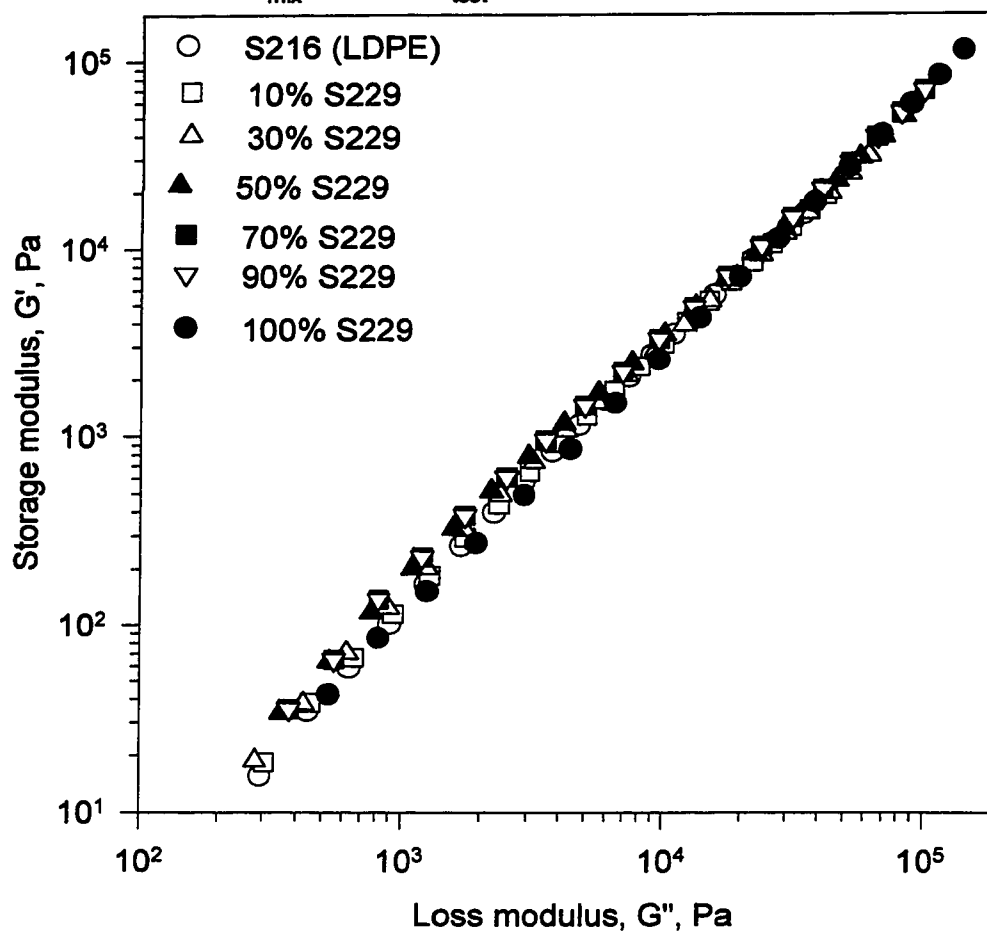
Third, the modified Casson equation was employed to evaluate the 'apparent' yield stress and calculate rheological functions free from yield stress phenomena. Fourth, the four-parameter Carreau model was used to model $\eta'(\omega)$ data, allowing the assessment of miscibility through $\eta_o(\phi)$. Finally, the mCC plots were also utilized. Although the technique is somewhat involved compared to the previous methods, yet it does <u>not</u> identify ϕ-regions of miscibility for the partially miscible systems.

Thus, the different methods of data treatment suggest that the high-M_w pair mixed at 190°C is likely <u>miscible</u> in the *LLDPE-rich* blends ($\phi\geq70\%$ LLDPE); and likely <u>immiscible</u> in the 50/50 and *LDPE-rich* blends ($\phi\geq50\%$ LDPE). The immiscibility of the blends can be explained by a simple emulsion model.

Furthermore, the effect of the mixing temperature (T_{mix}) was examined by testing another set of the high-M_w pair following melt blending at <u>220°C</u> (to compare with T_{mix}=190°C used in cases described above). Other blender and RMS testing conditions remained the same; and the dynamic shear data were analyzed in a similar fashion.

Plots of $\eta'(\omega)$ and $\eta'(\tau)$ are given in Appendix (Figures C.21 and C.22 respectively) for the high-M_w pair torqued at 220°C. At low ω (low τ), the LDPE-rich blends ($\phi<50\%$) showed viscosities that are closer to that of LDPE (high η_o) than at 190°C. However, the viscosity of the 10% S229 blend was again observed to be higher than that of LDPE ($\eta_{o,\ LDPE} > \eta_{o,\ LLDPE}$) over more than a decade of ω (or τ). This observation is visible in plots of $\eta'(\phi)_{\omega=const}$ that are shown in Figures 6.16 and C.23. Unlike the previous data with T_{mix}=190°C, blends torqued at 220°C also displayed PDB in the LLDPE-rich blends. The PDB was observed over the whole range of composition

Figure 6.16 $\eta'(\phi)$ for blends* of S229 (LLDPE) and S216 (LDPE)

$(T_{mix}=220°C; T_{test}=190°C, \gamma°=10\%, \omega=0.04 \text{ rad/s})$

**with additional 1000 ppm of A/O*

high-M_w pair

Dynamic viscosity, η', Pas

S229 (LLDPE), ϕ, %
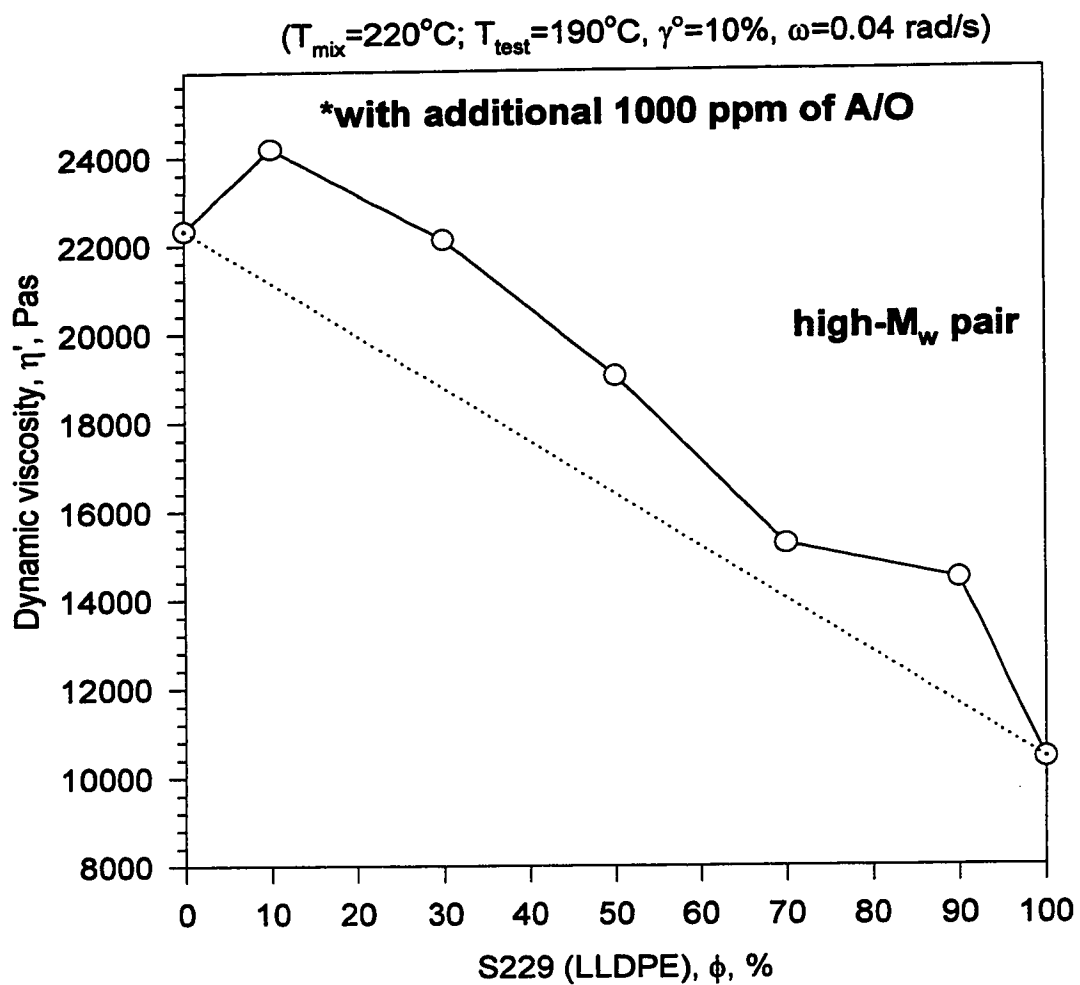
with less PDB at ϕ=70%. At high $\omega \geq 10$ rad/s, the linear additivity rule is almost followed (see Figures C.24 and C.25).

Further, the yield stresses, $\sigma_y{}'$ and $\sigma_y{}''$, were calculated using the modified Casson equations (6.6 a&b) following the previously described procedure. Results are given in Appendix D (Table D.2).

The values of $\sigma_y{}''$ were subtracted from the corresponding G'' and then the corrected $\eta'(\omega)$ were obtained and fitted to the Carreau Model (equation 6.4). SigmaPlot software was used to calculate the parameters of equations 6.4 and 6.5. Results are displayed in Table 6.4. The zero-shear viscosity, η_o, and the mean relaxation time, θ, are also shown in Figures 6.17 and C.26 respectively. Both η_o and θ showed PDB over the whole composition range except the 70% S229. These findings support the $\eta'(\phi)_{\omega<1}$ observations that were discussed earlier. The η_o for the 70% blend followed the linear additivity rule, suggesting its miscibility.

Table 6.4: Blends of S229 and S216: Parameters for Equation 6.4 (T_{mix}=220°C)

Composition	η_o (Pas)	θ (s)	m_1	m_2	n
S216 (LDPE)	31,430	19.1	0.93	0.60	0.44
10% S229	34,710	21.1	0.91	0.59	0.46
30% S229	32,480	20.7	0.79	0.62	0.51
50% S229	29,530	13.4	0.57	0.83	0.53
70% S229	18,170	6.81	0.67	0.62	0.58
90% S229	18,720	5.28	0.52	0.78	0.59
100% S229 (LLDPE)	12,260	0.14	0.39	1.61	0.37

Figure 6.17 $\eta_o(\phi)$ for blends* of S229 (LLDPE) and S216 (LDPE)

$(T_{mix}=220°C; T_{test}=190°C, \gamma°=10\%)$

*with additional 1000 ppm of AO
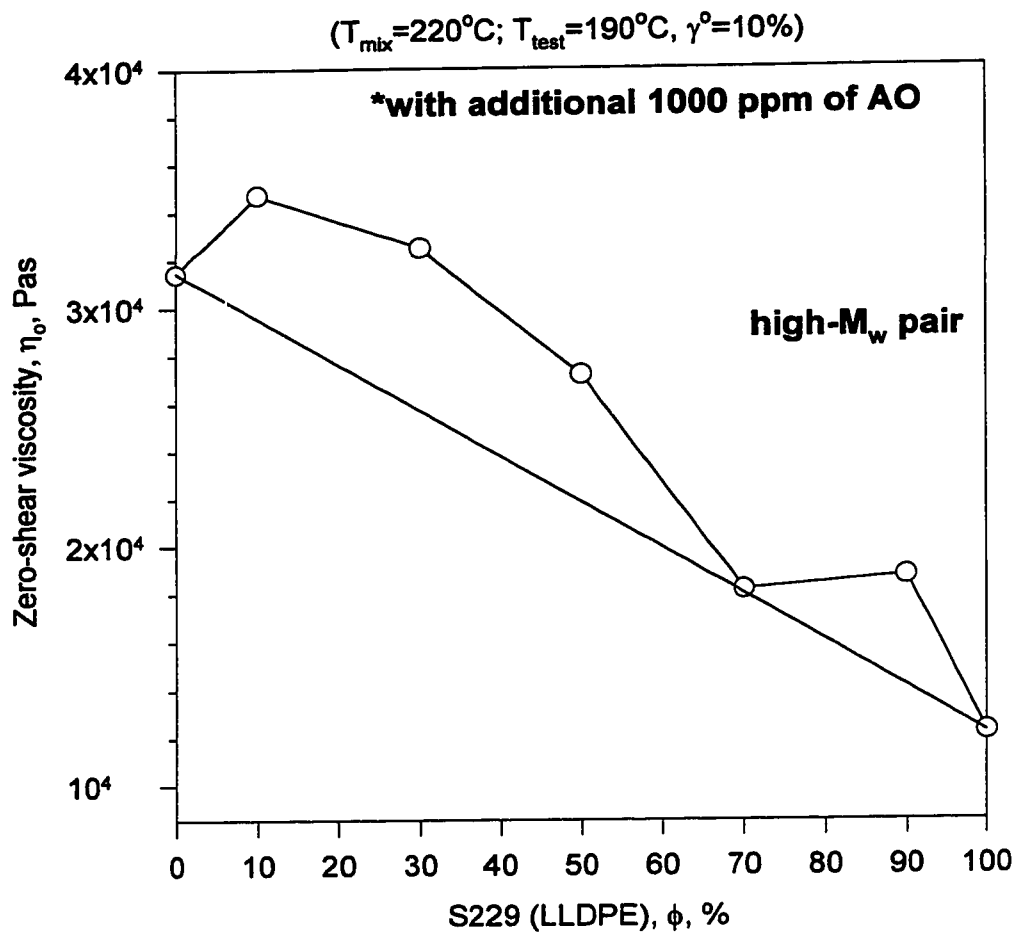
high-M_w pair

The dilute emulsion model was utilized to predict the viscosity of the 10% S229 and, hence, explain the observed increase (~10%) in the blend viscosity. Equations 6.7 and 6.8 were used and results are given in Table 6.5. For the high-M_w pair, the deviations from dilute emulsion predictions ($\Delta\eta'/\eta'_{theor}$) at T_{mix}= 220°C were less than those obtained for T_{mix}= 190°C (Table 6.3). This suggests that mixing at 220°C (above transition temperature, T_1) enhances the immiscibility.

Table 6.5: Viscosities for the 10% S229 Blend (T_{mix}=220°C)

ω rad/s	Matrix	η_1' Pas	η_2' Pas	η'_{theor} Pas	η'_{exp} Pas	$\Delta\eta'/\eta'_{theor}$ (%)
0	LDPE	31,430	12,260	35,896	34,710	3.3
0.04	LDPE	22,330	10,400	25,627	24190	5.6
0.1	LDPE	16,670	9,084	19219	18,160	5.5

Furthermore, plots of $G'(\omega)$ and $G'(\tau)$ shown in Figures C.27 and C.28 for the high-M_w pair (T_{mix}=220°C) display the same features of the corresponding η' plots discussed earlier. This is emphasized in plots of $G'(\phi)_{\omega=const}$ given in Figures 6.18 (ω=0.04 rad/s), C.29 (ω=0.1 rad/s) and C.30 (ω=100 rad/s).

Therefore, the immiscibility at T_{mix}= 220°C has increased to cover almost the whole range of composition (except the 70% LLDPE blend). It was originally believed possible that increased mixing temperatures might improve the miscibility, but unfortunately, this was not the case for these polyethylenes. In Chapter IV, polyethylene is shown to possess molecular order in the liquid state; and undergo high-temperature

Figure 6.18 G'(φ) for blends* of S229 (LLDPE) and S216 (LDPE)

$(T_{mix}=220°C; T_{test}=190°C, \gamma°=10\%, \omega=0.04 \text{ rad/s})$

*with additional 1000 ppm of A/O

high-M_w pair
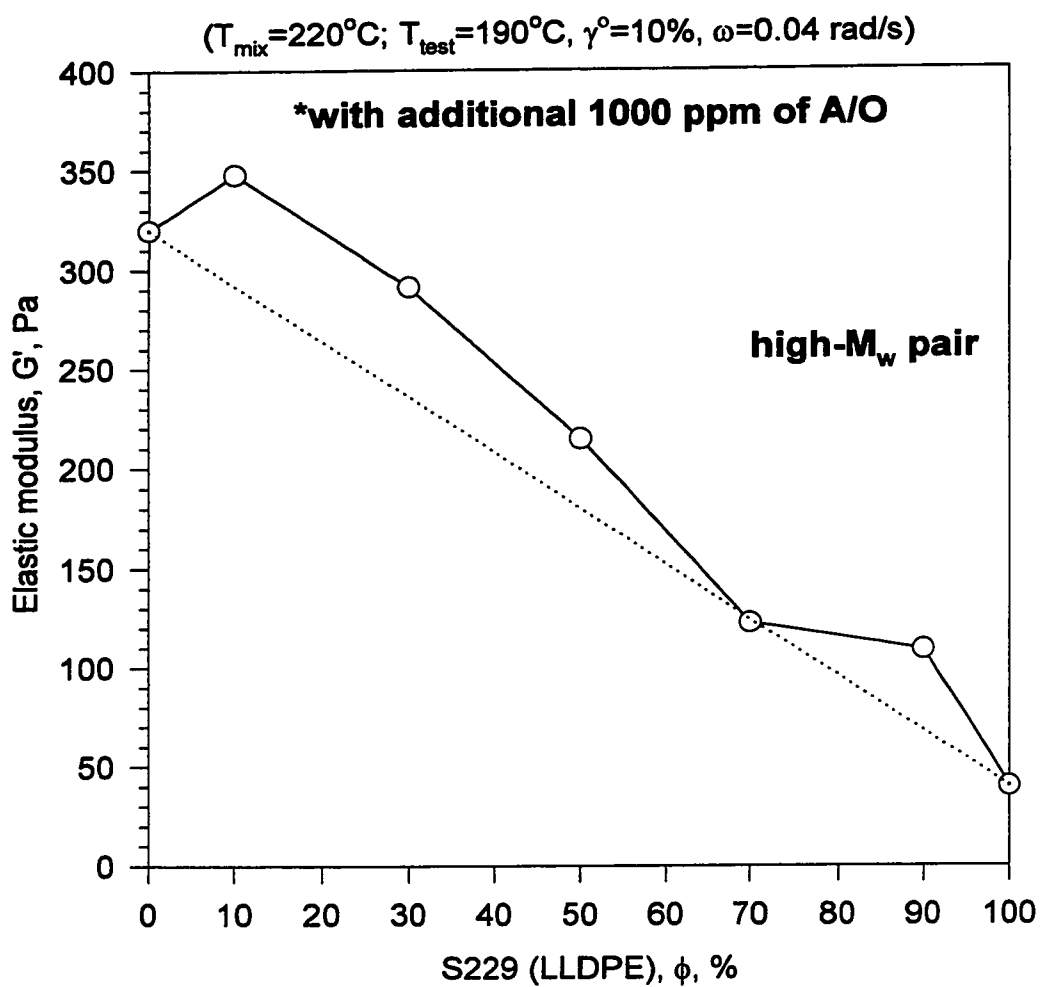
transitions. When T>T$_l$, a 'mismatch' in the molecular conformation of blend components would likely increase the degree of immiscibility.

C. ω-sweep Measurements for Blends of Nova S226 (Octene) and S216

After studying the effect of M$_w$ and T$_{mix}$ the current investigation turned to study the influence of the comonomer type (or branch length) on the miscibility of LLDPE/LDPE systems. For this purpose, an octene-LLDPE (S226) of the same M$_w$ (see Table 3.1) as that of the butene-LLDPE (S229) was selected for blending with S216 (LDPE). The S226/S216 blends were melt blended and the 'pure' polymers were conditioned for 10 minutes at 190°C and 50 rpm, followed by dynamic shear testing in the RMS at 190°C. The blends examined were 20, 50, and 80 % S226 (octene) in addition to the 'pure' polymers.

The dynamic viscosities of the octene blends, $\eta'(\omega)$ and $\eta'(\tau)$, are shown in Figures C.31 and C.32 respectively. At low ω (low τ), the LDPE-rich blends (φ<50%) showed viscosities that are approximately the same as that of LDPE (high η$_o$). The viscosity of the 20% S226 (octene-LLDPE) blend was higher than that of LDPE (η$_{o, LDPE}$ > η$_{o, LLDPE}$) over a decade of ω (or τ). This observation is more obvious in plots of $\eta'(\phi)_{\omega=const}$ that are given in Figures 6.19 and C.33. PDB was observed over the whole composition range, and the behavior is more pronounced in the LDPE-rich blends. Unlike the S229 (butene)/S216 set (mixed at 190°C, Figure 6.6a), the octene-rich blends of S226/S216 system did not follow the linear-additivity rule. However, the linear-additivity behavior was approached by the 80% S226 blend at low ω and achieved in the Newtonian limit (see Figure 6.20), suggesting miscibility. At high ω≥10 rad/s, the linear additivity rule is almost followed (see Figures C.34 and C.35).

Figure 6.19 $\eta'(\phi)$ for blends* of S226 (octene) and S216 (LDPE)

$(T_{mix}=190°C;\ T_{test}=190°C,\ \gamma°=10\%,\ \omega=0.04\ rad/s,\ C\&P)$

*with additional 1000 ppm of AO
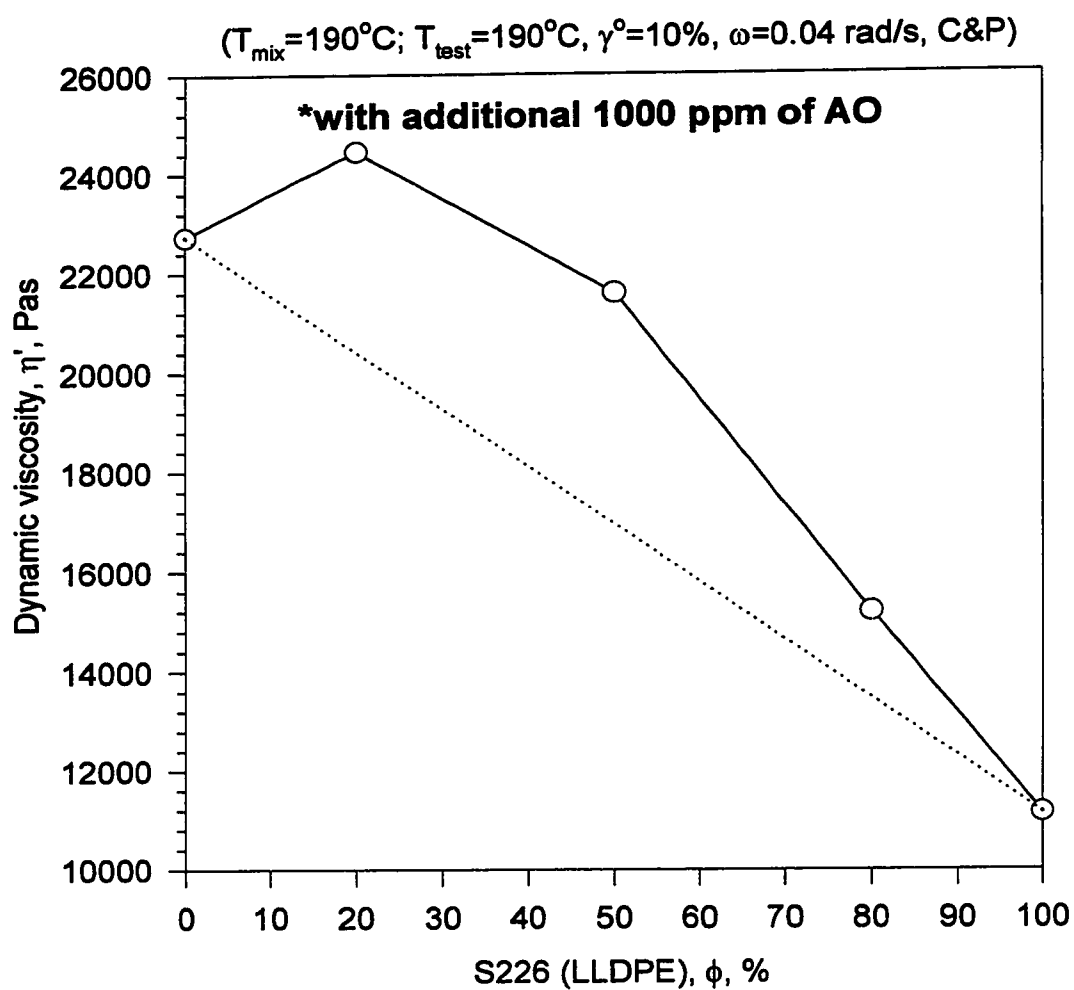
Figure 6.20 $\eta_o(\phi)$ for blends* of S226 (octene) and S216 (LDPE)

(T_{mix}=190°C; T_{test}=190°C, $\gamma°$=10%, C&P)

*with additional 1000 ppm of AO
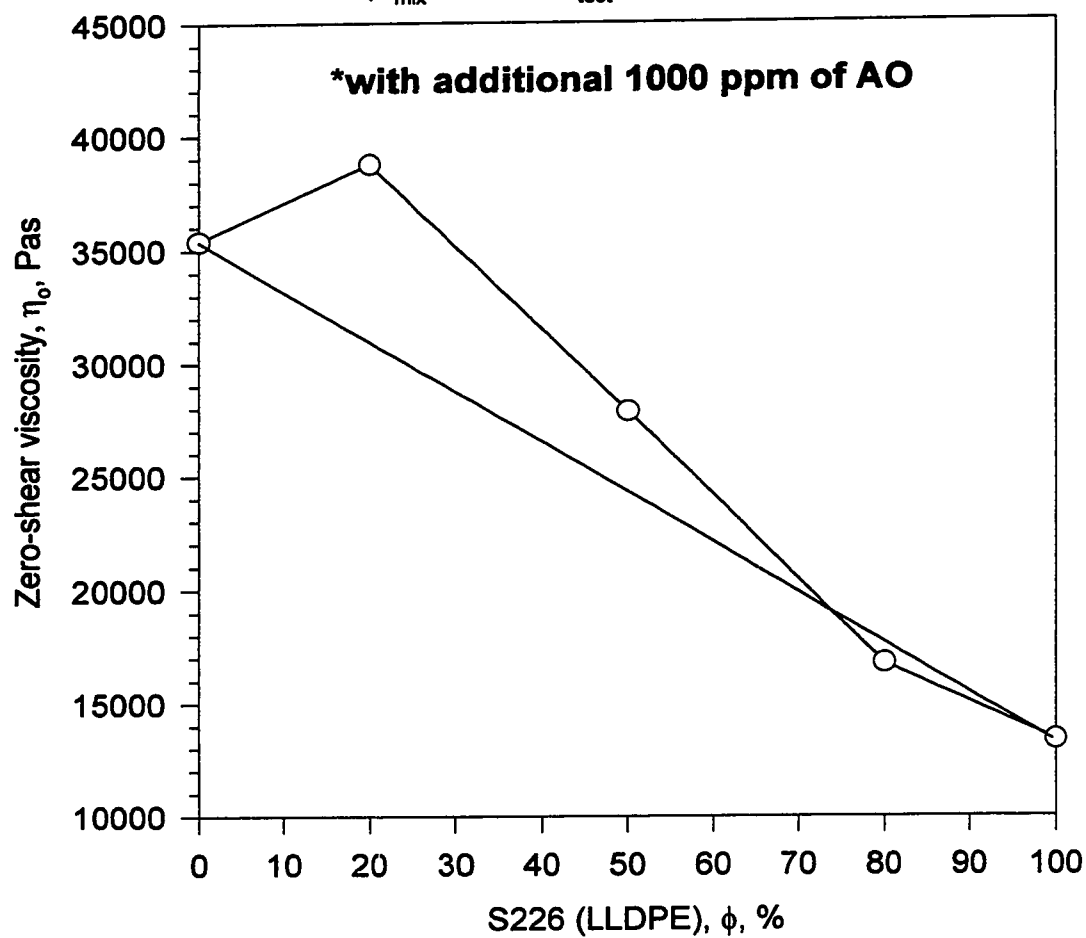
Furthermore, the yield stresses, σ_y' and σ_y'', were calculated using the modified Casson equations (6.6 a&b) and results are given in Appendix D (Table D.3).

The parameters of the Carreau Model were determined by fitting the corrected $\eta'(\omega)$ data to equations 6.4 and 6.5. Results are given in Table 6.6. The zero-shear viscosity, η_o, and the mean relaxation time, θ, are also shown in Figures 6.20 and C.36 respectively. Both η_o and θ showed PDB over the LDPE-rich blends, while η_o followed the linear-additivity for the 80% S226 blend.

Table 6.6: Blends of S226 and S216: Parameters for Equations 6.4 and 6.5

Composition	η_o (Pas)	θ (s)	m_1	m_2
S216 (LDPE)	35,390	19.6	0.78	0.74
20% S226	38,770	17.4	0.68	0.81
50% S226	23,970	11.3	1.03	0.43
80% S226	16,770	2.9	0.68	0.65
100% S226 (LLDPE)	13,370	0.01	0.36	3.0

The dilute emulsion model was used to estimate the viscosity of the 20% S226 blend, however, this composition may be outside the range of the applicability of the model (not sufficiently dilute). Equations 6.7 and 6.8 were again used and results are displayed in Table 6.7. The deviations from dilute emulsion predictions $(\Delta\eta'/\eta'_{theor})$ were much higher than those obtained for the 10% S229/S216 system mixed at the same temperature (Table 6.3). No conclusion could be drawn from this comparison since the composition is different.

Table 6.7: Viscosities for the 20% S226 (Octene) Blend (T_{mix}=190°C)

ω rad/s	Matrix	η_1' Pas	η_2' Pas	η'_{theor} Pas	η'_{exp} Pas	$\Delta\eta'/\eta'_{theor}$ (%)
0	LDPE	35,390	13,370	45,379	38,770	14.6
0.04	LDPE	22,730	11,140	29,518	24,450	17.2
0.1	LDPE	16,870	10,190	27,680	18,710	32.4

Moreover, plots of $G'(\omega)$ and $G'(\tau)$ are given in Figures C.37 and C.38. The same features of the previous η' are displayed. This is emphasized in plots of $G'(\phi)_{\omega=const}$ given in Figures 6.21 (ω=0.04 rad/s), C.39 (ω=0.1 rad/s) and C.40 (ω=100 rad/s). The $G'(\phi)_{\omega\leq0.1}$ data supported the η_0 results in suggesting the miscibility of the 80% S226 blend. The η_0 for the 50/50 blend exhibited less PDB from linear-additivity rule (14%) in comparison to that of the butene system (28%). This suggests that the degree of immiscibility of LLDPE/LDPE systems has weakened by increasing length of the branches from butene to octene.

In summary, the butene and octene-LLDPE blends with LDPE (mixed at the same temperature) both showed the following features:

a. immiscibility for the LDPE-rich blends and in the 50/50 range.

b. miscibility for the LLDPE-rich blends.

c. slightly reduced immiscibility with increased branch length (butene to octene).

D. T-*sweep Measurements for blends of Nova S229 (butene) and S226 (octene) with S216*

The T-sweep tests were carried out for blends of the butene and octene LLDPEs with LDPE. Both pairs were mixed at 190°C in the presence of 1000 ppm of additional

Figure 6.21 G'(ϕ) for blends* of S226 (octene) and S216 (LDPE)

(T_{mix}=190°C; T_{test}=190°C, γ°=10%, ω=0.04 rad/s, C&P)

*with additional 1000 ppm of AO
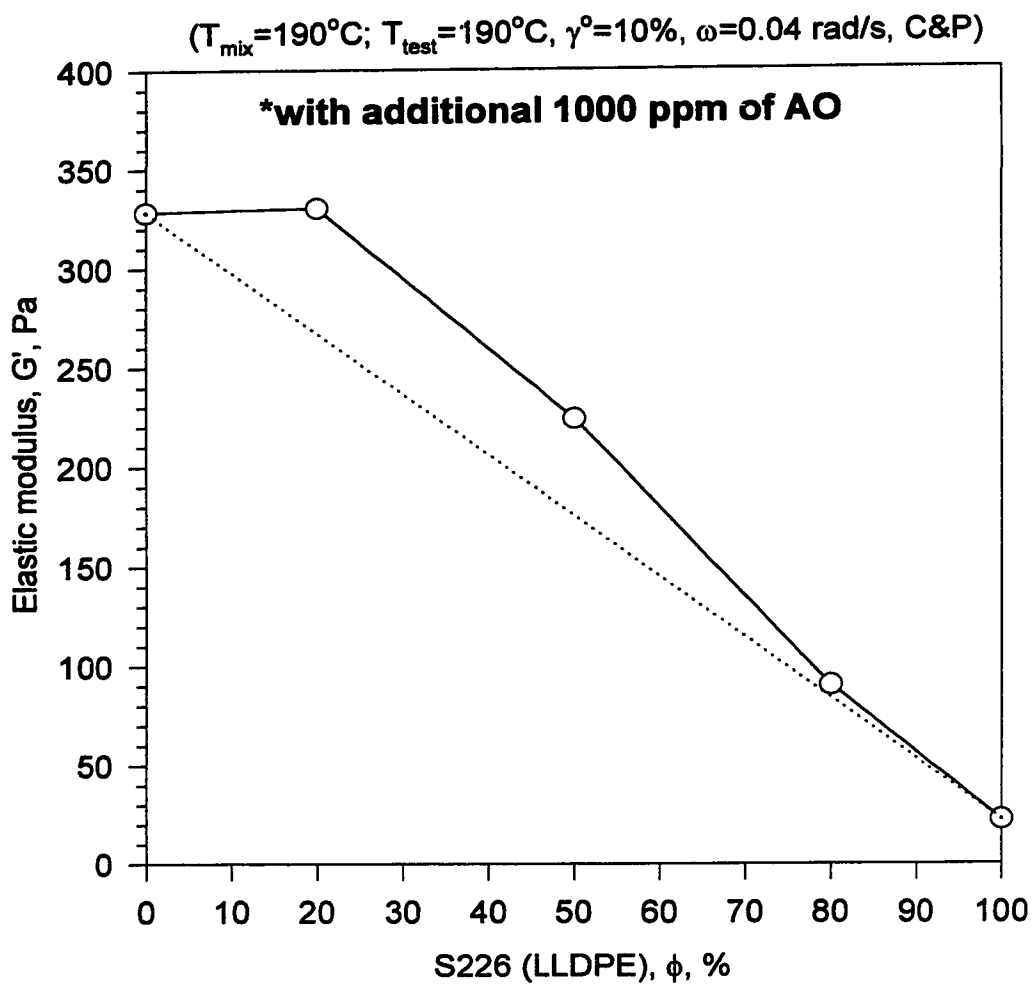
AO. The dynamic measurements ($\gamma^\circ=10\%$; $\omega=1$ rad/s) were performed in the range 160° to 260°C at a step of ~10°C. The previous test procedure (Chapter IV) that was used to investigate transition temperature T_1 in 'pure' PEs was utilized, here, for blends. The objective of this testing was to:

a. examine the presence of T_1 in blends of LLDPE and LDPE.

b. explore the influence of composition on flow activation energies.

The complex viscosity, η^*, was measured at constant ω and plotted for each blend as an Arrhenius plot of $\eta^*(1/T)$. A typical set of data is shown in Figure 6.22 for the 50/50 blend of S229 (butene) and S216 (LDPE). It is clear that the data can be represented by two straight lines intersecting at T_1. The activation energies above, E_a, (on the left side of the plot) and below, E_b, (on the right side of the plot) the transition as well as the corresponding values of A_a and A_b were extracted from the Arrhenius plots ($\eta^*=A$ $e^{E/RT}$). Results for blends of S229 and S216 are given in Table 6.8. Plots of $E(\phi)$ and $A(\phi)$ are given in the Appendix (see Figures C.42 and C.43)

Similarly, Arrhenius plots were used to analyze the data for the S226 (octene) and S216 (LDPE) pair. A typical plot is shown in Figure 6.23 for the 50/50 blend of S226 and S216. Results for the S226/S216 system are displayed in Table 6.9. Plots of $E(\phi)$ and $A(\phi)$ are shown in the Appendix (see Figures C.44 and C.45).

For both pairs, the flow activation energies E_a were higher than the corresponding values of E_b by ~22 to 39%. The transition temperature T_1 was found to lie between 200° and 208°C. It is difficult to draw any conclusions from the T_1-composition dependency since T_1 values for the 'pure' polymers were too close. In general, plots of $E(\phi)$ and $A(\phi)$ did not follow linear additivity behavior (see Figures C.42 to C.45).

Figure 6.22 Arrhenius plot of $\eta^*(1/T)$ for the 50% S229 (butene)[+]

$(T_{mix}=190^{\circ}C;\ \omega=1rad/s,\ \gamma^{\circ}=10\%,\ T=160^{\circ}-260^{\circ}C,\ PP)$

[+]with additional 1000 ppm of AO

$E_a=6.82$ kcal/mol ($r^2=0.9990$)

$E_b=5.29$ kcal/mol ($r^2=0.9972$)

$T_1=206^{\circ}C$

high-M_w pair
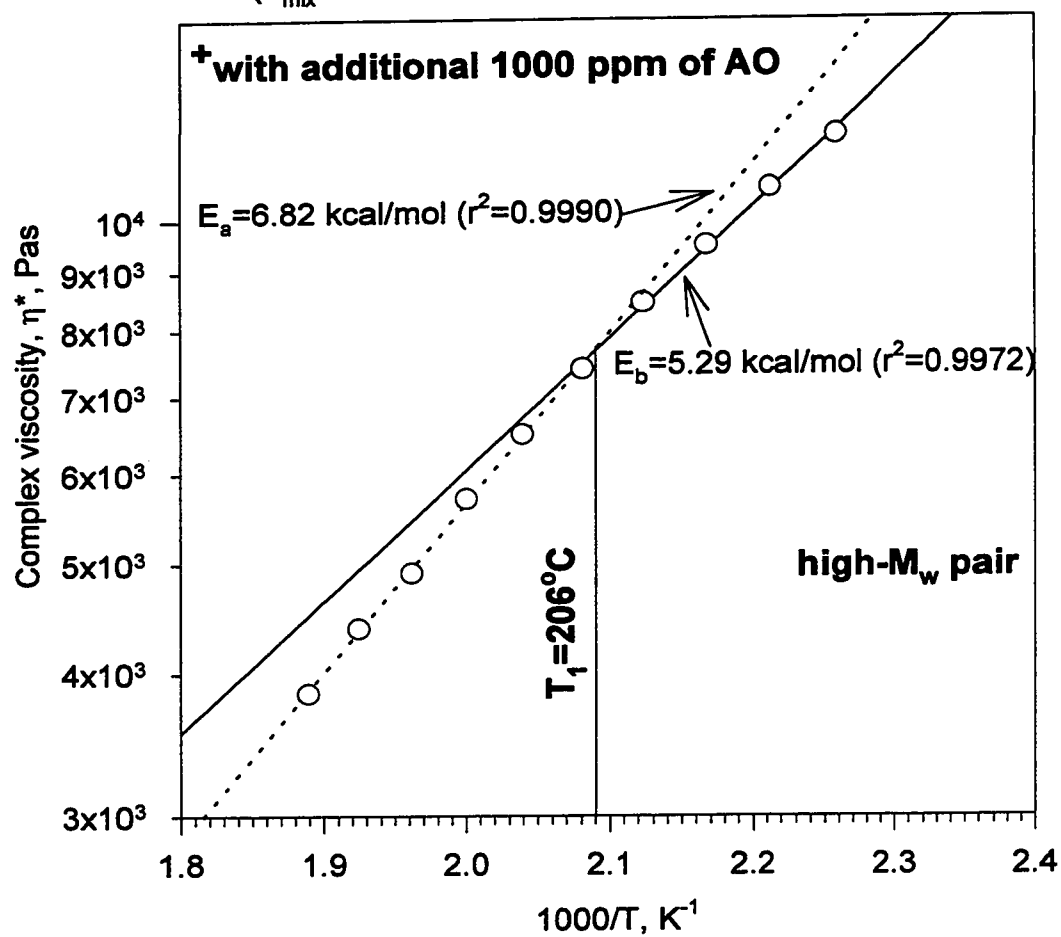
Figure 6.23 Arrhenius plot of $\eta^*(1/T)$ for the 50% S226 (octene)[+]

$(T_{mix}=190°C; \omega=1\text{rad/s}, \gamma°=10\%, T=160°-260°C, PP)$

[+]with additional 1000 ppm of AO

$E_a=6.66$ kcal/mol $(r^2=0.9996)$

$E_b=5.03$ kcal/mol $(r^2=0.9966)$

$T_1=203.5°C$

Complex viscosity, η^*, Pas

$1000/T$, K^{-1}
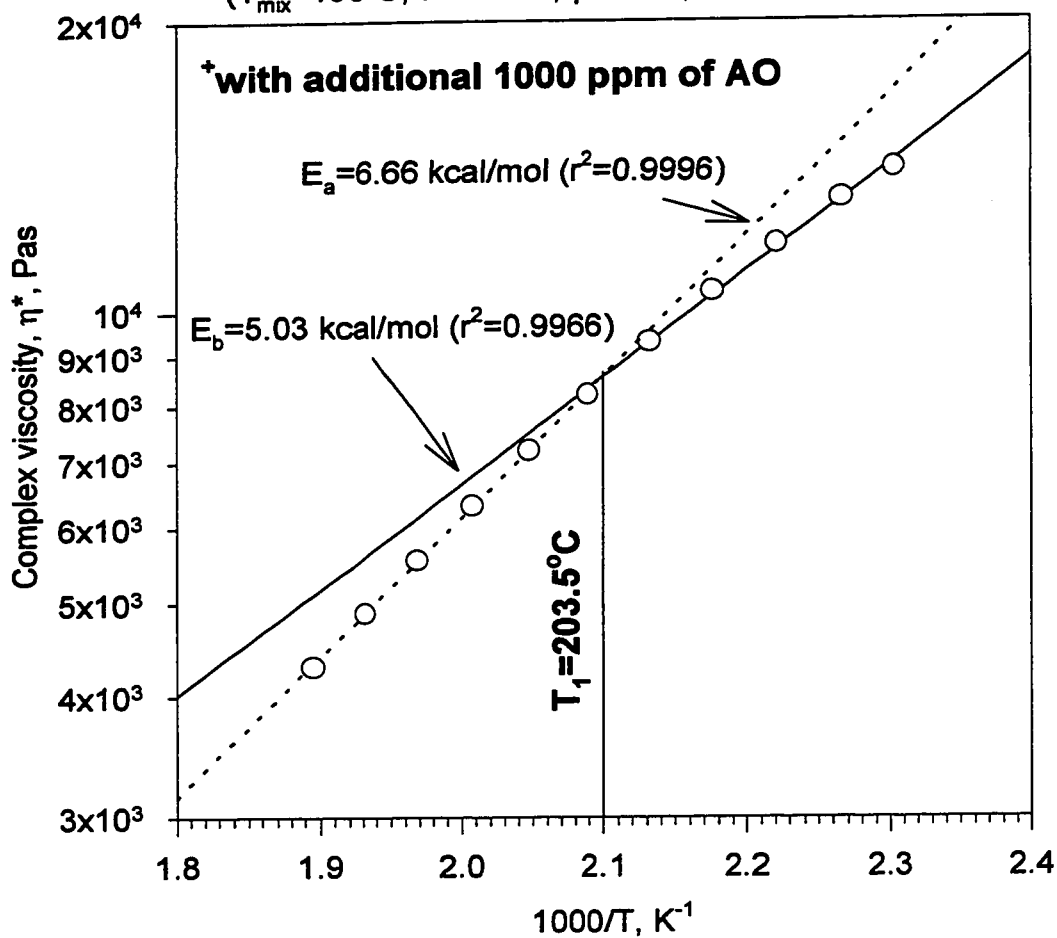
Table 6.8: Blends of S229 (Butene) and S216 (LDPE): T-sweeps (T_{mix}=190°C)

Composition	E_a (kcal/mol)	A_a (Pas)	r_a^2	E_b (kcal/mol)	A_b (Pas)	r_b^2	E_a/E_b	T_1, °C
S216 (LDPE)	8.05	1.33	0.9992	5.79	14.27	0.9979	1.39	206.0
10% S229	7.99	1.65	0.9990	5.94	14.05	0.9974	1.35	206.8
30% S229	7.20	3.98	0.9989	5.56	22.18	0.9968	1.29	206.6
50% S229	6.82	5.89	0.9990	5.29	29.48	0.9972	1.29	206.0
70% S229	6.42	8.15	0.9995	5.27	27.17	0.9978	1.22	207.8
90% S229	6.21	8.97	0.9997	4.78	41.2	0.9959	1.30	201.4
S229 (LLDPE)	5.99	10.47	0.9996	4.68	42.06	0.9981	1.30	203.5

Table 6.9: Blends of S226 (Octene) and S216 (LDPE): T-sweeps (T_{mix}=190°C)

Composition	E_a (kcal/mol)	A_a (Pas)	r_a^2	E_b (kcal/mol)	A_b (Pas)	r_b^2	E_a/E_b	T_1, °C
S216 (LDPE)	8.05	1.33	0.9992	5.79	14.27	0.9979	1.39	206.0
20% S226	7.35	3.43	0.9990	5.38	27.17	0.9951	1.37	203.5
50% S226	6.66	7.56	0.9995	5.03	42.14	0.9966	1.32	203.5
80% S226	6.18	11.69	0.9997	4.90	45.68	0.9966	1.26	202.8
S226 (LLDPE)	5.96	13.30	0.9998	4.66	52.78	0.9952	1.28	200.5

In conclusion, the effect of molecular weight, branch type, and mixing temperature on the miscibility of LLDPE/LDPE blends was investigated. The following

is a summary of the previous observations suggested by the different methods of data treatment:

a. Blends of low-M_w LLDPE (butene) and LDPE are likely *miscible*.

b. Blends of high-M_w LLDPE (butene) and LDPE mixed at $T<T_1$ (190°C) are *partially* miscible. *Immiscibilty* is likely to occur around the 50/50 composition and in the LDPE-rich blends. Blends are likely *miscible* in the LLDPE-rich range.

c. Blends of high-M_w LLDPE (butene) and LDPE mixed at $T>T_1$ (220°C) are almost *immiscible*. Miscibility is likely to occur for the *70% LLDPE* blend.

d. The immiscibility of the blends leads to $\eta(\phi)$ *can* be explained by a simple *emulsion* model.

e. The 'mismatch' in the molecular *conformation* of LLDPE and LDPE past T_1 is likely responsible for the increased degree of immiscibility at high mixing temperatures.

f. Increasing the branch length from butene to octene has *slightly* increased miscibility.

g. Blends as well as 'pure' components of high-Mw LLDPEs and LDPE *show* transition temperature T_1.

VII. Conclusions and Recommendations

A. Conclusions

In the first part of this thesis, molecular order in polyethylenes was discussed in light of new evidence of melt molecular order and high-temperature transitions. Thermal as well as different rheological techniques were used. Second, a comprehensive investigation was carried out to examine the influence of thermo-mechanical melt conditioning in the mixer on the structure and rheology of blends. The melt conditioning was studied at 50 rpm and for 10 minutes for different temperatures and blender conditions. Four different techniques were used. Finally, rheology was utilized to study the miscibility of LLDPE/LDPE blend systems. The influence of M_w, branch type, and mixing temperature were investigated by different data treatment methods. The following are the conclusions for each of the three parts of this study.

1. Molecular Order and high-temperature Transitions in Polyethylenes

a. The following measurements presented evidence for the existence of microstructural transitions near 208°C and 227°C in HDPE, LDPE, and LLDPE:

i. Thermal analysis in Differential Scanning Calorimetry (DSC).

ii. Torque measurements in the Rheocord 90 melt blender.

iii. Temperature sweeps in the Rheometrics Mechanical Spectrometer (RMS)

iv. Melt flow in a Melt Indexer over a range of temperatures.

v. Melt density in a densitometer.

b. Observation of anomalous normal force behavior at low shear and a 'kink' in the viscosity that mimic in many ways the characteristics of liquid-crystal polymers predicted by rheological theories.

c. Highly branched metallocene LLDPE (~40 CH_3/1000 C) do <u>not</u> show the above transitions.

d. Temperature sweep tests carried out in the RMS showed the existence of two different phases below and above the 208°C transition characterized by two different flow activation energies.

e. The temperature range 210°-230°C showed a unique torque-temperature dependence not reported before for any polymer other than thermotropic liquid crystal polymers. A flat temperature profile or an increase in torque with temperature following a flat profile was observed. This temperature range is of importance for processing and worth a more extensive study.

f. Examination of the rheology below and above the transition showed a behavior totally different from that of isotropic viscoelastic polymers and didn't show the attainment of the isotropic state at high temperature although more freedom of molecules and/or more molecular interactions are suggested by the higher activation energies above the transition.

g. This study used commercial PEs a range not investigated in the literature as for the low M_w PEs (waxes) and the UHMWPEs. Hence this study of structures in the melt is important to show that molten linear PE is a structured liquid regardless of the M_w although the M_w dependency of the transition(s) in the melt should be studied.

h. From the current study and the previously published work we conclude that linear HDPE is a Liquid Crystal Polymer with order in the melt that persists even at temperatures more than 100°C above its normal melting point.

i. The evidence for ordered structures in these commercial PE melts ($M_w=10^4$-10^5) should induce the melt processing industry to re-examine the conditions (e.g., the temperatures) at which their processes operate, in view of the potential to make those processes more effective and to optimize product quality.

2. Degradation of Polyethylenes during Melt Blending

a. Rheology, NMR, DSC and GPC were used.

b. In Ziegler-Natta LLDPEs, structural modifications accompanied by loss of branches and profound increase in viscosity at low shear were observed.

c. It was found that, the higher the mixing temperature, the higher the enhancement in viscosity.

d. Preliminary results show a correlation between the enhancement in viscosity and branch content.

e. No evidence of degradation in HDPEs or saturated LDPE produced by free radical polymerization.

f. Poor "batch reproducibility" is a possible reason for the peculiar negative deviation behavior in viscosity-composition plots for blends of LLDPE and LDPE.

g. Lack of 'batch reproducibility' could be a sign of degradation in one (or more) of the blend components. This test might be introduced as a routine quality control check for degradation in the polyethylene industry.

h. It is difficult to conclude anything about the miscibility of a blend if one (or more) of the components is undergoing degradation since the reproducibility of the data is very poor.

i. It is important to check the influences of melt conditioning or sample preparation steps on the 'pure' polymers before proceeding with melt blending.

j. Addition of adequate amounts of antioxidant is necessary to protect the polymers (particularly LLDPE) from degradation during melt blending.

3. Miscibility of LLDPE/LDPE Blend Systems

a. Blends of low-M_w LLDPE (butene) and LDPE are likely *miscible*.

b. Blends of high-M_w LLDPE (butene) and LDPE mixed at $T<T_1$ (190°C) are *partially* miscible. *Immiscibilty* is likely to occur around the 50/50 composition and in the LDPE-rich blends. Blends are likely *miscible* in the LLDPE-rich range.

c. Blends of high-M_w LLDPE (butene) and LDPE mixed at $T>T_1$ (220°C) are almost *immiscible*. Miscibilty is likely to occur for the *70% LLDPE* blend.

d. The 'mismatch' in the molecular conformation of LLDPE and LDPE past T_1 is likely responsible for the increased degree of immiscibility at high mixing temperatures.

e. Increasing the branch length from butene to octene has slightly increased the miscibility of LLDPE/LDPE blends (Maybe the longer octene branches look like the long chain branches).

f. Blends as well as 'pure' components of the high-M_w LLDPEs and LDPE show transition temperature T_1.

g. Molecular conformations in polyethylene melts range from ordered (chain-folded) linear HDPE to almost random coil highly-branched LLDPE. Hence, the miscibility of different polyethylenes is strongly influenced by their entropy of mixing.

B. Recommendations for Future Work

The future work is going to concentrate on the molecular order in 'pure' LLDPEs and its influence on the miscibility of polyethylene LLDPE/LDPE blend systems. The study will use Z-N and metallocene LLDPEs to investigate the following:

1. 'Pure' Polymers

a. Extend the current study of order in polyethylene melts to solutions. Negative normal force is expected to show in solutions of LCPs.

b. Study the influence of branch content and type on the molecular order, transitions, and conformations in the liquid state.

2. Blends of LLDPE and LDPE

Future work will study the influence of the following factors on the miscibility of blends:

a. Branch density and distribution.

b. Molecular weight distribution (MWD).

c. Catalyst type: Z-N vs. metallocene.

d. Mixing temperature.

References

Abraham D., K.E. George and D.J. Francis, 'Effect of chemical modification on the flow behavior of LDPE and its blends with linear LDPE', Polymer, 39(1), 117-121, **1998**.

Aharoni S.M., V. Kramer and D.A. Vernick, 'Instantaneous shape and segmental density of individual flexible linear macromolecules 4. tagged in untagged crystalline polymers', Macromolecules, 12, 265, **1979**.

Ajji A. and L. **Choplin**, 'Rheology and Dynamics near Phase Separation in a Polymer Blend: Model and Scaling Analysis', Macromolecules, 24, 5221-5223, **1991**.

Andrade E.N. DA C., 'The viscosity of liquids', Nature, 125, 309; 582, **1930**.

Ashcraft C.R and R.H. **Boyd**, 'A Dielectric study of molecular relaxation in oxidized and chlorinated polyethylenes', J. Polym. Sci., Polym. Phys. Ed., 14, 2153-2193, **1976**.

Bair H.E., 'Thermal analysis of additives in polymers', in 'Thermal characterization of polymeric materials', 2nd ed., edited by Edith Turi, Vol 2, Academic Press, **1997**.

Baird D.G., 'Concepts in rheological studies of polymeric liquid crystals', Polym. Sci. and Technology, Vol 28, published by Plenum Press, NY, 119-43, **1985**.

Baird D.G., A. Gotsis and G. Viola, 'Transient shear flow behavior of thermotropic liquid crystalline copolyesters', ACS, Div. of Polym. Chem., Washington DC, USA, August 28-31, 1983 and published by Plenum Press, Polymer Sci. and Technology, Vol 28, NY, 183-195, **1985**.

Balta'-Celleja F.J., K.D. Berling, H. Cackovic, R. Hosemann and J. Loboda-Cackovic, 'Diamagnetic susceptibility of solid and liquid paraffins', J. Macromol. Sci.-Phys., B12, 383-392, **1976**.

Barham P.J., M.J. Hill, G. Goldbeck-Wood, and J. van Ruiten, 'A qualitative scheme for the liquid phase separation in blends of homopolymers with their branched copolymers', Polymer, 34(14), 2981-88, **1993**.

Batschinski A.J., 'Untersuchungen Uber die innere Reibung der Flussigkeiten', Z. physik Chem., 84, 643-648, **1913**.

Bersted B.H., 'On the effect of very low levels of long chain branching on rheological behavior in polyethylene', J. Appl. Polym. Sci., 30, 3751-3765, **1985**.

Bestul A.B. and H.V. **Belcher**, 'Temperature coefficients of non-Newtonian viscosity at fixed shearing stress and at fixed rate of shear', J. Appl. Phys., 24(6), June **1953**.

Bharel R., R.C. Anand, V. Choudhary, and I.K. Varma, 'Performance evaluation of antioxidants in polyethylene by DSC', Polym. Deg. Stab., 38, 107-112, **1992**.

Bourgeois J. Rudy and Peter W. **Blackett**, 'High-Density Polyethylene (HDPE)', 'Engineered Materials Handbook', edited by J.N. Epel et al., Vol 2, Metal Park, Ohio, USA, p. 163, **1988**.

Boyd R.H., 'Relaxation processes in crystalline polymers: experimental behavior- a review', Polymer, 26, 323-347, **1985**.

Bremner T. and A. **Rudin**, 'Persistence of regions with high segment density in polyethylene melts', J. Polym. Sc., Polym. Phys. Ed., 30, 1247-60, **1992**.

Bremner T. and A. **Rudin**, 'Modification of high density polyethylene by reaction with dicumyl peroxide', Plastics and Rubber Processing and applications, 13(1), **1990**.

Carreau P.J., 'Rheological Equations from Molecular Network Theories', Trans. Soc. Rheol., 16 (1), 99-127, **1972**.

Chartoff R.P., 'Thermoplastic polymers', in 'Thermal characterization of polymeric materials', 2nd ed., edited by Edith Turi, Vol 2, Academic Press, **1997**.

Choi Phillip, Henk P. Blom, Tom A. Kavassalis, and Alfred Rudin, 'Immiscibility of Poly(ethylene) and Poly(propylene): A Molecular Dynamics Study', Macromolecules, 28, 8247-8250, **1995**.

Choi S.J., W.R. **Schowalter**, 'Rheological properties of nondilute suspensions of deformable particles', Phys. Fluids, 18(4), 420-427, **1975**.

Chuang C.I. and C.D. **Han**, 'Rheological Behavior of Polymer Blends', J. Appl. Polym. Sci., 29, 2205-2229, **1984**.

Coates D. and G.W. **Gray**, "The Structures and microscopic textures of smectic liquid crystals", Microscope, 24(2), 117-150, **1976**.

Cogswell F.N. and K.F. Wissbrun, 'Rheology and processing of liquid crystal polymer melts', in 'Rheology and Processing of Liquid Crystal Polymers', Eds. D. Acierno and A.A. Collyer, Chapman & Hall, **1996**.

Curto D., F.P. La Mantia and D. Acierno, 'The Rheological behavior of HDPE/LDPE blends. I. End effects and shear viscosity', Rheol. Acta, 22, 197-208, **1983**.

Datta N.K. and A.W. Birley, 'Polyethylene blends: low-density and linear low-density types', Plastics and Rubber Processing, 3(3), 1983.

D'Allest J.F., P. Sixon, A. Blumstein, R.B. Blumstein, Mol. Cryst. liq. Cryst., 229, **1988**.

Dealy J.M. and K.F. Wissbrun, 'Melt rheology and its role in plastics processing', Nelson Canada, ON, p. 174, **1990**.

Denn M. M., 'Fluid Mechanical issues in polymer processing', in 'Interdisciplinary issues in materials processing and Manufacturing', Vol 2, Edited by Samanta et al., 587-591, **1987**.

Dexter F.D., 'Rotational plastometry applied to molten polyethylenes', J. Appl. Phys., 25(9), Sept. **1954**.

Dobrescu, V, 'Influence of blending upon rheological properties of polymers in the melt', in Rheology, Edited by G. Astarita, G. Marrucci and L. Nicolais, Vol 2, Plenum Press, New York, **1980**.

Done D. and D.G. Baird, 'The effect of thermal history on the rheology and texture of thermotropic liquid crystalline polymers', Polym. Eng. and Sci., 27(11), 816-22, June **1987**.

Drake W.O., 'Antioxidants - Part I: General Aspects', in 'Plastics additives and modifiers handbook', revised ed., edited by Jesse Edenbaum, Chapman & Hall, **1996a**.

Drake W.O., 'Antioxidants - Part II: Formulation and evaluation considerations', in 'Plastics additives and modifiers handbook', revised ed., edited by Jesse Edenbaum, Chapman & Hall, **1996b**.

Dumoulin M, L.A. Utracki, and P.J. Carreau, 'Melt rheology and morphology of linear low density polyethylene/polypropylene blends', in 'progress in polymer processing' edited by L.A. Utracki, Hanser Publishers, **1991**.

Egorenkov N.I., D.G. Lin and V.A. Bely, 'Effect of metals on melt oxidation of polyethylene', J. Polym. Sci., Polym. Chem. Ed., 13, 1493-1498, **1975**.

El'darov E.G., V.M. Gol'dberg and G.E. Zaikov, 'The kinetics of the chemical changes during extrusion of polyethylene', Polym. Deg. Stab., 16, 291-296, **1986**.

Fan Z., I.A. Hussein, P. Choi and M.C. Williams, 'D.S.C. Study of the Miscibility of LDPE/LLDPE Blends', 47th Canadian Chemical engineering Conference, Edmonton, AB, Canada, October **1997**.

Fairley G.R and R.E. Prud'homme, 'Dynamic Melt Rheology of Polyethylene-Ionomer Blends', in 'Multiphase Polymers: Blends and Ionomers', edited by L.A. Utracki and R.A. Weiss, ACS, Washington, DC, **1989**.

Ferry J.D., 'Viscoelastic Properties of Polymers, John Wiley & Sons< New York, **1980**.

Flory P.J., "Principles of Polymer Chemistry", Cornell University Press, Ithaca, NY, **1953**.

Folland R. and A. Charlesby, "Entanglement effects on the NMR spin-spin relaxation polyethylene melts", J. Polym. Sci. Polym. Lett. Ed., 16, 339-344, **1978**.

Fredrickson G.H. and A.J. Liu, 'Design of Miscible Polyolefin Copolymer Blends', J. Polym. Sci.: Part B: Polym. Phys., 33, 1203-1212, **1995**.

Freed K.F. and J. Dudowicz, 'Influence of short chain branching on the miscibility of binary polymer blends: Application to polyolefin mixtures', Macromolecules, 29, 625-636, **1996**.

Franklin D. S., 'Liquid crystals the fourth state of matter', Marcel Dekker, NY, **1979**.

Frölich H. and Sack R., 'Theory of the rheological properties of dispersions', Proc. Roy. Soc., A185, 415-430, **1946**.

Fujiyama M. and Y. Kawasaki, 'Rheological properties of polypropylene/High-density polyethylene blend melts. I. Capillary flow properties', J. Appl. Polym. Sci., 42, 467-480, 1991a.

Fujiyama M. and Y. Kawasaki, 'Rheological properties of polypropylene/High-density polyethylene blend melts. II. Dynamic viscoelastic properties', J. Appl. Polym. Sci., 42, 481-488, 1991b.

Garcia-Rejon A. and C. Alvarez, 'Mechanical and flow properties of High-density polyethylene/Low-density polyethylene blends', Polym. Eng. Sci., 27(9), 1987.

Ghosh P., D. Dev, 'Reactive processing of polyethylene: effect of peroxide-induced graft copolymerization of some acrylic monomers on polymer structure melt rheology and relaxation behavior', Eur. Poly. J., 34(10), 1539-1547, 1998.

Ghosh P., D. Dev and A. Chakrabarti, 'Reactive melt processing of polyethylene: effect of peroxide action on polymer structure, melt rheology and relaxation behavior', Polymer, 38(25), 6175-6180, 1997.

Ghosh, Tamal, Jim C. Huang and Michael Williams', Melt Index for molecular weight quality control', proc. of the VII Int. Rheol. Conf., Quebec, Canada, August 1996.

Glasstone S., K.J. Laidler, and H. Eyring, 'The theory of rate processes', Mc Graw-Hill, New York, 1941.

Graebling D., R. Muller, and J.F. Palierne, 'Linear Viscoelastic Behavior of Some Incompatible Polymer Blends in the Melt. Interpretation of Data with a model of Emulsion of Viscoelastic Liquids', Macromolecules, 26, 320-329, 1993.

Gramespacher H. and J. Meissner, 'Interfacial tension between polymer melts measured by shear oscillations of their blends', J. Rheol., 36(6), 1127-1141, 1992.

Groves D.J., T.C.B. McLeish, R.K. Chohan, and P.D. Coates, 'Predicting the rheology of linear with branched polyethylene blends', Rheol. Acta, 35, 481-493, 1996.

Han Chang Dae, 'Rheology in Polymer Processing', Academic Press, 1976.

Han Chang Dae, 'Multiphase flow in polymer processing', Academic Press, 1981.

Han C.D. and J.K. Kim, 'On the use of time-temperature superposition in multicomponent/multiphase polymer systems', Polymer, 34, 2533-2539, **1993**.

Han W.H. and A.D. Rey, 'Simulation and validation of temperature effects on the nematorheology of aligning and nonaligning liquid crystals', J. Rheol., 39(2), 301-322, **1995**.

Hawkins W.L., 'Polymer degradation and stabilization', No. 8 in 'Polymer properties and applications' series, Springer-Verlag, Berlin, **1984**.

Heberer D.P., J.A. Odell and V. Percec, 'Rheology and flow-induced liquid crystalline phase transitions in thermotropic polyethers', J. of Materials Sci., 29, 3477-83, **1994**.

Heitmiller R.F., R.Z. Naar, and H.H. Zabusky, 'Effect of homogeneity on viscosity in capillary extrusion of polyethylene', J. Appl. Polym. Sci., 3, 873-880, **1964**.

Hill M.J. and P.J. **Barham**, 'Absence of phase separation effects in belends of linear polyethylene fractions of differing molecular weight', Polymer, 36, 1523-1530, **1995**.

Hill M.J. and P.J. **Barham**, 'Liquid-liquid phase segregation in blends of linear and branched polyethylene with a series of octene copolymers of differing branch content', Polymer, 34, 2975-80, **1993**.

Hill M.J. and P.J. **Barham**, 'Liquid-liquid phase separation in melts of blends of linear with branched polyethylenes: morphological exploration of the phase diagram', Polymer, 33(19), 4099-102, **1992**.

Hill M.J., P.J. Barham, A. Keller and C.C.A. Rosney, 'Phase segregation in melts of blends of linear and branched polyethylene', Polymer, 32(8), 1384-93, **1991**.

Hill M.J. and C.C. **Puig**, 'Liquid-liquid phase separation in blends of a linear low density polyethylene with a low density polyethylene', Polymer, 1921-1931, **1997**.

Hinsken H., S. Moss, J.R. Pauquet and H. Zweifel, 'Degradation of polyolefins during melt processing', Polym. Deg. Stab., 34, 279-293, **1991**.

Horio Masao, Tsuguo Fujii, and Shigeharu Onogi, 'Rheological properties of polyethylene melts: Effects of temperature and blending', J. Phys. Chem., 68(4), April 15, **1964**.

Horng Paul-Li and Peter P. Klemchuk, 'Investigation of thermal oxidation and stabilization of High-density polyethylene', in 'Polymer stabilization and degradation', edited by Peter P. Klemchuk, ACS, Washington D.C., **1985**.

Huang C.-M., J.J. Magda, and R.G. Larson, 'The effect of temperature and concentration on N_1 and tumbling in a liquid crystal polymer', J. Rheol., 43(1), 31-50, **1999**.

Hussein Ibnelwaleed A. and Michael C. Williams, 'Temperature Dependence of Complex Viscosity in HDPE melts and Evidence of Microstructural Transitions', to be presented at the EURORHEO99 Conference, Sophia Antipolis, France, May 3-7, **1999**.

Hussein Ibnelwaleed A. and Michael C. Williams, 'Rheological evidence for high-temperature phase transitions in melts of high-density polyethylene', Macromol. Rapid Commun., 19, 323-325, **1998a**.

Hussein Ibnelwaleed A. and Michael C. Williams, 'Anomalous Nonlinearities in Steady Shear Rheology of Polyethylene Melts', J. Non-Newtonian Fluid Mech., in press, **1998b**.

Hussein Ibnelwaleed A. and Michael C. Williams, 'Anomalous Nonlinearities in Polyethylene Melts', presented at 'Mechanics of Nonlinear Materials' Conference, Banff, Alberta, May 13-16, **1998c**.

Hussein Ibnelwaleed A. and Michael C. Williams, 'Evidence of Liquid Crystalline Rheology in Melts of Polyethylene', presented at the 70th Annual meeting of the Society of Rheology, Monterey, California, Oct. 4-8, **1998d**.

Hussein I.A., Z. Fan, P. Choi and M.C. Williams, 'Phase Behavior of LDPE/LLDPE Blends Prepared at Optimum Blending Conditions', presented at the 47th Canadian Chemical Engineering Conference, Edmonton, AB, Canada, October 5-8, **1997**.

Hussein Ibnelwaleed A. and Michael C. Williams, 'Rheology of Immiscible polyethylenes', presented at the 69th Annual Meeting of the Society of Rheology, Columbus, Ohio, USA, October 19-23, **1997**.

Kalyon D.M., Dong-Woo Yu, and F.H. Moy, 'Rheology and processing of linear low density polyethylene resins as affected by alpha-olefin comonomers', Polym. Eng. Sci., 28(23), **1988**.

Kamel I. and Charlesby, 'NMR spin-spin relaxation in solid and molten polyethylene structures', J. Polym. Sci. Phys. Ed.,19, 803-14, 1981.

Kamiya Y. and E. Niki, 'Oxidative degradation', in 'Aspects of degradation and stabilization of Polymers', edited by H.H.G. Jellinek, Elsevier Sci., 1978.

Karbashewski E., L. Kale, A. Rudin, and W.J. Tchir, 'Effects of additives of high-density polyethylene on the processability of linear low-density polyethylene', J. Appl. Polym. Sci., 47, 1143-1154, 1993.

Kauzmann Walter and Henry Eyring, 'The viscous flow of large molecules', American Chem. Soc. J., 62, 3113-3125, 1940.

Kavassalis T.A. and P.R. Sundararajan, 'A Molecular Dynamics study of polyethylene crystallization', Macromolecules, 26, 4144-50, 1993.

Keller A., 'A note on single crystals in polymers: Evidence for a folded chain configuration', Phil. Mag., 2, 1171-1175, 1957.

Keller A. and G. Ungar, 'A scheme for phase stability in liquid crystal polymers', J. of Appl. Polym. Sci., 42, 1683-93, 1991.

Keller A., G. Ungar and V. Percec, 'Liquid-Crystalline Polymers: A unifying thermodynamics-based scheme', Liquid-Crystalline Polymers, ACS symposium series 435 edited by R.A. Weiss and C.K. Ober, Washington, DC, 309-34, 1990.

Kiss Gabor, 'Anomalous Temperature Dependence of Viscosity of Thermotropic Polyesters', J. of Rheology, 30(3), 585-99, 1986.

Kiss G. and R.S. Porter, 'Rheology of Concentrated Solutions of Poly(γ-Benzyl-glutamate)', J. Polym. Sci.: Polym. Symp., 65, 193-211, 1978.

Kiss G. and R.S. Porter, 'Rheology of Concentrated Solutions of Polypeptides', J. Polym. Sci.: Phys. Ed., 18, 361-388, 1980.

Kolnaar J.W.H. and A. Keller, 'A temperature window of reduced flow resistence in polyethylene with implications for melt flow rheology: 1. The basic effect and principal parameters', Polymer, 35(18), 3863-74, 1994.

Kolnaar J.W.H. and A. Keller, 'A temperature window of reduced flow resistence in polyethylene with implications for melt flow rheology: 2. Rheological investigations in the extrusion window', Polymer, 36(4), 821-36, **1995.**

Kolnaar J.W.H. and A. Keller, A singularity in the melt flow of polyethylene with wider implications for polymer melt flow rheology', J. Non-Newtonian Fluid Mech., 67, 213-240, **1996.**

Kolnaar J.W.H. and A. Keller, 'A singularity in the melt flow of polyethylene with wider implications for polymer melt flow rheology', J. Non-Newtonian Fluid Mech., 69, 71-98, **1997.**

Konar J. and R. Ghosh, 'Oxidative degradation of polyethylene in the presence of phase transfer catalyst: Part I-Infrared studies', Polym. Deg. Stab., 21, 263-275, **1988.**

Konar J. R. Ghosh and S.K. Ghosh, 'Oxidative degradation of polyethylene in the presence of phase transfer catalyst: Part II-Thermal studies', Polym. Deg. Stab., 22, 43-52, **1988.**

Kresteva M., E. Nedkov and and A. Radilova, 'Melting of nascent and thermally treated super-high molecular weight polyethylene', Colloid & polymer Science, 263, 273-9, **1985.**

Krevelen D.W. van, 'Properties of Polymers: Correlations with Chemical Structure', Elsevier Publishing Co., Amsterdam, **1972.**

Krevelen D.W. van, 'Properties of Polymers: Their Estimation and Correlation with Chemical Structure', second Ed., Elsevier Publishing Co., Amsterdam, **1976.**

Kruger J.K., 'Evidence for structures in paraffin-melts by Brillouin-Spectroscopy', Solid State Communications, 30, 43-6, **1979.**

Kruger J.K., L. Peetz, W. Wildner and M. Pietralla, 'Evidence for structural transformations in polymer melts', J. Polymer, 21, 620-6, June **1980.**

Kumar Anil and Rakesh K. Gupta, 'Fundamentals of Polymers', McGraw-Hill Co., Toronto, p. 385, **1998.**

Lacoste J., Y. Deslandes, P. Black and D.J. Carlsson, 'Surface and bulk analyses of the oxidation of polyethylene', Polym. Deg. Stab., 49, 21-28, **1995**.

Larson R.G., 'Arrested Tumbling in Shearing Flows of Liquid Crystal Polymers', Macromolecules, 23, 3983-3992, **1990**.

Larson R.G., 'Flow-induced mixing, demixing, and phase transitions in polymeric fluids', Rheol. Acta, 31, 497-520, **1992**.

Lee Soo Y., Jae Y. Jho, and Young C. Lee, 'Effect of Comonomer distribution of LLDPE on miscibility behavior with HDPE', Polym. Mater. Sci. Eng., 76, 325-326, **1997**.

Lindner R.A., 'Low-molecular weight polyethylene', in 'Plastics additives and modifiers handbook', revised ed., ed. by Jesse Edenbaum, Chapman & Hall, London, **1996**.

Linster J.J. and J. Meissner, 'Melt elongation and structure of linear polyethylene (HDPE)', Polym. Bull., 16, 187-194, **1986**.

Lipatov Yu.S., A.E. Nestrov, V.F. Shumski, T.D. Ignatova, and A.N. Gorbatenko, 'Comparison of thermodynamic and rheological properties of binary polymer mixtures', Eur. Polym. J., 18, 981-986, **1982a**.

Lipatov Yu.S., A.E. Nestrov, T.D. Ignatova, V.F. Shumski, and A.N. Gorbatenko, 'The thermodynamic and rheological properties of polymer melt mixtures', Polym. Sci. USSR, 24(3), 607-613, **1982b**.

Lipatov Yu.S., V.F. Shumski, A.N. Gorbatenko, Yu.N., 'Viscoelastic properties of polystyrene-polycarbonate blends in melt', J. Appl. Polym. Sci., 26, 499-508, **1981**.

Macosko Christopher W., 'Rheology: Principles, Measurements, and Applications', VCH Publishers, Inc., New York, **1994**.

Macosko C.W. and D.J. Morse, in Proc. 7th Intern. Congress on Rheol.; C. Kalson and J. Hubat, Eds., Gothenberg, p. 376, **1976**.

Maffettone P.L. and Marrucci G., 'A two-dimensional approach to the constitutive equation of nematic polymers' J. Non-Newt. Fluid Mech., 38, 273-288, **1991**.

Malik J., K.H. Stoll, D. Cabaton, and A. Thürmer, 'Processing stabilization of HDPE: a complex study of an additive package', Polym. Deg. Stab., 50, 329-336, **1995**.

Manero O., C. Rangel-Nafaile and A. Garcia-Rejon, 'Analysis of the flow behavior of HDPE/LDPE blends using a kinetic network model', J. Appl. Polym. Sci., 33, 2053-2064, **1987**.

Manke C.W. and M.C. **Williams**, 'Transient Stress and Strain Responses Predicted by the Internal Viscosity Model in Shear Flows', J. Rheol., 33(6), 949-978, **1989**.

Mark H.F., N.M. Bikales, C.G. Overberger and G.Menges, 2nd ed., 'Encyclopedia of Polymer Science and Engineering', Vol 6, p. 477, John Wiley & Sons, **1986**.

Marrucci G. and F. **Greco**, 'A molecular approach to the polydomain structure of LCPs in weak shear flows', J. Non-Newt. Fluid Mech., 44, 1-13, **1992**.

Marrucci G. and P.L. **Maffettone**, 'Description of the Liquid-Crystalline Phase of Rodlike Polymers at high Shear Rates', Macromolecules, 22, 4076-4082, **1989**.

Marrucci G. and P.L. **Maffettone**, 'Nematic phase of rodlike polymers. II. Polydomain predictions in the tumbling regime', J. Rheol., 34, 1231-1244, **1990**.

Mathot Vincent B.F., Rolf L. Scherrenberg and Thijs F.J. Pijpers, 'Metastability and order in linear, branched and copolymerized polyethylenes', Polymer, 39(19), 4541-4559, **1998**.

McChesney Charles E., 'Liquid Crystal Polymers' in 'Engineered Materials Handbook', edited by J.N. Epel et al., Vol 2, Metal Park, Ohio, USA, p. 179, **1988**.

Meissner Joachim, 'The effect of temperature on the flow properties of the Low Density Polyethylene melt', proceedings of the 4th Intern. Congr. On Rheol., Brown, **1963**.

Mendelson Robert, 'Melt viscosity-temperature dependence of some Low Density Polyethylene', SPE Trans., 5(1), 34-38, **1965a**.

Mendelson Robert, 'Polyethylene melt viscosity: Shear rate-temperature superposition', Trans. Soc. Rheol., 9(1), 53-63, **1965b**.

Mendelson R.A., W.A. Bowles, and F.L. Finger, 'Effect of molecular structure on polyethylene melt rheology. II. Shear-dependent viscosity', J. Polym. Sci.: Part A-2, 8, 127-141, **1970**.

Mewis J. and P. **Moldenaers**, 'Transient rheological behaviour of a lyotropic polymeric liquid crystal', Mol. Cryst. Liq. Cryst., 153, 291-300, **1987**.

Micic P., S.N. Bhattacharya and G. Field, 'Melt strength and elastic behaviour of LLDPE/LDPE blends', Intern. Polym. Processing XI, 14-20, **1996**.

Minale M., P. Moldenaers, and J. Mewis, 'Effect of Shear History on the Morphology of Immiscible Polymer Blends', Macromolecules, 30, 5470-5475, **1997**.

Minkova L. and M. **Mihailov**, 'A calorimetric study of normal high density and ultra-high molecular weight polyethylene blends', Colloid & Polymer Sci., 265(1), 1-7, **1987**.

Moldenaers P. and J. **Mewis**, J. Rheol., 'Transient Behavior of Liquid Crystalline Solutions of Poly(benzylglutamate)', 30(3), 567-584, **1986a**.

Moldenaers P. and J. **Mewis**, 'Transient Rheological Behaviour of Polymeric Liquid Crystals', 3rd World Congress of Chem. Eng., Tokyo, **1986b**.

Muhammed M., unpublished work, University of Alberta, **1995**.

Muhammed M., I.A. Hussein, and M. C. Williams, 'Measuring density-temperature behavior of polymer solids and melts: Comparison of DSC and densitometer results for polyethylenes', 47th Canadian Chemical Engineering Conference, Edmonton, AB, October 5-8, **1997**.

Muñoz-Escalona A., P. Lafuente, J.F. Vega, M.E. Muñoz and A. Santamaria, 'Rheological behavior of metallocene catalyzed high density polyethylene blends', Polymer, 38(3), 589-594, **1997**.

Nakajima N. and E.R. **Harrell**, 'Modified Cole-Cole plot as a tool for rheological analysis of polymers' in 'Current Topics in Polymer Science', Vol II, 'Rheology and Polymer Processing/Multiphase Systems', Edited by R.M. Ottenbrite, L.A. Utracki, and S. Inoue, Hanser Publishers, NY, **1987**.

Nesarikar A.R., Ph.D. Thesis, 'Thermodynamics and Kinetics of Liquid-Liquid Phase Separation in Random Copolymers', Northwestern University, Evanston, IL, **1995a**.

Nesarikar A.R., 'Rheology of Polymer Blend Liquid-Liquid Phase Separation', Macromolecules, 28, 7202-7207, **1995b**.

Niemiec Jan M., Jean-Jacques Pesce, Gregory B. McKenna, Stephen Skocypec and Ronald F. Garritano, 'Anomalies in the normal force measurement when using a force rebalance transducer', J. Rheol., 40(3), 323-334, **1996**.

Nyden M.R., G.P. Forney and J.E. Brown, 'Molecular modeling of polymer flammability: Application to design of flame-resistant polyethylene', Macromolecules, 25, 1658-1666, **1992**.

Ober C.K. and R.A. Weiss, 'Current topics in liquid crystalline polymers' in 'liquid crystalline polymers' edited by Weiss and C.K. Ober, ACS symposium, Miami, USA, 1-11, Sept. **1989**.

Olabisi Olagoke, Lloyd M. Robeson, and Montgomery T. Shaw. "Polymer-Polymer Miscibility", Academic Press, NY, p. 54, **1979**.

Oldroyd J.G., 'The elastic and viscous properties of emulsions and suspensions', Proc. Roy. Soc. A, 128, 122-132, **1953**.

Onogi S. and T. Asada, 'in 'Rheology' vol 1, edited by G. Astarti, G. Marucci and L. Nicholais, Plenum Press, NY, 127-147, **1980**.

Percec Virgil and Dimitris Tomazos, 'Can the rigidity of a side-chain liquid-crystalline polymer backbone influence the mechanism of distortion of its random-coil conformation?', Polymer, 31, 1658-62, Sept. **1990**.

Perry R.H. and D.W. Green, 'Perry's Chemical Engineers' Handbook', 7th edition, McGraw-Hill, p. 3-74, **1997**.

Petermann J. and H. Gleiter, 'The molecular structure of molten polyethylene films', Phil. Mag. Series 8, 28(1), 271-276, **1973**.

Philippoff W. and F.H. Gaskins, 'Viscosity measurements on Molten Polyethylene', J. Polymer Sci., 21, 205-222, **1956**.

Phuong-Nguyen H. and G. Delmas, 'Arrested melting due to strain in ultrahigh molecular weight polyethylene', Macromolecules, 25, 408-13, **1992a**.

Phuong-Nguyen H. and G. Delmas, 'Thermal analysis and model of ultrahigh molecular weight polyethylene gels', Macromolecules, 25, 414-21, **1992b**.

Plochocki A.P., 'Polyolefin Blends: Rheology, Melt Mixing, and Applications', in Polymer Blends, Vol 2, Edited by D.R. Paul and S. Newman, Academic press, **1978**.

Polance R. and K. **Jayaraman**, 'Mixing in reactive extrusion of low-density polyethylene melts: linear vs. branched', Polym. Eng. Sci., 35(19), **1995**.

Popli R., M. Glotin, L.Mandelkem and R.S. Benson', 'Dynamic mechanical studies of α and β relaxations of polyethylenes', J. Polym. Sci., Polym. Phys. Ed., 22, 407-48, **1984**.

Porter Roger S. and Julian F. **Johnson**, 'Viscosity of polyethylenes: Dependence on molecular weight and temperature', J. Appl. Polym. Sci., 3(8), 194-199, **1960**.

Porter Roger S. and Julian F. **Johnson**, 'Temperature dependence of polymer viscosity. The influence of shear rate and stress', J. Polym. Sci.: Part C, No. 15, 365-371, **1966**.

Pospíšil J. and S. **Nešpůrek**, 'Chain-breaking stabilizers in polymers: the current status', Polym. Deg. Stab., 49, 99-110, **1995**.

Pospíšil J. and P.P. **Klemchuk**, 'Oxidation Inhibition in Organic Materials', CRC Press, Boca Raton, FL, **1990**.

Rabesiaka J. and A.J. **Kovacs**, 'Isothermal characterization kinetics of polyethylene: III Influence of the sample preparation', J. Appl. Phys., 32, 2314-20, **1961**.

Radian Corporation, 'Chemical additives for the plastic industry', Noyes data corp., NJ, **1987**.

Rudin Alfred, 'The Elements of Polymer Science and Engineering', Academic Press, Toronto, p. 445-446, **1982**.

Rudin A., 'Effect of processing history on melt flow defects', Polym. Eng. Sci., 10(2), 94-101, **1970**.

Sabia Raffaele, 'On the characterization of non-Newtonian flow. III', J. Appl. Polym. Sci., 8, 1651-1657, **1964**.

Scholz P., D. Froelich, and R. Muller, 'Viscoelastic Properties and Morphology of Two-Phase Polypropylene/Polyamide 6 Blends in the Melt. Interpretation of Results with an Emulsion Model', J. Rheol. 33(3), 481-499, **1989**.

Schott Hans and W.S. **Kaghan**, 'Viscous flow of molten polyethylene resins', J. Appl. Polym. Sci., 5(14) 175-183, **1961**.

Shah Vishu, Handbook of Plastics Testing Technology, Ch. 10, A Wiley-Interscience Publication, John Wiley & Sons, **1984**.

Shipman R.W.G., Morton M. Denn, and Roland Keunings, 'Free-Surface Effects in Torsional Parallel-Plate Rheometry', Ind. Eng. Chem. Res., 30, 918-922, **1991**.

Shumsky V.F., Ye. V. Lebedev and Yu.S. Lipatov, 'The viscoelastic properties of mixtures of crystallizable polymers', Polym. Sci. U.S.S.R, 21, 1085-1095, **1979**.

Strand S.R., S. Kim, and S.J. Karrila, 'Computation of Rheological Properties of Suspensions of Rigid Rods: Stress Growth after Inception of Steady Shear Flow', J. Non-Newt. Fluid Mech., 24, 311-329, **1987**.

Stupp S.I., 'Molecular organization in nematic polymers', Polym. Preprints, ACS Div., Polym. Chem., 30(2), 509-10, **1989**.

Stupp S.I., J.S. Moore and P.G. Martin', Chemical disorder and phase separation: A study of two liquid crystal Polymers', Macromolecules, 21, 1228-34, **1988**.

Taylor G.I., 'The viscosity of a fluid containing small Drops of Another Fluid', Proc. Roy. Soc., A138, 41-48, **1932**.

Thomas D., J. Williamson, M.J. Hill and P.J. Barham, 'Liquid-liquid phase separation in a ternary blend of polyethylene', Polymer, 34(23), 4919-23, **1993**.

Tsenoglou C., 'Viscoelasticity of binary homopolymer polymer blends, ACS Polymer Preprints, 28(2), 185-186, **1987**.

Tsenoglou C., 'Viscoelasticity and diffusion of miscible heteropolymer blends, ACS Polymer Preprints, 29(1), 405-406, **1988**.

Tsenoglou C., 'Molecular weight polydispersity effects on the viscoelasticity of entangled linear polymers, Macromolecules, 24, 17621767, **1991**.

Ungar G., 'From plastic-crystal paraffins to liquid-crystal polyethylene: Continuity of the mesophase in hydrocarbons', Macromolecules, 19, 1317-24, **1986**.

Utracki L.A., M.M. Dumoulin, and P. Toma, 'Melt Rheology of High Density Polyethylene/Polyamide-6 Blends', Polym. Eng. Sci., 26(1), 34-44, **1986**.

Usami T., Y. Gotoh, and S. Takayama, 'Generation Mechanism of Short-Chain Branching Distribution in Linear Low-Density Polyethylenes', Macromolecules, 19, 2722-2726, **1986**.

Utracki L.A., 'Rheology and processing of multiphase systems' in 'Current Topics in Polymer Science', Vol II, 'Rheology and Polymer Processing/Multiphase Systems', Edited by R.M. Ottenbrite, L.A. Utracki, and S. Inoue, Hanser Publishers, NY, **1987**.

Utracki L.A., 'Viscoelastic behaviour of polymer blends', Polym. Eng. Sci., 28(21), 1401-1404, **1988**.

Utracki L.A., 'Polymer Alloys and Blends: Thermodynamics and Rheology', Hanser Publishers, NY, **1989a**.

Utracki L.A., 'Melt flow of polyethylene blends' in 'Multiphase Polymers: Blends and Ionomers', ACS Symposium Series, edited by L.A. Utracki and R.A. Weiss, ACS Washington, DC, **1989b**.

Utracki L.A. and B. **Schlund**, 'Linear low density polyethylenes and their blends: Part 4 Shear flow of LLDPE blends with LLDPE and LDPE', Polym. Eng. Sci., 27(20), **1987**.

Van Oene, 'Rheology of polymer blends and dispersions', in Polymer Blends, Vol 1, Edited by D.R. Paul and S. Newman, Academic press, **1978**.

Vega J.F., A. Munoz-Escalona, A. Santamaria, M.E. Munoz, and P. Lafuente, 'Comparison of the rheological Properties of Metallocene-Catalyzed and Conventional Polyethylenes', Macromolecules, 29, 960-965, **1996**.

Vinckier Inge, Jan Mewis, Paula Moldenaers, 'Stress relaxation as a microstructural probe for immiscible blends', Rheol. Acta, 36, 513-523, **1997**.

Viola G.G. and D.G. **Baird**, 'Studies on the transient shear flow behavior of liquid crystalline polymers', J. Rheol., 30(3), 601-28, **1986**.

Waddon A.J. and A. **Keller**, J. Polym. Sci., 28, 1063-, **1990**.

Waddon A.J. and A. **Keller**, J. Polym. Sci.. Part B: Polym. Phys., 30, 923-, **1992**.

Walters K., 'Rheometry', Chapman and Hall, **1975**.

Wang Shi-Qing and Patrick A. **Drda**, 'Stick-slip transition in capillary flow of linear polyethylene: 3. Surface conditions', Rheol. Acta, 36, 128-134, **1997**.

Wanke S.E., Professor of Chemical Engineering, University of Alberta, Personal Communications, April **1999**.

Wardhaugh Leigh T. and Michael C. **Williams**, 'Blockiness of olefin copolymers and possible microphase separation in the melt', Polym. Eng. and Sci., 35(1),18-27, mid January **1995**.

Wasserman S.H. and G.N. **Foster**, 'Rheological detection of structure modification due to extrusion processing in polyethylene', In Proc. XII Int. Congr. On Rheology, Edited by: A. Aït-Kadi, J.M. Dealy, D.F. James and M.C. Williams, Quebec City, Canada, August 18-23, **1996**.

Wissbrun K.F. and A.C. **Griffin**, 'Rheology of a thermotropic polyester in the nematic and isotropic states', J. Polym. Sci., Polym. Phys. Ed., 20, 1835-45, **1982**.

Wissbrun K.F., 'Note: Negative extrudate swell of liquid crystal polymers', J. Rheol., 38(2), 247-52, **1994**.

Wissbrun K.F., 'Observations on the melt rheology of thermotropic aromatic polyesters', Br. Polym. J., 163-9, December **1980**.

Wissbrun K.F., 'Rheology of rod-like polymers in the liquid crystalline state', J. Rheol., 25(6), 619-62, **1981**.

Wissbrun K.F., G. Kiss, and F.N. Cogswell, 'Flow behavior of a thermotropic liquid crystal aromatic copolyester', Chem. Eng. Comm., 35, 149-73, **1987**.

Wunder Stephanie L. and Sofia D. **Merajver**,'Ultrahigh molecular weight polyethylene: Raman spectroscopic study of melt anisotropy', J. Polym. Sci., Polym. Phys. Ed., 24, 99-110, **1986**.

Wunderlich Bernhard, 'Macromolecular Physics', Vol 3, 'Crystal Melting', Academic Press, **1980**.

Wunderlich Bernhard, 'The basis of thermal analysis', in 'Thermal characterization of polymeric materials', 2ⁿᵈ ed., Ed. by Edith A. Turi, Vol 1, Academic Press, 347-63, **1997**.

Wunderlich Bernhard and Janusz **Grebowicz**, 'Thermotropic mesophases and mesophase transitions of linear, flexible macromolecules', Adv. Polym. Sci., 60/61, 1-59, **1984**.

Xanthos M., V. Tan, and A. Ponnusamy, "Measurement of melt viscoelastic properties of polyethylenes and their blends-A comparison of experimental techniques", Polym. Eng. and Sci., 37(6), 1102-1112, June **1997**.

Zachariades A.E. and **Logan**, 'The melt anisotropy of ultrahigh molecular weight polyethylene', J. Polym. Sci., Polym. Phys. Ed., 21, 821-30, **1983**.

Zoller P., P. Bolli, V. Pahud, and H. Ackermann, Apparatus for measuring pressure-volume-temperature relations of polymers to 350°C and 2200 kg/cm², Rev. Sci. Instrum., 47(8), 948-952, **1976**.

Appendix A

Supplement to Chapter IV

Figure A.1 Strain sweep test for Q-HDPE at 260°C

(as-received, ω=1 rad/s)
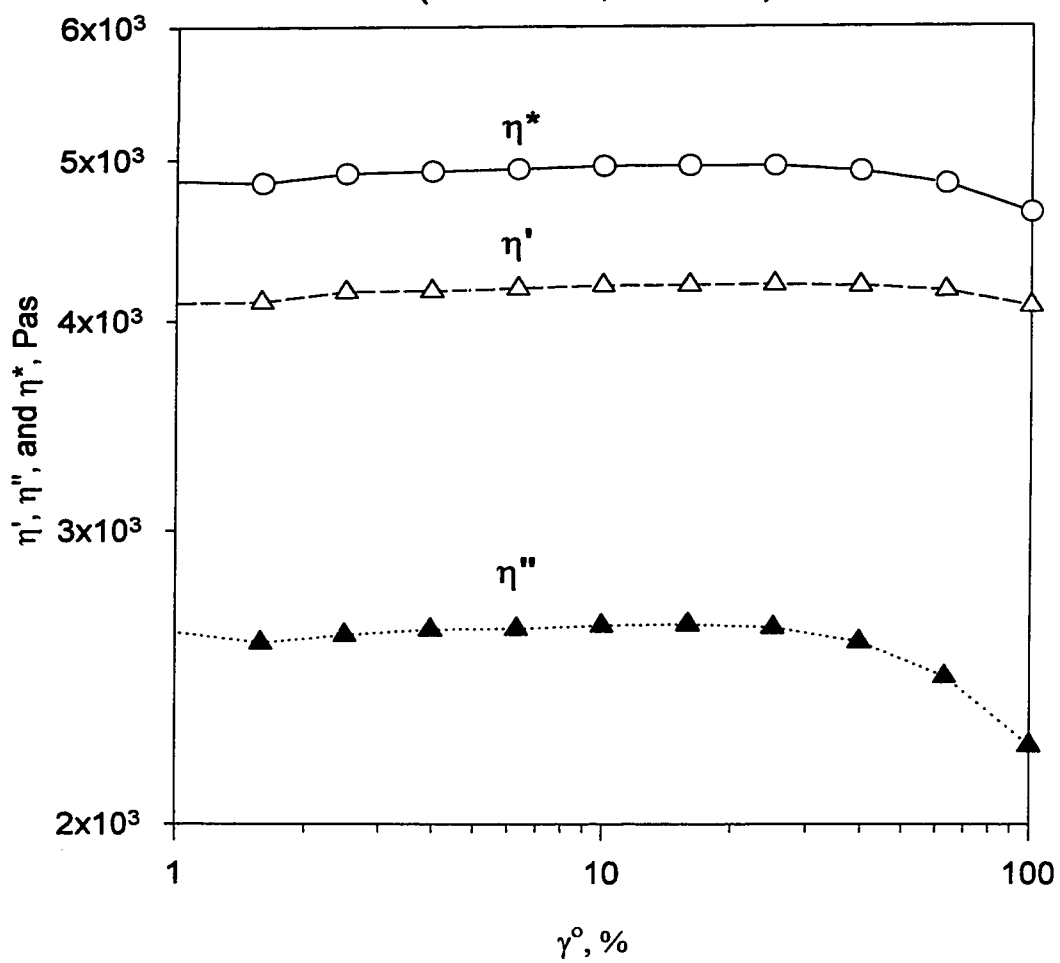
Figure A.2 Arrhenius plot of η*(1/T) for Nova S229 (butene)⁺

$(\gamma°=10\%, \omega=1rad/s, branches=22.1/1000C)$

Figure A.3 Arrhenius plot of $\eta^*(1/T)$ for S237 (hexene)[+]

(17.2 branches/1000 C, ω=1 rad/s, γ°=10%, 160°-260°C)

[+]with additional 1000 ppm of A/O
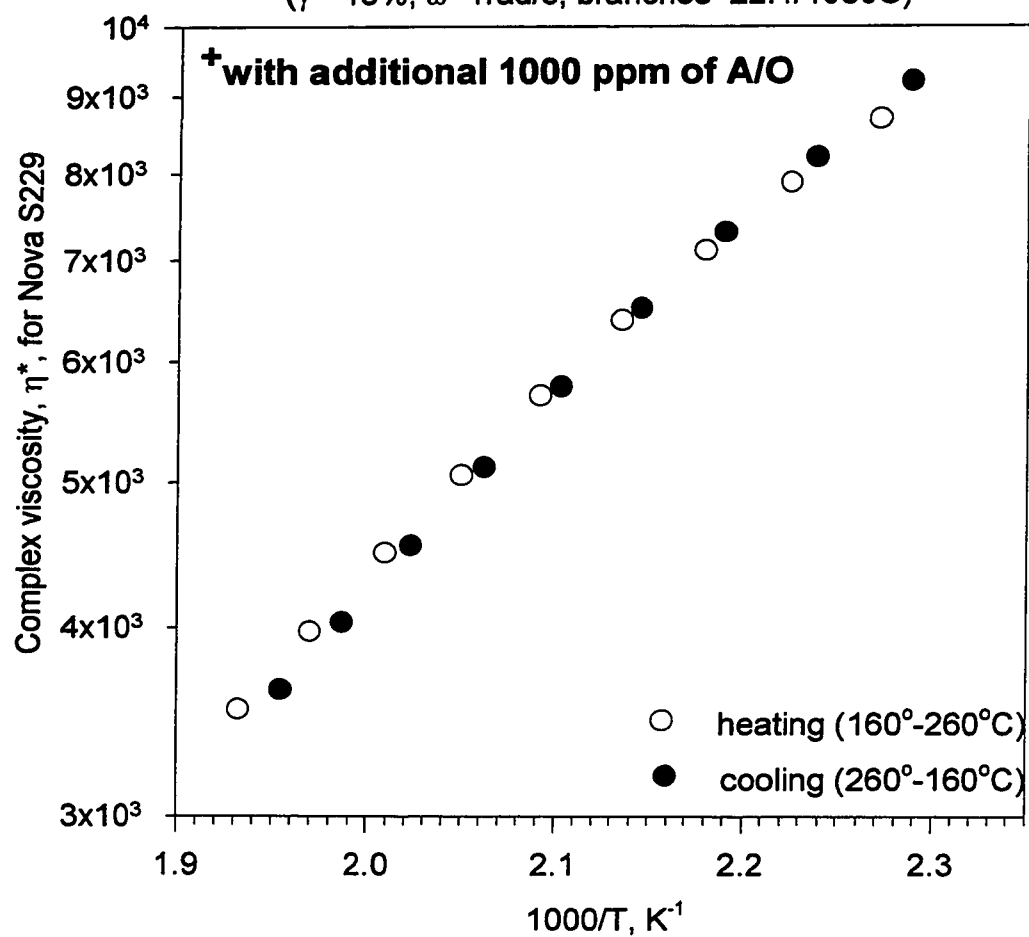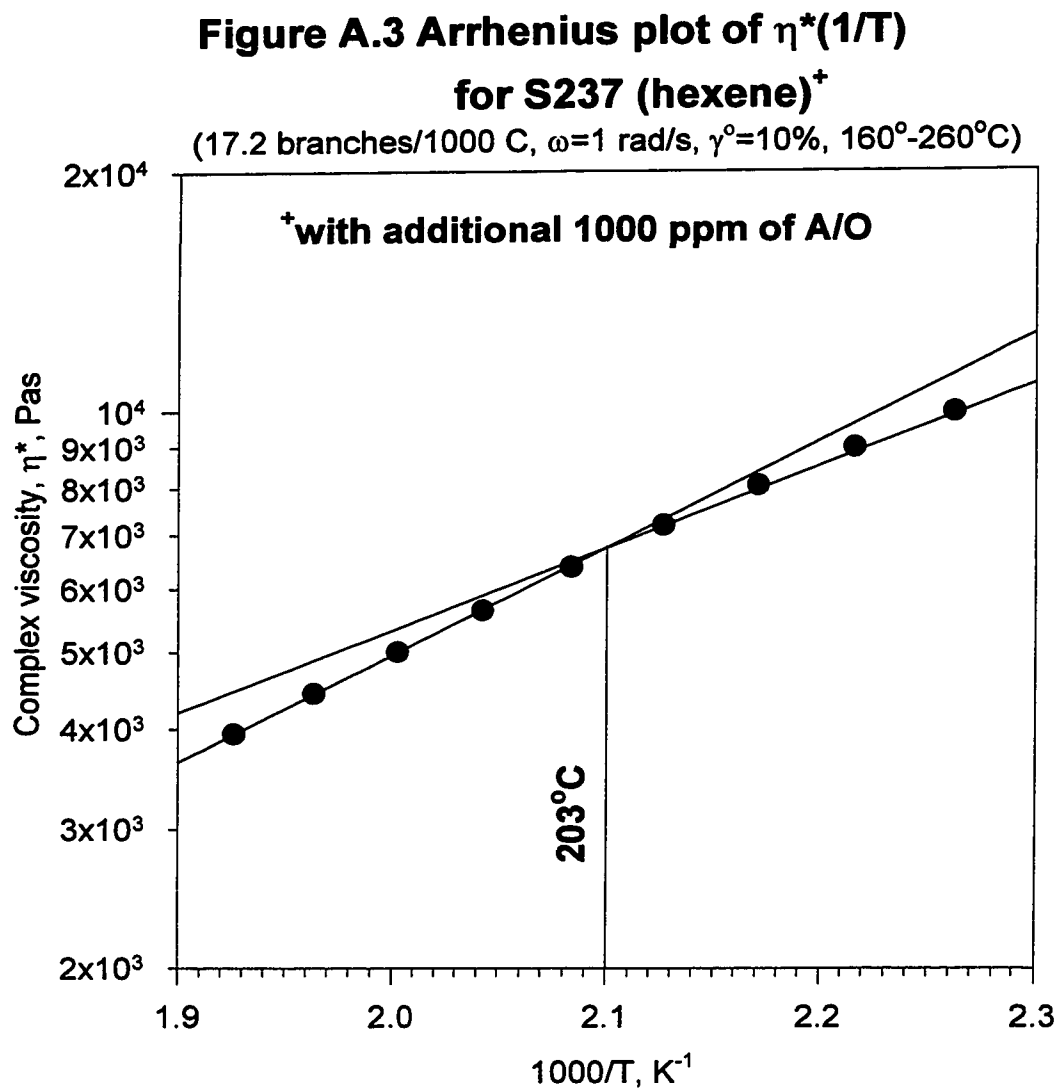
Figure A.4 Arrhenius plot of η*(1/T) for S226 (octene)⁺

(14.7 branches/1000 C, 160°-260°C, ω=1rad/s, γ°=10%)
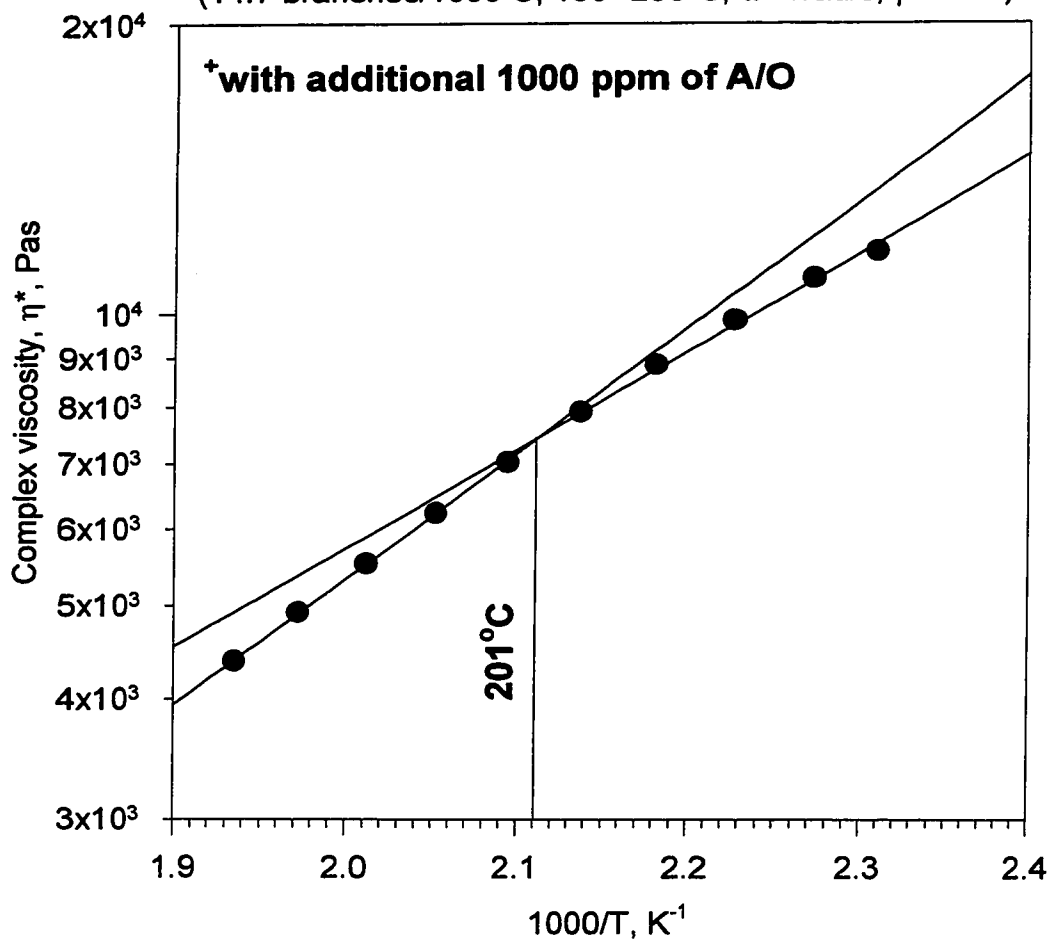
**Figure A.5 Arrhenius plot of η*(1/T)
for Exxon 4033 (Met.)⁺**

(γ°=10%, ω=1rad/s, Butene, 36.2 Branches/1000)

⁺with additional 6000 ppm of A/O

(E=6.744 kcal/mol, r²=0.9968)

○   heating (160°-260°C)

●   cooling (260°-160°C)
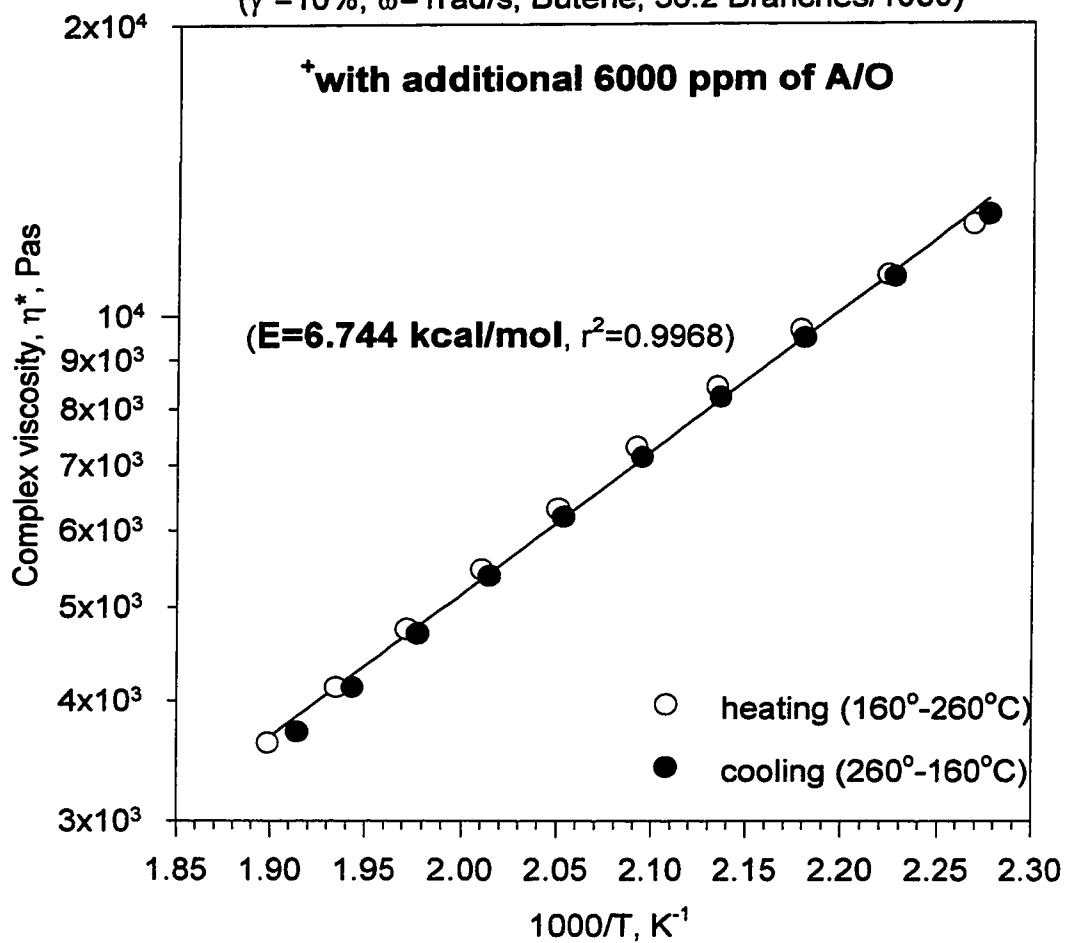
Figure A.6 Steady shear measurements for Solvay-HDPE

(T=250°C, PP, 1.5 mm gap, tbm=5 min., mt= 0.5 min.)
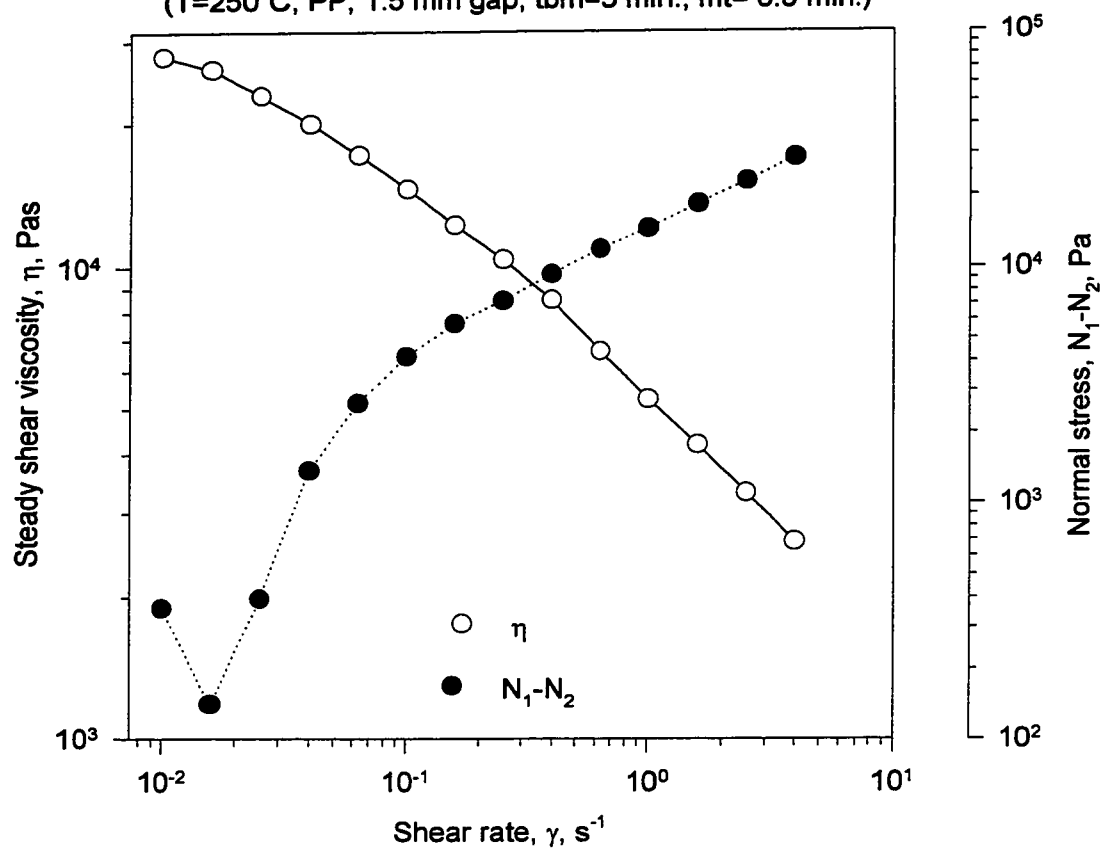
Figure A.7 Comparison of steady shear measurments in CP and PP for Q-HDPE at 190°C

Legend:
- ▲ η (C&P)
- ○ η (PP)
- △ N_1(C&P)
- ● N_1-N_2 (PP)

Y-axis (left): Steady shear viscosity, η, Pas
Y-axis (right): Normal stress, Pa
X-axis: shear rate,γ, s^{-1}
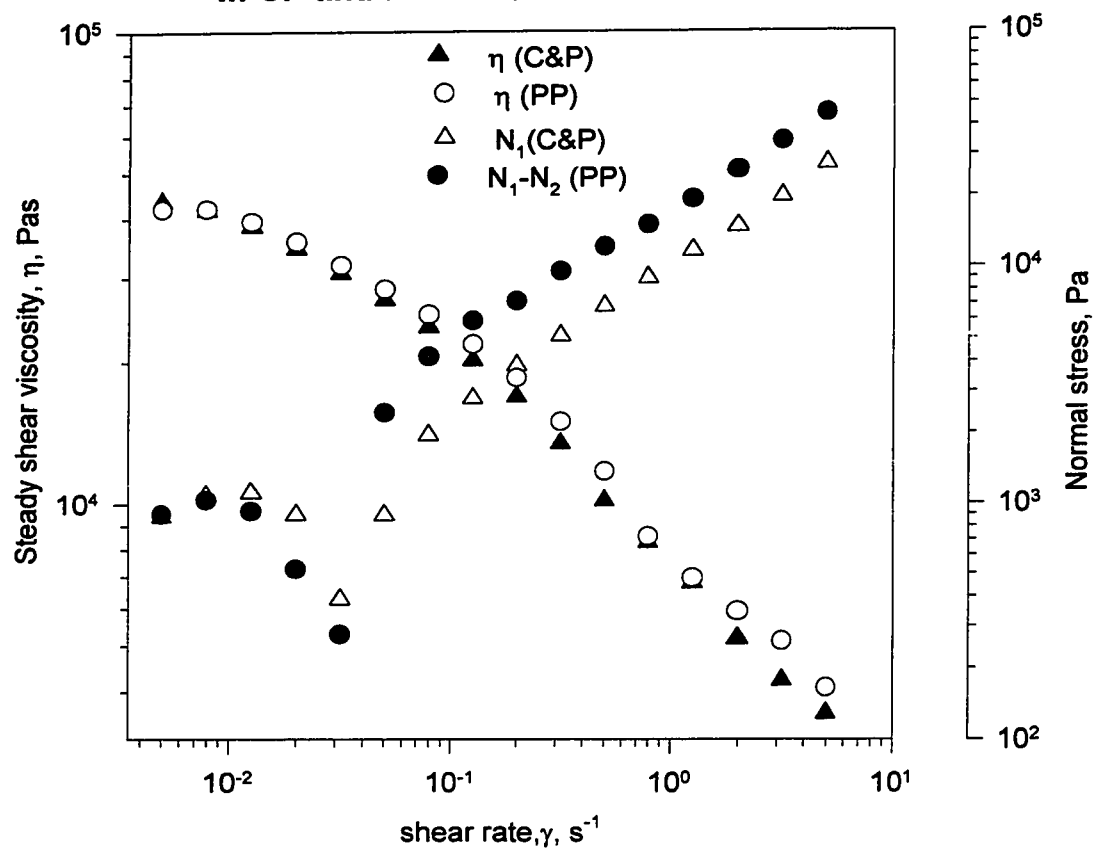
Figure A.8 Transient normal force for Paxon-HDPE
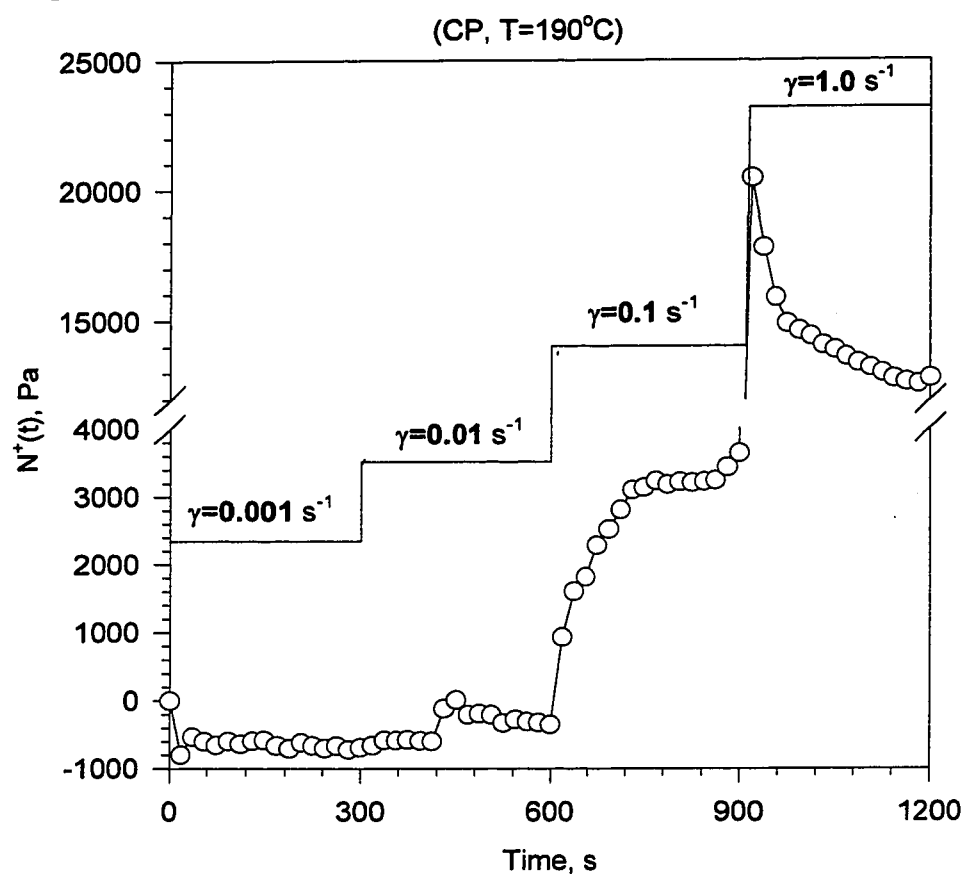
Figure A.9 Transient normal force for Dow-PS

(CP, T=190°C)
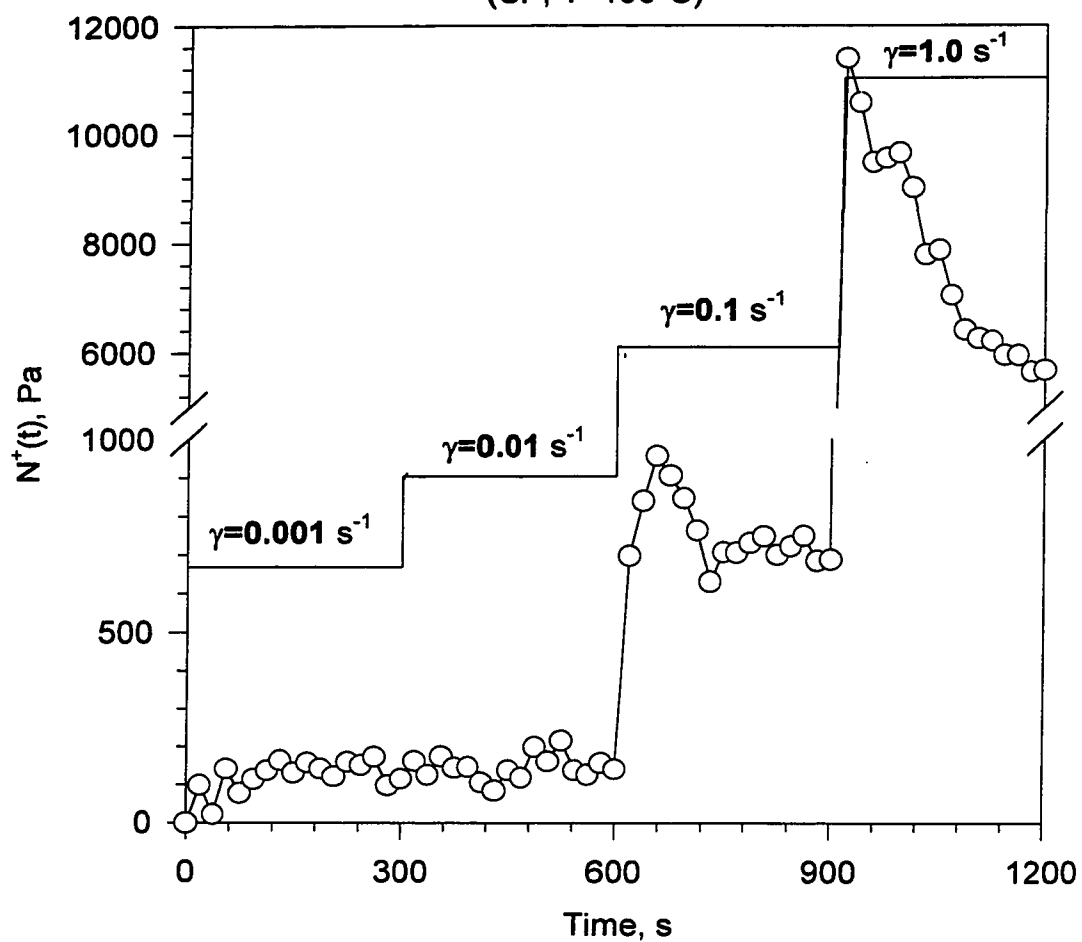
Figure A.10 Comparison of the ascending and descending dynamic testing at 190°C & 240°C
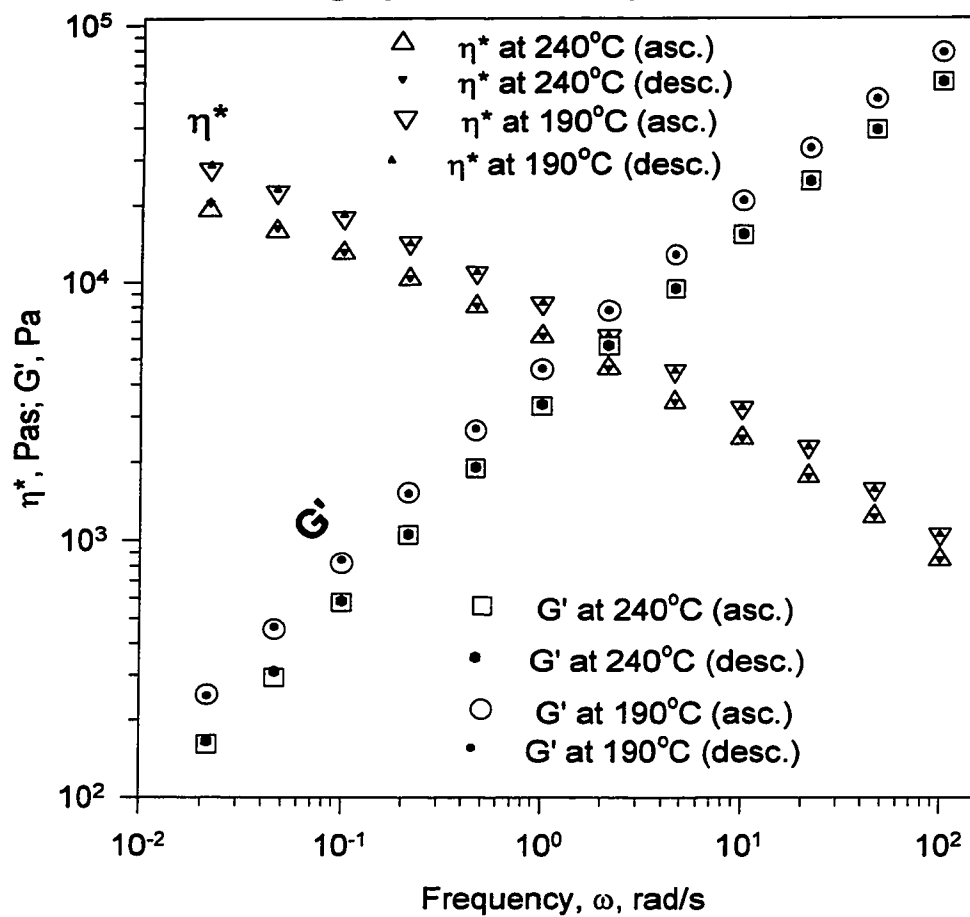
Figure A.11 Time sweep test for Q-HDPE

$(\gamma^{\circ}=6\%,\ \omega=0.1\ rad/s,\ T=190^{\circ}C)$
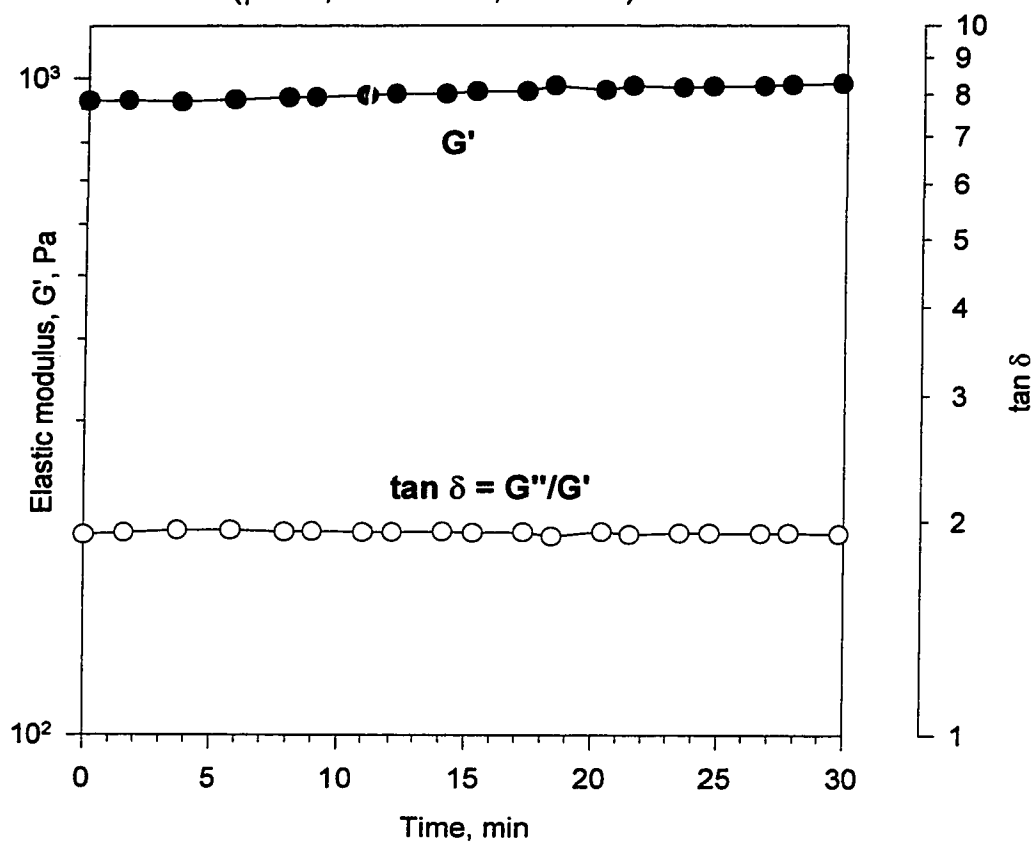
Figure A.12 Comparison of steady and dynamic shear for Solvay-HDPE

(T=250°C, PP, 1.5 mm gap, tbm=5 min., mt= 0.5 min.; γ^o=10%)

Frequency, ω; Shear rate, γ_R, s^{-1}

□ η (steady shear viscosity)

■ η^*(complex viscosity)
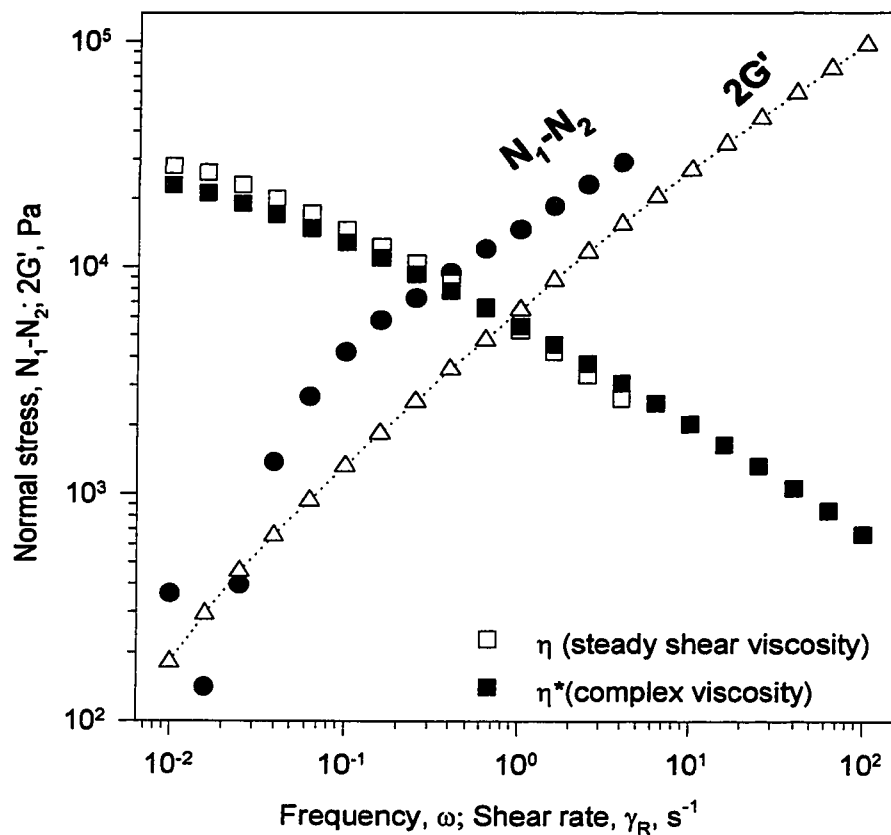
Figure A.13 Torque-melt temperature curve for Solvay-HDPE*

(T_{hold}=160°C, t_{hold}=3min., ramp to 260°C at 5°C/min)

*with additional 2000 ppm of A/O
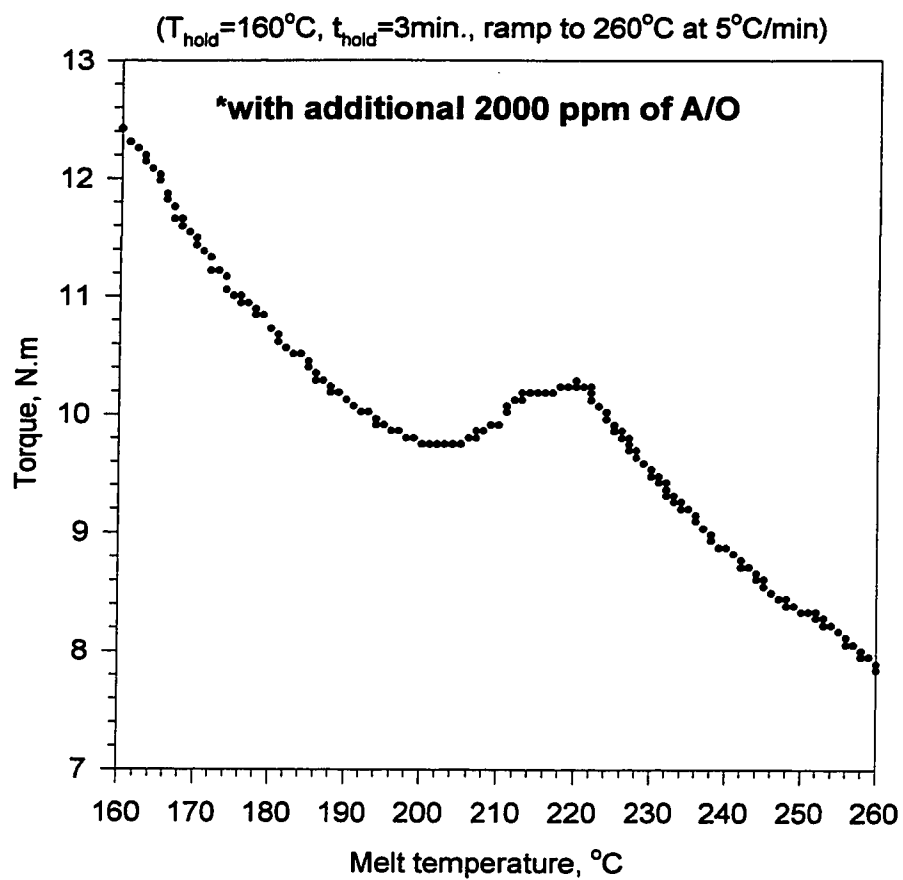
Figure A.14 Torque-melt temperature curve for UC-HDPE

(hold at 160°C for 3 min, 50 rpm, 5°C/min, with N_2)
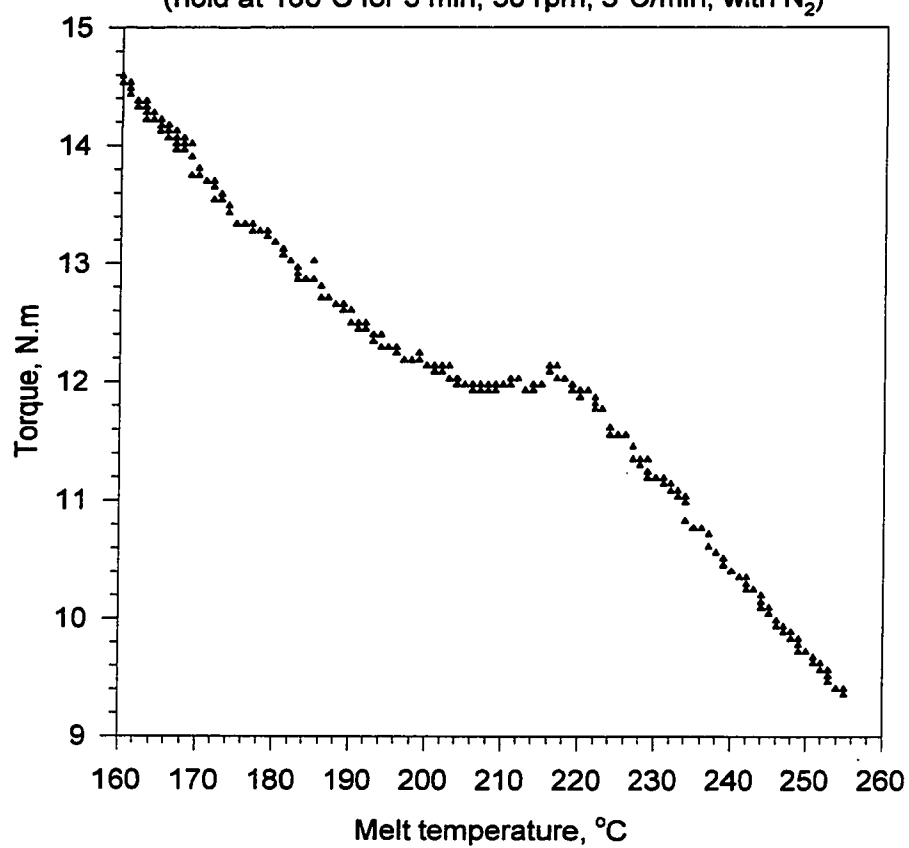
Melt temperature, °C

Figure A.15 Torque-melt temperature curve for Paxon-HDPE

(hold at 160°C for 3 min, 50 rpm, ramp=5°C/min, with N_2)
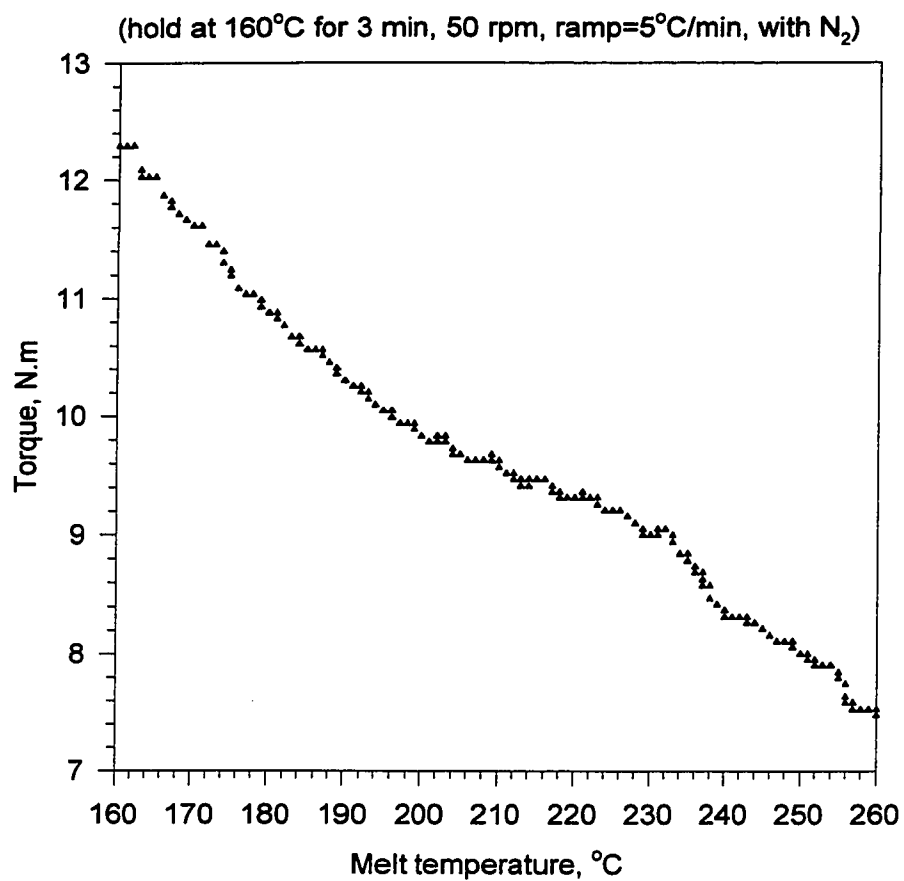
Figure A.16 Torque-Melt temperature curve for Q-HDPE

(as-received, 50 rpm, ramp=5°C/min)
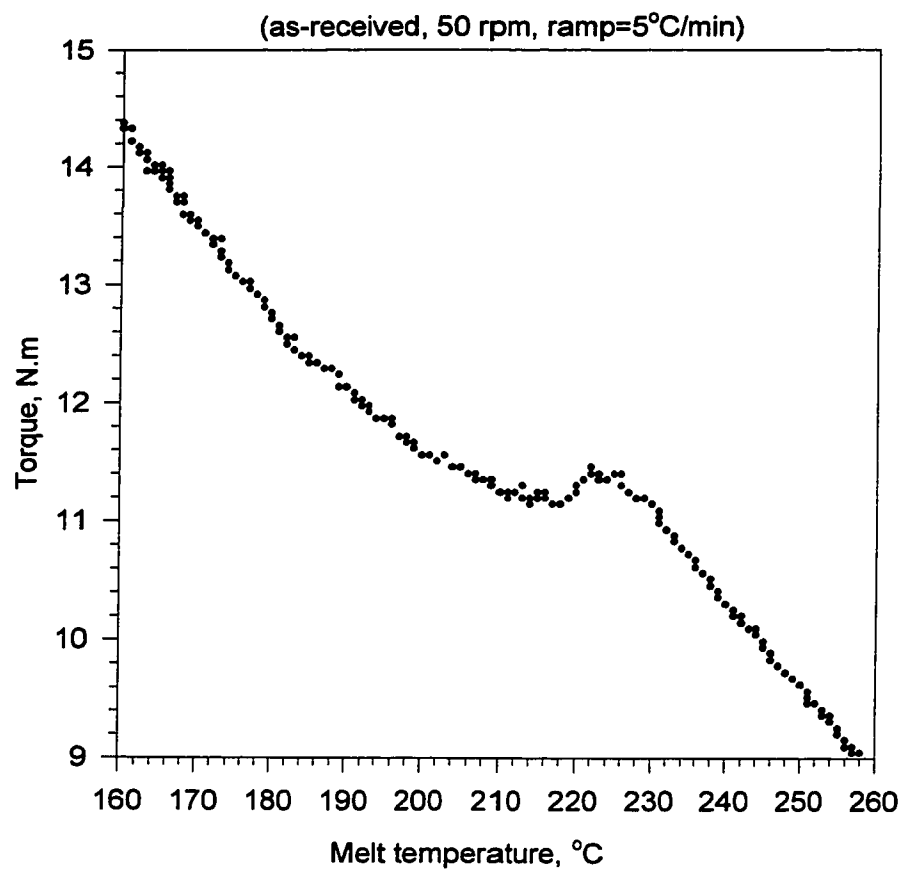
Figure A.17 Arrhenius torque-melt temperature curve for Q-HDPE

(50 rpm, hold at 160 for 10 min, 5°C/min)

1000/T, K⁻¹
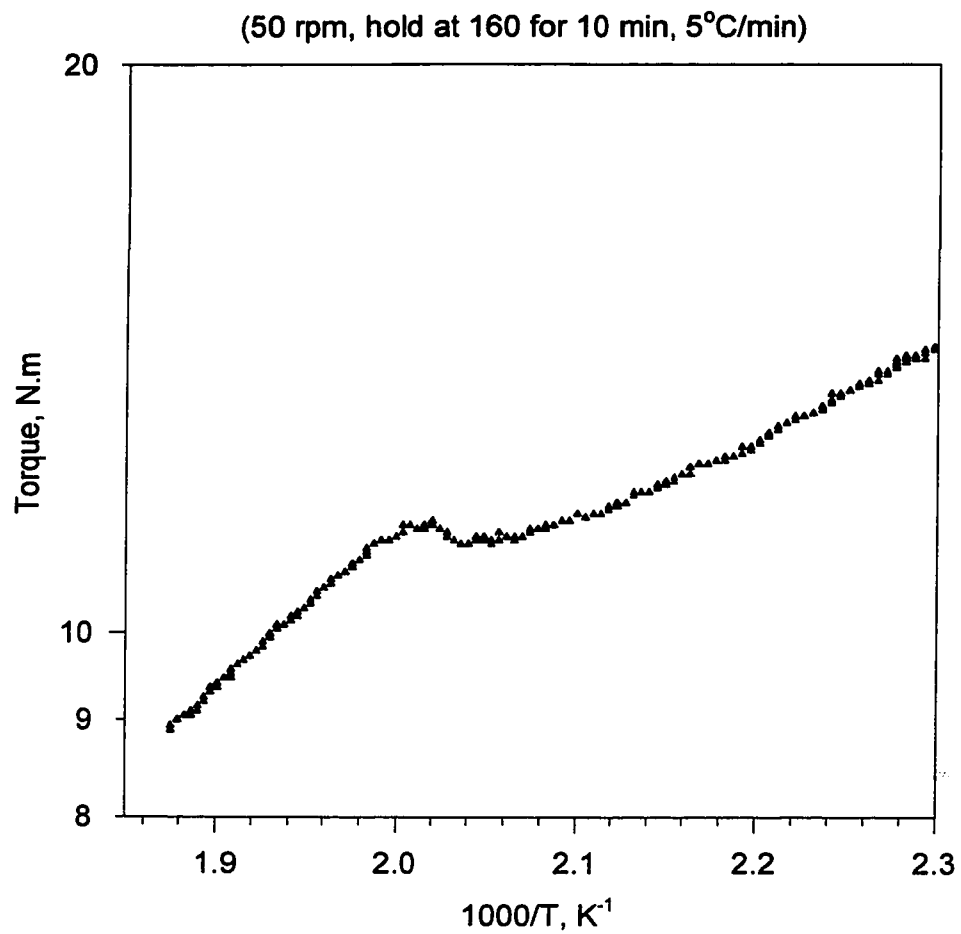
Figure A.18 Arrhenius torque-melt temperature curve for UC-HDPE
(50 rpm, hold at 160 °C for 10 min, 5°C/min)
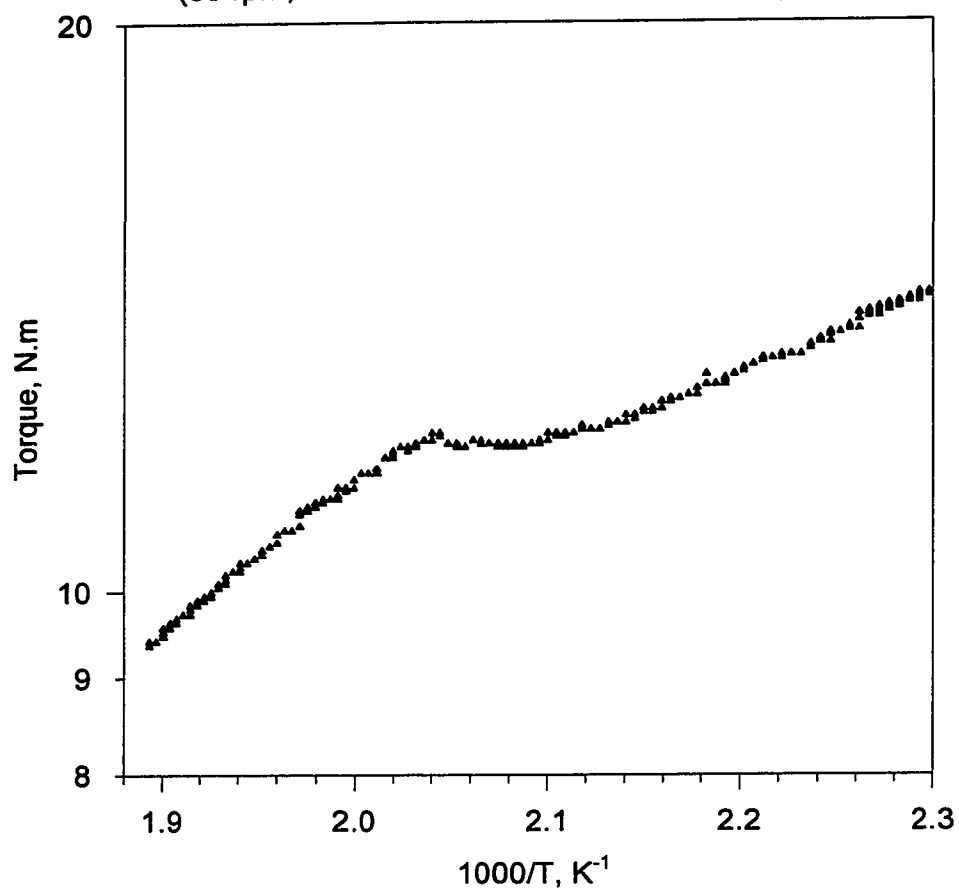
Figure A.19 Arrhenius torque-melt temperature curve for Phillips-HDPE

(50 rpm, hold at 160°C for 10 min, 5°C/min)
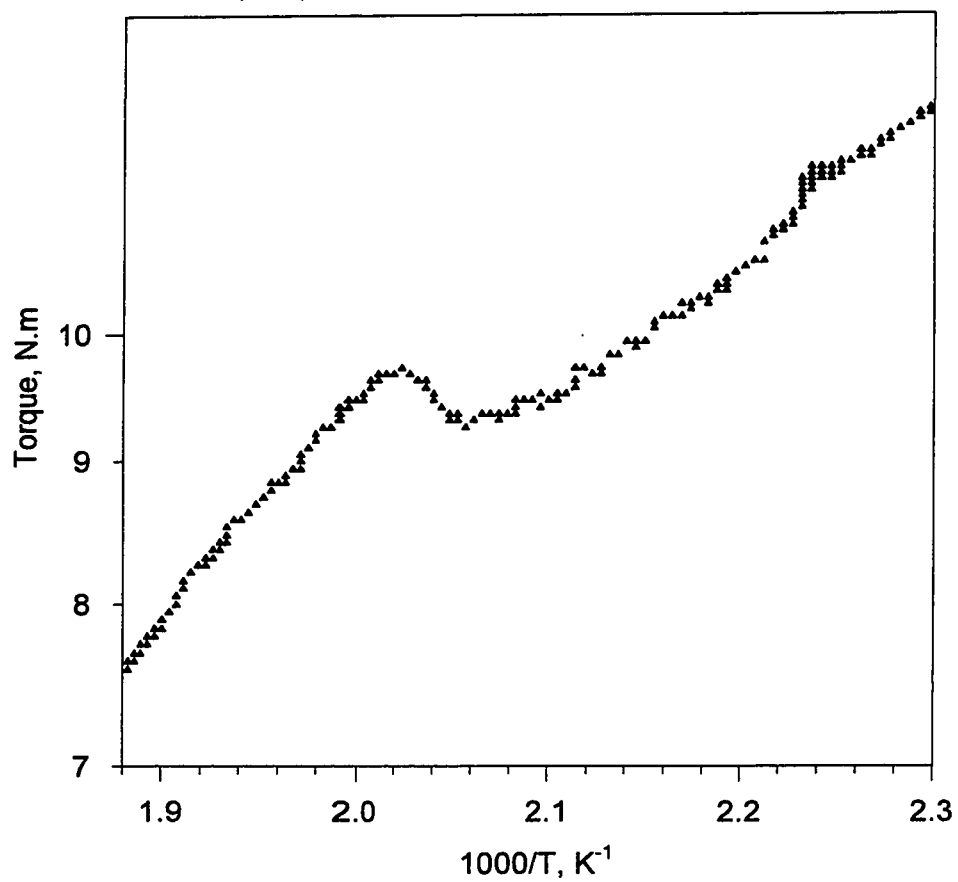
Figure A.20 Arrhenius Torque-melt temperature curve for Solvay-HDPE

(50 rpm, hold at 160°C for 3 min, 5°C/min)
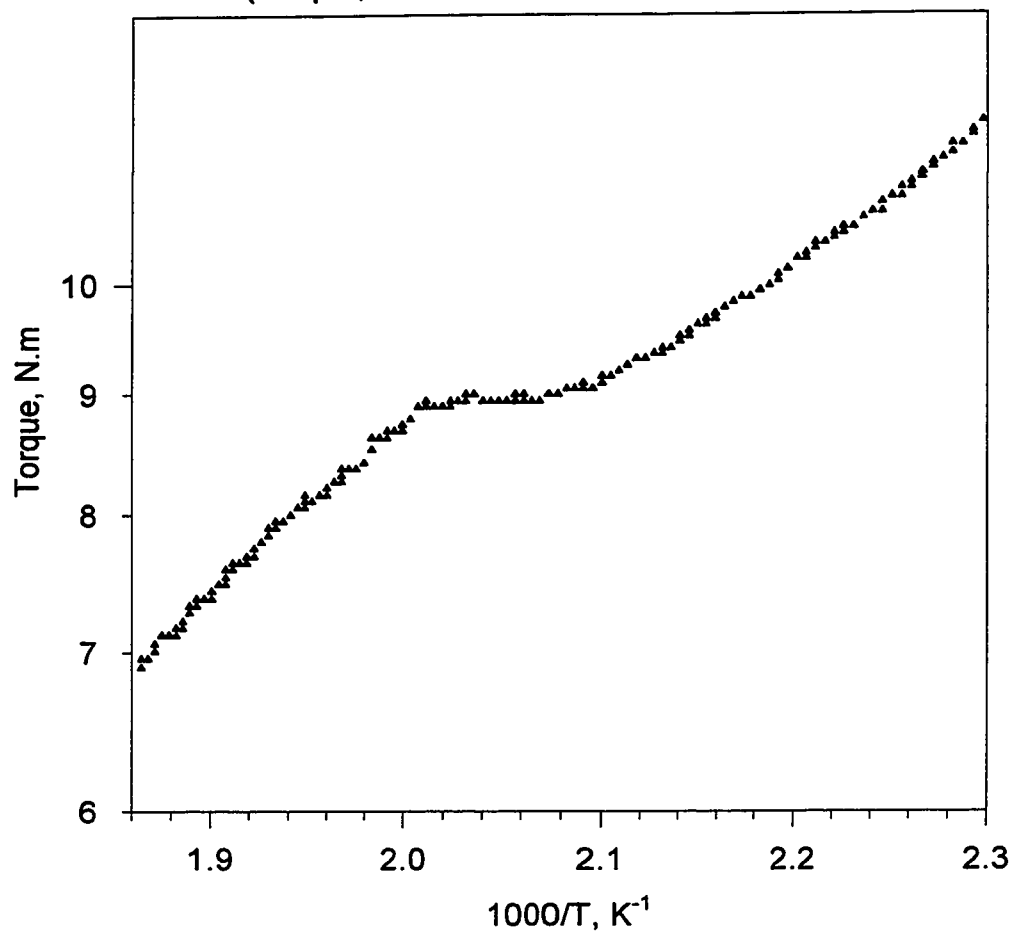
Figure A.21 Torque-Melt temperature curve for Solvay-HDPE at different rotor speeds

(hold at 160°C for 3 min, 5°C/min, with N_2)

100 rpm

50 rpm

20 rpm
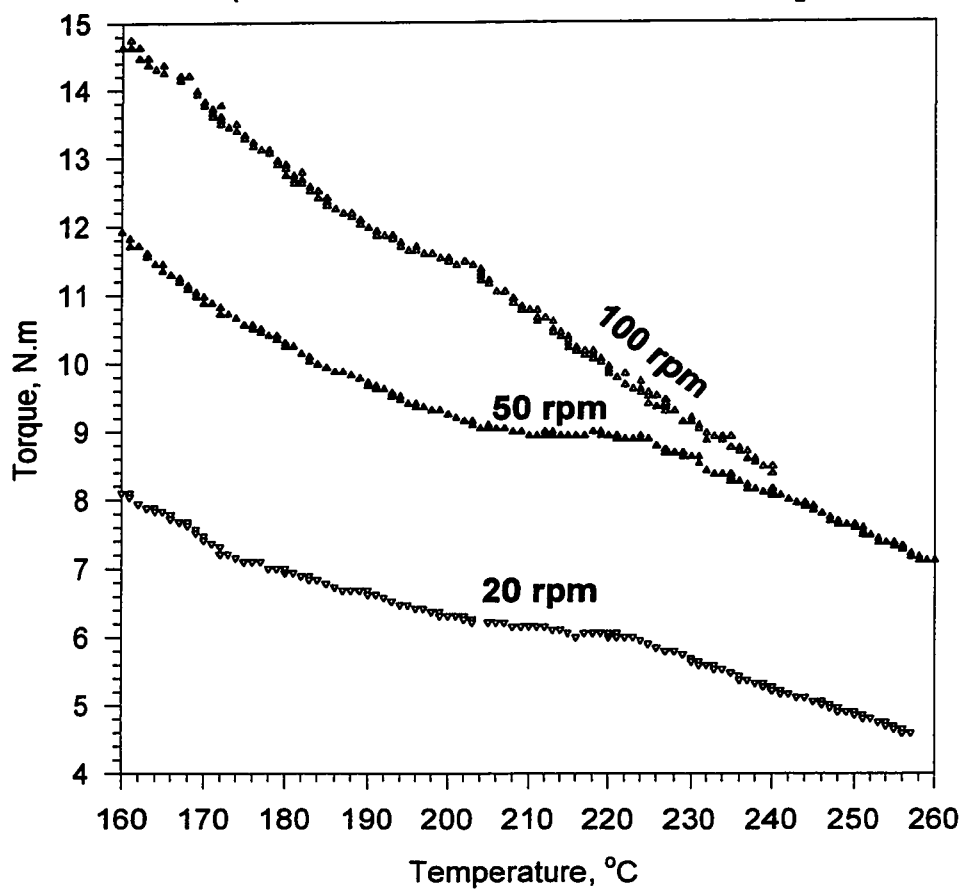
Figure A.22 Torque-Melt temperature curve for Phillips-HDPE with and w/o nitrogen
(hold at 135°C for 5 min, 50 rpm, 5°C/min)
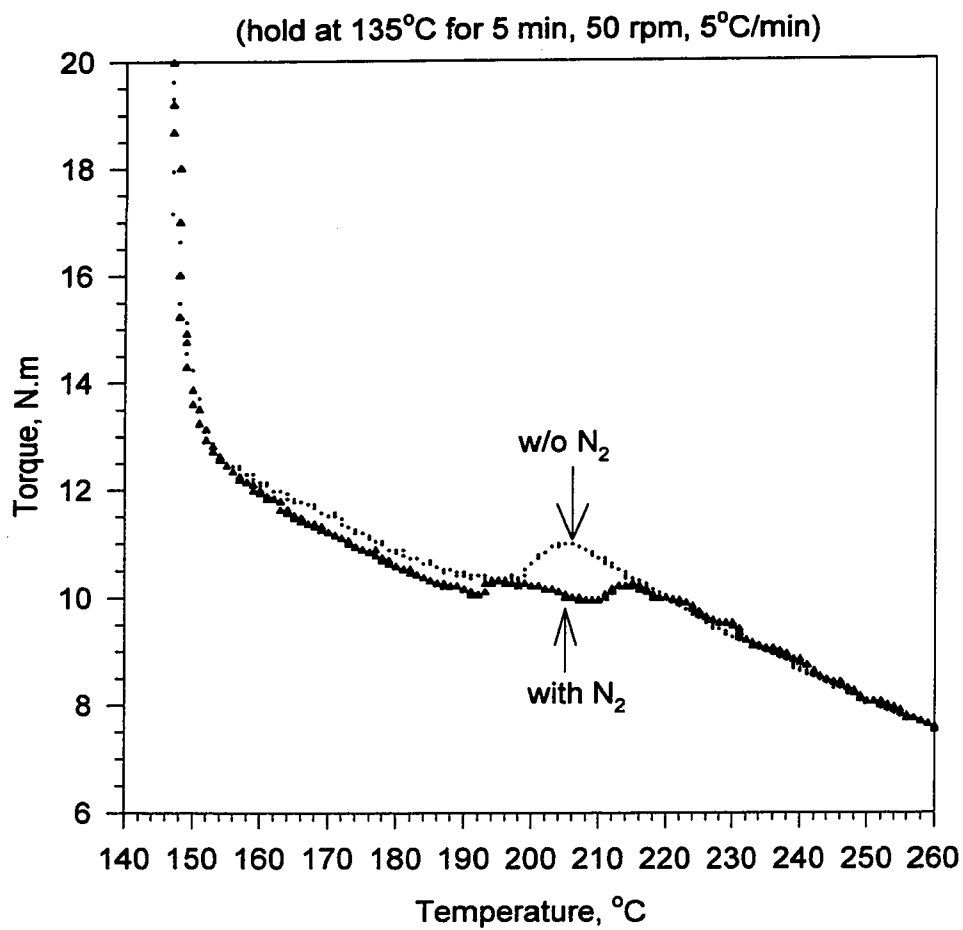
Figure A.23 Arrhenius plot of torque-T for Exxon(Met.)*

(30 rpm, hold at 160°C for 3 min., 3°C/min)

*with additional 6000 ppm of AO

$E=5.386$ kcal/mol ($r^2=0.9969$)
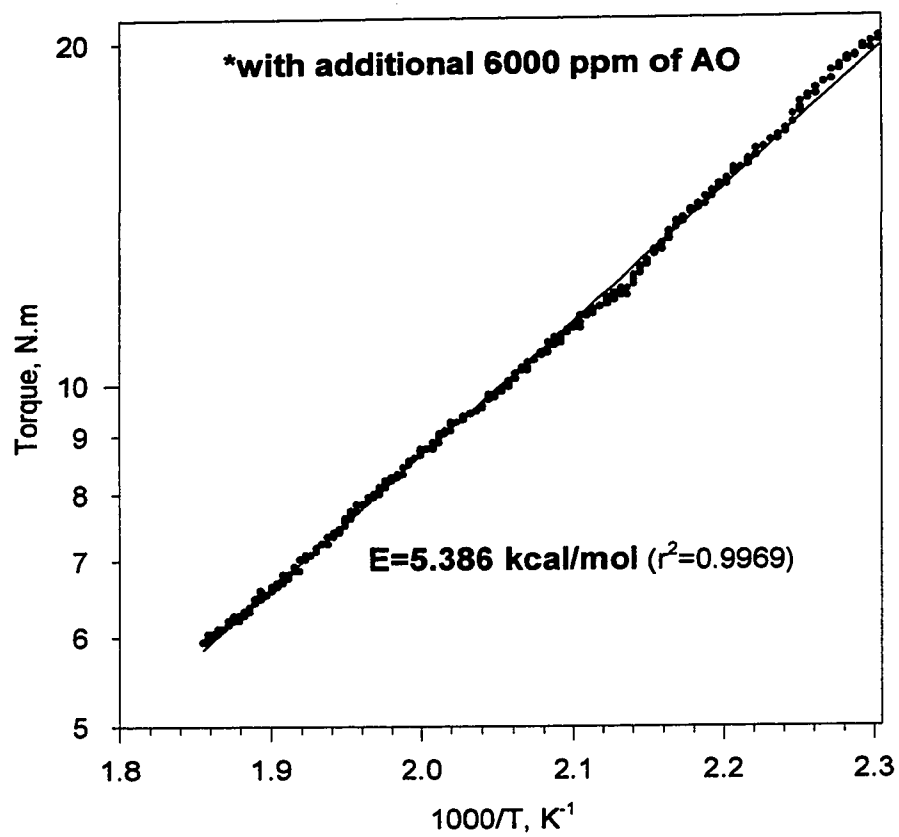
Figure A.24 Torque-T curve for Exxon (Met)*

(20 rpm, hold at 160°C for 3 min., 3°C/min.)

*with additional 6000 ppm of AO

Melt Temperature, °C
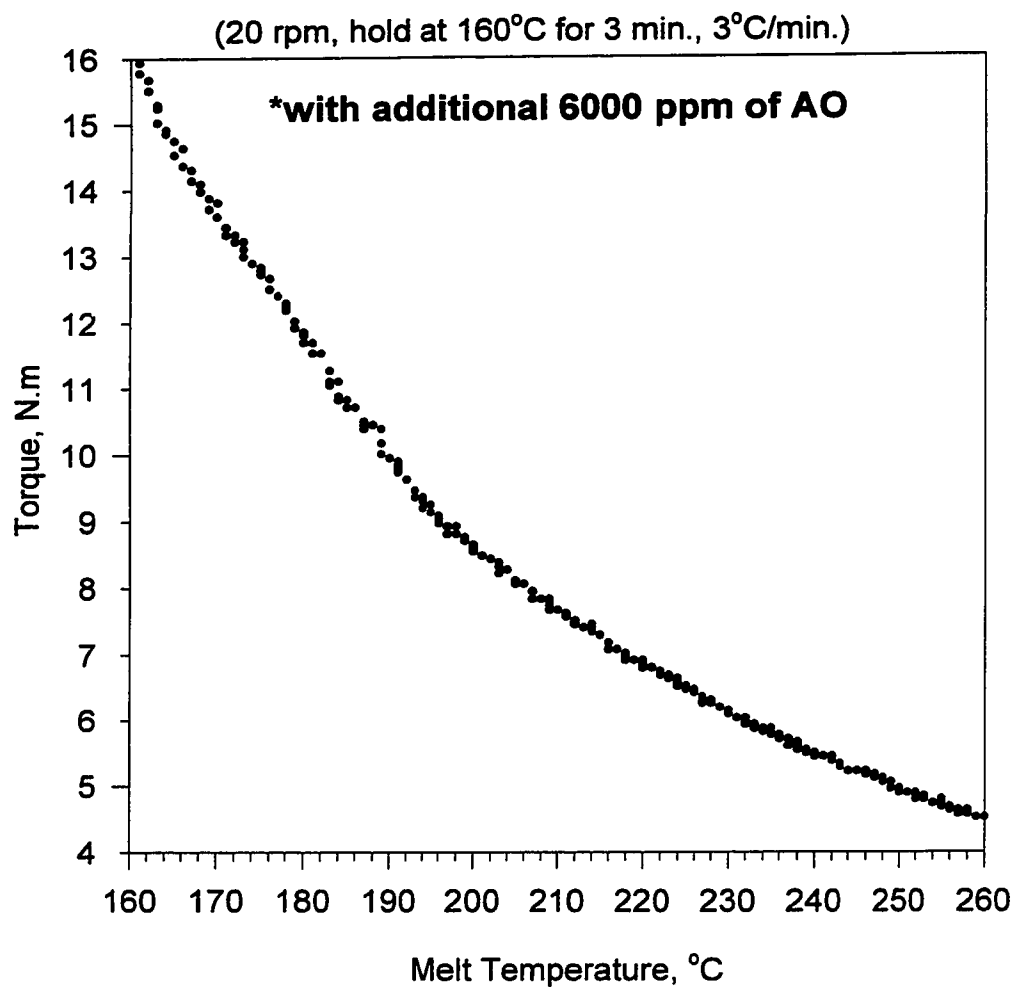
Figure A.25 Arrhenius plot of torque-T for Exxon(Met.)*

(20 rpm, hold at 160°C for 3 min., 3°C/min)

*with additional 6000 ppm of AO

E=5.778 kcal/mol (r^2=0.9977)

Torque, N.n

$1000/T$, K^{-1}
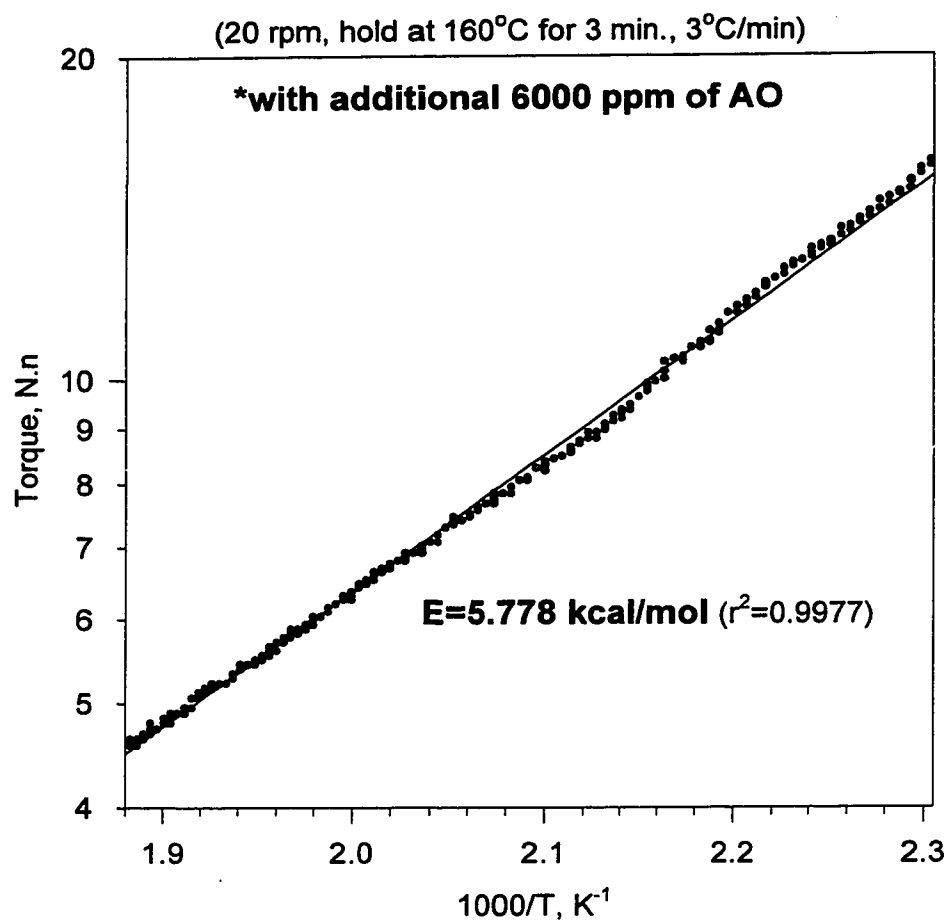
Figure A.26 Torque-T behavior of S216 (LDPE)
(hold at 160°C for 3 min., 20 rpm, 2°C/min.)

*with additional 6000 ppm of AO
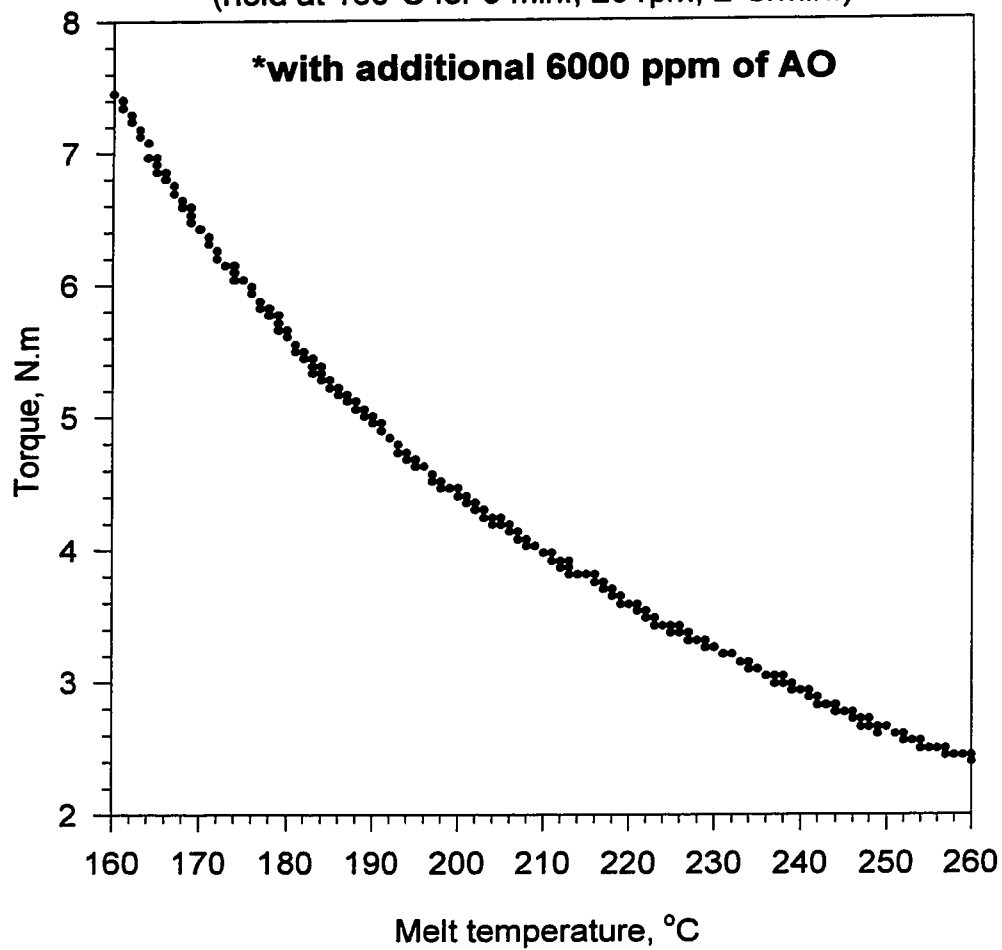
Figure A.27 Arrhenius torque-T plot for S216 (LDPE)

(hold at 160°C for 3 min., 20 rpm, 2°C/min.)

*with additional 6000 ppm of AO

$E=5.074$ kcal/mol ($r^2=0.9990$)
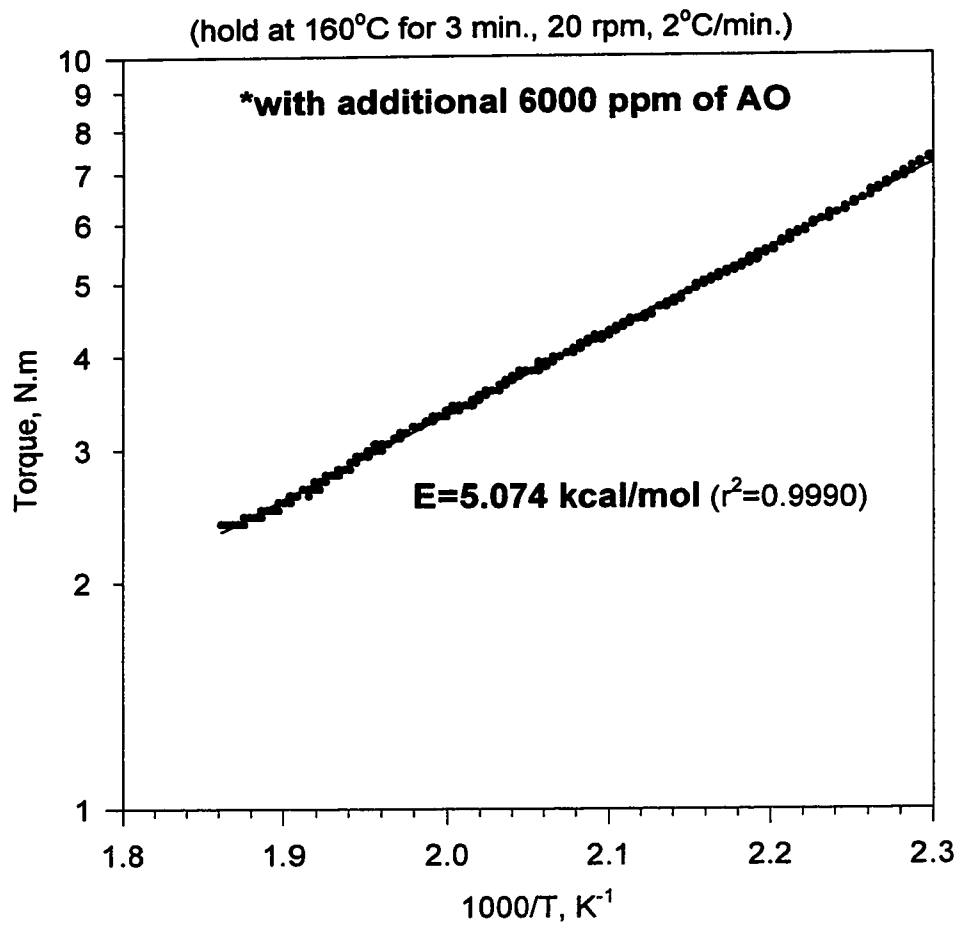
Figure A.28 Torque-T behavior of S225 (LLDPE)*

(hold at 160°C for 3 min., 30 rpm, 3°C/min)

*with additional 6000 ppm of AO
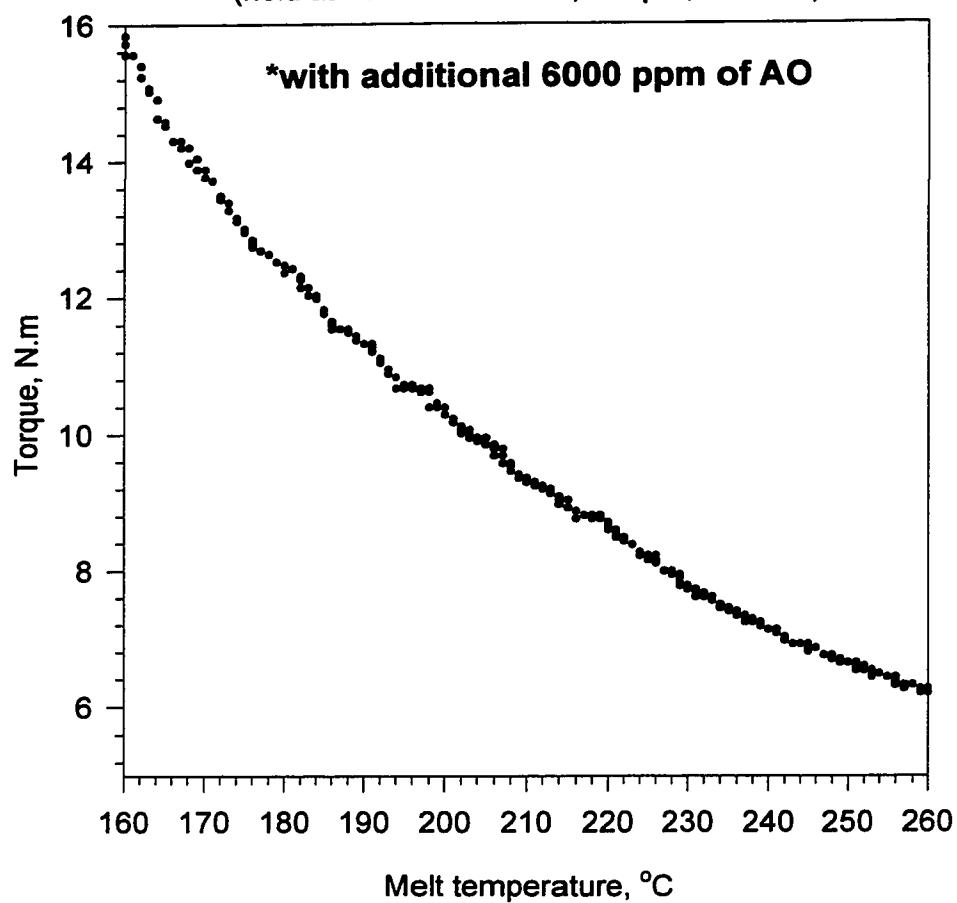
Figure A.29 Arrhenius torque-T behavior for S225 (LLDPE)

(hold at 160°C for 3 min., 30 rpm, 3°C/min.)

*with additional 6000 ppm of AO

$E=4.219$ kcal/mol ($r^2=0.9986$)

Torque, N.m

$1000/T_m$, K^{-1}
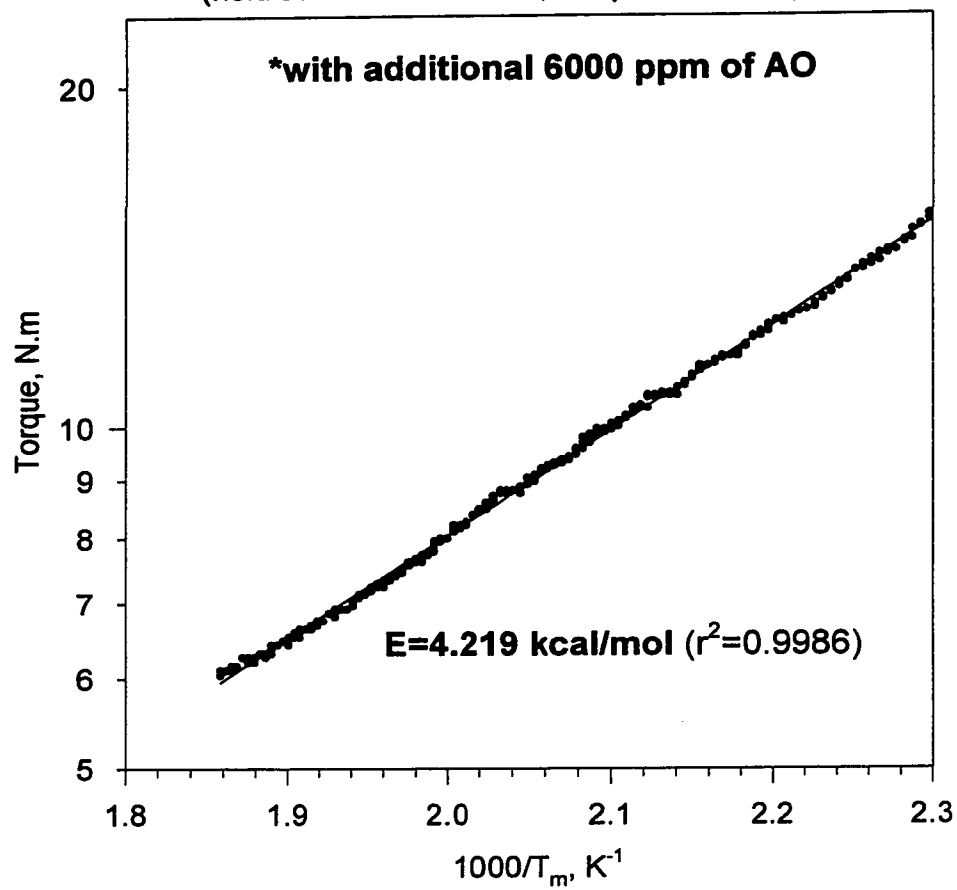
Figure A.30 Torque-T behavior of S229(LLDPE)*

(hold at 160°C for 3 min., 30 rpm, 3°C/min)

**with additional 6000 ppm of AO*
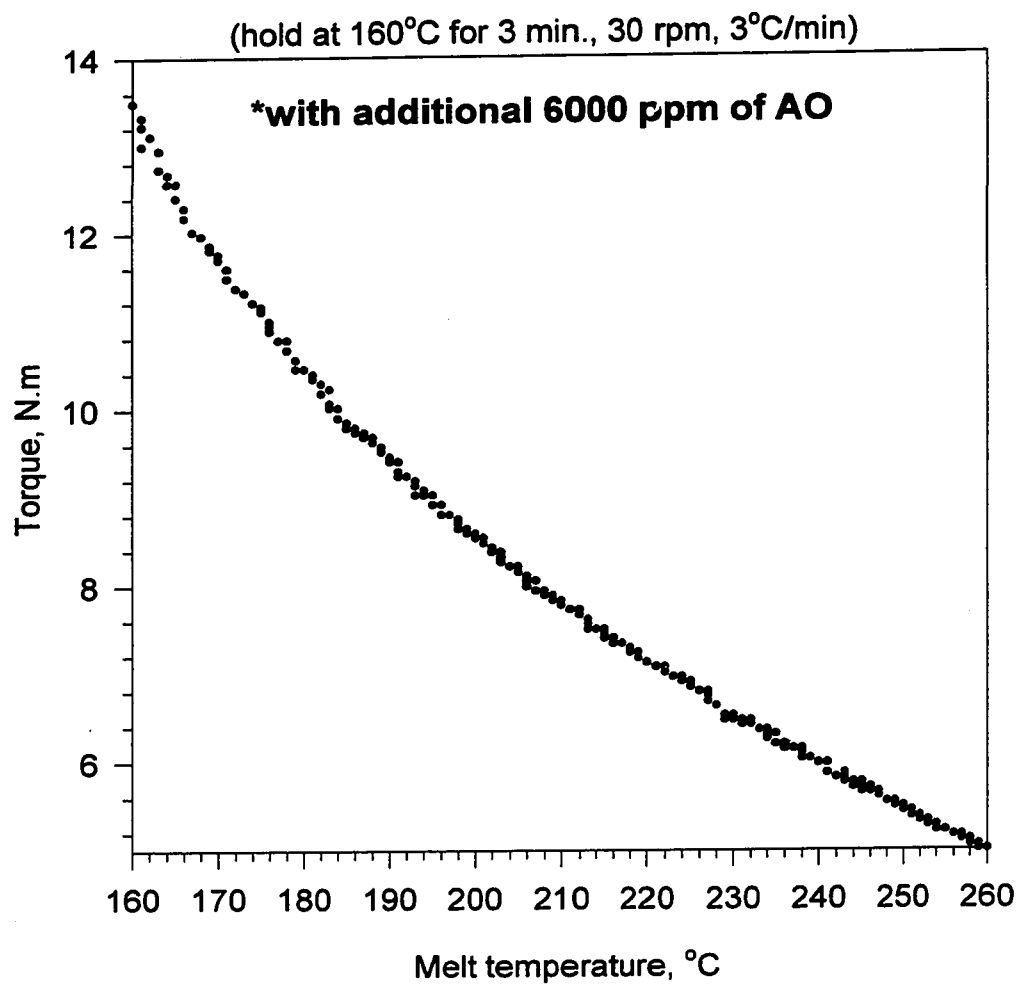
Figure A.31 Arrhenius torque-T plot for S229 (LLDPE)*

(hold at 160°C for 3 min., 30 rpm, 3°C/min.)

*with additional 6000 ppm of AO

$E=4.411$ kcal/mol ($r^2=0.9987$)
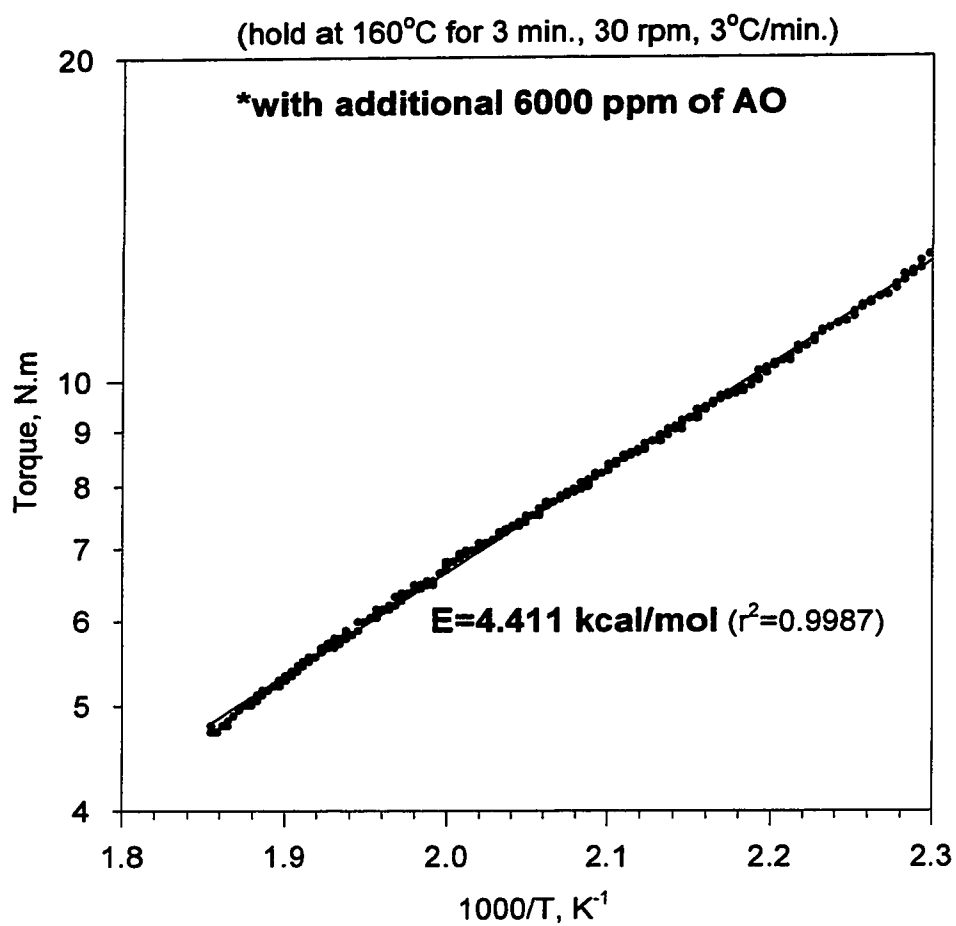
Figure A.32 Arrhenius plot of M.I.- T for PEs
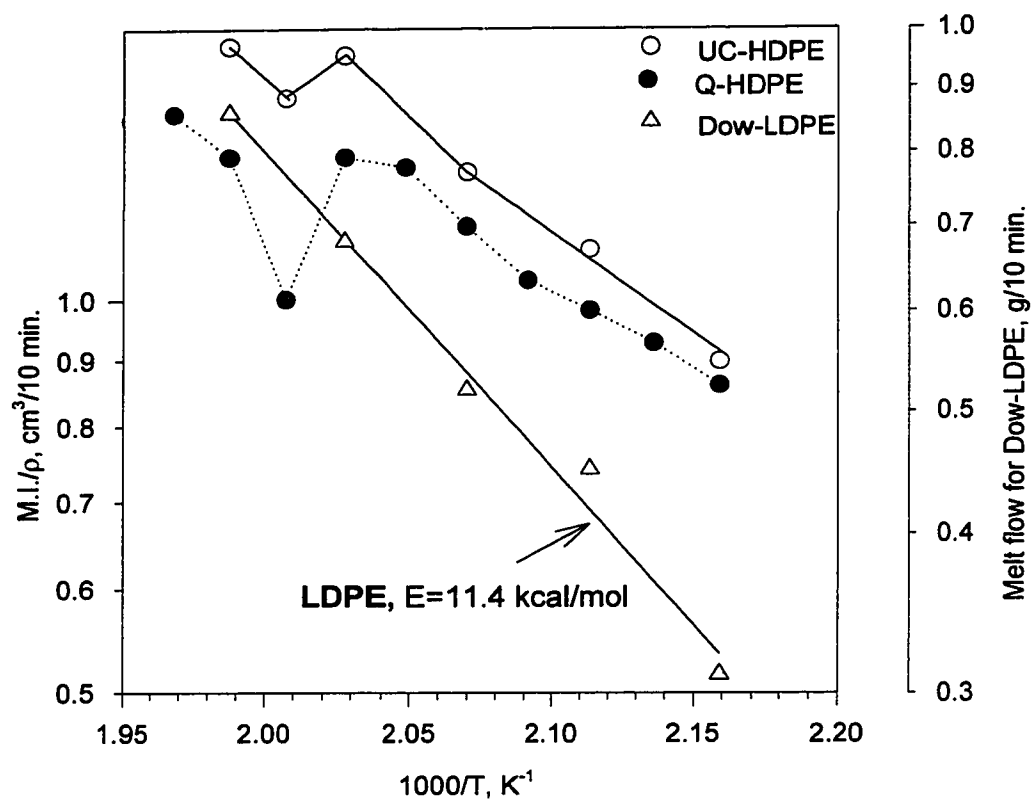
Figure A.33 Torque-T plot for Dow(LDPE)*

(hold at 160°C for 3 min., 50 rpm, ramp to 260°C at 5°C/min)

* highly stabilized
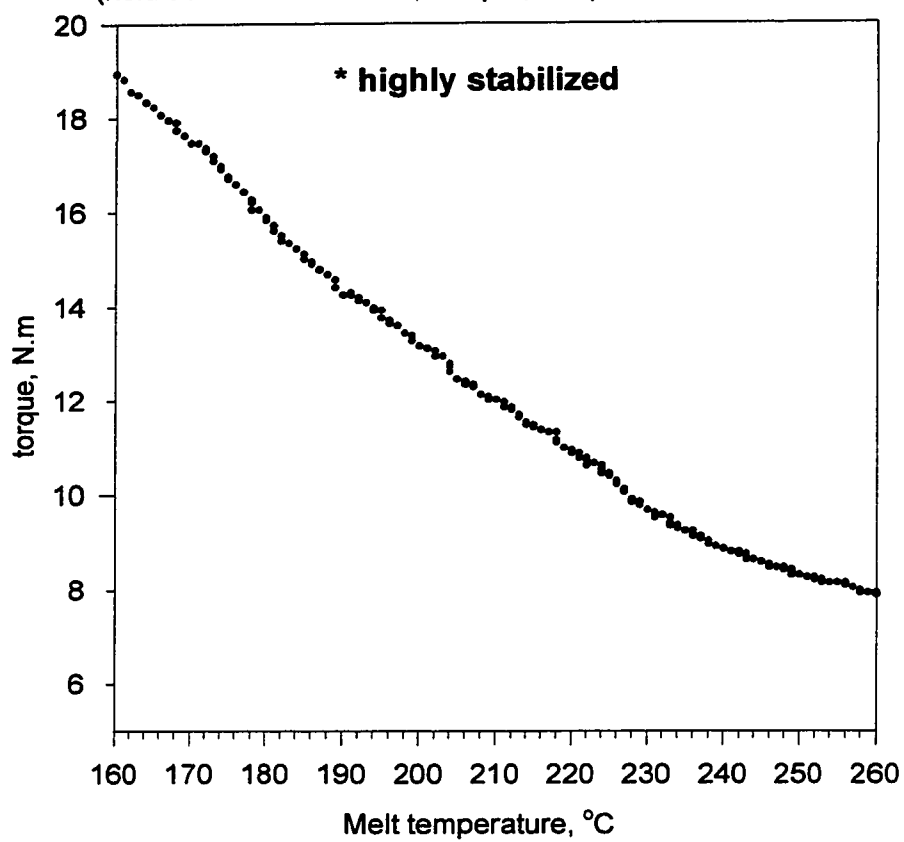
Figure A.34 Arrhenius torque-T plot for Dow(LDPE)*

(hold at 160°C for 3 min., 50 rpm, 5°C/min)
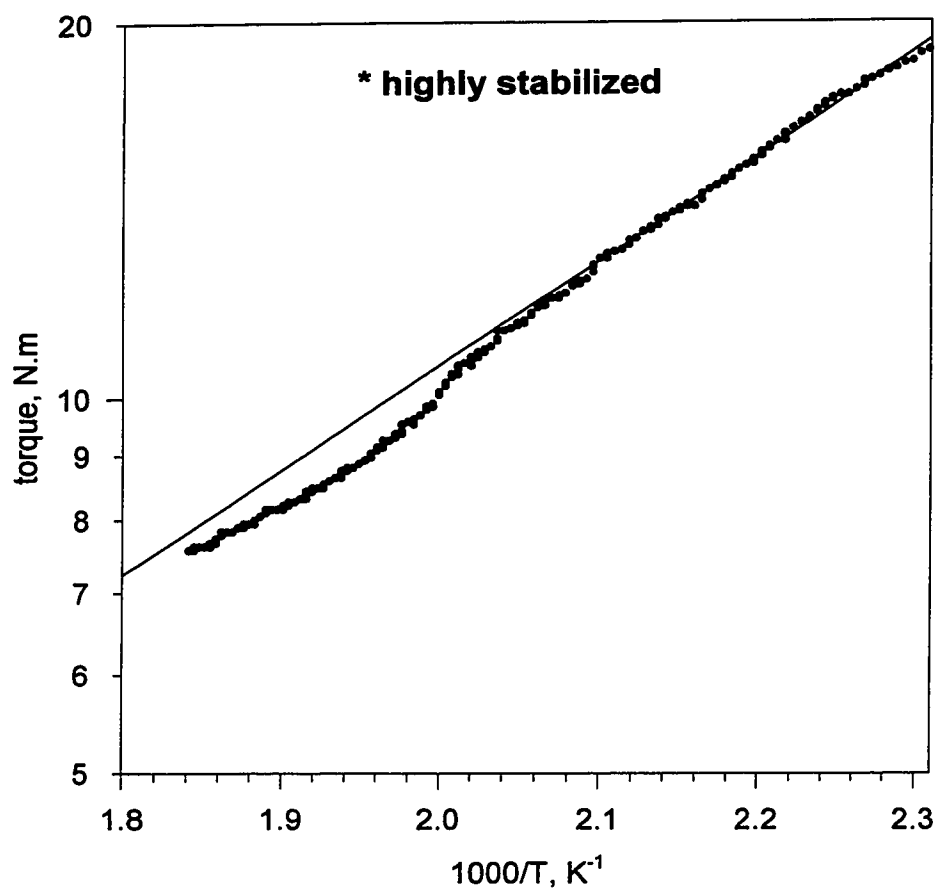
Figure A.35 Density calibration for mineral oil
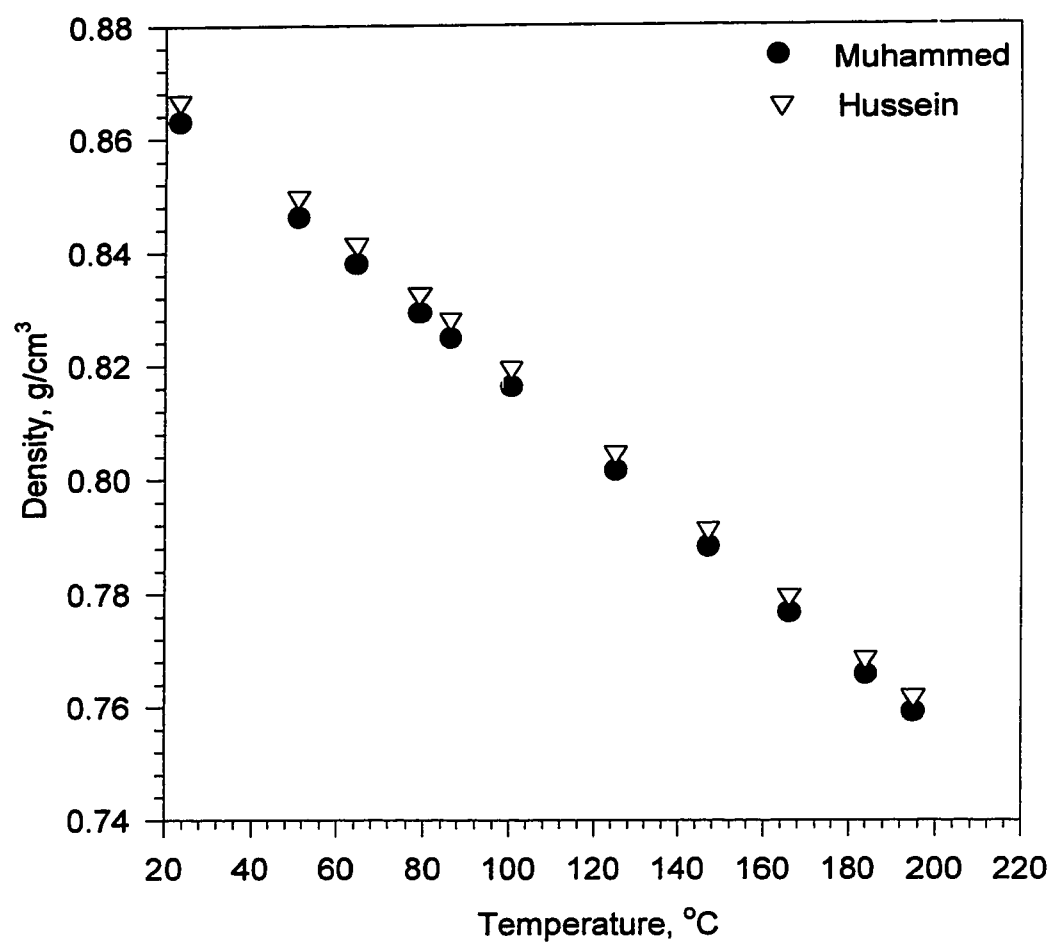
Figure A.36 Density calibration for silicone oil

The plot shows Density (g/cm^3) on the vertical axis (ranging from 0.78 to 0.98) versus Temperature ($°C$) on the horizontal axis (ranging from 20 to 240), with the fitted relationship:

$$\rho = 0.9811 - 8.34 \times 10^{-4}\, T \quad (r^2 = 0.997)$$
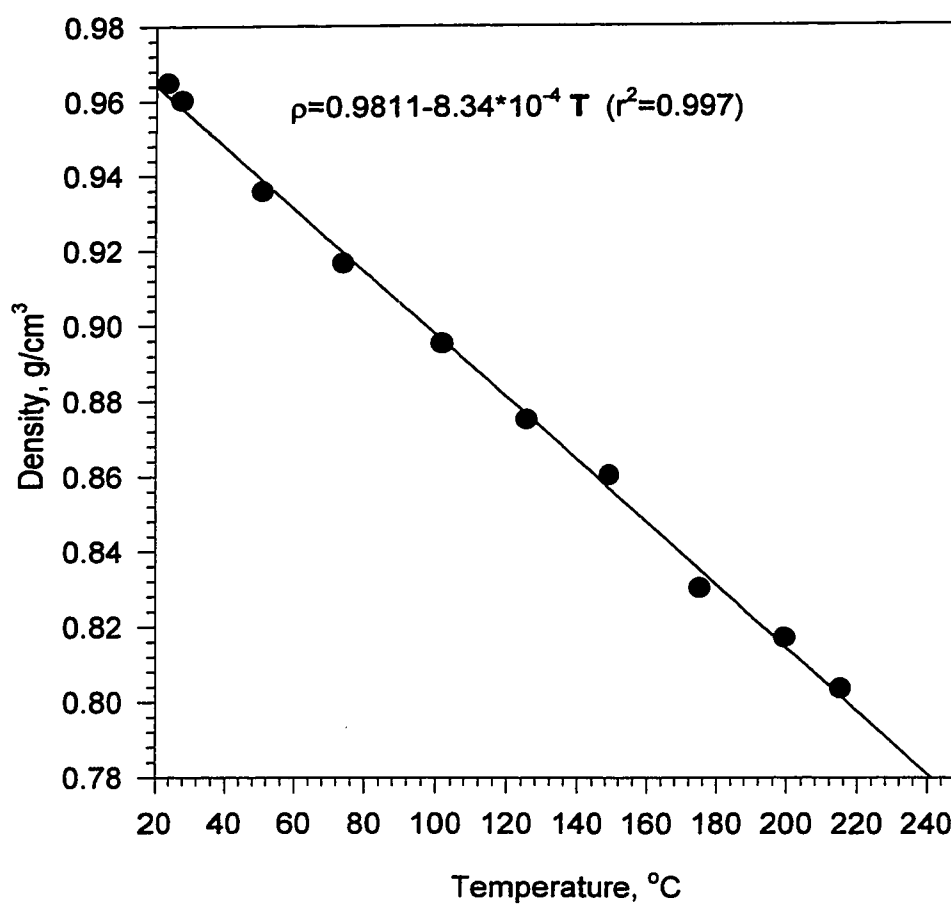
Figure A.37 ρ(T) for Q-HDPE in different oils
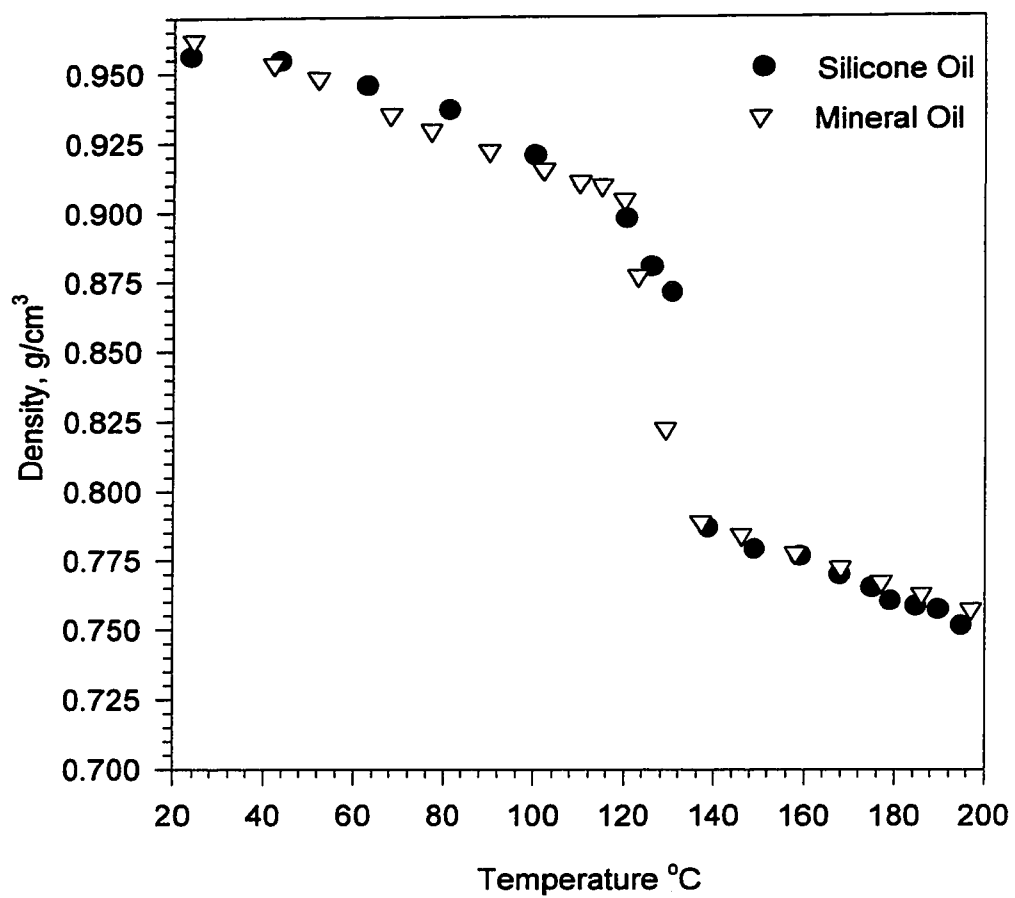
Figure A.38 ρ(T) for Q-HDPE
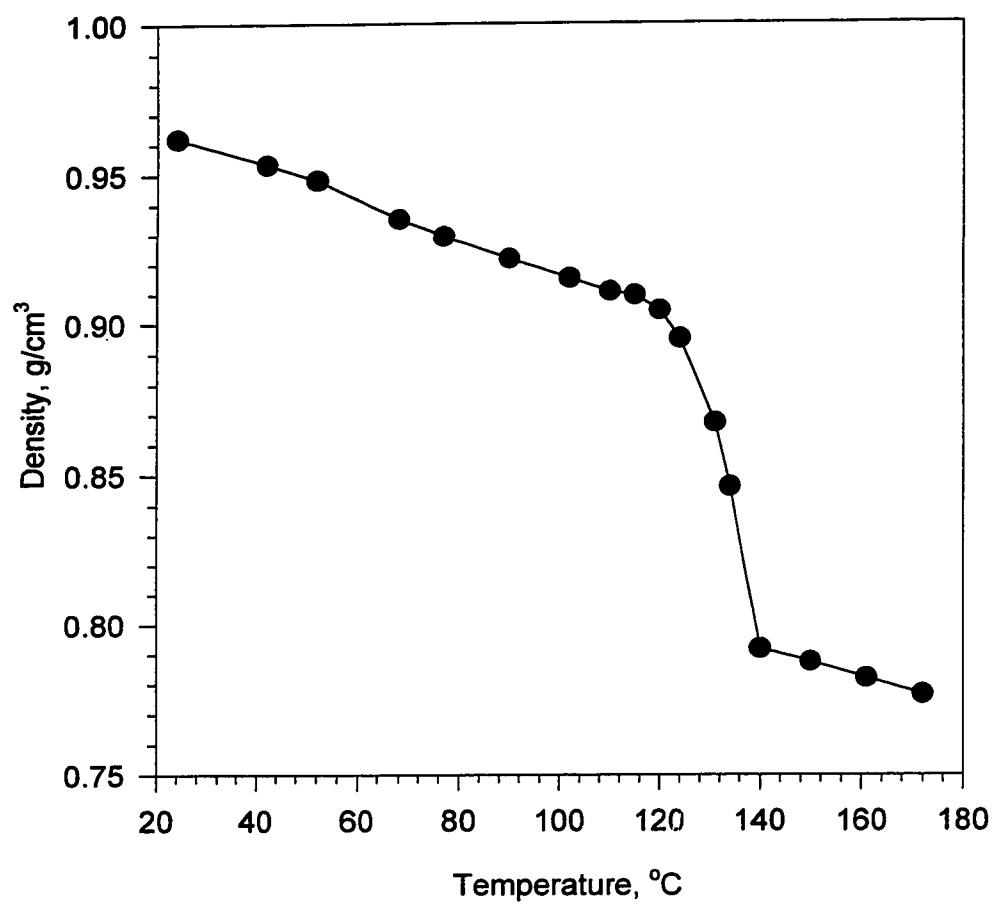
Figure A.39 DSC plot for Exxon (HDPE)
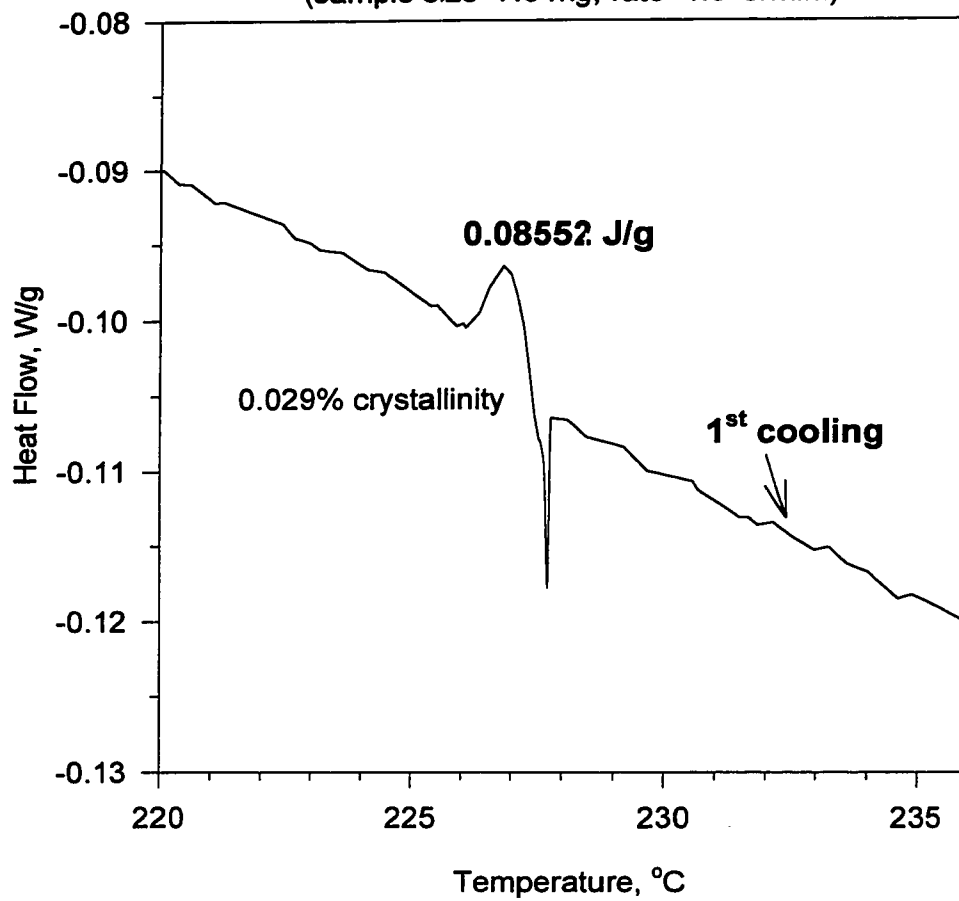
Figure A.40 DSC plot for Exxon (HDPE)
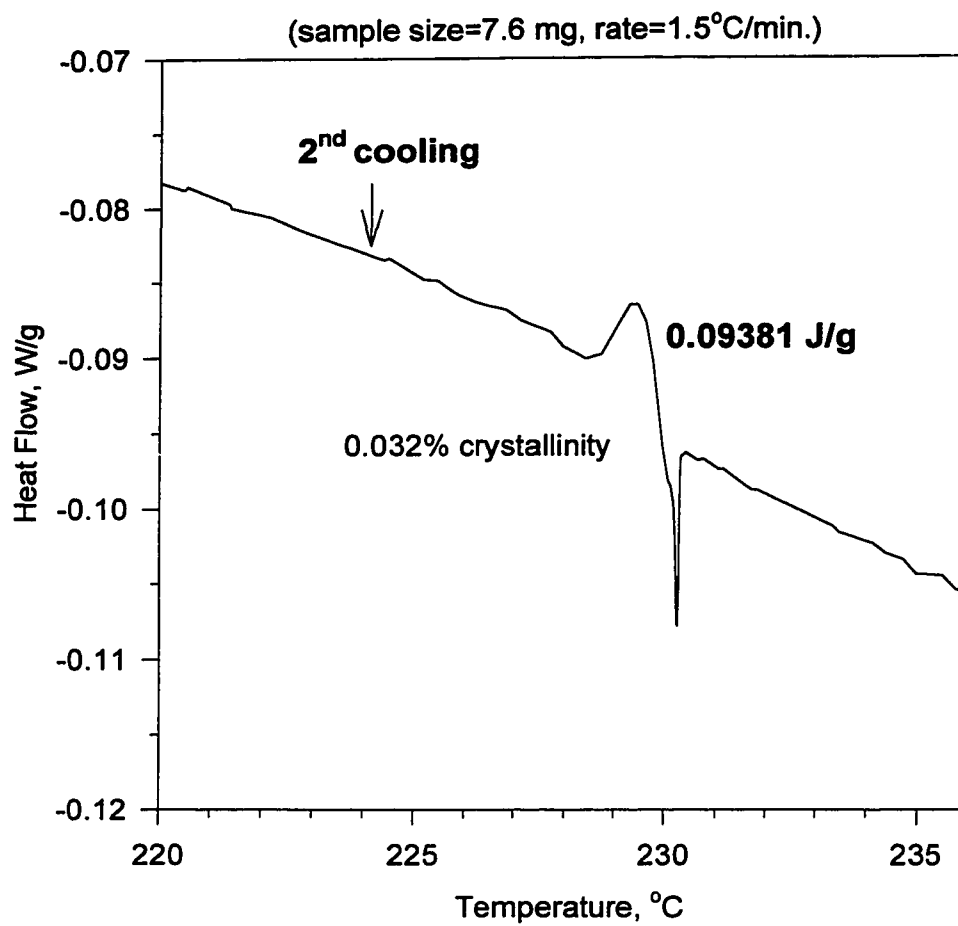
Figure A.41 DSC plot for Q-HDPE

(sample size 9.5 mg, rate=2°C/min)
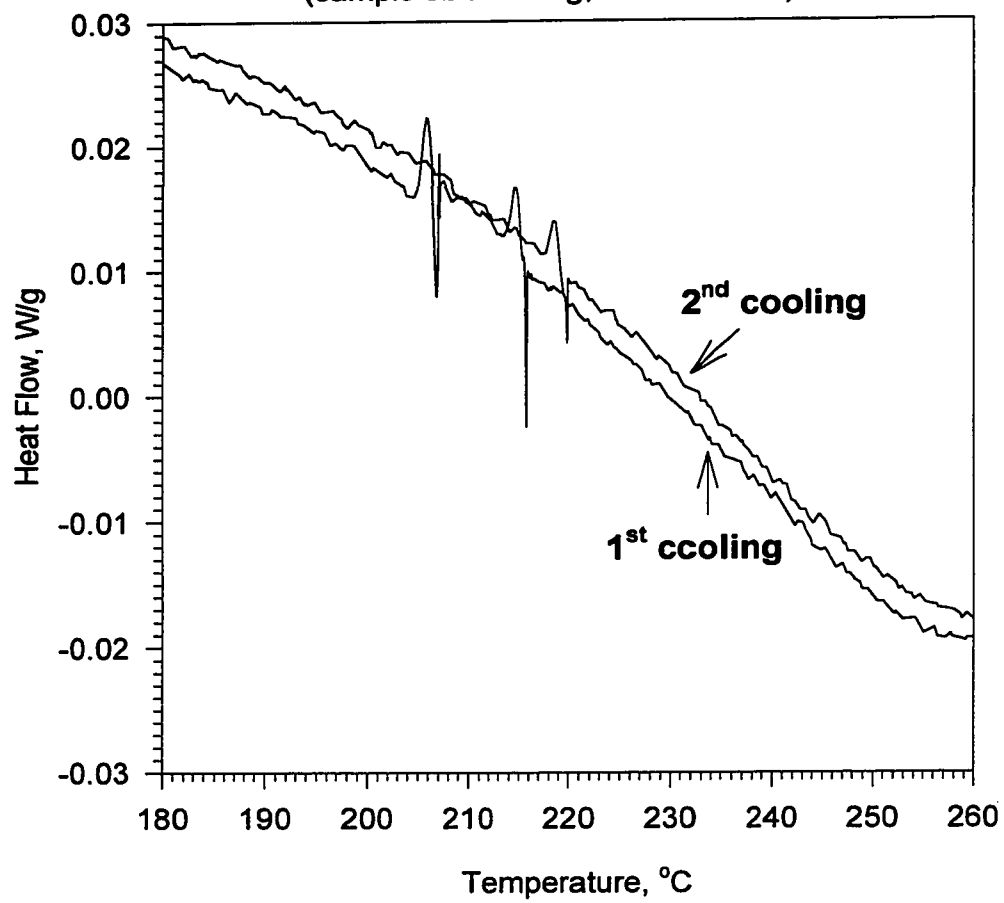
Figure A.42 DSC plot for Q-HDPE (1st cooling cycle)

(sample size=9.5 mg, rate=2°C/min.)
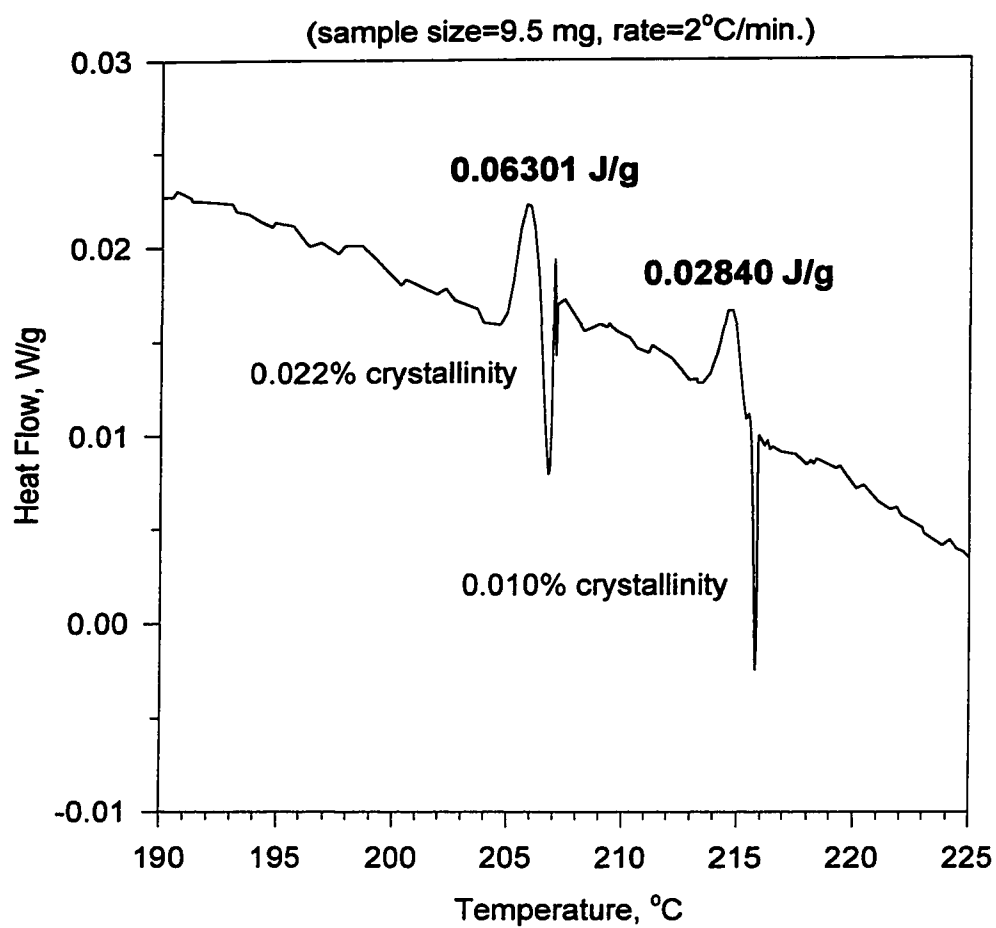
Figure A.43 DSC plot for Q-HDPE (2nd cooling)
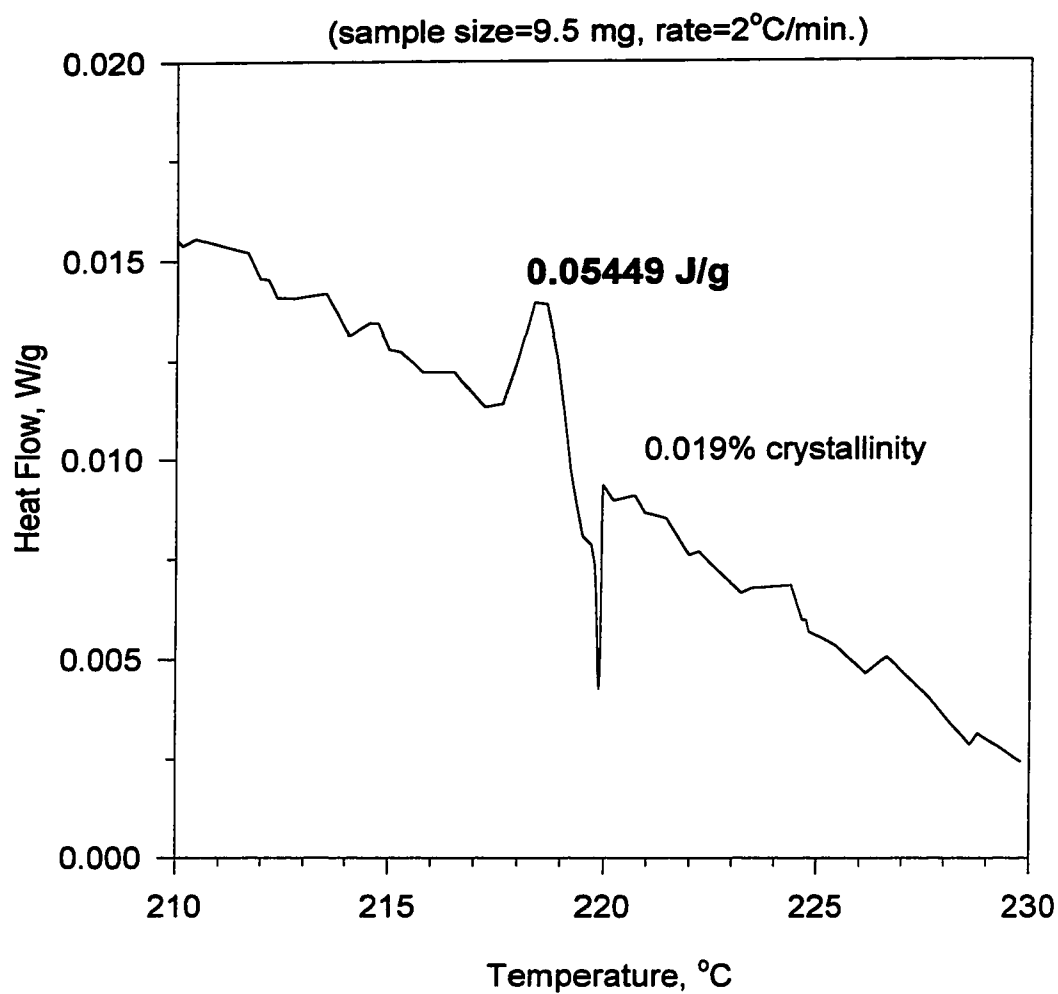
Figure A.44 DSC plot for Dow (LLDPE-A)

(sample size=9.6 mg, rate=2°C/min.)

0.07989 J/g

0.028% crystallinity

1st cooling

Heat Flow, W/g

Temperature, °C
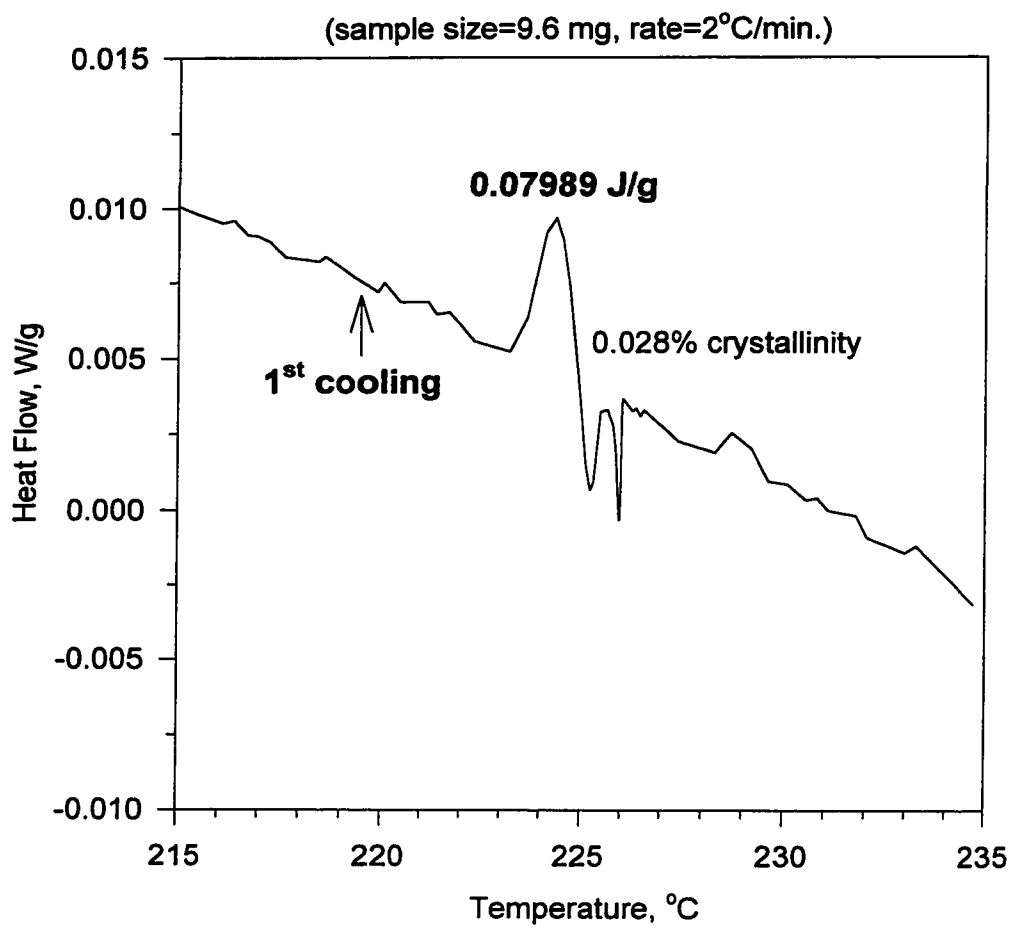
Figure A.45 DSC plot for Dow (LLDPE-A)

(sample size=9.6 mg, rate=2°C/min.)

322
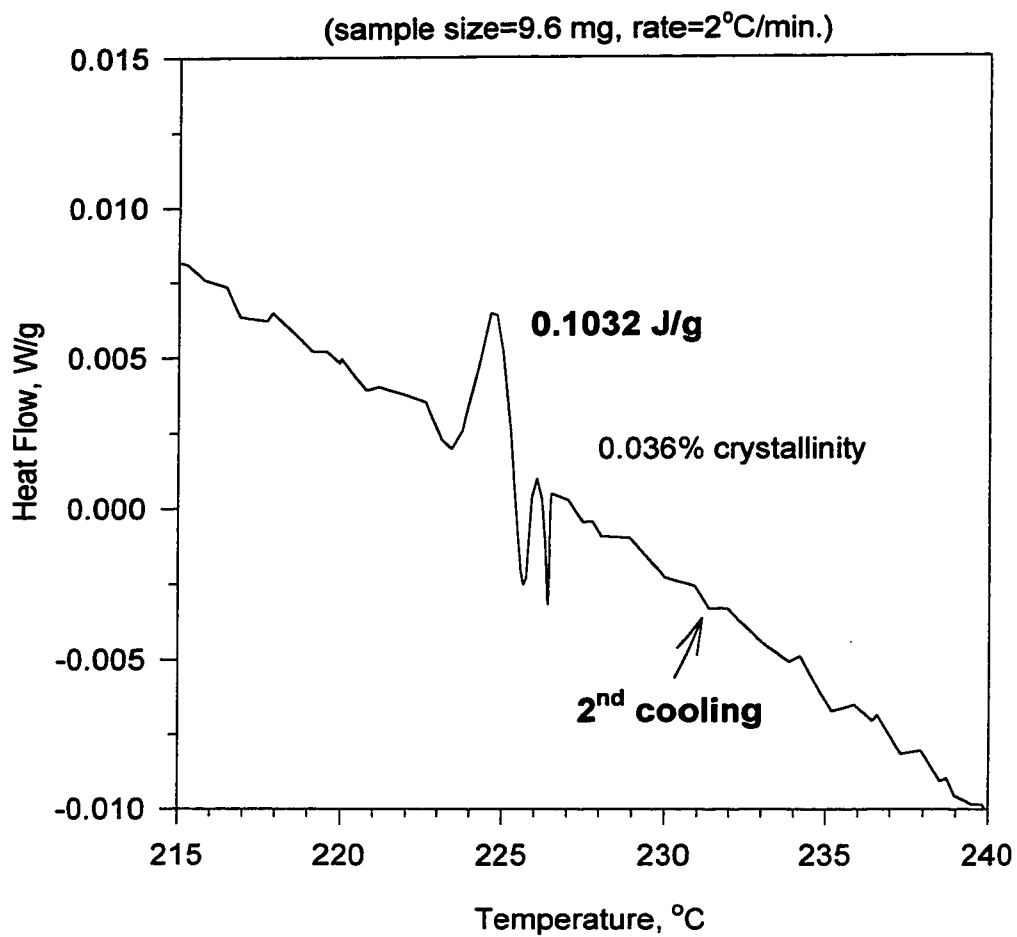
Figure A.46 DSC plot for Dow (LDPE)
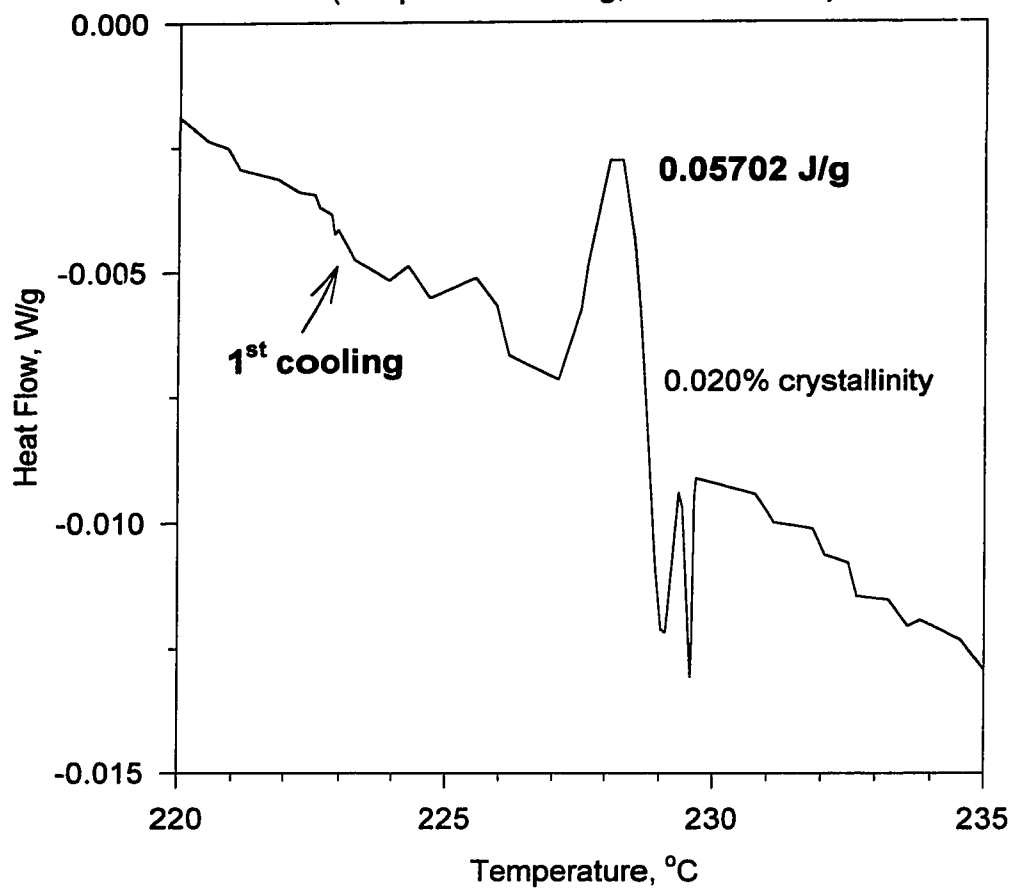
Figure A.47 DSC plot for Dow (LDPE)

(sample size=8.7 mg, rate=2°C/min.)

0.1097 J/g

0.038% crystallinity

2nd cooling
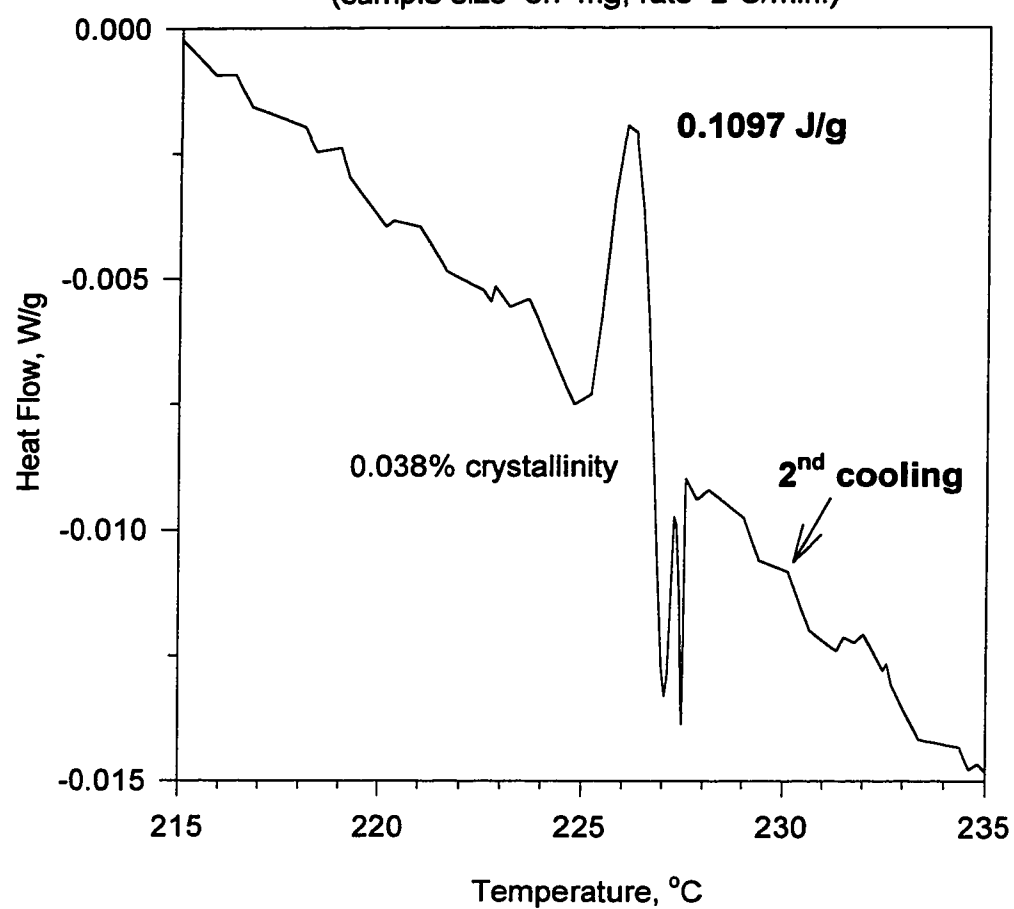
Figure A.48 DSC plot for S216 (LDPE)

(sample size=7 mg, rate=2°C/min.)

1st cooling

0.00899 J/g

0.003% crystallinity
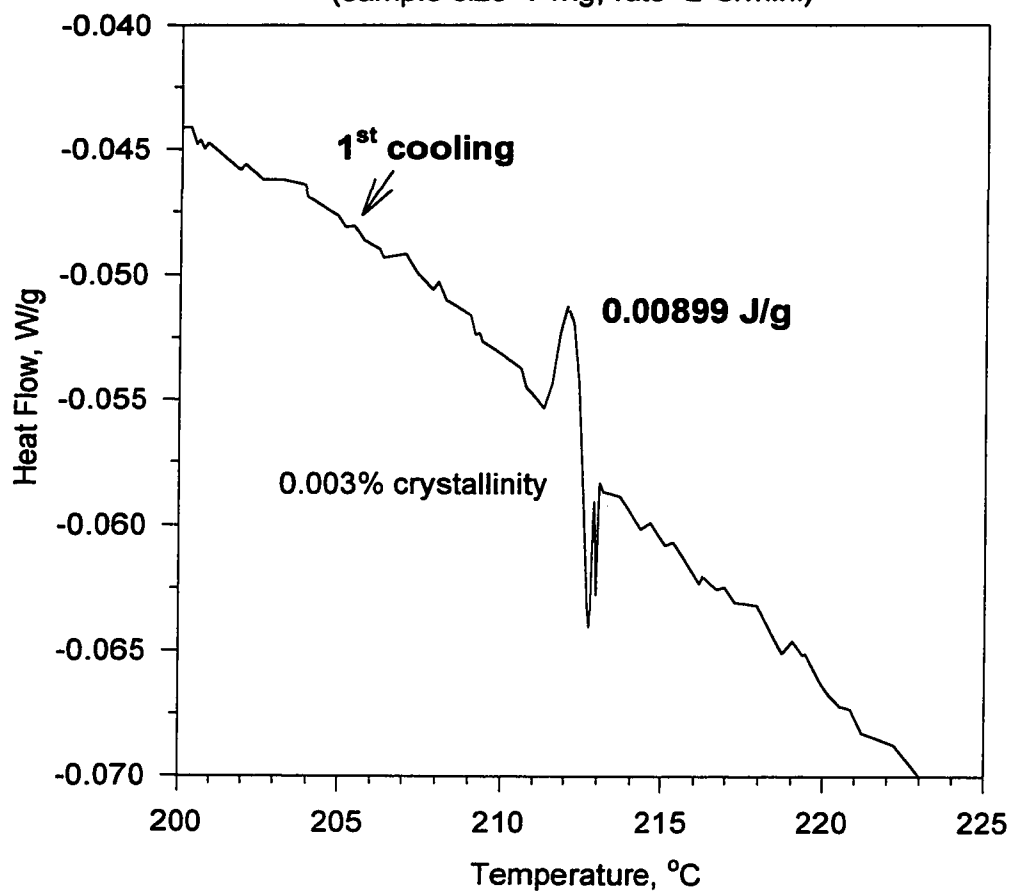
Figure A.49 DSC plot for S216 (LDPE)

(sample size=7 mg, rate=2°C/min.)
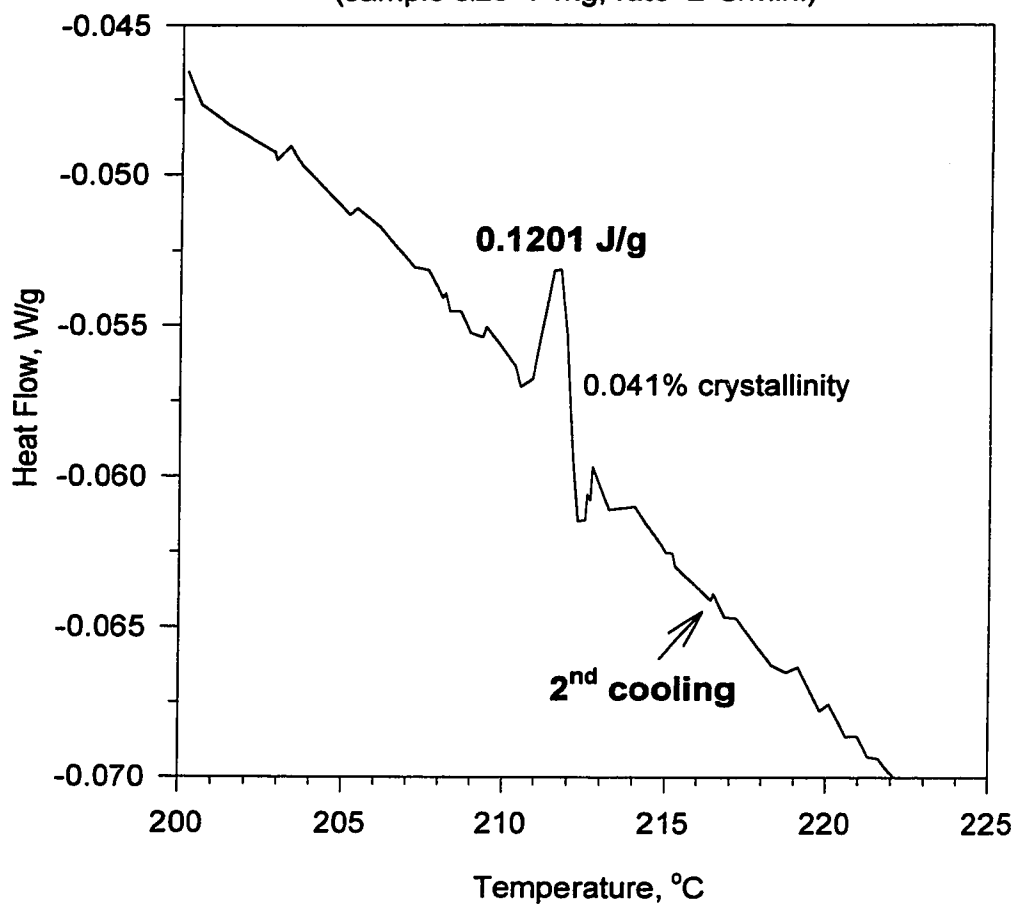
Appendix B

Supplement to Chapter V

Figure B.1 Strain sweep results for S214 (w/o ppa)

(Check for reproducibility)

(PP, ω=1 rad/s, T=190 $^\circ$C)
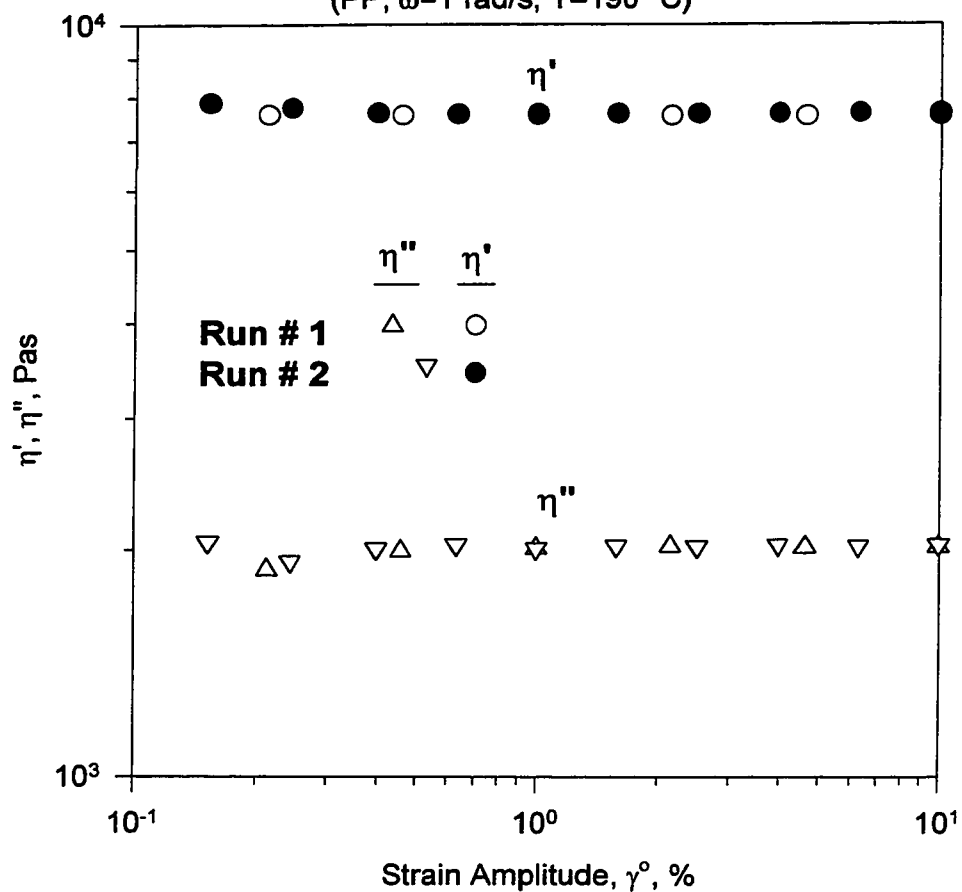
Figure B.2 Steady shear measurements for S214 (w/o ppa) (Check for reproducibility)

$(PP, T=190^{\circ}C, tbm=3 min., mt=30 sec)$
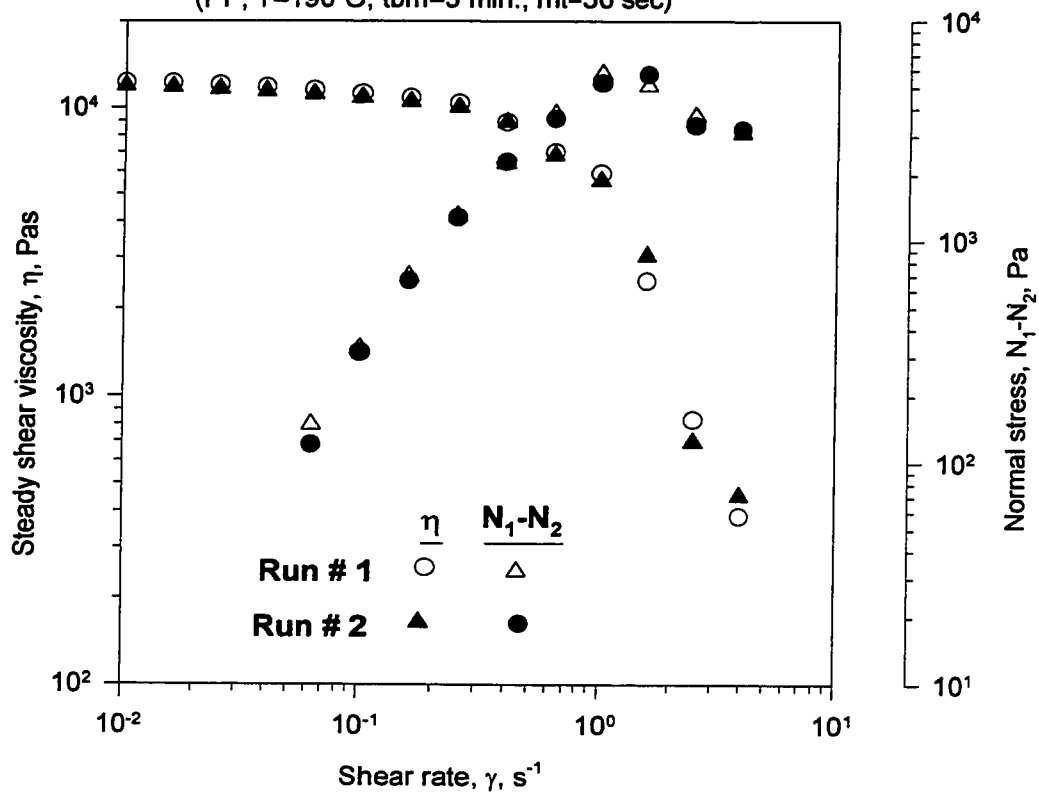
Figure B.3 γ^o-sweep measurements for S213 and S214

(PP, T=190°C, ω=1 rad/s)

Figure B.4 ω-sweep measurements for S213 and S214

(PP, T=190°C, γ°=1%)
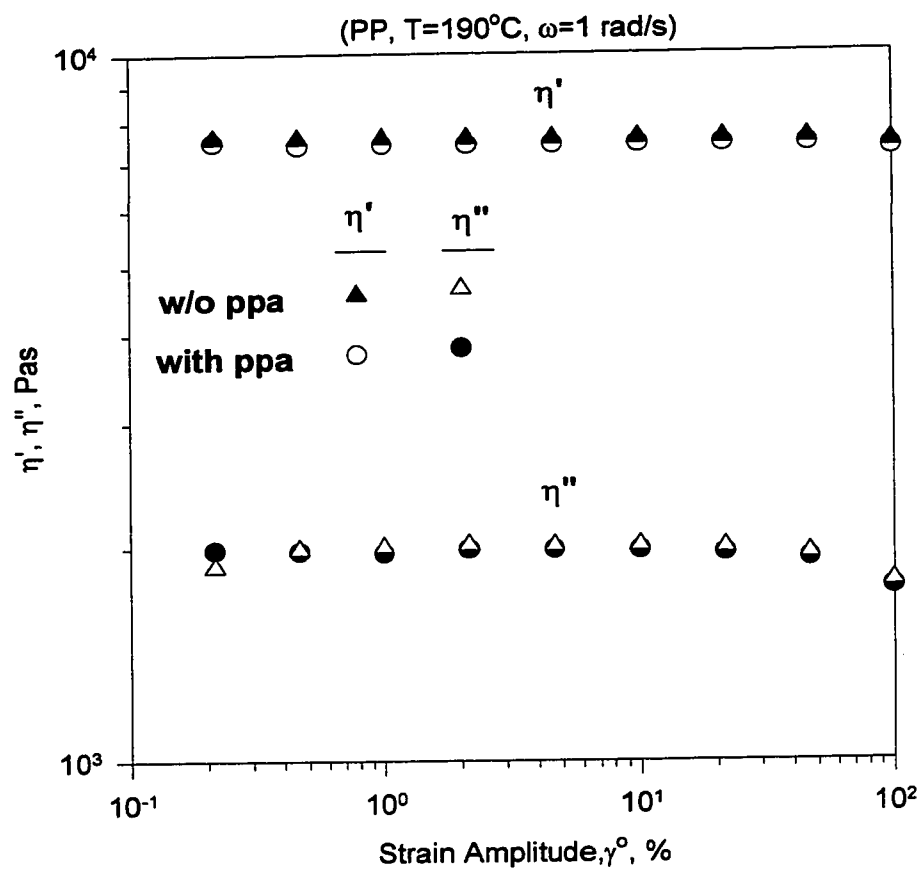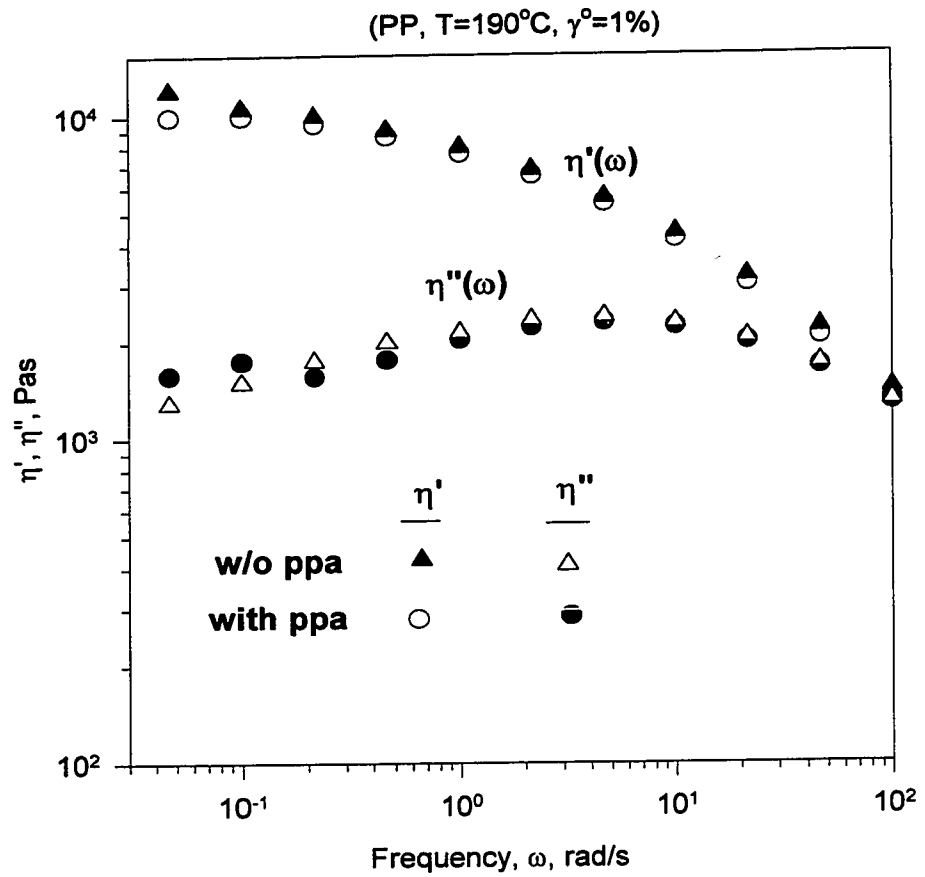
Figure B.5 Steady Shear measurements for S213 and S214
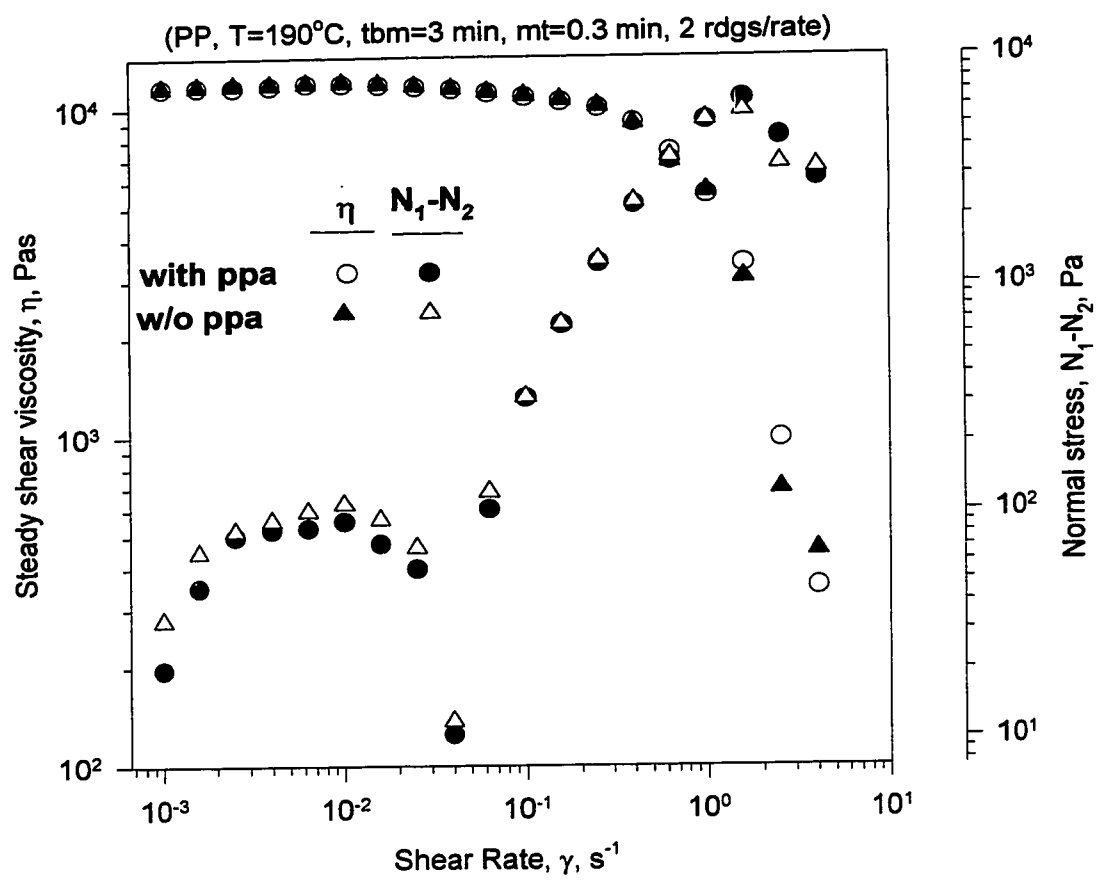
(PP, T=190°C, tbm=3 min, mt=0.3 min, 2 rdgs/rate)

Figure B.6 γ^o-sweep for S213 and S214

(PP, ω=0.1 rad/s, T=230°C)

Figure B.7 ω-sweep measurements for S213 and S214

(PP, T=230°C, γ^o=1%)
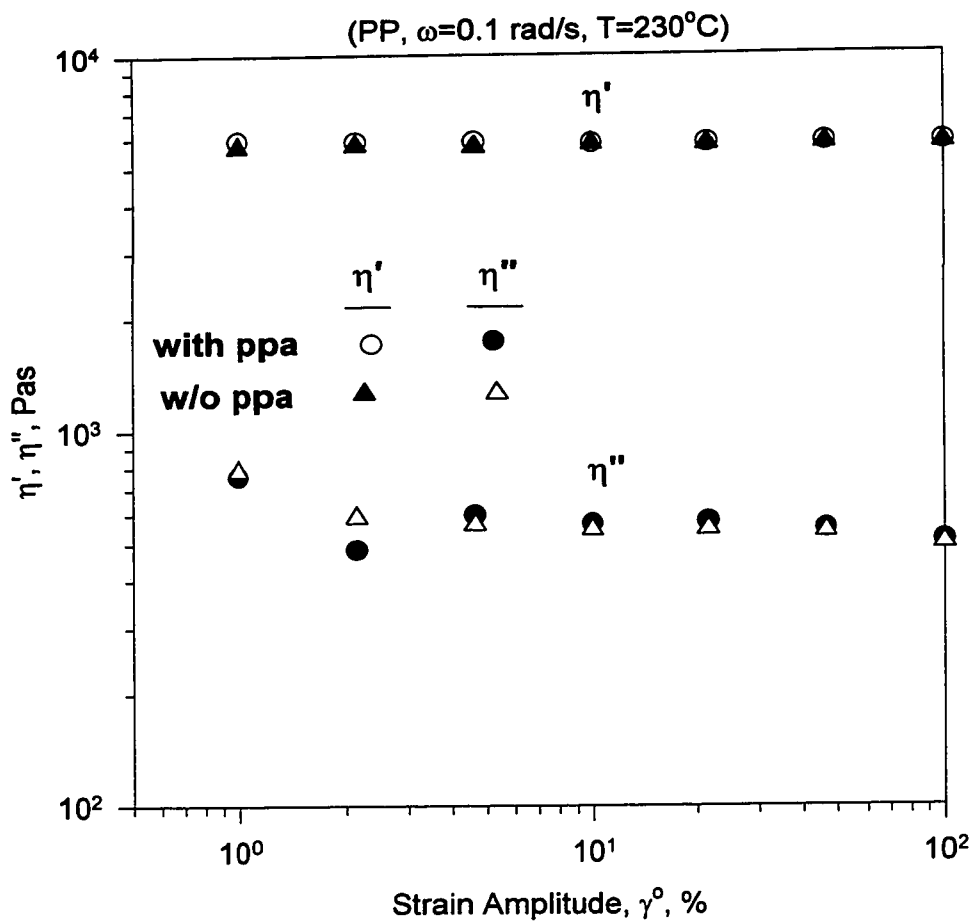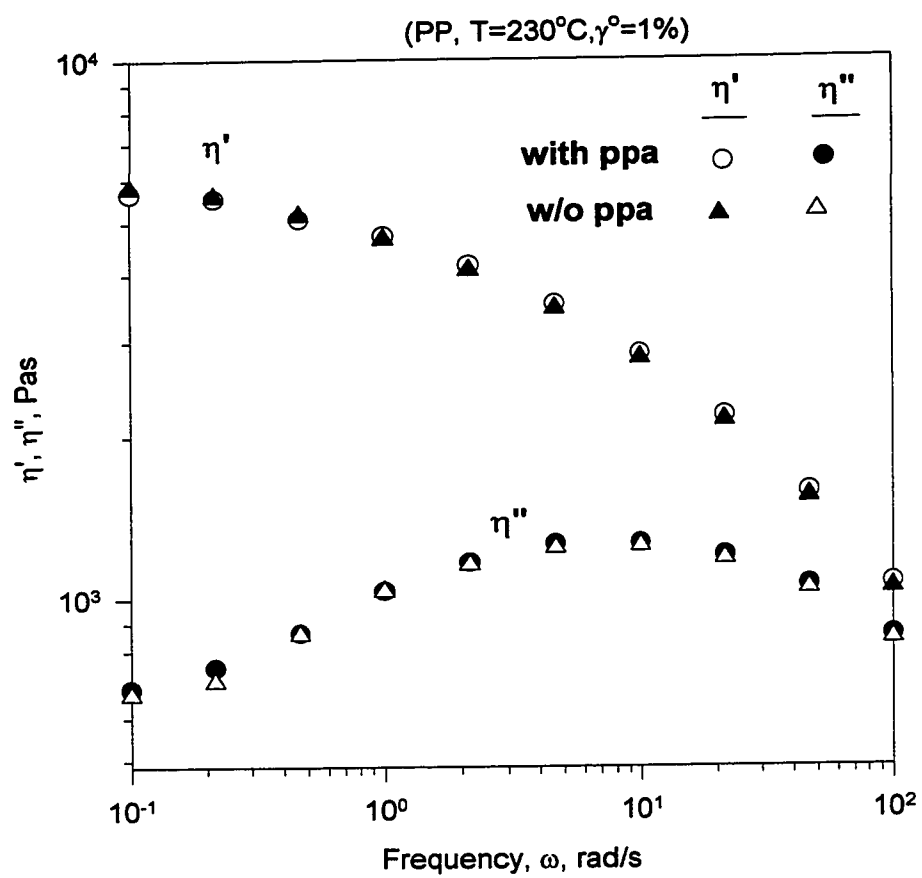
Figure B.8 Steady Shear for S213 and S214
(PP, T=230°C, tbm=3 min, mt=0.5 min, 2 rdgs/rate)
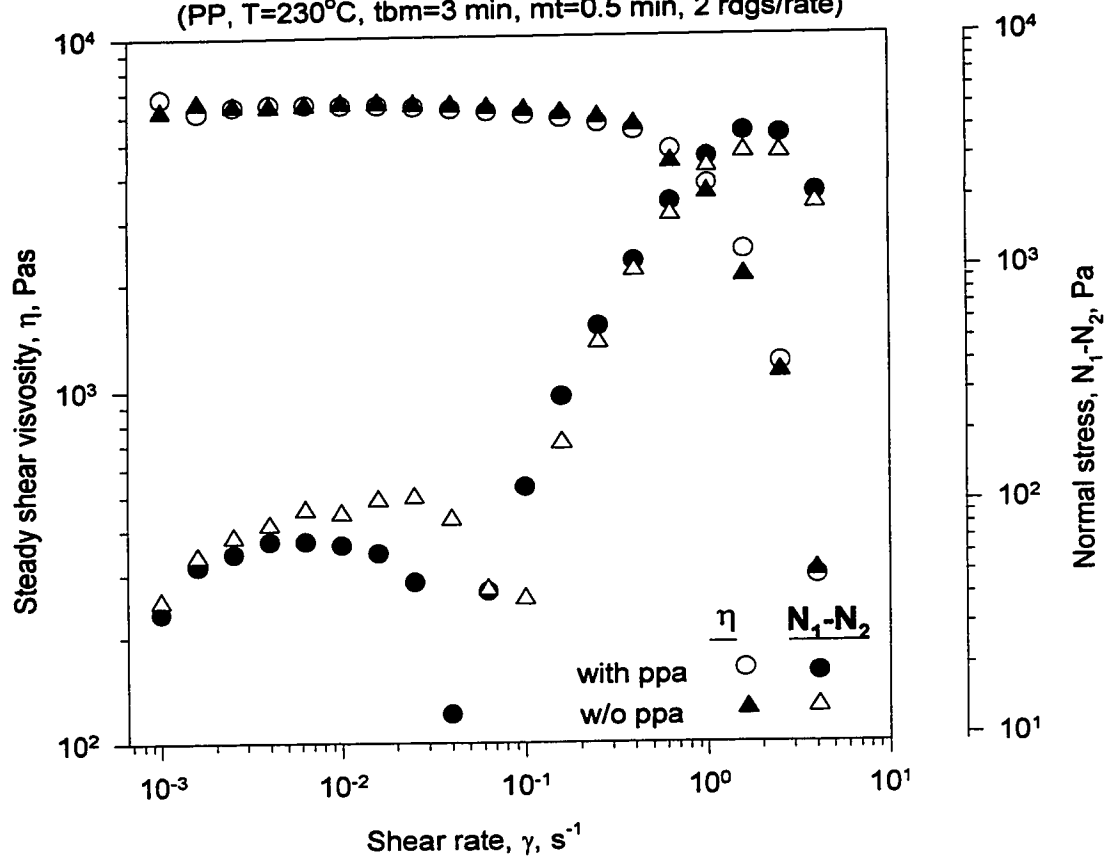
Figure B.9 DSC plot for S213 (with ppa)

(sample size=4.9 mg, rate=5°C/min.)

T_c=111°C

1st heating

2nd heating

T_m=123.6°C

T_m=124.2°C
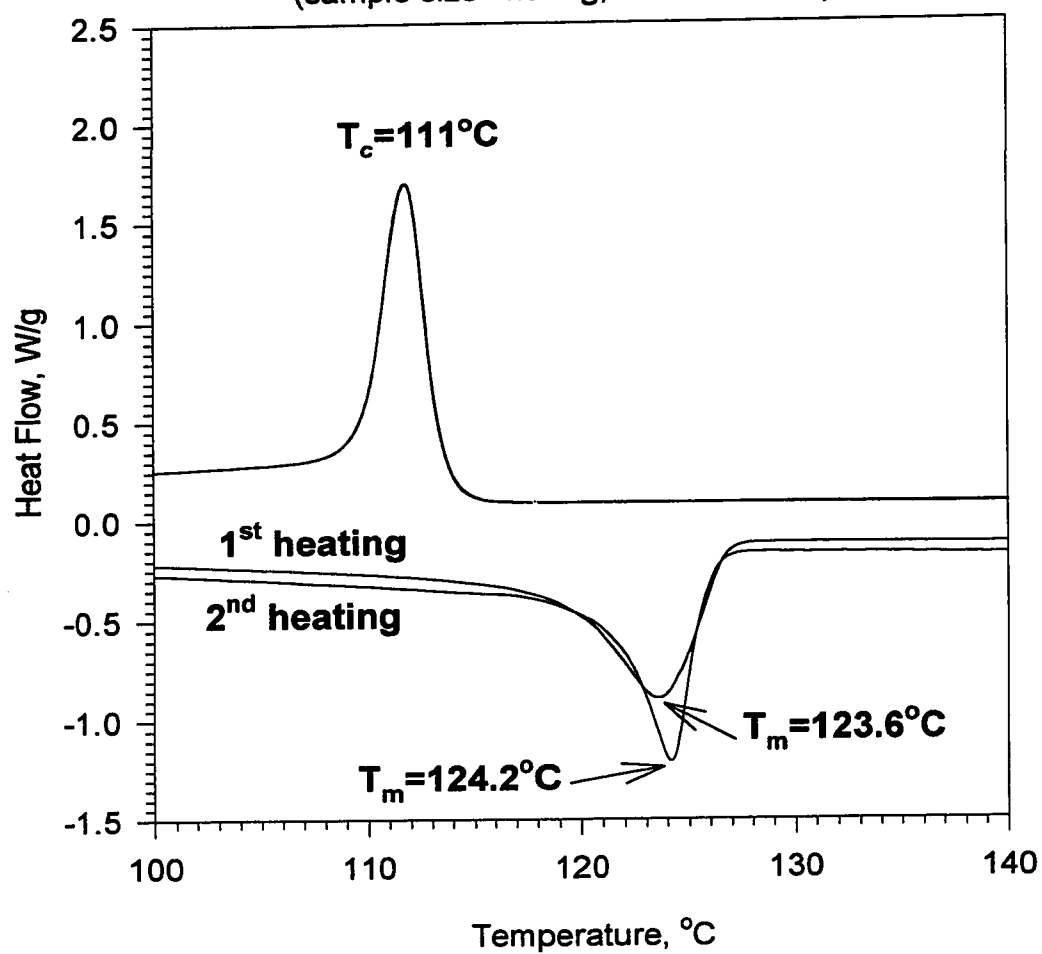
Figure B.10 DSC plot for S214 (w/o ppa)

(sample size=4.9 mg, rate=5°C/min.)

T_c=111°C

1st heating

2nd heating

T_m=123.7°C
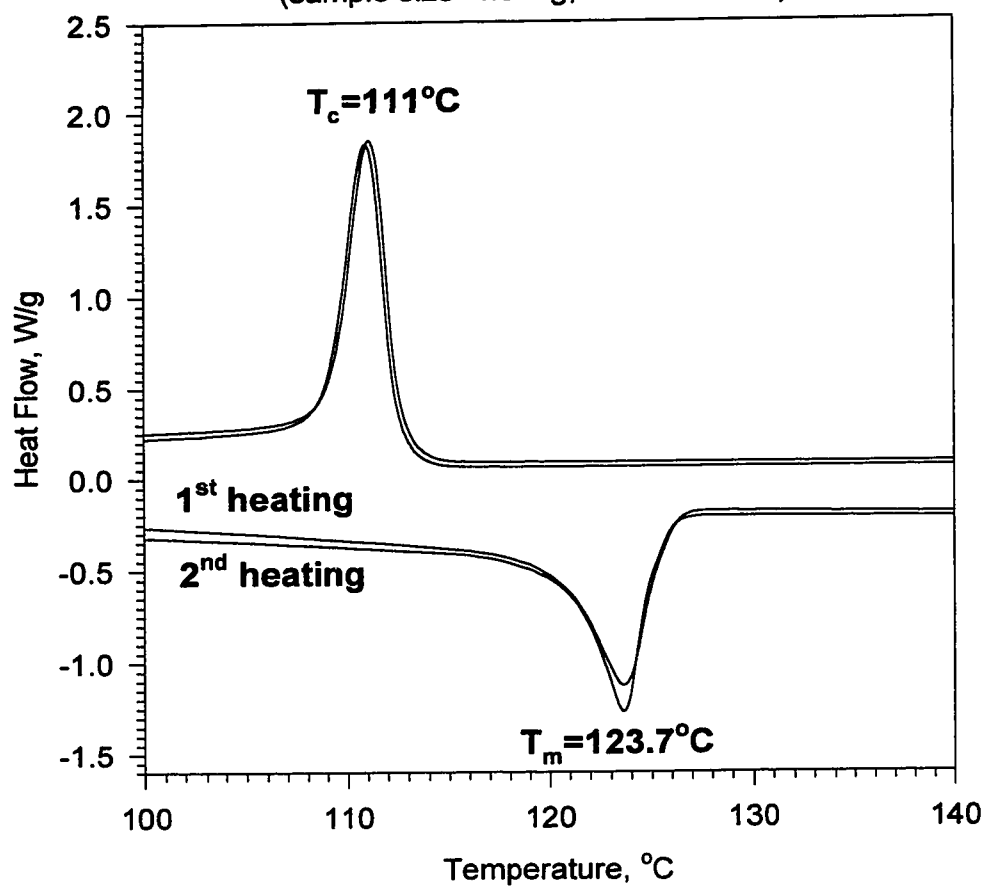
Figure B.11 DSC plot for S213 (with ppa)
(sample size=4.9 mg, rate=5°C/min)

Crystallinity=36.66%

T_m=124.2°C
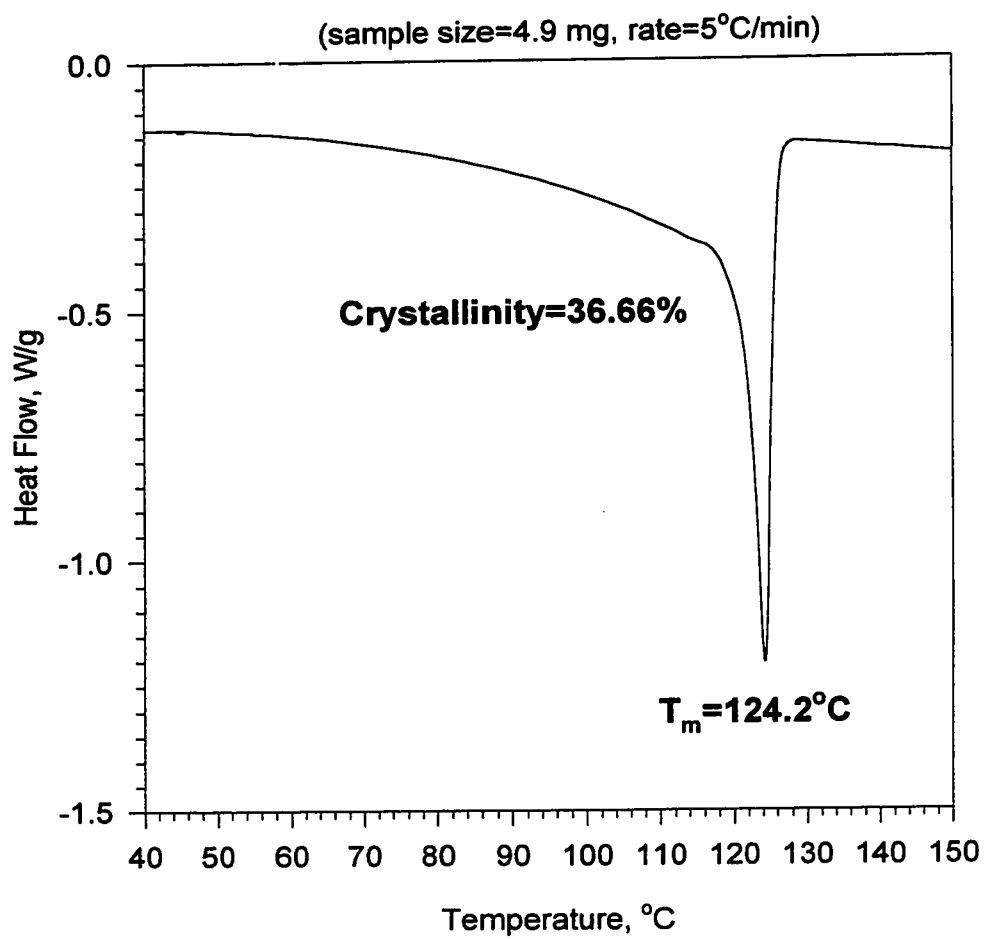
Figure B.12 DSC plot for S214 (w/o ppa)

(sample size=4.9 mg, rate=5°C/min)

Crystallinity=37.03%

T_m=123.6°C
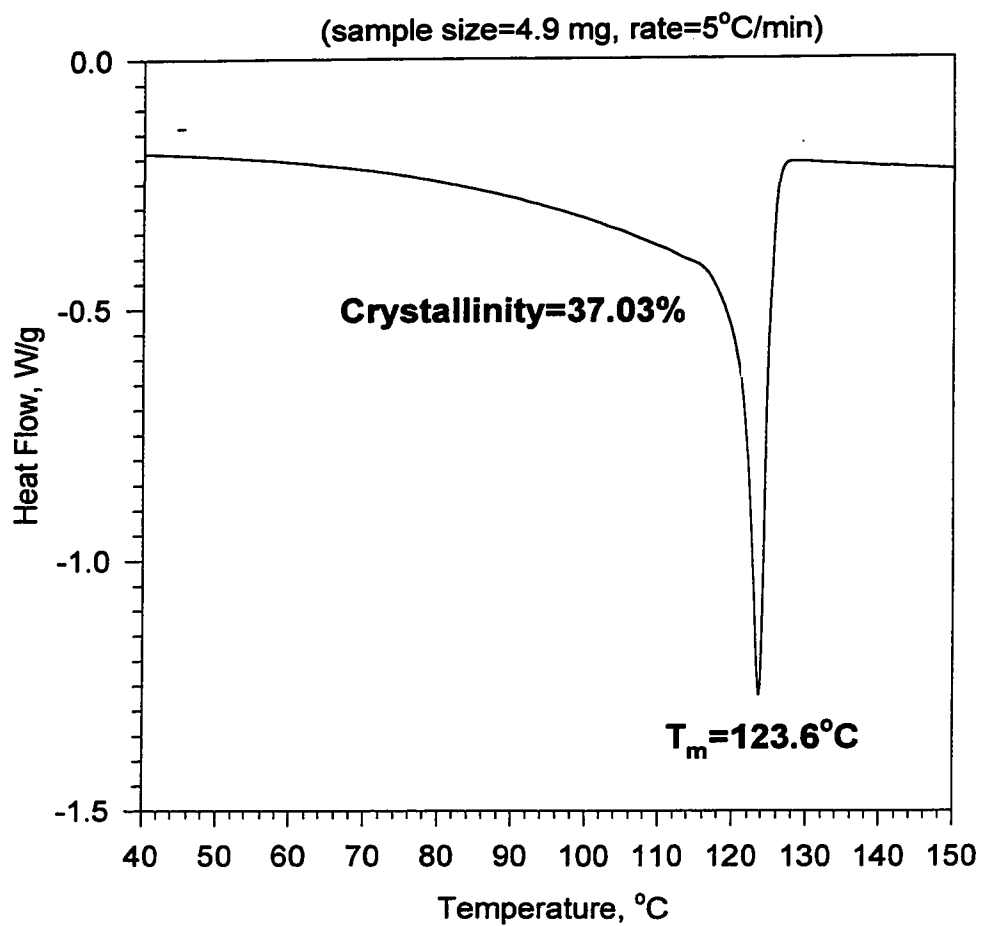
Figure B.13 Oxidation of Dowlex 2045 (w/o AO)

(sample size=5mg, rate=10°C/min., in air)

crystallinity=41%

T_{op}=235°C

T_{oo}=214°C

T_m=122°C

Heat Flow, W/g

Temperature, °C
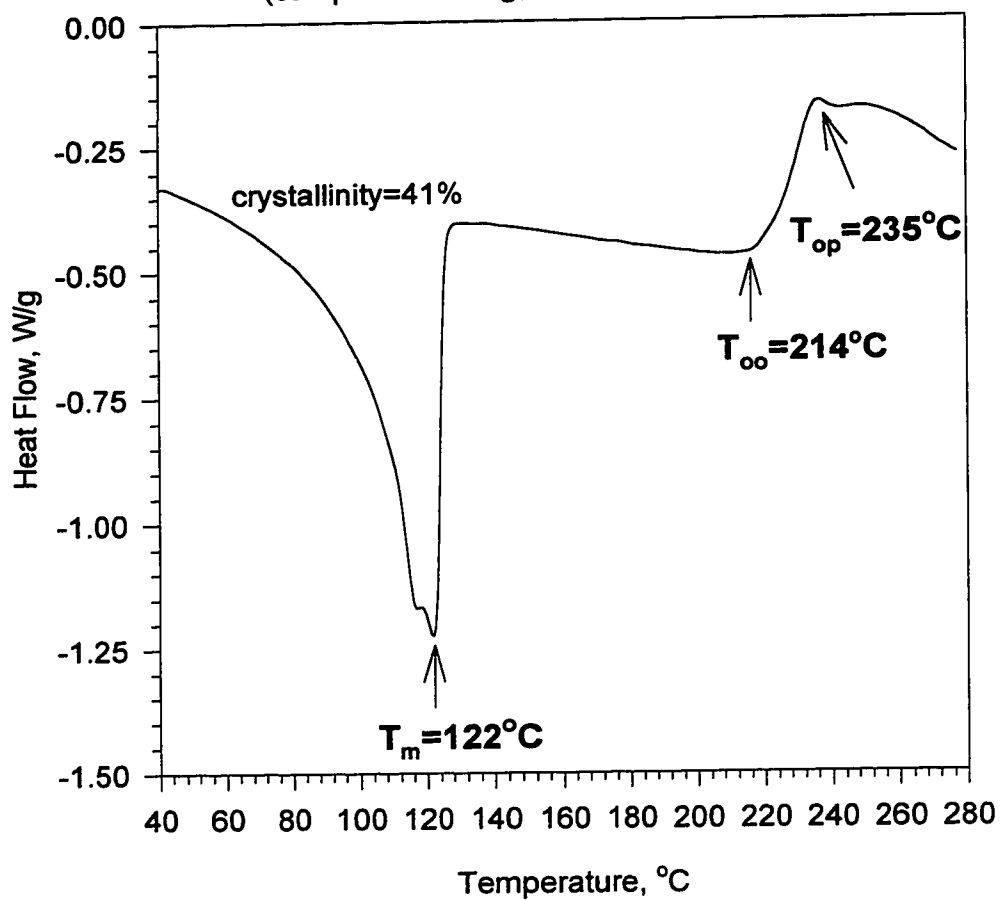
Figure B.14 Oxidation of Dowlex 2045AC

(sample size=4.5 mg, rate=10°C/min., in air)

crystallinity=40%

T_{op}=249°C

T_{oo}=228°C

T_m=122°C
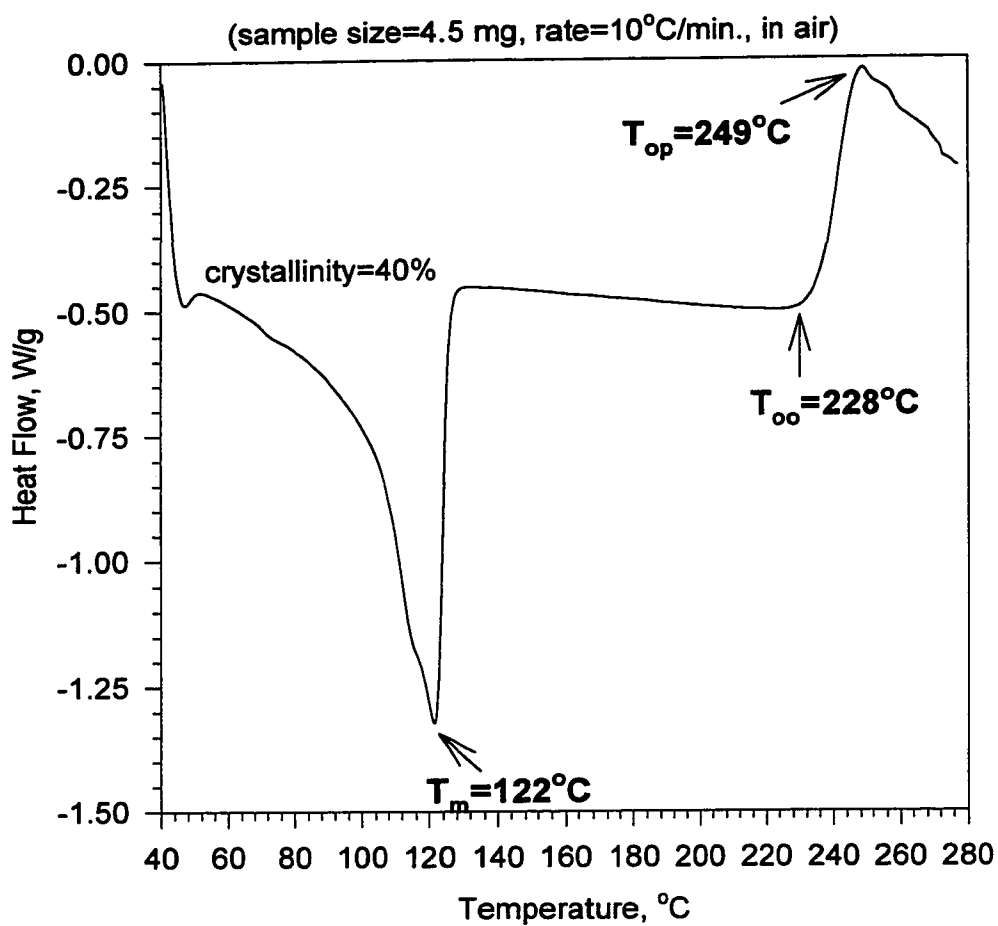
Figure B.15 $\eta^*(T)$ for Q-HDPE (160°-260°C)

(PP, gap=1.5 cm, γ°=6%, ω=0.1 rad/s)
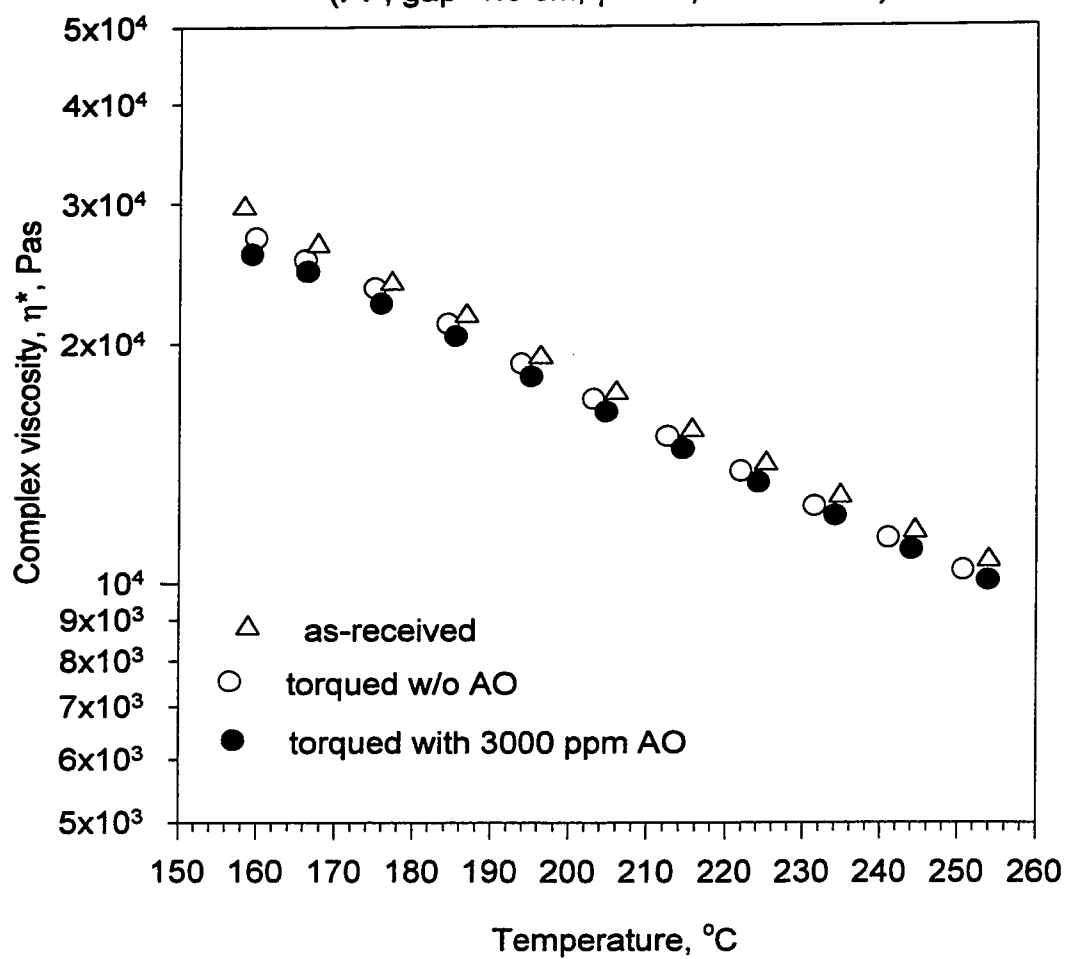
Figure B.16 η' for **S216 (LDPE) torqued at 220°C**
(Check for reproducibility)

(T_{mix}=220°C, no AO, no N_2; T_{test}=190°C, $\gamma°$=10%)
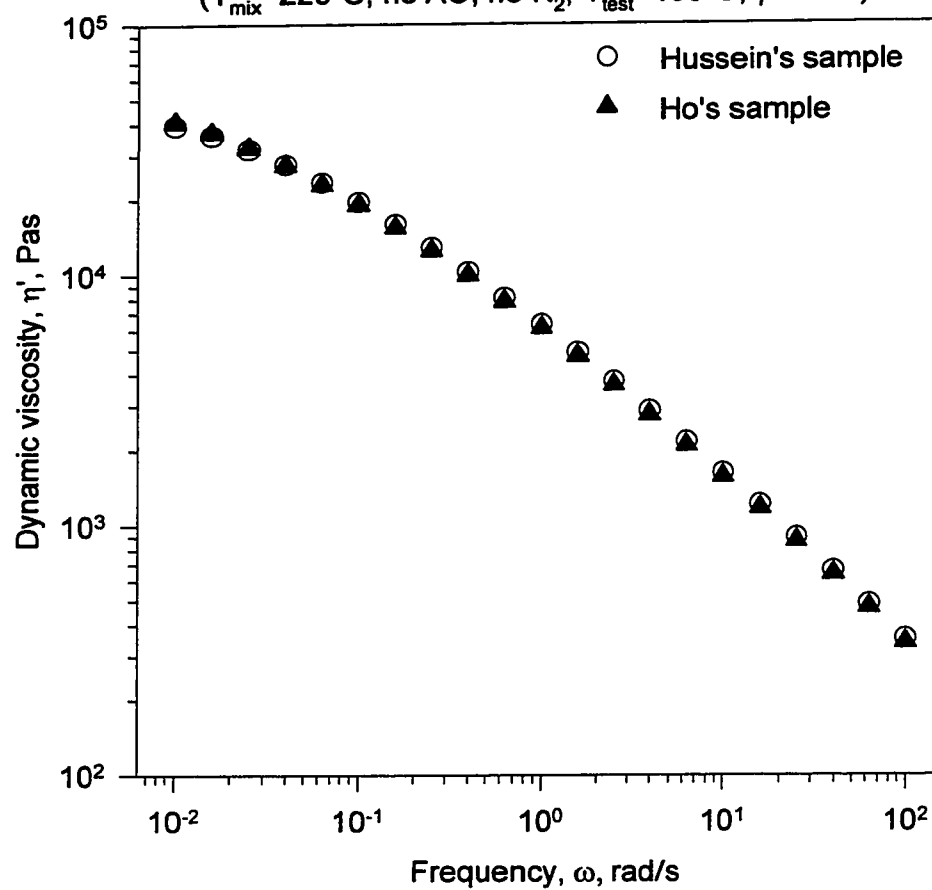
Figure B.17 η' for S229 mixed at 190° and 220°C
(Check for reproducibility within the same batch)

(no AO, no N_2; T_{test}=190°C, $\gamma°$=10%)

T_{mix} =220°C

T_{mix} = 190°C

T_{mix}	220°C	190°C
Run # 1	△	●
Run # 2	▼	○

Dynamic viscosity, η', Pas

Frequency, ω, rad/s
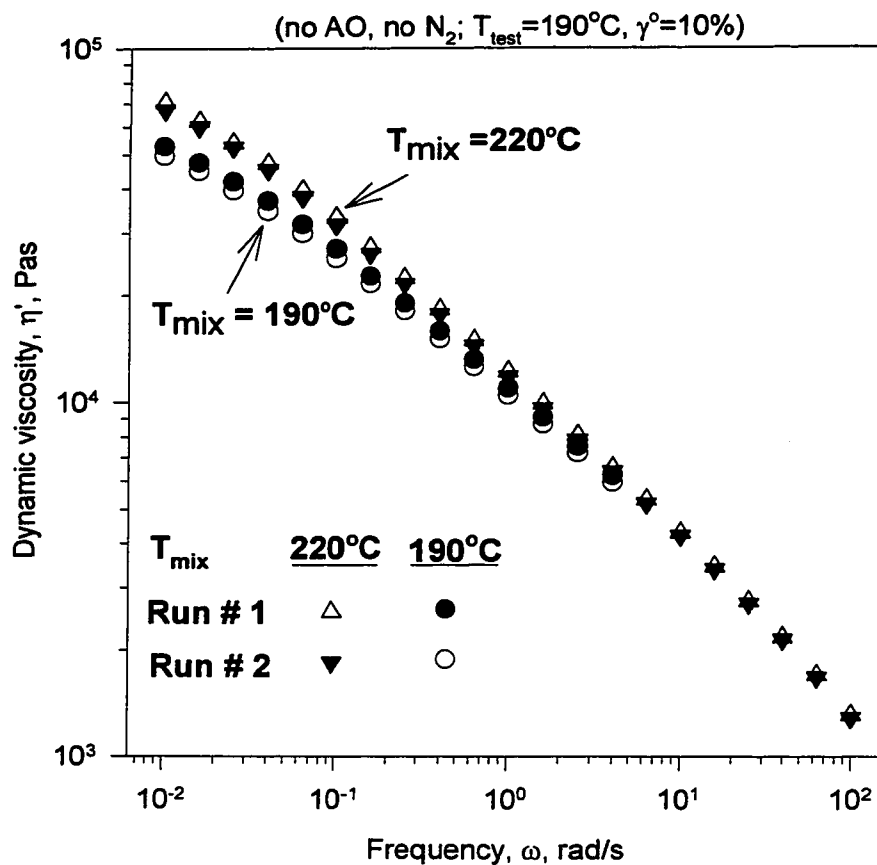
Figure B.18 Effect of T_{mix} on the rheology of S237

$(T_{test}=190^{\circ}C$, tbm=5min., mt=0.5 min., $\gamma^{\circ}=10\%$, C&P)

- $\bigcirc$ η (as-received)
- $\blacktriangle$ η' (as-received)
- $\triangle$ η' $(T_{mix}=190^{\circ}C)$
- $\square$ η' $(T_{mix}=220^{\circ}C)$

Dynamic viscosity, η'; Steady shear viscosity, η, Pas

Frequency, ω; Shear rate, γ, s^{-1}
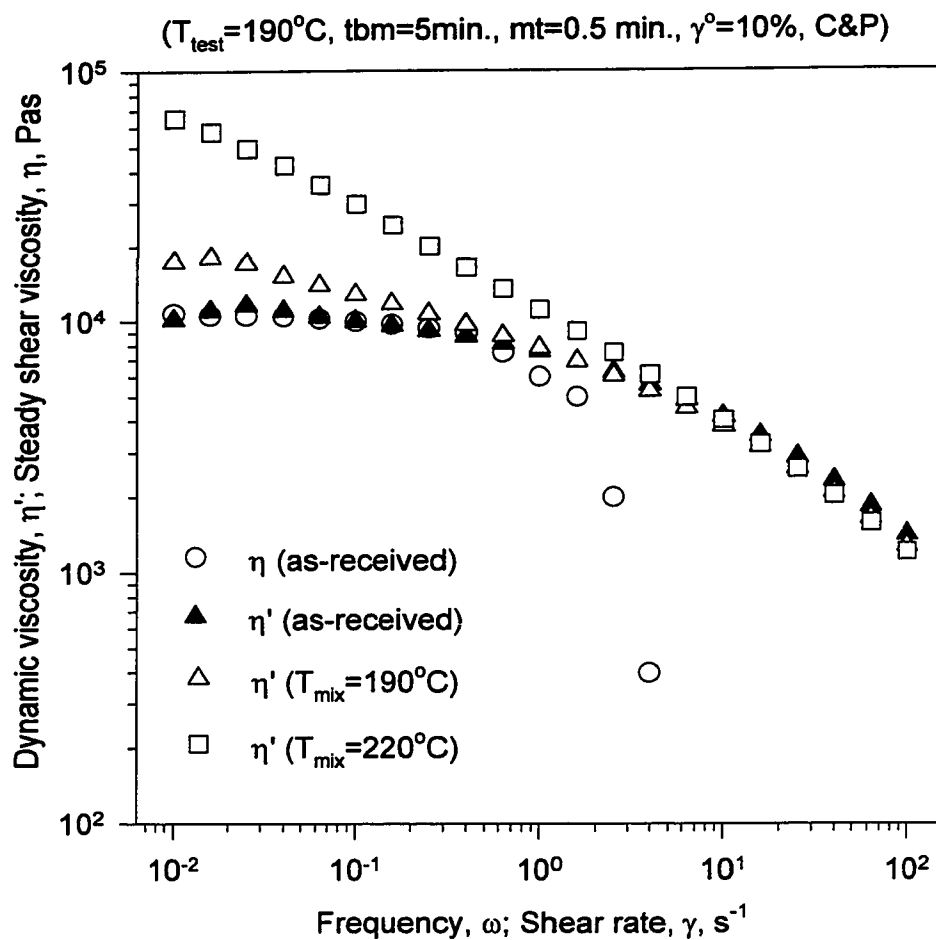
Figure B.19 NMR spectrum for as-received S229 (LLDPE)
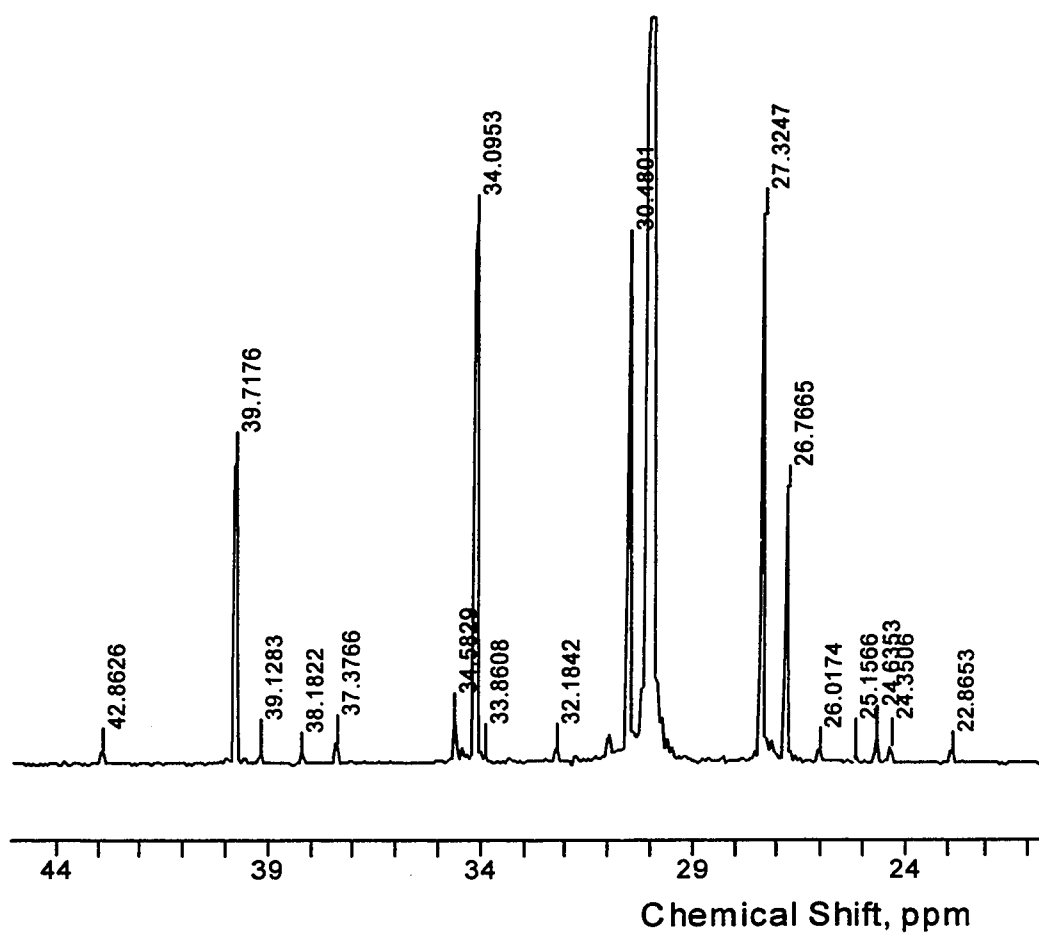
Figure B.20 NMR spectrum for S229 (LLDPE) mixed at 190°C with 1000 ppm of AO
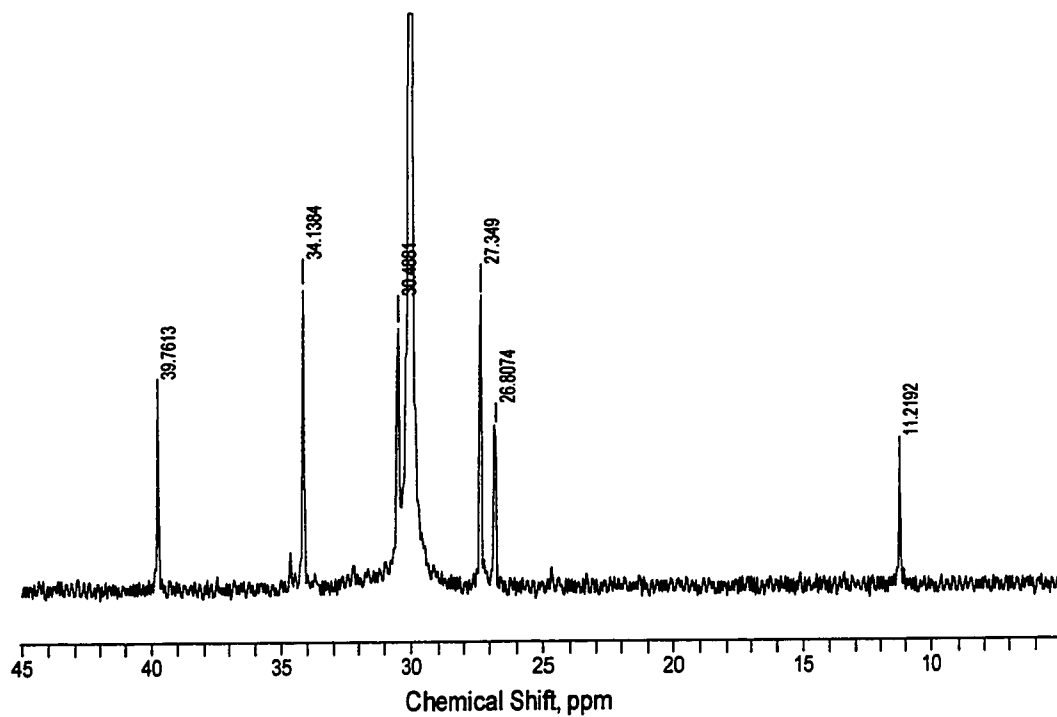
Figure B.21 NMR spectrum for S229 (LLDPE) torqued at 190°C w/o AO
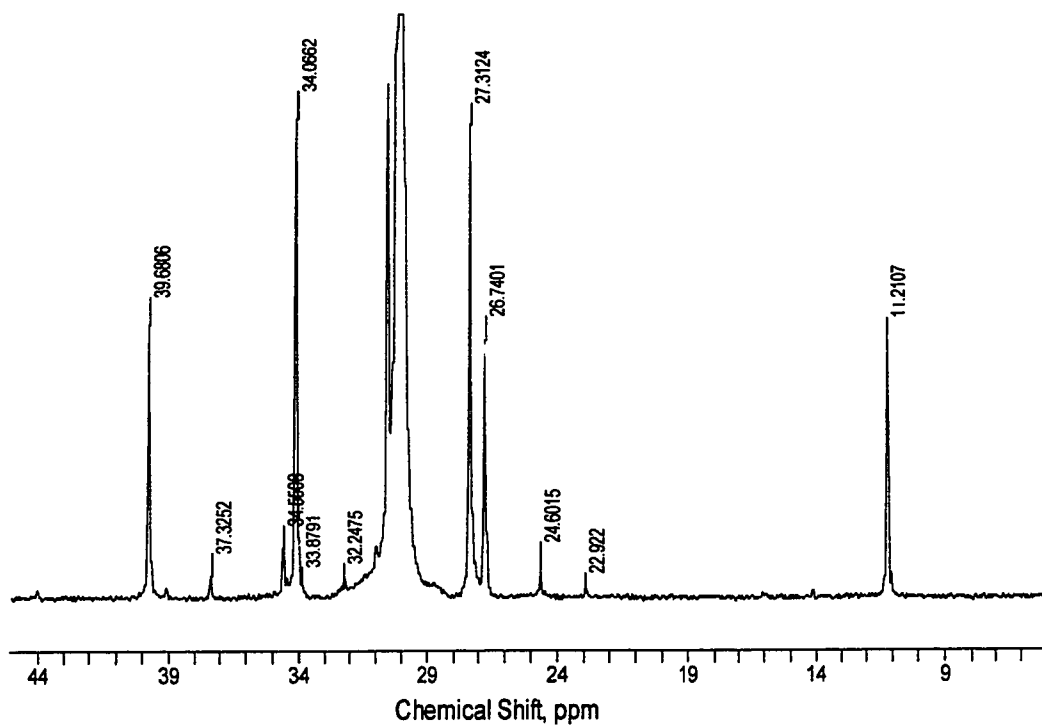
Figure B.22 NMR spectrum for S229 (LLDPE) torqued at 220°C w/o AO
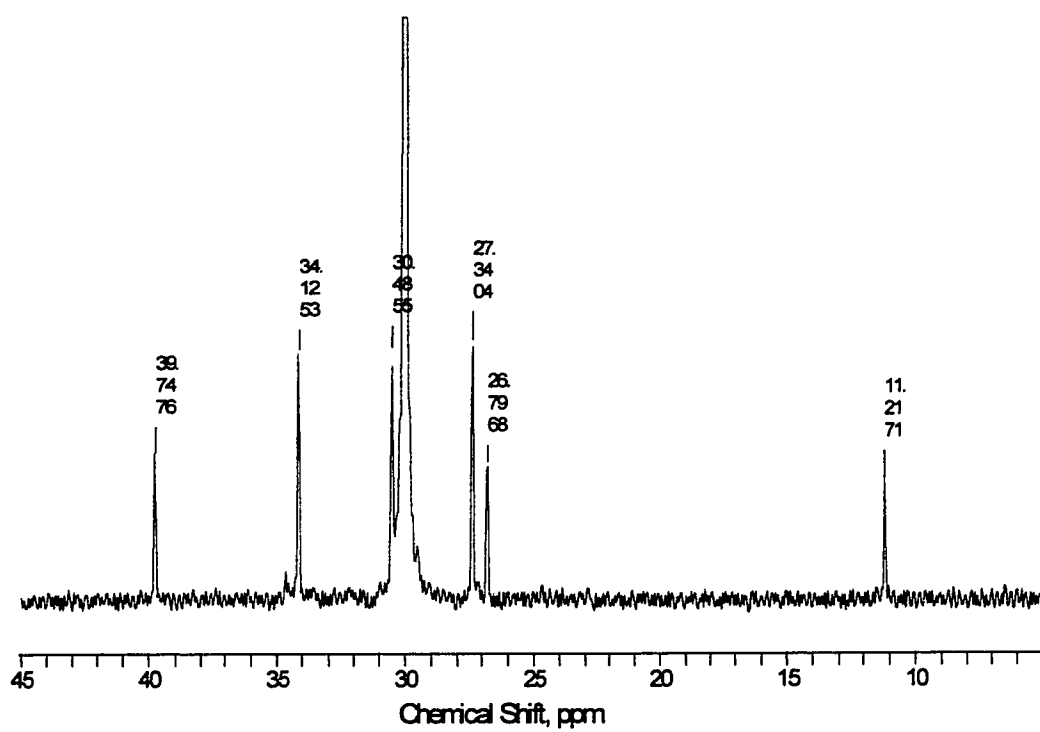
Figure B.23 NMR spectrum for S229 (LLDPE) mixed at 220°C with 2000 ppm of AO
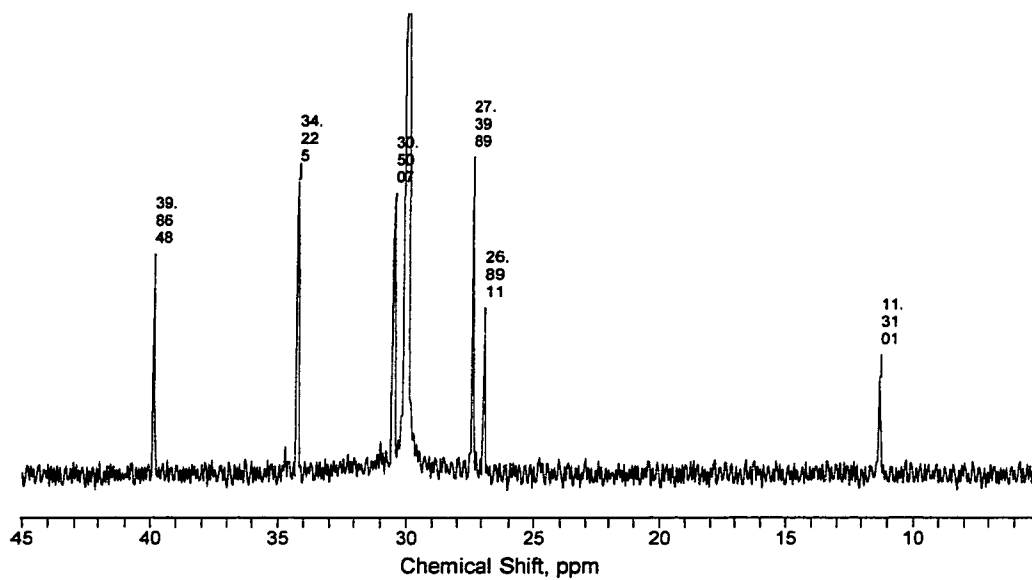
Figure B.24 NMR spectrum for S229 (LLDPE) mixed at 220°C with 1000 ppm of AO
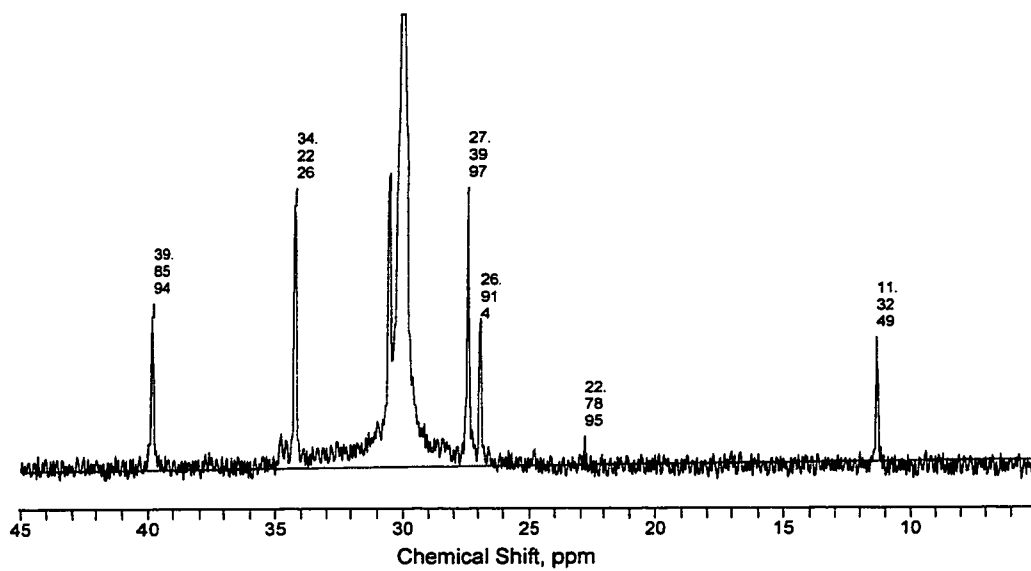
Figure B.25 DSC melting curve for as-received S229 (LLDPE)

(sample size=6.5 mg, heating rate=10°C)

X_c=39.7%

T_m=122.8°C
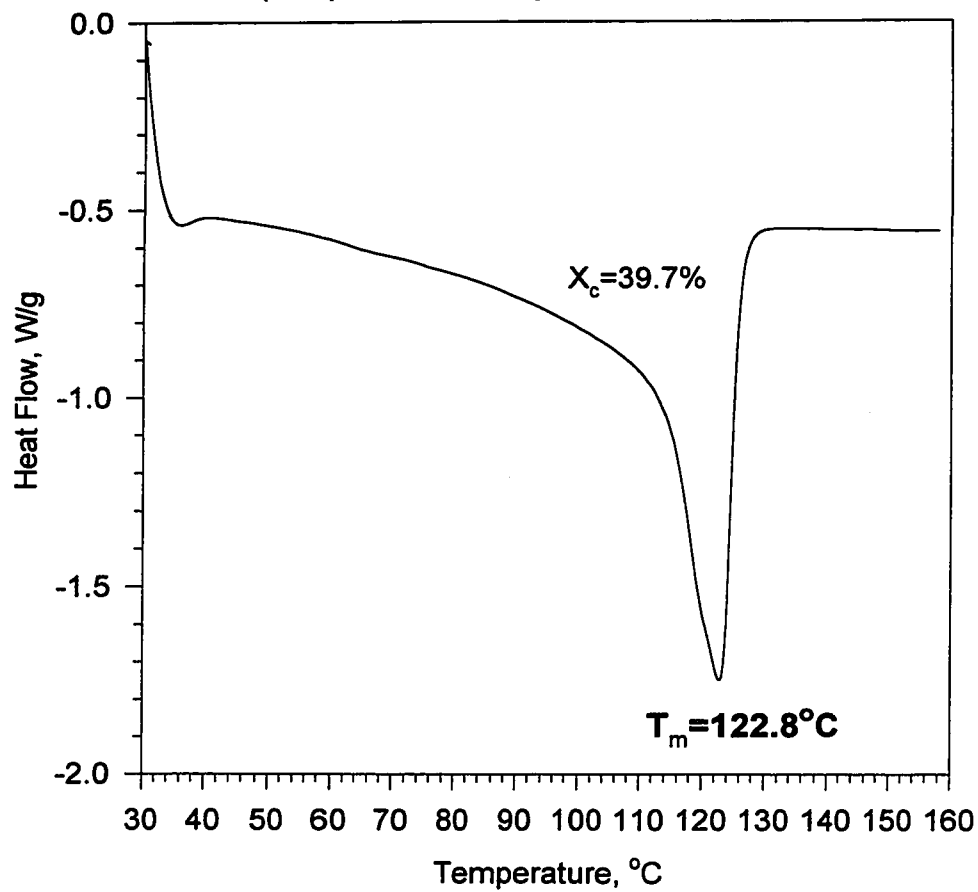
Figure B.26 DSC melting curve for as-received S216 (LDPE)

(sample size=6 mg, heating rate=10°C/min.)

X_c=41%

T_m=110.1°C
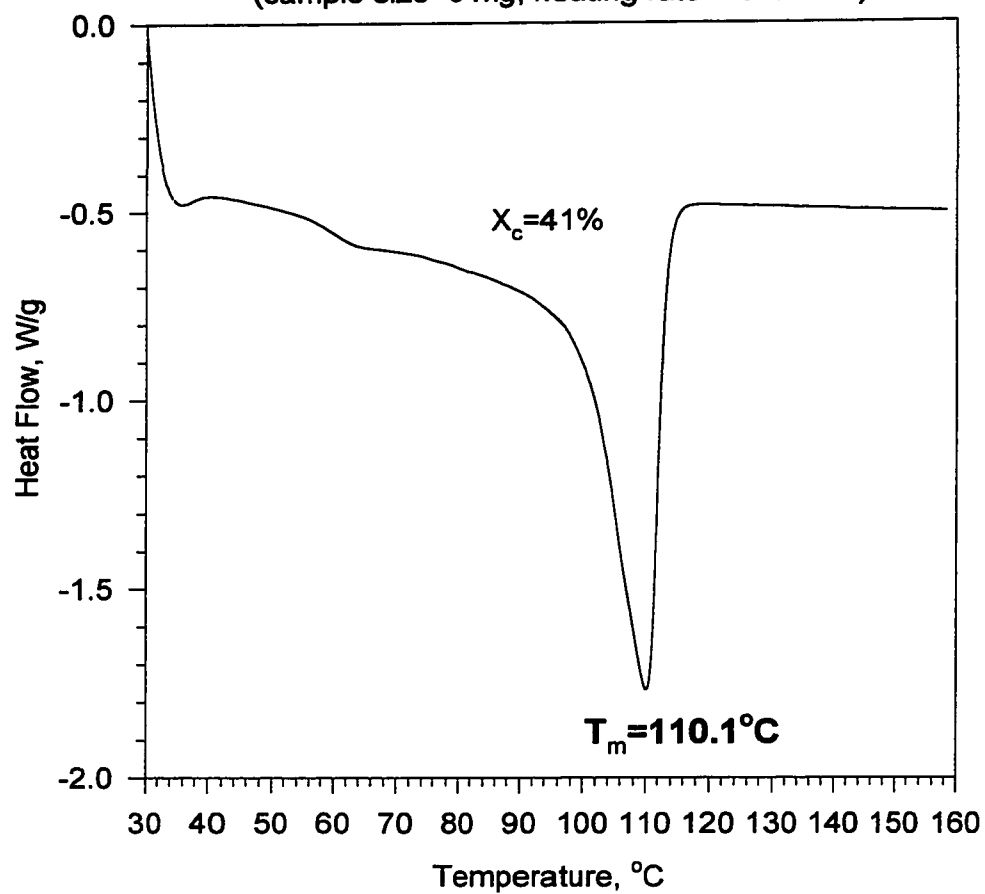
Figure B.27 DSC melting curve for S216 (LDPE) with added AO

$(T_{mix}=220^{\circ}C;$ sample size=5.1 mg, heating rate=$10^{\circ}C/min.)$

$X_c=40\%$

$T_m=109.6^{\circ}C$
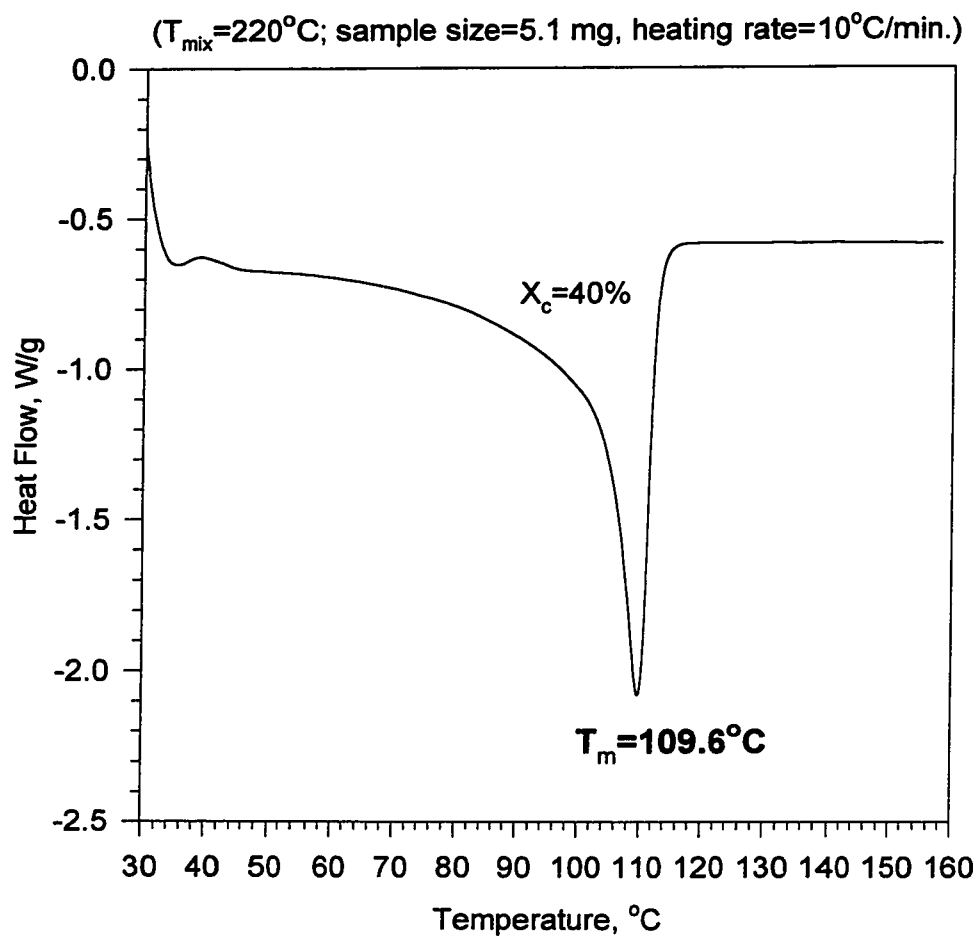
Figure B.28 DSC melting curve for S216 (LDPE) w/o added AO

$(T_{mix}=220^\circ C$; sample size=5.8 mg, heating rate=$10^\circ C$/min.)

$X_c=38\%$

$T_m=109.7^\circ C$
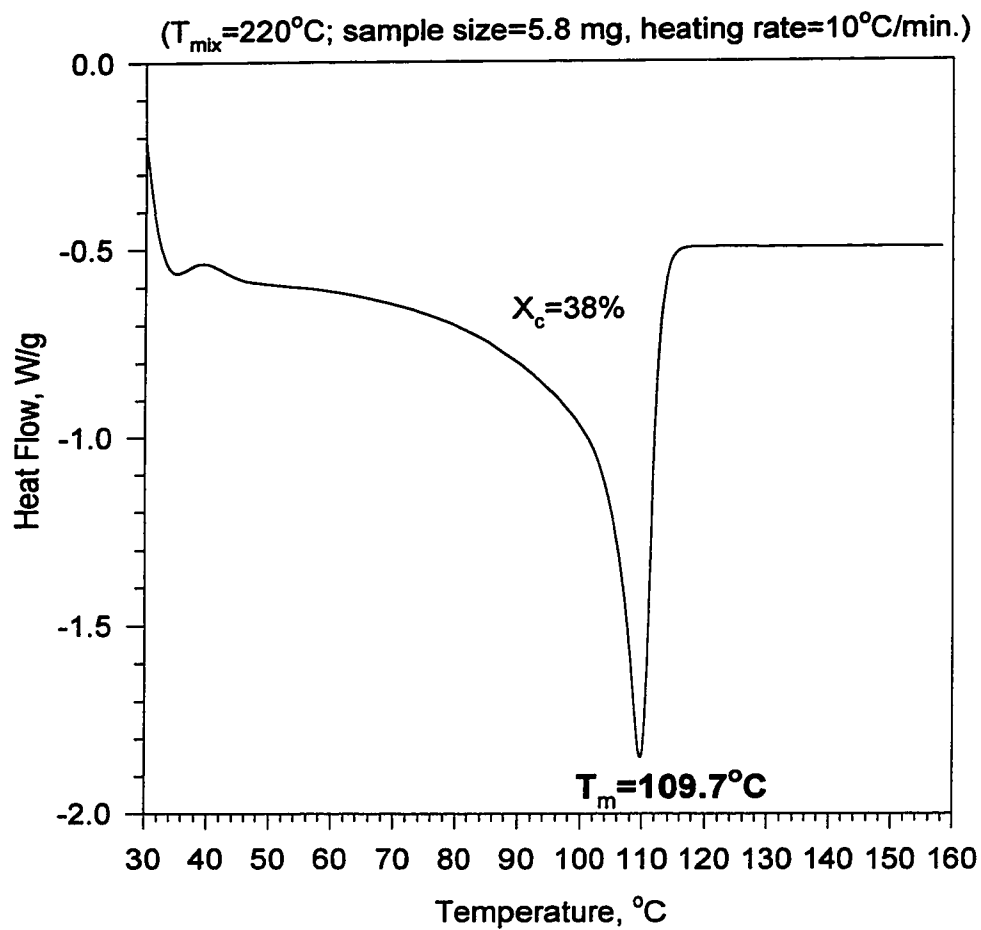
Figure B.29 Comparison of η' for S229 from different batches

$(T_{mix}=220°C; C\&P, T_{test}=190°C, \gamma°=10\%)$

Figure B.30 η' and G' for blends of LLDPE and LDPE

$(T_{mix}=220°C, T_{test}=190°C, \gamma°=10\%, \omega=1.0 \text{ rad/s, w/o AO})$
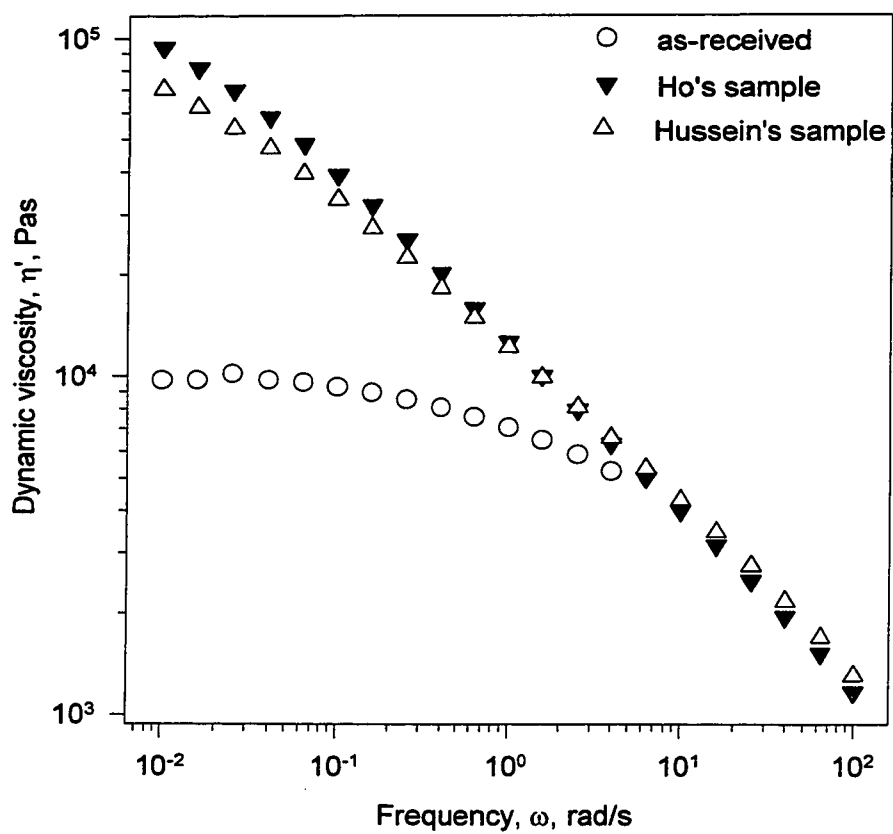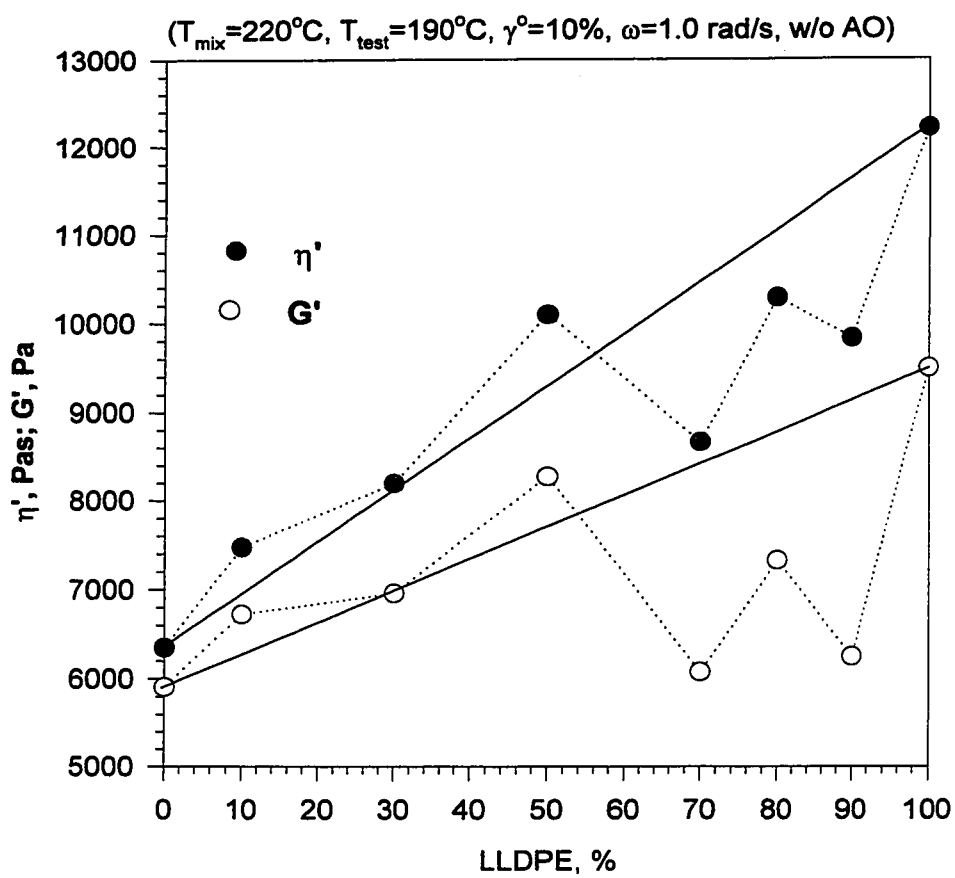
Figure B.31 Effect of T$_{test}$ on η' for blends of LLDPE and LDPE
(T$_{mix}$=220°C, w/o added AO, γ°=10%, ω=0.1 rad/s)
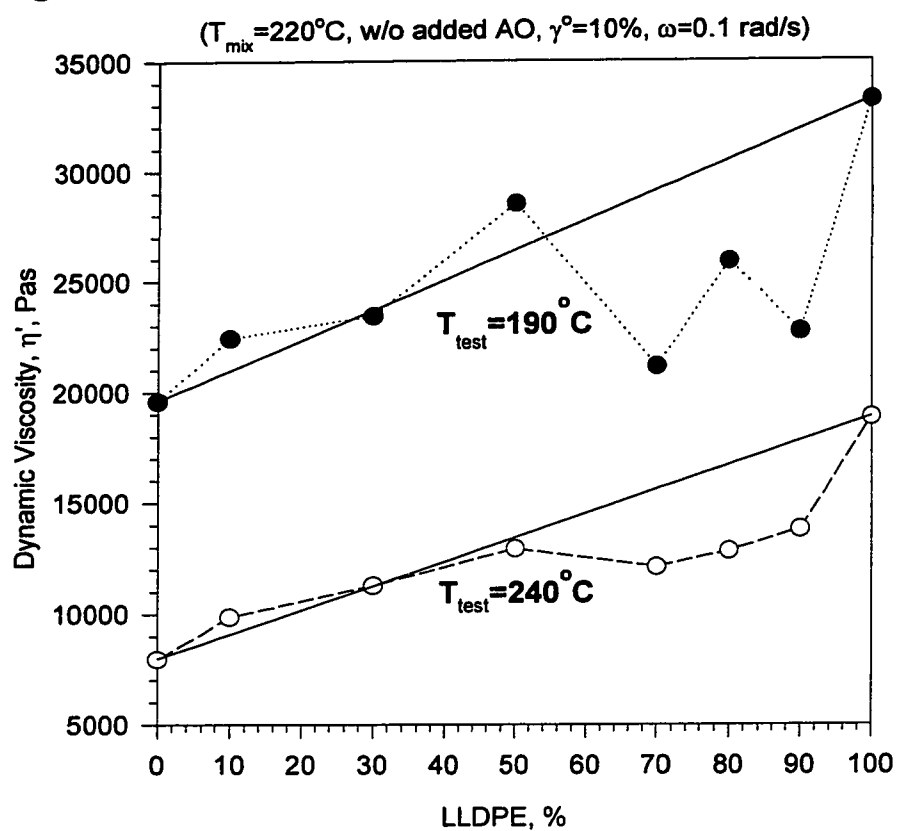
Appendix C

Supplement to Chapter VI

Figure C.1 Plot of G'(T) for a 50/50 blend*
of S226 (octene) and S216 (LDPE)
(test for degradation)
(T_{mix}=190°C; γ°=10%, ω=1 rad/s, gap=1.5 mm, PP)

*with additional 1000 ppm of A/O

○ heating (160°-260°C)
● cooling (260°-160°C)
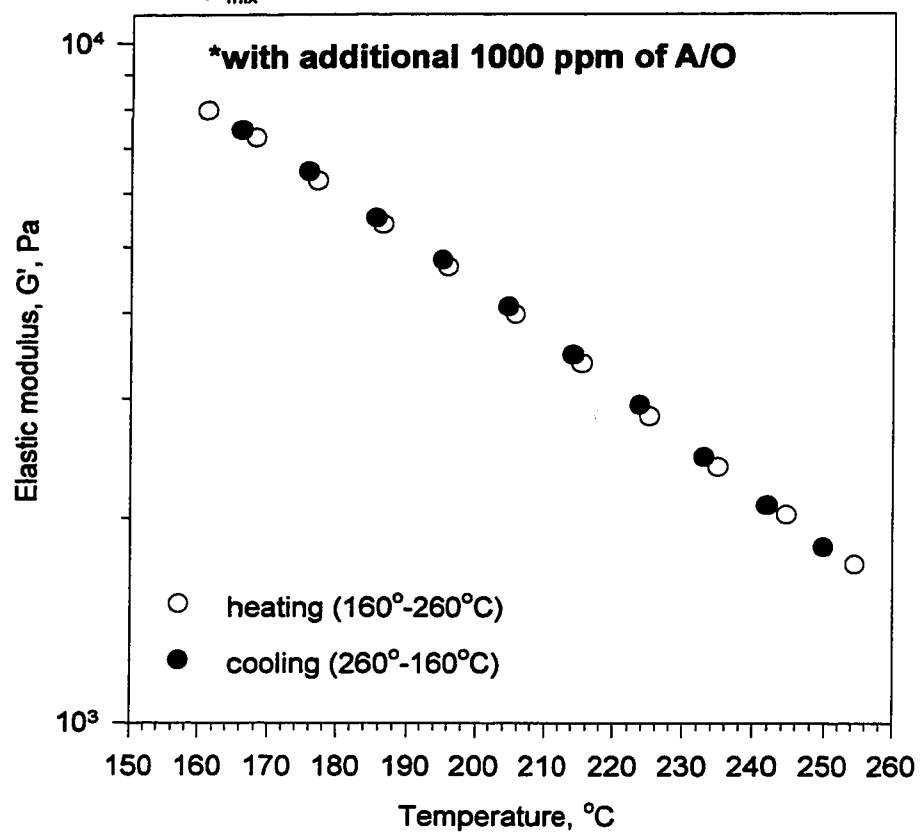
Figure C.2 $\eta'(\omega)$ and $G'(\omega)$ for 10% S229 (LLDPE)*

(T_{mix}=190°C, 50 rpm for 10 min.; T_{test}=190°C, $\gamma°$=10%, C&P)

*with additional 1000 ppm of A/O

Legend:
- $\triangledown$ η', 1st run
- $\blacktriangle$ η', 2nd run
- $\circ$ G', 1st run
- $\blacktriangledown$ G', 2nd run

Axes: Dynamic viscosity, η', Pas; Elastic modulus, G', Pa; Frequency, ω, rad/s
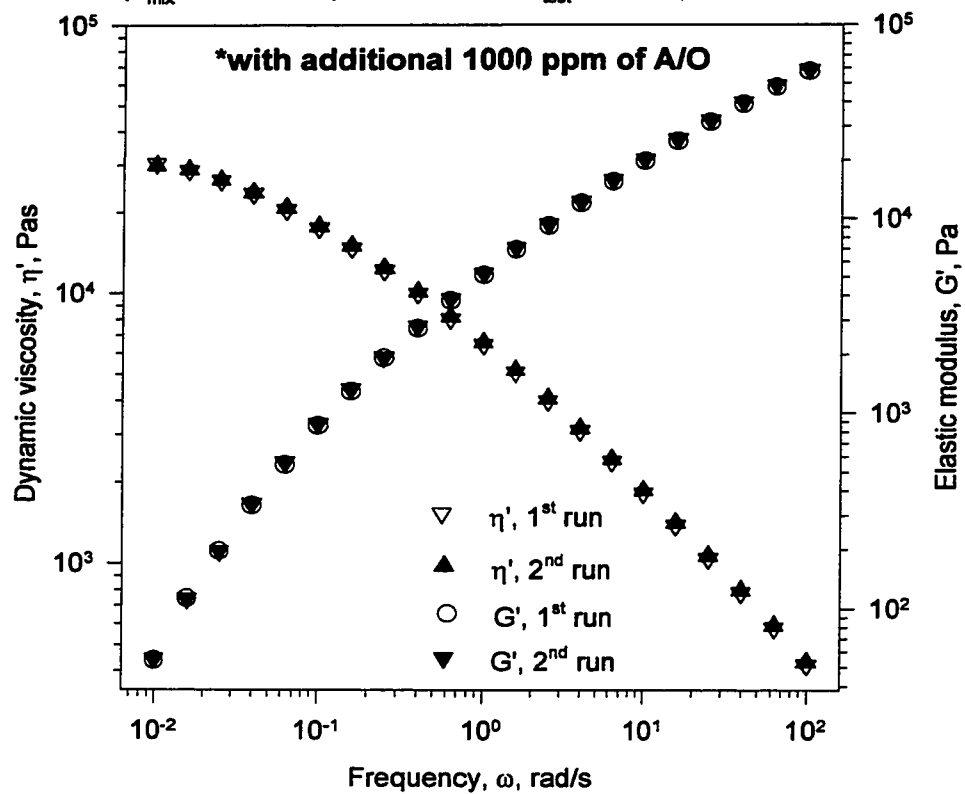
Figure C.3 $\eta'(\omega)$ and $G'(\omega)$ for 90% S227 (LLDPE)

(Reproducibility test)

$(T_{mix}=190°C; T_{test}=140°C, \gamma°=10\%)$
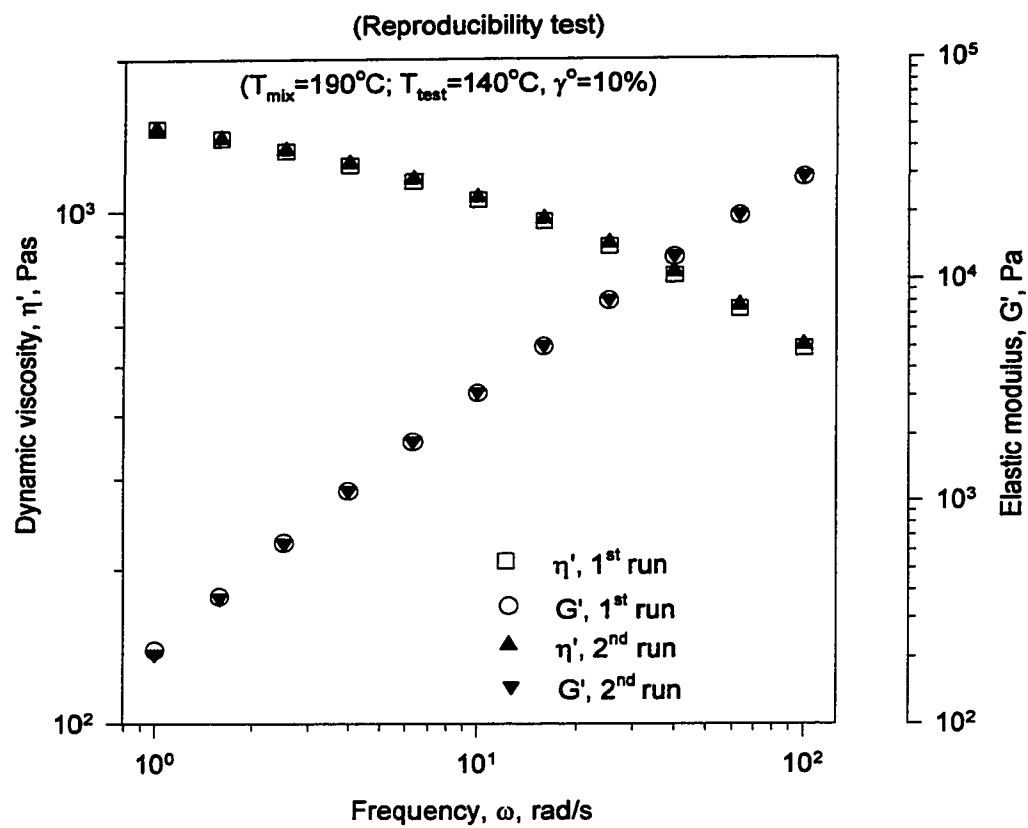
Figure C.4 $\eta'(\phi)$ for blends of S227 (LLDPE) and S231 (LDPE)

$(T_{mix}=190°C; T_{test}=140°C, \gamma°=10\%, \omega=100 \text{ rad/s})$
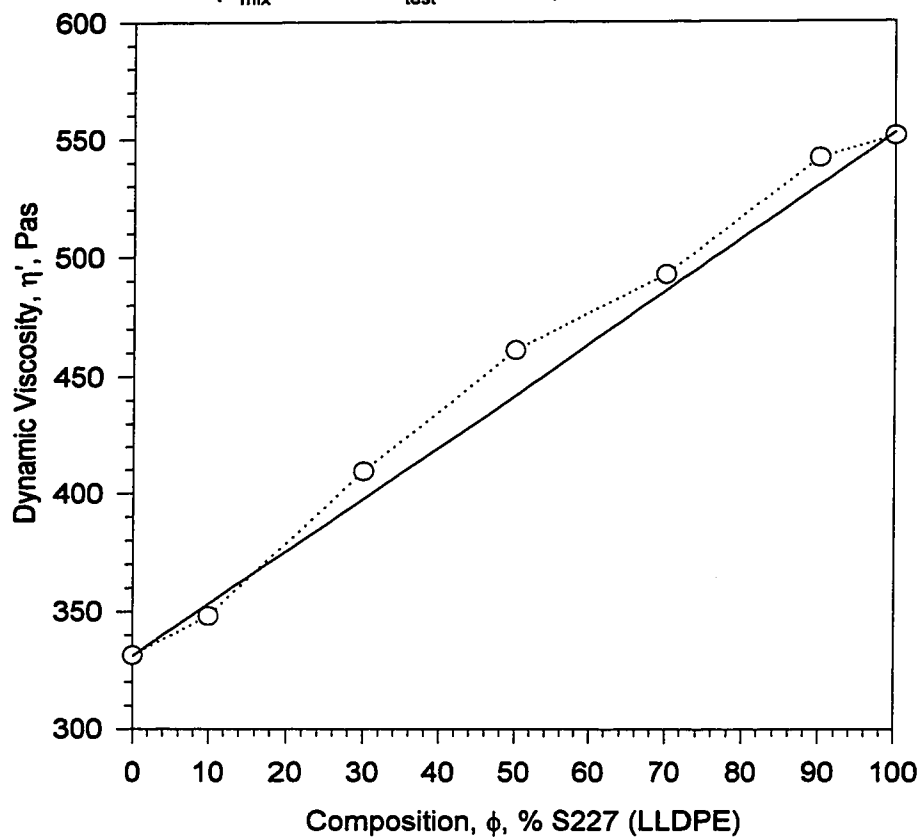
Figure C.5 $a_\phi(\phi)$ for blends of S227 (LLDPE) and S231 (LDPE)

$(T_{mix}=190^\circ C;\ T_{test}=140^\circ C,\ \omega=1\text{-}100\ rad/s)$
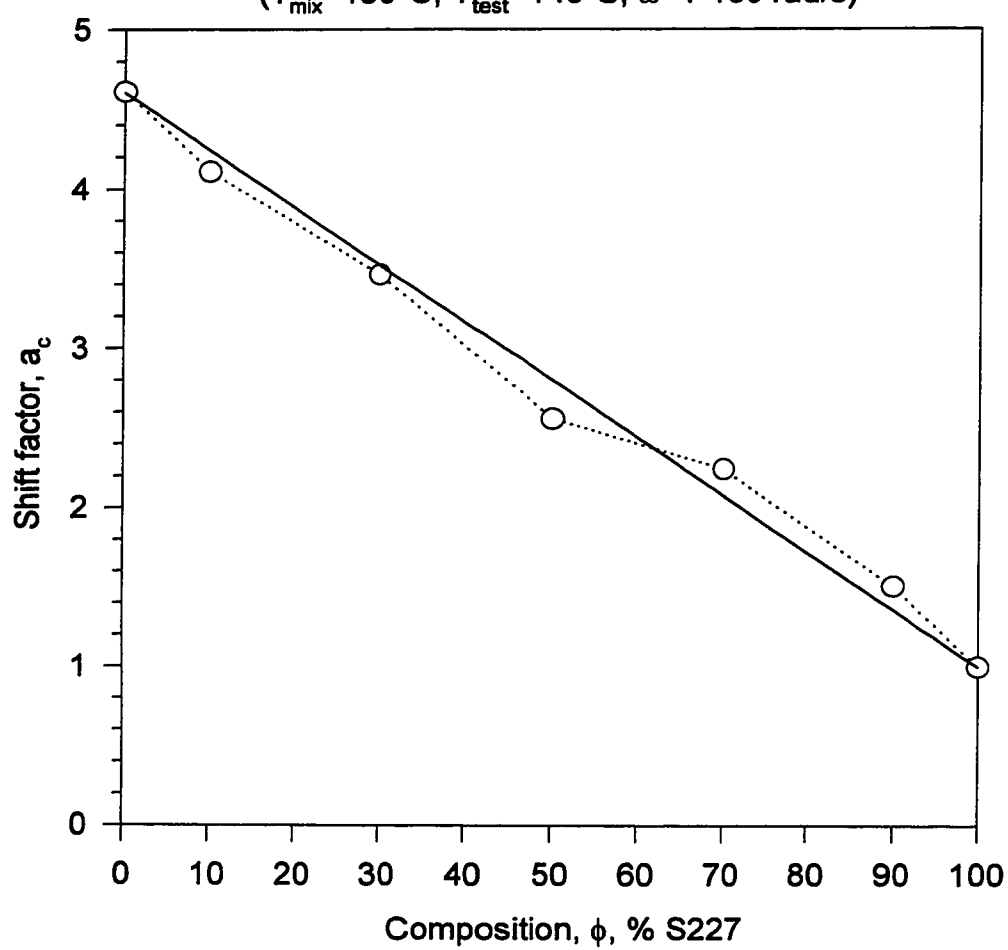
Figure C.6 $\eta'(\phi)$ for blends* of S229 (LLDPE) and S216 (LDPE)

$(T_{mix}=190°C; T_{test}=190°C, \gamma°=10\%, \omega=0.04 \text{ rad/s})$

*with additional 1000 ppm of A/O

Dynamic viscosity, η', Pas

2×10^4

10^4

9×10^3

8×10^3

0   10   20   30   40   50   60   70   80   90   100
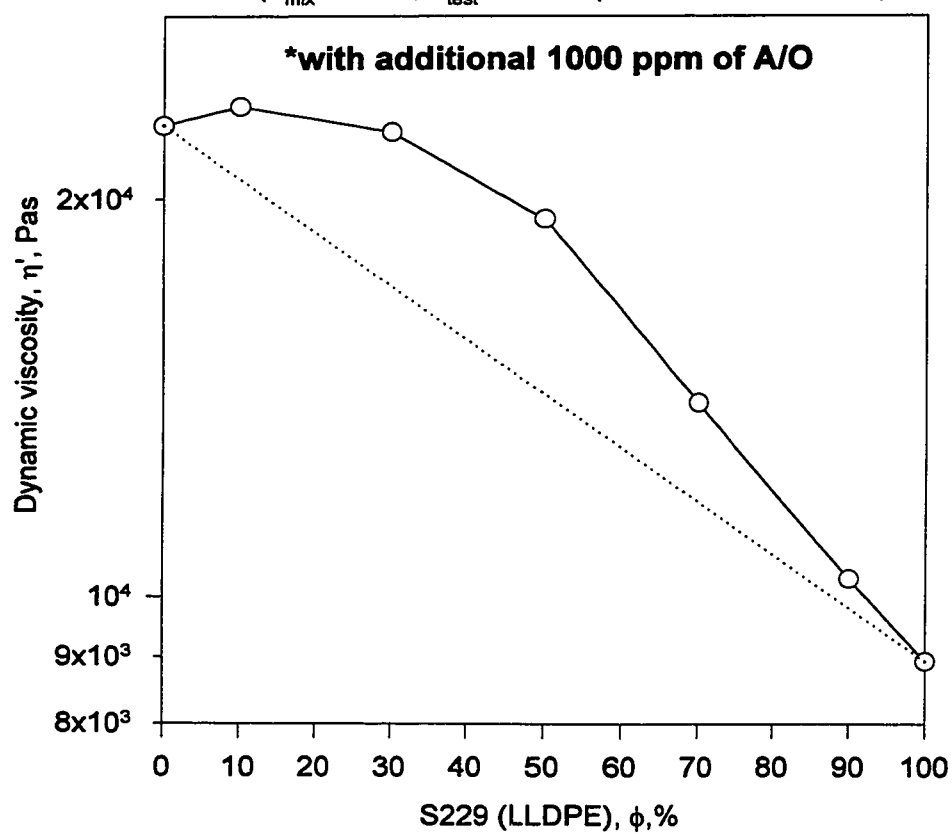
S229 (LLDPE), ϕ,%

Figure C.7 $\eta'(\phi)$ for blends* of S229 (LLDPE) and S216 (LDPE)

$(T_{mix}=190°C; T_{test}=190°C, \gamma°=10\%, \omega=0.1 \ rad/s)$

*with additional 1000 ppm of A/O

Dynamic viscosity, η', Pas

$2x10^4$

10^4

$9x10^3$

$8x10^3$

0 10 20 30 40 50 60 70 80 90 100

S229 (LLDPE), ϕ, %

Figure C.8 $\eta'(\phi)$ for blends* of S229 (LLDPE) and S216 (LDPE)

$(T_{mix}=190^\circ C; T_{test}=190^\circ C, \gamma^\circ=10\%, \omega=10 \text{ rad/s})$

*with additional 1000 ppm of A/O

Y-axis: Dynamic viscosity, η', Pas

X-axis: S229 (LLDPE), ϕ, %

Figure C.9 $\eta'(\phi)$ for blends* of S229 (LLDPE) and S216 (LDPE)

(T_{mix}=190°C; T_{test}=190°C, γ^o=10%, ω=100 rad/s)

*with additional 1000 ppm of A/O

Figure C.10 $\eta'(\phi)$ for blends of S229 and S216 for τ=1000 Pa

$(T_{mix}=190°C; T_{test}=190°C, \gamma°=10\%, \omega=0.01-100 \text{ rad/s})$

2×10^4

Dynamic viscosity, η', Pas

10^4
9×10^3
8×10^3
7×10^3
6×10^3

0   10   20   30   40   50   60   70   80   90   100

S229 (LLDPE), %

Figure C.11 Comparison of $\eta(\tau)$ and $\eta'(\tau)$
for blends* of S229 and S216

$(\gamma^\circ=10\%,\ \omega=0.01\text{-}100\ \text{rad/s; tbm=3 min., mt=30 s, } \gamma=0.01\text{-}1\ \text{s}^{-1})$

10% S229

90% S229

Shear viscosity, η or η', Pas

10^4

10^3

$\square$ η for 10% S229

$\bullet$ η' for 10% S229

$\bigcirc$ η for 90% S229

$\triangle$ η' for 90% S229

10^{-2} 10^{-1} 10^0 10^2 10^3 10^4 10^5

Shear stress, τ, Pa

Figure C.12 θ(φ) for blends of S229 (LLDPE) and S216 (LDPE)

$(T_{mix}=190°C; T_{test}=190°C, \gamma°=10\%)$

Figure C.13 $\eta'(\omega)$ **for S229 (LLDPE)**

$(T_{mix}=190^{\circ}C; T_{test}=190^{\circ}C, \gamma^{\circ}=10\%)$

○   Experimental data

——   Curve fit (Equation 6.4)

Dynamic viscosity, η', Pas

Frequency, ω, rad/s

Figure C.14 Calculation of $\sigma_y{}'$ for 90% S229 (LLDPE)

$$(T_{mix}=190^{\circ}C; \ T_{test}=190^{\circ}C, \ \gamma^{\circ}=10\%)$$

$(G'_{blend})^{0.5} = 1.077 + 0.989 \ (G'_{matrix})^{0.5}$ $(r^2=0.9995)$

Figure C.15 G'(φ) for blends* of S229 (LLDPE) and S216 (LDPE)

(T_{mix}=190°C; T_{test}=190°C, γ°=10%, ω=1.0 rad/s)

*with additional 1000 ppm of A/O

Elastic modulus, G', Pa

S229 (LLDPE), φ, %

Figure C.16 G'(φ) for blends* of S229 (LLDPE) and S216 (LDPE)

$(T_{mix}=190°C; T_{test}=190°C, \gamma=10\%, \omega=0.04$ rad/s)

*with additional 1000 ppm of A/O

Figure C.17 G'(φ) for blends* of S229 (LLDPE) and S216 (LDPE)

$(T_{mix}=190^{\circ}C; T_{test}=190^{\circ}C, \gamma^{\circ}=10\%, \omega=0.1\ rad/s)$

*with additional 1000 ppm of A/O

Figure C.18 G'(φ) for blends* of S229 (LLDPE) and S216 (LDPE)

Figure C.19 G'(φ) for blends* of S229 (LLDPE) and S216 (LDPE)

$(T_{mix}=190°C; T_{test}=190°C, γ°=10\%, ω=100 \text{ rad/s})$

*with additional 1000 ppm of A/O
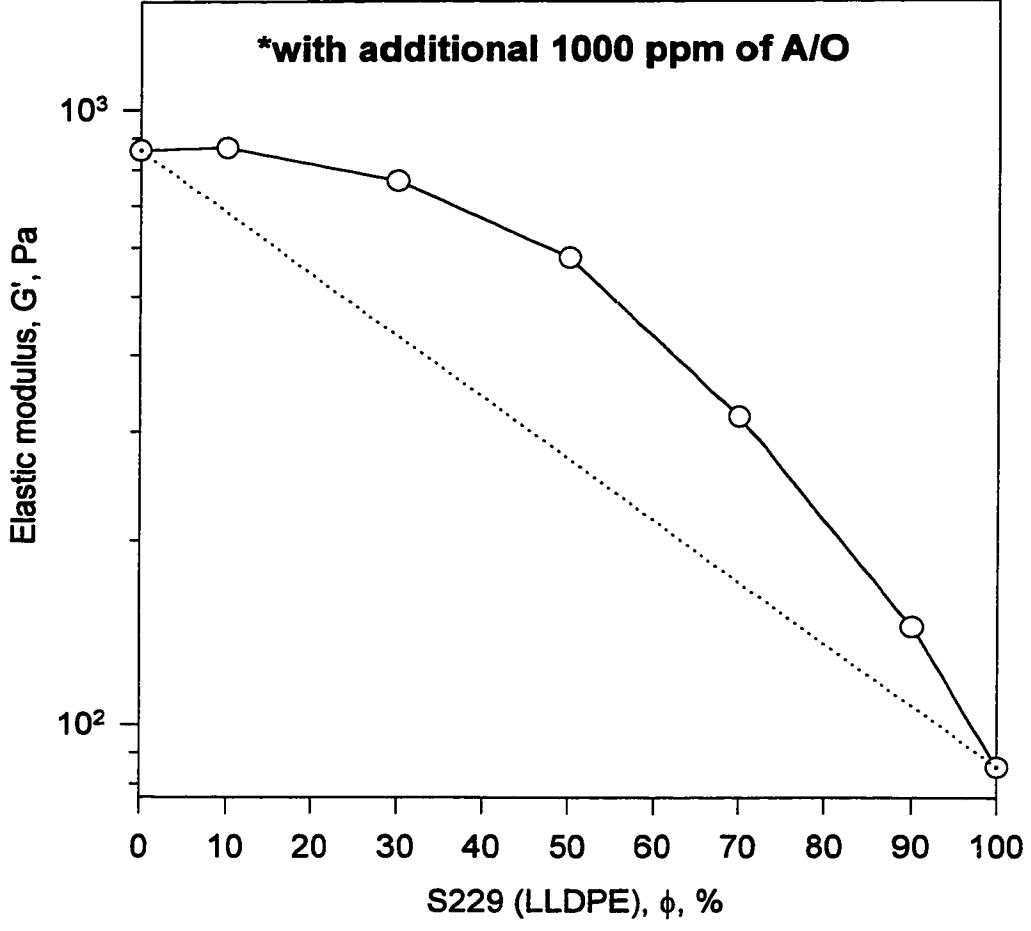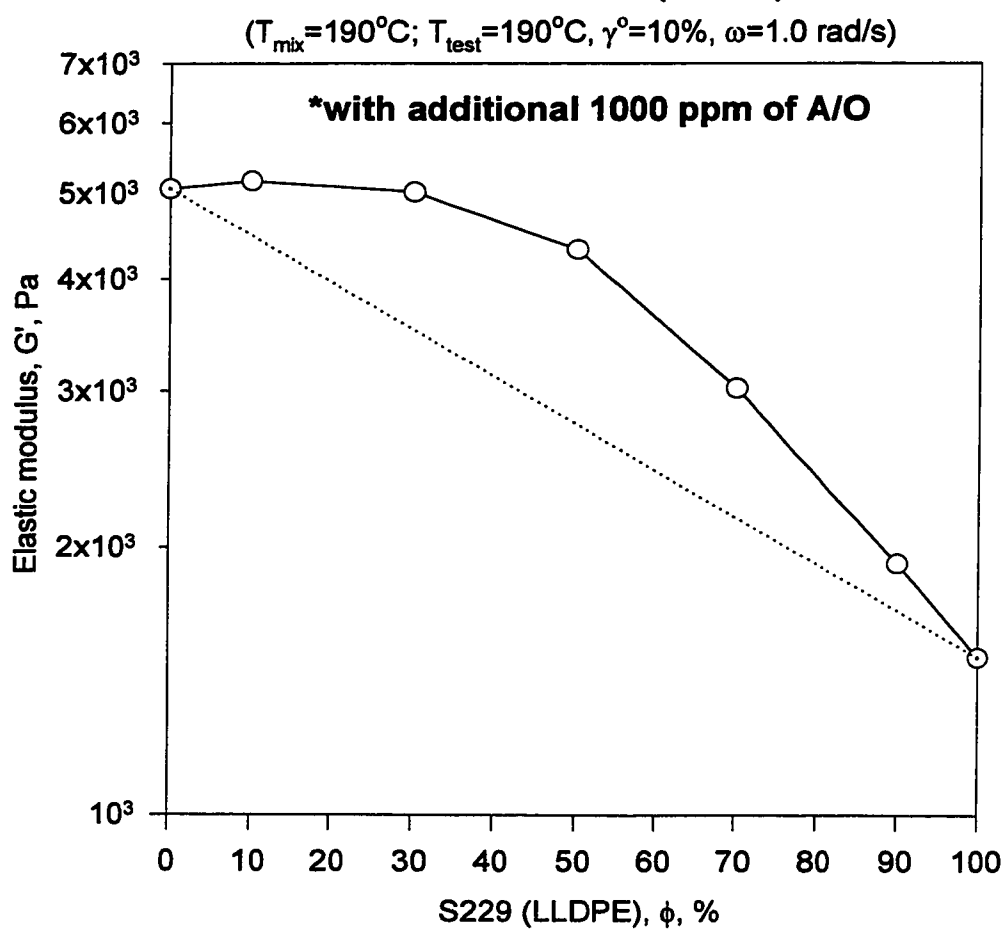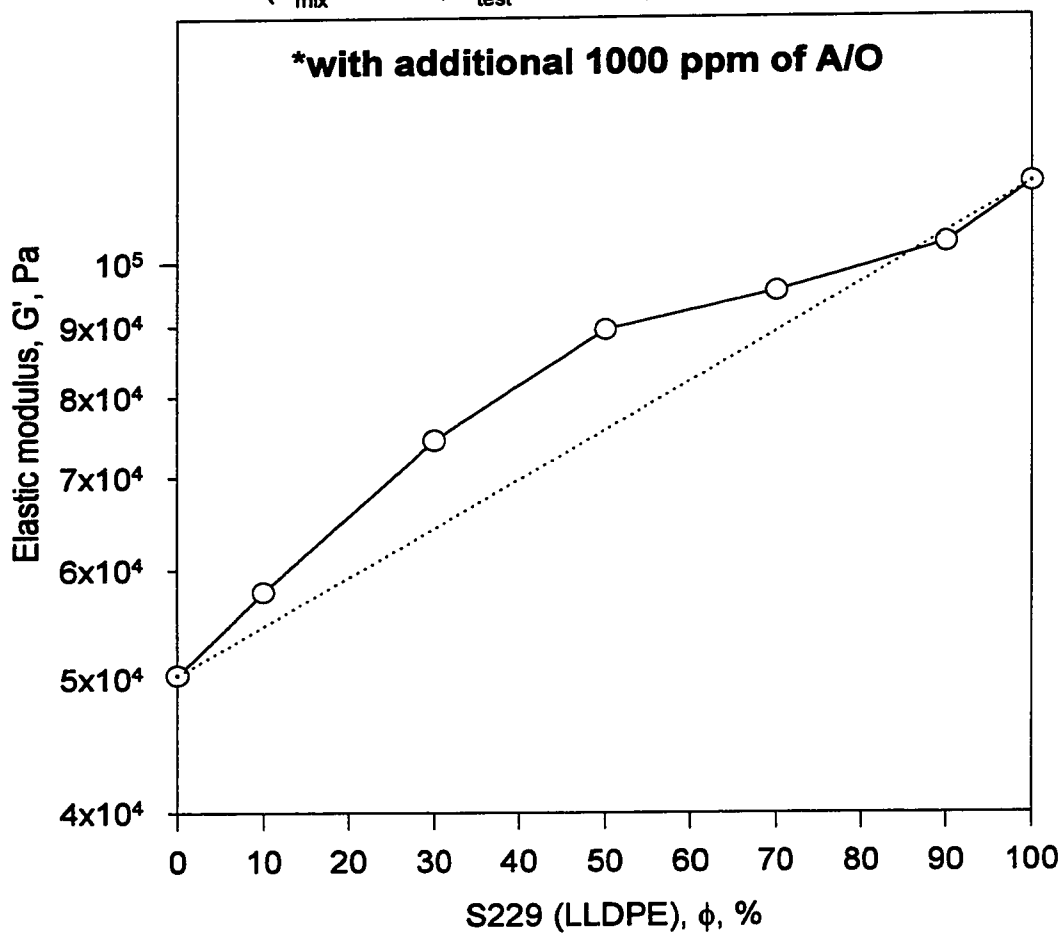
Figure C.20 $a_\phi(\phi)$ for blends of S216 (LDPE) and S229 (LLDPE)

$(T_{mix}=190°C; T_{test}=190°C, \omega=0.01\text{-}100 \text{ rad/s})$

Shift factor, a_ϕ

Composition, ϕ, % S229
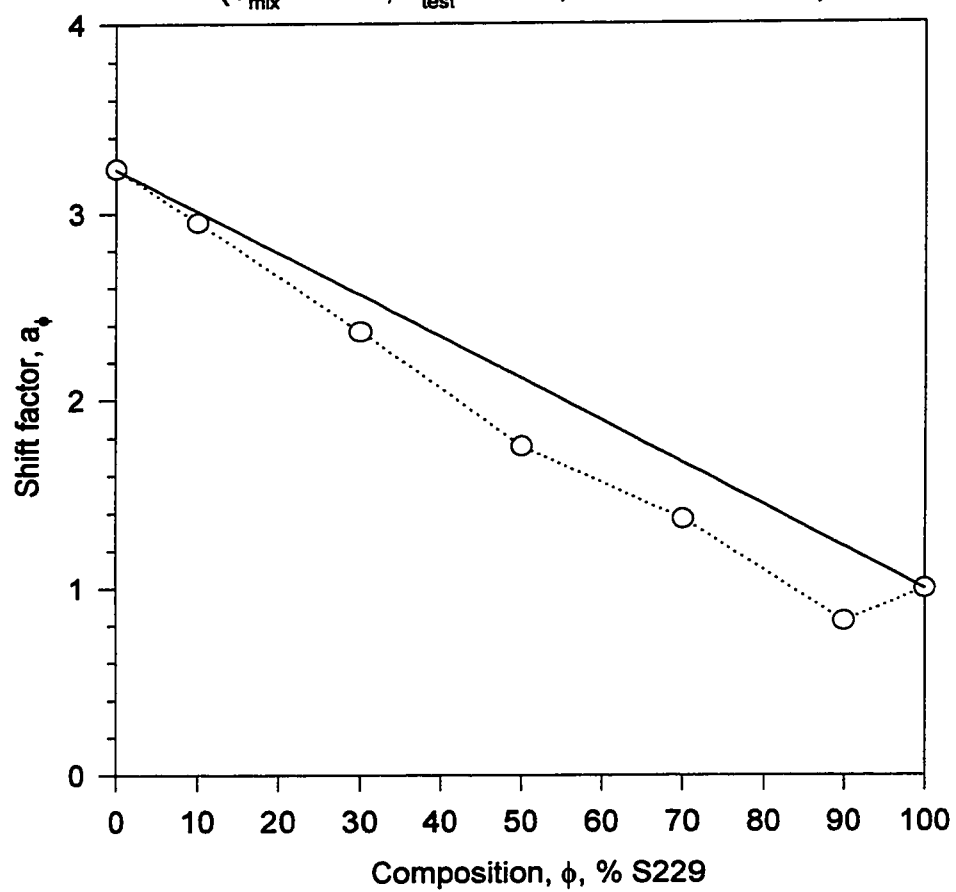
Figure C.21 η'(ω) for blends* of S229 (LLDPE) and S216 (LDPE)

$(T_{mix}=220°C; T_{test}=190°C, \gamma°=10\%, C\&P)$

Frequency, ω, rad/s
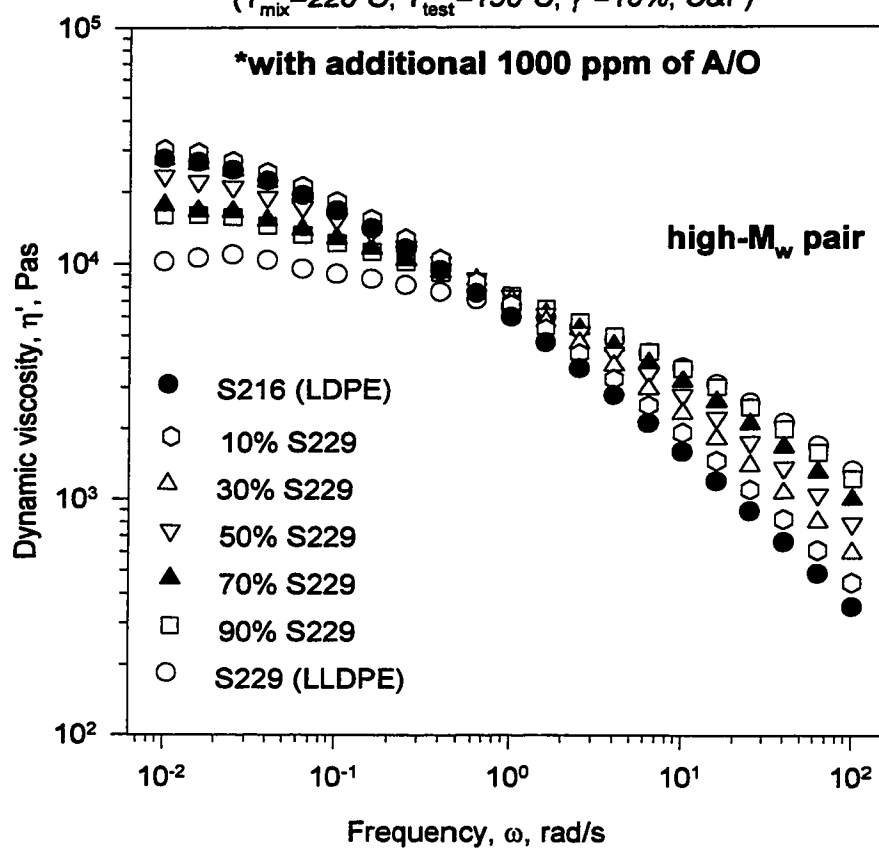
Figure C.22 $\eta'(\tau)$ for blends* of S216 (LDPE) and S229 (LLDPE)

$(T_{mix}=220^{\circ}C; T_{test}=190^{\circ}C, \gamma^{\circ}=10\%, \omega=0.01\text{-}100 \text{ rad/s})$

*with additional 1000 ppm of A/O

high-M$_w$ pair

Dynamic viscosity, η', Pas

10^4

10^3

10^2

○ S216 (LDPE)
▲ 10% S229
▽ 30%S229
▼ 50% S229
△ 70% S229
□ 90% S229
● S229 (LLDPE)

10^2 10^3 10^4 10^5

Stress,τ, ($\eta^* \times \omega$), Pa
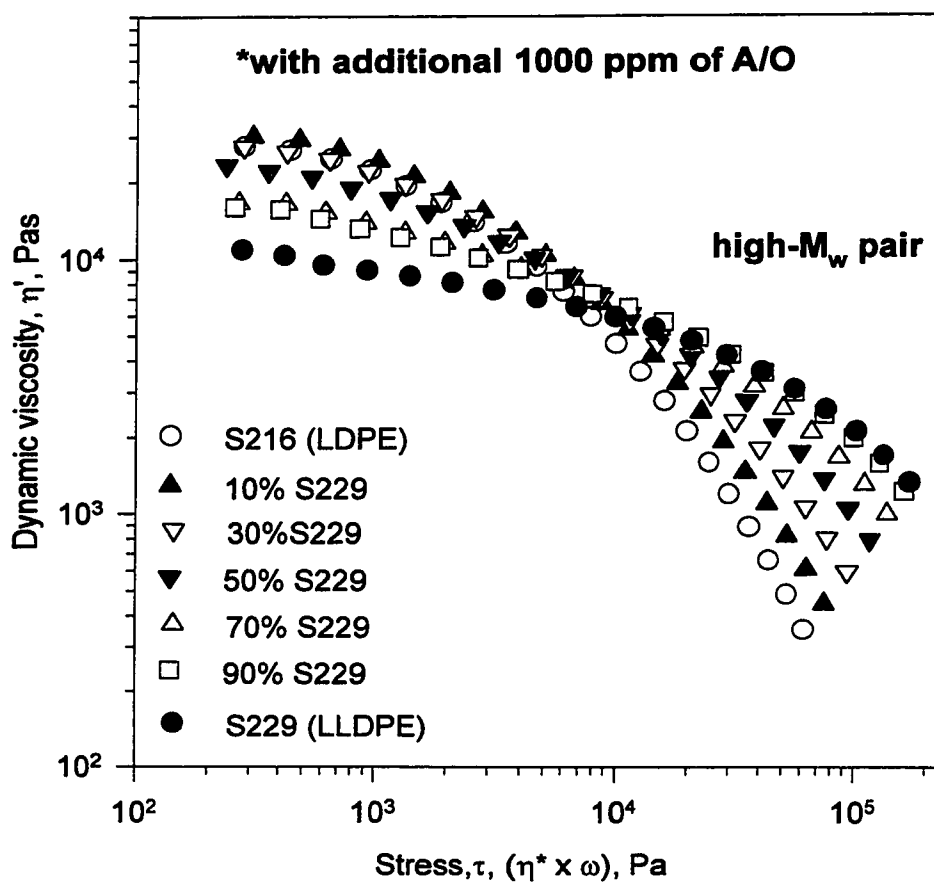
Figure C.23 $\eta'(\phi)$ **for blends* of S229 (LLDPE) and S216 (LDPE)**

$(T_{mix}=220°C; T_{test}=190°C, \gamma°=10\%, \omega=0.1 \text{ rad/s})$
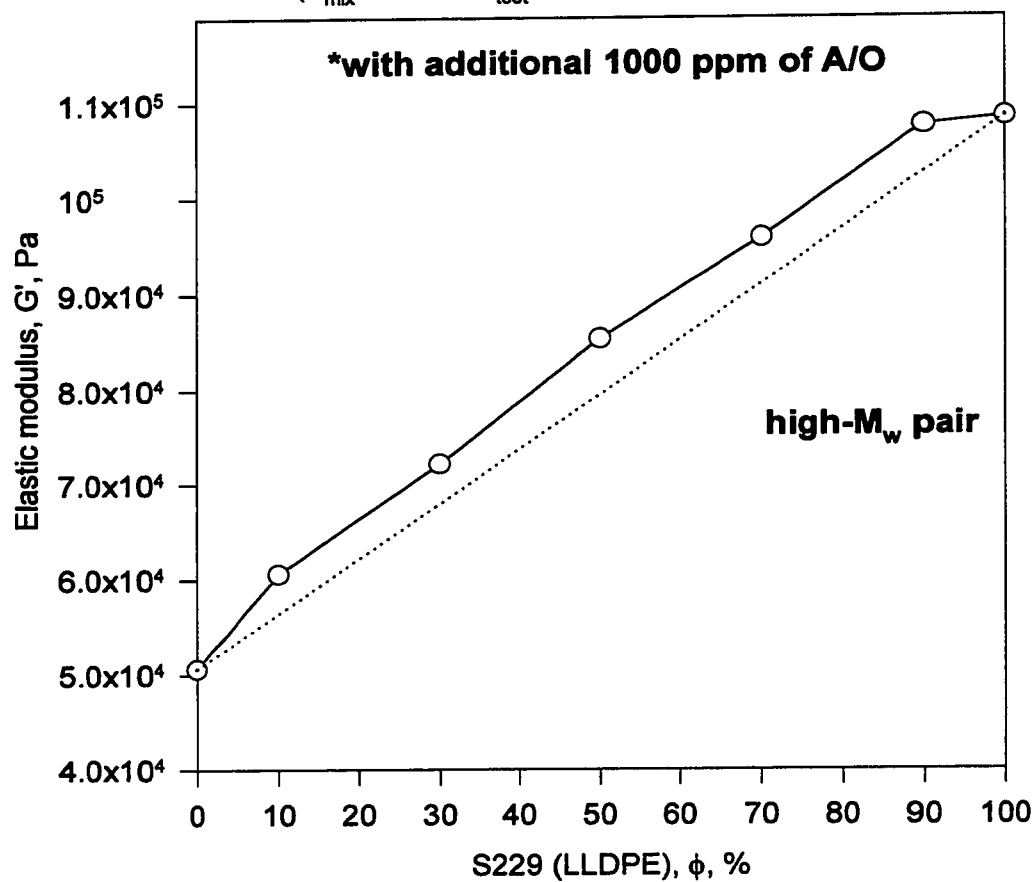
*with additional 1000 ppm of A/O

high-M_w pair
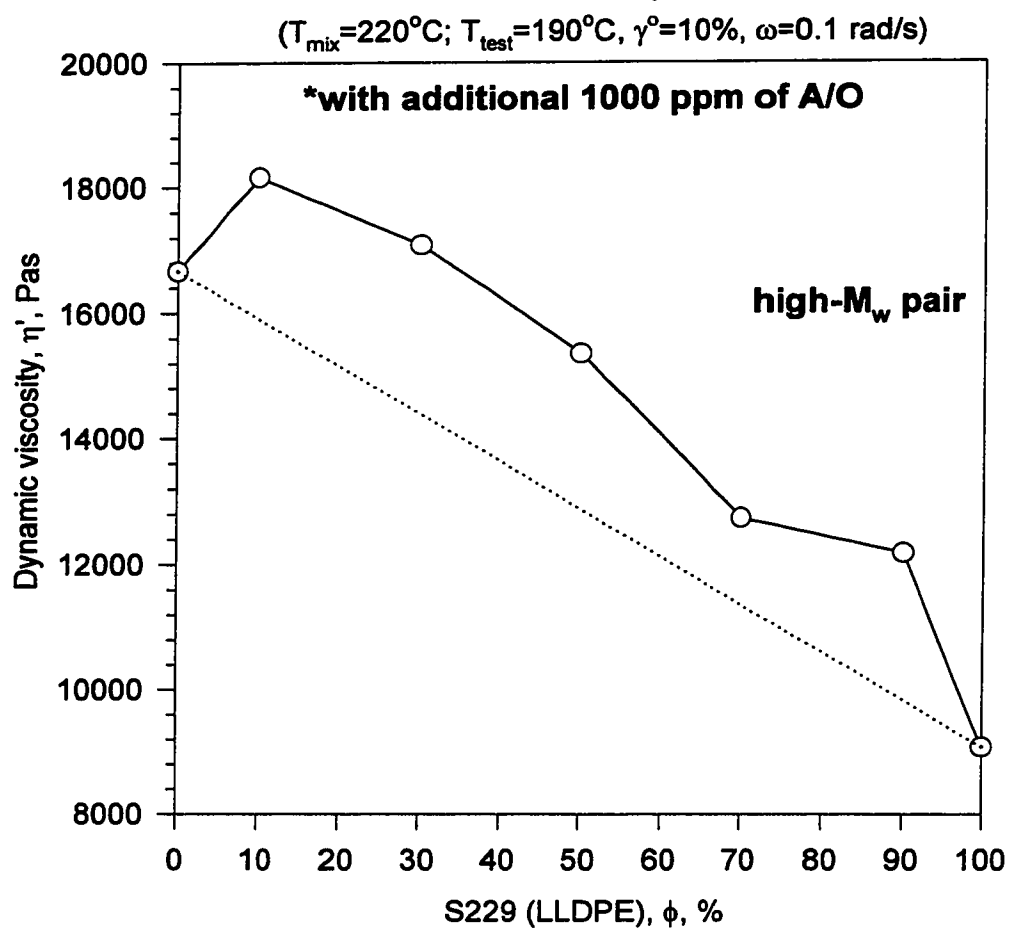
Figure C.24 $\eta'(\phi)$ for blends* of S229 (LLDPE) and S216 (LDPE)
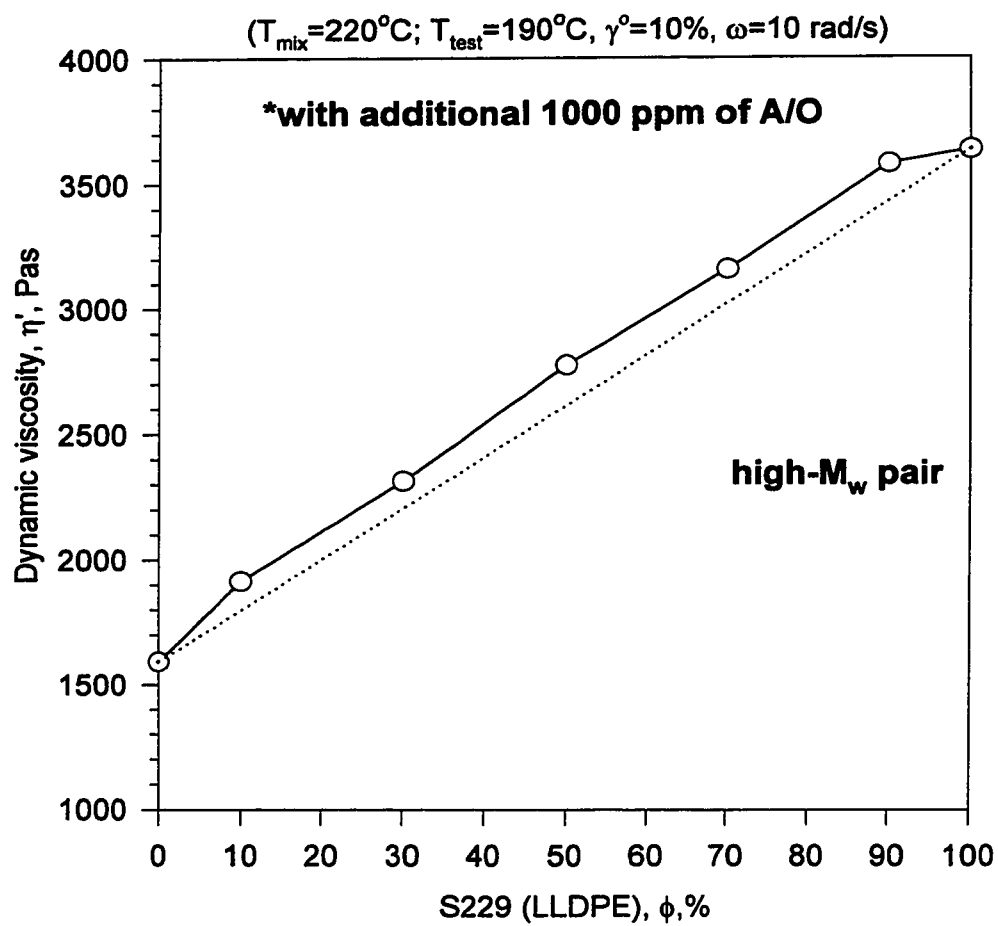
Figure C.25 $\eta'(\phi)$ for blends* of S229 (LLDPE) and S216 (LDPE)

$(T_{mix}=220°C; T_{test}=190°C, \gamma°=10\%, \omega=100$ rad/s$)$

*with additional 1000 ppm of A/O

high-M_w pair
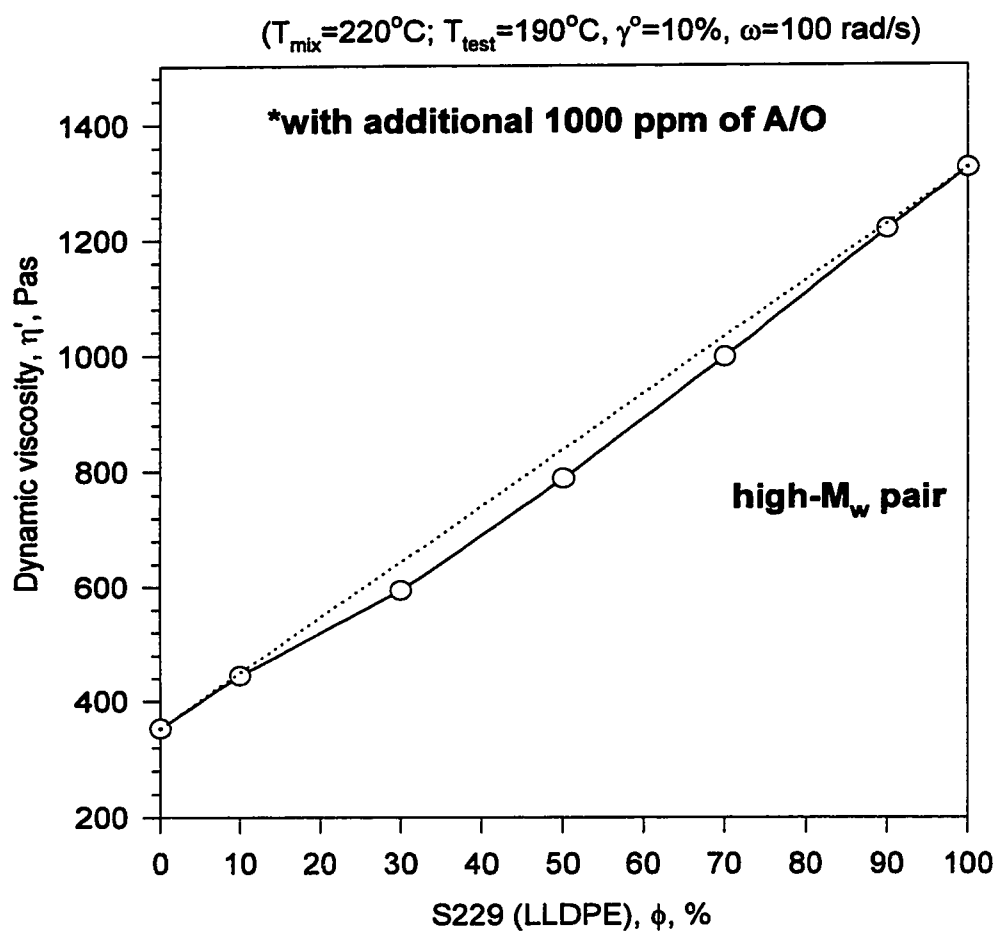
Figure C.26 $\theta(\phi)$ for blends* of S229 (LLDPE) and S216 (LDPE)

$(T_{mix}=220°C; T_{test}=190°C, \gamma°=10\%, C\&P)$

high-M_w pair

Mean relaxation time, θ, s

S229 (LLDPE), ϕ, %

Figure C.27 G'(ω) for blends* of S229 (LLDPE) and S216 (LDPE)

$(T_{mix}=220°C; T_{test}=190°C, \gamma°=10\%, C\&P)$

*with additional 1000 ppm of A/O

high-M_w pair

- ● S216 (LDPE)
- ⬡ 10% S229
- △ 30% S229
- ▽ 50% S229
- ▲ 70% S229
- □ 90% S229
- ○ S229 (LLDPE)

Figure C.28 G'(τ) for blends* of S216 (LDPE) and S229 (LLDPE)

(T_{mix}=220°C; T_{test}=190°C, $\gamma°$=10%,ω=0.01-100 rad/s)

Figure C.29 G'(φ) for blends* of S229 (LLDPE) and S216 (LDPE)

$(T_{mix}=220^{\circ}C; T_{test}=190^{\circ}C, \gamma^{\circ}=10\%, \omega=0.1$ rad/s)

*with additional 1000 ppm of A/O

high-M_w pair

Elastic modulus, G', Pa

S229 (LLDPE), φ, %

Figure C.30 G'(φ) for blends* of S229 (LLDPE) and S216 (LDPE)

$(T_{mix}=220°C; T_{test}=190°C, \gamma°=10\%, \omega=100\ rad/s)$

*with additional 1000 ppm of A/O

high-M_w pair
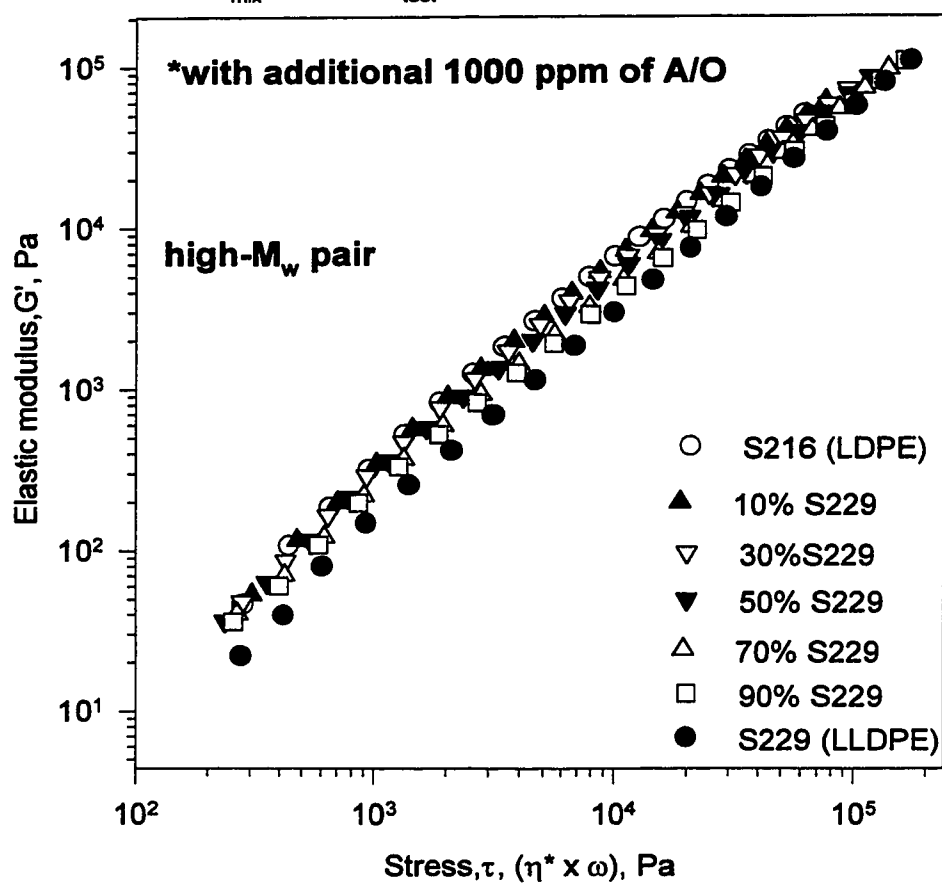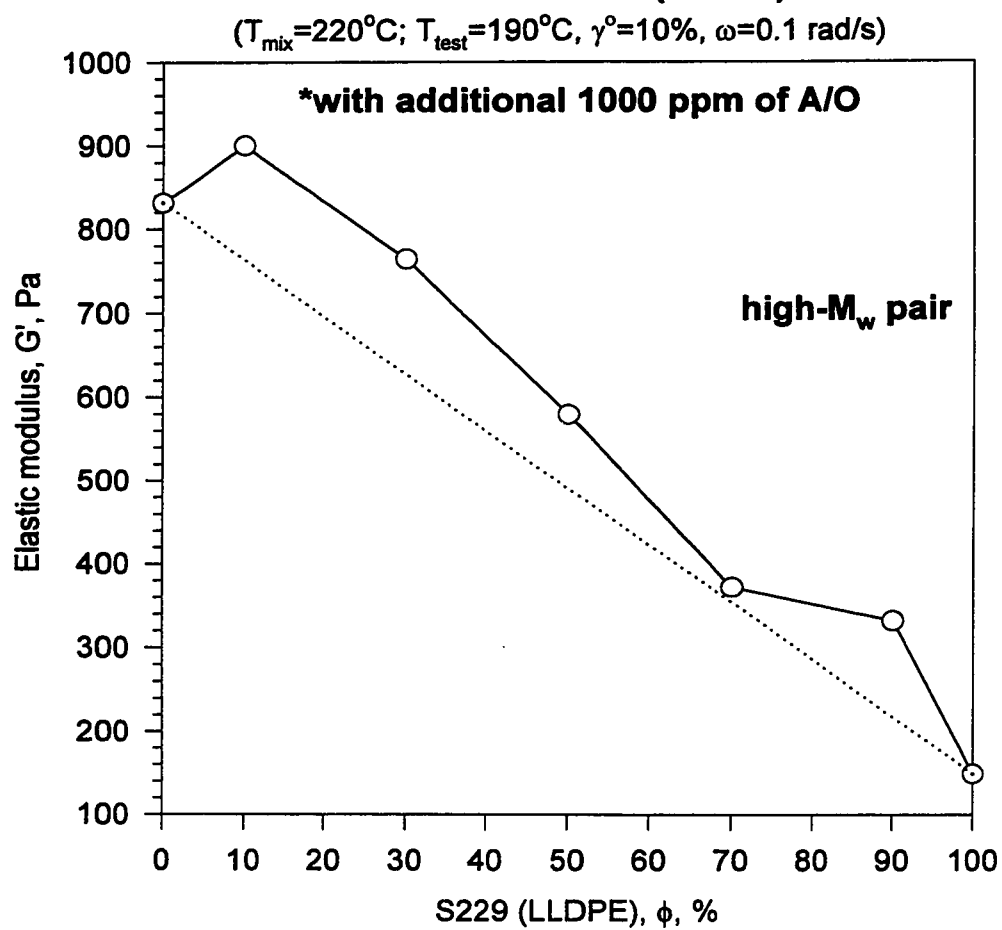
Figure C.31 η'(ω) for blends* of S226 (octene) and S216 (LDPE)

$(T_{mix}=190; T_{test}=190°C, \gamma°=10\%, C\&P)$

Figure C.32 $\eta'(\tau)$ for blends* of S226 (octene) and S216 (LDPE)

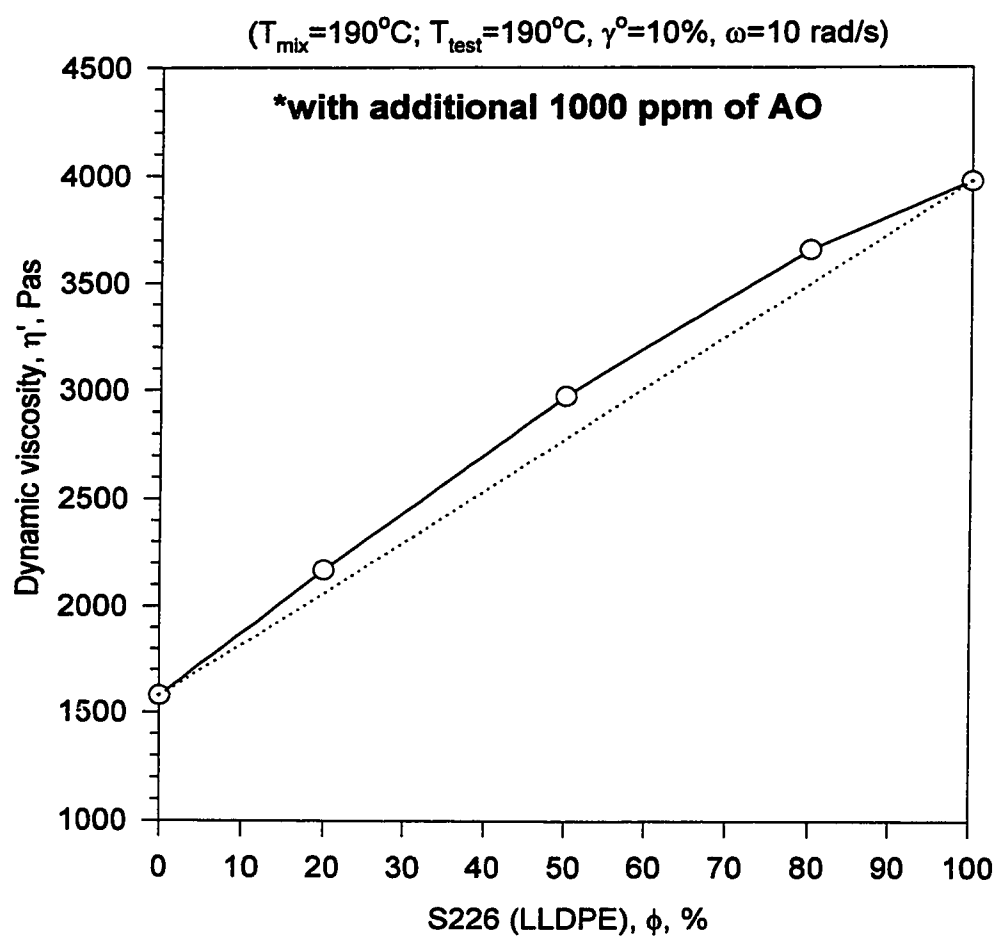$(T_{mix}=190^{\circ}C; T_{test}=190^{\circ}C, \gamma^{\circ}=10\%, C\&P)$

*with additional 1000 ppm of AO

○ S216 (LDPE)
▲ 20% S226
□ 50% S226
▽ 80% S226
● S226 (Octene)

]
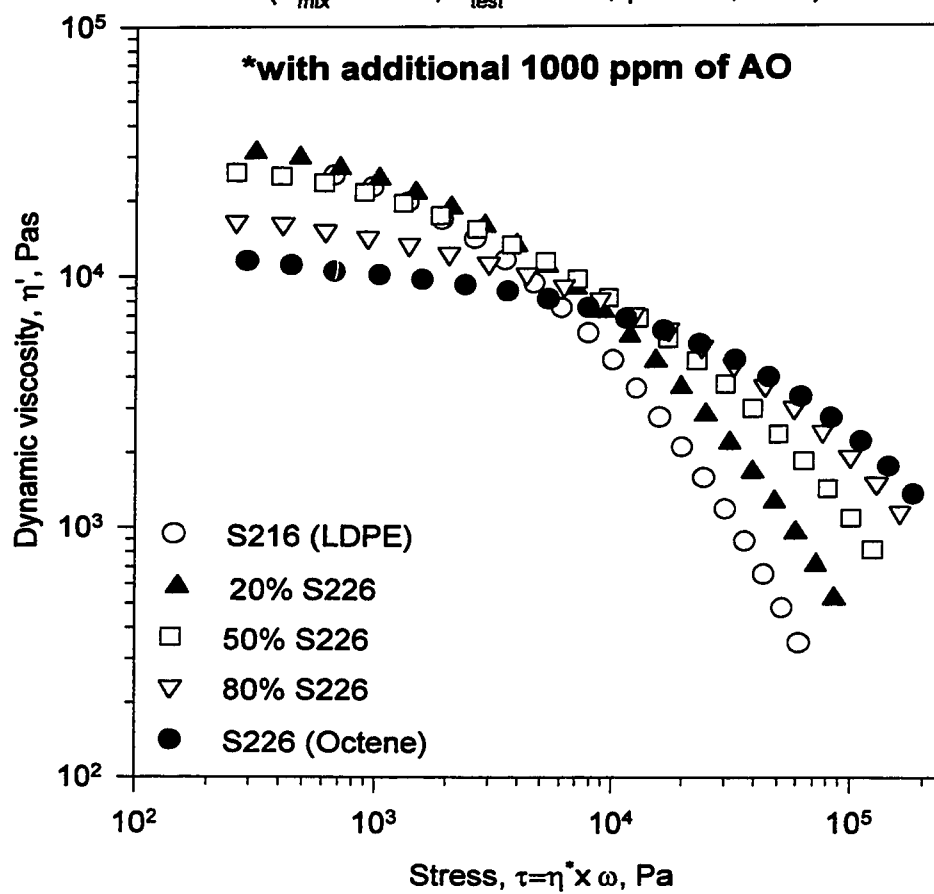
Figure C.33 $\eta'(c)$ **for blends* of S226 (octene) and S216 (LDPE)**

$(T_{mix}=190^{\circ}C;\ T_{test}=190^{\circ}C,\ \gamma^{\circ}=10\%,\ \omega=0.1\ rad/s)$

*with additional 1000 ppm of AO

Dynamic viscosity, η', Pas
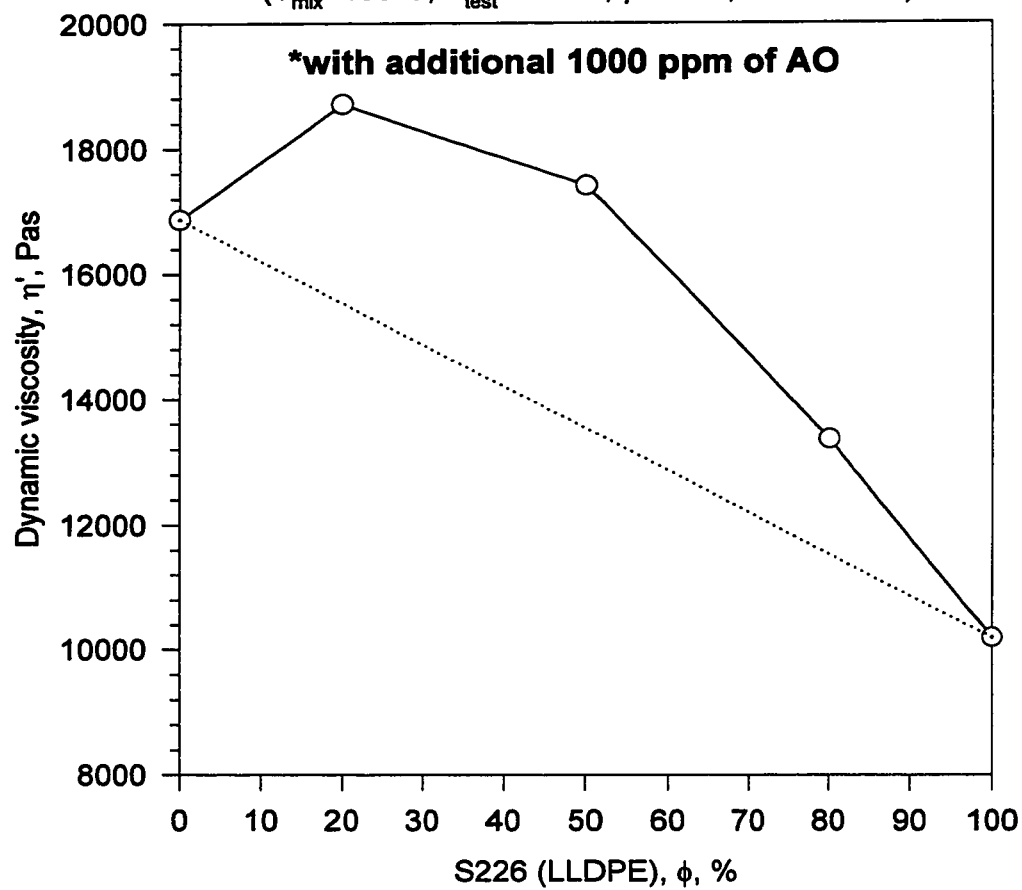
S226 (LLDPE), ϕ, %

Figure C.34 $\eta'(\phi)$ for blends* of S226 (octene) and S216 (LDPE)

$(T_{mix}=190^\circ C; T_{test}=190^\circ C, \gamma^\circ=10\%, \omega=10$ rad/s$)$

*with additional 1000 ppm of AO

Figure C.35 $\eta'(\phi)$ for blends* of S226 (octene) and S216 (LDPE)

$(T_{mix}=190°C; T_{test}=190°C, \gamma°=10\%, \omega=100$ rad/s)

*with additional 1000 ppm of AO
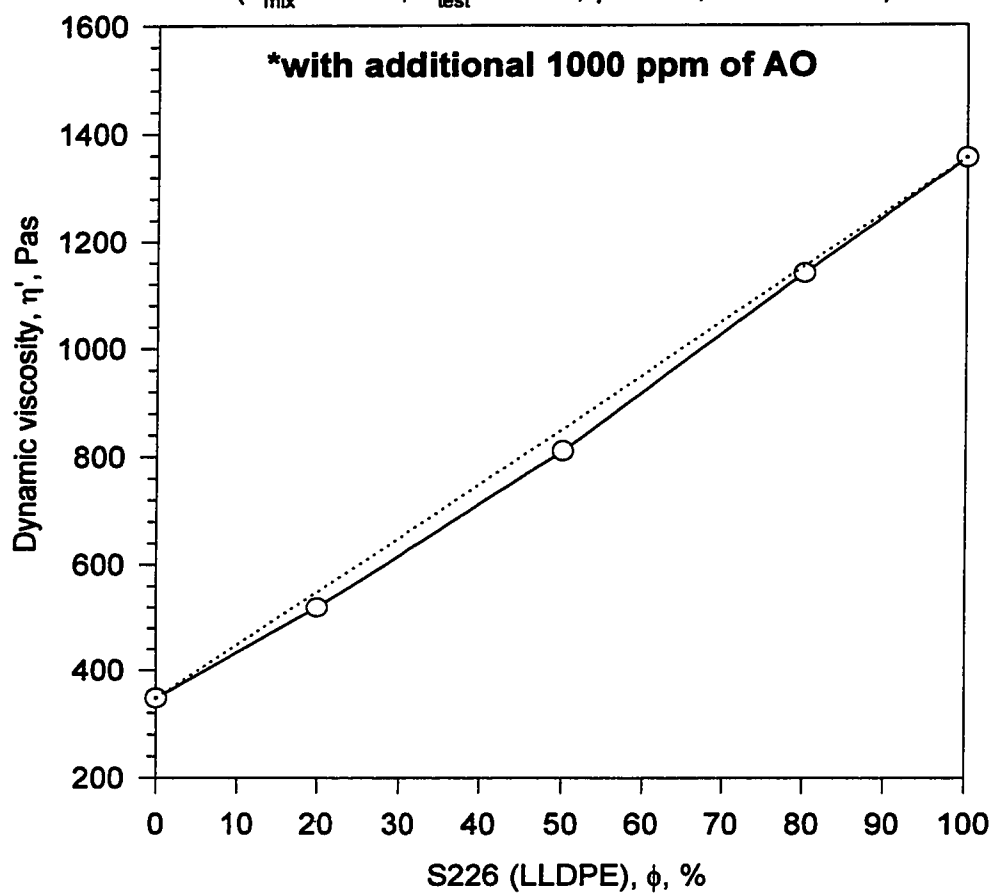
Figure C.36 $\theta(\phi)$ for blends of S226 (LLDPE) and S216 (LDPE)

$(T_{mix}=190^\circ C; T_{test}=190^\circ C, \gamma^\circ=10\%, \omega=0.01\text{-}100 \text{ rad/s})$
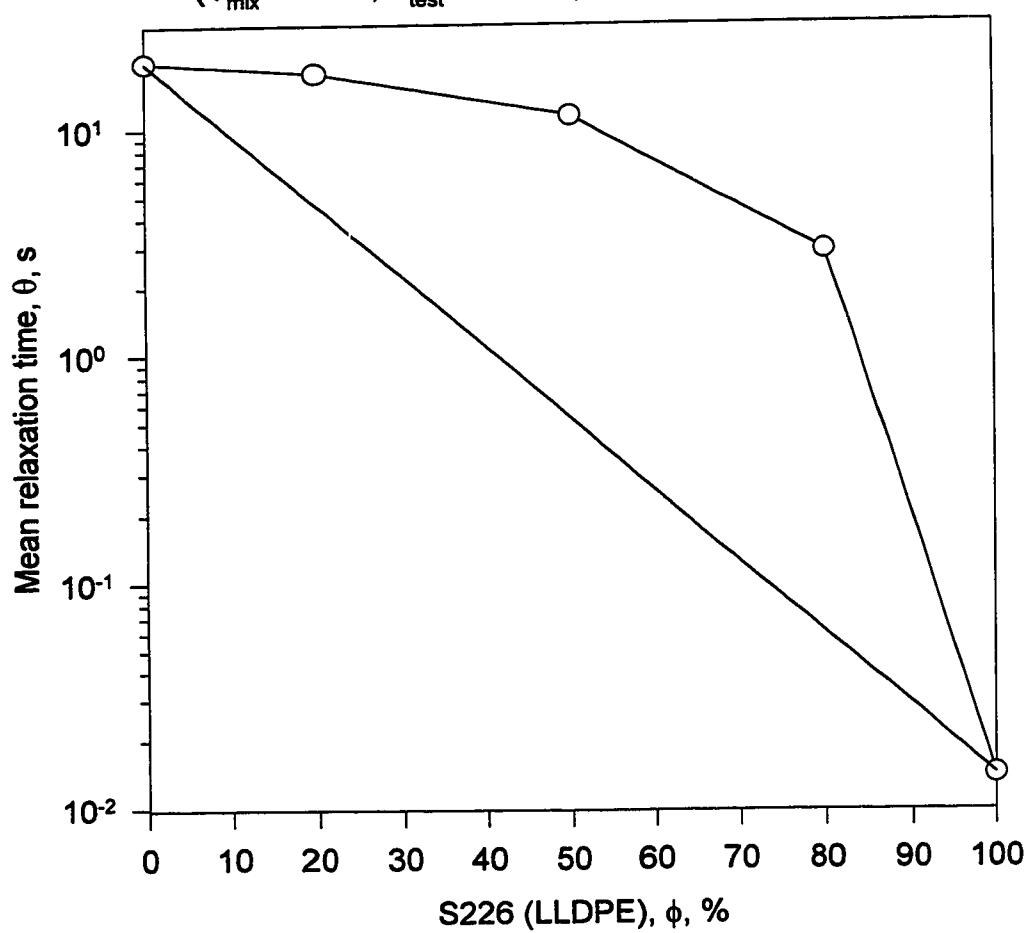
Figure C.37 G'(ω) for blends* of S226 (octene) and S216 (LDPE)

$(T_{mix}=190°C, T=190°C, \gamma°=10\%, C\&P)$
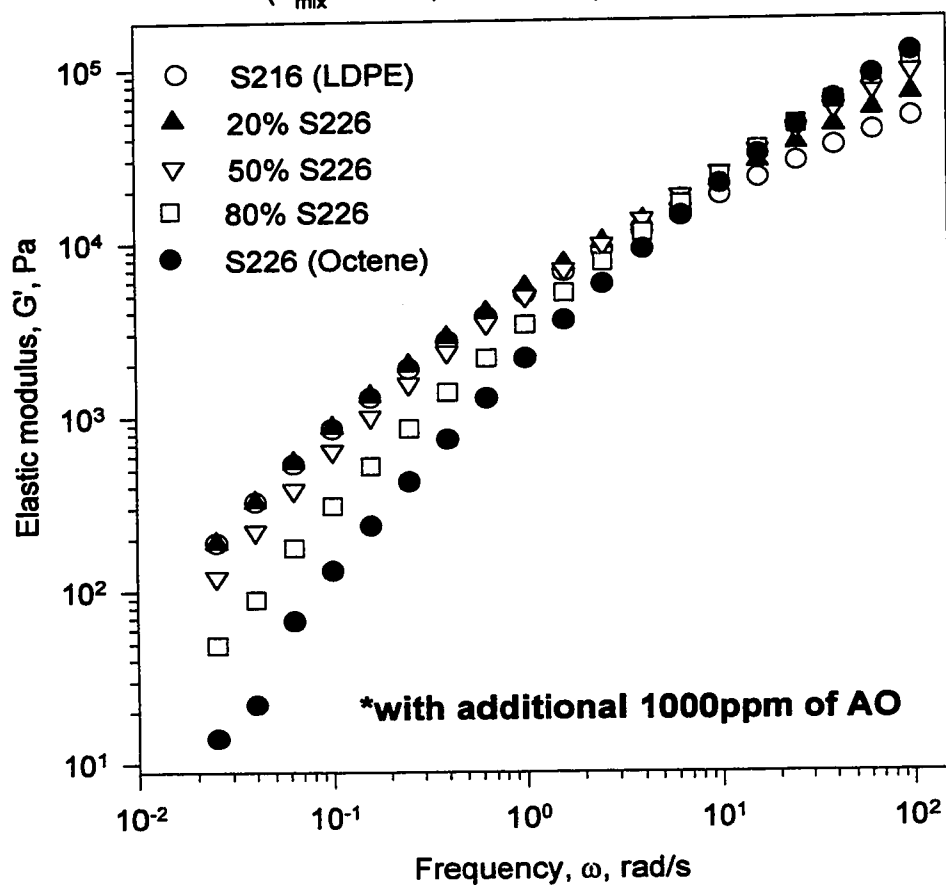
Figure C.38 G'(τ) for blends* of S226 (LLDPE) and S216 (LDPE)

$(T_{mix}=190°C; T_{test}=190°C, \gamma°=10\%, \omega=0.01\text{-}100 \text{ rad/s, C\&P})$
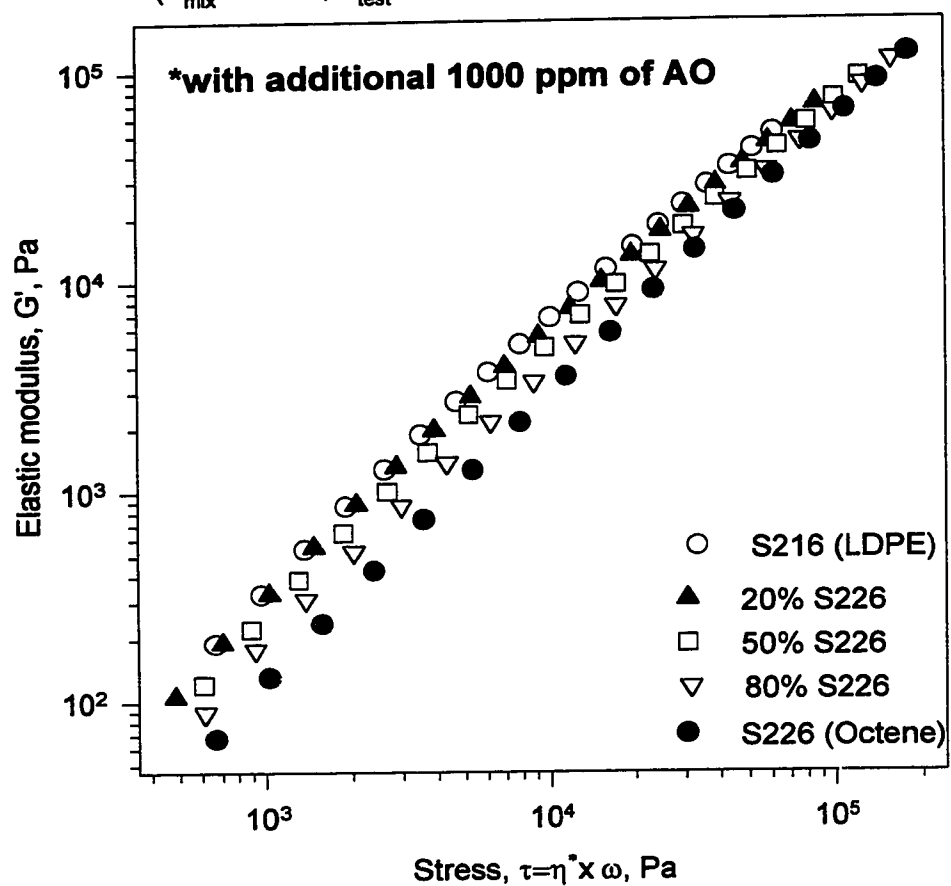
*with additional 1000 ppm of AO

Elastic modulus, G', Pa

○ S216 (LDPE)
▲ 20% S226
□ 50% S226
▽ 80% S226
● S226 (Octene)

Stress, τ=η*x ω, Pa

Figure C.39 G'(φ) for blends* of S226 (octene) and S216 (LDPE)

$(T_{mix}=190°C; T_{test}=190°C, \gamma°=10\%, \omega=0.1 \text{ rad/s})$

*with additional 1000 ppm of AO

Figure C.40 G'(ϕ) for blends* of S226 (octene) and S216 (LDPE)

(T_{mix}=190°C; T_{test}=190°C, γ°=10%, ω=100 rad/s)

*with additional 1000 ppm of A/O
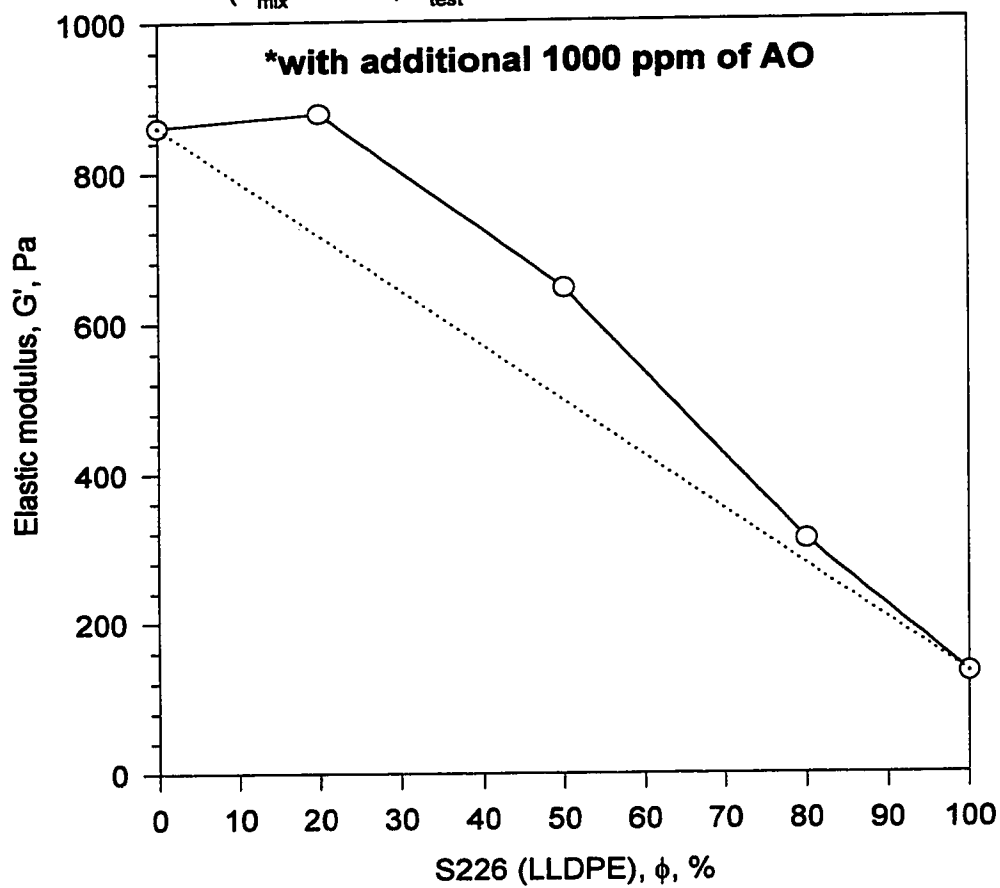
Figure C.41 Viscoelastic properties of S226 (Octene)

$(T_{mix}=190°C; T_{test}=190°C, \gamma°=10\%, C\&P)$

○   η' (as-received)

▲   η' (with 1000 ppm extra AO)

□   G' (as-received)

▼   G' (with 1000 ppm extra AO)
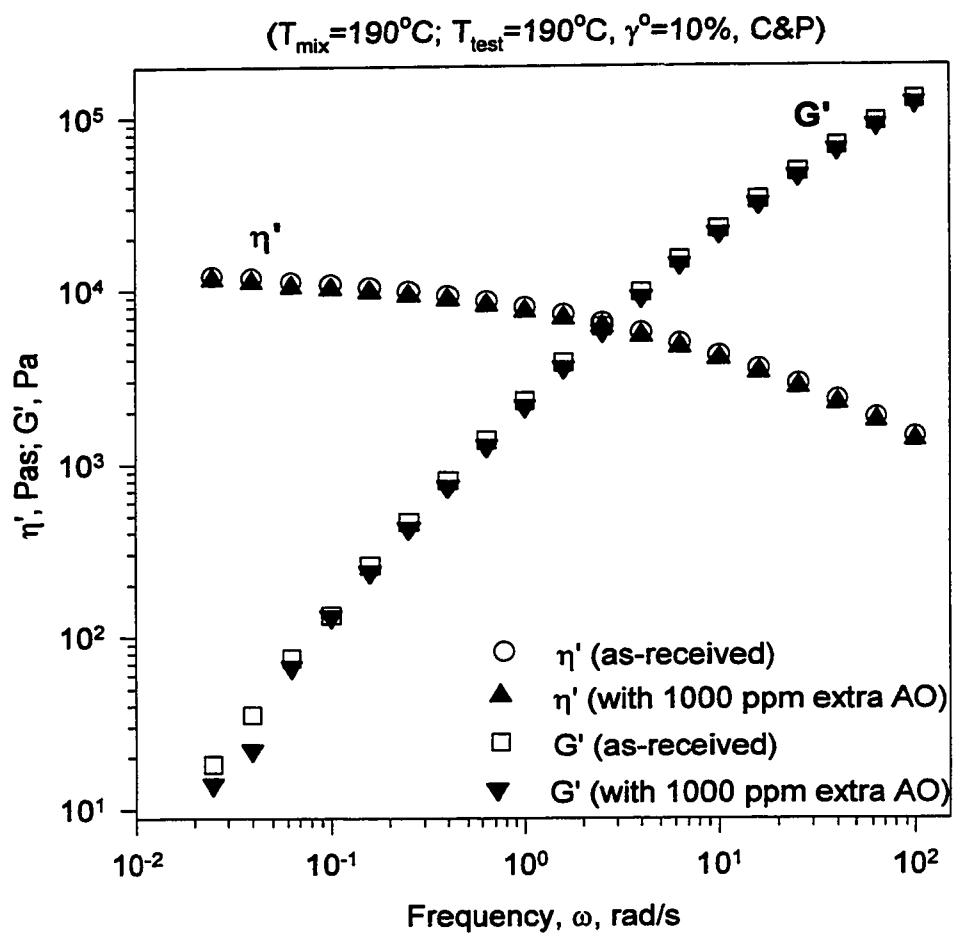
Figure C.42 $E_a(\phi)$ and $A_a(\phi)$ for blends* of S229 (butene) and S216 (LDPE)

$(T_{mix}=190°C; \omega=1$ rad/s, $\gamma°=10\%$, T=160°-260°C, PP)

*with additional 1000 ppm of AO
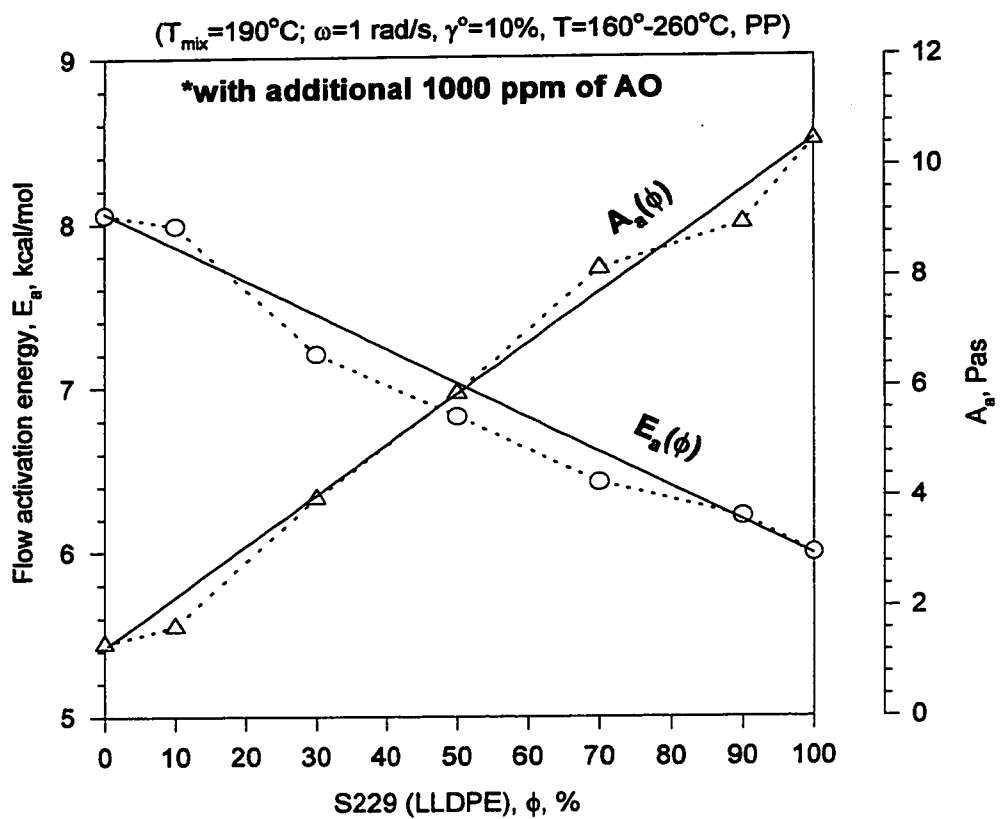
Figure C.43 $E_b(\phi)$ and $A_b(\phi)$ for blends* of S229 (butene) and S216 (LDPE) (T_{mix}=190°C; ω=1rad/s, $\gamma°$=10%, T=160°-260°C, PP)

*with additional 1000 ppm of AO
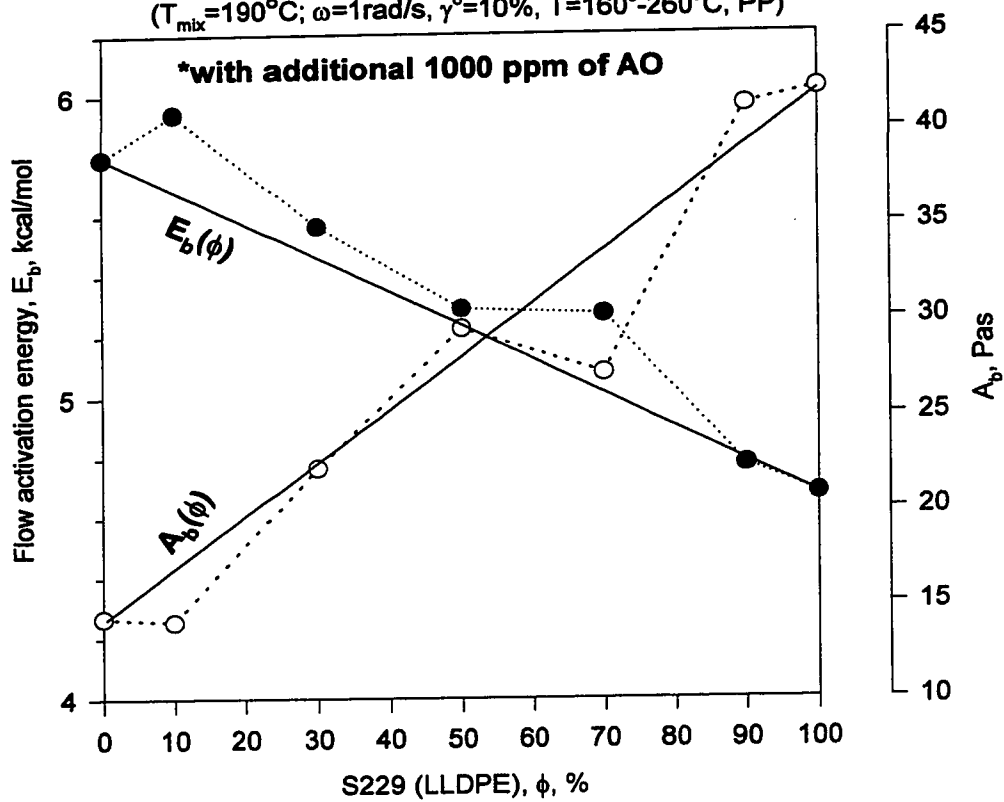
Figure C.44 $E_a(\phi)$ and $A_a(\phi)$ for blends* of S226 (octene) and S216

(T_{mix}=190°C; ω=1 rad/s, $\gamma°$=10%, T=160°-260°C, PP)
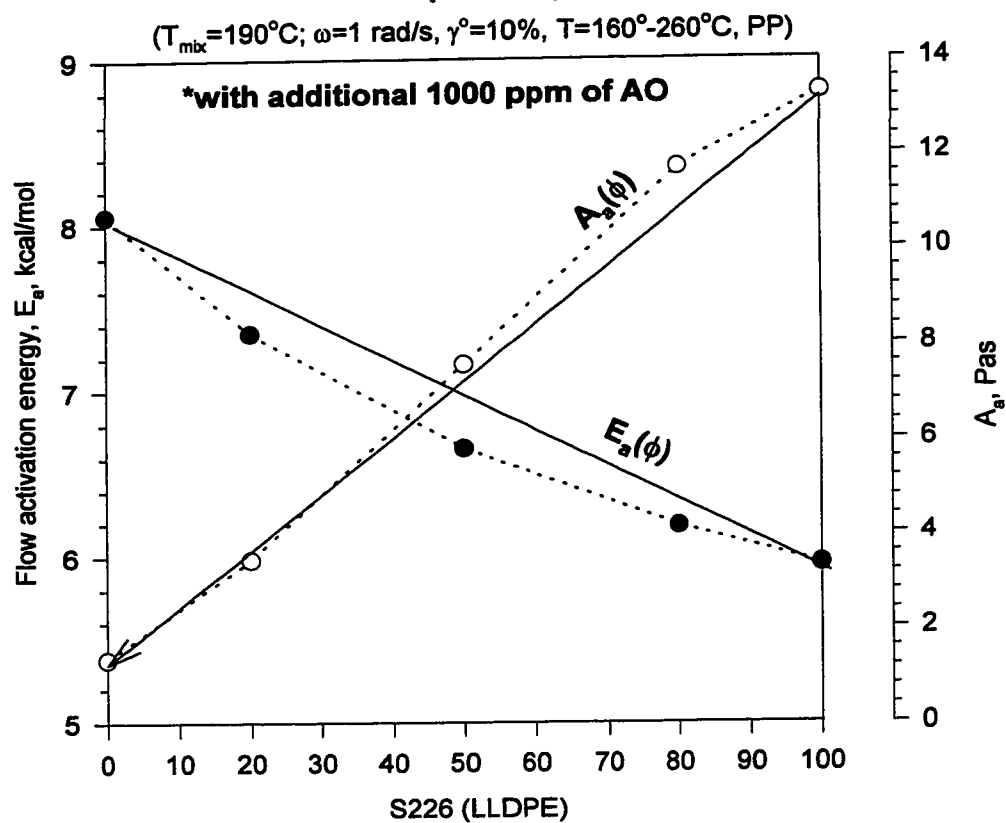
Figure C.45 $E_b(\phi)$ and $A_b(\phi)$ for blends*
of S226 (octene) and S216

$(T_{mix}=190°C; \omega=1 \text{ rad/s}, \gamma°=10\%, T=160°-260°C, PP)$
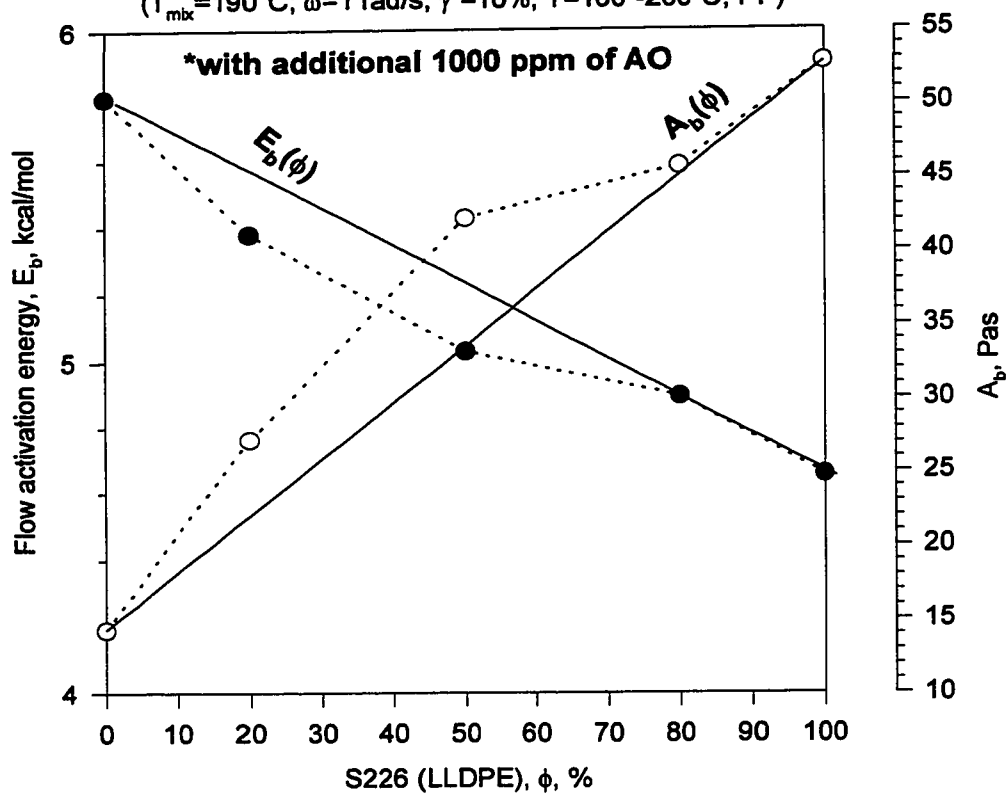
Appendix D

Supplement to Chapter VI

Calculation of Yield Stresses

Here, an alternative approach to finding σ_y' and σ_y'' is discussed. It calculates σ_y' and σ_y'' from a single dynamic measurement of $G''(\omega)$ and $G'(\omega)$ for each blend. Let us define stress:

$$\tau = \eta^* \times \omega \tag{D.1}$$

then, replace η^* by its viscous and elastic components η' and η'':

$$\tau = [(\eta')^2 + (\eta'')^2]^{1/2} \times \omega = [(\eta'\omega)^2 + (\eta''\omega)^2]^{1/2} \tag{D.2}$$

define:

$$\tau'(\omega) = \eta'(\omega) \times \omega = G''(\omega) \tag{D.3}$$

and

$$\tau''(\omega) = \eta''(\omega) \times \omega = G'(\omega) \tag{D.4}$$

Define yield stresses σ_y' and σ_y'' corresponding to τ' and τ'' respectively.

Therefore,

$$\sigma_y' = \lim \tau' \text{ as } \omega \to 0 \quad \text{or} \quad (\sigma_y')^{1/2} = \lim \tau'^{1/2} \text{ as } \omega^{1/2} \to 0 = \lim G''^{1/2} \text{ as } \omega^{1/2} \to 0 \tag{D.5}$$

$$\sigma_y'' = \lim \tau'' \text{ as } \omega \to 0 \quad \text{or} \quad (\sigma_y'')^{1/2} = \lim \tau''^{1/2} \text{ as } \omega^{1/2} \to 0 = \lim G'^{1/2} \text{ as } \omega^{1/2} \to 0 \tag{D.6}$$

Thus,

$$(\sigma_y')^{1/2} = \text{intercept of } G''^{1/2} \text{ vs. } \omega^{1/2} \tag{D.7}$$

$$\text{and } (\sigma_y'')^{1/2} = \text{intercept of } G'^{1/2} \text{ vs. } \omega^{1/2} \tag{D.8}$$

$(\sigma_y')^{1/2}$ calculated according to equation D.7 was found to be 1.9 $\text{Pa}^{1/2}$ which is the same as that obtained by the modified Casson approach (Figure 6.12). The yield stress σ_y can be calculated from σ_y' and σ_y'' $\{\sigma_y = [(\sigma_y')^2 + (\sigma_y'')^2]^{1/2}\}$.

Table D.1: Blends of S229 and S216: Yield Stresses ($T_{mix}=190^{\circ}C$)

Composition	$\sqrt{\sigma_y'}$, (Pa)$^{\frac{1}{2}}$	Matrix	$\sqrt{\sigma_y''}$, (Pa)$^{\frac{1}{2}}$
10% S229	0	LDPE	0
30% S229	0	LDPE	0
50% S229	0	LDPE	0
50% S229	4.8	LLDPE	6.0
70% S229	2.5	LLDPE	4.3
90% S229	1.1	LLDPE	1.9

Table D.2: Blends of S229 and S216: Yield Stresses ($T_{mix}=220^{\circ}C$)

Composition	$\sqrt{\sigma_y'}$, (Pa)$^{\frac{1}{2}}$	Matrix	$\sqrt{\sigma_y''}$, (Pa)$^{\frac{1}{2}}$
10% S229	0	LDPE	0
30% S229	0	LDPE	0
50% S229	0	LDPE	0
50% S229	5.4	LLDPE	3.9
70% S229	2.8	LLDPE	3.7
90% S229	2.5	LLDPE	2.2

Table D.3: Yield Stresses for S226 (octene)/S216 system

Composition	$\sqrt{\sigma_y'}$, (Pa)$^{\frac{1}{2}}$	Matrix	$\sqrt{\sigma_y''}$, (Pa)$^{\frac{1}{2}}$
20% S226	0	LDPE	0
50% S226	0	LDPE	0
50% S226	8.0	LDPE	6.0
80% S226	5.9	LLDPE	3.5

Figure D.1 Calculation of σ_y' for 90% S229 blend

$(T_{mix}=190°C; T_{test}=190°C, \gamma°=10\%)$

$(G'')^{0.5}=1.883+88.95 \, (\omega)^{0.5} \quad (r^2=0.9980)$

$\text{intercept}=(\sigma_y')^{0.5}=1.9 \, (Pa)^{0.5}$

Y-axis: $(\tau')^{0.5}= (\eta'\omega)^{0.5}, (Pa)^{0.5}$

X-axis: $\omega^{0.5}, (rad/s)^{0.5}$